ACS SYMPOSIUM SERIES 1101

Progress in Controlled Radical Polymerization: Materials and Applications

EDITED BY
Krzysztof Matyjaszewski
Brent S. Sumerlin
Nicolay V. Tsarevsky

Downloaded by 89.163.35.42 on May 30, 2012 | http://pubs.acs.org
Publication Date (Web): March 20, 2012 | doi: 10.1021/bk-2012-1101.fw001

Progress in Controlled Radical Polymerization: Materials and Applications

In Progress in Controlled Radical Polymerization: Materials and Applications; Matyjaszewski, K., et al.;
ACS Symposium Series; American Chemical Society: Washington, DC, 2012.

Downloaded by 89.163.35.42 on May 30, 2012 | http://pubs.acs.org
Publication Date (Web): March 20, 2012 | doi: 10.1021/bk-2012-1101.fw001

ACS SYMPOSIUM SERIES **1101**

Progress in Controlled Radical Polymerization: Materials and Applications

Krzysztof Matyjaszewski, Editor
Carnegie Mellon University
Pittsburgh, Pennsylvania

Brent S. Sumerlin, Editor
Southern Methodist University
Dallas, Texas

Nicolay V. Tsarevsky, Editor
Southern Methodist University
Dallas, Texas

Sponsored by the
ACS Division of Polymer Chemistry, Inc.

American Chemical Society, Washington, DC

Distributed in print by Oxford University Press, Inc.

Downloaded by 89.163.35.42 on May 30, 2012 | http://pubs.acs.org
Publication Date (Web): March 20, 2012 | doi: 10.1021/bk-2012-1101.fw001

In Progress in Controlled Radical Polymerization: Materials and Applications; Matyjaszewski, K., et al.;
ACS Symposium Series; American Chemical Society: Washington, DC, 2012.

Downloaded by 89.163.35.42 on May 30, 2012 | http://pubs.acs.org
Publication Date (Web): March 20, 2012 | doi: 10.1021/bk-2012-1101.fw001

Library of Congress Cataloging-in-Publication Data

Progress in controlled radical polymerization : materials and applications /
Krzysztof Matyjaszewski, editor ; Brent S. Sumerlin ; editor, Nicolay V. Tsarevsky, editor ;
sponsored by the ACS Division of Polymer Chemistry, Inc.
p. cm. -- (ACS symposium series ; 1101)
Includes bibliographical references and index.
ISBN 978-0-8412-2756-9 (alk. paper)
1. Polymerization. 2. Radicals (Chemistry) I. Matyjaszewski, K. (Krzysztof)
II. Sumerlin, Brent S. III. Tsarevsky, Nicolay V.
QD281.P6P76 2012
547′.7--dc23
2012005586

The paper used in this publication meets the minimum requirements of American National Standard for Information Sciences—Permanence of Paper for Printed Library Materials, ANSI Z39.48n1984.

Copyright © 2012 American Chemical Society

Distributed in print by Oxford University Press, Inc.

All Rights Reserved. Reprographic copying beyond that permitted by Sections 107 or 108 of the U.S. Copyright Act is allowed for internal use only, provided that a per-chapter fee of $40.25 plus $0.75 per page is paid to the Copyright Clearance Center, Inc., 222 Rosewood Drive, Danvers, MA 01923, USA. Republication or reproduction for sale of pages in this book is permitted only under license from ACS. Direct these and other permission requests to ACS Copyright Office, Publications Division, 1155 16th Street, N.W., Washington, DC 20036.

The citation of trade names and/or names of manufacturers in this publication is not to be construed as an endorsement or as approval by ACS of the commercial products or services referenced herein; nor should the mere reference herein to any drawing, specification, chemical process, or other data be regarded as a license or as a conveyance of any right or permission to the holder, reader, or any other person or corporation, to manufacture, reproduce, use, or sell any patented invention or copyrighted work that may in any way be related thereto. Registered names, trademarks, etc., used in this publication, even without specific indication thereof, are not to be considered unprotected by law.

PRINTED IN THE UNITED STATES OF AMERICA

Foreword

The ACS Symposium Series was first published in 1974 to provide a mechanism for publishing symposia quickly in book form. The purpose of the series is to publish timely, comprehensive books developed from the ACS sponsored symposia based on current scientific research. Occasionally, books are developed from symposia sponsored by other organizations when the topic is of keen interest to the chemistry audience.

Before agreeing to publish a book, the proposed table of contents is reviewed for appropriate and comprehensive coverage and for interest to the audience. Some papers may be excluded to better focus the book; others may be added to provide comprehensiveness. When appropriate, overview or introductory chapters are added. Drafts of chapters are peer-reviewed prior to final acceptance or rejection, and manuscripts are prepared in camera-ready format.

As a rule, only original research papers and original review papers are included in the volumes. Verbatim reproductions of previous published papers are not accepted.

ACS Books Department

Downloaded by 89.163.35.42 on May 30, 2012 | http://pubs.acs.org
Publication Date (Web): March 20, 2012 | doi: 10.1021/bk-2012-1101.fw001

Preface

This book and a preceding volume are addressed to chemists who are interested in radical processes and especially in controlled/living radical polymerization. They summarize the most recent accomplishments in the field.

The two volumes comprise the topical reviews and specialists' contributions presented at the American Chemical Society Symposium entitled *Controlled/ Living Radical Polymerization* that was held in Denver, Colorado, August 29- September 1, 2011. The Denver Meeting was a sequel to the previous ACS Symposia held in San Francisco, California, in 1997, in New Orleans, Louisiana, in 1999, in Boston, Massachusetts, in 2002, in Washington, DC, in 2005 and in Philadelphia, in 2008. They were summarized in the ACS Symposium Series Volume 685: *Controlled Radical Polymerization*, Volume 768: *Controlled/Living Radical Polymerization: Progress in ATRP, NMP and RAFT,* Volume 854: *Advances in Controlled/Living Radical Polymerization,* Volume 944: *Controlled/Living Radical Polymerization: From Synthesis to Materials,* Volume 1023: *Controlled/Living Radical Polymerization: Progress in ATRP*, and Volume 1024: *Controlled/Living Radical Polymerization: Progress in RAFT, DT, NMP and OMRP.* The Denver Meeting was very successful with 96 lectures and 83 posters presented. This illustrates a continuous growth in comparison with the San Francisco Meeting (32 lectures), the New Orleans (50 lectures), the Boston Meeting (80 lectures), the Washington Meeting (77 lectures) and the Philadelphia Meeting (90 lectures).

The 41chapters submitted for publication in the ACS Symposium series could not fit into one volume, and therefore we were asked by ACS to split them into two volumes. We decided to divide the chapters into volumes related to mechanisms and techniques (21 chapters) and materials (20 chapters).

Seven chapters in this volume are focused on macromolecular architecture, including sequence control, functionality and also shape of polymer chains in the form of stars or brushes. Two chapters discuss materials for electronic applications. Eight chapters present various aspects of polymeric/inorganic hybrid materials. The last four chapters describe bio-related materials.

The accompanying volume contains four chapters on general aspects of radical polymerization, nine chapters on ATRP, including two on ATRP commercial aspects, two chapters on organometallic radical polymerization and six chapters on reversible addition-fragmentation chain transfer polymerization and reversible iodine transfer polymerization.

Forty-one chapters published in two volumes show that CRP has made significant progress within the last 15 years. New systems have been discovered; substantial progress has been achieved in understanding the mechanism and

Downloaded by 89.163.35.42 on May 30, 2012 | http://pubs.acs.org
Publication Date (Web): March 20, 2012 | doi: 10.1021/bk-2012-1101.pr001

kinetics of reactions involved in all CRP systems. Significant progress has been made towards a comprehensive relationship between molecular structure and macroscopic properties. Some commercial applications of CRP were announced at the Denver Meeting, and it is anticipated that new products made by CRP will be soon on the market.

The financial support for the symposium from the following organizations is acknowledged: ACS Division of Polymer Chemistry, Inc., Boston Scientific, CSIRO, DSM, Evonik, General Electric, Lubrizol, the National Science Foundation, PPG, Royal Chemical Society and Wiley-VCH.

Krzysztof Matyjaszewski

Department of Chemistry
Carnegie Mellon University
4400 Fifth Avenue
Pittsburgh, Pennsylvania 15213

Brent Sumerlin

Department of Chemistry
Southern Methodist University
3215 Daniel Avenue
Dallas, Texas 75275

Nicolay V. Tsarevsky

Department of Chemistry
Southern Methodist University
3215 Daniel Avenue
Dallas, Texas 75275

Downloaded by 89.163.35.42 on May 30, 2012 | http://pubs.acs.org
Publication Date (Web): March 20, 2012 | doi: 10.1021/bk-2012-1101.pr001

Editors' Biographies

Krzysztof Matyjaszewski

Krzysztof Matyjaszewski is the J.C. Warner University Professor of Natural Sciences and Director of the Center for Macromolecular Engineering at Carnegie Mellon University. He developed atom transfer radical polymerization, commercialized in the U.S., Europe, and Japan. He has co-authored 700 publications (cited ca. 50,000 times, h-index 114), co-edited 14 books, and holds 40 U.S. and 120 international patents. Matyjaszewski received the 2011 Wolf Prize in Chemistry, 2009 Presidential Green Chemistry Challenge Award, and from the American Chemical Society: 2011 Hermann Mark Award, 2011 Award in Applied Polymer Science, 2002 Polymer Chemistry Award, and 1995 Creative Polymer Chemistry Award. He is a member of the USA National Academy of Engineering, Polish Academy of Sciences, and Russian Academy of Sciences.

Brent S. Sumerlin

Brent S. Sumerlin graduated with a B.S. from North Carolina State University (1998) and a Ph.D. from the University of Southern Mississippi (2003) under the direction of Charles McCormick. After serving as a Visiting Assistant Professor at Carnegie Mellon University under the direction of Krzysztof Matyjaszewski (2003-2005), he joined the Department of Chemistry at Southern Methodist University (Dallas, Texas, USA) as an assistant professor in 2005 and was promoted to associate professor in 2009. In 2012, Prof. Sumerlin joined the Department of Chemistry at the University of Florida. Prof. Sumerlin has received several awards, including a NSF CAREER Award and an Alfred P. Sloan Research Fellowship.

Nicolay V. (Nick) Tsarevsky

Nicolay V. (Nick) Tsarevsky obtained a M.S. in theoretical chemistry and chemical physics from the University of Sofia, Bulgaria (1999) and a Ph.D. in chemistry from Carnegie Mellon University (CMU, 2005, under Krzysztof Matyjaszewski). He was visiting assistant professor at the CMU Department of Chemistry (2005-2006), associate director of the CRP Consortium (2006-2007), and CSO of ATRP Solutions, Inc. (2007-2010). He joined the Department of Chemistry at Southern Methodist University in 2010. Research interests include polymerization techniques, functional materials, coordination chemistry, catalysis, and the chemistry of hypervalent compounds. He is the (co)author of over 65 peer-reviewed papers or book chapters, a textbook, and several patents.

Downloaded by 89.163.35.42 on May 30, 2012 | http://pubs.acs.org
Publication Date (Web): March 20, 2012 | doi: 10.1021/bk-2012-1101.ch001

Chapter 1

Controlling Polymer Primary Structure Using CRP: Synthesis of Sequence-Controlled and Sequence-Defined Polymers

Mirela Zamfir and Jean-François Lutz*

Precision Macromolecular Chemistry,
Institut Charles Sadron UPR22-CNRS, 23 rue du Loess,
BP 84047, 67034 Strasbourg Cedex 2, France
***E-mail: jflutz@unistra.fr**

In this chapter, we discuss the preparation of synthetic macromolecules with controlled comonomer sequences (i.e. controlled primary structures). In particular, we put an emphasis on the use of controlled radical polymerization (CRP) methods such as atom transfer radical polymerization (ATRP) and nitroxide mediated polymerization (NMP). Indeed, these straightforward polymerization techniques open interesting avenues for the design of sequence-defined (i.e. precisely ordered comonomer sequences ABCDEF) or sequence controlled (i.e. controlled microstructures, in which chain-to-chain sequence deviations may still exist) polymers. For instance, ATRP allows the design of tailor-made soluble polymer supports, which can be used for the synthesis of sequence-defined oligomers. In addition, some sequence-controlled kinetic options are available in ATRP and NMP. These novel synthetic opportunities are discussed herein and illustrated by recent results obtained in our laboratory.

Introduction

Over the last fifteen years, controlled radical polymerization techniques such as atom transfer radical polymerization (ATRP), nitroxide mediated polymerization (NMP) and reversible addition-fragmentation chain-transfer (RAFT) polymerization have changed our way to conceptualize and to synthesize macromolecules. Indeed, these techniques opened unprecedented avenues for macromolecular engineering, and in particular for the design of tailor-made polymer architectures (*1–4*), organic/inorganic hybrid materials (*5–7*) self-organized aggregates (*8*, *9*), and bio-hybrids (*10*, *11*). This broad range of possibilities is described in several chapters of the present volume but also in earlier volumes of the ACS symposium series (*12*).

However, some aspects of macromolecular structure are poorly-studied in the field of CRP. For instance, the control over tacticity and comonomer sequences remains challenging in CRP processes. These aspects, however, are extremely important for the design of highly-ordered polymer materials (*13*). For instance, the control over the monomer sequence during a polymerization is one of the last major synthetic challenges in polymer science (*14–16*). Indeed, CRP and other chain-growth polymerization methods do not allow precise control over polymer microstructures. Typically, statistical, alternating, gradient and block distributions are the most frequently obtained microstructures in controlled radical copolymerizations (*16*, *17*).

Nevertheless, interesting options for controlling sequences in radical chain-growth polymerizations have been reported over the last few years (*18–25*). In many of these examples, CRP conditions were selected. Indeed, CRP approaches allow precise control over molecular parameters such as chain-length, chain ends and molecular weight distribution. Hence, the combination of CRP processes with sequence-controlled methodologies should allow the design of tailor-made synthetic macromolecules with controlled primary structures. In the present chapter, some results recently obtained in our laboratory using CRP will be summarized. Yet, it is important to define at this stage the terms used in this chapter. Although there is no official IUPAC terminology for this particular field of research, we propose to rank polymers with a controlled primary structure in two categories:

Sequence-defined polymers are oligomers or polymers, which exhibit a perfectly defined comonomer sequence ABCDEF. For example, oligopeptides prepared by solid phase synthesis are sequence-defined macromolecules (*26*).

Sequence-controlled polymers are in our opinion slightly different. Such polymers exhibit controlled sequence distributions. However, defects as well as chain-to-chain deviations are still present. These types of polymers are typically obtained in a batch polymerization (e.g. in a chain-growth radical process).

Herein, two practical examples will be discussed. It will be first shown that CRP techniques are interesting tools for preparing macromolecular architectures containing sequence-defined segments. Indeed, CRP allows the design of well-defined soluble polymer supports, which can be utilized for the iterative synthesis of sequence-defined oligomers. For instance, tailored polystyrene supports prepared by ATRP will be presented in this chapter. Alternatively, comonomer sequences can be directly controlled in a CRP process. This aspect will be discussed in the second paragraph of this chapter. We recently demonstrated that sequences of donor and acceptor comonomers can be precisely controlled in ATRP and in NMP. This versatile sequence-controlled method allows preparation of tailor-made microstructures but also of complex topological polymers.

Downloaded by 89.163.35.42 on May 30, 2012 | http://pubs.acs.org
Publication Date (Web): March 20, 2012 | doi: 10.1021/bk-2012-1101.ch001

Downloaded by 89.163.35.42 on May 30, 2012 | http://pubs.acs.org
Publication Date (Web): March 20, 2012 | doi: 10.1021/bk-2012-1101.ch001

Synthesis of Sequence-Defined Polymers Using CRP-Made Soluble Supports

Solid-phase synthesis is today the most suitable route for preparing sequence-defined oligomers. However, this method is somewhat tedious for the preparation of complex macromolecular architectures. For instance, block copolymers containing sequence-defined segments are typically obtained by (*i*) synthesizing an oligomer on a solid support, (*ii*) cleavage of the formed oligomer and (*iii*) covalent attachment of the oligomer with another segment (i.e. using coupling- or macroinitiator- strategies). The latter step could be certainly bypassed if the sequence-ordered oligomers are directly grown on a soluble polymer segment. Indeed, linear macromolecules can be easily isolated from low molecular weight mixtures (e.g. via selective precipitation) and therefore used as efficient supports for organic synthesis (*27*). Such soluble polymer supports interestingly combine the advantages of solid-phase synthesis (i.e. facile isolation) and solution chemistry (i.e. accessibility). For instance, some examples of oligonucleotide and oligopeptide synthesis on soluble polymer supports have been described in past years (*28*). However, in these approaches, the soluble polymers have been principally used as sacrificial supports. Thus, in most cases, ill-defined commercial polymers have been exploited. Yet, modern polymerization approaches such as CRP certainly allows the design of more advanced macromolecular supports. However, CRP techniques have been barely explored to date for synthesizing tailored polymer supports (*29*). In this context, we recently underlined the advantages of ATRP for preparing advanced macromolecular architectures containing sequence-defined segments (*30*).

Linear polystyrene supports were prepared by ATRP and exploited for the synthesis of model sequence-defined oligomers (Figure 1). In particular, our aim was to demonstrate that these well-defined supports can either be used as (*i*) cleavable segment (i.e. standard sacrificial support, approach **b** in Figure 1) or (*ii*) as permanent segment (i.e. block copolymer synthesis; approach **c** in Figure 1). In all cases, the model oligomers contained alternating polar and apolar segments and were constructed stepwise via an AB + CD approach (Figure 1).

This synthetic strategy relies on two efficient chemical reactions, namely the 1,3-dipolar cycloaddition of terminal alkynes (A) and azides (D) and the amidation of carboxylic acids (B) with primary amines (C). These two reactions proceed chemoselectively in a ABCD multifunctional mixture (i.e. A reacts solely with D, whereas B reacts solely with C) (*31*). As a consequence, sequence-defined oligomers can be potentially prepared in the absence of protecting groups. However, these alternating oligomers were never synthesized before. Thus, a reference oligomer was first prepared using a standard solid-phase procedure (approach **a** in Figure 1). The bromide moieties of a commercial Wang resin were first transformed into azide functions by nucleophilic substitution in the presence of sodium azide (*32*). This modified resin was subsequently used to initiate the stepwise synthesis of an oligomer composed of 3 polar and 3 apolar building blocks (i.e. 6 consecutive iterative steps including 3 amidations and 3 cycloadditions). After each step the resin was characterized by FT-IR. These measurements confirmed that the iterative steps proceed in nearly quantitative yields. After the last step, the sequence-ordered oligomer was cleaved from the solid-support using a TFA/CH_2Cl_2 mixture, purified and analyzed by ^1H NMR, FT-IR, MALDI-TOF-MS and ESI-MS. All measurements indicated the formation of a monodisperse oligomer with a molecular weight of 1128 g·mol^{-1}. This corresponds to the targeted molecular structure containing 6 building blocks, an azide ω-end-group and a 4-hydroxybenzyl α-end-group (*30*). The latter is due to the cleavage of the aryl benzyl ether (*32*). The formed oligomer was found to be soluble in various solvents including water and methanol. These preliminary results indicated that the AB + CD strategy is rapid and efficient for synthesizing sequence-ordered oligomers.

Downloaded by 89.163.35.42 on May 30, 2012 | http://pubs.acs.org
Publication Date (Web): March 20, 2012 | doi: 10.1021/bk-2012-1101.ch001

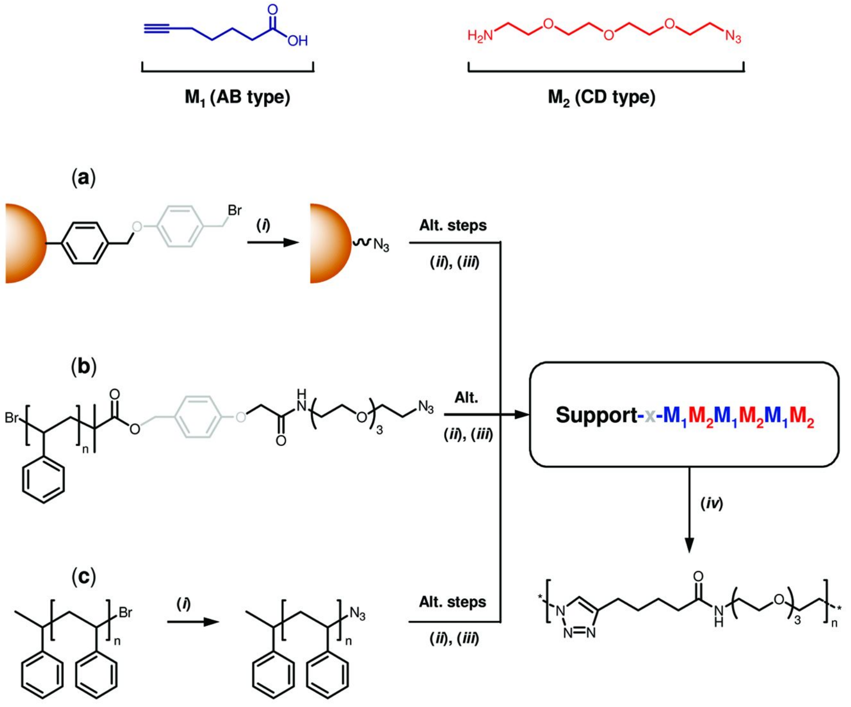

*Figure 1. Strategies for synthesizing sequence-defined oligomers via an AB + CD growth mechanism (30): (a) Conventional solid-phase approach based on an azido-functionalized Wang resin; (b) Liquid-phase approach based on a linear polystyrene support containing a cleavable linker; (c) Direct synthesis of block copolymers using an ω-azido functionalized polystyrene support. Light grey colors indicate cleavable moieties. Experimental conditions: (i) NaN_3, DMF; (ii) M_1, CuBr, dNBipy, THF; (iii) M_2, NHS, DCC, THF; (iv) TFA, CH_2Cl_2. This latter step was used in approaches **a** and **b**, only.*

Thus, oligomer synthesis was then performed on a well-defined soluble polystyrene support. In order to fully demonstrate the viability of this technique, a cleavable support, allowing oligomer isolation and characterization, was first investigated (approach **b** in Figure 1). This polystyrene support was synthesized by ATRP in the presence of an azido-functionalized ATRP initiator containing a labile *p*-alkoxybenzyl ester linker (*33*). The formed polymer was characterized by ^{1}H NMR, FT-IR and SEC. The former methods confirmed the presence of the "Wang initiator" at the α-chain end of the polymer, whereas the latter evidenced the formation of a well-defined macromolecule with a controlled molecular weight (M_n ~ 4300 g·mol^{-1}) and a narrow molecular weight distribution (M_w/M_n ~ 1.14). The azido-functionality of this linear polystyrene was exploited for initiating the sequential oligomerization of building blocks M_1 and M_2. Oligomers of different chain-length were synthesized on this linear support (i.e. 4 or 5 consecutive iterative steps). After each step, the modified polymer was isolated by precipitation in methanol. This purification procedure is rapid and allowed an efficient removal of the low molecular weight reactants together with a minimal polymer loss. Thus, the oligomer synthesis on this soluble polystyrene support was overall as fast as on a commercial Wang resin. Moreover, the products of each step were examined by ^{1}H NMR and FT-IR, which indicated high reaction yields in all cases. After the last step, the modified support was analyzed by ^{1}H NMR and SEC. Both techniques evidenced the formation of a well-defined block copolymer polystyrene-*b*-oligomer. For instance, SEC evidenced a clear difference in molecular weight between the formed diblock copolymer and the parent support. Although SEC only gives access to apparent molecular weight values, these differences roughly coincided with the theoretical molecular weights of the targeted oligomers (i.e. ~ 900 g·mol^{-1} after 4 iterative steps and ~1000 g·mol^{-1} after 5 iterative steps). Additionally, high molecular weight shoulders could also be detected on the chromatograms. These signals correspond to triblock copolymers oligomer-*b*-polystyrene-*b*-oligomer, which were initiated by α-ω-azido telechelic polystyrene (i.e. dead chains formed by bimolecular coupling during the ATRP). In order to fully characterize the formed oligomers, the diblock/triblock copolymers were cut using a TFA/CH_2Cl_2 mixture (Figure 1). After this treatment, the reaction mixture was reconcentrated and poured in a large volume of methanol. The polystyrene support precipitated out, whereas the cleaved oligomers remained in methanol solution. The former was dried in vacuo and characterized by ^{1}H NMR and SEC, while the latter were isolated by rotary evaporation and characterized by ^{1}H NMR, FT-IR, MALDI-TOF-MS and ESI-MS. SEC measurements clearly confirmed the quantitative cleavage of the block copolymers. Indeed, the chromatogram of the precipitate coincided with the one of the initial support. Furthermore, MALDI-TOF-MS and ESI-MS evidenced the formation of monodisperse oligomers. For example, after 5 iterative steps and cleavage, an oligomer with a molecular weight of 1160 g·mol^{-1} was detected. This value corresponds to the targeted alternating sequence with a *p*-alkoxybenzyl alcohol α-end-group. Yet, a second species with a molecular weight of 1174 g·mol^{-1} was also identified. This structure could be due to the partial esterification of the carboxylate end-group during the purification procedure (i.e. methanol + TFA).

Downloaded by 89.163.35.42 on May 30, 2012 | http://pubs.acs.org
Publication Date (Web): March 20, 2012 | doi: 10.1021/bk-2012-1101.ch001

Ultimately, soluble polystyrene supports were studied for preparing non-cleavable block copolymers containing sequence-defined oligomers (approach **c** in Figure 1). In this case, the bromine ω-end groups of ATRP polystyrene chains (M_n ~ 3900 g·mol^{-1}, M_w/M_n ~ 1.13) were first transformed into azide moieties by nucleophilic substitution with sodium azide. These functional chain-ends were then used as initiating sites for iterative oligomer synthesis. Six alternating iterative steps were performed on the soluble polystyrene support (3 amidations and 3 cycloadditions). As for previous approaches, the step-by-step oligomer growth was monitored by ^{1}H NMR and FT-IR. Both techniques evidenced high reaction yields in each step. After synthesis, ^{1}H NMR and SEC indicated the formation of a well-defined diblock copolymer containing sequence-ordered segment of approximately 1000 g·mol^{-1}. Contrary to the approach **b**, no triblock copolymers were formed in the present case. Indeed, approach **c** relies on a ω-chain end initiation, where dead-chains are simply inactive (i.e. they have initially no bromine terminal groups and therefore no azide initiating sites).

Sequence-Controlled CRP Processes

As discussed in the introduction of this chapter, comonomer sequences are usually poorly controlled in radical chain-growth polymerizations. For instance, for a conventional radical copolymerization of two monomers A and B, statistical or eventually alternating copolymers can be obtained, depending on the reactivity ratios (*16*). However, it was shown in recent years that the controlled/living mechanism of CRP reactions opens new opportunities for controlling polymer microstructures (*17*). Indeed, in CRP processes, the polymer chains grow in a kinetically controlled fashion and therefore their microstructures reflect the reactivity of the initial comonomer feed. Thus, unprecedented situations such as gradient copolymers (*34*) or one-pot block copolymers (*35*) can be obtained in a CRP process.

We recently pointed out that even more complex microstructures can be prepared by CRP of donor and acceptor comonomers (*36*). In particular, we emphasized that the CRP of styrenic monomers with *N*-substituted maleimides (MIs) is a very versatile sequence-controlled polymerization platform (Figure 2). This approach relies on the fact that *N*-substituted maleimides have a low tendency to homopolymerize but a very strong tendency to copolymerize with styrenics. This unusual feature has been used for decades for synthesizing AB alternating copolymers using equimolar or nearly-equimolar amounts of styrenics and MIs. However, we highlighted that this kinetic feature is even more interesting in non-equimolar situations. For instance, in comonomer feeds containing a very high excess of styrenics, the cross-propagation is still kinetically highly favored and therefore MIs are consumed extremely fast in the copolymerization process. This unusual kinetic feature is not very relevant in a conventional free radical polymerization. In such processes, polymer chains are initiated all along the reaction and therefore, if the comonomers have different reactivities, strong chain-to-chain deviations of composition can be expected (i.e. uncontrolled

Downloaded by 89.163.35.42 on May 30, 2012 | http://pubs.acs.org
Publication Date (Web): March 20, 2012 | doi: 10.1021/bk-2012-1101.ch001

Downloaded by 89.163.35.42 on May 30, 2012 | http://pubs.acs.org
Publication Date (Web): March 20, 2012 | doi: 10.1021/bk-2012-1101.ch001

microstructures). On the other hand, the non-equimolar copolymerization of styrene and MIs becomes very useful when combined with a controlled/living process such as ATRP or NMP (i.e. a polymerization mechanism, in which all chains are initiated simultaneously and grow at the same rate). In this case, the small amounts of ultra-reactive MIs can be locally incorporated in short sections of the growing chains (i.e. tailored microstructures can be synthesized). Yet, in such approaches, the control over sequences is not perfectly regulated, as in a biological process. As defined in the introduction of this chapter, the polymers synthesized in this process are not strictly sequence-defined but sequence-controlled. Nevertheless, the styrenics/MIs copolymerization platform constitutes a real step forward in the field of radical chain-growth polymerization.

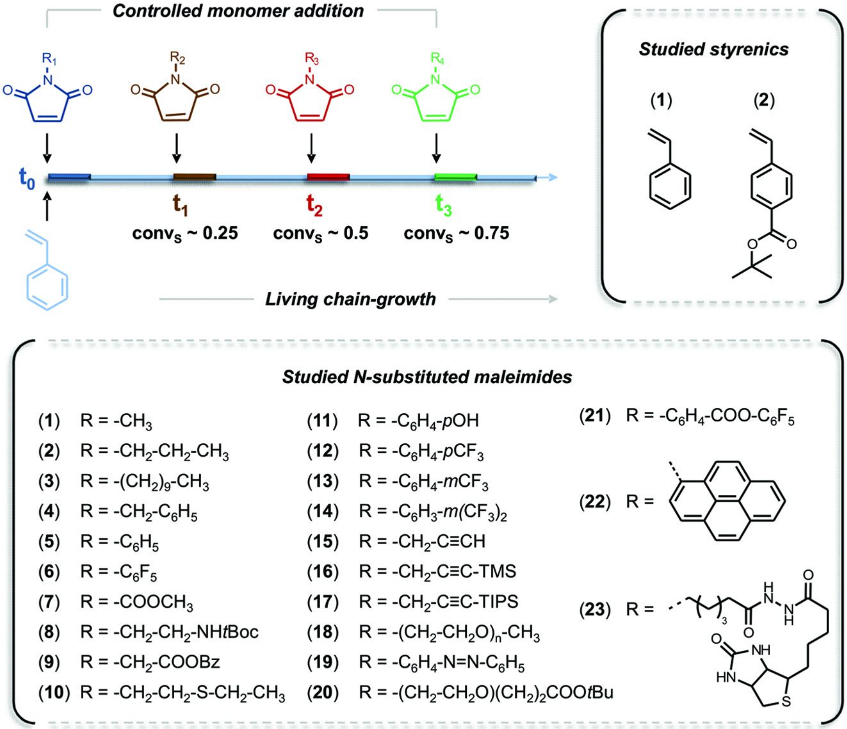
Controlled monomer addition
R_1
R_2
R_3
R_4
t_0
t_1
t_2
t_3
$conv_S$ ~ 0.25
$conv_S$ ~ 0.5
$conv_S$ ~ 0.75
Living chain-growth
Studied styrenics
(1)
(2)
Studied N-substituted maleimides
(1) R = -CH_3
(2) R = -CH_2-CH_2-CH_3
(3) R = -$(CH_2)_9$-CH_3
(4) R = -CH_2-C_6H_5
(5) R = -C_6H_5
(6) R = -C_6F_5
(7) R = -$COOCH_3$
(8) R = -CH_2-CH_2-NH*t*Boc
(9) R = -CH_2-COOBz
(10) R = -CH_2-CH_2-S-CH_2-CH_3
(11) R = -C_6H_4-*p*OH
(12) R = -C_6H_4-*p*CF_3
(13) R = -C_6H_4-*m*CF_3
(14) R = -C_6H_3-*m*$(CF_3)_2$
(15) R = -CH_2-C≡CH
(16) R = -CH_2-C≡C-TMS
(17) R = -CH_2-C≡C-TIPS
(18) R = -$(CH_2$-$CH_2O)_n$-CH_3
(19) R = -C_6H_4-N=N-C_6H_5
(20) R = -$(CH_2$-$CH_2O)(CH_2)_2$COO*t*Bu
(21) R = -C_6H_4-COO-C_6F_5
(22) R =
(23) R =

Figure 2. General concept for the synthesis of sequence-controlled polymers by CRP of donor (styrenics) and acceptor (N-substituted maleimides) comonomers. The insets show the molecular structures of the monomers, which have been already tested in our laboratory.

The initial proofs of concept were obtained with ATRP (*18*)(*19*). It was first shown that various MIs can be consecutively incorporated in a linear polystyrene backbone using successive addition steps (see main concept in Figure 2) (*18*). Hence, tailor-made single-chain microstructures can be easily created using this approach. It was afterwards demonstrated that this technique can be extended to a broad library of functional MIs (*19*). For instance, Figure 2 shows the molecular structure of the comonomers, which have been studied so far in our laboratory. Although some structures may lead to ill-defined situations (e.g. structures 11, 15 and 23 in Figure 2), most of the studied MIs can be locally incorporated in a chain constituted of donor styrenic momomers. Thus, a variety of functional groups can be potentially used to “write” on polymer single-chains. However, it should be noted that, although we target a local chain functionalization (i.e. the functional groups are typically carried by the MIs), the main chain of the polymer can also be functionalized. For instance, we recently reported that *t*-butyl 4-vinyl benzoate can be used instead of styrene (*37*). After sequence-controlled copolymerization with MIs, this monomer can be deprotected in acidic conditions, thus leading to water-soluble polyanions with a controlled microstructure. Nevertheless, it was noted that the local incorporation of the MIs in the chains was not as precise as in the case of styrene-based backbones (*37*).

NMP can also be utilized to synthesize sequence-controlled polymers by copolymerization of styrenics and MIs. For instance, we have shown in a recent series of papers (*37–39*), that the commercial alkoxyamine BlocBuilder MA® (i.e. an alkoxyamine based on the persistent nitroxide SG1 (*40*)) is particularly appropriate in that regard. Indeed, this compound allows a particularly fine control of the polymerization of styrenics and lead to the formation of macromolecules with a precisely controlled chain length and narrow molecular weight distribution (i.e. chromatograms are usually virtually exempt of bimolecular coupling). Moreover, for some particular MIs, an exceptionally precise degree of chain incorporation was observed (*38*).

The styrenics/MIs CRP platform can also be used to design folded polymer topologies. In general, synthetic polymer chains, prepared by chain-growth polymerization, do not contain precisely addressable sites, which can be used for controlling their intramolecular covalent folding. The only precisely localizable functions in chain-growth polymers are usually the chain-ends or, in the case of block copolymers, the spacers between the segments. Polymer chain-ends can be utilized to promote intramolecular covalent cyclization. However, this approach only leads to simple cyclic topologies (*42*, *43*). More advanced polymer origamis can be synthesized by combining intramolecular and intermolecular reactions employing chain-ends and chain-spacers (*44–46*). However, these syntheses are generally quite complex. In that regard, the styrene/MI platform is a much more flexible approach for synthesizing foldable linear macromolecules. Indeed, as highlighted above, reactive MIs can be placed virtually anywhere in a polymeric backbone. Thus, these positionable reactive functions can be easily exploited for controlling macromolecular folding. For example, we recently demonstrated that controllable covalent bridges can be prepared using the styrene/MI copolymerization platform (*41*). In this approach, small amounts of TMS- or TIPS-protected *N*-propargyl maleimide (structures 16 and 17 in Figure 2) were added during the course of styrene homopolymerization. Thus, various types of linear polystyrene precursors containing localized alkyne functions were synthesized. These reactive linear chains were afterwards involved in intramolecular reactions (e.g. Huisgen cycloaddition or Glaser coupling) in dilute solutions, thus affording different types of covalently folded polymer chains. For example, Figure 3 show examples of Q- and 8-shaped macromolecular origamis

Downloaded by 89.163.35.42 on May 30, 2012 | http://pubs.acs.org
Publication Date (Web): March 20, 2012 | doi: 10.1021/bk-2012-1101.ch001

Downloaded by 89.163.35.42 on May 30, 2012 | http://pubs.acs.org
Publication Date (Web): March 20, 2012 | doi: 10.1021/bk-2012-1101.ch001

prepared using the styrenics/MIs CRP platform. In all cases, FT-IR and SEC analyses indicated the successful formation of localized intramolecular covalent bridges (*41*). It was also recently shown that asymmetric covalent bridges could be created in between two different localized MIs (*39*). Alpha-shaped polystyrene origamis with variable sizes and loop diameters were synthesized through a series of consecutive chemical steps. Linear polystyrene precursors containing precisely incorporated reactive functions (i.e. alkyne and activated ester moieties) were first synthesized by sequence-controlled copolymerization of styrene with functional MIs. Discrete amounts (i.e. one molar equivalent as compared to the alkoxyamine) of TIPS-protected *N*-propargyl maleimide and pentafluorophenyl 4-maleimidobenzoate (structure 21 in Figure 2) were added at precise moments during the polymerization of a large excess of styrene. Afterwards the chains were folded in solution using a three-step strategy. The pentafluorophenyl activated ester moieties (*47*) were first reacted with 11-azido-3,6,9-trioxaundecan-1-amine, thus leading to azide-functionalized polymers. Subsequently, the alkyne function was deprotected and intramolecular azide-alkyne Huisgen cycloadditions were performed in dilute DMF solutions in the presence of a copper-based catalyst. SEC, ^{1}H NMR, and FT-IR measurements confirmed the formation of folded polymer chains containing asymmetric covalent bridges (*39*).

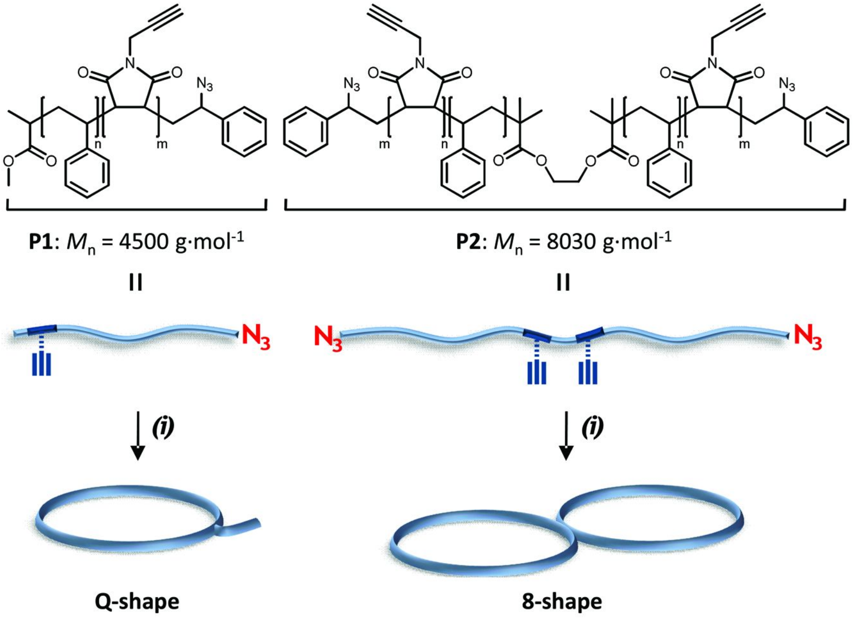
N
O
O
N₃
n
m
P1: M_n = 4500 g·mol^{-1}
P2: M_n = 8030 g·mol^{-1}
II
II
N₃
N₃
N₃
(i)
(i)
Q-shape
8-shape

Figure 3. Covalent folding of linear synthetic polymer chains (41). (top) Molecular structures of foldable linear polystyrene chains prepared by ATRP. For simplicity, these structural formulae display only the average comonomer composition of the precursors and do not give information about the localization of the MI units in the chains. (bottom) Schematic representation of the folded macromolecules. Experimental conditions: (i) copper-catalyzed azide-alkyne 1,3-dipolar cycloaddition: CuBr, bipy, DMF, ultra-diluted conditions, 80°C.

Downloaded by 89.163.35.42 on May 30, 2012 | http://pubs.acs.org
Publication Date (Web): March 20, 2012 | doi: 10.1021/bk-2012-1101.ch001

Conclusion

Controlled radical polymerization techniques offer interesting options for preparing synthetic polymers with a controlled primary structure. For instance, linear polymer chains prepared by CRP can be used as soluble supports for the iterative synthesis of sequence-defined oligomers. Therefore, complex macromolecular architectures containing sequence-defined segments can be prepared. Moreover, monomer sequences can also be directly controlled in a CRP process. For example, it was demonstrated that the atom transfer radical copolymerization or the nitroxide-mediated copolymerization of styrenics with *N*-substituted maleimides allows the design of sequence-controlled macromolecules. Hence, tailor-made microstructures and complex topological origamis can be synthesized. These findings broaden the scope of application of CRP reactions and suggest that new varieties of synthetic macromolecules could be attained within the next few years (*13*, *48*).

Acknowledgments

J.F.L thanks the CNRS, the University of Strasbourg, the international Center for Frontier Research in Chemistry and the European Research Council (ERC grant agreement n°258593) for financial support. Nezha Badi, Sebastian Pfeifer, Zoya Zarafshani, Bernhard Schmidt, Nina Fechler, Jana Falkenhagen, Laurence Oswald and Sansanee Srichan are also gratefully acknowledged for collecting some experimental data discussed in this chapter.

References

1. Matyjaszewski, K.; Tsarevsky, N. V. *Nature Chem.* **2009**, *1*, 276–288.
2. Ouchi, M.; Terashima, T.; Sawamoto, M. *Chem. Rev.* **2009**, *109*, 4963–5050.
3. Perrier, S.; Takolpuckdee, P. *J. Polym. Sci., Part A: Polym. Chem.* **2005**, *43*, 5347–5393.
4. Tebben, L.; Studer, A. *Angew. Chem., Int. Ed.* **2011**, *50*, 5034–5068.
5. Pyun, J.; Matyjaszewski, K. *Chem. Mater.* **2001**, *13*, 3436–3448.
6. Ghannam, L.; Parvole, J.; Laruelle, G.; Francois, J.; Billon, L. *Polym. Int.* **2006**, *55*, 1199–1207.
7. Beija, M.; Marty, J. D.; Destarac, M. *Prog. Polym. Sci.* **2011**, *36*, 845–886.
8. Lutz, J.-F. *Polym. Int.* **2006**, *55*, 979–993.
9. McCormick, C. L.; Sumerlin, B. S.; Lokitz, B. S.; Stempka, J. E. *Soft Matter* **2008**, *4*, 1760–1773.
10. Lutz, J.-F.; Börner, H. G. *Prog. Polym. Sci.* **2008**, *33*, 1–39.
11. Le Droumaguet, B.; Nicolas, J. *Polym. Chem.* **2010**, *1*, 563–598.
12. For a broader perspective on controlled radical polymerization methods, the reader is referred to volumes 685, 768, 854, 944, 1023 and 1024 of the ACS Symposium Series.
13. Ouchi, M.; Badi, N.; Lutz, J.-F.; Sawamoto, M. *Nature Chem.* **2011**, *3*, 917–924.
14. Badi, N.; Lutz, J.-F. *Chem. Soc. Rev.* **2009**, *38*, 3383–3390.

15. Lutz, J.-F. *Nature Chem.* **2010**, *2*, 84–85.
16. Lutz, J.-F. *Polym. Chem.* **2010**, *1*, 55–62.
17. Lutz, J.-F.; Pakula, T.; Matyjaszewski, K. *Advances in Controlled/Living Radical Polymerization*; Matyjaszewski, K., Ed.; ACS Symposium Series 854; American Chemical Society: Washington, DC, 2003; pp 268−282.
18. Pfeifer, S.; Lutz, J.-F. *J. Am. Chem. Soc.* **2007**, *129*, 9542–9543.
19. Pfeifer, S.; Lutz, J.-F. *Chem. Eur. J.* **2008**, *14*, 10949–10957.
20. Ida, S.; Terashima, T.; Ouchi, M.; Sawamoto, M. *J. Am. Chem. Soc.* **2009**, *131*, 10808–10809.
21. Ida, S.; Ouchi, M.; Sawamoto, M. *J. Am. Chem. Soc.* **2010**, *132*, 14748–14750.
22. Satoh, K.; Matsuda, M.; Nagai, K.; Kamigaito, M. *J. Am. Chem. Soc.* **2010**, *132*, 10003–10005.
23. Satoh, K.; Ozawa, S.; Mizutani, M.; Nagai, K.; Kamigaito, M. *Nature Commun.* **2010**, *1*, 1–6.
24. Hibi, Y.; Ouchi, M.; Sawamoto, M. *Angew. Chem., Int. Ed.* **2011**, *50*, 7434–7437.
25. Tong, X.; Guo, B.-h.; Huang, Y. *Chem. Commun.* **2011**, *47*, 1455–1457.
26. Börner, H. G. *Macromol. Rapid Commun.* **2011**, *32*, 115–126.
27. Wentworth, P., Jr.; Janda, K. D. *Chem. Commun.* **1999**, 1917–1924.
28. Gravert, D. J.; Janda, K. D. *Chem. Rev.* **1997**, *97*, 489–510.
29. Gravert, D. J.; Datta, A.; Wentworth, P.; Janda, K. D. *J. Am. Chem. Soc.* **1998**, *120*, 9481–9495.
30. Pfeifer, S.; Zarafshani, Z.; Badi, N.; Lutz, J.-F. *J. Am. Chem. Soc.* **2009**, *131*, 9195–9197.
31. Malkoch, M.; Thibault, R. J.; Drockenmuller, E.; Messerschmidt, M.; Voit, B.; Russell, T. P.; Hawker, C. J. *J. Am. Chem. Soc.* **2005**, *127*, 14942–14949.
32. Harju, K.; Vahermo, M.; Mutikainen, I.; Yli-Kauhaluoma, J. *J. Comb. Chem.* **2003**, *5*, 826–833.
33. Wang, S.-S. *J. Am. Chem. Soc.* **1973**, *95*, 1328–1333.
34. Matyjaszewski, K.; Ziegler, M. J.; Arehart, S. V.; Greszta, D.; Pakula, T. *J. Phys. Org. Chem.* **2000**, *13*, 775–786.
35. Benoit, D.; Hawker, C. J.; Huang, E. E.; Lin, Z.; Russell, T. P. *Macromolecules* **2000**, *33*, 1505–1507.
36. Lutz, J.-F.; Schmidt, B. V. K. J.; Pfeifer, S. *Macromol. Rapid Commun.* **2011**, *32*, 127–135.
37. Srichan, S.; Oswald, L.; Zamfir, M.; Lutz, J.-F., *Chem. Commun.* 2012, Advance article, DOI: 10.1039/C1CC14823K.
38. Kakuchi, R.; Zamfir, M.; Lutz, J.-F.; Theato, P. *Macromol. Rapid Commun.* **2012**, *33*, 54–60.
39. Zamfir, M.; Theato, P.; Lutz, J.-F., *Polym. Chem.* 2012, in press, DOI:10.1039/C1PY00514F.
40. Lutz, J.-F.; Lacroix-Desmazes, P.; Boutevin, B. *Macromol. Rapid Commun.* **2001**, *22*, 189–193.
41. Schmidt, B. V. K. J.; Fechler, N.; Falkenhagen, J.; Lutz, J.-F. *Nature Chem.* **2011**, *3*, 236–240.

Downloaded by 89.163.35.42 on May 30, 2012 | http://pubs.acs.org
Publication Date (Web): March 20, 2012 | doi: 10.1021/bk-2012-1101.ch001

42. Schappacher, M.; Deffieux, A. *Science* **2008**, *319*, 1512–1515.
43. Laurent, B. A.; Grayson, S. M. *Chem. Soc. Rev.* **2009**, *38*, 2202–2213.
44. Yamamoto, T.; Tezuka, Y. *Polym. Chem.* **2011**, *2*, 1930–1941.
45. Altintas, O.; Lejeune, E.; Gerstel, P.; Barner-Kowollik, C., *Polym. Chem.* 2012, Advance article, DOI: 10.1039/C1PY00392E.
46. Lonsdale, D. E.; Monteiro, M. J. *Chem. Commun.* **2010**, *46*, 7945–7947.
47. Theato, P. *J. Polym. Sci., Part A: Polym. Chem.* **2008**, *46*, 6677–6687.
48. Giuseppone, N.; Lutz, J.-F. *Nature* **2011**, *473*, 40–41.

Downloaded by 89.163.35.42 on May 30, 2012 | http://pubs.acs.org
Publication Date (Web): March 20, 2012 | doi: 10.1021/bk-2012-1101.ch001

Chapter 2

RAFT Polymerization: A Powerful Tool for the Synthesis and Study of Oligomers

Meiliana Siauw, Brian S. Hawkett, and Sébastien Perrier*

**Key Centre for Polymers & Colloids, School of Chemistry,
The University of Sydney, NSW 2006, Australia
*E-mail: sebastien.perrier@sydney.edu.au. Phone: +61 2 9351 3366.**

We demonstrate the ability of the reversible addition-fragmentation chain transfer (RAFT) process to produce well-defined oligomers of *n*-butyl acrylate (*n*BA) and styrene (St) of narrow molecular weight distribution (i.e., Đs ≤ 1.2) and degrees of polymerization (DPs) ranging from 9 to 27. We use these oligomers to study the effect of molecular weight (MW) and end groups on the thermal properties, in particular the glass transition temperature (T_g) of the materials. The T_g of P*n*BA oligomers is found to be relatively independent of end groups and MW, whilst the T_g of PSt oligomers is affected by the nature of end groups, and increases with MW. This work shows that, beyond its versatility for polymer synthesis, RAFT polymerisation can also be used to assess fundamental physical properties of materials.

Introduction

While it is often desired to prepare macromolecules with high MW and low dispersity, there is also sometimes a need to generate well-defined polymeric materials in the oligomeric range. According to IUPAC, an oligomer is a compound with a number of monomer repeating units typically varying from 3 to 10 (*1*). However, the term oligomer has been broadly expanded in the literature to be applied to short-chain polymers with a number average molecular weight (M_n) of approximately 6000 g/mol (*2*, *3*). Oligomers' properties are comparable to those of polymers, whilst their synthesis requires a smaller amount of raw material thus generally cheaper cost. With the growing concerns over the

In Progress in Controlled Radical Polymerization: Materials and Applications; Matyjaszewski, K., et al.;
ACS Symposium Series; American Chemical Society: Washington, DC, 2012.

sustainability of vinyl polymers, the use of shorter polymeric chains provides a simple and attractive solution to optimise monomer feedstock, whilst keeping the unique properties of polymers (*4*). The versatility of oligomers has been demonstrated in a range of applications, including in the design of branched polymeric architectures (*5–7*), peptide-polymer conjugates (*8–10*), surfactants (*11*) and in emulsion polymerization (*12*, *13*).

RAFT polymerization permits the preparation of well-defined and complex polymeric architectures (*14–20*), and in particular it is an ideal tool for the preparation of well-defined, high end group fidelity, low MW materials. The RAFT agent/monomer combination must be chosen such that hybrid behavior (*21*), a phenomenon that occurs when the addition rate of the propagating radicals with the initial RAFT agent is significantly lower than that of propagation, does not prevent the generation of very low MWs. According to the RAFT mechanism (*22*), very low dispersity (*Đ*) polymers in the oligomer range can be obtained when the radical concentration is kept low over the duration of the polymerization, the system features a relatively high rate of radical addition (k_{add}) to the RAFT agent, and a monomer of relatively low rate of propagation (k_p) is employed (*23*). The degree of low MW control with low dispersities is an advantage of RAFT over other living radical polymerization (LRP) methods, where, due to the persistent radical effect, control tends to increase only with increasing conversion and thus increasing MW. It is also worth noting that, as for other LRP techniques, since *Đ* is determined by the ratio of weight-average MW to number-average MW (M_w/M_n), it is likely that for the same value of *ĐPDI*, longer chain polymer would have narrower molecular weight distribution (MWD) compared to shorter chain polymers. Moreover, RAFT polymerization is arguably the most versatile of the LRP methods with respect to temperature (*24*), solvent (*25*) and monomer choice (*26*).

In this contribution, we demonstrate the capability of RAFT as a technique to produce short-chain homo-oligomers with well controlled MWs and narrow MWDs ($Đ \leq 1.2$). We then employ RAFT as a tool to produce well-controlled MW oligomers of a low T_g polymer, P*n*BA, and high T_g polymer, PSt, and study the effect of the chain length on the thermal properties.

Experimental Section

Materials

n-Butyl acrylate (*n*BA) and styrene (St) were obtained from Aldrich and were filtered through basic alumina (Aldrich) to remove the inhibitor. 2,2′-Azobisisobutyronitrile (AIBN; Aldrich) was recrystallised from ethanol. Benzoyl peroxide (BPO; Fluka) and lauroyl peroxide (LPO; Aldrich) were recrystallised from chloroform/methanol. 2-Propanoic acid butyl trithiocarbonate (PABTC) was supplied by Dulux, Australia. 2-Cyanopropan-2-yl dithiobenzoate (CPDB) (*27*) was prepared as reported previously. Toluene, 2-propanol, and tetrahydrofuran (THF) were of AR grade and were used as received. Water used for the experiment was purified by a Millipore Qplus water purification system (resistance 18.2 MΩcm).

Analyses

^{1}H-NMR analyses were done using either a Bruker Ultra Shield AVANCE200 spectrometer (1H 200 MHz) or a Bruker Ultra Shield AVANCE300 spectrometer (1H 300 MHz) at 25 °C. For P*n*BA oligomers and polymers, SEC analyses were performed on a Polymer Laboratories PL – GPC 50 Plus. DMF with 0.1% w/w LiBr was used as the eluent with a flow rate of 0.5 mL min^{-1} at 50 °C. For PSt oligomers, SEC analyses were performed on a Shimadzu LC10ATVP liquid chromatography system equipped with a guard column and two Polymer Laboratories PLgel 5 μm Mixed-C columns (MW range of 2,000,000 – 500) in an oven maintained at 40 °C. The columns were attached to a Shimadzu differential refractive index (DRI) detector (RID-10A) linked with a Shimadzu UV detector (APD-10AVP). THF was used as the eluent at a flow rate of 1 mL min^{-1} and toluene (0.5 wt%) was used as a flow rate marker. Electrospray Ionisation Mass Spectrometry (ESI-MS) was done on a Finnigan LCQ MS Detector with Finnigan LCQ Data Processing using Instrument Control Software. Ultraviolet-Visible Spectroscopy (UV/Vis) measurements were carried out using a Cary Bio50 UV-Vis spectrophotometer. Differential Scanning Calorimetry (DSC) analyses was undertaken using a TA Instruments DSC 2920 Modulated DSC under a nitrogen atmosphere (60 cm^3/min).

Typical Polymerization of nBA (Synthesis of PABTC-PnBA$_{10}$ Oligomer)

A solution containing *n*BA (5.4 g, 42.13 mmol), PABTC (1.0 g, 4.19 mmol), AIBN (70.0 mg, 0.43 mmol), and toluene (9.5 g) was placed in a schlenk tube, sealed, degassed with six freeze-evacuate-thaw cycles, and heated at 70 °C for 3 h. The conversion of the oligomer was 93%, which was determined by ^{1}H-NMR. The oligomer was purified by precipitation method using cold hexane to remove the unreacted monomer. The purified oligomer product was then dried overnight in a vacuum oven at 40 °C. For the characterisation of the purified oligomer: M_n can be obtained from ESI-MS, ^{1}H-NMR, and SEC; DP can be obtained from ESI-MS and ^{1}H-NMR; $Đ$ was obtained from SEC; and T_g was obtained from DSC. ESI-MS was used to provide a more accurate DP characterisation since the SEC was not calibrated against narrow dispersity poly(butyl acrylate) standards. ESI-MS: M_n = 1541 g/mol (gaining 1 Na^+) and DP P*n*BA = 10. ^{1}H-NMR: M_n = 1390 g/mol and DP P*n*BA = 9. SEC: M_n = 1300 g/mol and $Đ$ = 1.14. DSC: T_g P*n*BA = -50 °C. ^{1}H-NMR (200 MHz, $CDCl_3$): δ (ppm) 0.75-1.08 (t, 6H, $C\mathit{H_3}$-$(CH_2)_3$-S and $C\mathit{H_3}$-$(CH_2)_3$-COO), 1.10-1.24 (d, 3H, -CH($C\mathit{H_3}$)COOH), 1.24-2.19 (m, CH_3-$C\mathit{H_2}$-$(CH_2)_2$-S-C(S)-, CH_3-CH_2-$C\mathit{H_2}$-CH_2-S-C(S)-, P*n*BA backbone -$C\mathit{H}_2$, CH_3-$C\mathit{H_2}$-$(CH_2)_2$-COO and CH_3-CH_2-$C\mathit{H_2}$-CH_2-COO), 2.19-2.64 (P*n*BA backbone –C*H* and -C*H*(CH_3)(COOH)), 3.26-3.45 (t, 2H, CH_3-$(CH_2)_2$-$C\mathit{H_2}$-S-C(S)-S-), 3.83-4.30 (m, 2H, CH_3-$(CH_2)_2$-$C\mathit{H_2}$-COO), 4.74-4.95 (t, 1H, P*n*BA first chain length of –CH (-C(S)-S-C*H*(COO-$(CH_2)_3$-CH_3)CH_2).

Typical Polymerization of Styrene (Synthesis of PABTC-PSt$_9$ Oligomer)

A solution containing styrene (13.3 g, 127.70 mmol), PABTC (3.0 g, 12.58 mmol), and AIBN (208.5 mg, 1.27 mmol) was placed in a round-bottom flask, sealed with a rubber septum, degassed with nitrogen gas for 10 minutes, and heated at 65 °C for 17 h. The conversion of the oligomer was 84%, which was determined by ^{1}H-NMR. The oligomer was dissolved in THF and was purified twice by precipitation method using cold methanol to remove the unreacted monomer. The purified oligomer product was then dried overnight in a vacuum oven at 40 °C. For the characterisation of the purified oligomer: M_n and DP were obtained by ^{1}H-NMR and SEC, *Đ* was obtained from SEC, and T_g was obtained from DSC. ESI-MS was not used to determine the M_n and DP of the oligomer because the SEC was calibrated against narrow polystyrene standards thus it can provide accurate characterisation. ^{1}H-NMR: M_n = 1278 g/mol and DP PSt = 10. SEC: M_n = 930 g/mol, DP PSt = 9, and *Đ* = 1.13. DSC: T_g PSt = 62 °C. ^{1}H-NMR (300 MHz, $CDCl_3$): δ (ppm) 0.76-1.08 (t, 6H, $C\mathit{H}_3$-$(CH_2)_3$-S and -CH($C\mathit{H}_3$)-COOH), 1.20-2.52 (m, CH_3-$C\mathit{H}_2$-$(CH_2)_2$-S-C(S)-, CH_3-CH_2-$C\mathit{H}_2$-CH_2-S-C(S)-, -C*H*(CH_3)(COOH), PSt backbone –$C\mathit{H}_2$ and PSt backbone –C*H*), 3.14-3.40 (t, 2H, CH_3-$(CH_2)_2$-$C\mathit{H}_2$-S-C(S)-S-), 4.60-5.09 (m, PSt first chain length of –C*H*), 6.29-7.57 (m, PSt benzyl ring –$C_6\mathit{H}_5$ and 1H of C*H*Cl_3).

Typical Removal of Butyl Trithiocarbonate End Group: Modification of PABTC-PnBA$_n$ to H-PnBA$_n$

A mixture of PABTC-P*n*BA$_{10}$ (0.2 g, 0.13 mmol), BPO (0.5 g, 2.06 mmol (i.e., 13 molar equivalents)), and toluene (5.6 g) was placed in a round-bottom flask, sealed, and degassed with nitrogen gas for 10 minutes. 2-Propanol was degassed with nitrogen gas in a separate sealed round-bottom flask. The 2-propanol (5.2 g) was removed through a gas-tight syringe equipped with a long needle and injected to the mixture. The round-bottom flask containing the mixture was then heated to 100 °C for 1.4 h. The completion of butyl trithiocarbonate RAFT-end group removal was determined by ^{1}H-NMR after evaporating the volatile solvents from the product in a vacuum oven at 40 °C overnight. The ^{1}H-NMR spectrum of the product demonstrated the absence of signals associated with the butyl trithiocarbonate end group at 3.3 ppm (CH_3-$(CH_2)_2$-$C\mathit{H}_2$-S-C(S)-S-) and 4.8 ppm (the first chain length of C*H* oligomer backbone adjacent to the sulfur). The evaporated product was dissolved in 2-propanol and was purified by precipitation method in a cold methanol/water mixture (78/22 v/v %) to remove the unreacted BPO. The purified product was characterised by ^{1}H-NMR, ESI-MS, SEC, UV/Vis spectroscopy, and DSC. $M_{n\ \mathrm{ESI\text{-}MS}}$ = 1377 g/mol (gaining 1 Na^+). $M_{n\ \mathrm{1H\text{-}NMR}}$ = 1226 g/mol. SEC: M_n = 1100 g/mol and *Đ* = 1.14. T_g of the modified P*n*BA$_{10}$ (H-P*n*BA$_{10}$) = -52 °C. ^{1}H-NMR (300 MHz, $CDCl_3$): δ (ppm) 0.78-1.07 (t, 3H, $C\mathit{H}_3$-$(CH_2)_3$-COO), 1.07-2.15 (m, -CH($C\mathit{H}_3$)COOH, $C\mathit{H}_2$(COO$(CH_2)_3CH_3$)-CH_2-, P*n*BA backbone -$C\mathit{H}_2$, CH_3-$C\mathit{H}_2$-$(CH_2)_2$-COO and CH_3-CH_2-$C\mathit{H}_2$-CH_2-COO), 2.20-3.02 (m, P*n*BA backbone –C*H* and -C*H*(CH_3)(COOH)), 3.77-4.34 (m, 2H, CH_3-$(CH_2)_2$-$C\mathit{H}_2$-COO).

Results and Discussion

Synthesis of Oligomers *via* RAFT Polymerization

2-Propanoic acid butyl trithiocarbonate (PABTC) was used as RAFT agent to generate homo-oligomers of two common monomers, *n*-butyl acrylate (*n*BA) and styrene (St) with similar targeted degree of polymerization ($9 \leq DP \leq 27$). It is known that trithiocarbonates are effective RAFT agents for the polymerization of acrylic (acrylamides, acrylates and methacrylates) and styrenic monomers, given an appropriate choice of leaving group (R group) (*28*). Moreover, trithiocarbonates (Z = alkylthio) with 2-propanoic acid as the R group have been reported to be suitable RAFT agents for controlling the polymerization of acrylic acid, butyl acrylate and styrene (*29*). In oder to study the effect on thermal properties of the end group, RAFT polymerization of *n*BA was also mediated by a dithiobenzoate (CPDB) chain transfer agent.

Table 1. Synthesis of P*n*BA$_n$ oligomers

Theoretical DP	*Conv% ^{1}H-NMR*	*DP ^{1}H NMR*	*DP ESI-MS*	*M_n SEC*	*Đ SEC*	*Product*[f]
10[a]	93	9	10	1300	1.14	PABTC-P*n*BA$_{10}$
15[a]	96	14	14	2000	1.10	PABTC-P*n*BA$_{14}$
20[a]	95	19	18	2600	1.09	PABTC-P*n*BA$_{18}$
25[a]	91	23	21	3000	1.08	PABTC-P*n*BA$_{21}$
500[a],[c]	86	N/A[d]	N/A[e]	42400	1.18	PABTC-P*n*BA$_{331}$[g]
59[b], [c]	28	16	14	2000	1.12	CPDB-P*n*BA$_{14}$

Molar ratio of RAFT agent / AIBN = 10. [a] Polymerization mediated by PABTC in toluene at 70 °C for 3 h. [b] Polymerization mediated by CPDB at 70 °C for 6 h; all polymerizations were done in schlenk tubes using freeze pump thaw degassing (FPTD) technique, except for [c] which was done in a round-bottom flask (RBF) and degassed manually with nitrogen gas. [d] DP cannot be determined accurately from ^{1}H-NMR because the peaks belong to the butyl trithiocarbonate end group were too small compared to the P*n*BA peaks. [e] DP cannot be determined from ESI-MS because the MW of the polymer is outside the limit of ESI-MS (the maximum MW range of the ESI-MS is 4 000 g/mol). [f] DP values obtained from ESI-MS were used as the reference, except for [g] DP obtained from SEC was used as the reference.

DP characterisation by both ESI-MS and ^{1}H-NMR of the resulting oligomers showed a good agreement for all P*n*BA oligomers (Table 1). A small variation of DP (≤ 2 units) obtained from these two analytical techniques is reasonable, due to 10-15% error from ^{1}H-NMR (including integration error and signal to noise error). This error also contributes to the slight difference between the DP and the conversion % determined by ^{1}H-NMR. Thus the DP values of RAFT-capped P*n*BA oligomers obtained from ESI-MS were used as the reference. *Đ*s of RAFT-capped P*n*BA oligomers and polymer were obtained from SEC, and in all cases were lower than 1.2 (Table 1).

The DP of PABTC-PSt_n oligomers was characterised by SEC and ^{1}H-NMR. As in the case of P*n*BA, the variation in DP values between the two analytical techniques and conversion is attributed to integration errors and signal to noise ratio from ^{1}H-NMR (10-15% error). ESI-MS was not used to characterise the DP of PABTC-PSt_n oligomers since the SEC is calibrated against narrow polystyrene standards, thus offering accurate MW characterisation. Ðs of PABTC-PSt_n oligomers were obtained from SEC, and in all cases were below 1.2 (Table 2). These results were in agreement with the Ðs of PABTC-P*n*BA oligomers, confirming that RAFT is an excellent technique to create oligomers with well controlled MW and narrow MWD.

Table 2. Synthesis of PSt_n oligomers

Theoretical DP	*Conv%* *^{1}H-NMR*	*DP* *^{1}H-NMR*	*DP* *SEC*	*M_n* *SEC*	*Đ* *SEC*	*Product*[a]
10	84	10	9	930	1.13	PABTC-PSt_9
30	65	17	14	1500	1.12	PABTC-PSt_{14}
40	52	23	19	2000	1.13	PABTC-PSt_{19}
60	70	37	27	2800	1.16	PABTC-PSt_{27}

Polymerization mediated by PABTC at 65 °C for 17 h; molar ratio of PABTC / AIBN = 10. [a] DP values obtained from SEC were used as the reference.

Removal of Butyl Trithiocarbonate End Group by Radical-Induced Process

The thiocarbonylthio end group of PABTC-P*n*BA_n was substituted to a hydrogen atom in presence of BPO in toluene/2-propanol following a procedure reported by Chong et al. (Table 3) (*30*). Radicals formed from the decomposition of BPO add onto the oligomeric RAFT agent to form the intermediate radical, followed by fragmentation of the oligomeric group. This oligomeric radical can react irreversibly with a H-atom donor such as 2-propanol, which is ten times more effective than toluene as the hydrogen donor toward the P*n*BA propagating radical (*30*). The 2-hydroxyisopropyl radical can then disproportionate to form acetone and 2-propanol (*31*). Toluene is added to help solubilising BPO in the reaction mixture. Moreover, this oligomeric radical can also react irreversibly with small radicals (e.g., initiator-derived radicals, 2-hydroxyisopropyl radical, and benzyl radical) and another oligomeric radical (forming a product of double MW by termination by combination), although these side reactions are expected to be minor events.

^{1}H-NMR and ESI-MS indicated a complete removal of the butyl trithiocarbonate RAFT-end group, and replacement by an H atom. The ESI-MS showed the butyl trithiocarbonate end group was mostly replaced by H atom as the major distribution (with maximum relative abundance of 100%) and by benzyl radical from toluene as the minor distribution (with the maximum relative abundance of approximately 20%). An attempt to calculate the percentage of the minor population from the whole distribution was found to be difficult due to the strong intensity of the background peaks. The complete removal of the butyl trithiocarbonate RAFT end group was also illustrated by UV/Vis spectroscopy, which demonstrated that the PABTC and the PABTC-P*n*BA$_{18}$ have a maximum absorption at 307 nm, attributed to the trithiocarbonate group, while the H-P*n*BA$_{18}$ after purification has no adsorption at this wavelength. Finally, DRI traces of the SEC chromatograms of H-P*n*BA$_{n}$ showed monomodal peaks with narrow MWDs ($Đ$s ≤ 1.2), which suggested that there was formation of termination product by combination reactions.

Table 3. Summary of radical-induced reduction of PABTC-P*n*BA$_{n}$ to H-P*n*BA$_{n}$ in toluene/2-propanol (1:1 v/v%) with BPO initiator at 100 °C for 1.4 hours

Precursor[a]	*Precursor*		*BPO/ Precursor*	*Extent of end group removal % 1H-NMR*[c]	*H-PnBA$_n$*	
	M_n SEC g/mol	*Đ SEC*			*M_n SEC g/mol*	*Đ SEC*
PABTC-P*n*BA$_{10}$	1300	1.14	5	90%	N/A	N/A
PABTC-P*n*BA$_{10}$	1300	1.14	7.5	93%	N/A	N/A
PABTC-P*n*BA$_{10}$	1300	1.14	13	100%	1100	1.14
PABTC-P*n*BA$_{14}$	2000	1.10	12.5	100%	1500	1.15
PABTC-P*n*BA$_{18}$	2600	1.09	7.5	100%	2600	1.14
PABTC-P*n*BA$_{21}$	3000	1.08	7.5	100%	2400	1.13
PABTC-P*n*BA$_{331}$[b]	42400	1.18	7.5	100%	33500	1.24

[Precursor] = 0.0115 M for all experiments. [a] DP of the precursor was obtained from ESI-MS, except for [b] which was obtained from SEC. [c] The extent of end group removal was based on ^{1}H-NMR spectroscopic assessment of the disappearance of signals associated with the butyl trithiocarbonate end group.

A similar approach was used to remove the trithiocarbonate from the PSt oligomers. However, since PSt chains are more likely to terminate by combination and form higher molecular weight products, a combination of AIBN (20 molar equivalents) and BPO (5 to 12.5 molar equivalents) was used (*32*). Under these conditions, the BPO-generated radicals add to the RAFT polymer to form the intermediate radical, which fragments into the polymeric radical through the radical addition-fragmentation process. The generated polymeric radical may then be capped by the relatively high concentration of cyanoisopropyl radical instead of combining with another polymeric radical to form bimodal MWD. The molar ratio of AIBN to BPO should be high to ensure effective capping of the polymeric radical. This procedure led to the replacement of the trithiocarbonate group by a cyanoisopropyl radical, as demonstrated by ^{1}H-NMR and SEC analyses (Table 4). ^{1}H-NMR analysis after the radical induced reaction also revealed the termination products between oligostyryl radicals and initiator-derived radicals (benzoyloxy, phenyl, and cyanoisopropyl radicals), oligostyryl radical and benzyl radical from toluene, and two initiator-derived radicals. The low concentration and complexity of the resulting spectrum of these species made it impossible to assign each of these products to the ^{1}H-NMR signals. However, after purification, ^{1}H-NMR analysis showed that all these side products had disappeared.

Table 4. Summary of radical-induced reduction of PABTC-PSt$_n$ to $CN(CH_3)_2C$-PSt$_n$ in toluene with BPO and AIBN at 80°C for 4 h after purification

Precursor[a]	*Precursor*		*BPO/ Precursor*	*AIBN / Precursor*	*$CN(CH_3)_2C$-PSt$_n$*	
	M_n *SEC* *g/mol*	*Đ* *SEC*			M_n *SEC* *g/mol*[b]	*Đ* *SEC*[c]
PABTC-PSt$_9$	930	1.13	7.5	20	1660	1.36
PABTC-PSt$_{14}$	1500	1.12	7.5	20	2300	1.23
PABTC-PSt$_{14}$	1500	1.12	12.5	20	2350	1.24
PABTC-PSt$_{19}$	2000	1.13	7.5	20	2680	1.15
PABTC-PSt$_{27}$	2800	1.16	7.5	20	3760	1.19
PABTC-PSt$_{27}$	2800	1.16	5	20	3800	1.19

[Precursor] = 0.0115 M for all the experiments. Purification of $CN(CH_3)_2C$-PSt$_n$ was undertaken by precipitation in cold methanol, except for n = 9 where the purification was undertaken by precipitation in cold methanol/water mixture (95/5 v/v%). [a] DP of the precursor was obtained from SEC. [b] M_n and [c] $Đ$ of $CN(CH_3)_2C$-PSt$_n$ after purification.

Thermal Properties of P*n*BA

DSC analyses of the synthesised PABTC-P*n*BA*n* revealed similar T_g values ranging from -47 °C to -50 °C (Figure 1). The difference in heat capacity from one sample to another is attributed to the variation in sample weight, as increasing sample weight results in higher heat capacity. It was also noted that the T_g values of trithiocarbonate PABTC-P*n*BA$_{14}$ and dithiobenzoate CPDB-P*n*BA$_{14}$ were close, -49 °C and -46 °C respectively, thus suggesting that the T_g value of P*n*BA is relatively independent of the RAFT agent type (i.e. R and Z end groups). In addition, DSC analyses of the modified P*n*BA after butyl trithiocarbonate RAFT end group removal (H-P*n*BA$_n$) revealed T_g's ranging from -47 to -52 °C, and therefore close to those of PABTC-P*n*BA$_n$ (Figure 2). These values were also close to the T_g of P*n*BA obtained by free radical polymerization (M_n = 52,000 g/mol and $Đ$ = 11.09), -50°C. These results demonstrate that the T_g value of P*n*BA remains remarkably unchanged regardless of the MW (from values as low 1300 g/ mol, or DP 10) and chain end group.

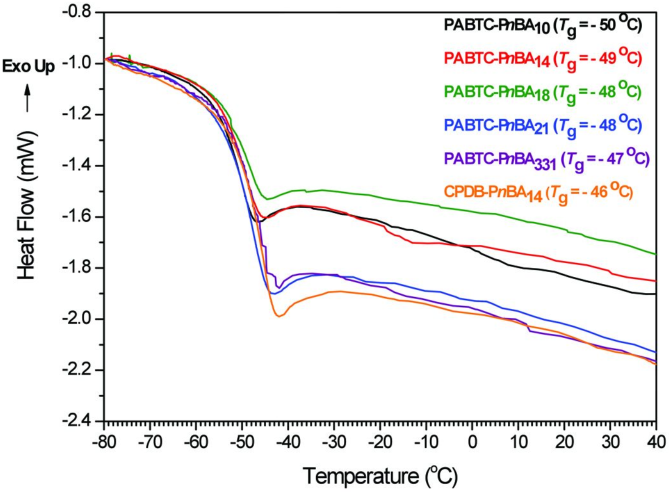

Figure 1. DSC curves of PABTC-PnBA$_n$ and CPDB-PnBA$_n$.

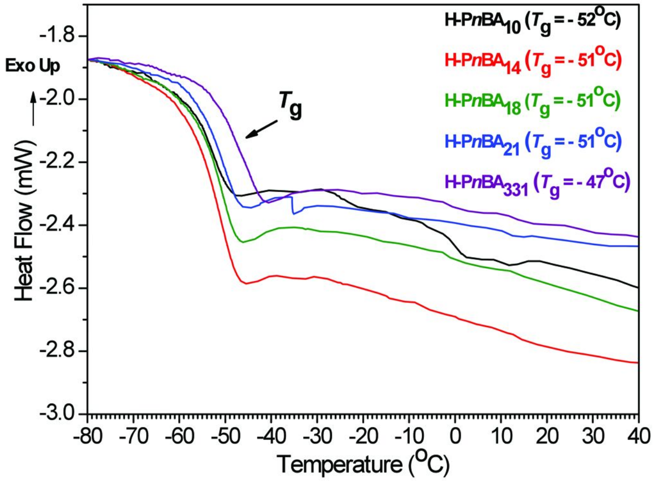

Figure 2. DSC curves of H-PnBA$_n$.

Thermal Properties of PSt

DSC analyses of PABTC-PSt$_n$ (Figure 3) and CN(CH$_3$)$_2$C-PSt$_n$ (Figure 4) showed that the T_g value of PSt increases with increasing MW. Such behavior can be explained by the overall bulkiness and stiffness of PSt, which increases with MW as the number of phenyl ring side group increases. Consequently, the restriction on segmental mobility increases, leading to an increase in T_g. Sokolov et al. (*33*) have also proposed that the rigidity of the polymer chains dictates how strongly segmental relaxation will be affected by the length of a polymer chain, and thus controls the MW dependence of T_g (*33*). Again, the difference in heat capacity from one PSt sample to another (Figure 3 and 4) was due to the variation of PSt sample weight; increasing sample weight resulted in higher heat capacity. Our results agree remarkably with the work of Fox and Flory, (*34*, *35*) who reported that the T_g of PSt increases rapidly with increasing MW up to 25,000 g/mol, then become cosntant. The variation in end group seems to have little influence on T_g, except for PSt$_9$, for which T_g varies from 62°C to 41°C after replacement of the trithiocarbonate by the isobutyronitrile group, in addition the appearance of a melting point (T_m = 61°C). We expect the introduction of the isobutyronitrile group at the chain end has a stronger effect on the shorter PSt chains. DSC analyses of PSt oligomers of similar DP synthesized by ionic polymerization, PSt$_8$ (T_g = 23°C), PSt$_{16}$ (T_g = 64°C) and PSt$_{22}$ (T_g = 73°C) confirmed the stronger effect of the end group on the T_g of shorter chains. In addition, the absence of T_m for PSt$_8$ also confirmed that the semi-crystalline structure of PSt$_9$ was imparted by the presence of the isobutyronitrile group.

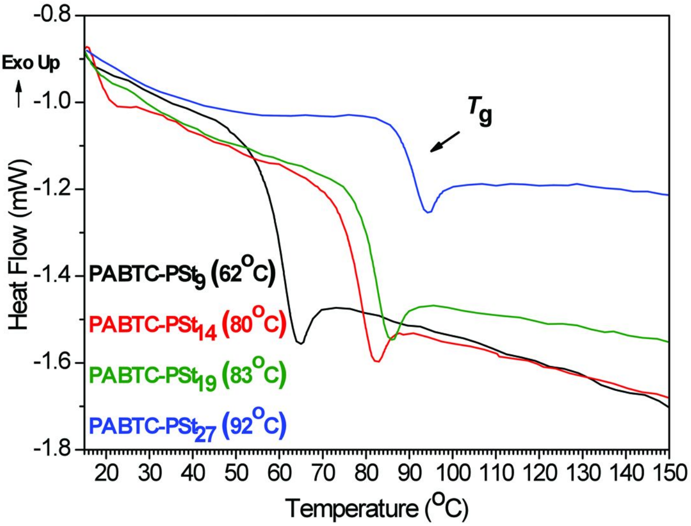

Figure 3. DSC curves of PABTC-PSt$_n$.

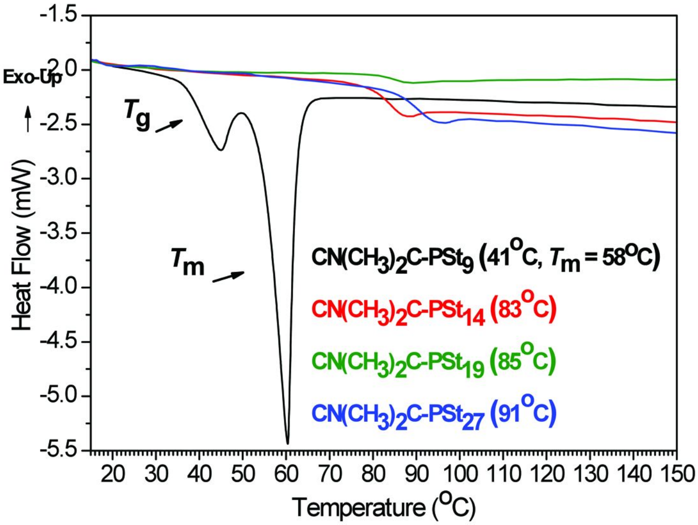

Figure 4. DSC curves of $CN(CH_3)_2C$-PSt_n. [Note: $CN(CH_3)_2C$-PSt_n was the modified PSt product after radical-induced reaction of PABTC-PSt_n in toluene with BPO (7.5 molar equivalents) and AIBN (20 molar equivalents).]

Conclusion

In this work, we have used RAFT polymerization as a tool to produce short chain oligomers, in order to study the effect of chain length on the glass transition of polymers. The capability of RAFT polymerization as a versatile technique to create short chain homo-oligomers was demonstrated by the synthesis of P*n*BA and PSt oligomers of well-controlled MW and narrow MWD ($Đ$s ≤ 1.2). A radical-induced reaction was performed to replace the butyl trithiocarbonate end group of the PABTC RAFT agent with an un-reactive end group on the oligomers. Chain length and end groups were fond to have little effect on the thermal properties of P*n*BA, whilst the T_g of PSt oligomers was established to depend strongly on both chain length and end groups, the latter also nucleating crystalline domains in the shorter PSt oligomers.

Acknowledgments

The authors aknowledge the Australian Research council Discovery and Linkage programmes and the University of Sydney for funding. MS aknowledge the Australian government for the provison of a scholarship.

References

1. McNaught, A. D.; Wilkinson, A. *IUPAC. Compendium of Chemical Terminology*, 2nd ed.; Blackwell Scientific Publications: Oxford, 1997.
2. Soeriyadi, A. H.; Li, G. Z.; Slavin, S.; Jones, M. W.; Amos, C. M.; Becer, C. R.; Whittaker, M. R.; Haddleton, D. M.; Boyer, C.; Davis, T. P. *Polym. Chem.* **2011**, *2*, 815–822.
3. Wang, H.; Han, Y. *Macromol. Rapid Commun.* **2009**, *30*, 521–527.
4. Semsarilar, M.; Perrier, S. *Nat. Chem.* **2010**, *2*, 811–820.
5. Kakwere, H.; Perrier, S. *J. Polym. Sci., Part A: Polym. Chem.* **2009**, *47*, 6396–6408.
6. Konkolewicz, D.; Poon, C. K.; Gray-Weale, A.; Perrier, S. *Chem. Commun.* **2011**, *47*, 239–241.
7. Konkolewicz, D.; Gray-Weale, A.; Perrier, S. *J. Am. Chem. Soc.* **2009**, *131*, 18075–18077.
8. Kakwere, H.; Chun, C. K. Y.; Jolliffe, K. A.; Payne, R. J.; Perrier, S. *Chem. Commun.* **2010**, *46*, 2188–2190.
9. Chapman, R.; Jolliffe, K. A.; Perrier, S. *Polym. Chem.* **2011**, *2*, 1956–1963.
10. Kakwere, H.; Payne, R. J.; Jolliffe, K. A.; Perrier, S. *Soft Matter* **2011**, *7*, 3754–3757.
11. Siauw, M.; Hawkett, B. S.; Perrier, S. *J. Polym. Sci., Part A: Polym. Chem.* **2012**, *50*, 187–198.
12. Ferguson, C. J.; Hughes, R. J.; Pham, B. T. T.; Hawkett, B. S.; Gilbert, R. G.; Serelis, A. K.; Such, C. H. *Macromolecules* **2002**, *35*, 9243–9245.
13. Ganeva, D. E.; Sprong, E.; De Bruyn, H.; Warr, G. G.; Such, C. H.; Hawkett, B. S. *Macromolecules* **2007**, *40*, 6181–6189.
14. Boyer, C.; Stenzel, M. H.; Davis, T. P. *J. Polym. Sci., Part A: Polym. Chem.* **2011**, *49*, 551–595.
15. Takolpuckdee, P.; Westwood, J.; Lewis, D. M.; Perrier, S. *Macromol. Symp.* **2004**, *216*, 23–35.
16. Barner-Kowollik, C.; Perrier, S. *J. Polym. Sci., Part A: Polym. Chem.* **2008**, *46*, 5715–5723.
17. Takolpuckdee, P.; Mars, C. A.; Perrier, S.; Archibald, S. J. *Macromolecules* **2005**, *38*, 1057–1060.
18. Barner-Kowollik, C. *Handbook of RAFT Polymerization*; Wiley-VGH: Weinheim, 2008.
19. Ebeling, B.; Vana, P. *Polymers* **2011**, *3*, 719–739.
20. Willcock, H.; O'Reilly, R. K. *Polym. Chem.* **2010**, *1*, 149–157.
21. Barner-Kowollik, C.; Quinn, J. F.; Nguyen, T. L. U.; Heuts, J. P. A.; Davis, T. P. *Macromolecules* **2001**, *34*, 7849–7857.
22. Theis, A.; Davis, T. P.; Stenzel, M. H.; Barner-Kowollik, C. *Polymer* **2006**, *47*, 999–1010.
23. Konkolewicz, D.; Siauw, M.; Gray-Weale, A.; Hawkett, B. S.; Perrier, S. *J. Phys. Chem. B.* **2009**, *113*, 7086–7094.
24. Arita, T.; Beuermann, S.; Buback, M.; Vana, P. *Macromol. React. Eng.* **2005**, *290*, 283–293.

25. Arita, T.; Buback, M.; Janssen, O.; Vana, P. *Macromol. Rapid Commun.* **2004**, *25*, 1376–1381.
26. Nguyen, D. H.; Wood, M. R.; Zhao, Y.; Perrier, S.; Vana, P. *Macromolecules* **2008**, *41*, 7071–7078.
27. Thang, S. H.; Chong, Y. K.; Mayadunne, R. T. A.; Moad, G.; Rizzardo, E. *Tetrahedron Lett.* **1999**, *40* (12), 2435–2438.
28. Postma, A.; Davis, T. P.; Li, G.; Moad, G.; O'Shea, M. S. *Macromolecules* **2006**, *39*, 5307–5318.
29. Moad, G.; Rizzardo, E.; Thang, S. H. *Aust. J. Chem.* **2009**, *62*, 1402–1472.
30. Chong, Y. K.; Moad, G.; Rizzardo, E.; Thang, S. H. *Macromolecules* **2007**, *40*, 4446–4455.
31. Liard, A.; Quiclet-Sire, B.; Zard, S. Z. *Tetrahedron Lett.* **1996**, *37*, 5877–5880.
32. Chen, M.; Moad, G.; Rizzardo, E. *J. Polym. Sci., Part A: Polym. Chem.* **2009**, *47*, 6704–6714.
33. Sokolov, A. P.; Novikov, V. N.; Ding, Y. *J. Phys.: Condens. Matter* **2007**, *19*, 205116.
34. Fox, T. G.; Flory, P. J. *J. Appl. Phys.* **1950**, *21*, 581–591.
35. Fox, T. G.; Flory, P. J. *J. Polym. Sci.* **1954**, *14*, 315–319.

Downloaded by CORNELL UNIV on June 1, 2012 | http://pubs.acs.org
Publication Date (Web): March 20, 2012 | doi: 10.1021/bk-2012-1101.ch003

Chapter 3

New Architectures and Applications of Organoboron Polymers Prepared via Controlled Radical Polymerization

Fei Cheng and Frieder Jäkle*

Department of Chemistry, Rutgers University-Newark,
73 Warren Street, Newark, New Jersey 07102
***E-mail: fjaekle@rutgers.edu**

Boron-containing polymers hold great potential for applications in the fields of controlled delivery, stimuli-responsive materials, luminescent materials, optoelectronics, catalysis, and chemical sensors. Organoboron polymers can be obtained by post-polymerization modification of precursor polymers or direct polymerization of boron-functionalized monomers. This chapter summarizes our efforts on the synthesis of organoboron block copolymers and star polymers via controlled radical polymerization. A series of amphiphilic block copolymers with boronic acid, borate and boronium functional groups were prepared by boron-silicon exchange of trimethylsilyl-functionalized block copolymer precursors, which were synthesized by ATRP. Direct RAFT polymerization of boron-containing monomers was employed to synthesize luminescent block and star polymers. The self-assembly of these novel organoboron block copolymers and star polymers was investigated.

Introduction

Over the past several decades, organoboron compounds have been widely studied with respect to applications as reagents in organic synthesis, Lewis acid catalysts, luminescent materials, chemical sensors, ceramic precursors and nuclear detectors (*1*). Besides the basic physical and chemical properties, materials for most practical applications require favorable processing characteristics. Polymeric materials are advantageous in this respect and especially, self-assembled functional polymeric nano-structures are promising for the development of new optical, electronic, biological and energy-related materials. Therefore, research on the synthesis and properties of well-defined boron-containing polymers is an emerging area that has drawn great interest of chemists and material scientists (*2–4*).

From a synthetic point of view, the preparation of organoboron polymers can be grouped into two catagories: post-polymerization modification and direct polymerization of boron-containing monomers (*4*). The former method allows one to synthesize polymers with different boron functionalities from a universal polymer precursor, but highly efficient reactions are required to minimize defects during modification. The latter method renders fully-functionalized polymers, but requires facile synthesis of boron-containing monomers and suitable methods for controlled polymerization. Taking advantage of the tremendous achievements of controlled/living radical polymerization, complex architectures of organoboron polymers have recently been introduced (*5*, *6*).

In this contribution, we discuss our recent work on the synthesis of functional organoboron block copolymers and star polymers and their self-assembly into nanostructures.

Downloaded by CORNELL UNIV on June 1, 2012 | http://pubs.acs.org
Publication Date (Web): March 20, 2012 | doi: 10.1021/bk-2012-1101.ch003

Results and Discussion

Boronic Acid, Borate, and Boronium Block Copolymers

In the family of organoboron polymers, boronic acid, borate and boronium-containing polymers are interesting, due to their ionic nature and solubility in water or other highly polar solvents. Boronic acid compounds can bind with sugars and other 1,2- or 1,3-diol compounds in basic aqueous solution, reversibly forming ionic boronate chelate structures (*7*). In dry organic solvents, the trimerization of boronic acids leads to cyclic boroxines, which dissociate back to boronic acids upon addition of trace amounts of water (*8*). Another interesting aspect of boronic acids lies in their pH-responsive solubility (for $PhB(OH)_2$ $pK_a \sim 9$). These concepts have been applied to boronic acid-containing block copolymers to construct multi-responsive self-assembled nanostructures. The ability to reversibly bind sugars makes boronic acid-containing block copolymers also promising candidates for drug delivery vehicles and therapeutic agents (*6*, *9*). On the other hand, anionic borate and cationic boronium polymers can act as supports for charged functional small molecules and macromolecules, such as organometallic catalysts, ionic clusters, synthetic polyelectrolytes and DNAs (*10*). The co-assembly of borate or boronium block copolymers with charge-reverse species also offers an attractive path to new functional nanomaterials (*11*). In spite of these promising potential applications, the exploration of boron-containing block copolymers is still in its infancy (*5*).

Our group developed a versatile post-polymerization modification approach (Scheme 1) to synthesize amphiphilic boronic acid, borate and boronium-functionalized block copolymers from a universal block copolymer precursor, poly(4-trimethylsilylstyrene)-*b*-polystyrene (PSTMS-*b*-PS) (*12–14*).

Downloaded by CORNELL UNIV on June 1, 2012 | http://pubs.acs.org
Publication Date (Web): March 20, 2012 | doi: 10.1021/bk-2012-1101.ch003

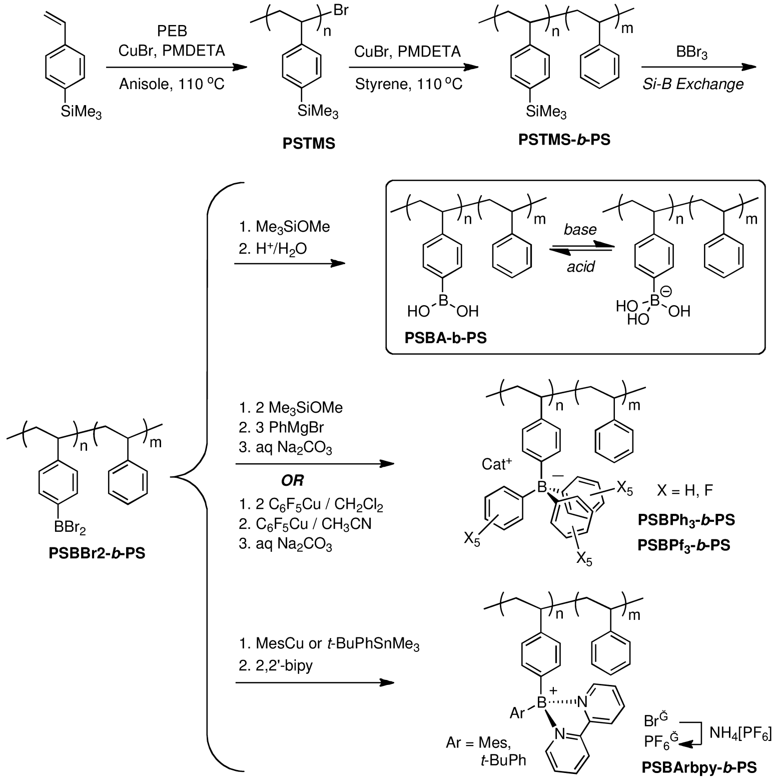
SiMe3
PEB
CuBr, PMDETA
Anisole, 110 °C
Br
n
SiMe3
PSTMS
CuBr, PMDETA
Styrene, 110 °C
n
m
SiMe3
PSTMS-b-PS
BBr3
Si-B Exchange
n
m
BBr2
PSBBr2-b-PS
1. Me3SiOMe
2. H+/H2O
base
acid
HO B OH
PSBA-b-PS
HO B OH HO
1. 2 Me3SiOMe
2. 3 PhMgBr
3. aq Na2CO3
OR
1. 2 C6F5Cu / CH2Cl2
2. C6F5Cu / CH3CN
3. aq Na2CO3
Cat+
B
X5
X5
X5
X = H, F
PSBPh3-b-PS
PSBPf3-b-PS
1. MesCu or t-BuPhSnMe3
2. 2,2'-bipy
Ar
B
N
N
Ar = Mes,
t-BuPh
Br−
PF6−
NH4[PF6]
PSBArbpy-b-PS

Scheme 1. Synthesis of boronic acid, borate, and boronium-functionalized block copolymers via post-polymerization modification.

The block copolymer precursor PSTMS-*b*-PS was synthesized by sequential ATRP polymerization (*13*, *14*). 4-Trimethylsilylstyrene was polymerized as the first block in anisole at 110 °C with 1-phenylethyl bromide (PEB) as the initiator and CuBr/*N,N,N,N',N'*-pentamethyldiethylenetriamine (PMDETA) as the catalyst system. Narrow homopolymers of PSTMS with molecular weights ranging from 3000 to 30000 g/mol were prepared. The polymerization kinetics were studied at a feed ratio of 4-trimethylsilylstyrene: PEB:CuBr:PMDETA = 150:1:1:1. The plot of $\ln([M]_0/[M])$ vs time (t) demonstrated the pseudo-first-order chain growth. Meanwhile, the molecular weight increased linearly with monomer conversion, and the polydispersity remained narrow (PDI < 1.2) over the polymerization, as shown in Figure 1a. The polymer PSTMS was then used as a macroinitiator to control the polymerization of styrene. Again, a kinetic analysis showed pseudo-first-order polymerization (Figure 1b). Narrow PSTMS-*b*-PS block copolymers were synthesized and used as precursors for subsequent post-polymerization modification.

Downloaded by CORNELL UNIV on June 1, 2012 | http://pubs.acs.org
Publication Date (Web): March 20, 2012 | doi: 10.1021/bk-2012-1101.ch003

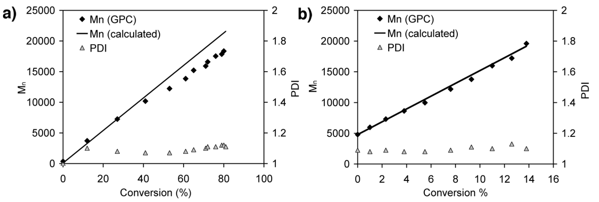

Figure 1. ATRP kinetics: Dependence of M_n and PDI on conversion of monomer. a) 4-Trimethylsilylstyrene with 1-phenylethyl bromide as initiator; b) styrene with poly(4-trimethylsilylstyrene) (PSTMS) as macroinitiator. (Adapted from refs. (13) and (15). Copyright 2004 American Chemicals Society and 2010 Wiley-VCH Verlag GmbH & Co. KGaA).

Chemical reactions on polymer chains are often not as efficient as small molecule reactions. Therefore, the post-modified polymers can be contaminated by unreacted sites and due to side reactions. To obtain defect-free post-modified polymers, quantitative reactions of high selectivity are necessary. A key step of our post-polymerization modification is the Si-B exchange, which was performed by treating PSTMS-*b*-PS with a slightly excess of BBr_3 in CH_2Cl_2. Since BBr_3 and any intermediates containing B-Br bonds are highly sensitive to moisture and oxygen, all reactions were carried out in dry solvents under inert atmosphere. The Si-B exchange was studied by multinuclear NMR spectroscopy. The complete disappearance of the Me_3Si signals in the ^{29}Si ($\delta = -4.4$), ^{13}C ($\delta = -0.5$) and ^{1}H NMR spectra ($\delta = -0.24$), and the appearance of Me_3SiBr indicated that the raction took place in a selective and quantitative fashion (Figure 2). The boron introduction was also evident from a broad signal in the ^{11}B NMR spectrum at $\delta = 54$, which is typical for arylboron dibromides.

The borane polymer $PSBBr_2$-*b*-PS was used for subsequent reactions to synthesize boronic acid, borate and boronium block copolymers, as shown in Scheme 1 (*12*, *15–17*). All reactions were chosen to be highly selective, to ensure defect-free final products. Treatment with Me_3SiOMe and further hydrolysis yielded the boronic acid block copolymer, PSBA-*b*-PS (*12*, *15*). Two different methods can be used for the synthesis of organoborate block copolymers (*16*). One method involves the treatment of boronates with an excess of organolithium or Grignard reagents. We converted the BBr_2 groups to $B(OMe)_2$ with Me_3SiOMe, then reacted the product *in situ* with an excess of PhMgBr to give the triphenylborate-modified block copolymer, $PSBPh_3$-*b*-PS. In another method, a triorganoborane was initially formed, which was further converted to tetracoordinated borates. A two-step reaction of C_6F_5Cu with $PSBBr_2$-*b*-PS in CH_2Cl_2 and then acetonitrile yielded $PSBPf_3$-*b*-PS. Acetonitrile coordinates to the copper reagent, and thereby facilitated the borate formation. The boronium block copolymers PSBArbpy-*b*-PS (Ar = mesityl, *t*-butylphenyl) were obtained by sequential post-modification of $PSBBr_2$-*b*-PS with organocopper/tin reagents and 2,2′-bipyridine (*17*, *18*). A particularly attractive aspect is the spontaneous formation of the boronium moieties upon treatment with 2,2′-bipyridine in what amounts to a “click-type” reaction.

Downloaded by CORNELL UNIV on June 1, 2012 | http://pubs.acs.org
Publication Date (Web): March 20, 2012 | doi: 10.1021/bk-2012-1101.ch003

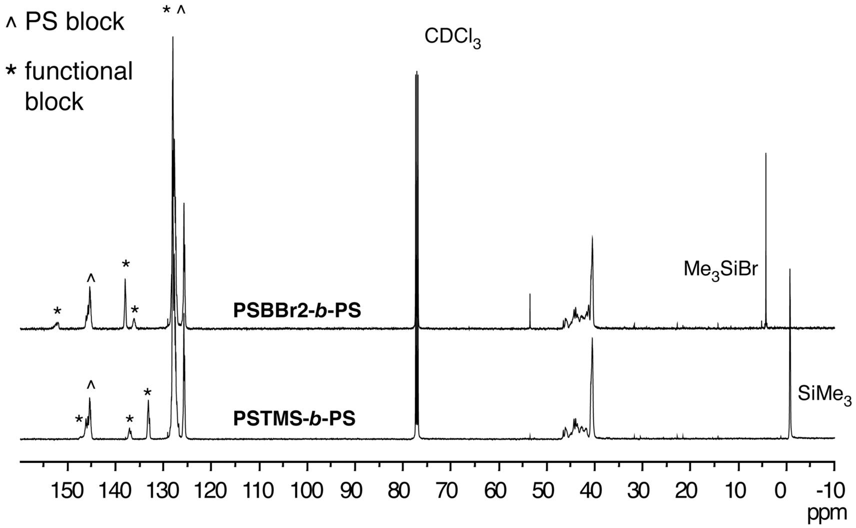

Figure 2. Comparison of ^{13}C NMR spectra of PSTMS-b-PS and $PSBBr_2$-b-PS in $CDCl_3$. (Adapted with permission from ref. (15). Copyright 2010 Wiley-VCH Verlag GmbH & Co. KGaA).

Since these boronic acid, borate and boronium block copolymers have hydrophobic polystyrene as the second block, they should be ideal as building blocks for amphiphilic self-assembly. Moreover, the PSBA-*b*-PS block copolymer can be expected to display pH and sugar-responsive behavior in aqueous solution. We investigated the pH and solvent-dependent self-assembly of PSBA-*b*-PS by transmission electron microscopy (TEM) and dynamic light scattering (DLS) (*15*). At high pH (0.1 M NaOH), we anticipated the boronic acid groups to be negatively charged as $R\text{-}B(OH)_3^-$ and thus hydrophilic. Indeed, self-assembly led to spherical micelles ($\langle D_h \rangle = 18$ nm) of high interface curvature, due to strong electrostatic repulsion (Figure 3a). In contrast, at lower pH (0.001 M NaOH), neutral $RB(OH)_2$ and ionic $R\text{-}B(OH)_3^-$ groups are expected to be randomly distributed along the boron-containing block. The decrease in electrostatic repulsion and possible H-bonding interaction between $RB(OH)_2$ moieties reduces the curvature, which led to shorter worm-like structures ($\langle D_h \rangle = 35$ nm). In organic solvent/water mixtures, other morphologies, including vesicles and larger compound micelles formed also (Figure 3b). Interactions of these micellar and vesicular structures with sugars is expected to lead to interesting phenomena. In related work, the Sumerlin and van Hest groups used boronic acid block copolymers, and investigated their sugar sensing and multi-responsive self-assembly (*9*).

Organoborate-stabilized cationic transition metal complexes are widely used as catalysts for chemical reactions and olefin polymerization (*19*). Organoborates are also promising as electrolytes in lithium ion batteries (*20*). Other new applications of organoborates include ionic liquids, electrochemical redox media, and membrane materials. We recently introduced the first amphiphilic organoborate block copolymers, PSBPh$_3$-*b*-PS and PSBPf$_3$-*b*-PS (Scheme 1) as supports for transition metal complexes (*16*). In toluene, a selective solvent for the PS block, the block copolymers formed reverse micelles with an organoborate-fucntionalized core and PS corona (Figure 4). The reverse micelles were loaded with Rh by treatment with the transition metal complex [Rh(cod)(dppb)]$^+$(OTf)$^-$. The uptake of the Rh complex was ascertained by TEM, which also confirmed the expected core-shell structure (Figure 4). The block copolymer micelles containing transition metal complexes may serve as potential nanoreactors with the advantage of high catalytic activity (high interface/volume ratio), good protection for the catalysts, ease of product separation and catalyst recovery.

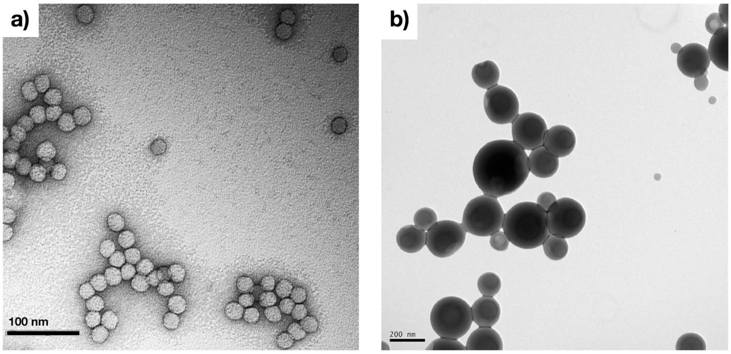

Figure 3. Self-assembly of PSBA-b-PS in different solvents. a) Spherical micelles in 0.1 M NaOH; b) vesicles and large compound micelles in THF/water mixture. (Adapted with permission from ref. (15) . Copyright 2010 Wiley-VCH Verlag GmbH & Co. KGaA).

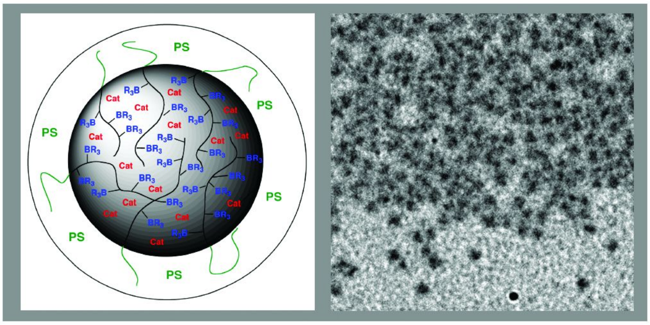

Figure 4. Schematic illustration and TEM image of borate block copolymer micelles loaded with [Rh(cod)(dppb)]$^+$ (Cat). (Adapted from ref. (16). Copyright 2010 American Chemical Society).

Downloaded by CORNELL UNIV on June 1, 2012 | http://pubs.acs.org
Publication Date (Web): March 20, 2012 | doi: 10.1021/bk-2012-1101.ch003

As the charge-reverse counterpart to the borate block copolymers, boronium block copolymers are potential candidates for fuel cell membranes, separation membranes, responsive surfaces and antimicrobial surfaces, which relate to the presence of cationic boronium moieties (*18*, *21*). We examined the self-assembly of the first boronium block copolymers PSBArbpy-*b*-PS (Scheme 1) in methanol and toluene (*17*). Highly regular spherical micelles were obtained.

Organoboron Quinolate Block Copolymers and Star Polymers

Another attractive class of functional polymers are luminescent polymers containing organoboron chromophores (*2*). Luminescent polymers and polymeric nanoparticles play important roles, for example, as chemical sensors, in microelectronic devices, and as bioimaging agents (*22*). Complexes of boron and conjugated organic ligands are often strongly colored and highly luminescent (*23*). With the wide selection of available ligands with different electronic structures, the photophysical properties of boron chromophores can be fine-tuned throughout almost the entire UV-visible-NIR window. Moreover, most tricoordinate boron chromophores bind to anionic and neutural electron-pair donors, such as fluoride, cyanide, or pyridines, which is known to result in remarkable changes in the absorption and emission characteristics (*24*). Other interesting optical properties, including two-photon absorption, room-temperature phosphorescence, and dual emission have been also discovered (*25*).

With their valuable properties, facile synthesis, and good stability, boron chromophores are ideal building blocks for luminescent boron-containing polymers. Compared to the impressive achievements with main-chain type conjugated boron polymers prepared via polycondensation or hydroboration polymerization, studies on polyolefin-based luminescent organoboron polymers, especially block copolymers and polymers of other complex topologies are still limited (*5*, *26*, *27*). In this section, we introduce our recent results on the synthesis of boron quinolate block copolymers and star polymers via RAFT polymerization.

We synthesized two different organoboron 8-hydroxyquinolate monomers, M1 and M2 (Scheme 2), in high yield using a three-step, one-pot method (*26*). To examine the polymerizability of these luminescent styryl monomers, we first carried out a kinetic study of the polymerization of M1. The reaction was performed in anisole at 80 °C, with AIBN as initiator and CTA1 as the trithiocarbonate chain transfer agent ([M1]:[CTA1]:[AIBN] = 33:1:0.33). The plot in Figure 5 revealed a pseudo-first-order polymerization up to ~73% monomer conversion; the molecular weight increased linearly with the monomer conversion, and the PDI remained narrow. After precipitation in diethyl ether, the product was isolated as a yellow powder (GPC-RI: 5840 g/mol, PDI = 1.21). M2 showed similar but slightly slower polymerization kinetics.

To prepare block copolymers, we used PEO terminated with the same CTA to control the polymerization of M1 and M2. In water, the resulting PEO block copolymers formed micelles with sizes of several tens of nanometers according to DLS analysis. The P1-*b*-PEO block copolymer solution was green-emissive and P2-*b*-PEO red-emissive, due to charge transfer from the dimethylamino phenyl

Downloaded by CORNELL UNIV on June 1, 2012 | http://pubs.acs.org
Publication Date (Web): March 20, 2012 | doi: 10.1021/bk-2012-1101.ch003

Downloaded by CORNELL UNIV on June 1, 2012 | http://pubs.acs.org
Publication Date (Web): March 20, 2012 | doi: 10.1021/bk-2012-1101.ch003

group to the quinolate moiety (Figure 6). Both block copolymer solutions showed good chemical and colloidal stability. Our current projects on this topic include the development of new luminescent boron monomers and corresponding block copolymer with various functional second blocks.

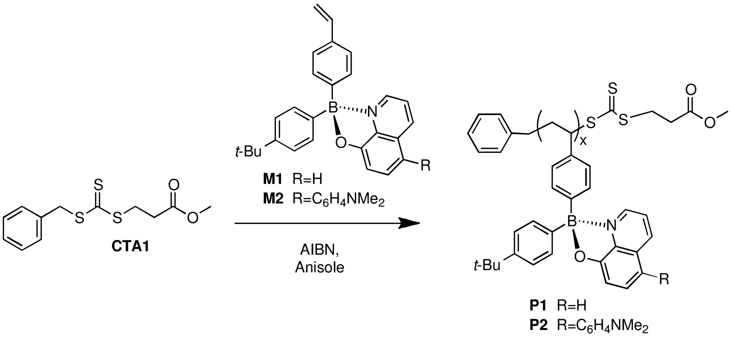

Scheme 2. RAFT polymerization of organoboron quinolate monomers.

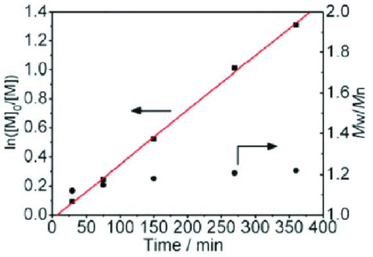

Figure 5. Kinetic plot for the polymerization of M1 in anisole at 80 °C. (ref. (26), http://dx.doi.org/10.1039/b920667a. Adapted by permission of The Royal Society of Chemistry).

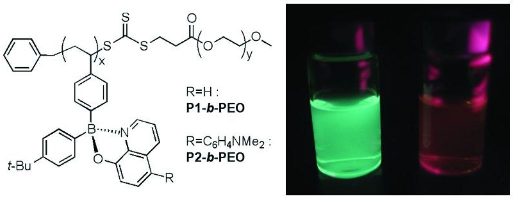

Figure 6. Photograph illustrating the emission of PM1-b-PEO (left) and PM2-b-PEO (right) in water. (ref. (26), http://dx.doi.org/10.1039/b920667a. Adapted by permission of The Royal Society of Chemistry).

Downloaded by CORNELL UNIV on June 1, 2012 | http://pubs.acs.org
Publication Date (Web): March 20, 2012 | doi: 10.1021/bk-2012-1101.ch003

Star polymers may be viewed as structural analogues to self-assembled block copolymer micelles. They have received much recent attention, due to their well-defined core-shell structure, which offers the possibility to precisely incorporate different functionalities into the core and/or shell regions (*28*, *29*). Star polymers find broad applications in the fields of catalysis, nanocontainers for encapsulation, drug delivery vehicles, coatings, and as self-assembly building blocks (*30*). Three major methods, “arm-first”, “core-first” and “graft-to”, can be used to synthesize star polymers. The advantages of the “arm-first” method lie in that: (1) a low polydispersity arm precursor of designed molecular weight is synthesized before the star formation; (2) the resulting star polymers typically possess a well-defined core-shell structure; and (3) the core fraction of the star polymers is high and can be controlled by the experimental conditions (*29*, *31*).

We synthesized the first organoboron star polymers by arm-first RAFT polymerization (Scheme 3) (*32*). A luminescent distyrylboron quinolate species (CL, λ_{em} = 505 nm) was used as a crosslinker. Four different RAFT-synthesized linear arm precursors, namely, PS, PNIPAM, P4VP, and PNIPAM-*b*-PS were used to control the crosslinking reaction of the boron quinolate crosslinker. As an example, a PS star polymer was synthesized in dioxane at 80 °C over 12h with a molar ratio of [crosslinker]:[PS-CTA]:[AIBN] = 24:1:0.1 ($M_{n,\,PS}$ = 9470 g/mol, PDI = 1.14).

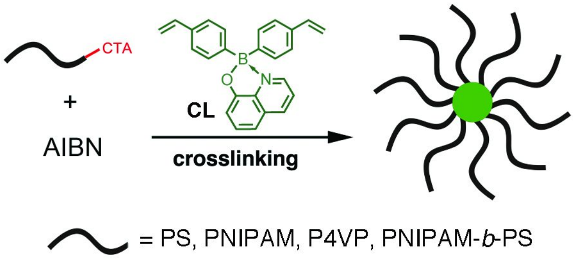

Scheme 3. Star polymer synthesis via arm-first RAFT polymerization nm. (ref. (32), http://dx.doi.org/10.1039/C2PY00556E. Adapted by permission of The Royal Society of Chemistry).

The crude product consisted of about 80% of star polymer and 20% of linear species, which could be easily removed by fractional precipitation. The GPC result of the purified product revealed a high molecular weight and low dispersity ($M_{n,\,PS}$ = 73800 g/mol, PDI = 1.21). The absolute molecular weight by GPC-MALLS (271000 g/mol) was much higher, which is a result of the nature of the crosslinker and the star architechture. PNIPAM, P4VP, and PNIPAM-*b*-PS star polymers were synthesized under similar conditions. A typical TEM image of PNIPAM-*b*-PS star polymers stained with RuO_4 vapour is shown in Figure 7a. A core-shell structure was clearly observed.

Downloaded by CORNELL UNIV on June 1, 2012 | http://pubs.acs.org
Publication Date (Web): March 20, 2012 | doi: 10.1021/bk-2012-1101.ch003

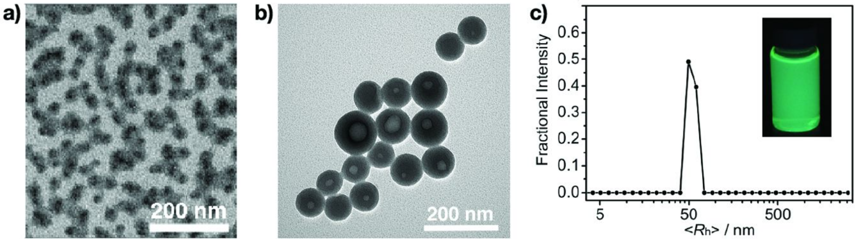

Figure 7. a) TEM image of PNIPAM-b-PS star polymers in $CHCl_3$ (stained with RuO_4 vapour. b) TEM image of PNIPAM-b-PS star polymer assemblies in water (stained with iodine vapour). c) Intensity-averaged size distribution of aggregates of PNIPAM-b-PS star polymers in water; inset: photograph of an aqueous solution excited with a UV lamp at 365 nm. (ref. (32), http://dx.doi.org/10.1039/C2PY00556E. Adapted by permission of The Royal Society of Chemistry).

Heteroarm and block-arm star polymers are also potential building blocks for higher nanostructures, which are challenging to obtain by block copolymer self-assembly. However, compared to the extensive studies on the self-assembly of block copolymer, star polymer self-assembly remains underdeveloped, and has mainly involved heteroarm star polymers (*33*). Our PNIPAM-*b*-PS star polymer serves as a model with unsymmetric amphiphilicity (short PNIPAM outer shell and long PS inner shell) and a covalently fixed core-shell structure. As shown by TEM in Figure 7b, in water, the PNIPAM-*b*-PS star polymer formed large vesicle-like aggregates (D_{TEM} = 97 nm). The aqueous self-assembly into large nanostructures that are strongly fluorescent was further confirmed by DLS (D_{DLS} = 108 nm) as illustrated in Figure 7c.

We proposed that in water the long, inner PS shell shrinks towards the crosslinked boron quinolate core, forming a thick hydrophobic layer. Given that the outer hydrophilic PNIPAM shell is much shorter than the PS inner shell, different star polymers aggregate to reduce the hydrophobic PS/water interface.

Conclusion

Using post-polymerization modification and direct polymerization methods, we synthesized new functional organoboron block copolymer, ranging from boronic acid, ionic borate and boronium polymers, to luminescent boron quinolate polymers. The first luminescent boron star polymers with different functional arms were obtained by arm-first RAFT polymerization. Our results demonstrate that both direct polymerization of boron monomers and post-polymerization modification procedures are powerful tools for the synthesis of organoboron polymers of complex architectures. The amphiphilic self-assembly of block and star polymers in selective solvents was exploited to generate higher-order structures with tailored functionality.

Downloaded by CORNELL UNIV on June 1, 2012 | http://pubs.acs.org
Publication Date (Web): March 20, 2012 | doi: 10.1021/bk-2012-1101.ch003

Acknowledgments

Financial support of our research program on nanostructured boron materials by the National Science Foundation (CHE-0346828, CHE-0956655, CHE-1112195, MRI-0116066) and the donors of the Petroleum Research Fund, administered by the American Chemical Society, is gratefully acknowledged. FJ thanks all his current and former students and collaborators for valuable contributions to the work summarized in here. Special thanks go to Prof. Yang Qin, Dr. Chengzhong Cui, and Prof. Edward Bonder for their efforts in the area of boron-containing block copolymer synthesis and characterization.

References

1. Jäkle, F., Boron: Organoboranes. In *Encyclopedia of Inorganic Chemistry*, 2nd ed.; Crabtree, R. H., Ed. Wiley: Chichester, U.K., 2005; pp 560−598.
2. (a) Jäkle, F. *Chem. Rev.* **2010**, *110*, 3985−4022. (b) Matsumi, N.; Chujo, Y. *Polym. J.* **2008**, *40*, 77−89.
3. Abd-El-Aziz, A. S.; Carraher Jr., C. E.; Pittman Jr., C. U.; Zeldin, M., *Macromolecules Containing Metal and Metal-Like Elements, Volume 8, Boron-Containing Polymers*; John Wiley & Sons: Hoboken, NJ, 2007.
4. (a) Jäkle, F. *Coord. Chem. Rev.* **2006**, *250*, 1107−1121. (b) Jäkle, F. *J. Inorg. Organomet. Polym. Mater.* **2005**, *15*, 293−307.
5. Cheng, F.; Jäkle, F. *Polym. Chem.* **2011**, *2*, 2011–2121.
6. Cambre, J. N.; Sumerlin, B. S. *Polymer* **2011**, *52*, 4631–4643.
7. Hall, D. G., *Boronic Acids: Preparation and Applications in Organic Synthesis and Medicine*; Wiley-VCH Verlag GmbH & Co. KGaA: Weinheim, Germany, 2005.
8. Korich, A. L.; Iovine, P. M. *Dalton Trans.* **2010**, *39*, 1423–1431.
9. (a) Bapat, A. P.; Roy, D.; Ray, J. G.; Savin, D. A.; Sumerlin, B. S. *J. Am. Chem. Soc.* **2011**, *133*, 19832−19838. (b) Roy, D.; Cambre, J. N.; Sumerlin, B. S. *Chem. Commun.* **2008**, 2477−2479. (c) Roy, D.; Cambre, J. N.; Sumerlin, B. S. *Chem. Commun.* **2009**, 2106−2108. (d) Kim, K. T.; Cornelissen, J. J. L. M.; Nolte, R. J. M.; van Hest, J. C. M. *J. Am. Chem. Soc.* **2009**, *131*, 13908−13909. (e) Kim, K. T.; Cornelissen, J. J. L. M.; Nolte, R. J. M.; van Hest, J. C. M. *Adv. Mater.* **2009**, *21*, 2787–2791.
10. (a) Kishi, N.; Ahn, C.-H.; Jin, J.; Uozumi, T.; Sano, T.; Soga, K. *Polymer* **2000**, *41*, 4005−4012. (b) Sablong, R.; van der Vlugt, J. I.; Thomann, R.; Mecking, S.; Vogt, D. *Adv. Synth. Catal.* **2005**, 347, 633−636. (c) Deore, B. A.; Yu, I.; Woodmass, J.; Freund, M. S. *Macromol. Chem. Phys.* **2008**, 209, 1094−1105.
11. Faul, C. F. J.; Antonietti, M. *Adv. Mater.* **2003**, *15*, 673–683.
12. Qin, Y.; Sukul, V.; Pagakos, D.; Cui, C.; Jäkle, F. *Macromolecules* **2005**, *38*, 8987–8990.
13. Qin, Y.; Cheng, G.; Achara, O.; Parab, K.; Jäkle, F. *Macromolecules* **2004**, *37*, 7123–7131.
14. Qin, Y.; Cheng, G.; Sundararaman, A.; Jäkle, F. *J. Am. Chem. Soc.* **2002**, *124*, 12672–12673.

15. Cui, C. Z.; Bonder, E. M.; Qin, Y.; Jäkle, F. *J. Polym. Sci., Part A: Polym. Chem.* **2010**, *48*, 2438–2445.
16. Cui, C.; Bonder, E. M.; Jäkle, F. *J. Am. Chem. Soc.* **2010**, *132*, 1810–1812.
17. Cui, C.; Bonder, E. M.; Jäkle, F. *J. Polym. Sci., Part A: Polym. Chem.* **2009**, *47*, 6612–6618.
18. Cui, C.; Jäkle, F. *Chem. Commun.* **2009**, 2744–2746.
19. Chen, E. Y.-X.; Marks, T. J. *Chem. Rev.* **2000**, *100*, 1391–1434.
20. Matsumi, N.; Sugai, K.; Miyake, M.; Ohno, H. *Macromolecules* **2006**, *39*, 6924–6927.
21. Piers, W. E.; Bourke, S. C.; Conroy, K. D. *Angew. Chem., Int. Ed.* **2005**, *44*, 5016–5036.
22. (a) Thomas, S. W., III; Joly, G. D.; Swager, T. M. *Chem. Rev.* **2007**, *107*, 1339–1386. (b) Kim, F. S.; Ren, G.; Jenekhe, S. A. *Chem. Mater.* **2011**, *23*, 682−732. (c) Liu, C.-L.; Lin, C.-H.; Kuo, C.-C.; Lin, S.-T.; Chen, W.-C. *Progr. Polym. Sci.* **2011**, *36*, 603−637.
23. (a) Benstead, M.; Mehl, G. H.; Boyle, R. W. *Tetrahedron* **2011**, *67*, 3573−3601. (b) Jäkle, F. *Chem. Sus. Chem.* **2011**, *4*, 325−326. (c) Zhang, G. Q.; Lu, J. W.; Sabat, M.; Fraser, C. L. *J. Am. Chem. Soc.* **2010**, *132*, 2160−2162. (d) Ulrich, G.; Ziessel, R.; Harriman, A. *Angew. Chem. Int. Ed.* **2008**, *47*, 1184–1201. (e) Wang, S. *Coord. Chem. Rev.* **2001**, *215*, 79−98.
24. (a) Wade, C. R.; Broomsgrove, A. E. J.; Aldridge, S.; Gabbai, F. P. *Chem. Rev.* **2010**, *110*, 3958−3984. (b) Hudson, Z. M.; Wang, S. *Acc. Chem. Res.* **2009**, *42*, 1584−1596. (c) Yamaguchi, S.; Akiyama, S.; Tamao, K. *J. Organomet. Chem.* **2002**, *652*, 3−9.
25. (a) Zhang, G.; Evans, R. E.; Campbell, K. A.; Fraser, C. L. *Macromolecules* **2009**, *42*, 8627−8633. (b) Entwistle, C. D.; Marder, T. B. *Chem. Mater.* **2004**, *16*, 4574−4585.
26. Cheng, F.; Jäkle, F. *Chem. Commun.* **2010**, *46*, 3717–3719.
27. (a) Nagai, A.; Kokado, K.; Miyake, J.; Chujo, Y. *Macromolecules* **2009**, *42*, 5446−5452. (b) Kersey, F. R.; Zhang, G. Q.; Palmer, G. M.; Dewhirst, M. W.; Fraser, C. L. *ACS Nano* **2010**, *4*, 4989−4996. (c) Zhang, G.; Fiore, G. L.; St. Clair, T. L.; Fraser, C. L. *Macromolecules* **2009**, *42*, 3162−3169. (d) Paris, R.; Quijada-Garrido, I.; Garcia, O.; Liras, M. *Macromolecules* **2011**, *44*, 80−86.
28. Altintas, O.; Vogt, A. P.; Barner-Kowollik, C.; Tunca, U. *Polym. Chem.* **2012**, *3*, 34–45.
29. Gao, H.; Matyjaszewski, K. *Progr. Polym. Sci.* **2009**, *34*, 317–350.
30. (a) Moad, G.; Chen, M.; Haussler, M.; Postma, A.; Rizzardo, E.; Thang, S. H. *Polym. Chem.* **2011**, *2*, 492−519. (b) Wiltshire, J. T.; Qiao, G. G. *Aust. J. Chem.* **2007**, *60*, 699−705.
31. Blencowe, A.; Tan, J. F.; Goh, T. K.; Qiao, G. G. *Polymer* **2009**, *50*, 5–32.
32. Cheng, F.; Doshi, A.; Jäkle, F. *Polym. Chem.* **2012**, DOI: 10.1039/C2PY00556E.
33. (a) Boyer, C.; Stenzel, M. H.; Davis, T. P. *J. Polym. Sci. A: Polym. Chem.* **2011**, *49*, 551−595. (b) Khanna, K.; Varshney, S.; Kakkar, A. *Polym. Chem.* **2010**, *1*, 1171−1185.

Downloaded by CORNELL UNIV on June 1, 2012 | http://pubs.acs.org
Publication Date (Web): March 20, 2012 | doi: 10.1021/bk-2012-1101.ch003

Chapter 4

Synthesis and Characterization of PE-b-POEGMA Copolymers Prepared by Linear/Hyperbranched Telechelic Polyethylene-Initiated ATRP of Oligo(ethylene glycol) Methacrylates

Pingwei Liu,[1] Weiqiang Lu,[1] Wen-Jun Wang,*,[1] Bo-Geng Li,[1] Zhibin Ye,*,[2] and Shiping Zhu*,[3]

[1]State Key Lab of Chemical Engineering, Institute of Polymerization and Polymer Engineering, Department of Chemical and Biological Engineering, Zhejiang University, Hangzhou, P R China 310027
[2]School of Engineering, Laurentian University, Sudbury, Ontario, Canada P3E 2C6
[3]Department of Chemical Engineering, McMaster University, Hamilton, Ontario, Canada L8S 4L7
***E-mails: wenjunwang@zju.edu.cn (W.-J.W.); zhuship@mcmaster.ca (S.Z.); zye@laurentian.ca (Z.Y.)**

Amphiphilic diblock copolymers consisting of linear or hyperbranched polyethylene (PE) and poly[oligo (ethylene glycol) methyl ether methacrylate] (POEGMA) were synthesized via atom transfer radical polymerization (ATRP) initiated by PE macroinitiators (MIs). The MIs contained an end-capping 2-bromoisobutyryl group per chain. Their linear and hyperbranched structures were first synthesized through a “living” polymerization of ethylene under pressure of 27.6 and 1 atm, respectively, using Pd–diimine catalyst, $[(ArN{=}C(Me)–(Me)C{=}NAr)Pd(CH_2)_3C(O)O(CH_2)_2OC(O)C(CH_3)_2Br]^+ SbF_6^-$ (Ar = 2,6-$(iPr)_2C_6H_3$) (**1**). In the ATRP of OEGMA, the effect of solvent, ligand, and MI concentration on the block copolymer formation were studied. The macroinitiator and block copolymer samples were characterized by GPC, 1H NMR, and DSC measurements. All samples

In Progress in Controlled Radical Polymerization: Materials and Applications; Matyjaszewski, K., et al.;
ACS Symposium Series; American Chemical Society: Washington, DC, 2012.

possessed well-defined topologies/structures with narrow molecular weight distributions and controlled lengths of PE and POEGMA blocks. The block structures were verified by an intrinsic viscosity study. Micelle formation and its temperature sensitivity were also analyzed by dynamic light scattering.

Introduction

Amphiphilic block copolymers (Amphiphilic BCs) consist of at least two blocks of distinct chemical nature like hydrophobicity versus hydrophilicity in most cases. In majority of solvents, such chains can have only one block dissolved and thus phase separation occurs, leading to the formation of various self-assembled nanostructures at interface or in solution (*1*, *2*). The nanostructures can be designed by tailoring amphiphilic BC's intrinsic parameters including chemical composition, microstructure, molecular weight, topology, and functionality of the covalently joined blocks. Amphiphilic BCs have advantages of enhanced stability and design flexibility over classical low-molecular-weight lipids and surfactants (*1–8*). Numerous amphiphilic BCs have been developed and used as advanced materials in applications such as emulsion stabilizer (*1*, *5*), detergency (*7*), drug delivery (*9–11*), template (*12*), nanoreactor (*11*, *13*).

Among amphiphilic BCs, the ones having hydrophobic olefinic block are of particular interest, due to high hydrophobicity, outstanding chemical stability, and excellent mechanical properties of the polyolefin materials (*14–17*). However, it is really challenging to prepare such amphiphilic BCs with a well-defined structure. The incompatibility between olefinic and water-soluble monomers is remarkable in terms of solvent solubility and polymerization mechanism. A block copolymerization strategy by combining different "living"/controlled polymerization techniques has been developed. There are a small number of well-defined amphiphilic BCs containing olefinic blocks reported in literatures. In most cases, the olefinic precursors were first prepared either by "living" anionic polymerization (LAP) (*17–25*) of 1,4-butadiene and/or 1,4-isoprene (Ip) or by "living" cationic polymerization of isobutylene (*26*). Further chain extension with various hydrophilic (or polar) monomers were carried out with "living" ring-opening polymerization (LROP) (*18–20*), atom transfer radical polymerization (ATRP) (*21–24*, *26*), reversible addition fragmentation transfer (RAFT) polymerization (*17*), or combined LROP and RAFT technique (*25*). Some resulted polar blocks required an additional hydrolysis process (*21*). In general, multiple reaction/modification steps were essentially required in these works, such as post-hydrogenation of the polymers produced by LAP and sequential transformation of olefinic chain end to desired functionality.

There are only a few reports for synthesis of the amphiphilic BCs directly from ethylene (E) and propylene (P) stocks. Chung et al. (*27*) reported the first synthesis of polyethylene and poly(ethylene oxide (EO)) block copolymer through borane–H chain transfer in metallocene polymerization of ethylene or ethylene/1-octene and subsequent interconversion of the borane chain end to an anionic ($–O^-K^+$) group for further LROP of EO. The obtained amphiphilic BCs had a polydispersity index (PDI) > 2.2. It was also reported (*28*) that epoxy- and diol-terminated low-molecular-weight PEs (number-average molecular weight (M_n) = 1.1 kg/mol, PDI = 1.8) were derived from linear vinyl-terminated PEs and used as precursors for further LROP of EO. Very recently, Zhu et al. (*29*) synthesized narrowly distributed amphiphilic BCs (PDI = 1.21) with linear crystalline PE block (weight-average molecular weight (M_w) = 1.0. and 2.1 kg/mol) and hydrophilic PEO (M_w = 1.6 and 6.5 kg/mol) by click coupling reaction between $PE–N_3$ and $PEO–CONHCH_2C≡CH$. The PEs were prepared by chain shuttling ethylene polymerization. In their work, multiple steps were involved in modification of chain-end group to obtain the clickable functionality. An efficiency of 65.4% was found in clicking PE (M_n = 2.1 kg/mol) with PEO of 1.6 kg/mol. Later, Zhu et al. (*30*) used similar PEs (after chain-end group transformation) of M_n = 0.9 kg/mol as macroinitiators (MIs) for ATRP of oligo(ethylene glycol) methacrylates (OEGMA). An amphiphilic BC sample (M_n = 8.0 kg/mol, PDI = 1.11) was prepared but no detailed kinetics and molecular weight control was given.

In general, the used olefinic precursors had relatively lower molecular weights with M_n values in the range of 0.9-4.0 kg/mol, except for Chung's case where M_n values were 10-27 kg/mol but their block copolymers had a broad PDI (> 2.2). Multi-step modifications of the olefinic blocks were also required for the chain extension. In this context, it is highly desirable to develop easier methods for synthesis of narrow amphiphilic BCs having a greater flexibility of molecular weight directly from ethylene or propylene stock. In addition, the above amphiphilic BCs had a linear chain topology (except for the coil-brush structure in Zhu's study (*30*)). Block polymers containing two or more different architectures such as dendritic (or hyperbranched) blocks have been demonstrated to possess novel interfacial properties, improved processability, and special phase separation behavior (*31*, *32*). There is no doubt that the synthesis of novel polymers with controlled molecular weight, composition, topology and functionality represents an emerging research area, leading to development of advanced nanostructured functional materials (*33*).

In this work, we report a simple approach to synthesize narrowly distributed amphiphilic BCs that contain a linear or hyperbranched PE block (with M_n up to 22.1 kg/mol) and a hydrophilic POEGMA brush block. It involves a two-step tandem polymerization process combining "living" polymerization of ethylene with ATRP of OEGMA as shown in Scheme 1. The first step takes advantage of the chain walking Pd–diimine catalyst that polymerizes ethylene in a "living" manner to form PE with controllable structure and chain topology (*34*–*38*). The catalyst $[(ArN=C(Me)–(Me)C=NAr)Pd-(CH_2)_3C-(O)O(CH_2)_2OC(O)C(CH_3)_2Br]^+ SbF_6^-$ ($Ar = 2,6-(iPr)_2C_6H_3$) (catalyst **1** in Scheme 1) (*39*), was used to polymerize ethylene at 27.6 atm (≈ 400 psi) and 1 atm. Well-defined PE MIs bearing 2-bromoisobutyryl terminal group and having linear and hyperbranched topologies were obtained. The MIs were subsequently used to initiate ATRP of OEGMA in the second step to render amphiphilic PE-b-POEGMAs with a narrow molecular weight distribution. The PEs and copolymers were characterized by gel permeation chromatography (GPC) equipped with differential refractive index (DRI), viscometer (IV), and light scattering (LS) and analyzed by ^{1}H NMR, differential scanning calorimetry (DSC). Micelle behaviors of the block copolymers in aqueous solution were studied by dynamic light scattering (DLS).

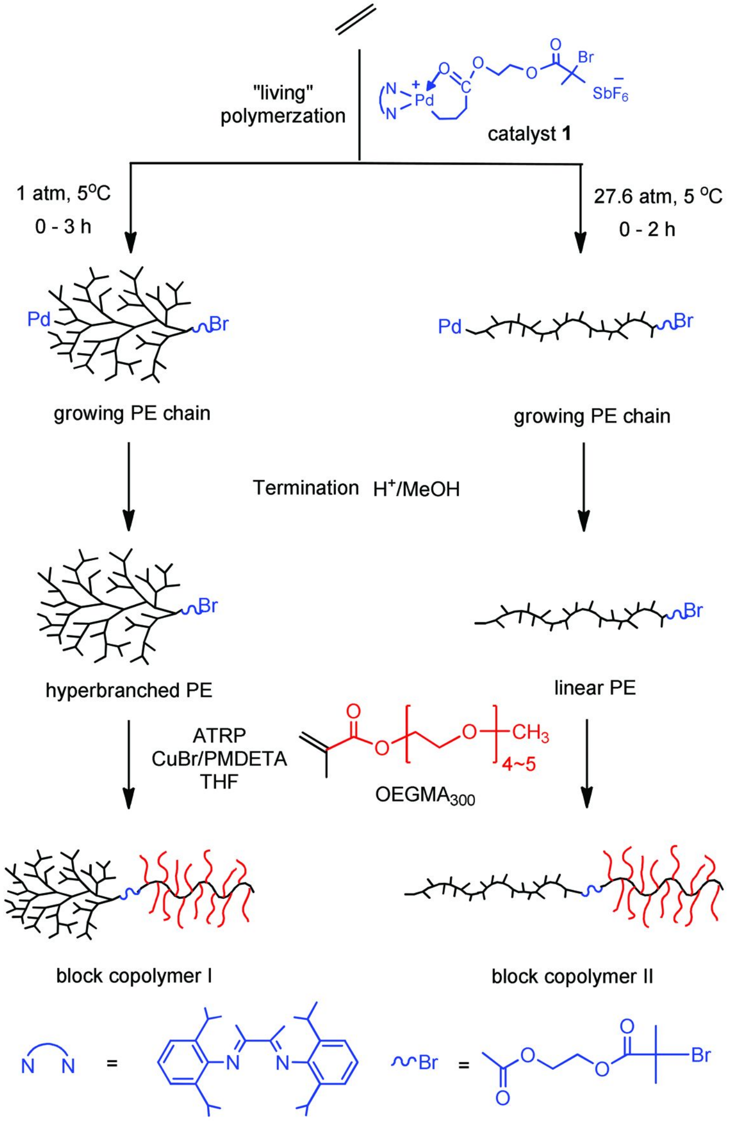
"living" polymerzation
catalyst 1
1 atm, 5°C
0 - 3 h
27.6 atm, 5 °C
0 - 2 h
Pd
Br
growing PE chain
growing PE chain
Termination H+/MeOH
hyperbranched PE
linear PE
ATRP
CuBr/PMDETA
THF
OEGMA300
4~5
block copolymer I
block copolymer II

Scheme 1. Synthesis of amphiphilic polyethylene-block-poly[oligo(ethylene glycol) methacrylate] (PE-b-POEGMA) through a combination of Pd-catalyzed "living" polymerization of ethylene and ATRP of OEGMA.

Experimental Section

Materials

Experiments involving air- or moisture-sensitive substances were conducted in a glove box or using Schlenk techniques. Functionalized Pd–diimine complex $[(ArN{=}C(Me){-}(Me)C{=}NAr){-}Pd(CH_2)_3C(O)O(CH_2)_2OC(O)C(CH_3)_2Br]^+ SbF_6^-$ ($Ar = 2,6\text{-}(iPr)_2C_6H_3$) was prepared as described (*39*). Dichloromethane (>99%, Sinopharm), diethyl ether (99.5%, Sinopharm) and chlorobenzene (99.5%, Aladdin) were refluxed over CaH_2 (98%, Sinopharm) for > 12 h and distilled prior to use. Tetrahydrofuran (THF, >99%, Sinopharm) was refluxed over sodium (CP, Sinopharm) with benzophenone (AR, Sinopharm) as an indicator. Ultra-high purity N_2 and polymerization-grade ethylene (Sinopec China) were purified by passing through CuO catalyst and 3Å molecular sieves. Oligo(ethylene glycol) methacrylates (average M_n = 300 g/mol, 99%, Sigma-Aldrich) were passed through a column filled with neutral alumina (100–200 mesh) to remove inhibitors. CuBr (99%, Sinopharm) was purified by washing successively with acetic acid, ethanol and diethyl ether. Methanol (>99.8%) and $CuBr_2$ (>99%, Sinopharm), ethyl 2-bromoisobutyrate (EBiB, 99%, Sigma-Aldrich), 2, 2′-bipyridine (BPY, >99%, Aladdin) and N,N,N′,N″,N″-pentamethyldiethylenetriamine (PMDETA, 99%, Sigma-Aldrich) were used directly without further purification.

Synthesis of PE MIs

For ethylene polymerization at 1 atm, a flame-dried flask (250 mL) with two manifold branches was evacuated and purged with ethylene three times. Dried chlorobenzene of 50 mL was then injected into the flask. The solution was stirred for 10 min to establish a temperature at 5 °C. A catalyst solution of 20 mL (0.2 mmol Pd–diimine in chlorobenzene) was added to catalyze polymerization with continuously feeding ethylene. After 2 h, the polymer solution was collected and poured into a large amount of 2%-acidified methanol to precipitate out the polymer product. The precipitate was re-dissolved in THF. The solution was then filtered with a 0.2 μm Teflon syringe filter to remove Pd particles, followed with precipitation in methanol. This dissolution-precipitation procedure was repeated until the polymer product was clear. After drying under vacuum at 50 °C for 2 days, 1.54 g MI2 was obtained. For the polymerization at 27.6 atm, a similar operation procedure was adopted as reported (*39*, *40*), except for the use of a 2 L reactor and 400 mL chlorobenzene as solvent each time. The separation and purification method of products were the same.

Typical Synthesis of PE-b-POEGMA by ATRP

Entry 1b in Table 2 is listed as an example. PE MI (MI1, 0.150 g, 0.0234 mmol), THF (8.0 mL), PMDETA (65.2 μL, 0.317mmol, 13.2 equiv) were added into a 20 mL glass tube reactor. The reactor was sealed with a rubber septum and the mixture was stirred with a magnetic stirrer. After PE MI was dissolved in THF, OEGMA (2.7 mL, 2.77 mmol, 400 equiv to MI1) was injected. The mixture was subjected to three freeze-pump-thaw cycles and finally filled with nitrogen.

CuBr (41.1 mg, 0.281 mmol, 12 equiv) and $CuBr_2$ (6.7 mg, 0.0293 mmol, 1.2 equiv) were then added under N_2 protection. After stirring at room temperature for several minutes, the frozen solvent was fully melted. The reactor was placed in a thermostated oil bath set to 50 °C to start polymerization. Throughout the polymerization, the reaction system was protected by dry nitrogen. Samples were taken at 15, 30, 60, and 120 min during the polymerization to monitor OEGMA conversion with ^1H NMR and molecular weight by GPC. The polymers were purified by dialysis (nominal molar mass cutoff = 1.0 kg/mol) of the reaction solution against deionized water and followed with freeze-drying. For the homopolymerization of OEGMA, the same polymerization procedure was adopted, except that EBiB was used as initiator and injected before heating the reaction mixture.

Preparation of Micelle Solution

The polymer product (10 mg) from run 5 (20 min) was dissolved in THF for 24 h and dialyzed against deionized water for 3 days. The solution concentration was determined by gravimetric method after lyophilisation, further adjusted to 1 g/L by adding deionized water.

Characterization

^1H NMR (400 MHz) spectra of Pd–diimine complex, polymerization solution, and polymer products were recorded using a Bruker Advance 400 spectrometer with $CDCl_3$ as solvent and tetramethylsilane as internal standard. Conversions were determined from the ^1H NMR spectra based on the molar ratio between unreacted OEGMA (from integration of double bond peak) and all OEGMA units (from integration of terminal $–OCH_3$ group peaks of unreacted OEGMA and POEGMA block in PE-b-POEGMA). Molecular weights and their distributions were determined at 30 °C by a Polymer Laboratory gel permeation chromatography PL-GPC50 system equipped with DRI, four-bridge capillary viscometer (IV) and laser detectors following the reported procedure (*40*). In molecular weight calculation, DRI increment (dn/dc) value of 0.078 mL/g was used for all PE MIs (*38*, *40*), and 0.180 mL/g for PS standard. The dn/dc value of POEGMA homopolymers was 0.060 mL/g at 30 °C, determined from sample concentration using Cirrus software. For the block copolymers, an average dn/dc value was calculated from the feed mass of PE MI (W_{MI}), feed mass of OEGMA (W_{OEGMA}) and its conversion (x) according to Equation 1.

$$dn/dc_{avg} = dn/dc_{PE} \times \frac{W_{MI}}{W_{MI} + xW_{OEGMA}} + dn/dc_{POEGMA} \times \frac{xW_{OEGMA}}{W_{MI} + xW_{OEGMA}} \quad (1)$$

In the calculation of PDI, DRI signals from the triple-detector GPC were used with a universal calibration based on narrow PS standards.

DSC analysis was conducted using a TA Instruments Q200 DSC equipped with a refrigerated cooling system under N_2. The temperature and heat capacity of the instrument were calibrated against an indium standard. The polymer samples were first heated to 120 °C at a rate of 10 °C/min to eliminate the thermal history effect, and then cooled down to −90 °C at 10 °C/min. The data were collected in the second heating cycle from −90 to 120 °C at a scanning rate of 10 °C/min. Glass transition temperature (T_g) was read from the middle of the heat capacity change, and the melting temperature (T_m) was determined from the maximum of the endothermic peak.

Hydrodynamic diameter and its distribution of the micelles were measured by dynamic light scattering (DLS). DLS spectrophotometer-Malvern Zetasizer Nano S90 was equipped with an argon ion laser operating at 633 nm at a fixed scattering angle of 90°. A temperature raising procedure with 5 °C each time before 50 °C followed by 2 °C each time until 70 °C, was adopted. Upon reaching desired temperature, the sample was maintained for 2 minutes before measurement.

Results and Discussion

Synthesis of PE MIs

Pd-diimine catalysts, first developed by Brookhart et al. (*41*), are a type of late transition metal-based single-site catalysts that have "living" feature and chain walking ability in ethylene polymerization (*34*, *36*, *42–45*). The "living" polymerization can be achieved under the conditions of T = 5-15 °C and ethylene pressure from 1 to 27.6 atm (~400 psi) (*36*, *38*, *45*). Chain walking takes place at the same time, in which Pd metal center isomerizes (i.e. "walking") along polymer chain during propagation, resulting in branched structures (*46*, *47*). Chain walking competes with propagation and its rate is a function of temperature only, the ethylene pressure (i.e., ethylene concentration) shows little influence, while the rate of propagation depends on both temperature and ethylene pressure. Therefore, a simple change of ethylene pressure can easily regulate the competition and enable tailoring of chain topology from dendritic at 0.1 atm, hyperbranched at 1 atm, to linear at 400 psi (*27*, *34*, *37*, *45*). In this work, by changing time and pressure, we prepared hyperbranched/linear PE MIs with the functionalized Pd–diimine complex previously developed by our group, which catalyzed the "living" polymerization of ethylene at 27.6 atm and 5 °C (*39*, *40*). The PE chains possessed a terminal 2-bromoisobutyryl functionality.

Table 1 summarizes the polymerization results. The corresponding GPC curves and ^{1}H NMR spectra were shown in Figures S1 and S2 in the appendix as supporting information. MI1-MI3 were prepared under 1 atm (PE1atm) while MI4-MI5 under 27.6 atm (~400 psi) (PE400psi). Compared to MI4-MI5, lower turnover frequencies (TOFs) and molecular weight values were found in MI1-MI3, due to slower ethylene propagation rate at lower ethylene pressure. The light scattering detector of the triple-detector GPC provided the absolute number-average molecular weight ($M_{n,LS}$), which is included in Figure S1, showing the molecular weight increase with time. Linear correlations of $M_{n,LS}$ versus time were found both at 1 atm and 27.6 atm, demonstrating "living" nature of the polymerization system. The PDIs determined from universal calibration against polystyrene standards were in the range of 1.16 to 1.32, further confirming the system "livingness".

In Progress in Controlled Radical Polymerization: Materials and Applications; Matyjaszewski, K., et al.;
ACS Symposium Series; American Chemical Society: Washington, DC, 2012.

Table 1. Hyperbranched/linear polyethylene macroinitiators with different chain lengths [a]

MI	*Time (h)*	*Ethylene pressure (atm)*	*TOF*[b] *(1/h)*	$M_{n,LS}$[c] *(kg/mol)*	$M_{w,LS}$[c] *(kg/mol)*	$M_{n,NMR}$[d] *(kg/mol)*	PDI_{PS}[e]	*Branching density*[f] *(/1000 C)*	$[\eta]_w$[g] *(mL/g)*
MI1	1	1	97	6.4	6.9	6.4	1.27	93	9.9
MI2	2	1	134	14.6	15.1	13.9	1.26	91	13.5
MI3	3	1	182	22.1	22.4	23.6	1.32	91	16.7
MI4	1	27.6	245	9.7	9.9	10.4	1.19	86	15.1
MI5	2	27.6	268	20.8	20.8	20.9	1.16	85	26.0

[a] Other conditions: solvent, chlorobenzene; total volume, 70 mL for MI1 (0.3 mmol catalyst **1** used), MI2 (0.2 mmol), and MI3 (0.15 mmol), 400 mL for MI4 (0.4 mmol) and MI5 (0.2 mmol); temperature, 5 °C. [b] Ethylene turnover frequency (TOF). [c] Absolute average molecular weights from light scattering detector of GPC. [d] Number-average molecular weight from ^1H NMR spectroscopy based on end group analysis. [e] PDI calculated using universal calibration against PS standards. [f] Branching density data determined with ^1H NMR spectroscopy. [g] Weight-average intrinsic viscosity ($[\eta]_w$) from viscosity detector of GPC.

MI4-MI5 had PDIs of 1.16-1.19, narrower than those of MI1-MI3 (1.26-1.32). This is probably because higher ethylene pressure resulted in more efficient initiation through ethylene substitution of the stable chelating carbonyl group of **1**. The substitution is usually much slower than chain propagation (*48*). The shorter low-MW tail in MI4-MI5 GPC curves further supports this assumption. A lower ethylene TOF of MI1 (97 in the first 1h compared to 182 of MI3 for 3h) can be also attributed to the slow rate of chelate opening and ethylene substitution at the early stage of polymerization at 1 atm.

Since each chain contains one end-capping 2-bromoisobutyryl functionality (*39*, *40*), the polymer number-average molecular weights, $M_{n,NMR}$, were also estimated from their ^1H NMR spectra. Figure S2 in Appendix shows a representative spectroscopy of MI2. The $M_{n,NMR}$ data plotted against time are in good agreement with the $M_{n,LS}$ data, suggesting the presence of one 2-bromoisobutyl end group per chain in the MIs.

Due to chain walking of Pd-diimine, the polymer samples were highly branched at low pressure, with a branching density of 85-93 per 1000 carbons as calculated from the resonance signals of the ethylene sequences in their ^1H NMR spectra. Similar to those reported (*34*, *35*, *37*), these polymers showed little change in total branch with the ethylene pressure, from about 91 at 1 atm to 85 at 27.6 atm. Compared to linear MI4 and MI5, lower weight-average intrinsic viscosities of hyperbranched MI2 and MI3 were evident and confirmed the difference in topology of the two sets of highly branched MIs (*45*).

ATRP of OEGMA

OEGMA-based polymers are very useful and intensively studied for biomaterials design (*49*). These polymers also have unique thermoresponsivity and thus receive remarkable attention in the recent years (*50*). OEGMAs can be readily polymerized with controlled radical polymerization techniques such as ATRP or RAFT polymerization (*51*, *52*). In this work, with the PE MIs above, we used ATRP to synthesize PE-b-POEMGAs from a commercially available OEGMA with an average M_n of 300 g/mol. It is a mixture of OEGMAs with 4 and 5 EO units in the side chain (*53–55*). There were some creative works reported on synthesis of amphiphilic core-shelled copolymers with a hyperbranched or dendritic polyethylene core and multiple POEGMA arms (*56–58*). In those cases, hyperbranched or dendritic PEs bearing multiple ATRP initiation sites were prepared by a coordinative copolymerization of ethylene and ATRP inimer (acting as both initiator and monomer in ATRP) and were served as MIs for a subsequent ATRP of OEGMA. It is challenging to synthesize well-defined PE-b-POEGMA diblock copolymers because there is only one initiation site per chain. Difficulties are radical coupling, incomplete chain initiation (*59*), as well as poor compatibility of the low Br content PE MIs with OEGMAs.

In order to facilitate ATRP, it is essential to use an organic co-solvent for both PE and OEGMA (*51*). THF (with a polarity index of 4.0), anisole (3.9), and toluene (2.4) meet the requirement (*60*). These solvents were used for ATRP of OEGMA with 2, 3 or more EO units in the side chain (*61–63*). Herein, in the ATRPs with MI5 as the initiator, we studied the effect of solvents (THF and toluene) and ligands (BPY and PMDETA) on the activity. Other strategies included low MI feed concentration ($[MI]_0 = 2.2$ mM), high ratio of $[Cu^+]_0/[MI]_0 = 12$, and initial addition of Cu^{2+} (10% of Cu^+) as deactivator to suppress radical concentration, reduce radical coupling, and thus enhance initiation efficiency (*39*). THF: OEGMA = 3:1 vol. was used to prevent the PE MIs from precipitation with the increased polarity of added OEGMA.

Figure 1 shows GPC results of the four runs with different solvents and ligands. When less active BPY was used as ligand, bimodal GPC curves were evident in Figure 1(a)&(b). The lack of control could be attributed to the low solubility of copper catalyst in nonpolar toluene. In contrast, when THF was used as solvent, a monomodal trace of lower molecular weight was obtained at 120 min, as shown in Figure 1(c). However, there was no obvious increase of molecular weight in the low-MW part (i.e., high elution volume) at 480 min, suggesting dead chains existed in the 120 min product. When ligand was changed to the higher activity PMDETA (*51*), the molecular weight continuously increased from 15 min to 120 min with a full shift of the block copolymer from MI5 clearly observed in 120 min. Both GPC curves had long tails and were unsymmetrical, indicating a relatively low initiation efficiency of MI5.

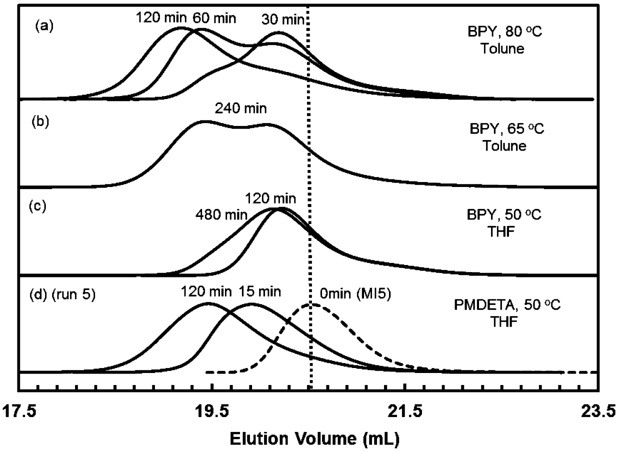

Figure 1. GPC curves in ATRP runs of OEGMA initiated by MI5 with different solvents and ligands. Other conditions: $[MI5]_0 = 2.2$ mM ($[MI5]_0:[OEGMA]_0 = 1:400$), $[MI5]_0:[CuBr]_0:[CuBr_2]_0:[Ligand]_0 = 1:12:1.2:13.2$, T = 50 °C, THF or toluene: OEGMA = 3:1 vol.

In further experiments with THF as solvent and PMDETA as ligand, we found that the initial $[MI]_0$ (or the molar ratio of OEGMA to MIs) affected the block copolymerization significantly. Figure 2 shows the kinetics of run 1a with $[MI1]_0$ = 4.4 mM and run 1b = 2.2 mM. Both runs did not follow simple first-order kinetics up to 120 min. The rate slowed down in 60 min with little increase of OEGMA conversion afterwards. In addition, the rate of run 1a with doubled $[MI]_0$ was not as twice as but only slightly higher than that of run 1b. Diffusion controlled reaction might play a role here. OEGMA experienced increasing difficulty in access to longer POEGMA.

Figure 3 shows the DRI traces of runs 1a and 1b recorded from triple-detector GPC. In agreement with the conversion data, an obvious increase of MW was seen in the first 60 min with only slightly increase afterwards. The continuous MW increase during polymerization demonstrated successful chain extension of MIs and formation of PE-*b*-POEGMA diblock copolymers. There was no remaining shoulder peak in the GPC traces at the early stage, e.g., 15 min, overlapped with the MI1 peak, suggesting a complete initiation of MIs. No high-MW shoulders were observed, suggesting absence of radical coupling. The monomodal PDIs confirmed that no POEGMA homopolymers were generated in the processes.

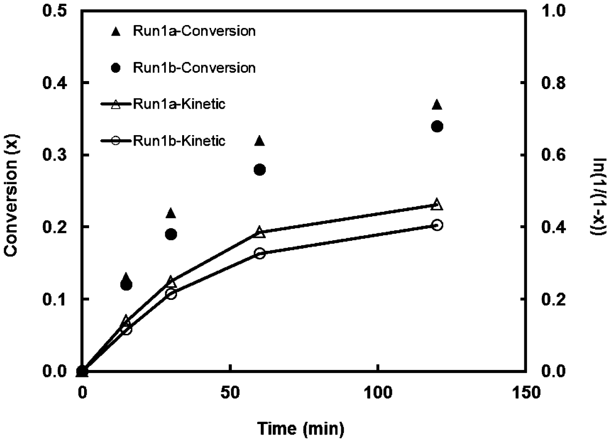

Figure 2. OEGMA conversion versus polymerization time and corresponding kinetic plots of run 1a ($[MI1]_0$ = 4.4 mM, $[MI1]_0$:$[OEGMA]_0$ = 1:200) and run 1b (2.2 mM, 1:400). Other ATRP conditions: $[MI1]_0$:$[CuBr]_0$:$[CuBr_2]_0$:$[PMDETA]_0$ = 1:12:1.2:13.2, T = 50 °C, THF: OEGMA = 3:1 vol.

There was a low-MW shoulder in the GPC curves at 60 and 120 min of run 1a, which could be attributed to dead chains resulting from deactivation. The dead chain amount, estimated from the difference between the curves and that of MI1 through de-convolution, accounted for about 30 wt% in the total polymer product of run 1a (120 min). When $[MI1]_0$ decreased to 2.2 mM, this shoulder peak disappeared, and the GPC curve overlapped with the theoretical trace at 120 min in run 1b with only 1.4% error. It suggested that the chain termination was dramatically reduced when $[MI1]_0$ was lowered from 4.4 to 2.2 mM.

Figure 4 shows the $M_{n,LS}$ and $M_{n, NMR}$ against OEGMA conversion of Runs 1a and 1b. Linear correlations were found for both runs, suggesting "livingness" of the ATRP system. $M_{n,NMR}$ appeared to be closer than $M_{n,LS}$ to the theoretical $M_{n, theory}$ (= $M_{n, MI}$ + 300 × conversion × $[OEGMA]_0/[MI]_0$). The reason might be that both $M_{n,NMR}$ and $M_{n, theory}$ were based on the chain end analysis, where the whole MI molecule was treated as a big terminal group for $M_{n,NMR}$ estimation. Because of complete initiation and no POEGMA homopolymer generated, the $M_{n,NMR}$ values must be accurate. The deviation of $M_{n,LS}$ data could be due to the fact that LS detector is more sensitive to high MW chains and thus overestimated M_n and underestimated PDI (*64*). We therefore used a universal calibration against polystyrene standards to determine the PDIs. Run 1b samples had PDI = 1.31-1.43 (MI1, PDI = 1.27), further suggesting the ATRP "livingness" at $[MI]_0$ = 2.2 mM. In comparison, run 1b produced narrower molecular weight distributions with the late two samples (60 and 120 min) of run 1a having PDI = 1.46 and 1.55, respectively.

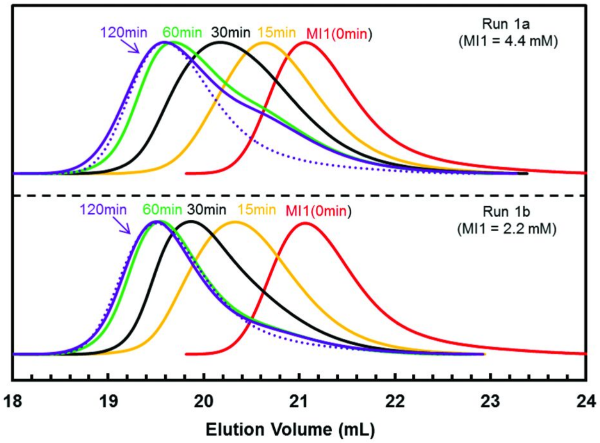

Figure 3. GPC elution traces of runs 1a ($[MI1]_0$ = 4.4 mM) and 1b (2.2 mM). The peak plotted by dotted line (with the same peak shape as MI1) is the expected trace for the block copolymers at 120min of each run.

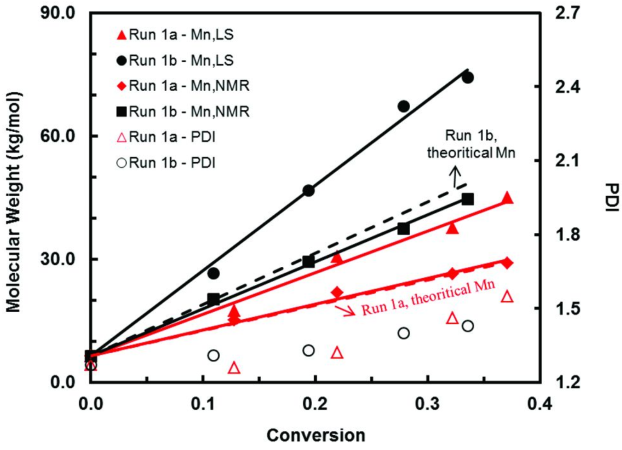

Figure 4. The number-average molecular weight measured by triple-detector GPC ($M_{n,LS}$) and NMR ($M_{n,NMR}$) versus conversion. The PDI data were obtained from a universal calibration against polystyrene standards. Runs 1a ($[MI1]_0$ = 4.4 mM) and 1b (2.2 mM).

Run 2 with hyperbranched MI2 ($M_{n,LS}$ = 14.6 kg/mol) and run 4 with linear MI4 (9.7 kg/mol) were also conducted to prepare block copolymers. Table 2 summarizes their results and Figure S3–S5 in Appendix show the respective conversion versus time, GPC curves and molecular weight development.

The ATRP results of hyperbranched MI3 (22.1 kg/mol) and linear MI5 (20.8 kg/mol) at a lower $[MI]_0$ = 1.5 mM ($[MI]_0$:$[OEGMA]_0$ = 1:600) were also summarized in Table 2 and plotted in SI.

Similar "living" nature was observed with PDIs of 1.18-1.43. The MI MW had a minor effect on the ATRP under the current experimental conditions, evident from the OEGMA conversion and molecular weight data of run 1b (MI1 as initiator, $M_{n,LS}$ = 6.4 kg/mol) and run 2 (MI2, 14.6 kg/mol) in Table 2. A slightly slower polymerization rate, i.e. 0.28 at 120 min of run 2 compared to 0.34 of run 1b, and a correspondingly lower $M_{n,NMR}$ of POEGMA block, i.e. 36.6 kg/mol versus 38.3 kg/mol were found. Slightly lower polymerization rate and $M_{n,NMR}$ of the POEGMA segment in run 5 (linear MI5, $M_{n,LS}$ = 20.8 kg/mol) than run 3R (hyperbranched MI3, 22.1 kg/mol) were also observed, suggesting a little influence of MI topology on the ATRP. The poorer solubility of MIs with a higher MW (having the same chain topology) or more linear chain topology (having similar molecular weights), the more likely for MIs to aggregate, and more difficult for OEGMA monomers to react.

Table 2. Synthesis of PE-b-POEGMA with linear/hyperbranched PE macroinitiators have different chain lengths and topologies by ATRP of OEGMA [a]

								GPC Characterization Results[g]				*Number-average block size/DP*[h]		
Run	***[MI]$_0$ (mM)***	***Time (min)***	***Conv.***[b]	***Cont.***[c]	***dn/dc***[d] ***(mL/g)***	***$M_{n,t}$***[e] ***(kDa)***	***$M_{n,NMR}$***[f] ***(kDa)***	*$M_{n,LS}$ (kDa)*	*$M_{w,LS}$ (kDa)*	*PDI_{PS}*	*$[\eta]_w$ (mL/g)*	*PE block (kDa)*	*POEGMA block (kDa)*	***Calculated $21.3[\eta]_w$***[i] ***(mL/g)***
1b	[MI1]$_0$	15	0.11	0.70	0.066	21.3	20.3	26.6	28.4	1.31	9.1	6.4/229	13.9/46	9.0
	2.2	120	0.34	0.87	0.062	48.6	44.7	74.3	93.1	1.43	13.0		38.3/128	11.7
2	[MI2]$_0$	15	0.09	0.46	0.070	25.7	25.6	31.8	32.9	1.26	13.1	13.9/496	11.7/39	13.2
	2.2	120	0.28	0.73	0.065	50.6	50.5	73.7	90.2	1.36	15.6		36.6/122	15.7
3	[MI3]$_0$	15	0.08	0.40	0.071	40.1	40.0	43.5	44.4	1.25	16.8	23.6/843	16.4/55	17.6
	1.5	60	0.20	0.62	0.067	62.5	63.6	81.1	88.0	1.30	18.6		40.0/133	18.7
3R[j]	[MI3]$_0$	20	0.09	0.43	0.070	40.4	42.3	47.1	48.6	1.28	18.3	23.6/843	18.7/62	18.1
	1.5	40	0.144	0.54	0.068	51.3	50.8	61.3	62.5	1.25	17.5		27.2/91	17.7

								GPC Characterization Results[g]				***Number-average block size/DP***[h]		
Run	***$[MI]_0$ (mM)***	***Time (min)***	***Conv.***[b]	***Cont.***[c]	***dn/dc***[d] ***(mL/g)***	***$M_{n,t}$***[e] ***(kDa)***	***$M_{n,NMR}$***[f] ***(kDa)***	*$M_{n,LS}$ (kDa)*	*$M_{w,LS}$ (kDa)*	*PDI_{PS}*	*$[\eta]_w$ (mL/g)*	*PE block (kDa)*	*POEGMA block (kDa)*	***Calculated $21.3[\eta]_w$***[i] ***(mL/g)***
4	$[MI4]_0$	15	0.12	0.57	0.068	24.5	23.2	38.3	38.8	1.18	15.6	10.4/371	12.8/43	17.0
	2.2	120	0.28	0.75	0.064	42.2	44.3	80.4	102.9	1.32	18.7		33.9/113	19.5
5	$[MI5]_0$	20	0.08	0.43	0.070	34.0	35.8	41.5	45.0	1.24	22.1	20.9/746	14.9/50	23.1
	1.5	40	0.13	0.56	0.068	46.2	46.1	54.0	62.5	1.26	22.2		25.2/84	22.8

[a] Polymerization conditions: $[MI]_0:[CuBr]_0:[CuBr_2]_0:[PMDETA]_0 = 1:12:1.2:13.2$ in all runs, run 1b, 2, 4 with a $[OEGMA]_0:[MI]_0 = 400$ and run 3, 5 = 600; THF: OEGMA = 3:1 vol.; T = 50 °C. [b] OEGMA conversion determined with ^{1}H NMR. [c] The mass content of POEGMA block in the copolymer calculated from OEGMA conversions. [d] Average refractive index increment of block copolymer estimated from Eq. 1. [e] Theoretical number-average molecular weight. [f] Number-average molecular weight calculated from ^{1}H NMR. [g] Number-average molecular weight ($M_{n,LS}$) and weight-average molecular weight ($M_{w,LS}$) from light scattering detector; weight-average intrinsic viscosity ($[\eta]_w$) from viscometer; polydispersity index (PDI_{PS}) calculated from GPC using universal calibration against PS standards. [h] The number-average molecular weight of PE and POEGMA blocks; DP is the degree of the polymerization, all based on $M_{n,NMR}$ results. [i] The calculated $[\eta]_w$ is obtained by using Ho-Duc and Prud′homme's combination rule (*65*) as shown in Eq. 2. [j] Run 3R is the repeat run of run 3.

Intrinsic Viscosity Study

The intrinsic viscosities of these polymers in THF, a good solvent for both PE and POEGMA blocks, were determined from the viscosity detector of the triple-detector GPC. Figure 5 shows their $[\eta]_w$ versus M_w data, wherein the Mark-Houwink curves of hyperbranched PE (PE1atm) prepared by Pd–diimine catalyst under 1 atm and 5 °C, linear PE (PE400psi) under 400 psi and 5 °C, POEGMA homopolymer by ATRP were also included for comparison.

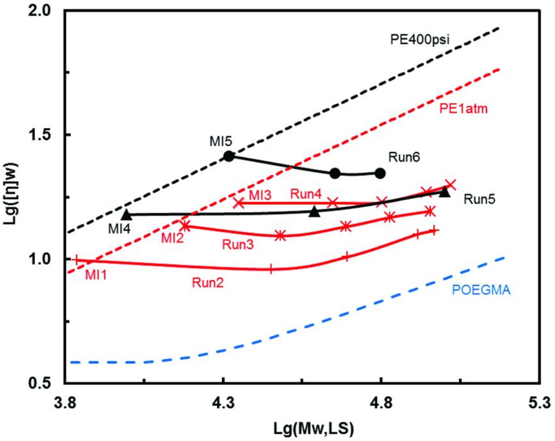

Figure 5. Mark-Houwink plots of the amphiphilic diblock copolymers synthesized in runs 1b-5 from Table 2. Three fitted intrinsic viscosity curves were also constructed for comparison, including PE400psi ($\log[\eta]_w = 0.603\log M_w - 1.19$ ($R^2 = 0.999$)) (45), PE1atm ($\log[\eta]_w = 0.600\log M_w - 1.34$ ($R^2 = 0.986$)), and POEGMA. There were two transition points in the POEGMA curve with $\log[\eta]_w = 0.586$ for $\log M_w < 4.05$ and $\log[\eta]_w = 0.459\log M_w - 1.38$ ($R^2 = 0.991$) for $\log M_w > 4.35$. The data determined from light scattering detector (LS) and viscometer.

With the same molecular weight, hyperbranched PE1atm had lower intrinsic viscosity (IV) than linear PE400psi (*34*, *35*, *37*). POEGMA had much lower IV in THF due to its bulky side chains. Similar observation was also reported for poly(styrene macromonomer) (*66*). The amphiphilic BC's $[\eta]_w$ values were all between those of the MIs' and POEGMA's. Compared to the linear increase of PE1atm and PE400psi, relatively flat curves were found from the copolymers. The samples prepared from larger- $[\eta]_w$ PE MI had higher IV values, but their difference became smaller with chain extension.

A combination rule for IV of diblock (AB) and symmetric triblock (ABA) copolymers in good or theta solvent has been developed by Ho-Duc and Prud′homme (*65*). Equation 2 was used to calculate the $[\eta]_w$ values of the amphiphilic BCs obtained in this work.

$$[\eta]^{2/3} = \omega_a[\eta]_a^{2/3} + (1-\omega_a)[\eta]_b^{2/3} \tag{2}$$

where ω_a and 1-ω_a are the weight fractions of A and B blocks determined from ^{1}H NMR; $[\eta]_a$ and $[\eta]_b$ are the respective IVs of A and B homopolymers having an equal molecular weight to amphiphilic BCs, which can be calculated from the Mark-Houwink equations as shown in Figure 5. The calculated intrinsic viscosity data listed in Table 2 were in good agreement with the measured ones, verifying this combination rule valid for the newly prepared amphiphilic BCs. Similar agreement was also reported in the IV study of "treelike" hyperbranched PE-b-linear PE block polymers (*45*). This also gave strong evidence for the presence of distinct hybrid PE-POEGMA diblock structures.

^{1}H NMR Characterization

The amphiphilic copolymer PE-b-POEGMAs were soluble in a very wide range of solvents, it was difficult to find a precipitant for separation of unreacted OEGMA from the block copolymers. Therefore, the separation and purification of the copolymer products were conducted by dialysis against deionized water to remove the unreacted monomers, THF, and copper catalysts. Figure 6 shows ^{1}H NMR spectra of the PE-b-POEGMA product of run 5 at 20 min after dialysis and freezing-drying. No signal of the vinyl bonds was found, suggesting an effective sample purification. The resonance peaks for PE and POEGMA blocks were all present in the spectra, such as the characteristic signals of the protons in –OCH_3 group at 3.38 ppm from POEGMA, the methylene peak at 1.26 ppm attributed to methylene protons from PE. This further confirmed successful chain extension in the ATRP of OEGMA.

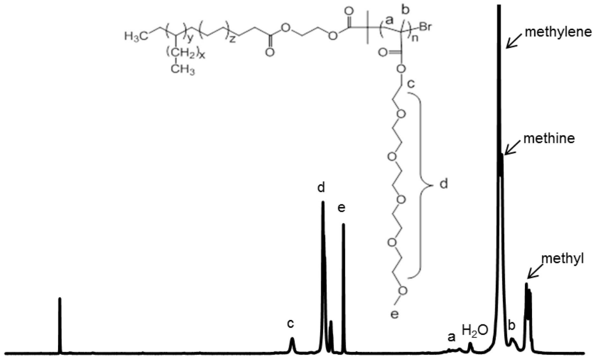

Figure 6. 6 ^{1}H NMR spectra of run 5 sample at 20 min with $CDCl_3$ as deuterated solvent.

DSC Characterization

DSC measurements were performed on run 3R sample collected at 40min (run 3R-40) and run 5 at 40min (run 5-40) to investigate thermal properties of the amphiphilic polymers. Figure 7 shows their DSC thermograms, together with those of MI3, MI5, and POEGMA for comparison.

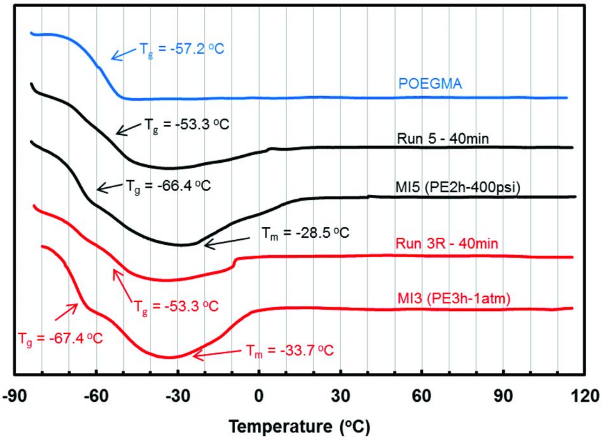

Figure 7. DSC thermograms of the polymer samples from (a) run 3R sample collected at 40min (Run 3R-40min, MI3 as initiator) and (b) run 5 at 40 min (Run 5-40min, MI5). The thermograms of corresponding MIs and POEGMA were also used for comparison.

Characteristic of Pd−diimine PEs, MI5 had a weak broad melting endotherm from −70 to 10 °C with a peak temperature (T_m) of −28.5 °C (*39*). MI3 had a T_m of −33.7 °C in the range of −70 to 0 °C (*44*, *45*), respectively. The variance on T_m could be attributed to the topology difference between hyperbranched MI3 and linear MI5 (*37*). For the two block copolymers having different PE topologies, some unique thermal properties were found in their thermograms. In particular, a weak glass transition at −70 to −50 °C and a reduced but visible broad melting endotherm from −70 to 0 °C, belonging to MI3 and MI5, still could be seen in run 3R–40 and run 5–40 samples, respectively. In addition, compared to MIs, there existed a vanished endotherm peak and an inclined glass transition change centered at −53.3 °C in both block copolymers in the range of −80 to −10 °C, resulted from POEGMA blocks with a similar length in run 3R–40 (DP = 91) and run 5–40 (DP = 84).

Micelle Behaviors in Aqueous Solution

When amphiphilic BCs are dissolved in a selective solvent thermodynamically good for one block and poor for the other, i.e., water for PE-b-POEGMA herein, the chains may form micellar aggregates (*4*). The micelle behavior of a selected PE-b-POEGMA sample (run 5, collected at 20min) in aqueous solution was studied. Figure 8 shows a monomodal distribution with its Z-average diameter of 71.4 nm and size polydispersity of 0.222 at 30 °C. These sizes (10–100 nm) are typical of the micelle formed by amphiphilic BCs (*2*).

To further study the thermo-sensitivity of these micelles with POEGMA coronas, the average micelle diameters at different temperatures were recorded. As shown in Figure 8, the hydrodynamic diameter increased drastically from 74.1 nm to 197.3 nm from 60 °C to 64 °C, suggesting formation of large particles by micellar aggregation, resulted from the sharply increased hydrophobicity of the POEGMA corona chains upon heated to its transition point (LCST). The aggregation also narrowed the size polydispersity of micelles from 0.222 to 0.029. However, this aggregation was not reversible and cooling the solution to room temperature did not lead to redispersion of the material and resumption of the micellar state.

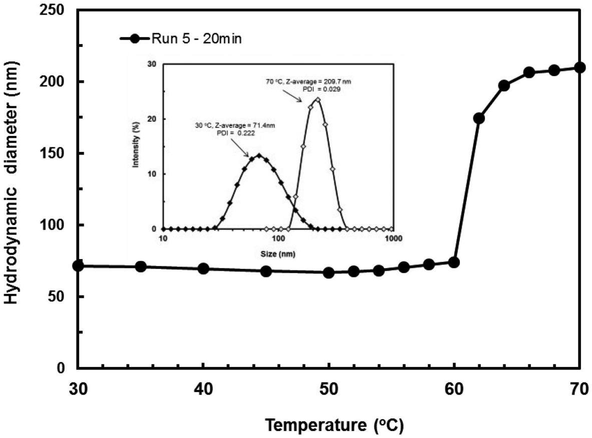

Figure 8. Micelle size distributions of run 5 PE-b-POEGMA sample collected at 20min in aqueous solution with a concentration of 1 mg/mL at 30 and 70 °C and the temperature dependency of Z-average hydrodynamic diameters.

Conclusion

We reported a facile method to synthesize well-defined amphiphilic diblock copolymers containing a linear or hyperbranched hydrophobic PE block and a hydrophilic OEGMA block. The method combined Pd–diimine catalyzed "living" polymerization of ethylene and ATRP of OEGMA. Catalyzed by the functionalized Pd–diimine catalyst **1** at 5 °C, hyperbranched PE having $M_{n,LS}$ of 6.4 to 22.1 kg/mol and PDI of 1.26-1.32, and linear PE having $M_{n,LS}$ of 9.7 to 20.9 kg/mol and PDI of 1.16-1.19 were successfully prepared by changing the ethylene pressure from 1 atm to 27.6 atm. In ATRP of OEGMA initiated by the 2-bromoisobutyryl-containing PEs, high MI concentration of 4.4 mM led to deactivation of 30% reactive chain ends with THF as solvent. Significant reduction of chain termination and "living" chain extension succeeded at lower MI concentrations of 1.5 or 2.2 mM (depending on the MI molecular weight). The MI chain topology and molecular weight slightly affected the ATRP kinetics and molecular weight development of the POEGMA block. With all the five MIs, narrow distributed PE-b-POEGMA copolymers (PDI = 1.18-1.43) having well-controlled block molecular weights were obtained. The presence of distinct block structure in the copolymers was confirmed through the study of intrinsic viscosity behaviors in THF, which was well described by the combination rule for common diblock polymers. The DLS study demonstrated that these copolymers formed micelles in water at room temperature and were thermoresponsive

Acknowledgments

This work is financially supported by National Basic Research Program of China (973 Program 2011CB606001), the National Natural Science Foundation of China (Key Grant 20936006), the Chinese State Key Laboratory of Chemical Engineering at Zhejiang University (Grant No. SKL-ChE-11D02 and SKL-ChE-08D02), and the Program for Changjiang Scholars and Innovative Research Team in University in China. P.L. thanks "Scholarship Award for Excellent Doctoral Student" granted by Ministry of Education and the financial support from "985 Project" innovative talent training program at Zhejiang University

Appendix

The GPC elution traces and plots of molecular weight versus time of the five MIs, ^{1}H NMR spectra of MI2, and conversion and kinetics, GPC elution traces, and plots of molecular weight versus time of runs 2 and 3 are included in this appendix.

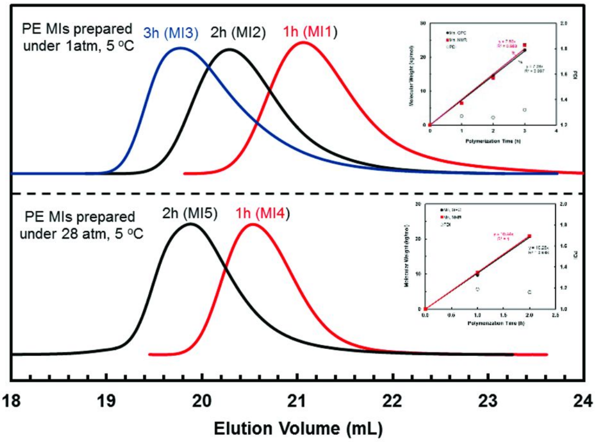

*Figure S1. GPC elution curves of five MIs (MI1–MI5 in Table 1) synthesized by ethylene polymerization with catalyst **1** at ethylene pressure of 1 atm (MI1, MI2, and MI3) or 400 psi (MI4 and MI5) and 5 °C; corresponding number-average molecular weight calculated from light scattering detector ($M_{n,LS}$) and NMR measurements ($M_{n,NMR}$), and polydispersity index (PDI) are also plotted against polymerization time.*

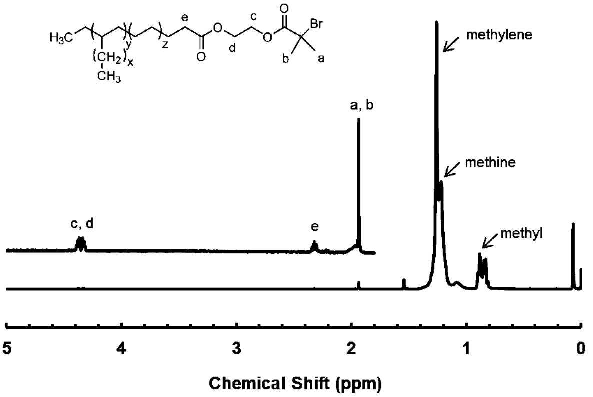

Figure S2. ^{1}H NMR spectra of MI2.

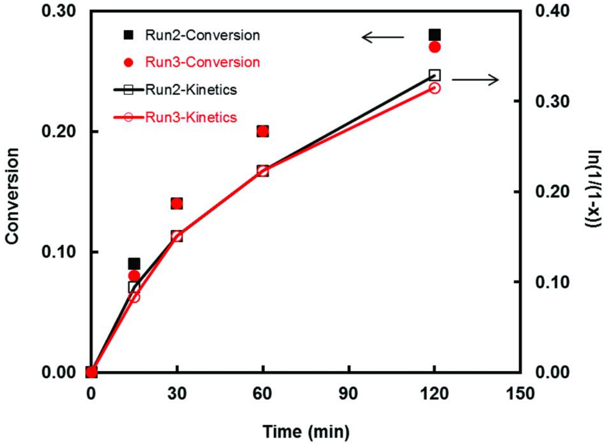

Figure S3. Kinetic plots of OEGMA conversion versus polymerization time in Run 2 ($[MI2]_0$ = 2.2 mM) and Run 3 ($[MI3]_0$ = 1.5 mM). Other conditions: $[MI2]_0$:[OEGMA]:$[CuBr]_0$:$[CuBr_2]_0$:$[PMDETA]_0$ = 1:400: 12:1.2:13.2; $[MI3]_0$:[OEGMA]:$[CuBr]_0$:$[CuBr_2]_0$:$[PMDETA]_0$ = 1:600: 12: 1.2:13.2; THF: OEGMA = 3:1 vol; T = 50 °C.

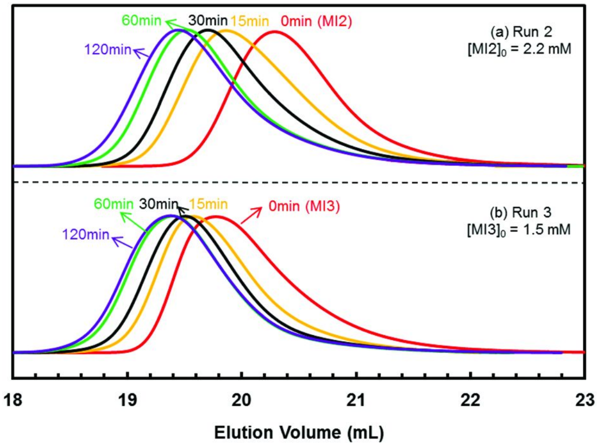

Figure S4. GPC elution traces of Run 2 ($[MI2]_0$ = 2.2 mM) and Run 3 ($[MI3]_0$ = 1.5 mM).

(a)

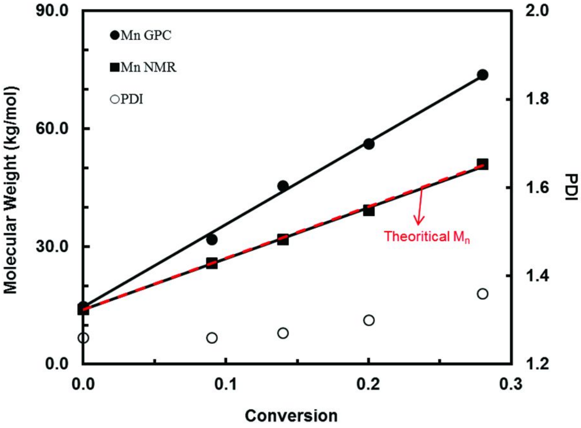

(b)

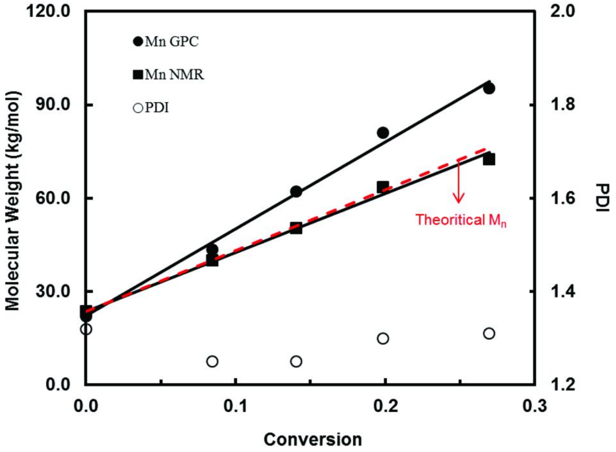

Figure S5. The dependencies of number-average molecular weight calculated from light scattering detector ($M_{n,GPC}$) and NMR measurements ($M_{n,NMR}$), and polydispersity using universal calibration against polystyrene standards (PDI_{PS}) of block copolymers versus OEGMA conversion in (a) Run 2 ($[MI2]_0$ = 2.2 mM) and (b) Run 3(($[MI3]_0$ = 1.5 mM).

References

1. Alexandridis, P.; Lindman, B. *Amphiphilic Block Copolymers: Self-Assembly and Applications*, 1st ed.; Elsevier: Amsterdam, Netherlands, 2000.
2. Letchford, K.; Burt, H. *Eur. J. Pharm. Biopharm.* **2007**, *65*, 259–269.
3. Riess, G. *Prog. Polym. Sci.* **2003**, *28*, 1107–1170.
4. Gohy, J. F. In *Block Copolymers II*; Abetz, V., Ed.; Adv. Polym. Sci.; Springer-Verlag: Berlin, Germany, 2005; Vol. 190, pp 65−136.
5. Hamley, I. W. *Block Copolymers in Solution: Fundamentals and Applications*; John Wiley & Sons, Ltd: New York, 2005.
6. Rodriguez-Hernandez, J.; Checot, F.; Gnanou, Y.; Lecommandoux, S. *Prog. Polym. Sci.* **2005**, *30*, 691–724.
7. Zana, R.; Kaler, E. W. *Giant Micelles: Properties and Applications*, 1st ed.; CRC Press: Boca Raton, FL, 2007.
8. Lodge, T. P.; Bang, J. A.; Li, Z. B.; Hillmyer, M. A.; Talmon, Y. *Faraday Discuss.* **2005**, *128*, 1–12.
9. Adams, M. L.; Lavasanifar, A.; Kwon, G. S. *J. Pharm. Sci.* **2003**, *92*, 1343–1355.
10. Kwon, G. S.; Forrest, M. L. *Drug Dev. Res.* **2006**, *67*, 15–22.
11. Blanazs, A.; Armes, S. P.; Ryan, A. J. *Macromol. Rapid Commun.* **2009**, *30*, 267–277.
12. Holder, S. J.; Sommerdijk, N. *Polym. Chem.* **2011**, *2*, 1018–1028.
13. Aseyev, V.; Tenhu, H.; Winnik, F. In *Self Organized Nanostructures of Amphiphilic Block Copolymers II*; Müller, A. H. E., Borisov, O., Eds.; Adv. Polym. Sci.; Springer-Verlag: Berlin, Heidelberg, Germany, 2011; Vol. 242, pp 29−89.
14. Chung, T. C. *Prog. Polym. Sci.* **2002**, *27*, 39–85.
15. Zhao, Y. L.; Wang, L.; Xiao, A. G.; Yu, H. J. *Prog. Polym. Sci.* **2010**, *35*, 1195–1216.
16. Lopez, R. G.; D'Agosto, F.; Boisson, C. *Prog. Polym. Sci.* **2007**, *32*, 419–454.
17. Yin, L. G.; Hillmyer, M. A. *Macromolecules* **2011**, *44*, 3021–3028.
18. Hillmyer, M. A.; Bates, F. S. *Macromolecules* **1996**, *29*, 6994–7002.
19. Allgaier, J.; Poppe, A.; Willner, L.; Richter, D. *Macromolecules* **1997**, *30*, 1582–1586.
20. Zhang, P.; Moore, J. S. *J. Polym. Sci., Part A: Polym. Chem.* **2000**, *38*, 207–219.
21. Jankova, K.; Kops, J.; Chen, X.; Batsberg, W. *Macromol. Rapid Commun.* **1999**, *20*, 219–223.
22. Haddleton, D. M.; Jarvis, A. P.; Waterson, C.; Bon, S. A. F.; Heming, A. M. Copper-Mediated Living Radical Polymerization Utilizing Biological and End Group Modified Poly(ethylene-co-butylene) Macroinitiators; Matyjaszewski, K., Ed.; *Controlled/Living Radical Polymerization*; American Chemical Society: Washington, DC, 2000; Vol. 768, pp 182−196.
23. Even, M.; Haddleton, D. M.; Kukulj, D. *Eur. Polym. J.* **2003**, *39*, 633–639.

24. Zhou, C.; Hillmyer, M. A.; Lodge, T. P. *Macromolecules* **2011**, *44*, 1635–1641.
25. Lenoir, S.; Pagnoulle, C.; Detrembleur, C.; Galleni, M.; Jerome, R. *J. Polym. Sci., Part A: Polym. Chem.* **2006**, *44*, 1214–1224.
26. Fang, Z.; Kennedy, J. P. *J. Polym. Sci., Part A: Polym. Chem.* **2002**, *40*, 3679–3691.
27. Lu, Y.; Hu, Y.; Wang, Z. M.; Manias, E.; Chung, T. C. *J. Polym. Sci., Part A: Polym. Chem.* **2002**, *40*, 3416–3425.
28. Matoishi, K.; Nakatsuka, S.; Nakai, K.; Isokawa, M.; Nagai, N.; Fujita, T. *Chem. Lett.* **2010**, *39*, 1028–1029.
29. Li, T.; Wang, W. J.; Liu, R.; Liang, W. H.; Zhao, G. F.; Li, Z. Y.; Wu, Q.; Zhu, F. M. *Macromolecules* **2009**, *42* (11), 3804–3810.
30. Wang, W. J.; Liu, R.; Li, Z. Y.; Meng, C. F.; Wu, Q.; Zhu, F. M. *Macromol. Chem. Phys.* **2010**, *211*, 1452–1459.
31. Gitsov, I. *J. Polym. Sci., Part A: Polym. Chem.* **2008**, *46*, 5295–5314.
32. Wurm, F.; Frey, H. *Prog. Polym. Sci.* **2011**, *36*, 1–52.
33. Matyjaszewski, K. *Science* **2011**, *333*, 1104–1105.
34. Guan, Z. B.; Cotts, P. M.; McCord, E. F.; McLain, S. J. *Science* **1999**, *283*, 2059–2062.
35. Cotts, P. M.; Guan, Z. B.; McCord, E.; McLain, S. *Macromolecules* **2000**, *33*, 6945–6952.
36. Gottfried, A. C.; Brookhart, M. *Macromolecules* **2003**, *36*, 3085–3100.
37. Ye, Z.; Zhu, S. *Macromolecules* **2003**, *36*, 2194–2197.
38. Wang, W.-J.; Liu, P.; Li, B.-G.; Zhu, S. *J. Polym. Sci., Part A: Polym. Chem.* **2010**, *48*, 3024–3032.
39. Zhang, K.; Ye, Z.; Subramanian, R. *Macromolecules* **2008**, *41*, 640–649.
40. Liu, P.; Landry, E.; Ye, Z.; Joly, H.; Wang, W.-J.; Li, B.-G. *Macromolecules* **2011**, *44*, 4125–4139.
41. Johnson, L. K.; Killian, C. M.; Brookhart, M. *J. Am. Chem. Soc.* **1995**, *117*, 6414–6415.
42. Ittel, S. D.; Johnson, L. K.; Brookhart, M. *Chem. Rev.* **2000**, *100*, 1169–1203.
43. Guan, Z. B. *Chem.-Asian J.* **2010**, *5*, 1058–1070.
44. Ye, Z. B.; Li, S. Y. *Macromol. React. Eng.* **2010**, *4*, 319–332.
45. Xu, Y. Q.; Xiang, P.; Ye, Z. B.; Wang, W. J. *Macromolecules* **2010**, *43*, 8026–8038.
46. Tempel, D. J.; Johnson, L. K.; Huff, R. L.; White, P. S.; Brookhart, M. *J. Am. Chem. Soc.* **2000**, *122*, 6686–6700.
47. Shultz, L. H.; Tempel, D. J.; Brookhart, M. *J. Am. Chem. Soc.* **2001**, *123*, 11539–11555.
48. Johnson, L. K.; Mecking, S.; Brookhart, M. *J. Am. Chem. Soc.* **1996**, *118*, 267–268.
49. Lutz, J.-F. *Adv. Mater.* **2011**, *23*, 2237–2243.
50. Lutz, J.-F. *J. Polym. Sci., Part A: Polym. Chem.* **2008**, *46*, 3459–3470.
51. Matyjaszewski, K.; Xia, J. H. *Chem. Rev.* **2001**, *101*, 2921–2990.
52. Moad, G.; Rizzardo, E.; Thang, S. H. *Polymer* **2008**, *49*, 1079–1131.
53. Hu, Z.; Cai, T.; Chi, C. *Soft Matter* **2010**, *6*, 2115–2123.
54. Han, S.; Hagiwara, M.; Ishizone, T. *Macromolecules* **2003**, *36*, 8312–8319.

55. Ishizone, T.; Seki, A.; Hagiwara, M.; Han, S.; Yokoyama, H.; Oyane, A.; Deffieux, A.; Carlotti, S. *Macromolecules* **2008**, *41*, 2963–2967.
56. Chen, G. H.; Huynh, D.; Felgner, P. L.; Guan, Z. B. *J. Am. Chem. Soc.* **2006**, *128*, 4298–4302.
57. Sun, G. B.; Guan, Z. B. *Macromolecules* **2010**, *43*, 9668–9673.
58. Zhang, L.; Su, J.; Zhang, W. Z.; Ding, M.; Chen, X. D.; Wu, Q. *Langmuir* **2010**, *26*, 5801–5807.
59. Huang, J.; Jia, S.; Siegwart, D. J.; Kowalewski, T.; Matyjaszewski, K. *Macromol. Chem. Phys.* **2006**, *207*, 801–811.
60. Barton, A. F. M. *CRC Handbook of Solubility Parameters and Other Cohesion Parameters*, 2nd ed.; CRC Press: Boca Raton, FL, 1991.
61. Yamamoto, S.; Pietrasik, J.; Matyjaszewski, K. *Macromolecules* **2007**, *40*, 9348–9353.
62. Yamamoto, S.-I.; Pietrasik, J.; Matyjaszewski, K. *J. Polym. Sci., Part A: Polym. Chem.* **2008**, *46*, 194–202.
63. Neugebauer, D.; Zhang, Y.; Pakula, T.; Sheiko, S. S.; Matyjaszewski, K. *Macromolecules* **2003**, *36*, 6746–6755.
64. Netopilík, M.; Podzimek, Š.; Kratochvíl, P. *J. Chromatogr., A* **2001**, *922*, 25–36.
65. Ho-Duc, N.; Prud′homme, J. *Macromolecules* **1973**, *6*, 472–474.
66. Terao, K.; Hokajo, T.; Nakamura, Y.; Norisuye, T. *Macromolecules* **1999**, *32*, 3690–3694.

Chapter 5

Microgel-Core Star Polymers as Functional Compartments for Catalysis and Molecular Recognition

Takaya Terashima* and Mitsuo Sawamoto*

Polymer Chemistry, Graduate School of Engineering, Kyoto University,
Kyotodaigaku-katsura, Nishikyo-ku, Kyoto 615-8510, Japan
***E-mails: terashima@living.polym.kyoto-u.ac.jp (T.T.);**
sawamoto@star.polym.kyoto-u.ac.jp (M.S.).

Core-functionalized star polymers were designed as functional compartments for molecular recognition and catalysis, focused on the unique environments of the microgel-cores that were spatially separated from outer environments by the surrounding linear arms. Due to the high tolerance to functional groups and the high controllability, ruthenium-catalyzed living radical polymerization afforded the one-pot synthesis and functionalization of microgel-core star polymers via the arm-linking reaction with functional monomers and/or linking agents. Typically, metal-bearing star polymers efficiently catalyzed various reactions including oxidation of alcohols, transfer hydrogenation of ketones, and living radical polymerization. Fluorine-condensed star polymers, in turn, worked as fluorous compartments to selectively recognize, and thus enclose perfluorinated compounds in the core and stimuli-responsively release the guests from the core.

Introduction

Design of a confined nano-space in globular macromolecules plays a critical role to reach unique properties in catalysis and molecular recognition (*1*–*3*). Microgel-core star polymers (*4*–*20*) are one of the most attractive polymeric materials to embed and condense functional groups, since they carry the nano-scale core in the center of the polymers that is compartmentalized from outer environments by linear polymeric arms. Due to the high tolerance to functional groups and high versatility, metal-catalyzed living radical polymerization (*21–33*) now affords the tailor-made design of functional polymers with precision primary structures on demand. Microgel-core star polymers can be also facilely prepared and functionalized, in one-pot, by ruthenium-catalyzed polymerization (*21–30*) via the linking reaction of linear arms in conjunction with functional linking agents and/or monomers. Focusing on these features, we have developed core-functionalized star polymers (*7–18*) as functional compartments for catalysis such as oxidation (*9*, *14*), hydrogenation (*15*, *16*), and living radical polymerization (*13*), and for molecular recognition of protic compounds (*6*, *8*), ionic dyes (*8*, *18*, *25*), and perfluorinated compounds (*17*). These star polymers performed intriguing functions originating from the unique environment of the microgel core.

In this paper, we thus report a brief overview on recent advances of core-functionalized star polymers applicable to catalysis and fluorous molecular recognition (Scheme 1).

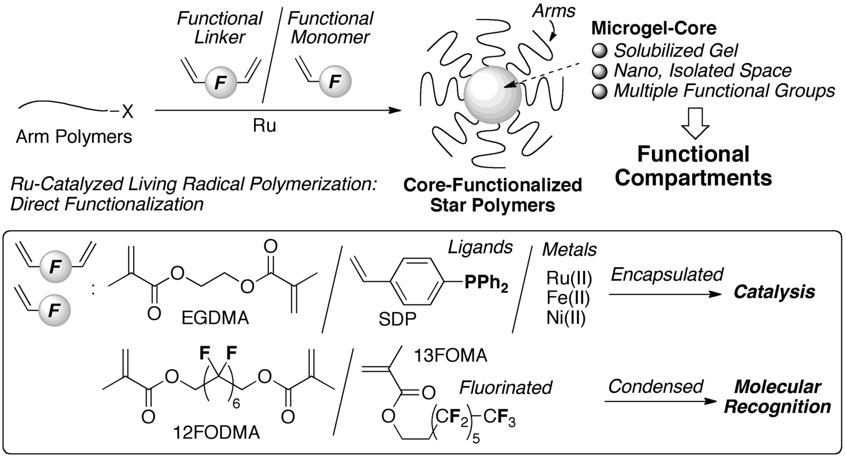

Functional Linker
Functional Monomer
F
Arm Polymers
X
Ru
Arms
Microgel-Core
Solubilized Gel
Nano, Isolated Space
Multiple Functional Groups
Functional Compartments
Ru-Catalyzed Living Radical Polymerization: Direct Functionalization
Core-Functionalized Star Polymers
EGDMA
Ligands
Metals
PPh2
SDP
Ru(II)
Fe(II)
Ni(II)
Encapsulated
Catalysis
12FODMA
13FOMA
Fluorinated
CF2
CF3
Condensed
Molecular Recognition

Scheme 1. Core-functionalized star polymers via Ru-catalyzed living radical polymerization for functional compartments.

Results and Discussion

Ru-Bearing Microgel-Core Star Polymers: Direct Ru-Encapsulation

In general, metal complexes-bearing polymer catalysts are prepared by the following two methods: 1) post introduction of metal species into ligand-bearing polymers; 2) polymerization of metal-bearing monomers (*34*, *35*). The former often suffers from the low efficiency of metal incorporation due to the steric hindrance around ligands by polymeric backbones and multiple side chains. The latter, in turn, requires not only the adaptability of monomer-bound metals on polymerization system but also the multistep synthesis of the monomers. Thus, such difficulties were normally inevitable to produce metal-bearing polymer catalysts.

To overcome these problems, we have developed novel one-pot strategy to create metal-bearing star polymer catalysts by ruthenium-catalyzed living radical polymerization with diphenylphosphinostyrene (SDP) (Scheme 2) (*9–11*, *13*). This method realizes the direct transformation of metal catalysts into the star polymer catalysts, in which SDP dynamically coordinates onto ruthenium catalysts during the polymerization to capture the ruthenium onto the resulting polymers. Typically, methyl methacrylate (MMA) was first polymerized with $RuCl_2(PPh_3)_3$ (catalyst) (*23*) and a chloride initiator [RCl: $(MMA)_2Cl$ or ethyl α-chlorophenylacetate (ECPA)] in toluene at 80 °C (Targeted $DP = [MMA]_0/[RCl]_0 = 100$) to give well-controlled PMMA with narrow molecular weight distribution ($M_n = 11300$, $M_w/M_n = 1.16$, Figure 1A). The arm polymers were then directly linked with ethylene glycol dimethacrylate (EGDMA) in the presence of SDP ($[RCl]_0/[EGDMA]_0/[SDP]_0/[RuCl_2(PPh_3)_3]_0 = 1/10/5/1$) to efficiently lead to star polymers (Ru-Star: **S1**) in high yield [star yield: ~90% by size-exclusion chromatography (SEC)] (*9*, *10*, *13*).

The star polymers had $M_w = 651{,}000$, arm numbers = 35, R_g (radius of gyration) = 9.8 nm, analyzed by multi-angle laser light scattering coupled with SEC (SEC-MALLS). A single star polymer cast on glass plate was observed as a round-shaped image by atomic force microscopy (Figure 1C) (*9*, *10*). The height (~6 nm) was close to the diameter of the core of similar PMMA-based star polymers in solution (*12*).

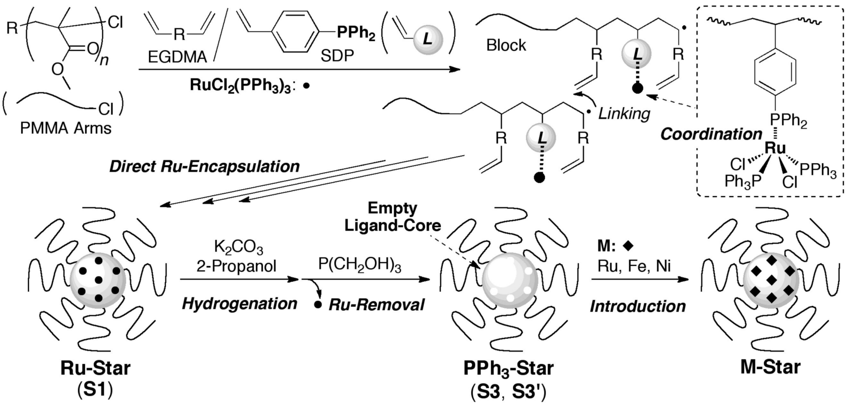
R
Cl
O
n
O
Cl
PMMA Arms
R
EGDMA
PPh₂
SDP
L
RuCl₂(PPh₃)₃: •
Block
R
L
R
Linking
R
L
R
Coordination
PPh₂
Ru
Cl
PPh₃
Ph₃P
Cl
Direct Ru-Encapsulation
Empty Ligand-Core
K₂CO₃
2-Propanol
Hydrogenation
P(CH₂OH)₃
Ru-Removal
M: ◆
Ru, Fe, Ni
Introduction
Ru-Star
(S1)
PPh₃-Star
(S3, S3')
M-Star

Scheme 2. Direct Ru-encapsulation into microgel-core star polymers via Ru-catalyzed living radical polymerization and interchange of core-bound metals.

The product (**S1**) exhibited red-brown color and UV-vis absorption originating from $RuCl_2(PPh_3)_3$ (Figure 1B), meaning that the core successfully supported the ruthenium during polymerization in one-pot. The amounts of the core-Ru was estimated as 75 μmol/g-polymer by inductively coupled plasma atomic emission spectroscopy (ICP-AES), meaning that the star polymers carried ~50 Ru per a single core. The contents of core-bound ruthenium can be controlled by the feed ratio of SDP in the arm-linking reaction (r_{SDP} = $[RCl]_0/[SDP]_0$ = 1.25-5.0), where the ruthenium contents increased with increasing the SDP feed ratio. Thanks to the high contrast, core-bound ruthenium was directly observed as black dots with 2-3 nm diameters without any staining by transmission electron micrograph (TEM) (Figure 1D) (*9*, *10*). A series of ruthenium-bearing star polymers were directly applied to various organic reactions shown later.

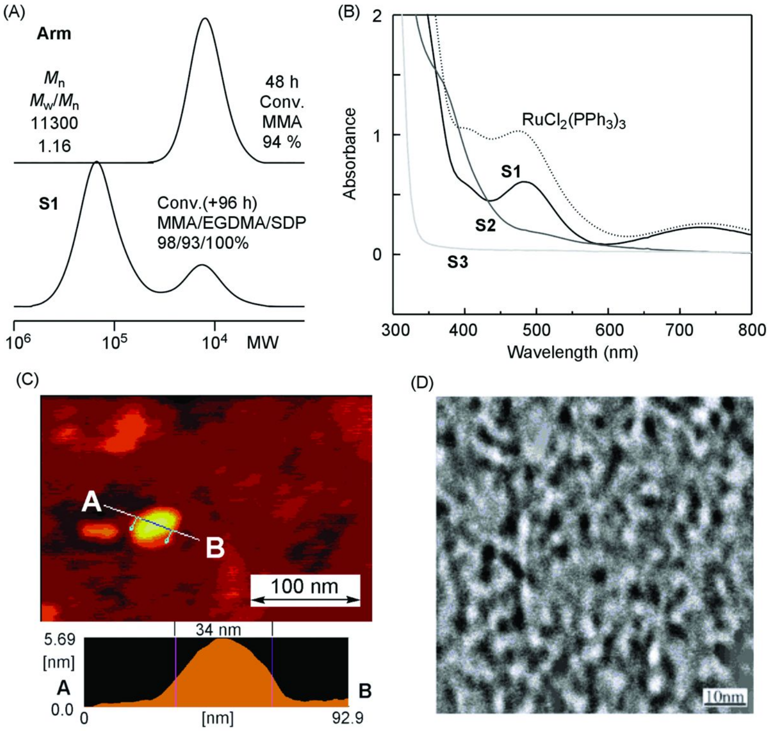

*Figure 1. (A) SEC curves of PMMA arms and Ru-star polymers (**S1**). (B) UV-vis spectra of star polymers (**S1**, **S2**: hydrogenated Star, **S3**: PPh_3-Star) and $RuCl_2(PPh_3)_3$: [Star] = 12.5 mg/mL; [Ru] = 0.98 mM in CH_2ClCH_2Cl at 25 °C. (C) AFM and (D) TEM images of **S1** cast on glass plate.*

Tandem Catalyst Interchange for Versatile Core-Reaction Vessel

Ruthenium catalysts in star polymers were immobilized by the coordination of the core-phosphine ligands onto the metal center. Thus, novel metal-bearing star polymer catalysts can be efficiently obtained from the interchange of core-bound metals via ruthenium removal and metal re-introduction. However, the core still contains chlorine terminals, derived from the living arms, and remaining pendant olefins, both of which are typically active for radical reaction. Ruthenium complexes are well-known to perform versatile catalysis not only living radical polymerization but also organic reaction such as hydrogenation, oxidation and so on (*36*). Focusing on the high versatility of ruthenium catalysts, we have recently developed in-situ hydrogenation of the terminal chlorine in PMMA-Cl to PMMA-H via ruthenium-catalyzed living radical polymerization (*37*). Importantly, the polymerization catalysts were sequentially transformed into hydrogenation catalysts in one-pot without any isolation.

Based on the in-situ hydrogenation technique, we successfully synthesized PPh_3-Star (**S3**) with an empty core from $RuCl_2$-Star (**S1**) via the following tandem catalyst interchange (*13*): 1) the in-situ hydrogenation of a $RuCl_2$-Star (**S1**) core with the core-bound Ru into a hydrogenated star (**S2**) via the direct addition of K_2CO_3 and 2-propanol into **S1**; 2) the removal of **S2**-bound Ru via ligand exchange reaction with a basic and hydrophilic phosphine compound [$P(CH_2OH)_3$] (Scheme 2). Efficient removal of core-Ru was confirmed by UV-vis (Figure 1B), ICP-AES (<6 μmol/g-polymer, > 90% Ru removal), and ^1H and ^{31}P nuclear magnetic resonance (NMR) spectroscopy. The empty star polymer (**S3**) still maintain the shape and size identical to those of **S1**, confirmed by SEC and MALLS. Similarly, non-hydrogenated PPh_3-Star (**S3′**) was also obtained.

Metal Encapsulation

We first investigated the encapsulation of an iron salt ($FeCl_2$) into the empty cores of PPh_3-Star (**S3′**) (Figure 2) (*13*). **S3′** efficiently solubilized and captured $FeCl_2$ into the core in toluene, though $FeCl_2$ was originally insoluble in toluene. The core-bound iron complexes showed UV-vis absorption similar to $FeCl_2(PPh_3)_2$ (Figure 2B). The empty core of **S3′** further worked as versatile polymeric ligands for various metal complexes [$FeX_2(PPh_3)_2$, $NiX_2(PPh_3)_2$, $NiBr_2(P\textit{n}\text{-}Bu_3)_2$] and salts ($FeX_2$, NiX_2) (X = Cl, Br, Figure 2C). As well as **S3′**, **S3** also efficiently enclosed pentamethylcyclopentadienyl ruthenium chloride (RuCp*Cl) into the core (core-Ru: ~100/star), where the ligation involved two phosphines in the core, confirmed by UV-vis and ^1H and ^{31}P NMR spectroscopy.

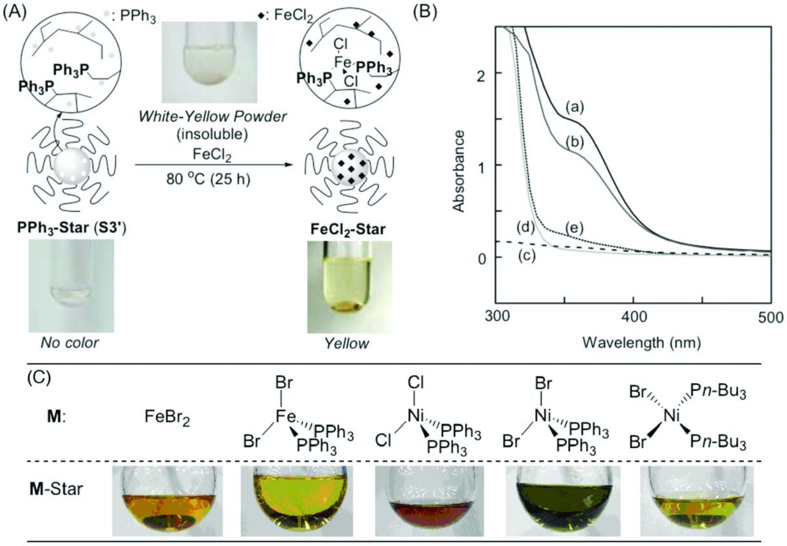

*Figure 2. (A) Introduction of FeCl$_2$ into PPh$_3$-Star (**S3'**). (B) UV-vis spectra of FeCl$_2$-Star obtained with (a) FeCl$_2$ or (b) FeCl$_2$(PPh$_3$)$_2$, (c) PMMA-Star treated with FeCl$_2$, (d) **S3'**, and (e) FeCl$_2$(PPh$_3$)$_2$ in toluene at 25 °C: [Star] = 12.5 mg/mL. (C) Photographs of various metal-star polymers.*

Microgel-Core Catalysis

Star polymer catalysts carried multiple metal complexes in the core that are spatially isolated from outer environments (Figure 3). The metal complexes were enclosed in the tightly cross-linked space but were solubilized by lots of arms in solution. As a result, the core uniquely behaves as a totally homogeneous system, but with locally isolated compartments. Thus, the star polymer catalysts could not only be compatible with activity (high yield, fast reaction) and stability (catalyst recycle) but also provide unique functions different from conventional polymer-bound catalysts. Motivated by these aspects, we applied star polymer catalysts to the following reactions: 1) oxidation of sec-alcohols (*9*, *14*); 2) hydrogenation of ketones in organic (*15*) or aqueous media (*16*); 3) living radical polymerization (*13*) (Figure 3). The organic reactions 1), 2) were investigated with ruthenium-bearing star polymer catalysts that were directly obtained from ruthenium-catalyzed living radical polymerization, whereas the polymerization 3) was, in turn, done with metal-bearing star polymer catalysts obtained through tandem catalyst interchange and metal-encapsulation.

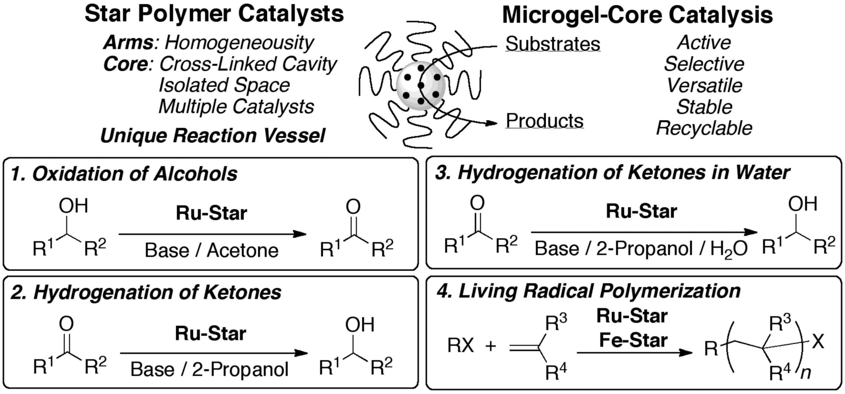
Star Polymer Catalysts
Arms: Homogeneousity
Core: Cross-Linked Cavity
Isolated Space
Multiple Catalysts
Unique Reaction Vessel
Microgel-Core Catalysis
Substrates
Products
Active
Selective
Versatile
Stable
Recyclable
1. Oxidation of Alcohols
Ru-Star
Base / Acetone
2. Hydrogenation of Ketones
Ru-Star
Base / 2-Propanol
3. Hydrogenation of Ketones in Water
Ru-Star
Base / 2-Propanol / H2O
4. Living Radical Polymerization
RX +
Ru-Star
Fe-Star
OH
O
R1
R2
R3
R4
X
n

Figure 3. Microgel-core catalysis with metal-bearing star polymers.

Oxidation of sec-Alcohols

A ruthenium-bearing star polymer with PMMA arms [Ru-Star: M_w = 390,000; 24 arms (M_n = 10000); Ru = 24 μmol/g-polymer, 15Ru/star] efficiently catalyzed the oxidation of sec-alcohols (**A1-A7**) in acetone at 65 °C even in the small feed ratio of Ru to substrates ([substrates]/[Ru] = 1000/1, Figure 4A) (*14*). Typically, the oxidation of 1-phenylethanol (**A1**) reached over 90% conversion. The high activity is probably due to the homogeneity of the polymer catalyst. More importantly, the star polymer can be reused three times without any loss of catalytic activity even via the catalyst recovery under air (Figure 4B). The high stability, in turn, most likely arises from the tight ligation of metal catalysts with cross-linked phosphines. Confirmed by SEC and ^{1}H NMR, the star polymer was tough enough to maintain the original structure after the catalysis. Thus, the polymer catalyst was active, versatile, stable, and recyclable in the oxidation of sec-alcohols.

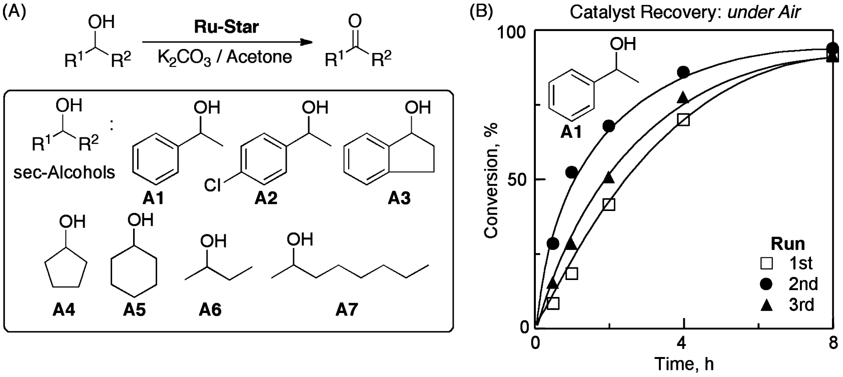

*Figure 4. (A) Oxidation of sec-alcohols catalyzed by ruthenium-bearing star polymers. (B) Recycle of a star polymer catalyst in oxidation of **A1**: **A1**/Ru_{star}/K_2CO_3 = 12/0.012/1.2 mmol in acetone (12 mL) at 65 °C.*

Transfer Hydrogenation of Ketones

Design of the reaction space surrounding a catalytic center would be quite innovative compared to conventional catalysis in terms of activity combined with selectivity approaching that of enzymes (*38*). Spatial control is a unique advantage to use microgel-core star polymers as catalyst-immobilizing agents, in addition to practical considerations including catalyst recycling and product recovery.

To design a reaction space suitable for transfer hydrogenation of ketones, we produced ruthenium-bearing star polymers with poly(ethylene glycol) (PEG)-carrying arms (Ru-PEG Star, Figure 5) via ruthenium-catalyzed living radical polymerization (*11*, *15*). The key is to create a ruthenium-bearing hydrophobic core covered by amphiphilic PEG arms. In addition to Ru-Star (**S1**) with PMMA arms, Ru-PEG Star was successfully obtained from $RuCl_2(PPh_3)_3$-catalyzed block copolymerization of poly(ethylene glycol) methyl ether methacrylate (PEGMA) and MMA (Targeted DP = $[PEGMA]_0/[RCl]_0$ = 50, $[MMA]_0/[RCl]_0$ = 10) and the subsequent linking reaction of the block arms with EGDMA and SDP ($[EGDMA]_0/[SDP]_0/[RCl]_0$ = 15/1.25/1) (Yield = 76%, M_w = 772,000, R_g = 15 nm, 16 arms, Ru = 24 µmol/g-polymer, 19Ru/star) (*11*). Here, ruthenium catalysts were directly embedded in the core even in the presence of the polar arms. This approach is namely the direct transformation of hydrophobic polymerization catalysts into amphiphilic and thermosensitive star polymer catalysts. The resulting polymer was well soluble in polar solvents such as alcohols and water, and showed upper critical temperature (UCST: ~31 °C) in 2-propanol.

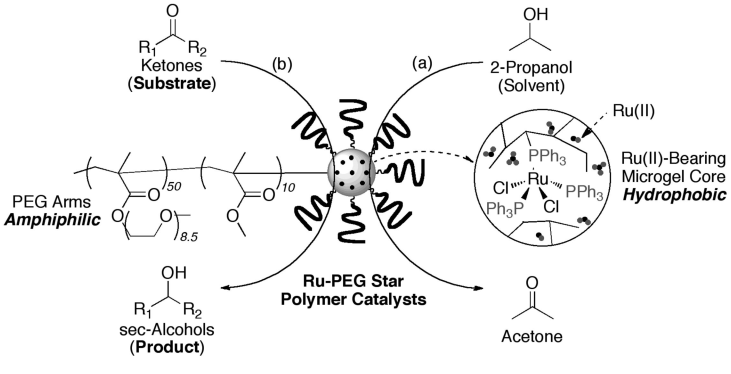

Figure 5. Ru-PEG Star-catalyzed transfer hydrogenation of ketones.

Ru-PEG Star efficiently and homogeneously catalyzed the transfer hydrogenation of wide variety of ketones (**K1**-**K12**) in 2-propanol at 100 °C ([ketones]/[Ru] = 1000/1, Figure 5 and 6) (*15*). Typically, acetophenone (**K1**) was reduced into 1-phenylethanol in high yield (~90%) and the turn over frequency (TOF) reached over 200 (h^{-1}) (Figure 6). Intriguingly, Ru-PEG Star induced the reaction faster than an original ruthenium catalyst [$RuCl_2(PPh_3)_3$] and the other polymer-bound catalysts [Ru-MMA Star: PMMA arm version of Ru-PEG Star; Ru-Gel: Cross-linked PSt-bound Ru (insoluble); Ru-Random: Ru-bearing

MMA/SDP random copolymer]. The high activity may be explained by the following possibility. Because 2-propanol works as a hydrogen donor in this reaction, the efficient catalytic cycle requires a sufficient supply of solvent at the ruthenium center. In this case, the hydrogen source is effectively donated to the core-bound ruthenium owing to the homogeneous solubility of the star catalyst originating from the affinity between the amphiphilic PEG-based arms and 2-propanol (Figure 5a). Additionally, the hydrophobic acetophenone (**K1**) can easily enter the reaction space, comprising a hydrophobic Ru(II)-bearing microgel core, while 1-phenylethanol, the product from **K1**, can efficiently escape because the alcohol product favors the polar PEG-based arm area over the hydrophobic microgel core (Figure 5b). Such a polarity difference between the core and arms of the star catalysts might effectively diffuse the substrate and the product around the microgel-core reaction space, contributing to higher catalytic activity. The high activity of Ru-PEG Star was remarkable for **K2** and **K8**, where the TOF in their hydrogenation reached about 1000 (h^{-1}). Ru-PEG Star was further recyclable three times for **K1** or **K10**.

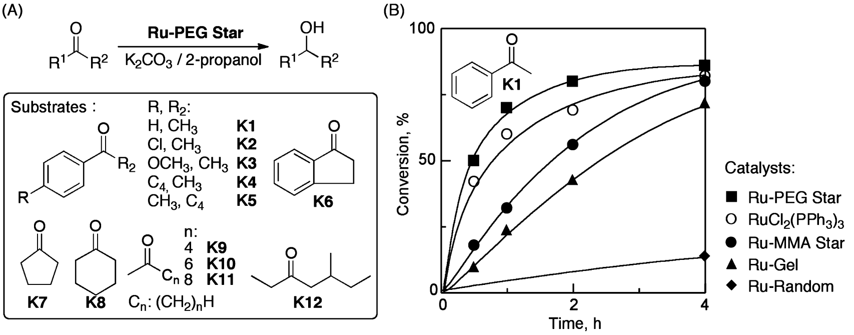

*Figure 6. (A) Transfer hydrogenation of various ketones catalyzed by Ru-PEG Star. (B) Effects of catalyst structures on transfer hydrogenation of **K1**: **K1**/Ru/K_2CO_3 = 10/0.01/1.0 mmol in 2-propanol (10 mL) at 100 °C.*

Thermoregulated Phase-Transfer Catalysis in Water

Due to the thermosensitive solubility, Ru-PEG Star realized unique thermoregulated phase-transfer catalysis for the transfer hydrogenation of 2-octanone in aqueous media (Figure 7) (*16*). The star was homogeneously soluble in 2-propoanol (hydrogen source)/H_2O (1/1, v/v) at room temperature. To this solution was added 2-octanone (substrate; a hydrophobic long-alkyl ketone), to induce a biphasic separation into an organic layer (upper) and aqueous counterpart (lower) (Figure 7A). In this stage, the lower layer was red-brown, while the upper layer was transparent and colorless, indicating that the star catalyst completely stayed in the aqueous phase. Upon heating the solution to reflux at 100 °C (resulting in a dispersion), the polymer was quickly transferred to the organic phase, as judged from the color change (Figure 7B). During the phase transfer, the star thereby efficiently catalyzed the reduction of 2-octanone to the corresponding sec-alcohol (73% yield in 24 h), despite the low catalyst/substrate mole ratio [2-octanone/Ru = 1000/1]. Upon cooling the solution to room temperature, the star polymer moved down to the aqueous layer again. Catalyst recycle was successful via the thermoregulated phase-transfer by the removal of the upper organic layer (product and 2-propanol, Figure 7C) and the additional feed of a substrate and 2-propanol for second cycle (Figure 7D).

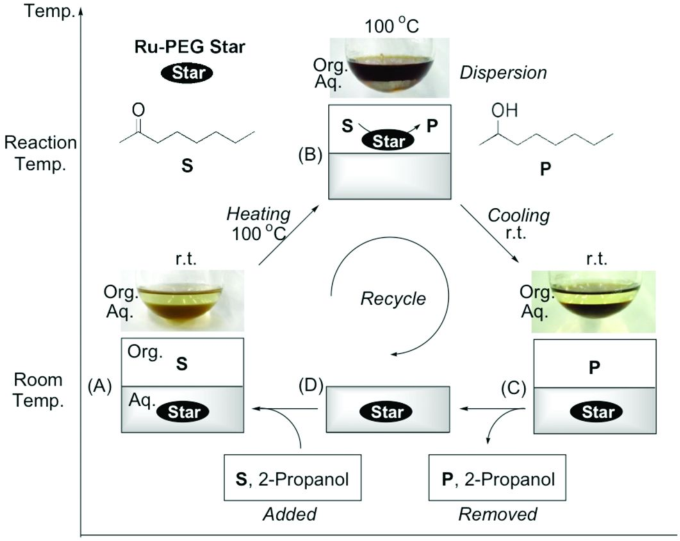
Temp.
Ru-PEG Star
Star
100 °C
Org.
Aq.
Dispersion
O
OH
Reaction Temp.
S
(B)
S
Star
P
P
Heating 100 °C
Cooling r.t.
r.t.
r.t.
Org.
Aq.
Recycle
Org.
Aq.
Org.
S
Room Temp.
(A)
Aq.
Star
(D)
Star
(C)
P
Star
S, 2-Propanol
Added
P, 2-Propanol
Removed

*Figure 7. Thermoregulated phase-transfer catalysis on transfer hydrogenation of 2-octanone (**K10**) with Ru-PEG Star in water: **K10**/Ru/K_2CO_3 = 10/0.01/1.0 mmol in 2-propanol/H_2O (5/5 mL) at 100 °C.*

Living Radical Polymerization

Star polymer catalysts were also applicable to living radical polymerization (Figure 8, Table 1) (*13*). To eliminate unfavorable side reactions such as star-star coupling and macroscopic gelation, we utilized hydrogenated PPh_3-Star ligands (**S3**). Pentamethylcyclopentadienyl ruthenium chloride (RuCp*Cl) was embedded into **S3** in toluene to lead to RuCp*Cl-Star (**S4**: $[RuCp^*Cl]_0/[Core\text{-}PPh_3]_0 = 1/2$), since RuCp*Cl derivatives with phosphine ligands [$RuCp^*Cl(PR_3)_2$] is efficient for living radical polymerization (*21*, *22*, *24*–*30*).

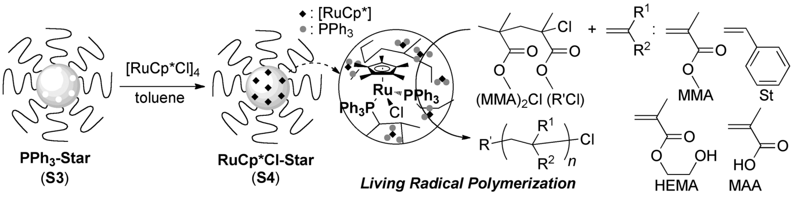
◆: [RuCp*]
●: PPh_3
[RuCp*Cl]$_4$
toluene
PPh_3-Star
(S3)
RuCp*Cl-Star
(S4)
Ru
PPh_3
Ph_3P
Cl
Cl
(MMA)$_2$Cl (R'Cl)
+
R^1
R^2
MMA
St
R'
R^1
R^2
n
Cl
OH
HO
HEMA
MAA
Living Radical Polymerization

Figure 8. Star polymer-catalyzed living radical polymerization.

Table 1. RuCp*Cl-Star-Catalyzed Living Radical (Co)polymerization[a]

Entry	*Monomer*	*Catalyst (in-core complex)*	*Time (h)*	*Conversion (%)*	M_n[b]	M_w/M_n[b]	*Olefin (%)*[c]
1	MMA	**S1** ($RuCl_2$)	10	74	Gel	-	-
2	MMA	**S3** (none)	24	0	-	-	-
3	MMA	**S4** (RuCp*Cl)	72	90	11200	1.11	<3
4	MMA	**S4** (RuCp*Cl)	144	197	20000	1.11	-
5	MMA	$RuCp^*Cl(PPh_3)_2$	94	73	12000	1.16	~30
6	MMA	$[RuCp^*Cl]_4$	96	18	4800	2.27	-
7	MMA	RuCp*-Gel	72	89	20600	2.62	-
8	MMA/MAA	**S4** (RuCp*Cl)	144	75/72	8300	1.15	-
9	MMA/MAA	$RuCp^*Cl(PPh_3)_2$	144	29/28	not determined		-
10	MMA/ HEMA	**S4** (RuCp*Cl)	144	72/96	8000	1.13	-
11	MMA/ HEMA	$RuCp^*Cl(PPh_3)_2$	144	33/70	4400	1.17	-
12	St	**S4** (RuCp*Cl)	168	85	9700	1.11	~0
13	St	**S4** (RuCp*Cl)	168	80	9300	1.21	-

[a] (entry 1): [MMA]/[ECPA]/[Ru]/[*n*-Bu_3N] = 2000/20/10/40 mM; (entry 2): [MMA]/ [$(MMA)_2Cl$]/ [**S3**-PPh_3] = 4000/40/8 mM; (entry 3-7): [MMA]/[$(MMA)_2Cl$]/[Ru] = 4000 (+4000: entry 5; monomer addition)/40/4 mM in toluene at 80 °C. (entry 8,9): [MMA]/[MAA]/[$(MMA)_2Cl$]/[Ru] = 1900/100/2.0/4.0 mM in THF at 80 °C. (entry 10,11): [MMA]/[HEMA]/[$(MMA)_2Cl$]/[Ru] = 1700/ 300/2.0/4.0 mM in toluene at 80 °C. (entry 12,13): [St]/[$(MMA)_2Cl$]/[Ru] = 4000/40/4.0 mM in toluene at 100 °C. [b] Determined by SEC. [c] Terminal olefin: determined by ^1H NMR.

The resulting **S4** was directly applied to living radical (co)polymerization of MMA, 2-hydroxyethyl methacrylate (HEMA), methacrylic acid (MAA), and styrene (St) (Table 1). **S4** showed higher activity and controllability in MMA polymerization than a core-forming analogue [$RuCp^*Cl(PPh_3)_2$] (entry 3-5). As expected, $RuCl_2$-Star without core-hydrogenation (**S1**) induced gelation (entry 1). The microgel-core encapsulation of RuCp*Cl dramatically enhanced the catalyst stability to acid functions (MAA) (entry 8, 9). It should be noted that this is the first example of direct living radical copolymerization of MAA with metal catalysts. RuCp*Cl-Star was effective for St in spite of the precipitation of the catalyst over 50% conversion, giving almost pure poly(St) via the simple decantation of the solution (entry 12, Ru residue: 56 ppm; over 95% Ru removal). Due to the spontaneous precipitation, **S4** was facilely reused (entry 13). Now, we further designed iron-bearing star polymer catalysts suitable for living radical polymerization.

Fluorine-Condensed Star Polymers

Microgel-core star polymers can be employed as nano capsules to recognize functional molecules. The key is to condense functional groups such as amide (*7*), poly(ethylene glycol) (PEG) (*25*), and quaternary ammonium groups (*18*) in the core, which enhances the hydrogen-bonding and ionic interaction for protic and/or ionic guests. Fluorination of organic (macro)molecules is intriguing to provide so called "fluorous" character, the incompatibility with aqueous and common organic phases (*39*). The fluorous nature might be another trigger to recognize perfluorinated molecules, as typically giving the intriguing functions: facile separation in catalysis (*40*); stable formation of micelles and vesicles in solution (*41*).

Thus, we designed fluorine-condensed microgel-cores star polymers via ruthenium-catalyzed living radical polymerization, to construct nano-scale fluorinated compartments for efficient and selective molecular recognition (Figure 9, 10) (*17*). Direct fluorination of the core was successfully achieved by the linking reaction of poly(MMA) arms (M_n ~13000, M_w/M_n <1.2) with a fluorinated linker (12FODMA) and monomer (13FOMA) (Star yield: ~80%, $[\text{12FODMA}]_0/[\text{13FOMA}]_0/[\text{arm}]_0 = 5/10/1$, M_w = 2,000,000, 75 arms, R_g = 20 nm by SEC-MALLS). The number of core-bound fluorine (N_F) and that of CF_3 groups (N_{CF3}) were estimated as about 17000 and 700, respectively, from the feed ratio of 12FODMA and 13FOMA to arms and the arm numbers.

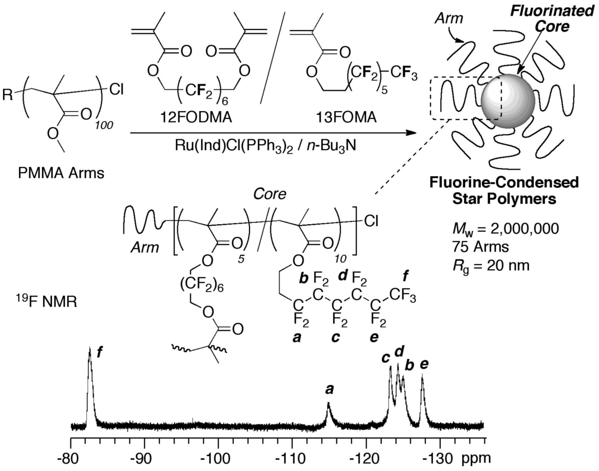
R
Cl
100
PMMA Arms
$(CF_2)_6$
12FODMA
$(CF_2)_5$–CF_3
13FOMA
$Ru(Ind)Cl(PPh_3)_2$ / n-Bu_3N
Arm
Fluorinated Core
Fluorine-Condensed Star Polymers
M_w = 2,000,000
75 Arms
R_g = 20 nm
Core
Arm
5
10
Cl
$(CF_2)_6$
b F_2 d F_2 f
CF_3
F_2 F_2 F_2
a c e
^{19}F NMR
f
a
c d b e
-80
-90
-100
-110
-120
-130 ppm

Figure 9. Fluorine-condensed star polymers via ruthenium-catalyzed living radical polymerization and the core analysis by ^{19}F NMR in $CDCl_3$ at r.t.

Thanks to the high sensitivity, ^{19}F NMR and diffusion-ordered NMR spectroscopy (DOSY) measurements of the resulting star polymers give us critical information in terms of the core environment (diffusion, space-confinement, thermal movement, etc.), that has been unknown so far (Figure 9). To clarify the core-unit mobility, the signal intensity I(***a***) of the innermost pendent CF_2 [–O–$(CH_2)_2$–CF_2 in 13FOMA units; peak ***a***] was compared with its estimated maximum [I(***a***)$_{calcd}$] based on the signal intensity of the tip CF_3 (peak ***f***) assuming that this group can freely move even within a tight network and thus exhibit unperturbed NMR signals. I(***a***) for the star polymer was about 60 % of I(***a***)$_{calcd}$, whereas that for MMA/13FOMA random copolymer (MMA/13FOMA = 100/10; M_n = 14000; M_w/M_n =1.18; N_F = 118; N_{CF3} = 9) was close to I(***a***)$_{calcd}$. The decreased mobility of the core was further supported by the fact that the spin-lattice relaxation time (T_1) for the core-bound CF_3 (***f***) was smaller than that for random counterpart [T_1 = 0.50 s (star), 1.48 s (random) in $CDCl_3$ at 30 °C].

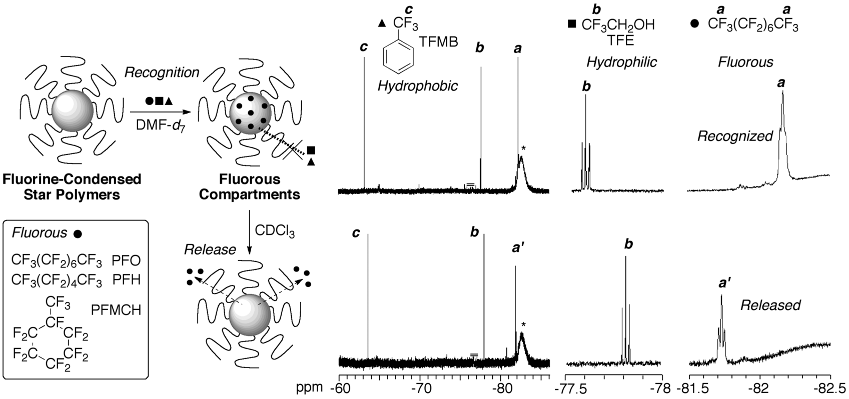

Figure 10. Fluorous recognition of perfluorinated compounds with fluorine-condensed star polymers and stimuli-responsive release of guests from the core.

Fluorous Molecular Recognition

Recognition of perfluorinated guest compounds [perfluorooctane (PFO), perfluorohexane (PFH), perfluoromethylcyclohexane (PFMCH)] was examined with fluorine-condensed star polymers in DMF-d_7 at room temperature (Figure 10) (*17*). The star polymer efficiently solubilized PFO, PFH, and PFMCH (their perfluorinated guests alone: insoluble in DMF) in DMF-d_7. Typically, the CF_3 signal of PFO with a fluorinated star turned broader than that in $CDCl_3$ without the star, indicating a strong interaction between PFO and the fluorinated core. Such a fluorous recognition was still effective and selective for PFO even in the presence of other guests [trifluoromethylbenzene (TFMB): hydrophobic; 2,2,2-trifluoroethanol (TFE): hydrophilic]; the tip CF_3 signal (***a***: -82.3 ppm) of PFO broadened, while that of TFE remained sharp triplet (***b***) (Figure 10). The addition of $CDCl_3$ into DMF-d_7 (up to 1/1 v/v), in turn, interferes the PFO recognition and thereby triggers release of once entrapped PFO from the core, as indicated by the reappearance of a sharp triplet of CF_3 (***a'***: -81.7 ppm).

Conclusion

We have successfully produced core-functionalized star polymers via ruthenium-catalyzed living radical polymerization in one-pot, to create functional compartments for catalysis and molecular recognition. Due to the unique environment of the core that is totally homogeneous but locally cross-linked and isolated from outer environment, metal-bearing star polymers efficiently catalyzed organic reaction and polymerization, compatible with high activity, versatility, stability, and recyclability. Fluorine-condensed star polymers worked as fluorous compartments to efficiently and selectively recognize perfluorinated guests. The core-bound fluorine served as a unique probe for not only molecular recognition but also characterization of the structure and dynamics of the core. Marriage of catalytic sites and molecular recognition units in a star polymer core would provide multifunctional nano compartments to open new vistas in catalysis.

Acknowledgments

This research was supported by the Ministry of Education, Science, Sports and Culture through a Grant-in Aid for Creative Scientific Research (18GS0209), and through Grant-in Aids for Young Scientist (Start-up) (No.19850010) and Young Scientist (B) (No.20750091), for which T.T. is grateful. We thank Hokko Chemical for the kind supply of diphenylphosphinostyrene (SDP). We extend our thanks: to Professor Hideki Matsuoka (Department of Polymer Chemistry, Kyoto University) and Professor Kozo Matsumoto (Molecular Engineering Institute, Kinki University) for AFM observation; to Professor Hirokazu Hasegawa (Department of Polymer Chemistry, Kyoto University) for TEM analysis; and Dr. Takeshi Niitani (Nippon Soda Co., Ltd.) and Mr. Tomohiro Ono (Kurarey Co. Ltd.) for ICP-AES analysis. We appreciate to Mr. Akihisa Nomura and Mr. Yuta Koda for their experimental works.

References

1. Bosman, A. W.; Janssen, H. M.; Meijer, E. W. *Chem. Rev.* **1999**, *99*, 1665–1688.
2. Grayson, S. M.; Fréchet, J. M. J. *Chem. Rev.* **2001**, *101*, 3819–3867.
3. Van Dongen, S. F. M.; de Hoog, H.-P. M.; Peters, R. J. R. W.; Nallani, M.; Nolte, R. J. M.; van Hest, J. C. M. *Chem. Rev.* **2009**, *109*, 6212–6274.
4. Gao, H.; Matyjaszewski, K. *Prog. Polym. Sci.* **2009**, *34*, 317–350.
5. Blencowe, A.; Tan, J. F.; Goh, T. K.; Qiao, G. G. *Polymer* **2009**, *50*, 5–32.
6. Kanaoka, S.; Sawamoto, M.; Higashimura, T. *Macromolecules* **1992**, *25*, 6414–6418.
7. Baek, K.-Y.; Kamigaito, M.; Sawamoto, M. *Macromolecules* **2001**, *34*, 7629–7635.
8. Baek, K.-Y.; Kamigaito, M.; Sawamoto, M. *Macromolecules* **2002**, *35*, 1493–1498.
9. Terashima, T.; Kamigaito, M.; Baek, K.-Y.; Ando, T.; Sawamoto, M. *J. Am. Chem. Soc.* **2003**, *125*, 5288–5289.

10. Terashima, T.; Ouchi, M.; Ando, T.; Kamigaito, M.; Sawamoto, M. *J. Polym. Sci., Part A.: Polym. Chem.* **2006**, *44*, 4966–4980.
11. Terashima, T.; Ouchi, M.; Ando, T.; Kamigaito, M.; Sawamoto, M. *Macromolecules* **2007**, *40*, 3581–3588.
12. Terashima, T.; Motokawa, R.; Koizumi, S.; Sawamoto, M.; Kamigaito, M.; Ando, T.; Hashimoto, T. *Macromolecules* **2010**, *43*, 8218–8232.
13. Terashima, T.; Nomura, A.; Ito, M.; Ouchi, M.; Sawamoto, M. *Angew. Chem., Int. Ed.* **2011**, *50*, 7892–7895.
14. Terashima, T.; Ouchi, M.; Ando, T.; Sawamoto, M. *J. Polym. Sci., Part A.: Polym. Chem.* **2011**, *49*, 1061–1069.
15. Terashima, T.; Ouchi, M.; Ando, T.; Sawamoto, M. *Polym. J.* **2011**, *43*, 770–777.
16. Terashima, T.; Ouchi, M.; Ando, T.; Sawamoto, M. *J. Polym. Sci., Part A.: Polym. Chem.* **2010**, *48*, 373–379.
17. Koda, Y.; Terashima, T.; Nomura, A.; Ouchi, M.; Sawamoto, M. *Macromolecules* **2011**, *44*, 4574–4578.
18. Fukae, K.; Terashima, T.; Sawamoto, M. *Polym. Prepr. Jpn* **2011**, *60*, 1328.
19. Bosman, A. W.; Vestberg, R.; Heumann, A.; Fréchet, J. M. J.; Hawker, C. J. *J. Am. Chem. Soc.* **2003**, *125*, 715–728.
20. Rodionov, V.; Gao, H.; Scroggings, S.; Unruh, D. A.; Avestro, A.-J.; Fréchet, J. M. J. *J. Am. Chem. Soc.* **2010**, *132*, 2570–2572.
21. *Advances in Controlled/Living Radical Polymerization*; Matyjaszewski, K., Ed.; ACS Symposium Series 854; American Chemical Society: Washington, DC, 2003.
22. *Controlled/Living Radical Polymerization: From Synthesis to Materials*; Matyjaszewski, K., Ed.; ACS Symposium Series 944; American Chemical Society: Washington, DC, 2006.
23. Kato, M.; Kamigaito, M.; Sawamoto, M.; Higashimura, T. *Macromolecules* **1995**, *28*, 1721–1723.
24. Kamigaito, M.; Ando, T.; Sawamoto, M. *Chem. Rev.* **2001**, *101*, 3689–3746.
25. Ouchi, M.; Terashima, T.; Sawamoto, M. *Acc. Chem. Res.* **2008**, *41*, 1120–1132.
26. Ouchi, M.; Terashima, T.; Sawamoto, M. *Chem. Rev.* **2009**, *109*, 4963–5050.
27. Watanabe, Y.; Ando, T.; Kamigaito, M.; Sawamoto, M. *Macromolecules* **2001**, *34*, 4370–4374.
28. Ouchi, M.; Ito, M.; Kamemoto, S.; Sawamoto, M. *Chem. Asian. J.* **2008**, *3*, 1358–1364.
29. Yoda, H.; Nakatani, K.; Terashima, T.; Ouchi, M.; Sawamoto, M. *Macromolecules* **2010**, *43*, 5595–5601.
30. Fukuzaki, Y.; Tomita, Y.; Terashima, T.; Ouchi, M.; Sawamoto, M. *Macromolecules* **2010**, *43*, 5989–5995.
31. Tsarevsky, N. V.; Matyjaszewski, K. *Chem. Rev.* **2007**, *107*, 2270–2299.
32. Matyjaszewski, K.; Tsarevsky, N. V. *Nat. Chem.* **2009**, *1*, 276–288.
33. Rosen, B. M.; Percec, V. *Chem. Rev.* **2009**, *109*, 5069–5119.
34. Bergbreiter, D. E.; Tian, J.; Hongfa, C. *Chem. Rev.* **2009**, *109*, 530–582.
35. Leadbeater, N. E.; Marco, M. *Chem. Rev.* **2002**, *102*, 3217–3274.
36. Naota, T.; Takaya, H.; Murahashi, S. *Chem. Rev.* **1998**, *98*, 2599–2660.

37. Terashima, T.; Ouchi, M.; Ando, T.; Sawamoto, M. *J. Am. Chem. Soc.* **2006**, *128*, 11014–11015.
38. Terashima, T.; Mes, T.; De Greef, T. F. A.; Gillissen, M. A. J.; Besenius, P.; Palmans, A. R. A.; Meijer, E. W. *J. Am. Chem. Soc.* **2011**, *133*, 4742–4745.
39. Krafft, M. P.; Riess, J. G. *Chem. Rev.* **2009**, *109*, 1714–1792.
40. Horváth, I. T.; Rábai, J. *Science* **1994**, *266*, 72–75.
41. Kraff, M. P. *Adv. Drug Delivery Rev.* **2001**, *47*, 209–228.

In Progress in Controlled Radical Polymerization: Materials and Applications; Matyjaszewski, K., et al.;
ACS Symposium Series; American Chemical Society: Washington, DC, 2012.

Chapter 6

Synthesis and SEC Characterization of Poly(methyl methacrylate) Star Polymers

James A. Burns, David M. Haddleton,* and C. Remzi Becer*

Department of Chemistry, University of Warwick,
CV4 7AL Coventry, United Kingdom
***E-mails: c.r.becer@warwick.ac.uk (C.R.B.);**
d.m.haddleton@warwick.ac.uk (D.M.H.)

The use of multi detector SEC for the determination of the functionality (number of arms) of PMMA star polymers, made using ATRP and a core first technique is described. Multifunctional 3-arm, 5-arm, 8-arm and 21-arm initiators were used for the polymerisation of MMA to result in star polymers with narrow dispersity when the reaction was terminated at low conversion. Use of Zimm and Stockmayer theory with multi-detector SEC, the number of arms on each star polymer has been estimated using the reduction in intrinsic viscosity of a star polymer relative to a linear polymer equivalent.

Introduction

There are a number of techniques which can be used to characterise the molecular weight of polymers. These include multi angle laser light scattering (MALLS) and membrane osmometry as ways to determine the absolute weight average (M_w) and number average (M_n) molecular weights respectively, to sedimentation equilibrium and matrix assisted laser desorption ionisation (MALDI) mass spectroscopy. However, the characterisation of star polymers and copolymers presents a demanding challenge for the most commonly used method to analyse the molecular weight of polymers, gel permeation chromatography/size exclusion chromatography (GPC/SEC).

The principle of SEC is that a dilute solution of analyte is introduced into a stream of eluent flowing through a column of packed porous beads and separation occurs depending on the size of the analyte molecule in solution. The beads have pores of varying sizes of approximately the same size as the molecularly dissolved analyte. The elution time of the analyte is determined by the number of pores the analyte can enter and thus the pathlength through the column (*1–4*). A smaller analyte enters more pores and therefore elutes at a later time (*5*).

In conventional SEC analysis typically a concentration detector (often a differential refractometer (DRI)) is used to determine the concentration of polymer as it elutes from the column (Eq. 1). The elution time is related to the molecular weight of the analyte through a calibration curve (Figure 1) and the calibration is usually made using a range of linear narrow molecular weight standards.

$$\mathrm{RI} = \mathrm{B}\,(\mathrm{dn}/\mathrm{dc})\,\mathrm{c} \qquad \text{(Eq. 1)}$$

Where RI is the refractive index; c is the concentration of polymer in the sample; dn/dc is the change in the refractive index of the solution as a function of concentration. This value varies for each polymer-solvent pair under constant conditions.

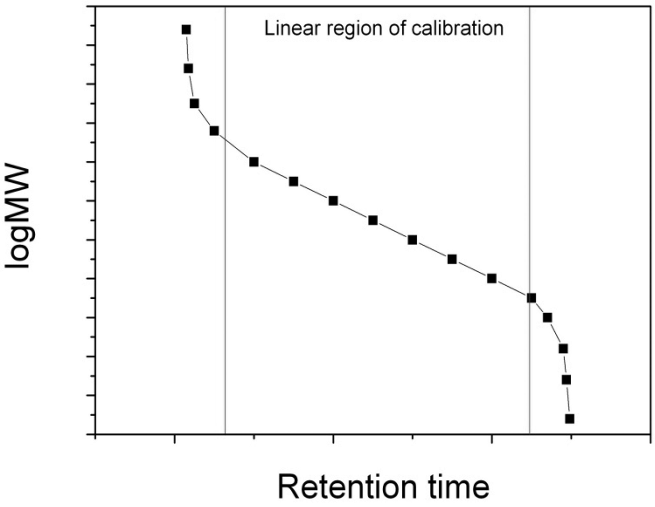

Figure 1. M_p of various linear calibration standards as a plot of log(MW) against retention time (retention time = retention volume at 1 mL.min^{-1}) in the SEC. These plots are used as a calibration curve for conventional SEC.

As the SEC columns separate the polymer by the size in solution, any variation in architecture or chemistry between calibrant and polymer analyte causes discrepancies from the calibration curve where linear random coils are required (*6–9*). This is particularly problematic when analysing novel polymers and copolymers where the two constituent monomers have different refractive indices, although averaging of the dn/dc has been shown to be effective for some studies (*10*). Likewise, different architectures can be difficult to analyse by conventional SEC due to geometrical constraints arising from covalent bonding.

When compared to their linear analogues with the same molecular weight, branched polymers have smaller dimensions (Figure 2) leading to a reduction in solution viscosity. The molecular weight of branched polymers determined by conventional GPC is often underestimated due to this reduction in hydrodynamic volume (*9*, *11*). The use of multiple detectors with SEC, such as MALLS and viscometry, can be used to observe these changes (*12*, *13*).

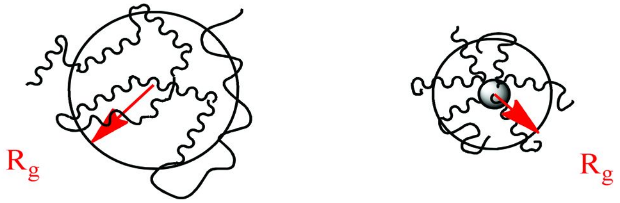

Figure 2. Schematic representation of the difference in root mean square radius of gyration of linear and star polymers of the same molecular weight.

It has been known for a long time that the use of a differential viscometer with SEC can be used to form a "universal calibration" (*6*) which has been shown to give more accurate analysis of the molecular weight, removing the need for the calibrant and polymer analyte to have the same chemistry and architecture (Figure 3).

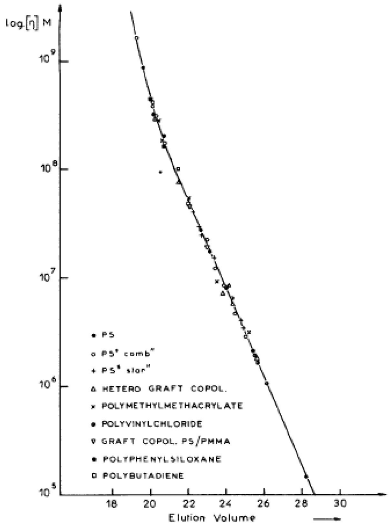

Figure 3. Plot of log[η].M vs elution volume for polymers of different molecular weights/functionalities and architectures. Taken without editing from reference (6).

This universal calibration is based upon Einstein's viscosity theory from his 1905 dissertation for the university of Zurich and subsequent corrections of 1911. This theory is utilisedby Benoit and Grubisic in their seminal paper (*6*), summarised below; using a simple form of Einstein's viscosity theory to show a relationship between viscosity and molecular weight. Modelling the polymer as hard spheres in dilute solution:

$$\eta_{sp} = 2.5\frac{N_B V_\eta}{V} \qquad \text{(Eq. 2)}$$

Where η_{sp} is the specific viscosity, N_B is the number of spheres, V_η is the volume of the spheres, and V is the total volume.

The volume of the spheres V_η is the effective hydrodynamic volume of the polymer in solution. Allowing the number of moles of polymer (n_B) to be $n_B = N_B/N_A$ then:

$$\eta_{sp} = 2.5\frac{n_B V_\eta N_A}{V} \qquad \text{(Eq. 3)}$$

Introducing a factor for the concentration into Eq. 3, using concentration, $c = n_B\, N_A/M$, where M is the molecular weight and N_A is Avagadro's number, gives:

$$\eta_{sp} = 2.5\frac{n_B M}{V}\,\frac{V_\eta N_A}{M}$$

$$\eta_{sp} = 2.5c\frac{V_\eta N_A}{M}$$

$$\frac{\eta_{sp}}{c} = [\eta] = 2.5\frac{V_\eta N_A}{M} \qquad \text{(Eq. 4)}$$

Therefore, extrapolating to zero concentration to yield intrinsic viscosity, and assuming that the effective hydrodynamic volume is proportional to the mean it can be written that:

$$[\eta] = k\frac{V_h}{M} \text{ or } V_h = \frac{[\eta]M}{k} \qquad \text{(Eq. 5)}$$

Where $[\eta]$ is the intrinsic viscosity, k is constant, and V_h is the hydrodynamic volume of the polymer.

As emphasised earlier, SEC separation is due to the size of the polymer in solution (provided there is no unwanted chemical interactions). Therefore, using the hydrodynamic volume of the polymer (log([η].M)) vs. elution volume (Figure 3), rather than the molecular weight (log(M)) creates a calibration independent of chemistry and architecture (*6*, *14*, *15*). Therefore, this technique should give a closer representation of the molecular weight of a star polymer compared to conventional SEC.

Multi Angle Laser Light Scattering (MALLS) in SEC

Light scattering is a powerful technique for determining the molecular weight of a polymer and can be used to determine the absolute weight averaged molecular weight, M_w. When electromagnetic radiation hits an atom or a molecule, the electrons emit the radiation in all directions.

$$R(\theta) = \frac{I_\theta r^2}{I_0} \qquad \text{(Eq. 6)}$$

Where I_θ is scattering intensity per unit of scattering volume, I_0 is the intensity of incident light, r is the distance between the scattering volume and the detectors.

The amount of scattered light is measured using detectors at varying angles to the incident light, and is proportional to the size of the analyte molecule, with larger molecules scattering more than smaller molecules. The amount of light scattered by a dilute solution of analyte at a given angle, θ, is termed the excess Raleigh ratio, $R(\theta)$, Eq. 6.

$$\frac{K^* c}{R(\theta)} = \frac{1}{M_w} \qquad \text{(Eq. 7)}$$

Where c is the concentration of the scattering volume.

$$K^* = \frac{4\pi^2 n_0^2 (dn/dc)^2}{\lambda_0^4 N_A} \qquad \text{(Eq. 8)}$$

Where N_A is Avogadro's number, N_0 is the refractive index of the solvent, λ_0 is the vacuum wavelength of the incident radiation, and (dn/dc) is the specific refractive index increment.

The excess Raleigh scattering and concentration of the solution can be used to determine the absolute molecular weight, M_w through the Raleigh-Gans-Debye approximation, Eq. 7.

The angular dependence of the scattered light and inverse absolute molecular weight, M_w^{-1} are related by a Zimm plot. By varying concentration of the polymer and angle of scattered light, the inverse absolute molecular weight, M_w^{-1}, is calculated by extrapolating to zero concentration and an angle of 0° (*16*). Using SEC-MALLS, the scattered light is detected at different angles for each eluting segment. When used in conjunction with a concentration detector it is possible to calculate the M_w and $\langle R_g^2 \rangle_z$ for each integral slice of the SEC separation. If the local dispersity of the polymer in the SEC separation is unknown, or much greater than unity due to co-elution of different architectures of the same hydrodynamic volume, then these values must be treated as averages.

For star polymers, the radius of gyration has been related to the molecular weight by Daoud and Cotton (*17*) where they deduced a dependence of R_g on $N^{3/5} f^{1/5}$ where N is the number of segments in each arm. This led to the conclusion that for systems where N is constant this results in $R_g \; \mu \; M^{1/5}$ (*18*).

Radius of Gyration Contraction Factor

By comparing the radius of gyration of a branched (star) polymer sample with a linear analogue at the same molecular weight it is possible to resolve branching information (*19*). The extent of the branching is described by the radius of gyration contraction factor, g, (Eq. 9).

$$g = \frac{< r_g^2 >_s}{< r_g^2 >_l} \qquad \text{(Eq. 9)}$$

Where $< r_g^2 >_s$ is the square mean radius of gyration of a star polymer, $< r_g^2 >_l$ is the square mean radius of gyration of a linear polymer of the same composition and molecular weight.

Mays and co-workers synthesised a range of highly branched PMMA polymers by varying the amount of ethylene glycol dimethacrylate (EGDMA) divinyl crosslinker used in the polymerisation. Then, using multi detector SEC the radius of gyration contraction factor was investigated and seen to increase with increasing branching (*20*).

Mark-Houwink Plots

The use of a capillary viscometer (*21*, *22*) allows determination of the intrinsic viscosity across the MWD of the polymer and is an easy way to produce a Mark-Houwink plot for a polymer from the Mark-Houwink equation, $[\eta] = KM^{\alpha}$. For a polymer with a constant amount of branching the contraction in solution is consistent, and the exponent of the Mark-Houwink equation will be reduced by a consistent amount (*23*). Thus, a Mark-Houwink plot of a perfect core first star polymer should result in a parallel line to the linear one, but shifted to lower viscosity. The Mark-Houwink exponent, α, depends on the structure of the polymer in solution. Its value can be in the range from 0 (solid sphere) to 2 (rigid rod).

Simon *et al.* (*24*) synthesised highly branched PMMA using 2-(2-methyl-1-triethylsiloxy-1-propenyloxy)-ethyl methacrylate (MTSHEMA) divinyl crosslinker. They then validated the use of multi-detector SEC to determine a Mark-Houwink plot, by separation of a highly branched polymer by preparative SEC. Using high concentration light scattering experiments on the nine resulting narrow polydispersity polymers gave the absolute Mw and viscosity measurements gave the intrinsic viscosity. Both multi-detector SEC and the preparative SEC gave Mark-Houwink exponents in THF that are considerably lower than those for linear PMMA of $\alpha = 0.40$ (for linear PMMA, $\alpha = 0.688$) highlighting the branched structure of the polymers (*24*).

Intrinsic Viscosity Shrink Factor

The use of intrinsic viscosity and ascertain an intrinsic viscosity shrink factor, g^I, defined in Eq. 10, can also be effective.

$$g^I = \frac{[\eta]_s}{[\eta]_l} \qquad \text{(Eq. 10)}$$

Where $[\eta]_s$ is the intrinsic viscosity of a star polymer, $[\eta]_l$ is the intrinsic viscosity of a linear polymer of the same composition and molecular weight.

The radius of gyration contraction factor is predominantly used in quantify branching, however the intrinsic viscosity is often more accessible. As viscosity has some dependence on the size of a molecule in solution (*25*), there have been attempts to relate g^I back to the radius of gyration contraction factor, g, to allow its use in quantifying branching. Zimm and Stockmayer's work (*19*) has been used as the foundation for a number of investigations into dilute polymer solution properties (*12*, *26*, *27*). The relationship between g^I and g is currently disputed in literature, but has been described by an exponential relationship $g^I = g^\varepsilon$, where ε can has a value of 3/2 based on Flory-Fox theory (*28*). Zimm and Kilb calculated ε = ½, and argued that it was a universal value; however, it has been calculated experimentally as between 0.8 and 1 by Mays *et al.* (*20*) and also as 0.83 for PMMA by Millequant and coworkers (*25*, *26*). Complicating the argument further, several researchers have developed and used a different relationship between g^I and g based on experimental data, (Eq. 11) (*29–32*).

$$g = [a + (1 - a){g^I}^b]\, {g^I}^c \qquad \text{(Eq. 11)}$$

Where g is the radius of gyration contraction factor, g^I is the intrinsic viscosity shrink factor, and a, b and c are constants derived from experiment.This relationship has been particularly studied for PMMA, where Robello *et al.* have determined that for the above equation a= 0.2625, b= 1.088 and c= 0.6087 (*30*).

Determining the Functionality of Star Polymers

Determination of the functionality of star polymers has been achieved in a variety of ways. Using the core first methodology, the functionality is determined using ^{1}H NMR to ensure that all initiating sites on the core have initiated polymerisation, and hence the functionality of the star is estimated to be equal to the functionality of the core. Using the arm first approach the functionality can be determined during synthesis. A crude final product using this technique contains both star and unreacted arm polymers. Comparison of the M_n of the linear arms with the star polymer, and dividing the star molecular weight by the one by the other is used to estimate the functionality (*33*). A novel technique for determining the functionality using multi detector SEC has been used with varying success (*12*, *26*, *27*). This approach, described below, has the advantage of allowing analysis of unknown polymers post-synthesis.

Determining the Number of Arms Using Multi Detector SEC

The relationship between the radius of gyration contraction factor and functionality (*f*) of a star polymer is dependent on the model used to simulate the star polymer. Zimm and Stockmayer proposed a relationship between g and *f* by modelling the star polymer as a singular core with arms of equal length (Eq. 12) (*19*).

$$g = \frac{3}{f} - \frac{2}{f^2} \qquad \text{(Eq. 12)}$$

Robello *et al.* have used this relationship to characterise 3, 5, 6 and 10 arm stars synthesised by ATRP using sulfonyl chloride initiators with defined functionality (*30*). They found that the functionality, *f*, changed over the molecular weight distribution of the polymer, but at the M_p of the star polymer the functionality calculated by the above equation was within ± 1 of the initiator functionality. This approach to determining the functionality using multi detector SEC was investigated here using core first PMMA made using ATRP.

Experimental

Instruments

SEC was used to determinate the molecular weight averages and the dispersity of polymers using one of two systems. System 1; with a 390-LC Polymer Laboratories system equipped with a PL-AS RT/MT autosampler, a PL- gel 3 μm (50 × 7.5 mm) guard column, two PL-gel 5 μm (300 × 7.5 mm) mixed-D columns (suitable for separations up to MW = 2.0×10^6 $g.mol^{-1}$), a differential refractometer, 4 capillary viscometer and MALLS were used. Eluent used was chloroform / triethylamine 95 : 5 (v/v) as the eluent with a flow rate of 1.0 mL.min-1. System 2; with a 390-LC Polymer Laboratories system equipped with a PL-AS RT/MT autosampler, a PL- gel 3 μm (50 × 7.5 mm) guard column, two PL-gel 5 μm (300 × 7.5 mm) mixed-D columns (suitable for separations up to MW = 2.0×10^6 $g.mol^{-1}$), a differential refractometer, MALLS, and a photodiode array were used. Solvent used was tetrahydrafuran / triethylamine 95 : 5 (v/v) as the eluent with a flow rate of 1.0 $mL.min^{-1}$, unless otherwise stated. Calibrations were set using a single injection of narrow molecular weight PMMA standards (1000 – 1×10^6 $g.mol^{-1}$) of known concentration, with a minimum of 10 points to form the curve.

All ^1H and ^{13}C NMR spectra were recorded on Bruker DPX300, Bruker DPX400 and Bruker DRX500 spectrometers as solutions in deuterated NMR solvents. Chemical shifts are cited as parts per million (ppm). The following abbreviations are used to represent multiplicities; s = singlet, d = doublet, t = triplet, q = quartet, m = multiplet.

FTIR was recorded on a VECTOR-22 Bruker spectrometer using a Golden Gate diamond attenuated total reflection cell.

Synthesis of 1,1,1-Tris(methyl-O-isobutyryl bromide) Ethane

1,1,1-Tris(hydroxymethyl) ethane (12.01 g, 100 mmol), triethylamine (56.20 mL, 350 mmol) and THF (200 mL) were placed into a round bottom flask and cooled to 0 °C in an ice bath. 2-Bromoisobutyryl acid bromide (41.70 mL, 330 mmol) was added dropwise with stirring over 30 minutes, and the reaction left over night at ambient temperature. The reaction mixture was filtered, and the filtrate passed through a column of basic aluminium oxide. The organic solution was washed with acidified water (pH 4.5, 2 x 300 ml) and dried with magnesium sulphate. The organic solvent was removed under reduced pressure. ^1H NMR ($CDCl_3$) δ (ppm), 4.20 (s, 6H, $-COOC\underline{H}_2-$), 1.98 (s, 18H, $-C\underline{H}_3$), 1.21 (s, 3H, $C\underline{H}_3$).

^{13}C NMR ($CDCl_3$) δ (ppm), 171.2 ($-\underline{C}OO-$), 66.6 ($COO\underline{C}H_2$), 55.4 ($-C(CH_3)_2$ Br), 39.7 ($\underline{C}(C_4H_8O_2Br)_3CH_3$), 30.7 ($C(\underline{C}H_3)Br$), 17.1 ($C(C_4H_8O_2Br)_3\underline{C}H_3$). FT-IR (ν): 2975 cm^{-1}, 1732 cm^{-1}, 1461 cm^{-1} , 1389 cm^{-1}, 1265 cm^{-1}, 1153 cm^{-1}, 1102 cm^{-1}.

Synthesis of Methyl Methacrylate 3 Arm Star Polymer

Methyl methacrylate (11.82 g, 118 mmol), 1,1,1-tris(hydroxymethyl)ethane derived initiator 1 (0.17 g, 0.30 mmol), *N*-(n-propyl)-2-pyridylmethanamine (0.26 g, 1.77 mmol) and toluene (10 mL) as the solvent, were placed in a dry Schlenk tube containing a magnetic stirrer. The tube was sealed with a rubber septum and subjected to five-freeze-pump thaw cycles to degas the solution. Copper(I) bromide (0.13 g, 0.89 mmol) was added to the degassed, frozen solution against a flow of nitrogen. The sealed tube was then immersed in an oil bath heated to 70 °C, and samples taken periodically using a degassed syringe for molecular weight and conversion analysis. At the end of the reaction, after 8 hours, the mixture was diluted with toluene (20 mL) and air was bubbled through for 1 hour. Neutral alumina (10 g) was added to the reaction mixture and stirred for 2 hours. The mixture was filtered, and the solution was concentrated under reduced pressure. The polymer was precipitated in water/methanol to yield a white powder. Yield = 4.30 g. Conversion of the polymer was followed by comparing the decreasing singlet at 4.60 ppm (corresponding to the $C(O)OCH_2$ protons in the monomer) with the broad signal at 4.40 ppm increasing with time (corresponding to the $C(O)OCH_2$ protons in the polymer). M_n (SEC) = 20300 $g.mol^{-1}$; dispersity (SEC) = 1.51; Conversion = 49%; Initiator efficiency = 94%

Results and Discussion

Synthesis of Core First PMMA Stars by ATRP

PMMA star polymers were synthesised using a well established core first approach. Core initiators were synthesised by reaction of polyols with 2-bromo-isobutyryl bromide in the presence of base (Scheme 1). An 3-arm initiator was synthesised from 1,1,1 tris(hydroxymethyl) ethane by the esterification of 3 equivalents of 2-bromoisobutyryl bromide in anhydrous THF, with triethyleneamine used as the base catalyst.

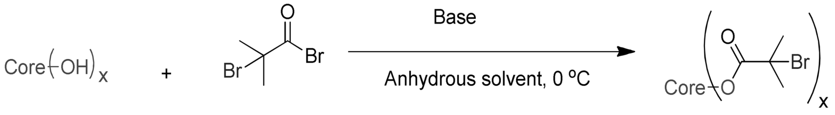

Scheme 1. General synthesis of multi functional initiator from the esterification of alcohols with a tertiary bromide functionalised acid bromide.

CFStar1 was made by polymerisation of MMA using this initiator in toluene at 65 °C (Scheme 2). The initiator, monomer, ligand and solvent were placed into a Schlenk tube and degassed by freeze-pump-thaw and filled with nitrogen to ensure the absence of oxygen. The copper(I) bromide was added against a flow of nitrogen to start the reaction.

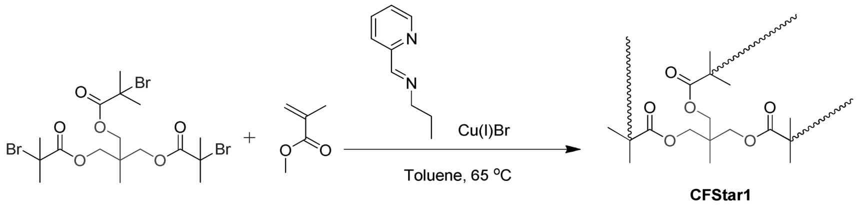

Scheme 2. Polymerisation of MMA from a trifunctional initiator to form a 3 arm PMMA star, CFStar1. 〰 *= PMMA.*

Aliquots were taken periodically to allow the polymerisation to be monitored by ^1H NMR and SEC throughout the reaction. The polymerisation reactions were seen to progress in a pseudo living manner with molecular weight growth with conversion, dispersity < 1.2, and a linear plot of $\ln([M]_0/[M]_t)$ against time. From the fit of the kinetic plot we can get a propagation rate of 4960 s^{-1} (Figure 4). CFStar2 was made similarly, using a 5-arm initiator derived from glucose with 1 equivalent of Cu(I)Br, and 2.1 equivalents of pyridineimine ligand per initiating site. The 8-arm initiator, made from lactose, was used to make the 8-arm star CFStar3 which has also been used in this study. Finally, CFStar4 was formed using a 21-arm initiator, derived from β-cyclodextrin (Figure 5).

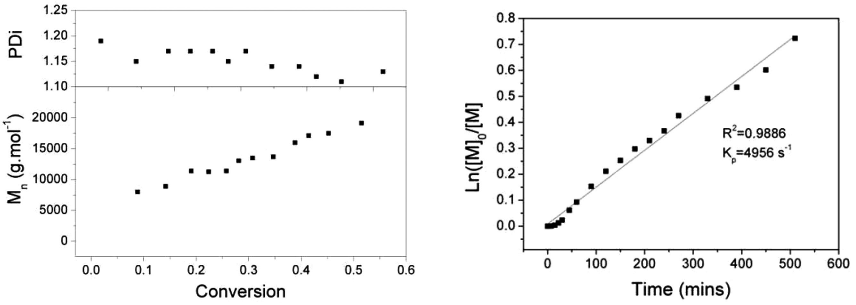

Figure 4. Polymerisation of MMA using 3 arm initiator; (left) Molecular weight, from conventional SEC, evolution with conversion, (right) Plot of $\ln([M]_0/[M]_t)$ against time as a kinetic plot.

Using the universal calibration to analyse the polymers gives a higher M_n, M_w and dispersity than the conventional SEC calibration (Table 1). This is thought to be due to the increased density of the star polymer in solution resulting in larger retention times compared to the linear PMMA calibrants. Increasing the functionality causes an increase in polymer density, which causes greater discrepancies between these two SEC calibration methods. This can be seen in table 1, where the M_n calculated by the 2 methods for the 3 arm star polymer differ by 29%, and the discrepancies increase for the 5, 8 and 21-arm stars which are 52%, 64%, and 89% respectively.

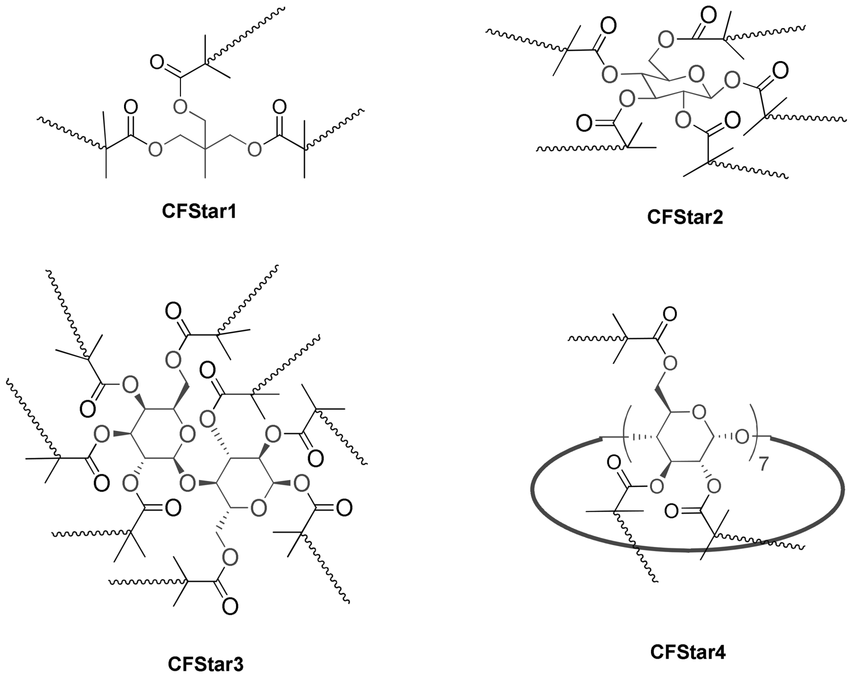

Figure 5. Star polymers synthesised using a core first approach ATRP, using initiators with 3, 5, 8 and 21 initiating sites. 〰 *= PMMA.*

The substantial apparent increase in dispersity between conventional calibration and universal calibration was also of interest. This was assumed at first to be due to an increase in band broadening (*34*); an effect caused by lateral diffusion in 'dead' volume of the SEC, as a competitive process to the steric separation by columns. With the multi detector SEC, the 'dead' volume is increased with the same steric separation, therefore the relative influence is greater than before and band broadening is increased. However, it is also inherent to the universal calibration of branched materials. In conventional calibration, the calibration "curve" should be linear through the area of interest with a gradient, m_{con} and in universal calibration the calibration "curve" will be a straight line with a gradient, m_{univ}. It holds true for any given SEC column that $m_{univ} > m_{con}$ for a branched molecule. The gradient of the calibration curve is a function of the number of arms (branches) therefore the same peak shape and retention will not only have a higher molecular weight, but also greater relative difference between M_n and M_w.

Table 1. SEC results 3, 5, 8 and 21-arm star PMMA by both conventional SEC using a differential refractometer and linear PMMA standards to create a calibration curve, and by universal calibration using a differential refractometer and a four capillary viscometer

Polymer	*Functionality, f*	*Conventional SEC*		*Universal Calibration*	
		M_n (g.mol^{-1})	*Disperisty*	*M_n (g.mol^{-1})*	*Dispersity*
CFStar1	3	15700	1.22	20300	1.51
CFStar2	5	19200	1.22	29200	1.45
CFStar3	8	34800	1.23	57100	1.67
CFStar4	21	21100	1.14	39800	1.29

Dilute Solution Properties of Core First PMMA Stars

It is possible to elucidate information concerning a polymer using multi-detector SEC. Calculation of the radius of gyration contraction factor can provide information about the structure of the polymer in solution. However, it has been shown that for polymers with high dispersity, calculation of the bulk R_g for comparison with linear polymers is ineffective (*35*). Conveniently, SEC provides a method for rapidly fractionating a polymer solution, and the use of MALLS allows the R_g to be determined for each eluting slice. One consideration to be noted is that for a randomly branched polymer, i.e. a star formed by core crosslinking, the fractionation may not be complete. This is because the separation is based on hydrodynamic size. Core cross-linked star polymers can have very similar hydrodynamic volume but have different *f* and therefore different molecular weights. Therefore, it's possible that these polymers will not be separated on the chromatograph and will co-elute. Simon *et al.* showed that this co-elution does not occur for highly branched poly(methyl methacrylate-co-2-(2-methyl-1-triethylsiloxy-1-propenyloxy)-ethyl methacrylate) using light scattering data (*24*). Likewise, Radke *et al.* synthesised comb shaped polymers by anionic polymerisation and characterised them by multi-detector SEC, including viscometry and MALLS (*33*). Using UV tagging of the side chains, they deduced that there was direct correlation between the number of side chains and the SEC elution. Therefore the branching was correlated to the molecular weight. Although local dispersity has not been calculated for the current study, the synthesis technique aims to yield only one architecture, and minimise any co-elution. Therefore, it is assumed that local dispersity in the SEC is low.

Assuming no co-elution, analysis of the core first star polymers by multi detector SEC with MALLS provides information on the absolute M_w and the R_g of the eluting polymer fractions. However, the specific refractive index increment of PMMA in common SEC solvents is particularly low; the dn/dc of PMMA in $CHCl_3$ is 0.056 mL.g^{-1} at T=30 °C and λ_0 = 436 nm (*36*), and in THF is 0.089 mL.g^{-1} at T=25 °C and λ_0 = 436 nm (*37*, *38*). The inverse 2nd power dependence of light scattering on the specific refractive index increment of the analyte (Eq. 7, Eq. 8) hinders its use for PMMA in common SEC solvents at the low concentration needed for successful SEC.

The use of a capillary viscometer in-line on the SEC detector train allows the intrinsic viscosity of each fraction eluting from the SEC to be determined. A Mark-Houwink plot of log(intrinsic viscosity) against log(MW) has been produced for each of the polymers analysed.

A Mark-Houwink plot for the 3 arm star polymer, CFStar1, shows that the intrinsic viscosity increases with molecular weight. The data is more uniform in areas of higher polymer concentration, but becomes more scattered and therefore less reliable at areas of low concentration (Figure 6). CFStar2 has a bimodal MWD due to star-star coupling. This bimodal nature can be seen in the Mark-Houwink plot, which shows the transition from single star to aggregates at approximately 40000 g.mol^{-1}. The single star region shows a shallow increase in intrinsic viscosity over the MWD of the polymer (Figure 6), and the high molecular weight region of the plot shows a step up to higher intrinisic viscosity that coincides with the star-star coupling shoulder on the MWD (Figure 6).

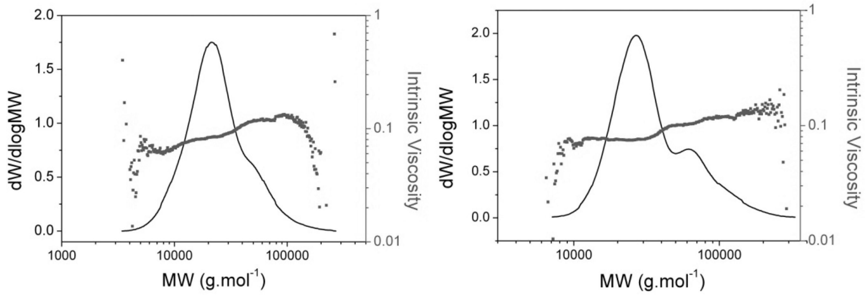

Figure 6. (left) CFStar1, 3 arm star PMMA and (right) CFStar2, 5-arm star PMMA: From multi detector SEC, scatter trace is the Mark-Houwink plot, solid trace is the molecular weight distribution calculated by universal calibration, dW/dlogMW.

The Mark-Houwink plot of CFStar3 (Figure 7) shows a decreasing intrinsic viscosity in the low molecular weight region, followed by a shallow increase in intrinsic viscosity over the remainder of the MWD. The low molecular weight region however is less reliable as the concentration of polymer is very low, therefore only high concentration areas were used for calculating the alpha value of the Mark-Houwink plot.

CFStar4 has a much higher functionality than the other stars synthesised here. It shows an interesting trend, where the intrinsic viscosity of the polymer decreases slightly with increasing MW over the MWD of the polymer (Figure 7). Like CFStar2, CFStar4, has a high molecular weight shoulder due to star-star coupling. The Mark-Houwink plot shows the same step in intrinsic viscosity as CFStar2. As in the 5-arm star, it coincides with the beginning of high molecular weight shoulder of the MWD (Figure 7).

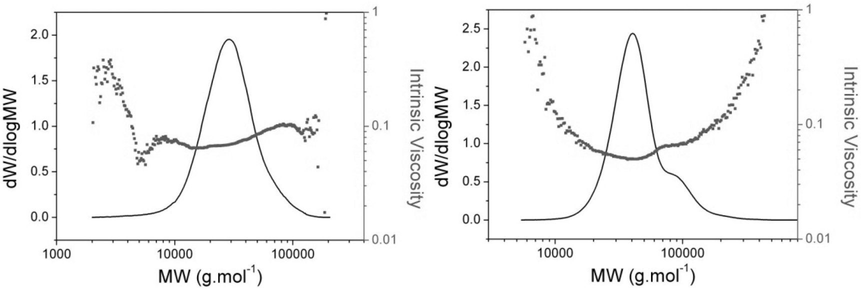

Figure 7. (left) CFStar3, 8-arm star PMMA and (right) CFStar4, 21 arm star PMMA: From multi detector SEC, scatter trace is the Mark-Houwink plot, solid trace is the molecular weight distribution calculated by universal calibration, dW/dlogMW.

An overlay of the Mark-Houwink plots allows for the comparison of the effect molecular weight has on intrinsic viscosity of the various star polymers (Figure 8). The Mark-Houwink plots for the star polymers shift to lower intrinsic viscosity with increasing functionality at the same molecular weights. This is expected as the polymers of the same molecular weight will contract in size with increasing functionality. Unexpectedly, there is also a decrease in the exponent, α, suggesting a change in architecture over the MWD. The decrease in α is more pronounced for the polymers with bimodal MWD, CFStar2 and CFStar4 suggesting that it could be related to the occurrence of star-star coupling. The Mark-Houwink plots provide a lot of relative information about the differences in the star polymers; however, to elucidate any quantifiable data further analysis is required.

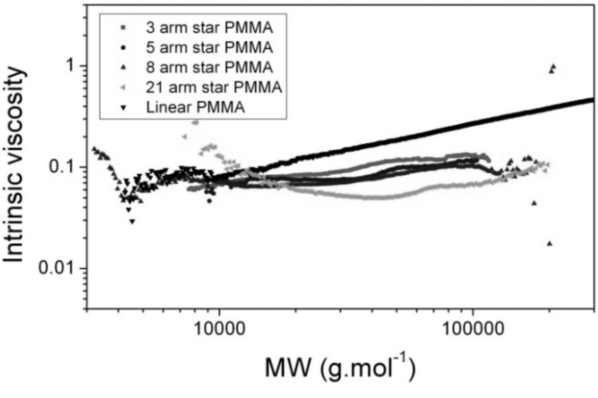

Figure 8. Mark- Houwink plot of linear PMMA, and 3, 5, 8 and 21 arm star PMMA.

Quantifying the Number of Arms on PMMA Core First Star Polymers

The intrinsic viscosity of both the star and the linear polymer at the same molecular weight can be used to determine the intrinsic viscosity shrink ratio, g^I for each integral slice of the MWD (Eq. 10). This shrink ratio can be useful as a further representation of the contraction of the star polymers in solution, however is still only shows the contractions relative to the other stars; to quantify the functionality of the star polymers, it is necessary to convert gI to the radius of gyration contraction factor, g. This was carried out using a relationship derived from experiment in the literature (Eq. 11), using the parameters utilised by Robello *et al.* (*30*), where a = 0.2624, b= 1.088 and c = 0.6087.

The functionality, *f*, was determined using Zimm and Stockmayer's quadratic solution for relating g and *f* for regular arm stars (Eq. 12) for a 3 arm star, CFStar1 (Figure 9). As expected, the data is seen to be most consistent at areas of high concentration of polymer close to the M_p on the MWD. The functionality, *f*, increases with increasing molecular weight, from 3 at low MW to 5 at high MW. At the M_p the functionality is approximately 4, 1 higher than the number of initiating sites on the multifunctional initiator. This could be accounted for by the star-star coupling which is evidenced by a high molecular weight shoulder on the MWD (Figure 9).

Using the analogous calculations to those used for CFStar1, the functionality was quantified for each slice of the MWD of CFStar2 (Figure 9). The polymer was synthesised using a 5-arm initiator, therefore the functionality of the PMMA polymer should be quantified to be close to 5. The functionality is seen to increase with the molecular weight, with the functionality at M_p quantified as 6. The increase in functionality over the MWD has been seen before by Robello *et al.* who report it to be due to imperfect initiator efficiency resulting in lower than expected functionality and star-star coupling resulting in higher than expected functionality (*30*).

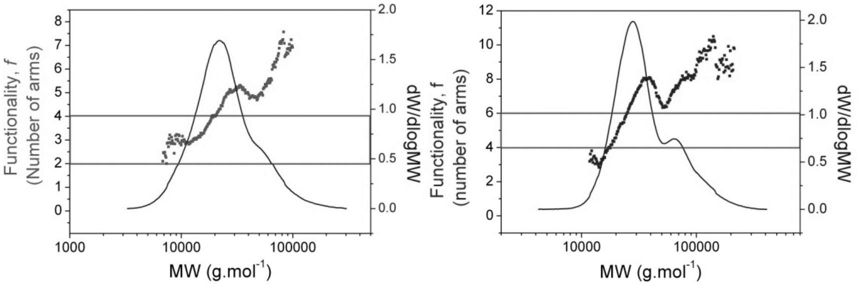

Figure 9. (left) PMMA 3-arm star polymer and (right) PMMA 5-arm star polymer: The estimated functionality, f, plotted over the distribution of the polymer, estimated from the radius of gyration contraction factor, g. The Zimm and Stockmayer solution for regular arm star polymers was used to relate g to f. The box shows the functionality of the initiator ±1.

The functionality of the star PMMA made using an 8 arm initiator, CFStar3, has also been quantified (Figure 10). The functionality is seen to change from 4 to 14 over the MWD, indicating that the initiator is inefficient at initiating every site, and that star-star coupling is occurring. Interestingly, there is no shoulder on the polymer to indicate large quantities of star-star coupling.

It was expected that CFStar4 would have a much higher functionality than the other PMMA star polymers as a 21-arm initiator was used in the synthesis. Using Zimm Stockmayer theory (Eq. 12) to quantify the functionality shows a wide range of functionality over the MWD of the polymer; from 4 to 27. The low functionality calculated at the lower MW of the MWD suggests that the initiator efficiency for each initiating site in the multi functional initiator is very variable, or termination is occurring early on in the reaction to leave low MW dead arms on the stars. As mentioned earlier, there is a high MW shoulder on the MWD of CFStar4 evidencing star-star coupling. This can explain why the functionality exceeds the maximum of 21, related to the number of initiating sites on the star polymer.

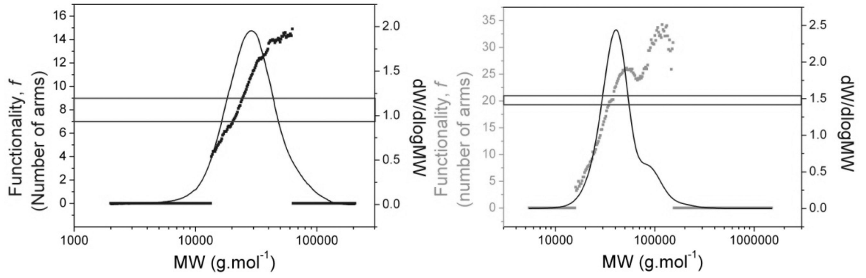

Figure 10. (left) PMMA 8-arm star polymer and (right) PMMA 21-arm star polymer: The estimated functionality, f, plotted over the distribution of the polymer, estimated from the radius of gyration contraction factor, g. The Zimm and Stockmayer solution for regular arm star polymers was used to relate g to f. The box shows the functionality of the initiator ±1.

Conclusion

Core first stars have been synthesised by polymerisation of MMA using different multifunctional initiators. These star polymers have been analysed using multi-detector SEC using a universal calibration and conventional SEC. Universal calibration was seen to estimate the MW more accurately than conventional SEC.

Although star-star coupling was seen to occur in the reaction, this was minimised by terminating the reactions at low conversions, below 50%. Interestingly, there is a visible change in the Mark-Houwink plots for these two polymer architectures, with a step up in the intrinsic viscosity. However, there is no evidence of a decrease in the gradient, α, which would be expected with coupling due to increased polymer density in solution. Comparison of the plots shows that at the same MW on the MWD of the polymers, the intrinsic viscosity is lower for a star with more arms.

Each star polymer's functionality was determined using their intrinsic viscosity contraction factor (Eq. 10) and Zimm Stockmayer theory (Eq. 12), and seen to agree with the functionality of the core initiator at the M_p. At the highest concentration at the peak molecular weight, M_p, the functionality is approximately 4 for the 3-arm star (Figure 9), approximately 6 for the 5-arm star (Figure 9) approximately 8 for the 8-arm star (Figure 10), and approximately 21 for the 21-arm star (Figure 10). The determination of functionality using this technique uses a number of approximations and assumptions, however the error of ± 1 at the M_p was in agreement with a previous study of PMMA core first star polymers by Robello and coworkers (*30*).

The functionality of the stars was seen to change over their MWD, which is thought to be because of initiator efficiency, and termination, and star-star coupling occurring in the reaction. This could cause co-elution of star polymers and coupled stars with the same hydrodynamic volume, and increase local SEC dispersity.

Acknowledgments

Some equipment used in this research was supported by the Innovative Uses for Advanced Materials in the Modern World (AM2), with support from Advantage West Midlands (AWM) and part funded by the European Regional Development Fund (ERDF). The authors thank Lubrizol (JAB) for funding. CRB is currently a Science City Research Fellow and DMH a Royal Society/Wolfson Fellow.

References

1. Moore, J. C. *J. Polym. Sci., Part A: Gen. Pap.* **1964**, *2*, 835–843.
2. Moore, J. C.; Hendrickson, J. G. *J. Polym. Sci., Part C: Polym. Symp.* **1965**, *8*, 233–241.
3. Moore, J. C. *Sep. Sci.* **1970**, *5*, 723–730.
4. Striegel, A. M.; Yau, W. W.; Kirkland, J. J.; Bly, D. D. In *Modern Size-Exclusion Liquid Chromatography*; John Wiley & Sons, Inc.: Hoboken, NJ, 2009, pp 18−48.
5. Manfred, J. R.; Cantow, R. S. P.; Johnson, Julian F. *J. Polym. Sci., Part A: Polym. Chem.* **1967**, *5*, 987–991.
6. Grubisic, Z.; Benoit, H.; Rempp, P. *J. Polym. Sci., Polym. Lett. Ed.* **1967**, *5*, 753–759.
7. Saunders, G. In *LC-GC Europe*; Advanstar Communications, Inc.: New York, 2004; Vol. 17, pp 650−655.
8. Castignolles, P.; Graf, R.; Parkinson, M.; Wilhelm, M.; Gaborieau, M. *Polymer* **2009**, *50*, 2373–2383.
9. Guillaneuf, Y.; Castignolles, P. *J. Polym. Sci., Part A: Polym. Chem.* **2008**, *46*, 897–911.
10. Liu, P.; Landry, E.; Ye, Z.; Joly, H.; Wang, W.-J.; Li, B.-G. *Macromolecules* **2011**, *44*, 4125–4139.
11. Netopilík, M.; Kratochvíl, P. *Polymer* **2003**, *44*, 3431–3436.

12. Saunders, G.; Cormack, P. A. G.; Graham, S.; Sherrington, D. C. *Macromolecules* **2005**, *38*, 6418–6422.
13. Fazeli, N.; Mohammadi, N.; Taromi, F. A. *Polym. Test.* **2004**, *23*, 431–435.
14. Samay, G.; K., M.; Podescaronva, J. *Angew. Makromol. Chem.* **1978**, *72*, 185–198.
15. Mourey, T. H.; Miller, S. M.; Balke, S. T. *J. Liq. Chromatogr. Relat. Technol.* **1990**, *13*, 435–452.
16. Zimm, B. H. *J. Chem. Phys.* **1948**, *16*, 1093–1099.
17. Roovers, J.; Burchard, W. In *Branched Polymers II*; Springer: Berlin/Heidelberg, 1999; Vol. 143, pp 113−194.
18. Held, D.; Müller, A. H. E. *Macromol. Symp.* **2000**, *157*, 225–238.
19. Zimm, B. H.; Stockmayer, W. H. *J. Chem. Phys.* **1949**, *17*, 1301–1314.
20. Jackson, C.; Chen, Y.-J.; Mays, J. W. *J. Appl. Polym. Sci.* **1996**, *59*, 179–188.
21. Haney, M. A. *J. Appl. Polym. Sci.* **1985**, *30*, 3037–3049.
22. Haney, M. A. *J. Appl. Polym. Sci.* **1985**, *30*, 3023–3036.
23. Roovers, J.; Zhou, L. L.; Toporowski, P. M.; van der Zwan, M.; Iatrou, H.; Hadjichristidis, N. *Macromolecules* **1993**, *26*, 4324–4331.
24. Simon, P. F. W.; Müller, A. H. E.; Pakula, T. *Macromolecules* **2001**, *34*, 1677–1684.
25. Bruno, H.; Zimm, R. W. K. *J. Polym. Sci.* **1959**, *37*, 19–42.
26. Lesec, J.; Millequant, M. *Int. J. Polym. Anal. Charact.* **1996**, *2*, 305–321.
27. Balke, S. T.; Mourey, T. H.; Robello, D. R.; Davis, T. A.; Kraus, A.; Skonieczny, K. *J. Appl. Polym. Sci.* **2002**, *85*, 552–570.
28. Flory, P. J. *Principles of Polymer Chemistry*; 16 ed.; Cornell University Press: Ithaca, 1953.
29. Grest, G. S.; Fetters, L. J.; Huang, J. S.; Richter, D. *Adv. Chem. Phys.* **1996**, *94*, 67.
30. Robello, D. R.; Andre, Alix; McCovick, T. A.; Mourey, T. H. *Macromolecules* **2002**, *35*, 9334–9344.
31. Weissmuller, M.; Burchard, W. *Polym. Int.* **1997**, *44*, 380–390.
32. Burchard, W. *Adv. Polym. Sci.* **1999**, *143*, 113.
33. Radke, W.; Müller, A. H. E. *Macromolecules* **2005**, *38*, 3949–3960.
34. Striegel, A. M.; Yau, W. W.; Kirkland, J. J.; Bly, D. D. *Modern Size-Exclusion Liquid Chromatography*; 2nd ed.; Wiley: Hoboken, NJ, 2009.
35. Kilb, R. W. *J. Polym. Sci.* **1959**, *38*, 403–415.
36. Kisakürek, D.; Baysal, B. M. *Polymer* **1984**, *25*, 693–697.
37. Bodmann, O. *Makromol. Chem.* **1969**, *122*, 196–198.
38. Cantow, H. J.; Bodmann, O. *Z. Phys. Chem. (Frankfurt)* **1955**, *3*, 65–69.

Downloaded by OHIO STATE UNIV LIBRARIES on June 1, 2012 | http://pubs.acs.org
Publication Date (Web): March 20, 2012 | doi: 10.1021/bk-2012-1101.ch007

Chapter 7

Synthesis of ω-End Functionalized Polymers through Tellurium-Metal Transmetallation Reaction

Eiichi Kayahara and Shigeru Yamago*

Institute for Chemical Research, Kyoto University,
Uji, Kyoto 611-0011, Japan, and
CREST, Japan Science and Technology Agency, Tokyo, Japan
***E-mail: yamago@scl.kyoto-u.ac.jp**

Synthesis of ω-end functionalized polymers via tellurium-metal transmetallation reaction was examined. The transmetallation reaction of poly(methyl methacrylate) (PMMA), poly(*n*-butyl acrylate) (PBA), and poly(*N*-isopropylacrylamide) (PNIPAM) bearing organotellurium ω-polymer end groups, which were prepared by organotellurium-mediated living radical polymerization (TERP), with organometallic reagent proceeded quantitatively without affecting polar functional groups in the polymers. Subsequent trapping of the resulting anionic species with electrophiles afforded the desired ω-end functionalized polymers. ^{1}H NMR, GPC, and MALDI TOF MS analyses revealed the quantitative transformation while keeping the controlled molecular weights and narrow molecular weight distributions of the starting polymers.

In Progress in Controlled Radical Polymerization: Materials and Applications; Matyjaszewski, K., et al.;
ACS Symposium Series; American Chemical Society: Washington, DC, 2012.

Downloaded by OHIO STATE UNIV LIBRARIES on June 1, 2012 | http://pubs.acs.org
Publication Date (Web): March 20, 2012 | doi: 10.1021/bk-2012-1101.ch007

Introduction

Synthesis of structurally well-defined polymers with controlled molecular weights, molecular weight distributions, and chain-end functionalities have attracted great deal of attention because such polymers would enhance the ability of macromolecular engineering leading to various polymer materials with new and/or improved properties (*1*). They are conventionally synthesized by transformations of living polymer-end prepared by living anionic (*2*) and cationic (*3*) polymerizations. However, requirement of stringent polymerization conditions and low functional group compatibilities limit the synthetic utilities of these methods. With the development of living radical polymerization (LRP) which enables the precise control of molecular weight and its distribution in radical polymerization (*4–9*), applications of LRP to the end-functionalized polymers have been increasing due to its high versatility in polymerizable monomer families and tolerance to functional groups. Polymer-end carbanion species would be an attractive species for the end-functionalization among various reactive intermediates, as carbanions occupy a central position in organic synthesis (*10*, *11*). However, due to the low tolerance of carbanions to polar functional groups which are present in polymers prepared by LRP, the synthetic utility of the polymer-end carbanions is unclear.

We have already developed organotellurium- (*12–22*), organostibine- (*23–26*), and organobismuthine- (*27*, *28*) mediated LRP (TERP, SBRP, and BIRP, respectively) (*9*, *29*). Among various LRP methods so far developed (*4–9*), they are one of the most synthetically valuable methods (*30*, *31*) as exemplified in high versatility of monomer families, high compatibility towards functional groups and solvents (*17*, *32–35*), and ease of the living-end transformation for the synthesis of block copolymers (*18*, *36–38*) and end-functionalized polymers (*25*, *39–41*). We have also reported that organostibines and organobismuthines are highly reactive to stibine-metal and bismuthine-metal transmetallation reaction, respectively, and that the reaction at the polymer ends prepared by SBRP and BIRP proceeded selectively in the presence of polar functional groups in the polymer backbone (*41*). Furthermore, trapping of the resulting carbanions gave various end-functionalized polymers with quantitative end-group fidelity. These results prompted us to investigate the transformation of organotellanyl polymer-end group prepared by TERP to anionic species by tellurium-metal transmetallation reaction. The reactivity of organotellurium compounds towards the transmetallation reaction is very similar to organostibine and organobismuthine compounds (*41*), but transmetallation in the presence of many of polar functional groups has never be tested (*31*). We report here the chemoselective tellurium-metal transmetallation reaction at the polymer-end group for polymers prepared by TERP, giving ω-end functionalized polymers with highly controlled and defined structure in terms of molecular weight, molecular weight distribution, and end group functionality (Scheme 1).

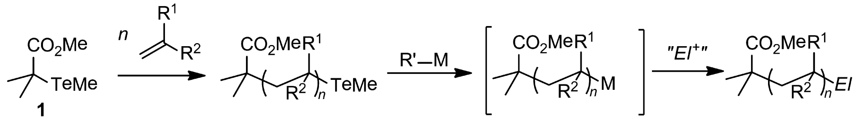

Scheme 1. Synthesis of ω-end functionalized polymer via tellurium-metal transmetallation reaction.

Downloaded by OHIO STATE UNIV LIBRARIES on June 1, 2012 | http://pubs.acs.org
Publication Date (Web): March 20, 2012 | doi: 10.1021/bk-2012-1101.ch007

Results and Discussion

Tellurium-Metal Transmetallation Reaction at ω-Polymer Ends

The generation of carbanion from ω-methyltellanyl group of poly(methyl methacrylate) (PMMA) **2** prepared by TERP was initially examined (Table 1). Thus, **2** (M_n = 3,300, M_w/M_n = 1.19, where M_n and M_w are the number-average and weight average molecular weight, respectively, and M_w/M_n represents molecular weight distribution), which was prepared in 99% yield from methyl 2-methyltellanyl-2-methylpropionate (**1**) (*42*) and MMA (30 equiv) by heating at 80 °C for 12 h in the presence of $(TeMe)_2$ (1.0 equiv) (*13*). Then, it was treated with *n*-BuLi (1.1 equiv) in THF at -78 °C for 0.5 h, and the resulting anionic species was quenched by the addition of DCl (2.0 equiv) in D_2O. Extractive workup and precipitation from hexane gave the ω-end deuterated PMMA **3a** with M_n = 3,300 and M_w/M_n = 1.18 as a white powder (Table 1, entry 1). The similarity of the molecular weight and molecular weight distribution (MWD) before and after the transmetallation reaction indicates that no apparent decomposition occurred during the transmetallation reaction. Matrix-assisted laser-desorption ionization time-of-flight mass (MALDI-TOF MS) spectroscopy showed only the series of peaks possessing the molecular ion masses of **3a** were observed (Figure 1). The ^{2}H NMR spectrum of **3a** showed characteristic signal at 2.46 ppm as a broad singlet which can be assigned as the deuterium at α to the ester group. All these results clearly revealed the quantitative generation and selective formation of the anionic species from **2**, respectively. It is worth mentioning that the transmetallation reaction exclusively occurs at the organotellurium polymer end group despite of the existence of excess number of ester groups in **2**. All these results clearly indicated the high reactivity of organotellurium compounds toward the transmetallation reaction.

Transmetallation of **2** with zinc reagent, *t*-Bu_4ZnLi_2 (*43*), and magnesium reagent, *i*-PrMgCl·LiCl (*44*), were also effective for the generation of the corresponding carbanion species. End deuterated **3a** formed quantitatively after treatment of the anionic species with DCl/D_2O (entries 2 and 3).

Downloaded by OHIO STATE UNIV LIBRARIES on June 1, 2012 | http://pubs.acs.org
Publication Date (Web): March 20, 2012 | doi: 10.1021/bk-2012-1101.ch007

Table 1. Synthesis of ω-end functionalized PMMA

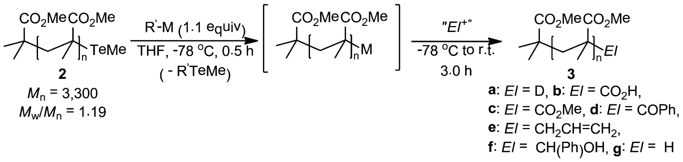
CO2MeCO2Me
TeMe
n
2
Mn = 3,300
Mw/Mn = 1.19
R'-M (1.1 equiv)
THF, -78 °C, 0.5 h
(- R'TeMe)
CO2MeCO2Me
M
n
"El+"
-78 °C to r.t.
3.0 h
CO2MeCO2Me
El
n
3
a: El = D, b: El = CO2H,
c: El = CO2Me, d: El = COPh,
e: El = CH2CH=CH2,
f: El = CH(Ph)OH, g: El = H

Entry	R'-M	Electrophile (equiv)	Product	$M_n/(M_w/M_n)$	Incorp. (%)[a]
1	*n*-BuLi	DCl/D_2O (2.0)	**3a**	3,300/1.18	>99
2	*t*-Bu_4ZnLi_2	DCl/D_2O (2.0)	**3a**	3,300/1.17	>99
3	*i*-PrMgCl · LiCl	DCl/D_2O (2.0)	**3a**	3,200/1.19	>99
4	*n*-BuLi	CO_2 (excess)	**3c**[b]	3,500/1.17	>99 (94)
5	*n*-BuLi	PhCOCl (5.0)	**3d**	3,500/1.18	98 (92)
6	*n*-BuLi	Allyl Iodide (5.0)	**3e**	3,400/1.18	98 (91)
7	*n*-BuLi	PhCHO (5.0)	**4**	3,100/1.20	94[c]

Downloaded by OHIO STATE UNIV LIBRARIES on June 1, 2012 | http://pubs.acs.org
Publication Date (Web): March 20, 2012 | doi: 10.1021/bk-2012-1101.ch007

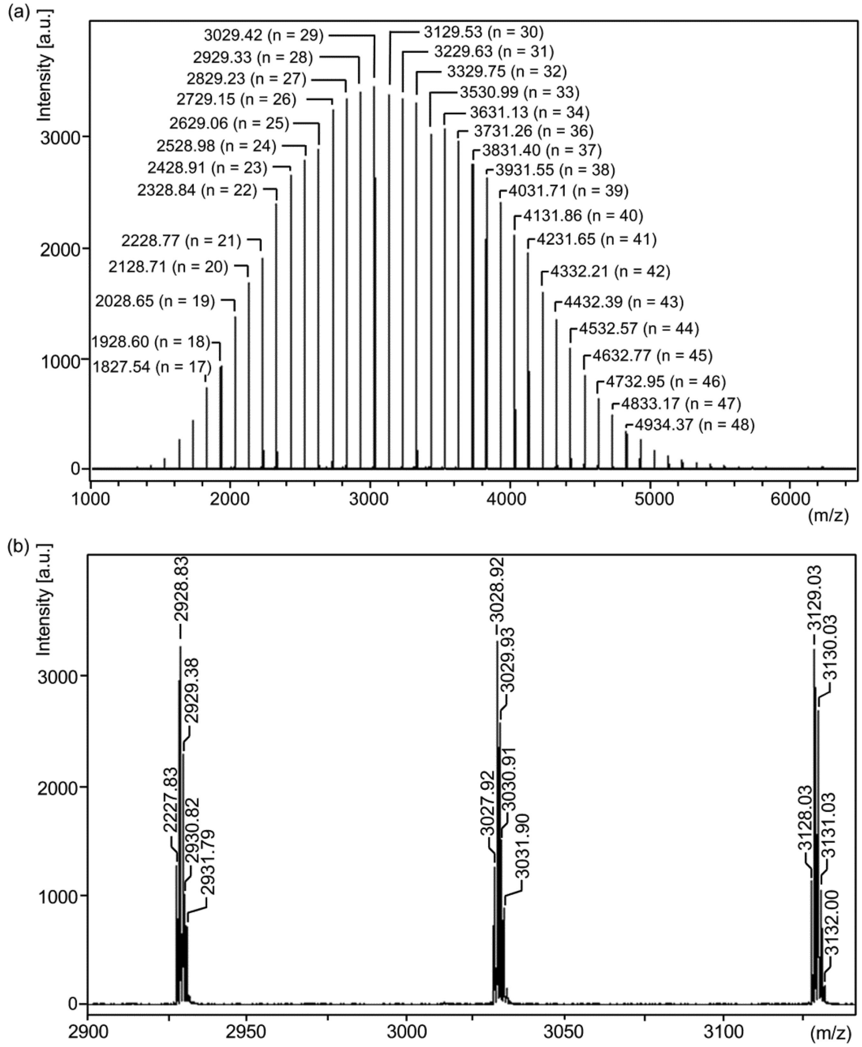

*Figure 1. MALDI-TOF MS spectra of ω-deuterated PMMA **3a**. A major series of peaks as indicated by average mass number in TOF MS spectrum are observed as sodium ion adduct $(M + Na)^+$.*

Downloaded by OHIO STATE UNIV LIBRARIES on June 1, 2012 | http://pubs.acs.org
Publication Date (Web): March 20, 2012 | doi: 10.1021/bk-2012-1101.ch007

Application to the Synthesis of ω-End Functionalized Polymers

The current method was successfully applied to the synthesis of ω-end functionalized PMMA by employing various electrophiles after the transmetallation reaction. Thus, treatment of the anionic species generated from **2** and *n*-BuLi with excess CO_2 afforded ω-carboxylic acid PMMA **3b**, which was fully characterized after converting to the corresponding methyl ester **3c** (M_n = 3,500 M_w/M_n = 1.17, entry 4). The ^1H NMR and MALDI-TOF MS analyses indicated a quantitative conversion from **2** to **3c**. The anionic species was also trapped with benzoyl chloride (5 equiv) and allyl iodide (5 equiv) giving the corresponding ω-end functionalized PMMA **3d** (M_n = 3,500, M_w/M_n = 1.18) and **3e** (M_n = 3,400, M_w/M_n = 1.18), respectively (entries 5 and 6). The quantitative formation of these ω-end functionalized polymers was unambiguously confirmed by using ^1H NMR and MALDI-TOF MS analyses (*45*). When benzaldehyde (5 equiv) was employed as an electrophile, PMMA **4** bearing δ-lactone was obtained as a major product (Chart 1), which was formed by an intramolecular cyclization of the initially formed addition product (entry 7). MALDI-TOF MS analysis indicated the formation of two minor products, which were assigned to PMMA **3f** having β-hydroxy ester structure and end-protonated PMMA **3g** (**4**/**3f**/**3g** = 94:5:1). A minor alcohol **3f** was quantitatively transformed into **4** upon treatment with trifluoroacetic acid. The molecular weight, MWD, and functionalities of the pendant group were preserved during the transformation in all cases. These results clearly reveal the high efficiency and versatility of polymer-end anionic species in synthesizing varieties of ω-end functionalized PMMAs.

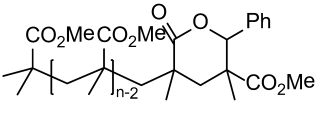

4

Chart 1

Downloaded by OHIO STATE UNIV LIBRARIES on June 1, 2012 | http://pubs.acs.org
Publication Date (Web): March 20, 2012 | doi: 10.1021/bk-2012-1101.ch007

The scope of the transmetallation reaction was further examined by employing polyacrylates and polyacrylamides, which possessing acidic hydrogen in the main chain as well as the side chain. *t*BuZnLi$_2$ was used as the organometallic reagent, because we have already clarified that lithium species generated at the polyacrylate polymer-end underwent a side reaction involving an intramolecular condensation. Thus, poly(*n*-butyl acrylate) (PBA) **5** (M_n = 4,100, M_w/M_n = 1.11) prepared by TERP was treated with *t*-Bu$_4$ZnLi$_2$ (1.1 equiv) in THF at -78 °C followed by the addition of benzoyl chloride (5 equiv) gave desired ω-benzoyl PBA **6** (M_n = 4,200, M_w/M_n = 1.12) (Scheme 2a). TOF MS and NMR spectra clearly revealed the quantitative transformation of ω-polymer end group.

Poly(*N*-isopropylacrylamide) (PNIPAM) **7** (M_n = 3,100, M_w/M_n = 1.09) prepared by TERP was also transmetallated by *t*-Bu$_4$ZnLi$_2$ (1.1 equiv) in DMF at -60 °C for 0.5 h without protection of the amide proton. Reaction of the resulting anionic species with benzoyl chloride (5.0 equiv) gave the desired ω-benzoyl PNIPAM **8** (M_n = 3,200, M_w/M_n = 1.10) in quantitative transformation (Scheme 2b). Trapping of the anionic species by 5-iodo-1-pentyne (5.0 equiv), on the other hand, afforded end-alkynylated PNIPAM **9** (M_n = 3,100, M_w/M_n = 1.08) in nearly quantitatively (Scheme 2c). The desired products formed in quantitatively (>99%) as judged by MALDI-TOF MS analysis (Figure 2). The alkyne group in **9** would be used to conjugate varieties of functionalities by the click reaction (*46*, *47*). Since PNIPAM is a thermosensitive polymer and has a lower critical solution temperature in water (*48*), the conjugated tailor-made polymers would find various applications.

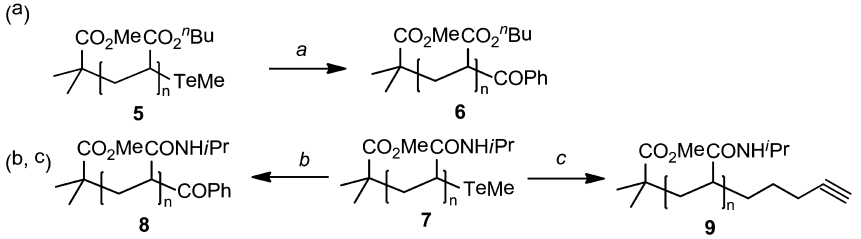

Scheme 2. Functionalization of PBA and PNIPAM. Reaction conditions; a) 1. tBu$_4$ZnLi$_2$ (1.1 equiv), THF, –78 °C, 0.5 h, 2. PhCOCl (5 equiv), –78 °C to rt, 3 h. b) 1. tBu$_4$ZnLi$_2$ (1.1 equiv), DMF, –60 °C, 0.5 h, 2. PhCOCl (5 equiv), –60 °C to rt, 3 h. c) 1. tBu$_4$ZnLi$_2$ (1.1 equiv), DMF, –60 °C, 0.5 h, 2. HC≡CH(CH2)$_3$I (5 equiv), –60 °C to rt, 3 h.

Downloaded by OHIO STATE UNIV LIBRARIES on June 1, 2012 | http://pubs.acs.org
Publication Date (Web): March 20, 2012 | doi: 10.1021/bk-2012-1101.ch007

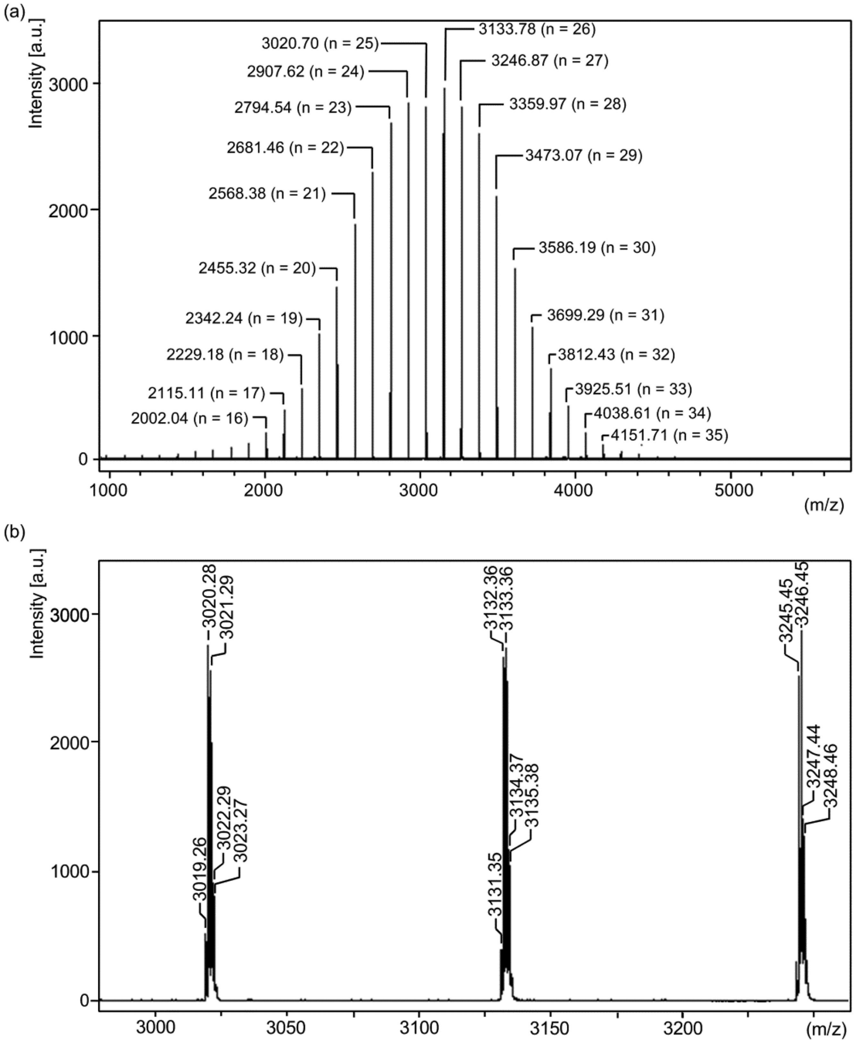

*Figure 2. MALDI-TOF MS spectra of ω-alkynylated PNIPAM **9**. A major series of peaks as indicated by average mass number in TOF MS spectrum are observed as sodium ion adduct (M + Na)$^+$.*

Conclusion

The precise synthesis of ω-end functionalized polymers through tellurium-metal transmetallation reaction was achieved. Due to the high reactivity of organotellurium compounds, transmetallation reaction occurred highly chemoselectivity even in the presence of various polar functional groups in poly(meth)acrylates and polyacrylamides. Furthermore, the reaction of the resulting anions with various electrophiles proceeded quantitatively giving structurally well controlled polymers with defined ω-polymer end groups. We believe that this work combined with the high versatility of TERP opens new possibilities in providing varieties of functional polymeric materials.

Downloaded by OHIO STATE UNIV LIBRARIES on June 1, 2012 | http://pubs.acs.org
Publication Date (Web): March 20, 2012 | doi: 10.1021/bk-2012-1101.ch007

Experimental Section

General

All reaction conditions dealing with air- and moisture sensitive compounds were carried out in a dry reaction vessel under nitrogen atmosphere. ^1H NMR (400 MHz) spectra was measured for a $CDCl_3$ or CD_2Cl_2 solution of a sample and are reported in parts per million (δ) from internal tetramethylsilane or residual solvent peak. MALDI-TOF MS spectrum was obtained on a spectrometer in the positive reflection mode and at 20 kV acceleration voltage. Samples were prepared from THF solution by mixing sample (5 mg/mL), dithranol (10 mg/mL), and sodium trifluoroacetate (5 mg/mL) in a ratio of 1:2:1. The GPC was performed with two linearly connected polystyrene mixed gel columns, which were calibrated with PMMA standards. Analyses were made using chloroform as an eluant for PMMA and PBA samples with a flow rate of 0.3 mL/min and 0.01 mol/L lithium chloride solution of DMF as an eluant for PNIPAM sample with a flow rate of 1.0 mL/min with a refractive-index detector at 40 °C.

Materials

Unless otherwise noted, chemicals obtained from commercial sources were used without purification. THF was distilled from sodium benzophenone ketyl and stored under nitrogen atmosphere. DMF was distilled successively over P_2O_5 and calcium hydride under reduced pressure and stored over molecular sieves. MMA and BA were washed with 5% aqueous sodium hydroxide solution and were distilled over calcium hydride under reduced pressure and stored under nitrogen atmosphere. NIPAM and dimethyl 2,2′-azobis(2-methylpropionate) (V-601) were recrystallized from hexane and cold methanol, respectively, and were stored under nitrogen. Methyl 2-methyltellanyl-2-methylpropionate **1** (*42*) and 5-iodo-1-pentyne (*49*) were prepared as described. *n*-BuLi in hexane and *t*-BuLi in pentane were titrated before use. *t*-Bu_4ZnLi_2 (*43*) and *i*-PrMgCl·LiCl (*44*) were prepared as reported and used immediately after preparation.

Downloaded by OHIO STATE UNIV LIBRARIES on June 1, 2012 | http://pubs.acs.org
Publication Date (Web): March 20, 2012 | doi: 10.1021/bk-2012-1101.ch007

Typical Procedure for Synthesis of ω−Deuterated PMMA 3a (Table 1, Entry 1)

A solution of **2** (M_n = 3,300, M_w/M_n = 1.19, 165.0 mg, 0.050 mmol) in THF (1.0 mL) was treated with *n*-BuLi (36 μL , 1.51 M solution in hexane, 0.055 mmol) at -78°C. After stirring for 0.5 h at this temperature, DCl (16 μL, 6.49 M in D_2O, 0.10 mmol) was added by a syringe. The resulting mixture was stirred for 1 h at this temperature, and was slowly warmed to room temperature over 2 h. The reaction mixture was quenched with saturated aqueous $NaHCO_3$ solution (0.50 mL), and was extracted with $CHCl_3$ (1.00 mL x 3). The organic layer was washed with saturated aqueous NaCl solution, dried over $MgSO_4$, filtered and concentrated under reduced pressure. The residue was dissolved in $CHCl_3$ (1 mL) and poured into vigorously stirred hexane (50 mL). The precipitated polymer was collected by suction and was dried under vacuum at 40 °C to give **3a** in 96% (155.2 mg) with M_n = 3,300 and M_w/M_n = 1.18. Incorporation of ω-deuterium was confirmed by ^{2}H NMR (δ = 2.46 ppm) and MALDI-TOF MS analyses (Figure 1).

Transmetallation of **2** with *t*-Bu_4ZnLi_2 or *i*-PrMgCl·LiCl was also carried out according to the above general procedure to give **3a**.

General Procedure for the Synthesis of ω-End Functionalized Polymers: ω-Carboxylic Acid PMMA 3b and ω-Methylester PMMA 3c (Table 1, Entry 4)

A solution of **2** (204.5 mg, 0.062 mmol) in THF (3.0 mL) was treated with *n*BuLi (45.0 μL, 1.51 M solution in hexane, 0.068 mmol) at -78°C. After stirring for 0.5 h at this temperature, to this solution was bubbled into carbon dioxide for 5 min. The resulting mixture was stirred for 1 h at this temperature, and was slowly warmed to room temperature over 2 h. Extractive work up and purification afforded ω-carboxylic acid PMMA **3b** in 94% (192.2 mg). A solution of **3b** (99.1 mg, 0.030 mmol) in MeOH/Toluene (0.5/0.5 mL) was treated with $TMSCHN_2$ solution (30.0 μL, 2.0 M solution in Et_2O, 0.060 mmol) at room temperature. After stirring for 2.0 h at this temperature, the reaction mixture was quenched with acetic acid. Extractive work up and purification afforded **3c** in 91% (90.2 mg) with M_n = 3500 and M_w/M_n = 1.17. Incorporation ratio of methylester group was determined to be 94 and >99% by ^{1}H NMR and MALDI-TOF MS analyses, respectively (Figure 3).

ω-Benzoyl PMMA 3d (Table 1, Entry 5)

The reaction of **2** (204.4 mg, 0.062 mmol), *n*BuLi (45.0 μL, 1.51 M solution in hexane, 0.068 mmol), and benzoyl chloride (35.4 μL, 0.305 mmol) in THF (1.5 mL) afforded **3d** in 94% isolated yield (189.9 mg) with M_n = 3,500 and M_w/M_n = 1.18. Incorporation of benzoyl group determined by ^{1}H NMR and MALDI-TOF MS (Figure 4) was 92% and 98%, respectively.

Downloaded by OHIO STATE UNIV LIBRARIES on June 1, 2012 | http://pubs.acs.org
Publication Date (Web): March 20, 2012 | doi: 10.1021/bk-2012-1101.ch007

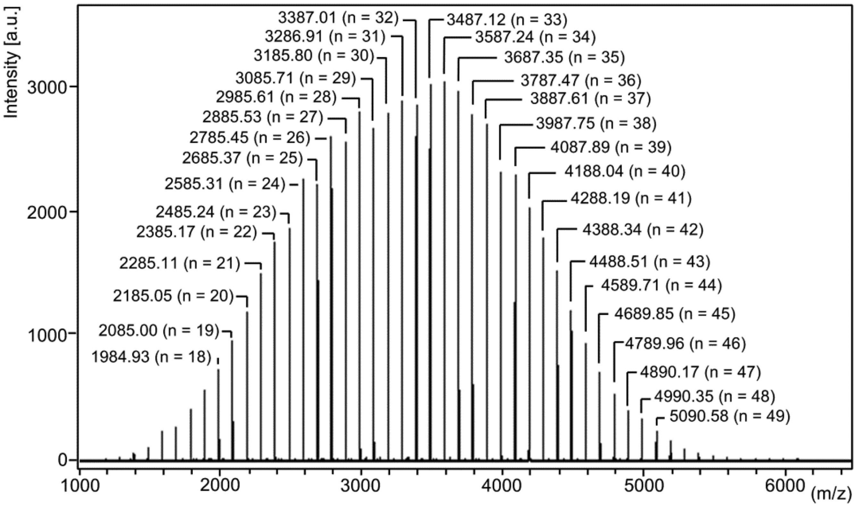

*Figure 3. MALDI-TOF MS spectra of ω-methylester PMMA **3c**. A major series of peaks as indicated by average mass number in TOF MS spectrum are observed as sodium ion adduct (M + Na)$^+$.*

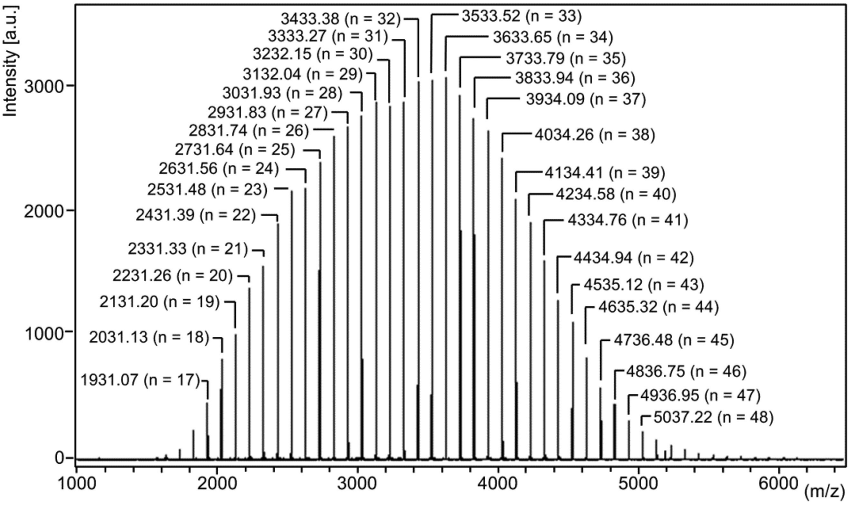

*Figure 4. MALDI-TOF MS spectra of **3d**. A major series of peaks as indicated by average mass number in TOF MS spectrum are observed as sodium ion adduct (M + Na)$^+$.*

Downloaded by OHIO STATE UNIV LIBRARIES on June 1, 2012 | http://pubs.acs.org
Publication Date (Web): March 20, 2012 | doi: 10.1021/bk-2012-1101.ch007

ω-Allyl PMMA 3e (Table 1, Entry 6)

The reaction of **2** (212.4 mg, 0.064 mmol), *n*BuLi (46.9 μL, 1.51 M solution in hexane, 0.071 mmol), and allyl iodide (29.2 μL, 0.320 mmol) in THF (1.5 mL) afforded **3e** in 92% isolated yield (195.4 mg) with M_n = 3,300 and M_w/M_n = 1.19. Incorporation of the allyl group determined by ^{1}H NMR and MALDI-TOF MS (Figure 5) was 91% and 98%, respectively.

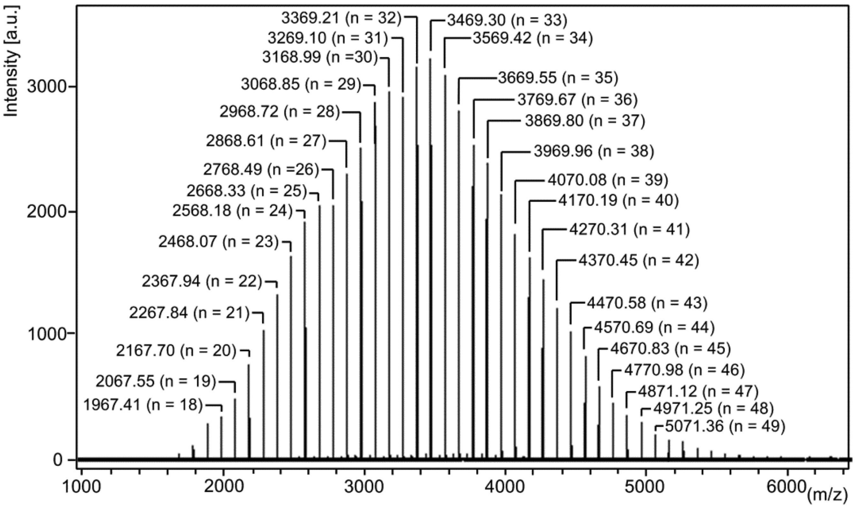

*Figure 5. MALDI-TOF MS spectra of **3e**. A major series of peaks as indicated by average mass number in TOF MS spectrum are observed as sodium ion adduct (M + Na)$^+$.*

ω-(δ-Lacton)-Substituted PMMA 4 (Table 1, Entry 7)

The reaction of **2** (197.8 mg, 0.060 mmol), *n*BuLi (43.7 μL, 1.51 M solution in hexane, 0.066 mmol), and benzaldehyde (30.4 μL, 0.300 mmol) in THF (1.5 mL) afforded a mixture of **4**, **3f**, and **3g** in 98% combined yields (193.8 mg) with M_n = 3,300 and M_w/M_n = 1.19 in a ratio of 94:5:1 by the MALDI-TOF MS analysis. Treatment of the polymer mixture (**4**/**3f**/**3g** = 94/5/1, 99.0 mg, 0.030 mmol) in CH_2Cl_2 (1.0 mL) with trifluoroacetic acid (4.4 μL, 0.060 mmol) in reflux for 3 h quantitatively converted **3f** to **4**. Extractive work up afforded **4** in 94% (192.2 mg) with M_n = 3,300 and M_w/M_n = 1.19. Incorporation of δ-lacton group determined by ^{1}H NMR and MALDI-TOF MS (Figure 6) was 91 and 98%, respectively.

ω-Benzoyl PBA 6

The reaction of 5 (M_n = 4,100, M_w/M_n = 1.11, 209.3 mg, 0.051 mmol), *t*-Bu_4ZnLi_2 (0.37 mL, 0.15 M solution in THF, 0.056 mmol), and benzoyl chloride (29.6 μL, 0.255 mmol) in THF (1.3 mL) afforded **6** in 99% isolated yiled

(207.2 mg) with M_n = 4,200 and M_w/M_n = 1.12. Incorporation of benzoyl group determined by ^{1}H NMR and MALDI-TOF MS (Figure 7) was 95% and 99%, respectively.

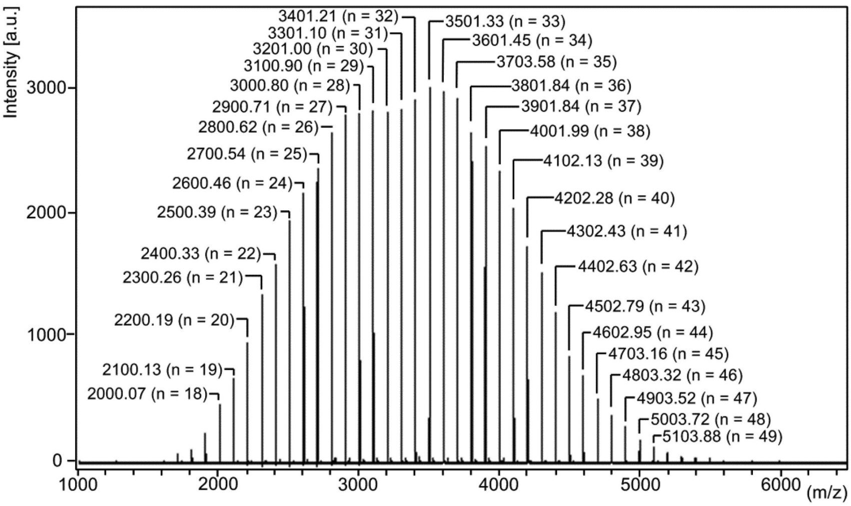

*Figure 6. MALDI-TOF MS spectra of **4**. A major series of peaks as indicated by average mass number in TOF MS spectrum are observed as sodium ion adduct (M + Na)*$^+$.

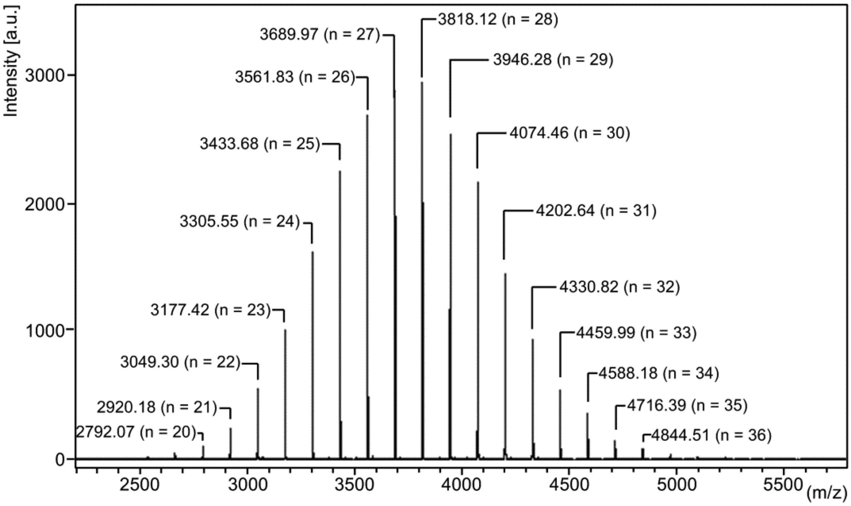

*Figure 7. MALDI-TOF MS spectra of PBA **6**. A major series of peaks as indicated by average mass number in TOF MS spectrum are observed as sodium ion adduct (M + Na)*$^+$.

Downloaded by OHIO STATE UNIV LIBRARIES on June 1, 2012 | http://pubs.acs.org
Publication Date (Web): March 20, 2012 | doi: 10.1021/bk-2012-1101.ch007

Downloaded by OHIO STATE UNIV LIBRARIES on June 1, 2012 | http://pubs.acs.org
Publication Date (Web): March 20, 2012 | doi: 10.1021/bk-2012-1101.ch007

ω-Benzoyl PNIPAM 8

The reaction of **7** (M_n = 3,100, M_w/M_n = 1.09, 145.6 mg, 0.047 mmol), *t*-Bu_4ZnLi_2 (0.52 mL, 0.10 M solution in THF, 0.052 mmol), and benzoyl chloride (27.3 μL, 0.235 mmol) in DMF (1.0 mL) gave **8** in 93% isolated yield (135.6 mg) with M_n = 3,200 and M_w/M_n = 1.10. Incorporation of the benzoyl group determined by ^{1}H NMR and MALDI-TOF MS (Figure 8) was 91% and 99%, respectively.

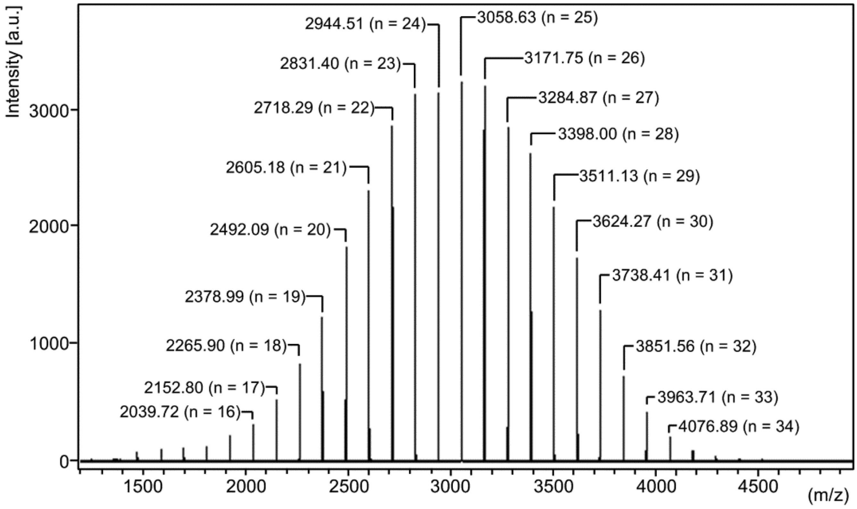

*Figure 8. MALDI-TOF MS spectra of PNIPAM **8**. A major series of peaks as indicated by average mass number in TOF MS spectrum are observed as sodium ion adduct (M + Na)$^+$.*

ω-Alkynylated PNIPAM 9

The reaction of **7** (M_n = 3,100, M_w/M_n = 1.09, 139.4 mg, 0.045 mmol), *t*-Bu_4ZnLi_2 (0.50 mL, 0.10 M solution in THF, 0.050 mmol), and benzoyl chloride (27.3 μL, 0.235 mmol) in DMF (1.0 mL) gave **9** in 93% isolated yield (135.6 mg) with M_n = 3,200 and M_w/M_n = 1.10. Incorporation of the alkynyl group determined by MALDI-TOF MS (Figure 3) was 99%.

Acknowledgments

This work was partly supported from the Core Research for Evolution Science and Technology (CREST) and Nagase Science and Technology Foundation.

Downloaded by OHIO STATE UNIV LIBRARIES on June 1, 2012 | http://pubs.acs.org
Publication Date (Web): March 20, 2012 | doi: 10.1021/bk-2012-1101.ch007

References

1. Matyjaszewski, K.; Gnanou, Y.; Leibler, L. *Macromolecular Engineering*; Wiley-VCH: Weinheim, 2007.
2. Hsieh, H. L.; Quirk, R. P. *Anionic Polymerization: Principles and Practical Applications*; Marcel Dekker: New York, 1996.
3. *Cationic Polymerizations: Mechanisms, Synthesis, and Applications*; Matyjaszewski, K., Ed.; Marcel Dekker: New York, 1996.
4. *Handbook of Radical Polymerization*; Matyjaszewski, K., Davis, T. P., Eds.; Wiley-Interscience: New York, 2002.
5. Moad, G.; Solomon, D. H. *The Chemistry of Radical Polymerization*; Elsevier: Amsterdam, 2006.
6. Braunecker, W. A.; Matyjaszewski, K. *Prog. Polym. Sci.* **2007**, *32*, 93.
7. Ouchi, M.; Terashima, T.; Sawamoto, M. *Chem. Rev.* **2009**, *109*, 4963.
8. Rosen, B. M.; Percec, V. *Chem. Rev.* **2009**, *109*, 5069.
9. Yamago, S. *Chem. Rev.* **2009**, *109*, 5051.
10. Negishi, E. *Organometallics in Organic Synthesis*; John Wiley and Sons: New York, 1980.
11. *Main Group Metals in Organic Synthesis*; Yamamoto, H.; Oshima, K., Eds.; Wiley-VCH: Weinheim, 2005.
12. Yamago, S.; Iida, K.; Yoshida, J. *J. Am. Chem. Soc.* **2002**, *124*, 2874.
13. Yamago, S.; Iida, K.; Yoshida, J. *J. Am. Chem. Soc.* **2002**, *124*, 13666.
14. Goto, A.; Kwak, Y.; Fukuda, T.; Yamago, S.; Iida, K.; Nakajima, M.; Yoshida, J. *J. Am. Chem. Soc.* **2003**, *125*, 8720.
15. Yamago, S.; Iida, K.; Nakajima, M.; Yoshida, J. *Macromolecules* **2003**, *36*, 3793.
16. Kwak, Y.; Goto, A.; Fukuda, T.; Kobayashi, Y.; Yamago, S. *Macromolecules* **2006**, *39*, 4671.
17. Sugihara, Y.; Kagawa, Y.; Yamago, S.; Okubo, M. *Macromolecules* **2007**, *40*, 9208.
18. Yusa, S.; Yamago, S.; Sugahara, M.; Morikawa, S.; Yamamoto, T.; Morishima, Y. *Macromolecules* **2007**, *40*, 5907.
19. Kayahara, E.; Yamago, S.; Kwak, Y.; Gota, A.; Fukuda, T. *Macromolecules* **2008**, *41*, 527.
20. Hasegawa, J.; Kanamori, K.; Nakanishi, K.; Hanada, T.; Yamago, S. *Macromolecules* **2009**, *42*, 1270.
21. Yamago, S.; Ukai, Y.; Matsumoto, A.; Nakamura, Y. *J. Am. Chem. Soc.* **2009**, *131*, 2100.
22. Hasegawa, G.; Kanamori, K.; Nakanishi, K.; Yamago, S. *Polymer* **2011**, *52*, 4644.
23. Yamago, S.; Ray, B.; Iida, K.; Yoshida, J.; Tada, T.; Yoshizawa, K.; Kwak, Y.; Goto, A.; Fukuda, T. *J. Am. Chem. Soc.* **2004**, *126*, 13908.
24. Ray, B.; Kotani, M.; Yamago, S. *Macromolecules* **2006**, *39*, 5259.
25. Yamago, S.; Yamada, T.; Togai, M.; Ukai, Y.; Kayahara, E.; Pan, N. *Chem. Eur. J.* **2009**, *15*, 1018.
26. Kayahara, E.; Kondo, N.; Yamago, S. *Heteroatom Chem.* **2011**, *22*, 307.

Downloaded by OHIO STATE UNIV LIBRARIES on June 1, 2012 | http://pubs.acs.org
Publication Date (Web): March 20, 2012 | doi: 10.1021/bk-2012-1101.ch007

27. Yamago, S.; Kayahara, E.; Kotani, M.; Ray, B.; Kwak, Y.; Goto, A.; Fukuda, T. *Angew. Chem., Int. Ed.* **2007**, *46*, 1304.
28. Kayahara, E.; Yamago, S. *J. Am. Chem. Soc.* **2009**, *131*, 2508.
29. Yamago, S. *J. Polym. Sci. Part A: Polym. Chem.* **2006**, *44*, 1.
30. Yamago, S. *J. Polym. Sci., Part A: Polym. Chem.* **2006**, *44*, 1.
31. Yamago, S.; Iida, K.; Yoshida, J. *J. Am. Chem. Soc.* **2002**, *124*, 2874.
32. Yamago, S.; Ray, B.; Iida, K.; Yoshida, J.; Tada, T.; Yoshizawa, K.; Kwak, Y.; Goto, A.; Fukuda, T. *J. Am. Chem. Soc.* **2004**, *126*, 13908.
33. Yamago, S.; Kayahara, E.; Kotani, M.; Ray, B.; Kwak, Y.; Goto, A.; Fukuda, T. *Angew. Chem., Int. Ed.* **2007**, *46*, 1304.
34. Yamago, S.; Ukai, U.; Matsumoto, A.; Nakamura, Y. *J. Am. Chem. Soc.* **2009**, *131*, 2100.
35. Mishima, E.; Yamago, S. *Macromol. Rapid Commun.* **2011**, *32*, 893.
36. Yamago, S.; Iida, K.; Yoshida, J. *J. Am. Chem. Soc.* **2002**, *124*, 13666.
37. Ray, B.; Kotani, M.; Yamago, S. *Macromolecules* **2006**, *39*, 5259.
38. Kumar, S.; Changez, M.; Murthy, C. N.; Yamago, S.; Lee, J.-S. *Macromol. Rapid Commun.* **2011**, *32*, 1576.
39. Yamada, T.; Mishima, E.; Ueki, K.; Yamago, S. *Chem. Lett.* **2008**, 650.
40. Yamago, S.; Kayahara, E.; Yamada, H. *React. Function. Polym.* **2009**, *69*, 416.
41. Kayahara, E.; Yamada, H.; Yamago, S. *Chem. Eur. J.* **2011**, *17*, 5272.
42. Mishima, E.; Yamada, T.; Watanabe, H.; Yamago, S. *Chem. Asian J.* **2011**, *6*, 445.
43. Uchiyama, M.; Furuyama, T.; Kobayashi, M.; Matsumoto, Y.; Tanaka, K. *J. Am. Chem. Soc.* **2006**, *128*, 8404.
44. Krasovskiy, A.; Knochel, P. *Angew. Chem., Int. Ed.* **2004**, *43*, 3333.
45. The trapping of the anionic species potentially gives *O*-acylataed and *O*-allylated products. However, lack of olefinic signals by the ^{1}H NMR analysis and control experiments by using polymer-end model compounds clearly ruled out this possibility. See Ref. 41.
46. Kolb, H. C.; Finn, M. G.; Sharpless, K. B. *Angew. Chem., Int. Ed.* **2001**, *40*, 2004.
47. Hoogenboom, R. *Angew. Chem., Int. Ed.* **2010**, *49*, 3415.
48. Schild, H. G. *Prog. Polym. Sci.* **1992**, *17*, 163.
49. Mancini, I.; Cavazza, M.; Guella, G.; Pietra, F. *J. Chem. Soc., Perkin Trans. 1* **1994**, 2181.

Downloaded by CORNELL UNIV on May 31, 2012 | http://pubs.acs.org
Publication Date (Web): March 20, 2012 | doi: 10.1021/bk-2012-1101.ch008

Chapter 8

Poly(glycidyl methacrylate-*block*-styrene) for Photolithographically Patternable Resist Materials

Qin Lou and Devon A. Shipp*

**Department of Chemistry and Biomolecular Science, and
Center for Advanced Materials Processing, Clarkson University,
Potsdam, New York 13699-5810, USA
*E-mail: dshipp@clarkson.edu**

Poly(glycidyl methacrylate-*block*-polystyrene) (PGMA-*b*-PS) acts as both a lithographic UV (365 nm) photoresist and a self-assembly material, thus it is demonstrated that this photoresist block copolymer material can be used for patterning by either top-down or bottom-up fabrication techniques. It is shown that PGMA homopolymer can undergo photoinitiated cationic ring-opening crosslinking and act as a negative-tone photoresist, and that PGMA-*b*-PS block copolymers also have the ability to produce micro-patterns from the same photolithographic process. TEM analysis of PGMA-*b*-PS thin films shows that the block copolymers have ability to undergo cylindrical or lamellar phase separations.

Introduction

Conventional photolithography is widely used in the semiconductor industry for fabricating nano-meter scale dimensions of microelectronic integrated circuit elements. This technique can make sub-micron to sub-100 nm features, and state-of-the-art photolithography using 193 nm immersion techniques are able to fabricate 50 nm patterns (*1*, *2*). The key to successful conventional photolithography is the ability to transfer patterns from a mask to a thin polymer film (the photoresist) that either crosslinks (producing a negative resist) or hydrolyzes (producing a positive resist) upon irradiation. The non-crosslinked or non-hydrolyzed material may then be washed out, leaving behind a negative

In Progress in Controlled Radical Polymerization: Materials and Applications; Matyjaszewski, K., et al.;
ACS Symposium Series; American Chemical Society: Washington, DC, 2012.

or positive image of the mask. As such, conventional photolithography is often referred to as a "top-down" approach. However, the inherent limitation of optical diffraction works against conventional photolithography techniques when attempting to fabricate sub-45 nm features. Furthermore, feature sizes are dictated by the mask, which become expensive and difficult to produce as feature sizes decrease. Thus, finding alternative techniques to conventional photolithography in order to access sub-45 nm feature sizes is a major goal for the microelectronics and other industries.

In recent years, several groups (*1*, *3–6*) have examined the use of block copolymers as a "bottom-up" approach that may overcome the pattern size limitation in conventional photolithography. The first example of industrial application of block copolymer (self-assembly) lithography is reported by IBM in which air gap insulators were fabricated using nano-porous templates derived from self-assembly of poly(styrene-*b*-methyl methacrylate) (PS-*b*-PMMA) block copolymers (*7*). However, a limitation of block copolymer self-assembly techniques compared to conventional photolithography is that block copolymer self-assembled patterns consist of only a single morphology, typically spheres, cylinders, gyroids, or lamellae (*3*).

A combination of block copolymer lithography and conventional photolithography may be a possible approach for hierichial patterning by using both top-down and bottom-up fabrication techniques. Using block copolymers that contain photoresist materials may provide compatibility with the conventional photolithography industry at the same time as giving potential to access sub-30 nm patterning. For example, Ober and coworkers (*3–5*) use poly(α-methylstyrene)-*block*-poly(4-hydroxystyrene) (PαMS-*b*-PHOST) as both lithographic deep UV photoresist and block copolymer self-assembly material. The PαMS-*b*-PHOST block copolymer thin film can either form horizontal fingerprint patterns by using nonselective THF for solvent annealing or hexagonally arranged dot pattern when using acetone (good for PHOST) for solvent annealing. Furthermore, the diblock copolymer PαMS-*b*-PHOST can be used as conventional deep UV (250 nm) negative-tone photoresist with 4 wt% tetramethoxymethyl glycouril as a crosslinker (*5*).

Mercury lamp i-line (365 nm-based) UV lithography is still widely used and can produce features sizes ranging from sub-microns to microns. The diblock copolymer poly(glycidyl methacrylate-*block*-styrene) (PGMA-*b*-PS) is a distinctive material because it is patternable by both UV (365 nm) lithography and self-assembly techniques. The epoxy groups from poly(glycidyl methacrylate) blocks can undergo cationic ring-opening polymerization with initiation by a photoacid generator (PAG) and behaves as a chemically amplified negative-tone photoresist (*8*). As with many block copolymers, the PGMA-*b*-PS may undergo nanometer phase separation and different self-assembly phase morphologies may be obtained by changing the constituent polymer block volume fractions. This can be controlled during reversible-deactivation radical polymerizations (RDRPs, or sometimes referred to as living radical polymerizations) (*9*, *10*). Thus, the PGMA-*b*-PS block copolymer can merge "top-down" and "bottom-up" approaches producing hierarchical features based on micropatterning from conventional photolithography and nanostructured features from block

Downloaded by CORNELL UNIV on May 31, 2012 | http://pubs.acs.org
Publication Date (Web): March 20, 2012 | doi: 10.1021/bk-2012-1101.ch008

copolymer phase separation. We report here the synthesis of poly(glycidyl methacrylate-*block*-styrene) photoresist block copolymers with various segment volume fractions using atom transfer radical polymerization (ATRP) (*11*, *12*) and show that this polymer is capable of acting as a negative-tone photoresist and undergoes nanophase separation.

Experimental

Materials

Styrene and glycidyl methacrylate (GMA) were passed through a basic alumina column to remove the inhibitors and purified by vacuum distillation prior to use. *N,N,N',N'',N''*-pentamethyldiethylenetriamine (PMDETA), ethyl 2-bromoisobutyrate (EBriB), methyl 2-bromopropionate (MeBrP), 2,2′-bipyridine (Bpy), copper (I) chloride (CuCl), copper (I) bromide (CuBr), copper (II) chloride ($CuCl_2$), diphenyl ether and other solvents were purchased from VWR or Aldrich, and used as received. Irgacure 250 photoacid generator was purchased from Ciba and used without further purification.

Instrumentation

Gel permeation chromatography (GPC) was performed on a modular system comprised of the following: a Waters 515 high-pressure liquid chromatographic pump operating at room temperature, a Waters 717 autosampler, and a Viscotek LR40 refractometer. THF was used as a continuous phase at a flow rate of 1.0 mL/ min. The columns were calibrated with commercial linear polystyrene and poly(methyl methacrylate) standards. ^1H (400 MHz) and ^{13}C (100 MHz) nuclear magnetic resonance (NMR) spectroscopy were performed on a Bruker Avance 400 with a BBO probe. Sample concentrations were about 25% (w/v) in $CDCl_3$ containing 1% TMS as an internal reference. Differential scanning calorimetry (DSC) was performed using a TA Instruments Q100 using a scan rate of 10°C/ minute. The UV light source for photolithography was an Oriel Instruments, model 68811, 500W mercury xenon arc lamp (intensity ~90mW/cm^2, as measured by a Dymax Corp. Accu-Cal-30 intensity meter). Ellipsometry was performed on a Multiskop null- elipsometer (Optrel, Germany) equipped with a HeNe laser (λ=633 nm). A JEOL JEM-2010 transition electron microscope (TEM) instrument operating at 200 kV was used to obtain the plane view of block copolymer thin film. The film was then exposed to iodine for 6 hours.

Synthesis of Poly(glycidyl methacrylate) ATRP Macro Initiator (PGMA)

CuCl (0.06 g, 0.6 mmol.) and $CuCl_2$ (0.015 g, 0.11 mmol.) were placed in a 25 mL Schlenk flask equipped with magnetic stir bar and sealed with rubber septum. The Schlenk flask was deoxygenated with three vacuum-nitrogen cycles. GMA (13.11 mL, 96 mmol.), EBriB (88.5 µL, 0.6 mmol.), bpy (0.243 g, 1.44 mmol.) and 5 mL of acetone (solvent) were placed in a 25 mL round bottom flask and purged with nitrogen for 30 mins. A degassed syringe was used to transfer the

Downloaded by CORNELL UNIV on May 31, 2012 | http://pubs.acs.org
Publication Date (Web): March 20, 2012 | doi: 10.1021/bk-2012-1101.ch008

monomer mixture into the Schlenk flask and the polymerization was initiated by placing the Schlenk flask into a 30 °C oil bath for 2 hrs. Once the polymerization was done, the mixture was diluted with THF and then passed through the basic alumina column to remove the catalyst and then rotary evaporated to concentrate the polymer solution. The PGMA was finally precipitated into cold hexanes, filtered and dried in a vacuum oven.

Synthesis of Block Copolymers (PS-b-PGMA) Using PGMA Macro-Initiator

Cu (I) Br (14 mg, 0.1 mmol.) and Cu (II) Br_2 (9 mg, 0.04 mmol.) were weighed into a 10 mL Schlenk flask equipped with magnetic stir bar and sealed with a rubber septum. The Schlenk flask was deoxygenated with three vacuum-nitrogen cycles. Styrene (4.6 mL, 40 mmol.), PGMA-Cl (0.6 g, 0.1 mmol.), bpy (0.04 g, 0.28 mmol.) and 6 mL of acetone (solvent) was placed in a 10 mL round bottom flask and purged with nitrogen for 30 mins. A degassed syringe was used to transfer the monomer mixture into the Schlenk flask and the polymerization was initiated by placing the Schlenk flask into a 60°C oil bath for 12 hrs. After this time, the mixture was cooled to room temperature, diluted with THF and then passed through a basic alumina column to remove the catalyst and then rotary evaporated to concentrate the polymer solution. The block copolymer was finally precipitated into an excess of cold methanol/hexanes mixture (50/50 vol.%), filtered and dried in vacua.

Photolithography Patterning

A THF solution containing 4.0 wt.% polymer and 1.0 wt.% Irgacure 250 PAG was prepared and used to spin coat a polymer film (2,000 rpm on a Si substrate). Block copolymer thin films were heat annealed at 180°C for 24 hrs and slowly cooled to room temperature. Photolithography was performed by placing a TEM grid on top of the film and exposing it to UV light source for 5 min and then immersing it in THF for 10 seconds. The resulting features of the polymer film on Si substrate were observed using an optical microscope (Olympus VANOX).

Analysis of Block Copolymer Phase Separation

The block copolymer films were spin coated and heat annealed using the same conditions as photolithography procedures. TEM samples were prepared by allowing the block copolymer thin film to float to the surface from the silicon substrate in a 5 wt % aqueous HF solution, and then collecting the film onto the carbon coated TEM copper grid. The film was stained with OsO_4 for 15 hrs before analysis.

Downloaded by CORNELL UNIV on May 31, 2012 | http://pubs.acs.org
Publication Date (Web): March 20, 2012 | doi: 10.1021/bk-2012-1101.ch008

Downloaded by CORNELL UNIV on May 31, 2012 | http://pubs.acs.org
Publication Date (Web): March 20, 2012 | doi: 10.1021/bk-2012-1101.ch008

Results and Discussion

Design and Synthesis of Glycidyl Methacrylate-Containing Resist Polymers

Glycidyl methacrylate (GMA) was polymerized using ATRP to give PGMA homopolymers with halogen (Br/Cl) end groups (*13*). The PGMA was then used as macro-initiator in the ATRP of styrene, thus forming PGMA-*b*-PS block copolymers (Scheme 1). Table 1 summerizes these reactions and molecular weight data obtained from the polymers. Representative GPC traces of a PGMA macro-initiator and the resultant PGMA-*b*-PS block copolymer (**BCP1**) are shown in Figure 1. These indicate that the molecular weight of polymer increases after the extension of the PGMA with styrene to form the block copolymer. The clear increase to higher molecular weight is an indication of successful chain extension. Furthermore, the width of the molecular weight distribution does not change significantly, resulting in the block copolymer having a relatively low polydispersity. Indeed, after copolymerization with styrene, the GPC results show that the M_n increased from 9,500 to 21,700 and the polydispersity remained at approximately 1.3. The synthesis of two other samples, **BCP2** and **BCP3**, was also successful, although both these samples have broader molecular weight distributions. This appears to be a result of using PGMA macroinitiators with relatively high M_w/M_n values; this, in turn, might be due to the larger equilibrium constant of methacrylates during ATRP when compared to acrylates and styrene, increasing [radical] and thus termination.

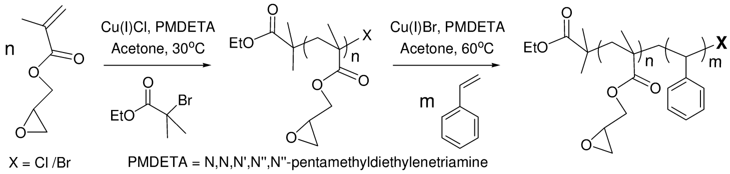

Scheme 1. Synthesis of PGMA-b-PS block copolymers using ATRP.

The ^1H NMR spectrum of the block copolymer **BCP1** is shown in Figure 2. These data clearly show that the PGMA-*b*-PS block copolymer has been formed. The spectrum shows signals from both the PGMA polymer (δ ~ 2.65, 2.85, 3.25, 3.8 and 4.4 ppm) and polystyrene (δ ~ 6 - 7.5 ppm). The protons from the block copolymer backbone are at δ ~ 0.9 -2.0 ppm. Peaks at δ ~ 6 -7.5 ppm indicate the aromatic protons from styrene monomer and peak at δ ~ 3.25 ppm indicates the -CH proton in the epoxy ring from glycidyl methacrylate residues. By integrating these peaks we obtain the mole ratio for the styrene and glycidyl methacrylate residues, from which the mole % of each monomer residue can be calculated (Table 2).

Downloaded by CORNELL UNIV on May 31, 2012 | http://pubs.acs.org
Publication Date (Web): March 20, 2012 | doi: 10.1021/bk-2012-1101.ch008

Table 1. Reaction conditions and results for the ATRP of poly(glycidyl methacrylate) (homopolymerization) and poly(glycidyl methacrylate-*block*-styrene) (block copolymerizations)

Entry	*Monomer (mmol.)*	*R-X (mmol.)*	*Cu(I)X (mmol.)*	*Ligand (mmol.)*	*Time (h)*	M_n[a]	M_w/M_n[a]
PGMA1[b]	96	0.60	0.6	0.14	1.5	9,500	1.32
BCP1[c]	21	0.11	0.11	0.25	11	21,700	1.33
PGMA2[d]	96	0.60	0.60	0.20	1	6,300	1.53
BCP2[e]	40	0.11	0.11	0.25	10.5	12,900	1.70
PGMA3[d]	96	0.60	0.60	0.20	1	6,800	1.41
BCP3[e]	40	0.11	0.11	0.25	10.5	13,100	1.43

[a] M_n and M_w/M_n data calculated from GPC data calibrated by poly(methyl methacrylate) or polystyrene standards. [b] Mole ratios (GMA: EBiB: Cu(I)Cl: bpy: Cu(II)Cl_2)= 160:1:1:2:0.2; solvent = 5 ml Acetone; temperature = 30°C. [c] Mole ratios (St: PGMA-X: bpy: Cu(I)Br: Cu(I)Br_2) = 200:1:2.4:1:0.2; solvent = 2.5 ml Acetone; temperature = 60°C. [d] Mole ratios (GMA: EBiB: Cu(I)Cl: bpy: Cu(II)Cl_2)= 160:1:1:2.8:0.4; solvent = 7 ml Acetone; temperature = 30°C. [e] Mole ratios (St: PGMA-X: bpy: Cu(I)Br: Cu(I)Br_2) = 400:1:2.4:1:0.2; solvent = 6 ml Acetone; temperature = 60°C.

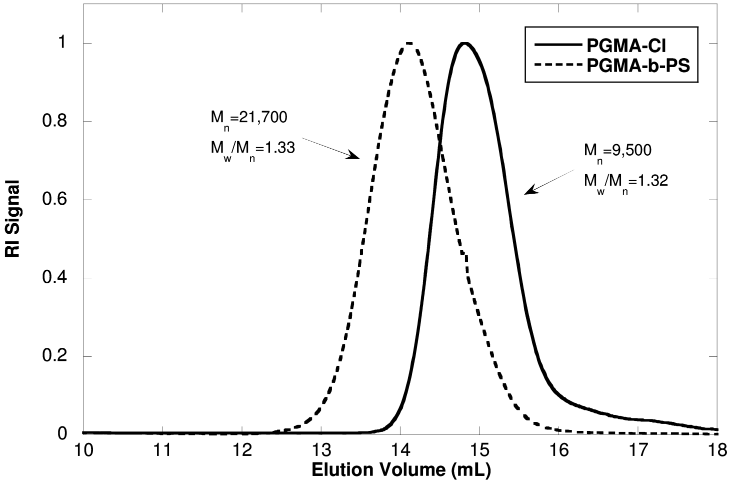

Figure 1. GPC traces of PGMA macro-initiator (solid line) and the resulting PGMA-b-PS block copolymer (dashed line) after the copolymerization of styrene.

Downloaded by CORNELL UNIV on May 31, 2012 | http://pubs.acs.org
Publication Date (Web): March 20, 2012 | doi: 10.1021/bk-2012-1101.ch008

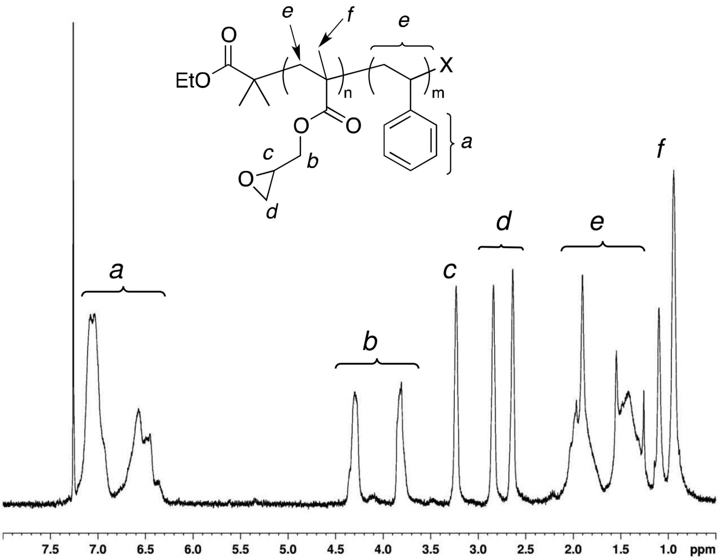

*Figure 2. ^{1}H NMR spectrum of PGMA-b-PS block copolymer **BCP1**.*

Table 2. % Styrene & GMA in PGMA-*b*-PS samples

PGMA-b-PS	***n** (Styrene)/ **n** (GMA)*[a]	*mol. % of GMA*[b]
BCP1	0.34	75%
BCP2	0.95	51%
BCP3	0.85	54%

[a] The mole (**n**) ratios are calculated from the integrations of styrene peaks at δ ~ 6-7.5 ppm (5H) and glycidyl methacrylate peak at δ ~ 3.25 ppm (1H) from ^{1}H NMR spectrum. [b] The mol.% values are calculated from mole ratios which are obtained from the ^{1}H NMR spectra.

Thermal Properties

The thermal properties of the PGMA and PGMA-*b*-PS resist materials were examined by differential scanning calorimetry (DSC) (Figure 3). DSC analysis of the **PGMA1** homopolymer and block copolymer (**BCP1**) were carried out as examples. The **PGMA1** homopolymer gives a clear transition, resulting in T_g ~ 60°C. This is at the generally accepted value for PGMA which is usually 60~ 70°C. The PGMA-*b*-PS (**BCP1**) shows a broad transition at 65~105°C, which appears to consist of two transitions at 69°C and 103°C, most likely due to the PGMA and PS segments, respectively. The PGMA segment in **BCP1** DSC trace shows a little higher T_g may be due to the covalently bonded PS segment affected its thermal behavior and result in the slightly higher T_g than the PGMA homopolymer.

Downloaded by CORNELL UNIV on May 31, 2012 | http://pubs.acs.org
Publication Date (Web): March 20, 2012 | doi: 10.1021/bk-2012-1101.ch008

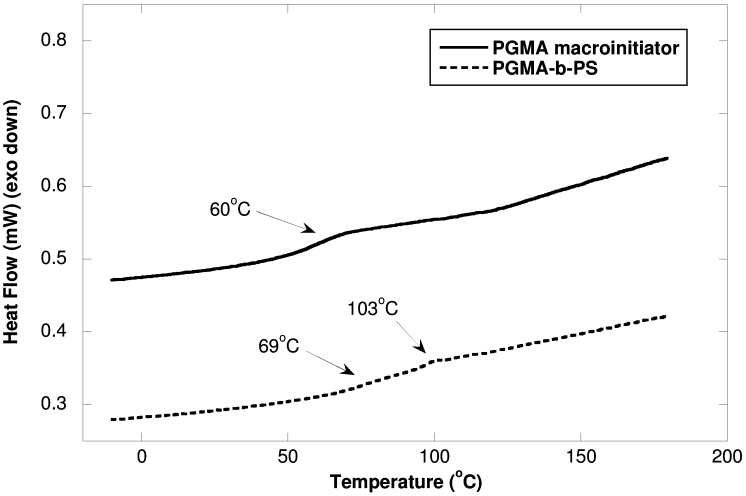

Figure 3. DSC curves for PGMA macro initiator (solid line) and PGMA-b-PS block copolymer (dashed line).

Evaluation of Photolithographic Patterning Using 365 nm UV Photolithography

PGMA can be potentially used as a negative-tone photoresist since the epoxy ring can undergo cationic ring-opening reaction in the presence of a photoacid generator (e.g. Irgacure 250 (*14*)), and thus crosslinked into an infinite network. To evaluate the photolithographic patterning performance, we demonstrated that PGMA homopolymer photoresists can be easily dissolved in THF but once the epoxy rings have been polymerized it is no longer soluble in THF. The PGMA-*b*-PS was dissolved in THF to form a 4.0 wt. % solution then spin coated on a Si substrate at 2,000 rpm for 1 min. The thickness of the block copolymer film after spin coating, as measured by ellipsometry, was ~ 300 nm with refractive index of ~ 1.1. A TEM grid was used as a mask (providing a simple pattern of 60 × 60 μm squares) and placed on top of PGMA polymer film. The UV light passing through the grid initiates cationic ring-opening polymerization of the epoxy groups, producing a crosslinked PGMA polymer network which is no longer soluble in THF (Scheme 2). In contrast, the areas of the PGMA resist polymer that are not irradiated with UV light because of the mask are not crosslinked and therefore THF soluble. After UV (λ = 365 nm) exposure with a dose of 90 mW/cm^2, the exposed films were developed in THF to give fine negative-tone images, the surface morphology of polymer film can be observed through optical microscopy. Figure 4A displays optical images indicating that the grey squares are the crosslinked PGMA and white areas are the surface of Si substrate, confirming that the features processed by photolithography using the PGMA homopolymer can be achieved successful.

Downloaded by CORNELL UNIV on May 31, 2012 | http://pubs.acs.org
Publication Date (Web): March 20, 2012 | doi: 10.1021/bk-2012-1101.ch008

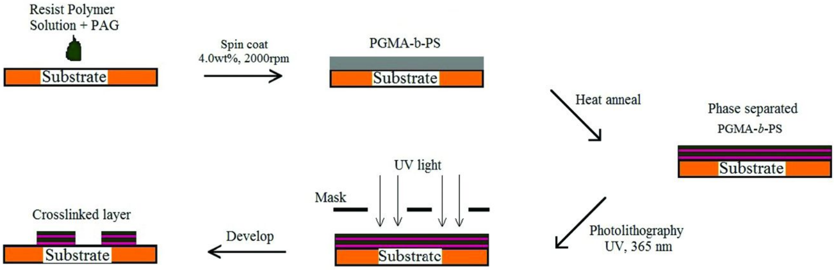
Resist Polymer
Solution + PAG
Substrate
Spin coat
4.0wt%, 2000rpm
PGMA-b-PS
Substrate
Heat anneal
Phase separated
PGMA-b-PS
Substrate
Photolithography
UV, 365 nm
UV light
Mask
Substrate
Develop
Crosslinked layer
Substrate

Scheme 2. The photolithography process for PGMA-b-PS photoresist block copolymers.

It is also of interest to determine if the PGMA-*b*-PS block copolymers perform as successfully in the photolithography experiments under the same conditions as the PGMA homopolymers. As can be seen in Figure 4B, the optical microscope image shows that the surface features of the PGMA-*b*-PS block copolymer film after photolithography is very similar to the PGMA homopolymer, indicating that the block copolymer also has the ability to be used in 365 nm UV photolithography. The squares from PGMA-*b*-PS block copolymer photolithography shown in Figure 4B have the same shape and size as those shown in Figure 4A (PGMA homopolymer photolithography).

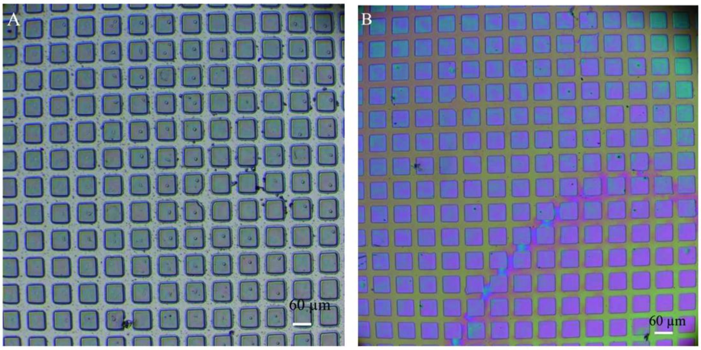
A
60 μm
B
60 μm

Figure 4. Optical microscope images for PGMA and PGMA-b-PS photoresist films which spin coated with 4.0 wt% polymer solution contain 1.0 wt% PAG at 2,000 rpm exposed at 365 nm UV light for 5 mins and then developed in THF for 10s: (A) Optical microscope image of PGMA photoresist homopolymer; (B) Optical microscope image of PGMA-b-PS photoresist block copolymer.

Phase Separation of PGMA-*b*-PS Block Copolymers

To examine phase separation of the photoresist block copolymers, TEM analysis of block copolymers thin films were performed. As shown in Figure 5, TEM measurements show nano-sized patterning of the phase separated PGMA-*b*-PS block copolymer films after heat annealing at 180°C. These films were prepared without photolithography, and the high temperature annealing is

Downloaded by CORNELL UNIV on May 31, 2012 | http://pubs.acs.org
Publication Date (Web): March 20, 2012 | doi: 10.1021/bk-2012-1101.ch008

likely to produce a crosslinked PGMA phase. The films were stained with OsO_4 so that the dark area in the TEM images are the PGMA, while the lighter areas are the PS. The TEM images of **BCP1**, **BCP2** and **BCP3** are shown in Figure 5A, 5B and 5C, respectively. The **BCP1** block copolymer shows what appears to be cylindrical worm-like phase separation, while **BCP2** and **BCP3** appear to exhibit something like horizontal lamellar phase separation, although the exact morphology requires further investigation by other methods to confirm the structure. These TEM results are consistent with expected morphologies based on the volume fractions estimated from ^{1}H NMR data (Table 2). The volume fraction of PGMA segments of **BCP1** is 0.75, which should yield cylindrical phase separation. The volume fraction of PGMA segments for **BCP2** and **BCP3** are 0.51 and 0.54, respectively, thus both block copolymers should give lamellar phase separation (it is worth noting, however, that these block copolymers may yield complex phase separation morphologies in part because their polydispersities are not as low as those of block copolymers that have had their phase diagrams extensively studied, e.g. < 1.10).

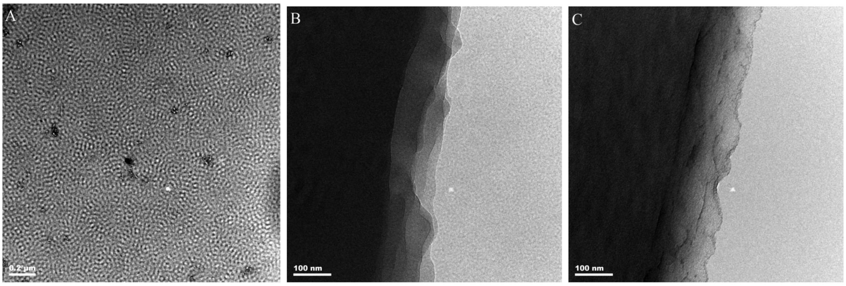

*Figure 5. TEM images of self-assembled PGMA-b-PS thin films after heat annealing at 180°C and then stained with OsO_4 for 15 hrs: (A) TEM image of phase separated **BCP1**; (B) TEM image of phase separated **BCP2**; (C) TEM image of phase separated **BCP3**.*

Conclusions

We have demonstrated the synthesis, characterization, and patterning properties of a series of poly(glycidyl methacrylate) (PGMA) and poly(glycidyl methacrylate-*block*-styrene) (PGMA-*b*-PS) resist materials synthesized by atom transfer radical polymerization (ATRP). DSC analysis of the PGMA and PGMA-*b*-PS resist materials ensured that the materials have glass transition temperature (T_g) of 60 °C and 65 ~105°C , respectively. TEM measurements showed lamellar/cylindrical patterning of the phase separated PGMA-*b*-PS block copolymer films after heat annealing at 180°C. Photolithographic patterning of the PGMA resist materials were performed under UV ($\lambda = 365$ nm) exposure with dose of 90 mW/cm^2 to give proof-of-concept negative-tone images with cationic ring-opening crosslinking mechanisms on a micrometer scale. The PGMA-*b*-PS block copolymers also have the ability to produce micro-patterns from the same photolithographic process as well. We expect that such block copolymers will have the ability to form hierarchical features based on micropatterning from photolithography and nanostructured features from block copolymer phase separation. This is the first report of PGMA containing polymeric lithographic patternable materials and their patterning performance for both 365 nm UV lithography and block copolymer phase separations.

Acknowledgments

We thank the U.S. Army Research Office (Grant # W911NF-05-1-0339), the Center for Advanced Materials Processing (a New York State Center for Advanced Technology) and the Department of Chemistry & Biomolecular Science at Clarkson University for financial support.

Downloaded by CORNELL UNIV on May 31, 2012 | http://pubs.acs.org
Publication Date (Web): March 20, 2012 | doi: 10.1021/bk-2012-1101.ch008

References

1. Bang, J.; Jeong, U.; Ryu, D. Y.; Russell, T. P.; Hawker, C. J. *Adv. Mater.* **2009**, *21*, 4769–4792.
2. Stoykovich, M. P.; Nealey, P. F. *Mater. Today* **2006**, *9*, 20–29.
3. Bosworth, J. K.; Black, C. T.; Ober, C. K. *ACS Nano* **2009**, *3*, 1761–1766.
4. Bosworth, J. K.; Paik, M. Y.; Ruiz, R.; Schwartz, E. L.; Huang, J. Q.; Ko, A. W.; Smilgies, D.-M.; Black, C. T.; Ober, C. K. *ACS Nano* **2008**, *2*, 1396–1402.
5. Du, P.; Li, M.; Douki, K.; Li, X.; Garcia, C. B. W.; Jain, A.; Smilgies, D. M.; Fetters, L. J.; Gruner, S. M.; Wiesner, U.; Ober, C. K. *Adv. Mater.* **2004**, *15*, 953.
6. Lou, Q.; Kishpaugh, M. A.; Shipp, D. A. *J. Polym. Sci., Part A: Polym. Chem.* **2010**, *48*, 943–951.
7. Bates, F. S.; Fredickson, G. H. *Phys. Today* **1999**, *52*, 32.
8. Hayek, A.; Xu, Y.; Okada, T.; Barlow, S.; Zhu, X.; Moon, J. H.; Marder, S. R.; Yang, S. *J. Mater. Chem.* **2008**, *18*, 3316–3318.
9. Shipp, D. A. *J. Macromol. Sci., Part C: Polym. Revs.* **2005**, *45*, 171–194.
10. Shipp, D. A. *Polym. Rev.* **2011**, *51*, 99–103.
11. Matyjaszewski, K.; Xia, J. *Chem. Rev.* **2001**, *101*, 2921–2990.
12. Ayres, N. *Polym. Rev.* **2011**, *51*, 138–162.
13. Cañamero, P. F.; Fuente, J. L. d. l.; Madruga, E. L.; Fernández-García, M. *Macromol. Chem. Phys.* **2004**, *205*, 2221–2228.
14. Moon, S. Y.; Kim, J. M. *J. Photochem. Photobiol., C* **2007**, *8*, 157–173.

Chapter 9

Nanoscale Functional Patterning of Thin Films Using Block Copolymers Prepared through CRP

Brigitte Voit,*[,1,2] Maria Riedel,[1,2] and Jan Stadermann[1,3]

[1]**Leibniz-Institut für Polymerforschung Dresden e.V., Hohe Strasse 6,**
D-01069 Dresden, Germany
[2]**Technische Universität Dresden, Organic Chemistry of Polymers,**
01062 Dresden, Germany
[3]**Current address: GRAFE Advanced Polymers GmbH,**
Waldecker Strasse 21, D-99444 Blankenhain, Germany
***E-mail: voit@ipfdd.de**

The synthesis of block copolymers suitable for the formation of nanostructured multifunctional thin films is described. For that, phase-separating block copolymers which contain further functionalities being able to react in polymer-analogous reactions have been prepared by a controlled radical polymerization method, namely RAFT polymerization. Functionalities like pentafluorostyrene, alkyne or carboxylic acid groups were introduced into the respective segments. Techniques like NMR, GPC and DSC were applied to verify structure, molar masses, molar mass distributions and thermal properties. Finally, thin films consisting of block copolymers that showed strong phase-segregation behavior and ordered nanostructured surfaces were obtained.

Introduction

In recent years, block copolymers attracted more and more attention for micro- and nanotechnology because of their ability to self-assemble into regular structures of mesoscopic dimensions (*1*). Furthermore, combining self-assembly on the nanoscale with functionality will open up new possibilities

In Progress in Controlled Radical Polymerization: Materials and Applications; Matyjaszewski, K., et al.;
ACS Symposium Series; American Chemical Society: Washington, DC, 2012.

for more complex functional surface pattern with the option to use them in high integration micro- and nanosystems. Chemical surface patterning attracts particular importance in such fields of biotechnology in which a controlled surface immobilization of biomolecules like enzymes or proteins is desired (*2–4*), e.g. for the development of biosensors (*5*) and microfluidic devices.

Controlled radical polymerizations are distinguished methods to realize such phase-separating block copolymers with narrow polydispersities as well as the incorporation of functional groups. Advantages of CRP compared to ionic polymerizations are the tolerance towards functional groups and their insensitivity against traces of water and small amounts of contaminations.

The additional chemical functionalities being present in the prepared block copolymers offer various modifications via polymer-analogous reactions. Thus, we introduced functionalities like alkyne groups, which are addressable by azides in a click-reaction (*6–9*) and pentafluorostyrene groups for reactions with thiols (*10–12*).

Here we describe the synthesis of several amphiphilic block copolymers via RAFT polymerization mainly based on a polymethylacrylate-*block*-polystyrene or pentafluorostyrene structure and containing groups for efficient post-modification. The phase-separation behavior in thin films prepared from those multifunctional block copolymers as well as the surface composition has been intensively studied.

Experimental

Details of the materials and characterization can be found in references (*13*) and (*14*). The polymers reported here have been prepared by RAFT polymerization and were characterized in detail by NMR, GPC, DSC and SAXS. Thin films of the polymers were prepared and analyzed by AFM and XPS.

Results and Discussion

Synthesis of the Block Copolymers

For phase-separating block copolymers, hydrophilic acrylic based blocks as well as a poly(4-vinylpyridine) segment were synthesized first by RAFT polymerization. These polymers were used as macro-CTAs for the synthesis of the second block which is based on styrene derivatives. In Chart 1 the block copolymers synthesized in this study are shown.

The polymers contain in the polar blocks acid groups (**BC1**, **BC3**, **BC4**, **BC5**), vinylpyridine groups (**BC2**) and hydroxystyrene groups (**BC3**). Acid groups induce a high polarity in the block and can also be used for specific reactions, e.g. with amines. The vinylpyridine group in **BC2** has two advantages. On the one hand it gives a strong polarity to the respective block. This is required to induce the incompatibility to the non-polar counter block being a prerequisite for block copolymer self-assembly (*15*, *16*) and on the other hand this group can be used for crosslinking in thin films (*17*, *18*). Another crosslinking group present in **BC3** is the 4-hydroxystyrene group. It can be cross-linked with a photoacid generator and tetramethoxymethyl glycuril under UV irradiation (*19*). The second non-polar block consists of pentafluorostyrene (PFS) (**BC1-BC3**) or (fluoro-) styrene and propargyloxystyrene groups (**BC4/BC5**). The PFS groups as well as the alkyne groups represent the main functionalities in the block copolymer. Both groups can be modified effectively in a polymer-analogous reaction. The alkyne groups are able to react with azides in the Cu(I) catalyzed 1,3-dipolar cycloaddition whereas the PFS group can be converted selectively in *para*-position with thiols in a nucleophilic substitution.

The characterization of the polymers was done by ^{1}H NMR and GPC using refractive index (RI) detection (PS calibration) and light scattering (LS) detection. In Table I the results of the block copolymer characterization are summarized.

The prepared macro-CTAs show narrow molar mass distributions and the molar masses determined by GPC (LS detection) are in good consistency with the NMR-calculated molar masses.

Molar mass distributions of the block copolymers were determined via GPC using RI detection (**BC1, BC2**) as well as LS detection (**BC3-BC5**). The PDI values are still in a very good range indicating a controlled polymerization process. The molar masses obtained from the LS detector confirmed the NMR-calculated values. In contrast, the molar masses determined by a RI detector with a PS calibration ($M_{n,GPC}$ for **BC1** and **BC2**) do not confirm the NMR-calculated values, because the PS calibration is not suited for our new multifunctional block copolymers.

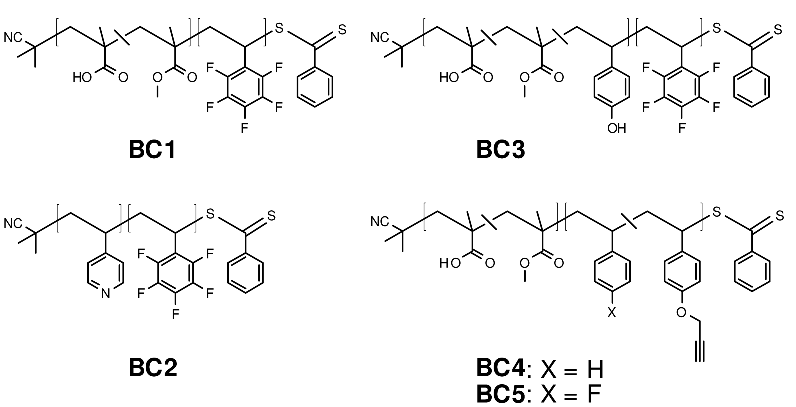

BC1

BC3

BC2

BC4: X = H
BC5: X = F

Chart 1. Structure of the synthesized block copolymers.

Table I. Characterization of the block copolymers BC1 – BC5

Sample	*Macro-CTA*				*Block copolymer*			
	$M_{n,NMR}$[a] *[g/mol]*	*$M_{n,GPC}$* *[g/mol]*	*PDI*	*Segment mol ratio*[e]	*$M_{n,NMR}$*[g] *[g/mol]*	*$M_{n,GPC}$* *[g/mol]*	*PDI*	*Block ratio*[k]
BC1	11,000	11,000[c]	1.08[c]	MMA/MAA= 1.8/1	70,000	39,000[h]	1.24[h]	1/5[m] 1 / 2.6[n]
BC2	-[b]	22,000[d]	1.17[d]	-[f]	99,000	30,000[h]	1.19[h]	1/3[m] 1/1.9[n]
BC3	-[b]	29,000[c]	1.14[c]	-	-[b]	200,000[i]	1.09[i]	1/ 6[m]
BC4	25,500	24,500[c]	1.10[c]	MMA/MAA = 2.2 / 1	110,000	138,000[i]	1.18[i]	1/3.3[m]
BC5	25,500	24,500[c]	1.10[c]	MMA/MAA = 2.2 / 1	95,000	98,000[i]	1.14[i]	1/2.7[m]

[a] Determined by ^{1}H NMR via end-group method. [b] Determination by NMR via end-group method (macro-CTA) or block ratio (BC) not possible. [c] Determined by a LS detector. [d] Determined by a RI detector using a PVP calibration. [e] Determined by ^{1}H NMR. [f] Determination by NMR not possible. [g] Determined by ^{1}H NMR via block ratio referred to the repeating units. [h] Determined by a RI detector and PS calibration. [i] Determined by a LS detector. [k] polar block/nonpolar block. [m] Referred to the molar masses of both blocks. [n] Referred to the repeating units of both blocks.

Phase Separation Behaviour

Prior to the film preparation, the phase separation behaviour of the block copolymers could be confirmed from the DSC analysis. In Figure 1 the DSC curves of the block copolymers **BC1** – **BC5** can be seen. **BC1** to **BC4** show two separated glass transition temperatures (T_gs), indicating strong phase segregation in bulk. The lower T_gs can be assigned to the unpolar styrene-based block and the higher T_gs are attributed to the polar methacrylate-based or vinylpyridine block. For **BC5** only one glass transition could be found.

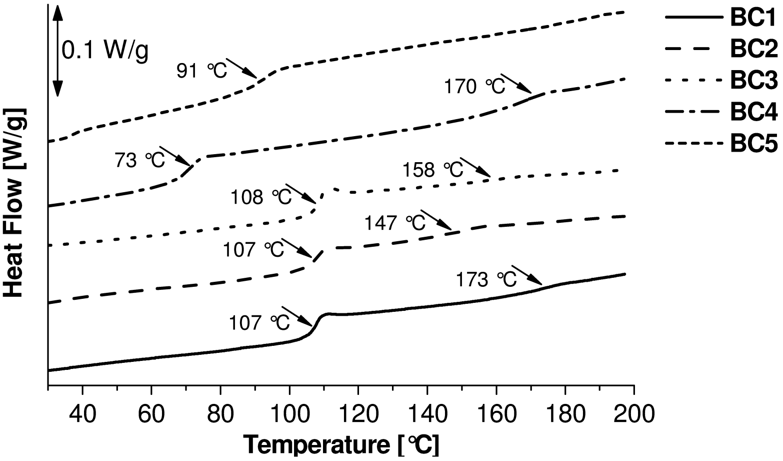

*Figure 1. DSC curves of the block copolymers **BC1** - **BC5** with the glass transition temperatures.*

Additional, SAXS measurements have been carried out to verify the phase separation behaviour. For that, THF solutions of the block copolymers **BC1**, **BC2**, **BC3** and **BC5** were slowly vaporized at room temperature in small Teflon bowls. The resulting polymer films were scratched out and this material was analyzed. Figure 2 shows the SAXS results and in Table II the corresponding morphologies as well as the structure parameters are summarized. The unit cell parameters were determined from reflection positions using Bragg's law and symmetry conditions of the related morphology.

For all four block copolymers, distinct scattering reflections were detected. Thus, it could be confirmed, that these materials undergo phase separation. **BC1** und **BC2** show lamellar structures. In **BC2** also hexagonal cylinder packages can be assigned to the scattering pattern (broad/asymmetric maxima). Whereas in block copolymer **BC3** hexagonally ordered (closed packed) cylinders were detected in correspondence to the higher molar mass of this polymer. Because of the absence of further scattering maxima for **BC5**, no well-ordered morphology could be suggested for that sample.

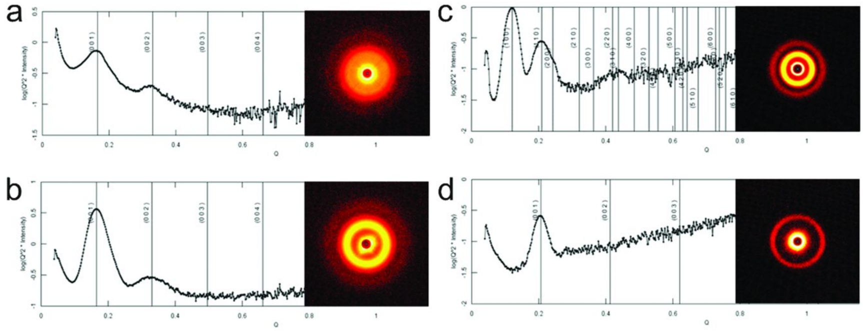

Figure 2. SAXS diagrams as Iq^2 vs. q of the block copolymers (a)* ***BC1****, (b)* ***BC2****, (c)* ***BC3****, and (d)* ***BC5****, each with assignment of reflections and insertion of primary 2D-SAXS pattern. (Please note: this figure was compiled including results adapted from ref. (13) and (14))*

Table II. Morphologies and structure parameters of the block copolymers BC1-BC3 and BC5

Sample	*Morphology*	*Parameter*	*d-value [nm]*
BC1	lamellae (LAM)	repeat unit L	38.0
BC2	lamellae (LAM) (Figure 2b) *or/and*	repeat unit L	38.0
	hex. closed packed cylinders (HCPC)	a_{hex}	39.8
BC3	hex. closed packed cylinders (HCPC)	a_{hex}	58.8
BC5	(could not be determined)	(max.)	30.4

Film Preparation

Preparation of Nanostructured Polymer Films and AFM Studies of Block Copolymers BC1 – BC5

The synthesized block copolymers **BC1 – BC5** were used for the preparation of thin polymer films on silicon wafers via spin-coating or dip-coating from dioxane or THF solution. The thickness of the obtained films was determined via optical ellipsometry. Table III shows the parameters of the preparation of the polymer films. AFM studies were carried out in Tapping Mode, recording height image and phase image simultaneously.

Table III. Film parameters

Sample	*Molar mass [g/mol]*	*Block ratio polar/non polar*	*Preparation method*	*Solvent*	*Concentration [wt%]*	*Film thickness[a] [nm]*	*Domain size [nm]*
BC1	70,000	1/5	dip coating	THF	0.5	34	38
BC2	99,000	1/ 3	dip coating	THF	0.5	19	37
BC3	200,000	1/6	dip coating	THF	0.5	14[b]	62
BC4	110,000	1/1.3	dip coating	dioxane	0.5	22[b]	43
BC5	95,000	1/2.7	spin coating	dioxane	0.5	30	42

[a] Measured by optical ellipsometry. [b] The film thickness of the dip-coated films was observed to be not uniform over the samples.

In Progress in Controlled Radical Polymerization: Materials and Applications; Matyjaszewski, K., et al.;
ACS Symposium Series; American Chemical Society: Washington, DC, 2012.

Figure 3 shows the AFM phase images of the five block copolymers. In all pictures one can observe phase-separated structures. The block copolymers **BC1**, **BC3**, **BC4** and **BC5** form thin film structures assembled by laying-down cylinders. The domain sizes are listed in Table III and the values are consistent with the molar masses of the respective block copolymer. In Figure 3c the strong tendency for dewetting of the block copolymer **BC3** is visible. This behavior originates from the very hydrophobic nature of the long PPFS block (170,000 g/mol). Block copolymer **BC2** also forms a phase separated film, but this structure resembles standing cylinders which appear in the thin films more as dots in a matrix. SAXS measurements of **BC2** in bulk revealed a mix of lamellae and hcp cylinders indicating that confinement effects as well as surface interactions in thin films influence the morphology of the phase-separated films.

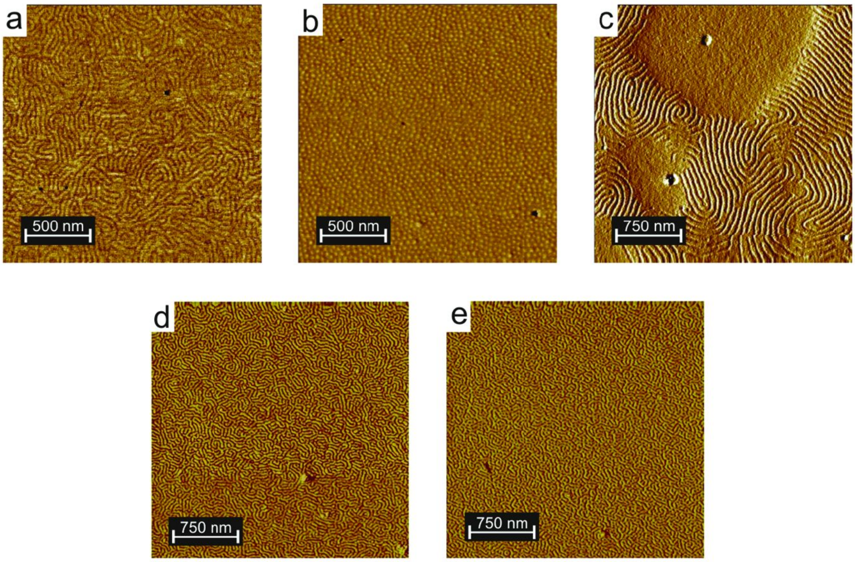

Figure 3. AFM phase images of the block copolymer films (a) ***BC1*** *(2µm²), (b)* ***BC2*** *(2µm²), (c)* ***BC3*** *(3µm²), (d)* ***BC4*** *(3µm²) and (e)* ***BC5*** *(3µm²). (Please note: this figure was compiled including results adapted from ref. (13) and (14))*

Regarding the aimed for use of the patterned surfaces for further modification, the structures were examined for their stability upon solvent exposure. For that, films of **BC5** were immersed into different non-solvents for 54 hours. After drying, the films were reviewed by AFM. Water, ethanol, acetonitrile, DMSO and *n*-hexane were chosen for the solvent treatment and in all cases no detachment of the film from the substrate was observed. However, only in the case of ethanol AFM measurements showed the same phase-separated surface morphology after the solvent treatment (Figure 4a).

The film of **BC2** was chemically cross-linked within a vapour of dibromobutane under reduced pressure for 3 days. After this procedure, the film was immersed in DMF for 24 hours. In this case, the AFM pictures also show the same morphology as before the solvent exposure (Figure 4b) and the film thickness determined by ellipsometry before and after the treatment remained constant. This result indicates a successful cross-linking of the vinyl pyridine phase in the film.

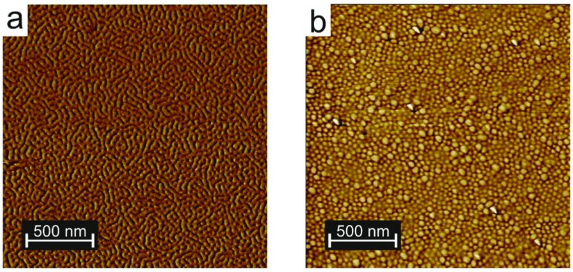

Figure 4. AFM phase images of the (a) ***BC5*** *film after ethanol treatment for 54 hours and (b)* ***BC2*** *film after crosslinking and 24 h DMF treatment.*

XPS Studies of the Films of Block Copolymers BC1 – BC5

For realization of phase-selective surface interactions, it is necessary to verify, whether both phases, the polar and the nonpolar phase, are exposed to the surface accessible for further chemical modification. Therefore, the composition of the film surface was determined by X-ray photoelectron spectroscopy (XPS) addressing the first few nm of the film surface (details see ref. (*14*)).

In Figure 5 the XPS wide scan as well as the high-resolution C1s spectra of the block copolymers films **BC1**, **BC2**, **BC3** and **BC5** are shown. In the wide-scan XPS spectra the photoelectron peaks of carbon, oxygen and fluorine are clearly found. From the high-resolution C1 spectra different component peaks were separated. In Table IV the correlations of the component peaks of the block copolymers are listed.

On the surface of the block copolymer film of **BC1** all three integrated monomers MMA, MAA and PFS are present. The sum of the intensities of the component peaks of G, H and a fifth of F results in the intensity of component peak B. The monomer ratio of MMA to MAA is reflected in the ratio of component peak G to H (1.8:1 *vs*. 1.89:1). The ratio of sum of component peak G and H to a fifth of component peak F (1:2.63) shows, that the surface consists of the same composition as the bulk block copolymer (block ratio: 1:2.6).

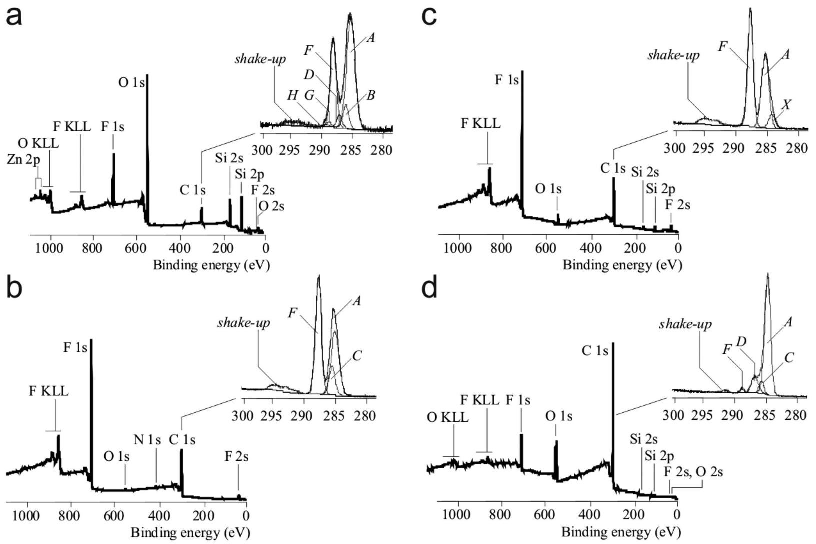

Figure 5. XPS wide-scan and high-resolution C1s spectra of the block copolymer films (a) ***BC1****, (b)* ***BC2****, (c)* ***BC3*** *and (d)* ***BC5****. (Please note: this figure was compiled including results adapted from ref. (13) and (14)).*

In the film of **BC2**, both monomers vinylpyridine and PFS were detected at the surface, but the atomic composition was not the same as in the bulk block copolymer. The ratio of component peak C to F is 1 to 3.65 (block ratio: 1:1.9), that means that the PPFS block is enriched at the surface. The C1s spectrum of **BC3** shows, that only the high molar mass PPFS block is existent at the film surface.

For the block copolymer film of **BC5** the ratio of the relative atomic concentration of oxygen and fluorine was determined from the wide-scan spectrum to be O:F = 2.1:1. The calculated value in the block copolymer is O:F = 2.0:1. The result shows that the surface exposure of the two phases is balanced. For the ethanol treated film of **BC5**, the obtained XPS data revealed a changed surface composition (Figure 6). The ratio of the relative atomic concentration of oxygen and fluorine has changed to be O:F = 7.6:1. This result shows that the polar phase is enriched at the surface as a consequence of the ethanol treatment.

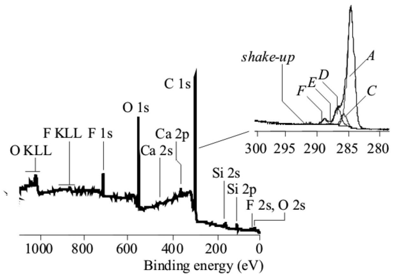

Figure 6. XPS wide-scan and high-resolution C1s spectra of the block copolymer film ***BC5*** *after ethanol treatment for 24 hours.*

Table IV. Correlation of the component peaks of the block copolymers BC1, BC2, BC3 and BC5

Component Peak[c]	*BC1*	*BC2*	*BC3*[b]	*BC5*
A	$\underline{C}_xH_y$[a]	$\underline{C}_xH_y$[a]	$\underline{C}_xH_y$[a]	$\underline{C}_xH_y$[a]
B	1-$\underline{C}$-atom of pentafluorophenyl $\underline{C}$-$COOCH_3$, $\underline{C}$-COOH	-	-	-
C	-	$\underline{C}$-atoms of pyridine	-	$\underline{C}$-$COOCH_3$, $\underline{C}$-COOH
D	$COO\underline{C}H_3$	-	-	$\underline{C}$-F, Ph-O-$\underline{C}H_2$-C≡CH
F	$\underline{C}$-F	$\underline{C}$-F	$\underline{C}$-F	$\underline{C}OOH$
G	$\underline{C}OOCH_3$	-	-	-
H	$\underline{C}OOH$	-	-	-

[a] Saturated and unsaturated hydrocarbons. [b] X: silicon organic impurities. [c] Shake-up peaks: Resulting from carbon atoms, which are involved in conjugated π-bonds.

Conclusion

In summary, we have demonstrated the synthesis of new amphiphilic and multifunctional block copolymers via RAFT polymerization. The block copolymers are equipped with functional groups suitable for post-modifications (pentafluorostyrene and propargyloxystyrene) and crosslinking (hydroxystyrene and vinylpyridine). DSC and SAXS measurements have shown that the block copolymers undergo phase separation in bulk. These polymers were used to prepare thin films on silica, where they form nanostructures. For one film, the stability of the self-assembled nanostructure in ethanol was observed. Another film was chemically cross-linked before a subsequent exposure to DMF resulting in a stable film with unchanged surface morphology. XPS analysis revealed the presence of both phases at the surface in four of five cases. That means, all functionalities are available for post-modifications. However, after the ethanol exposure the polar phase was enriched on the surface. Thus, the strategy of film crosslinking could lead to a better phase stability against solvents which is a necessary prerequisite of using those nanostructured, multifunctional films for post-modification reactions on the nanoscale and microfluidics applications.

Acknowledgments

The authors thank Ms. P. Treppe for GPC studies, Ms. L. Häußler for DSC analysis and Mr. Roland Schulze and Dr. M. Erber for ellipsometry measurements. Dr. D. Jehnichen and Dr. F. Simon are thanked for measurement and interpretation of SAXS and XPS, respectively. The partial financial support of the work by the Saxon State Excellence Initiative European Centre for Emerging Materials and Processes (ECEMP) and the European Regional Development Fund (ERDF) is gratefully acknowledged.

References

1. Kim, H. C.; Park, S. M.; Hinsberg, W. D. *Chem. Rev.* **2010**, *110*, 146–177.
2. Mendes, P. M.; Yeung, C. L.; Preece, J. A. *Nanoscale Res. Lett.* **2007**, *2*, 373–384.
3. Ober, C. K.; Senaratne, W.; Andruzzi, L. *Biomacromolecules* **2005**, *6*, 2427–2448.
4. Offenhausser, A.; Bocker-Meffert, S.; Decker, T.; Helpenstein, R.; Gasteier, P.; Groll, J.; Moller, M.; Reska, A.; Schafer, S.; Schulte, P.; Vogt-Eisele, A. *Soft Matter* **2007**, *3*, 290–298.
5. Niemeyer, C. M.; Jonkheijm, P.; Weinrich, D.; Schroder, H.; Waldmann, H. *Angew. Chem. Int. Ed.* **2008**, *47*, 9618–9647.
6. Bock, V. D.; Hiemstra, H.; van Maarseveen, J. H. *Eur. J. Org. Chem.* **2006**, *2006*, 51–68.
7. Huisgen, R. *Angew. Chem., Int. Ed.* **1963**, *2*, 565–598.
8. Rostovtsev, V. V.; Green, L. G.; Fokin, V. V.; Sharpless, K. B. *Angew. Chem.* **2002**, *114*, 2708–2711.

9. Tornoe, C. W.; Christensen, C.; Meldal, M. *J. Org. Chem.* **2002**, *67*, 3057–3064.
10. Becer, C. R.; Babiuch, K.; Pilz, D.; Hornig, S.; Heinze, T.; Gottschaldt, M.; Schubert, U. S. *Macromolecules* **2009**, *42*, 2387–2394.
11. Becer, C. R.; Hoogenboom, R.; Schubert, U. S. *Angew. Chem., Int. Ed.* **2009**, *48*, 4900–4908.
12. Ott, C.; Hoogenboom, R.; Schubert, U. S. *Chem. Commun.* **2008**, 3516–3518.
13. Riedel, M.; Stadermann, J.; Komber, H.; Simon, F.; Voit, B. *Eur. Polym. J.* **2011**, *47*, 675–684.
14. Stadermann, J.; Riedel, M.; Komber, H.; Simon, F.; Voit, B. *J. Polym. Sci., Part A: Polym. Chem.* **2011**in print.
15. Ishizu, K. *Prog. Polym. Sci.* **1998**, *23*, 1383–1408.
16. Shoji, M.; Eguchi, M.; Layman, J. M.; Cashion, M. P.; Long, T. E.; Nishide, H. *Macromol. Chem. Phys.* **2009**, *210*, 579–584.
17. Ishizu, K.; Ikemoto, T.; Ichimura, A. *Polymer* **1999**, *40*, 3147–3151.
18. Lam, Y. M.; Song, L. X.; Moy, Y. C.; Xi, L. F.; Boothroyd, C. *J. Colloid Interface Sci.* **2008**, *317*, 255–263.
19. Du, P.; Li, M. Q.; Douki, K.; Li, X. F.; Garcia, C. R. W.; Jain, A.; Smilgies, D. M.; Fetters, L. J.; Gruner, S. M.; Wiesner, U.; Ober, C. K. *Adv. Mater.* **2004**, *16*, 953–957.

Chapter 10

Synthesis and Characterization of Polyhedral Oligomeric Silsequioxane-Core Star Polystyrene via Nitroxide-Mediated Polymerization

David Glé,[1] Trang N. T. Phan,*,[1] Valérie Monier,[2] Laurence Charles,[1] Denis Bertin,[1] and Didier Gigmes*,[1]

[1]UMR-CNRS 7273, Institut de Chimie Radicalaire Fédération des Sciences Chimiques de Marseille, Aix-Marseille Universités, Service 542, Avenue Escadrille Normandie Niémen, 13397 Marseille Cedex 20, France
[2]Spectropole, Fédération des Sciences Chimiques de Marseille, Aix-Marseille Universités, Service 542, Avenue Escadrille Normandie Niémen, 13397 Marseille Cedex 20, France
***E-mails: trang.phan@univ-amu.fr, didier.gigmes@univ-amu.fr.**
Phone: 33 (0)491 288 097. Fax: 33 (0)491 288 758.

Multifunctional NMP initiator with a core of cubic silsesquioxane (POSS) was synthesized starting from the coupling of Octa(3-aminopropyl)octasilsesquioxane with 2-Methyl-2-[N-tert-butyl-N-(1-diethoxyphosphoryl-2,2-dimethylpropyl)aminoxy]-N propionyloxysuccinimide. The obtained POSS-based multialkoxyamine was then used as NMP initiator for the polymerization of styrene leading to the formation of star polystyrenes of narrow dispersity with a core consisting of dispersed nanosized hard particles. We demonstrated that stars with a predetermined molecular weight and a control of dispersity could be synthesized by simply controlling reaction parameters and restricting the monomer conversion typically below 30 - 35%. The precise structure of POSS based star polystyrenes was analyzed by the characterization of the individual arms obtained after etching the Si-O-Si bonds of the core. The influence of POSS core on the glass transition temperature of nanocomposites was investigated and compared to that of their cleaved products using differential scanning calorimetry.

Introduction

Star polymers are a class of branched polymers consisting of at least three linear polymeric chains radiating from one single multifunctional branching point, usually called the core or the central nodule (*1*). They differ from the linear analogues of identical molecular weight not only on the compact structure but also on the multiple functionality that is useful in some of their applications. Synthesis of star polymers is most often accomplished by living ionic polymerization (*2*, *3*) or controlled/living radical polymerization (*4–8*). There are essentially two strategies to synthesize star polymers: the "arm-first" method (*9*, *10*), which cross-links preformed macroinitiators using divinyl molecules and the "core-first" method (*4*, *5*), which uses an active multifunctional core to initiate the polymerization of monomers. A variation of "arm-first" technique, the "coupling-onto" method, involves attaching of preformed arms onto a multifunctional core (*11*, *12*). Although the "arm-first" approach is the easiest way to synthesize star polymer containing multiple arms and functionalities, they unfortunately lead to star polymers having statistical distribution of the number of arms and a relatively broad molecular weight distribution. The final product is also contaminated by the residual unreacted starting linear polymers. These problems come from the difficulty of achieving 100 % linkage of the chains to the core caused by increasing steric hindrance of the aldready attached long chains.

Recently, Matyjaszewski et al. (*13*, *14*) developed an other varation of "arm-first" method which consists in a copolymerization of linear macromers with a divinyl cross-linker using low molar mass initiators. With this method, the number of initiating sites and number of arms per star molecule are independently controlled. Thus, the star-star coupling reactions could be minimized by lowering the molar ratio of initiator to macromer, providing star polymers with low-polydispersities. As for most of the variant of "arm-first" method, the contamination of the final product by the residual unreacted macromer is inevitable unless macromer conversion reaches the high values (> 95%), but that requires often a long reaction time (about 24h or even several days for some macromers).

Well-defined star polymers offer many interesting properties such as lower melting points, lower solution viscosities, more processable and superior mechanical properties compared to the corresponding linear polymer of similar molecular weight. Their synthesis requires the use of initiator with precise functionality. "Core-first" approach has been proved to be efficient to prepare a series of star polymers with precise arm numbers and lengths via controlled radical polymerization techniques such as nitroxide mediated polymerization (NMP) (*15*), atom transfer radical polymerization (ATRP) (*4*, *5*), and reversible addition-fragmentation chain transfer polymerization (RAFT) (*8*) as well ring opening polymerization (ROP) (*16–18*). The synthesis of star polymers with 3-, 4-, 6-, 7-, 8-, and even 12-arms has been described by several research groups using either organic or inorganic initiators. The synthesis of star polymers initiated by inorganic cores would have the advantages of combining the unique characteristics of both the organic/inorganic materials and star-like polymers.

Polyhedral oligomeric silsesquioxanes (POSS) reagents combine unique hybrid (inorganic–organic) chemical compositions with nano-sized cage structures that have dimensions comparable with those of most polymer segments. A typical POSS molecule possesses the structure of cube-octameric frameworks represented by the formula ($R_8Si_8O_{12}$) with an inorganic silica-like core (Si_8O_{12}) surrounded by eight organic corner groups, which can be functionalized by a variety of organic reactive groups. POSS in polymer matrix has been found various applications in the areas such as liquid crystals (*19*), nanocomposites (*20*), photo-resists in lithographic technologies (*21*), based on their high thermal stability and oxidation resistance properties (*22–24*). A numbers of reports have been published on organic/inorganic hybrids containing pendant POSS (*25–27*). However, little work reported on the synthesis of well-defined hybrid star-like polymers by controlled radical polymerization using POSS as core. The first report on the used of POSS-based octafunctional ATRP initiator for the polymerization of methyl methacrylate was published by Laine et al (*28*). The resulting hybrid star-like polymers had polydispersity increasing as the polymerization progressed, additionally; the star-star coupling was observed for conversion as low as 20%, indicating a poor control on the synthesis. Recently, He et al. (*29*) and Liu et al. (*30*) reported the synthesis of POSS-$(Br)_8$ initiators and their use as multifunctional initiator for the ATRP of methyl methacrylate in acetonitrile/water mixture and that of styrene in anisole. In both reports, the authors obtained hybrid star polymers with low polydispersity (1.17 and 1.08, respectively). However, to obtain well-defined hybrid star polymers, these authors had stopped polymerization at quite low monomer conversion about 23%. Compared to ATRP techniques, there are relatively few studies that have exploited NMP for the synthesis of POSS-core star polymers. Indeed, we are only aware of one report in which Kuo et al. (*31*) described the synthesis of an octa-N-alkoxyamine POSS through the hydrosilylation of octakis(dimethylsiloxy) silsesquioxane (with 1-(2-(allyloxy)-1-phenylethoxy)-2,2,6,6-tetramethylpiperidine (allyl-TEMPO) in the presence of Karstedt's agent. This multifunctional initiator was further used for the synthesis of POSS based star polystyrene as well as several diblock copolymers. Bulk styrene polymerization was achieved at 80% monomer conversion after 17h at 120°C for a target molecular weight of 80000 g/mol. Interestingly, these authors didn't observe any star coupling reactions for a monomer conversion as high as 63% while other studies demonstrated that inter or intra-star coupling reactions appear once monomer conversion exceeds 25% (*4*, *28*, *30*). The occurrence of star coupling reaction is usually evidenced by detection of shoulder in the chromatographic traces at the high molecular weigh region.

With the growing interest of POSS based materials in various applications and the desire to investigate different convenient alternative of the NMP process in such system for successful synthesis of POSS based star polymers, we describe, in this paper, the synthesis of star polystyrene from a cubic silsequioxane NMP initiator using the "core-first" method. The strategy for the synthesis of hybrid star polystyrene with POSS core consist of three main steps depicted in Scheme 1. i) synthesis of octa(3-ammoniumpropyl)octasilsesquioxane octachloride [POSS-$(NH_3^+Cl^-)_8$]; ii) neutralization of POSS-$(NH_3^+Cl^-)_8$ followed immediately by its coupling with an alkoxyamine bearing a *N*-succinimidyl (NHS) ester group **1** to prepare the corresponding POSS-alkoxyamine initiator **2**; iii) solution or bulk polymerization of styrene by NMP using POSS-alkoxyamine **2** as initiator.

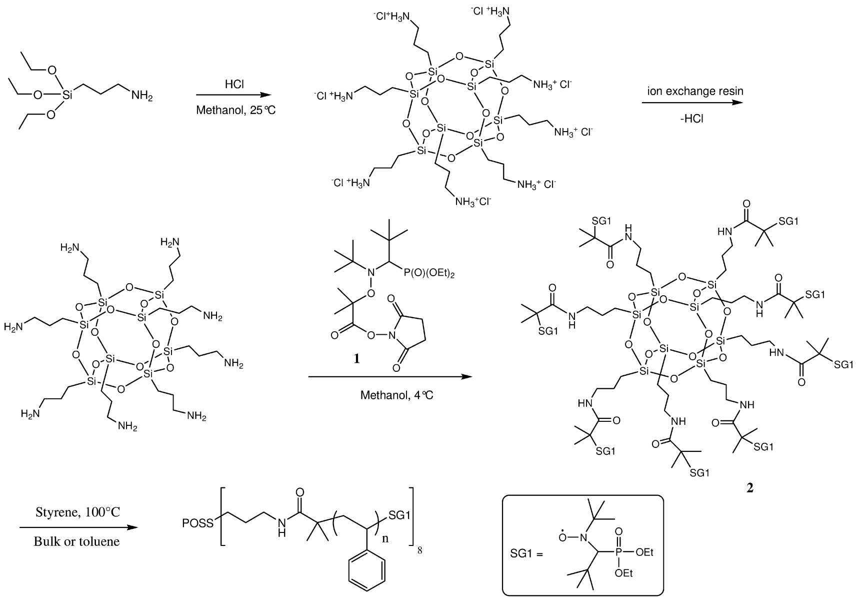

Scheme 1. Schematic illustration for the preparation of Octa(3-ammoniumpropyl)octasilsesquioxane Octachloride [POSS-$(NH_3^+Cl^-)_8$] and POSS-based octafunctional NMP initiator [POSS-$(SG1)_8$].

Experimental Section

Materials

MAMA-SG1 (Blocbuilder MA™ >99%), (scheme 1) derived was kindly provided by Arkema (France). 3-aminopropyltrimethoxysilane (97%), styrene (99%), dicyclohexylcarbodiimide (99%), and N-hydroxysuccinimide (98%) were purchased from Aldrich and used as received. All solvents and other chemicals were of reagent-grade quality and were obtained commercially and used without further purification.

Characterization

All ^1H, ^{31}P and ^{29}Si NMR were run either in DMSO-d_6 or in $CDCl_3$ and recorded in a Bruker AV400 MHz spectrometer. Number-average molecular weights (M_n) and molecular weights distribution (M_w/M_n) of resulting hybrid star polystyrene were determined by size exclusion chromatography operated at 30°C. The chromatographic device was equiped with a Waters 515 liquid chromatograph pump, a guard column and two Nucleogel (HR4 and HR5) columns in series. Detection systems were a differential refractive index detector (Waters Model 410) and a ultra-violet (UV) detector (Waters Model 468). The mobile phase was tetrahydrofuran with a flow rate of 1.0 mL min^{-1}. Calibration based on polystyrene standards from Polymer Laboratories (molecular weight range: 580 - 377 400 g mol^{-1}) was applied for the determination of molecular weights of star polymers.

Electrospray ionization mass spectroscopy (ESI-MS) experiments were performed with a QStar Elite mass spectrometer (Applied Biosystems SCIEX, Concord, ON, Canada) equipped with an electrospray ionization source operated in the positive ion mode. The capillary voltage was set at 5500 V and the cone voltage at 20 V. In this hybrid instrument, ions were measured using an orthogonal acceleration time-of-flight (oa-TOF) mass analyzer. Nitrogen was used as the nebulizing gas (10 psi) and the curtain gas (20 psi). POSS samples were dissolved in methanol at a concentration of 5 mg/mL; this solution was then diluted in 1:10 volume ratio with a acidified methanol (0.5 % formic acid). The sample solution was then infused into the electrospray interface by a syringe pump at a flow rate of 5 **µ**L/min.

The Differential Scanning Calorimetry (DSC) studies were carried out using a TA Instruments 2920 Modulated DSC. Typical sample masses for modulated DSC were 3-5 mg. The samples were first heated from room temperature to 130°C at a heating rate of 5°C/min under nitrogen atmosphere, followed by cooling to 40°C at a cooling rate of 5°C/min after stopping at 130°C for 5 min to erase any prior thermal history. Finally, samples were analyzed by subsequent heating to 130°C under modulation mode. The modulation conditions include period of 60 sec, modulation amplitudes of ± 0.8°C, and a scanning rate of 3°C/min. The glass transition temperature (T_g) was determined on the transition of the final heating process and was chosen at the 50% change of the heat capacity that is close to the point of inflection.

Octakis(3-ammoniumpropyl)octasilsesquioxane Octachloride (POSS-$NH_3^+Cl^-$)

POSS-$NH_3^+Cl^-$ was prepared in a round bottom two neck-flask equipped with a magnetic stirrer and nitrogen purge. First, 400 mL of methanol was placed in the flask, and then 50 mL (0.213 mol) of 3-aminopropyltrimethoxysilane was introduced dropwise. After the complete addition of silane, 67.5 mL of concentrated hydrochloric acid (36.5 wt%, 12 *M*) was poured quickly and the flask was closed when the fume production stopped (about 5 minutes). The reaction mixture was then stirred under nitrogen at room temperature for one week. POSS-*$NH_3^+Cl^-$* precipitated as a white powder and was formed after 5 days. The crude product obtained after filtration, washing with cold dry methanol, and drying was spectroscopically pure in 30% yield (9.6 g). Recrystallization from hot dry methanol afforded POSS-*$NH_3^+Cl^-$* (4.29 g, 3.66 mmol, 6.88%) as a white solid. ^{29}Si NMR (DMSO-d_6, δ, ppm): -66.44. ^{1}H NMR (DMSO-d_6, δ, ppm): 8.23 (s, 24H, $\underline{NH_3}^+Cl^-$), 2.76 (t, 16H, NH_3^+-$\underline{CH_2}$-CH_2), 1.71 (m, 16H, $\underline{CH_2}$-CH_2-Si), 0.72 (t, 16H, $\underline{CH_2}$-Si).

Octakis(2-Methyl-2-(N-tert-butyl-N-(1-diethoxyphosphoryl-2,2-dimethylpropyl)aminoxy)-N-propyl propionamide)octasilsesquioxane (POSS-*MAMA-SG1,* 2)

Amberlite IRA-400 ion-exchange resin (30 g) was prepared by successive washing with water (4 x 150 mL), 1M NaOH (3x150 mL), water (6x150 mL), and methanol (6x150 mL), which was the elution solvent; the resin was suspended in eluent and chilled (-10 °C, 2 h) before use. Half of the resin beads were loaded onto a column (3.5 cm outside diameter), and the other half were used to dissolve a suspension of neutralized POSS-*$NH_3^+Cl^-$* (1.43 g, 1.22 mmol) in the minimum amount of eluent below 0°C. Elution across the column produced a methanol solution of neutralized POSS-*NH_2*. Immediately, NHS-MAMA-SG1 **1**, previously prepared in a straightforward manner from the commercially available MAMA-SG1 according to the literature method (*32*) (6.46g, 9.76 mmol, 8 equiv) was added to a solution of neutralized POSS-*NH_2*, and the resulting mixture was kept under magnetic stirring at 4°C during 2h. Methanol was then evaporated under reduced pressure and the product was precipitated in cold pentane. The obtained solid was respectively washed with distilled water to remove N-hydroxysuccinimide and with diethyl ether to remove the unreacted NHS-MAMA-SG1. POSS-*MAMA-SG1* **2** was obtained as a white powder after drying under vacuum at room temperature. Yield: 50%. ^{31}P NMR ($CDCl_3$, δ, ppm): 27.51. ^{29}Si NMR (DMSO-d_6, δ, ppm): -66.22. ^{1}H NMR ($CDCl_3$, δ, ppm): 5.58 (broad peak, 8H, $\underline{NH}$-C=O), 3.95 – 4.46 (m, 32H, CH_3-$\underline{CH_2}$-O-P), 3.30 (d, J(H,P) = 27 Hz, 8H, N-$\underline{CH}$-P), 2.74 -3.08 (m, 16H, $\underline{CH_2}$-NH-C=O), 1.48 – 2.02 (m, 64H, $\underline{CH_3}$-C-CO and $\underline{CH_2}$-CH_2-Si), 0.98 –1.45 (m, 192H, $\underline{CH_3}$ of *tert*-butyl and $\underline{CH_3}$-CH_2-O-P), 0.67 (t, 16H, $\underline{CH_2}$-Si).

Synthesis of Star Polystyrene Using POSS-MAMA-SG1 as NMP Initiator

Styrene (3.0g, 2.86 x10^{-2} mols), POSS-MAMA-SG1 (127mg, 2.78 x10^{-5} mols), and toluene (2g) were weighted and mixed to generate a solution that contained 60 wt % of monomer. This solution was placed in a three-neck flask equipped with a reflux condenser and a magnetic stir bar. The mixture was purged for 20 min with argon at room temperature to remove oxygen. In kinetic studies, samples were collected from the reaction mixture at given time intervals by a syringe through a septum. Styrene conversion was determined by $_1$H NMR in $CDCl_3$. Average molar mass and molecular weight distribution were determined by size exclusion chromatography (SEC). The polymerization was stopped by quenching the reactor in an ice bath. The polymer was purified by precipitation in ethanol, filtered to remove the volatiles and dried under high vacuum at room temperature to a constant weight.

Cleavage of POSS-PS Star Polymer

50 mg POSS-PS star polymer was dissolved in 2 mL of THF in a polypropylene tube, and then 40 μL HF solution (40 wt %) was added to the solution (**Caution : Hydrofluoric acid is extremely corrosive**). After stirring at 50 °C for 15h and then removing all the solvents by vacumn, the residues were dissolved in 0.5 mL CH_2Cl_2 and precipitated into an excess of methanol. The solid was collected by filtration and dried in a vacuum at room temperature before analyze by SEC.

Results and Discussion

NMP Initiator Syntheses

POSS-$(NH_3^+Cl^-)_8$ was prepared according to the reported method (*33*, *34*). The produced POSS-$(NH_3^+Cl^-)_8$ had appearance of a white solid and was spectroscopically pure in 30 % yield; as might be expected for an octa-(ammonium chloride) salt, it was highly hydroscopic. Neutralization of POSS-$(NH_3^+Cl^-)_8$ was accomplished by eluting it as a methanol solution across a column of Amberlite IRA-400 resin according to the reported method (*34*, *35*). The preparation of NHS-activated ester alkoxyamine was previously reported by our group (*32*) in which we demonstrated the effectiveness of this alkoxyamine in the polymerization of styrene and *n*-butyl acrylate and especially its potential in the synthesis of hydroxyl-functionalized polystyrene and OH-functional alkoxyamine. This latter was easily obtained in a high yield by reaction of alkoxyamine **1** and ethanolamine. Thus, following this strategy, we synthesized POSS-alkoxyamine **2**. Typicallly, to a methanol solution of the freshly prepared POSS-$(NH_2)_8$ was added the NHS-activated ester alkoxyamine **1**, and the resulting mixture was held at 0°C for 2 hours. After removal of the solvent under reduced pressure, the POSS-alkoxyamine **2** was isolated as a white powder, easy to store and handle after precipitation in pentane. Two experiments were carried out, the first one with an equimolar ratio of amine group and alkoxyamine **1** and the second one with a molar ratio of alkoxyamine **1** to amine group equals to 1.5. The ^{31}P NMR analysis of the crude products after removal of methanol solvent allows the determination of the reaction yield (Figure 1). Typically, by comparison of the integral value of the peak at $\delta = 27.5$ ppm corresponding to the POSS-MAMA-SG1 alkoxyamine **2** with the one of the peak at $\delta = 25$ ppm corresponding to the starting alkoxyamine **1**, the reaction yield for the two experiments was respectively 83 mol % and 100 mol %. The unreacted NHS-MAMA-SG1 was removed from POSS-MAMA-SG1 alkoxyamine **2** by rinsing out the crude product with cold diethyl ether. This treatment was only efficient for the purification of crude product resulting from the experiment with an equimolar of POSS amine groups and alkoxyamine **1** as shown in the ^{31}P NMR spectra of the resulting POSS-MAMA-SG1 alkoxyamine (Figure 2). However, it was more difficult to remove completely the excess alkoxyamine **1** in the crude product resulting from the experiment with an excess of alkoxyamine **1** compared to POSS amine groups. In such case, the work up of the reaction mixture was accompanied with an important loss of the formed POSS-MAMASG1 alkoxyamine **2**. This is probably due to a similar affinity of the POSS that has all the avaible sites reacted with MAMA-SG1 and the excess alkoxyamine **1** towards diethyl ether.

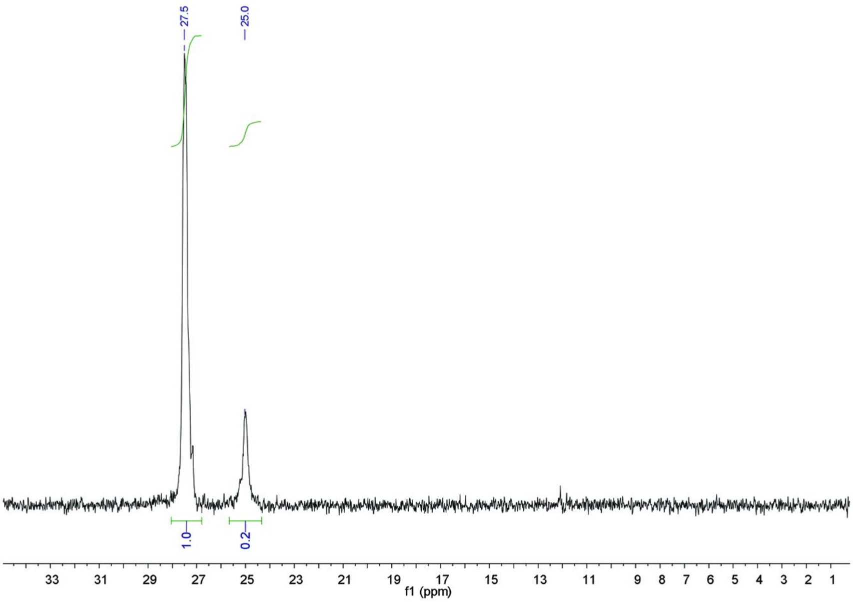

*Figure 1. ^{31}P NMR spectrum from the crude product of POSS-MAMA-SG1 alkoxyamine **2**, product obtained in the experiments with an equimolar ratio of amine group and alkoxyamine **1,** in CDCl$_3$.*

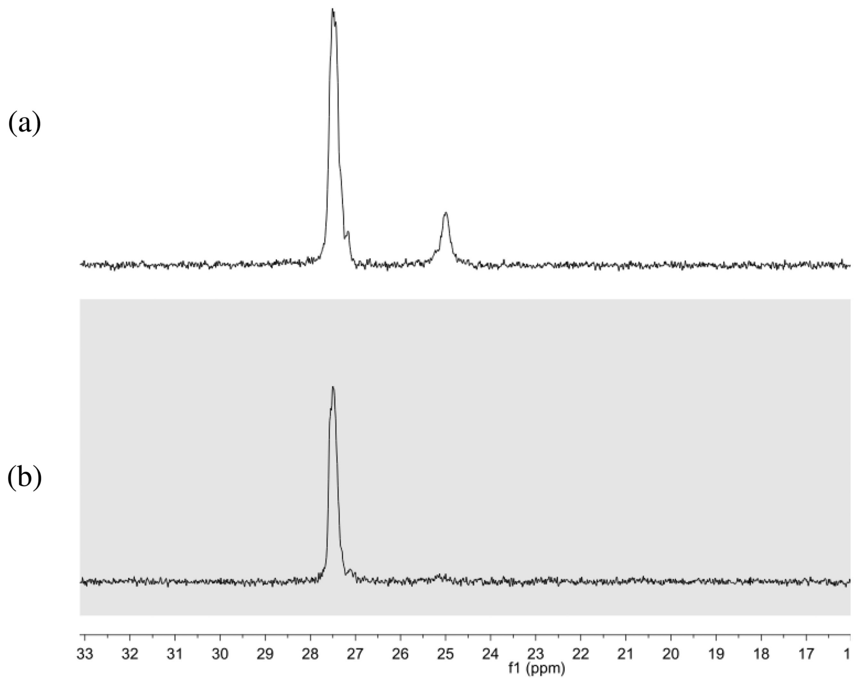

Figure 2. ^{31}P NMR spectra of POSS-MAMA-SG1 alkoxyamine ***2 (a)*** *before and* ***(b)*** *after washing with diethyl ether, products resulting from the experiment working with an equimolar ratio of amine group and alkoxyamine* ***1****, in $CDCl_3$.*

In addition to NMR analysis, ESI-MS was used to characterize the functionality of POSS based alkoxyamines. The ESI mass spectrum of POSS-MAMA-SG1, product resulting from experiment 1 (Figure 3), indicated the absence of a peak corresponding to the unreacted NHS-MAMA-SG1 but also the presence of different POSS based alkoxymine species with 3 to 6 initiating sites (MAMA-SG1) per POSS molecule. As expected, the ESI mass spectrum of POSS-MAMA-SG1 (not shown here), product resulting from experiment 2, shown the peak corresponding to the unreacted NHS-MAMA-SG1 ($[M + H]^+$ at *m/z* 479.2) that could not be completely eliminated from the crude product as well as the presence of several peaks corresponding to POSS based alkoxyamine with 5, 6, 7 and 8 initiating sites. By combination of these different characterizations, we denote afterwards, POSS-MAMA-SG1*(a)* as the “pure” alkoxyamine **2** having about 5 - 6 initiating sites (NMR value) per POSS molecule and POSS-MAMA-SG1*(b)* as the sample containing both NHS-MAMA-SG1 and 7 - 8 initiating sites (NMR value) per POSS molecule.

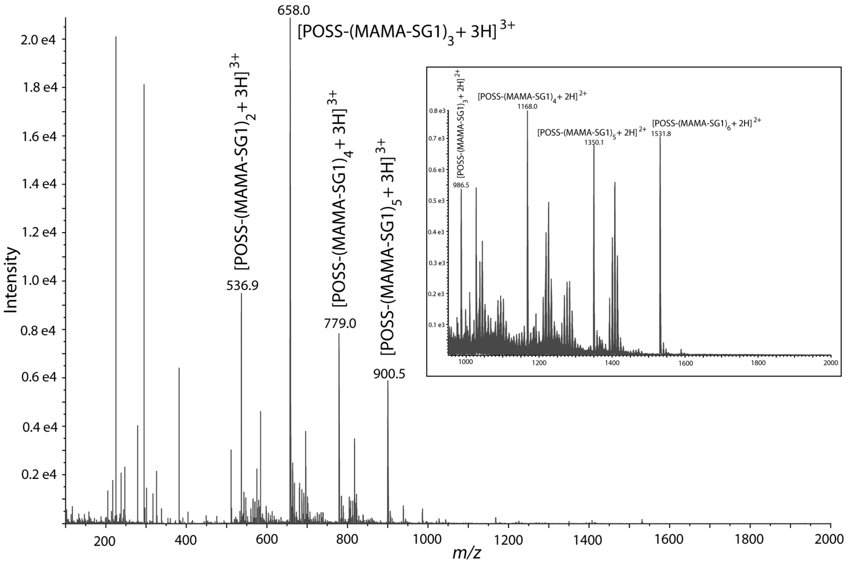

Figure 3. ESI mass spectrum of POSS-based alkoxyamine prepared in the experiment working with an equimolar ratio of amine group and alkoxyamine ***1****. The spectrum indicates the formation of POSS-(MAMA-SG1)$_n$, with n ranging from 2 to 6. Inset : zoom of the mass spectrum in the m/z range 900-2000.*

Synthesis of Star PS

The advent of controlled radical polymerization techniques, such as NMP, ATRP, and RAFT, has rendered the preparation of well-defined star polymers much easier, starting from proper multifunctional initiators with known number of initiating sites. Most star polymers with varying number of arms have been prepared via ATRP "grafting-from" strategy (*4*–*6*, *36*). Starting from POSS-based octafunctional ATRP initiator, organic/inorganic nanocomposite star polymers have been recently prepared by Laine et al. (*28*), He et al. (*29*), and Liu et al (*30*).

The obtained POSS-MAMA-SG1 alkoxyamine **2** was then used as multifunctional initiator for the NMP of styrene. Five different polymerizations of styrene were carried out either in bulk or in solution using toluene or ethyl benzene as solvent. The reaction conditions are detailed in Table 1. Whatever the targeted molecular weight and polymerization process, the kinetic curves relative to ln([M]$_0$/[M]) versus time was of first order with respect to monomer (Figure 4), indicating a constant concentration of active species throughout the reaction. As expected, the polymerization rate was significantly higher in bulk than in solution polymerization at the same polymerization temperature (Figure 4, entries (1) and (2)) as well as when the initiator concentration is high (Figure 4, entries (2) and (3)). Indeed, polymerization rate is proportional to monomer and initiator concentration, and these concentrations were lower in the solution polymerization than in the bulk one.

Table 1. Reaction conditions tested for the synthesis of star PS using POSS-MAMA-SG1 alkoxyamine 2 as initiator

Entry	*Styrene g (mol)*	*POSS-MAMA-SG1 mg (mol)*	*Solvent*	*target M_n*[c] *(g.mol^{-1})*	*T (°C)*	*over-all time (min)*
(1)[a]	3.00 (2.86 x10^{-2})	127 (2.78 x10^{-5})	Toluene	110 000	100	420
(2)[a]	3.00 (2.86 x10^{-2})	127 (2.78 x10^{-5})	/	110 000	100	210
(3)[a]	3.00 (2.86 x10^{-2})	71 (1.57 x10^{-5})	/	190 000	100	210
(4)[a]	3.00 (2.86 x10^{-2})	127 (2.78 x10^{-5})	Ethyl-benzene	110 000	120	180
(5)[b]	3.00 (2.86 x10^{-2})	127 (2.78 x10^{-5})	Toluene	110 000	100	420

[a] Studies (1), (2) and (3) were performed using POSS-MAMA-SG1*(a)* resulting from the experiment with an equimolar of POSS amine groups and alkoxyamine **1**. [b] Study (5) was performed using POSS-MAMA-SG1*(b)* resulting from the experiment with an excess of alkoxyamine **1** compared to POSS amine groups, it means that the product contains both mono and multifunctional initiators. [c] Expected star-polymer molar mass at 100% conversion. Monomer concentration in solvent was fixed at 60 wt % for all solution polymerisations.

Control over the growth of polymer chains was furthermore evidenced by the linear evolution of molecular weight with conversion as well as a low polydispersitiy of 1.14 at monomer conversion of 40% (Figure 5). Experiments (1) and (2) have the same theoretical line because they only differ on the polymerization conditions (bulk or solution polymerization), it may only affect the reaction kinetic. As it can be seen, the experimental molecular weights data corresponding to experiments (1), (2) and (3) are slightly below the theoretical ones which were calculated from the relation $M_{n(th)} = ([M]/[I]_o \times MW_{monomer}) + MW_{initiator}$. It has been pointed out that the radius of gyration of a star molecule is lower than that of a linear molecule with the same molecular weight due to the packing of the chains attached to the same core. Therefore, the hydrodynamic properties are affected, and SEC analyses based on linear polystyrene standards give molecular weights lower than expected, causing the experimental data to shift to the region below the theoretical line.

There is not significant increase of polymer dispersity with monomer conversion in the experiments (2) and (3) which only differ to each other on the initiator concentration. Dispersities of 1.14 and 1.17 are obtained for polymers generated from entry (2) and (3) respectively. The obtained polymers with broader M_n distribution are usually expected when initiator concentrations is increased as noted by Laine et al. (*28*) in the ATRP of methyl methacrylate using POSS based initiator. Indeed, the increase of catalyst and initiator concentrations engenders radicals with longer average lifetime and a higher concentration of active stars present in the reaction medium. In consequence, the occurrence of termination reactions increases and polymers with broader M_n distribution were obtained.

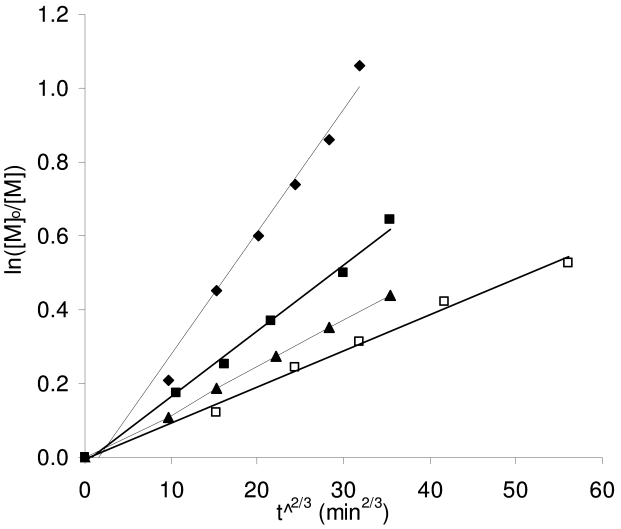

Figure 4. Semilogarithmic kinetics plot for the synthesis of star PS initiated by POSS-MAMA-SG1 under different polymerization conditions. □*: (1) solution polymerization in toluene at 100°C with $M_{n\ targeted}$ = 110 000 g.mol^{-1},* ■*: (2) bulk polymerization at 100°C with $M_{n\ targeted}$ = 110 000 g.mol^{-1};* ▲*: (3) bulk polymerization at 100°C with $M_{n\ targeted}$ = 190 000 g.mol^{-1};* ♦*: (4) solution polymerization in ethylbenzene at 120°C with $M_{n\ targeted}$ = 110 000 g.mol^{-1}. For detailed conditions of these studies, refer to Table 1.*

SEC traces shown in Figure 6 display unimodal and relatively symmetrical peaks for PS star polymers resulting from experiment (1). We note that chromatographic peaks became less and less symmetric with the increase of styrene conversion. Beyond 35% conversion, the base of peak trace becomes broader and a very slight shoulder appears in the high molar mass side of the SEC traces. This result can be attributed to the inter or intra-star coupling of the growing radicals due to irreversible termination reactions that are never totally negligible. Similar results have been already observed during the preparation of star polymers from POSS based or calixaren derivative octafunctional initiators (*4*, *28*, *30*). Nevertheless, the presence of higher molecular weight species derived from termination coupling observed in the chromatograms for experiments (1) (Figure 6), (2) and (3) (not shown here) were less pronounced than that reported in the literature at the same conversion.

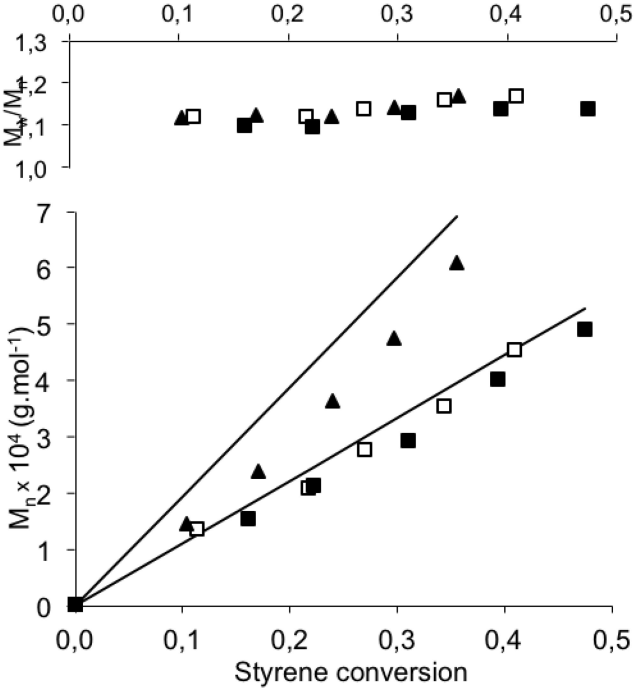

Figure 5. $M_{n(th)}$ (drawn line); M_n (symbols) and M_w/M_n versus conversion for star PS initiated by POSS-MAMA-SG1(a) under different polymerization conditions. □: (1) solution polymerization in toluene at 100°C with $M_{n\ targeted}$ = 110 000 g.mol^{-1}, ■: (2) bulk polymerization at 100°C with $M_{n\ targeted}$ = 110 000 g.mol^{-1}; ▲: (3) bulk polymerization at 100°C with $M_{n\ targeted}$ = 190 000 g.mol^{-1}.

Experiments (1) and (4) were carried out in the same experimental conditions but at two different temperatures 100°C and 120°C. As expected, the polymerization rate was significantly higher at 120°C than at 100°C (Figure 4). Indeed, the cleavage rate constant k_d depends on the dissociation energy of the alkoxyamine bond and Arrhenius temperature while cross-combination constant k_c shows non-Arrhenius temperature dependencies (*37*). The polymerization proceeds to high conversion (65%) within three hours at 120°C. Figure 7 shows the chromatograms of polymers generated from polymerizations performed at 100°C and 120°C having similar molecular weight. As we can see, polymer formed from polymerization at 120°C exhibited broader distribution than that obtained by polymerization at 100°C, indicating that high temperature increases growing radical reactivity, thus favouring termination reactions and leads to more polydisperse materials. We also noted that the shoulder appearing in the high molar mass side of the SEC traces was visible since 60 min, corresponding to 32% monomer conversion, of polymerization carrying out at 120°C.

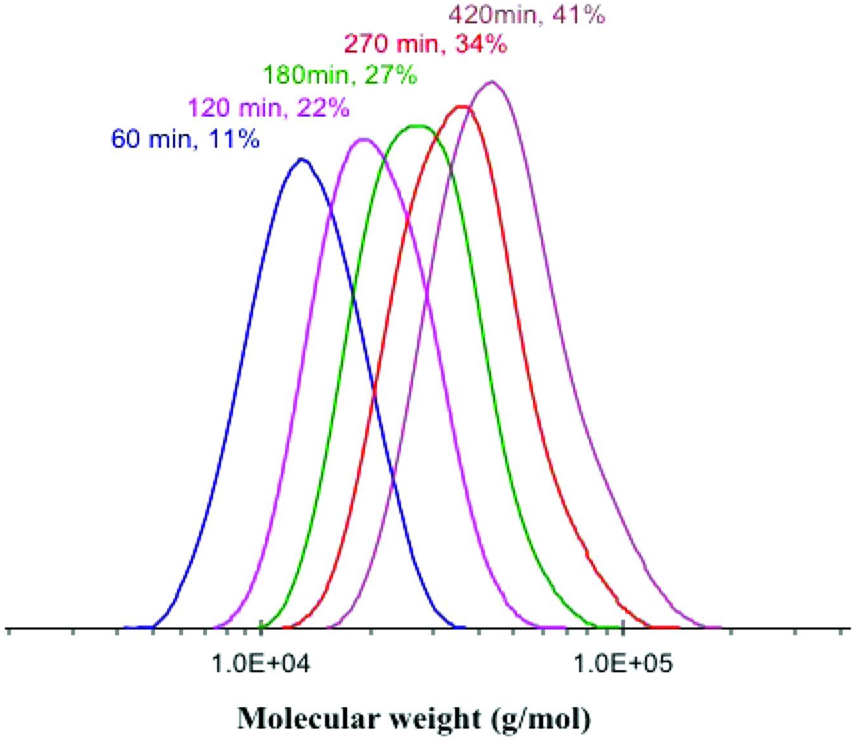

Figure 6. Evolution of SEC traces during synthesis of PS star polymer. Experimental conditions: [POSS-MAMA-SG1]$_o$/[styrene]$_o$ = 1 : 1023 ; in toluene at 100°C; monomer concentration in solution = 60wt %; linear polystyrene standards were used for calibration of the THF SEC.

Through these different polymerizations, it seems that the optimum reaction conditions to obtain better control of the star architecture are low monomer conversion (not exceeding 30%) and low reaction temperature. These parameters are quite important because they permit us to generate nanocomposite materials with the highest degree of control of dispersion and hence of mechanical properties.

The effect of the presence of both mono- and multifunctional initiators in the polymerization of styrene was investigated in a solution polymerization of styrene carried out at 100°C using POSS-MAMA-SG1*(b)* as initiator (experiment (5), Table 1). Recall that POSS-MAMA-SG1*(b)* was obtained from the experiment of alkoxyamine **1** with POSS amine in a molar ratio of 12 alkoxyamines **1** for 8 amino groups. Because of the unsuccessful attempt of purification of the resulting product, sample POSS-MAMA-SG1*(b)* contains both mono and multifunctional initiators in a molar proportion of 1:2 with respect to the initiating site. Thus, in the same experiment using POSS-MAMA-SG1*(b)* as initiator, we generate both star and linear polymers. Similar experiment reported by Gnanou et al. (*4*), used a mixture that was equimolar in mono and octafunctional initiators with respect to the initiating sites to polymerize styrene. Their objective was to generate both star and linear polymers in the same experiment and by comparing the molar masses of star and linear polymers, they deduced the functionality of star polystyrenes in the condition knowing the real number-average molecular weight of the stars.

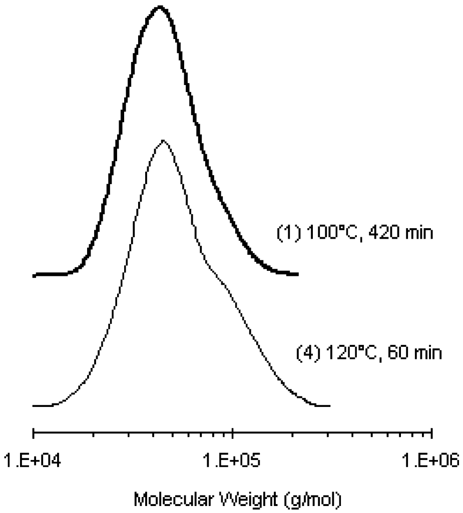

Figure 7. SEC traces of star polymers with similar M_n but obtained under different polymerization conditions. (1) solution polymerization in toluene at 100°C with $M_{n\ targeted}$ = 110 000 g.mol^{-1}, (4) solution polymerization in ethylbenzene at 120°C with $M_{n\ targeted}$ = 110 000 g.mol^{-1}. For detailed conditions of studies (1) and (4), refer to Table 1.

As we can see, SEC traces shown in Figure 8 exhibited two peaks, the one appearing at lower elution volumes corresponding to the star and the other one to the linear polymer. The SEC elugrams shift steadily to lower elution volumes with increasing conversion as well as for the peaks corresponding to the star than that corresponding to the linear polymers. The multiple Gaussian functions of the chromatography peaks were deconvoluted using Origin software. The molar mass of star and linear polystyrenes, determined by THF SEC according to the relative calibration curve established with linear polystyrene standards, increase linearly with the conversion (Figure 9). The ratios of area under the curve at lower elution volumes to that of the peak at higher elution volumes (RI detector) increase progressively from the value of 0.84 to 1.21 at the beginning to the end of polymerization. This implies that the rates of polymerization of styrene with respect to mono- and multifunctional initiators were reversed during polymerization. We attributed rather this result by the decrease of the accessibility of stars growing radicals compared to that of linear ones when monomer conversion is increased. Similarly to experiment (1), we also observed a slight shoulder appearing in the high elution volumes of the peaks corresponding to the star polystyrenes (Figure 8) with increasing reaction reaction time. On the other hand, we did not detect any shoulders or even peaks widening for the peaks corresponding to linear polystyrenes. The shoulder observed in the high elution volumes of the peaks corresponding to the star polystyrenes is putatively attributed to the star coupling of the growing radicals due to the proximity of star arms.

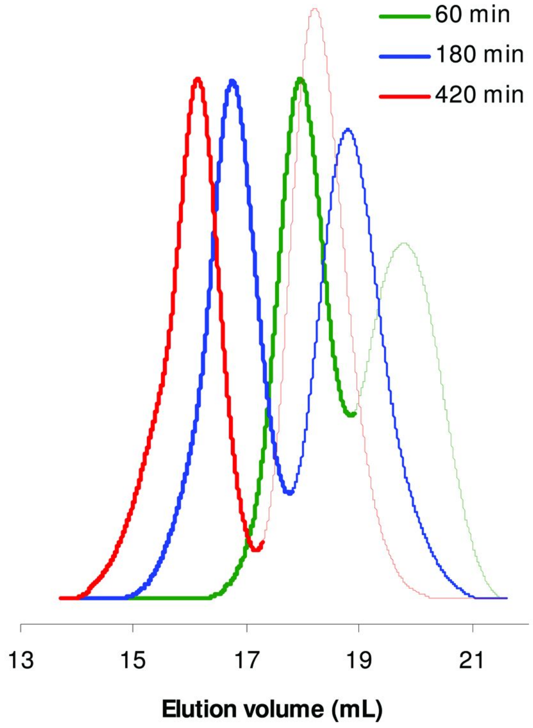

Figure 8. Evolution of the SEC traces (RI detector) at different states of the solution polymerization of styrene using POSS-MAMA-SG1(b) as initiator. Polymerization was carried out in toluene at 100°C with $M_{n\ targeted}$ = 110 000 g.mol^{-1} (study (5), Table 1). Analyzed samples contain a mixture of linear and star polystyrene, peaks in bold lines corresponding to star polystyrene and those in thin lines corresponding to linear one.

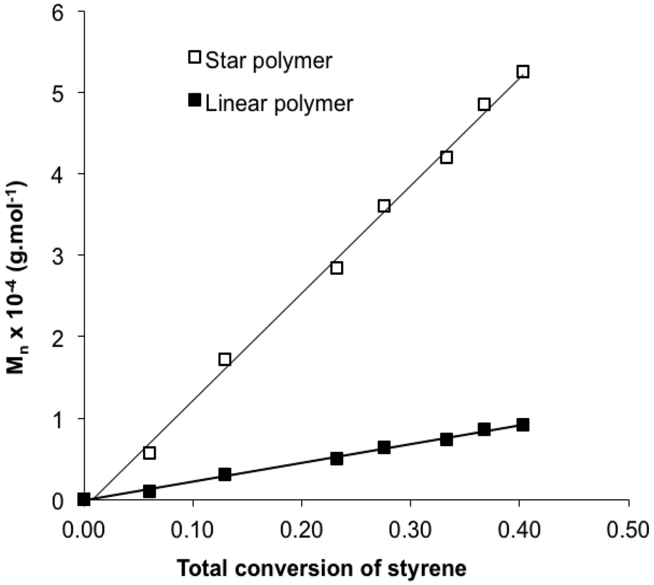

Figure 9. Evolution of M_n (symbols) versus conversion for star and linear PS initiated by POSS-MAMA-SG1(b) in the same solution polymerization of styrene in toluene at 100°C with $M_{n\ targeted}$ = 110 000 g.mol^{-1}. Lines are used only to guide the eyes.

Determination of Numbers of Arms

Core destruction has been reported as a useful method to determine the number of branches in star structure (*4*, *28*, *30*). The cubes offer a unique opportunity to do this because the PS arms can be disintegrated from the core by cleaving the siloxane bonds of the cubic silsesquioxane with concentrated HF. By comparing the molecular weight of stars before and after core destruction, one can obtain another proof for the star structure. Figure 10 compares the THF SEC traces of the star and cleaved product from experiment (1). Elugram of the cleaved product exhibited a relatively symmetric peak, reporting a dispersity, M_w/M_n of 1.2 and an M_n of 8900 g/mol. The ratio between the molar masses obtained before (M_n = 45300 g/mol) and after hydrolysis (M_n = 8900 g/mol) was found to be 5.1 which is slightly below the maximum of 6 arms possible (remind that POSS-MAMA-SG1*(a)* initiator used in study (1) contained about 5 - 6 initiating sites for each initiator molecule). The problem with this calculation is that star polymers present a lower hydrodynamic volume than a linear polymer with the same molecular weight. This implies that the real number-average molecular weight of the star polymer is higher than 45300 g/mol determined by THF SEC. Besides, once the silsesquioxane is cleaved, the resulted “high” molecular weight product can precipitate as silica gel. If not taken into account, these both factors would contribute to give an incorrect estimation of the number of arms.

Hydrolysis of poorly defined star, product of experiement (4), (in which a shoulder in the high molecular weight region was seen in it SEC trace) also resulted in linear polymers, but the SEC trace, unlike the case of well-defined stars, was not monomodal and presented a shoulder on the high molecular weight region (not shown here). The presence of this shoulder further substantiates the occurrence of star-star coupling during the radical propagation process. Similar results have also been observed by other authors (*28*, *30*) during the preparation of star polymers from POSS-based octafunctional ATRP initiator. In addition, the error in the determination of the number of arms can be affected by star-star coupling. Indeed, when star-star coupling occurs, double or even triple stars could be formed and impedes the propagation of one or two arms, the Mn of coupling arm doubles instantly, thus decreasing the average number of arms.

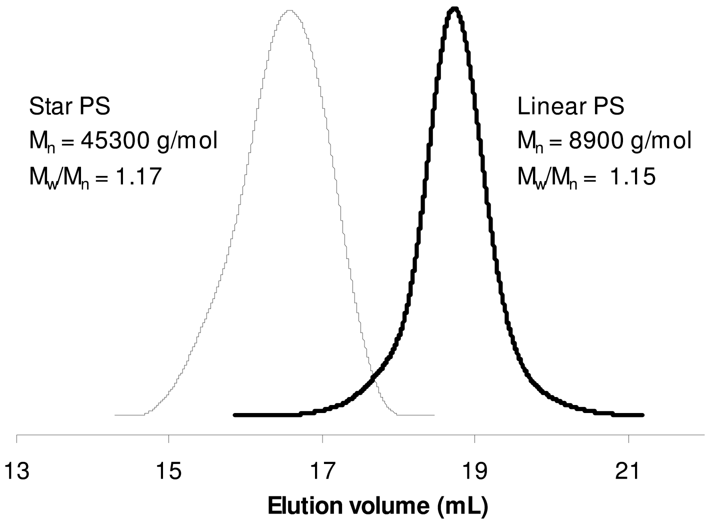

Figure 10. THF SEC traces of one star PS obtained from study (1) $[POSS\text{-}MAMA\text{-}SG1]_o/[styrene]_o = 1 : 1023$; in toluene at 100°C; and of the cleaved product resulting from reaction of the star with concentrated HF at 40°C.

DSC Studies of Star PS and Their Cleaved Products

Glass transition temperature (T_g) of star-PS1 (well-defined star PS issue from study (1)), star-PS4 (poorly defined star PS issue from study (4)) and their corresponding cleaved products was determined by DSC. Figure 11 shows DSC thermograms of these samples. The data revealed similar T_g values between star-PS1 and star-PS4, they exhibited respectively a T_g of 101 and 99°C. We expected a higher T_g for the poorly defined star PS4 compared to that of the well-defined star PS1 because the inter- and intrastar coupling reactions were more pronounced during the polymerization leading to star PS4 (see Figure 7). When the star coupling reactions occur, the free chain ends of PS arms decrease, which will reduce the chain mobility and thus increase the T_g value. This did not happen in our case because the proportion of chain end decrease resulting from intra or interstar coupling was maybe to low to have a significant effect on the star PS thermal behaviour. Nevertheless, the measured T_g values are largely higher than T_g of a linear PS having the same molecular weight than that of PS arms which means 9000 g/mol. The chemical bonding between PS arms and POSS core that reduces the chains mobility can explain this. This trend was already observed for poly(ethylene oxide) (*38*), poly(methyl methacrylate) (*29*) and polystyrene (*31*) when the latter are attached to the inorganic POSS surface. After etching with HF, T_g values for the cleaved products from well-defined star PS1 and poorly defined star PS4 were determined to be 95 and 89°C, respectively. The treatment with HF resulted in the release of PS arms covalently attached at the POSS surface. Thus, the number of chain ends is doubled; the chains mobility is increased as well as the decrease of overall molecular weight. All of these factors contribute propably to the decrease of T_g for the cleaved products. However, a deeper investigation study is required to understand the underlining mechanism of “confinement” caused by the POSS core on polystyrene segments.

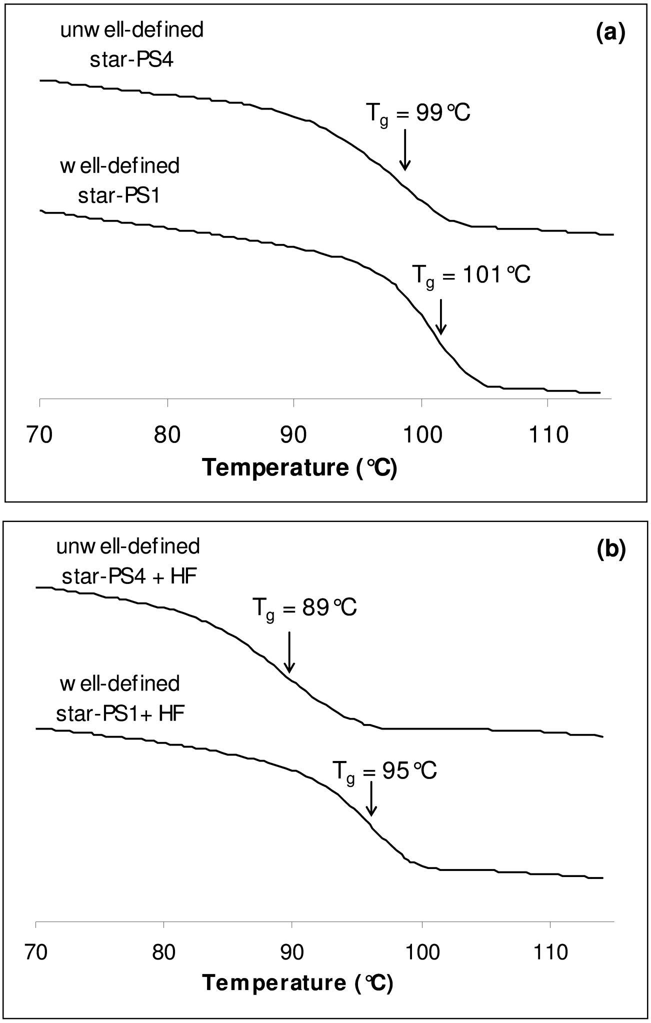

Figure 11. Differential scanning calorimetry thermograms recorded for ***(a)*** *star polystyrenes and* ***(b)*** *the corresponding cleaved products obtained by treating star PS with HF at 40°C in tetrahydrofuran.*

Conclusion

We have successfully synthesized the well-characterized POSS based multifunctional NMP initiator for the first time. The use of the latter in the NMP of styrene allowed producing POSS-core star polystyrenes, which are considered as organic/inorganic hybrid nanocomposites. Well-defined star polystyrenes could be synthesized by maintaining the monomer conversion below 30% and working at a mild temperature about 100°C, beyond which star-star coupling occurs as a result of inevitable termination led to the formation of product with large distribution. By cleaving the core structure with HF solution, the average number of arms was determined to be 5, below the maximum of 6.5 arms possible corresponding to the average number of initiating sites for each initiator molecule. DSC results revealed significantly higher glass transition temperature of POSS-cored star polystyrene as compared with linear PS of comparable molecular weight.

Acknowledgments

This work was financially supported by GENESIS project, University of Provence and CNRS

References

1. Hadjichristidis, N.; Pitsikalis, M.; Pispas, S.; Iatrou, H. *Chem. Rev.* **2001**, *101*, 3747–3792.
2. Charleux, B.; Faust, R. *Adv. Polym. Sci.* **1999**, *142*, 1–69.
3. Hirao, A.; Hayashi, M.; Matsuo, A. *Polymer* **2002**, *43*, 7125–7131.
4. Angot, S.; Murthy, K. S.; Taton, D.; Gnanou, Y. *Macromolecules* **1998**, *31*, 7218–7225.
5. Ueda, J.; Kamigaito, M.; Sawamoto, M. *Macromolecules* **1998**, *31*, 6762–6768.
6. Matyjaszewski, K.; Miller, P. J.; Pyun, J.; Kickelbick, G.; Diamanti, S. *Macromolecules* **1999**, *32*, 6526–6535.
7. Ohno, K.; Wong, B.; Haddleton, D. M. *J. Polym. Sci., Part A: Polym.Chem.* **2001**, *39*, 2206–2214.
8. Stenzel-Rosenbaum, M.; Davis, T. P.; Chen, V.; Fane, A. G. *J. Polym. Sci., Part A: Polym.Chem.* **2001**, *39*, 2777–2783.
9. Zhang, X.; Xia, J.; Matyjaszewski, K. *Macromolecules* **2000**, *33*, 2340–2345.
10. Baek, K. Y.; Kamigaito, M.; Sawamoto, M. *Macromolecules* **2001**, *34*, 215–221.
11. Gao, H.; Matyjaszewski, K. *Macromolecules* **2006**, *39*, 4960–4965.
12. Whittaker, M. R.; Urbani, C. N.; Monteiro, M. J. *J. Am. Chem. Soc* **2006**, *128*, 11360–11361.
13. Gao, H.; Ohno, S.; Matyjaszewski, K. *J. Am. Chem. Soc* **2006**, *128*, 15111–15113.
14. Gao, H.; Matyjaszewski, K. *Macromolecules* **2007**, *40*, 399–401.

15. Kakuchi, T.; Narumi, A.; Matsuda, T.; Miura, Y.; Sugimoto, N.; Satoh, T.; Kagas, H. *Macromolecules* **2003**, *36*, 3914–3920.
16. Celik, A.; Kemikli, N.; Ozturk, R.; Muftuoglu, A. E.; Yilmaz, F. *React. Funct. Polym.* **2009**, *69*, 705–713.
17. Kim, K. M.; Ouchi, Y.; Chujo, Y. *Polym. Bull.* **2003**, *49* (5), 341–348.
18. Liu, Y.; Yang, X.; Zhang, W.; Zheng, S. *Polymer* **2006**, *47* (19), 6814–6825.
19. Zhang, C.; Bunning, T. J.; Laine, R. M. *Chem. Mater* **2001**, *13*, 3653–3662.
20. Zheng, L.; Farris, R. J.; Coughlin, E. B. *Macromolecules* **2001**, *34*, 8034–8039.
21. Gonsalves, K. E.; Merhari, L.; Wu, H.; Hu, Y. *Adv. Mater.* **2001**, *13*, 703–714.
22. Lichtenhan, J. D.; Otonari, Y. A.; Carr, M. J. *Macromolecules* **1995**, *28*, 8435–8437.
23. Mather, P. T.; Jeon, H. G.; Romo-Uribe, A.; Haddad, T. S.; Lichtenhan, J. D. *Macromolecules* **1999**, *32*, 1194–1203.
24. Franchini, E.; Galy, J.; Gérard, J. F.; Tabuani, D.; Medici, A. *Polym. Degrad. Stab.* **2009**, *94*, 1728–1736.
25. Pyun, J.; Matyjaszewski, K.; Wu, J.; Kim, G. M.; Chun, S. B.; Mather, P. T. *Polymer* **2003**, *44*, 2739–2750.
26. Xu, H.; Kuo, S. W.; Lee, J. S.; Chang, F. C. *Macromolecules* **2002**, *35*, 8788–8793.
27. Huang, C. F.; Kuo, S. W.; Lin, F. J.; Huang, W. J.; Wang, C. F.; Chen, W. Y.; Chang, F. C. *Macromolecules* **2006**, *39*, 300–308.
28. Costa, R. O. R.; Vasconcelos, W. L.; Tamaki, R.; Laine, R. M. *Macromolecules* **2001**, *34* (16), 5398–5407.
29. Hussain, H.; Mya, K. Y.; Xiao, Y.; He, C. *J. Polym. Sci., Part A: Polym. Chem.* **2008**, *46*, 766–776.
30. Ge, Z.; Zhou, Y.; Liu, H.; Liu, S. *Macromolecules* **2009**, *42* (8), 2903–2910.
31. Lu, C. H.; Wang, J. H.; Chang, F. C.; Kuo, S. W. *Macromol. Chem. Phys.* **2010**, *211*, 1339–1347.
32. Vinas, J.; Chagneux, N.; Gigmes, D.; Trimaille, T.; Favier, A.; Bertin, D. *Polymer* **2008**, *49*, 3639–3647.
33. Gravel, M. C.; Zhang, C.; Dinderman, M.; Laine, R. M. *Appl. Organomet. Chem.* **1999**, *13*, 329–336.
34. Naka, K.; Fujita, M.; Tanaka, K.; Chujo, Y. *Langmuir* **2007**, *23*, 9057–9063.
35. Feher, F. J.; Wyndham, K. D. *Chem. Commun.* **1998**, *1998*, 323–324.
36. Matyjaszewski, K.; Miller, P. J.; Fossum, E.; Nakagawa, Y. *Appl. Organomet. Chem.* **1998**, *12*, 667–673.
37. Ananchenko, G. S.; Souaille, M.; Fischer, H.; Le Mercier, C.; Tordo, P. *J. Polym. Sci: Part A: Polym. Chem.* **2002**, *40* (19), 3264–3283.
38. Maitra, P.; Wunder, L. S. *Chem. Mater.* **2002**, *14*, 4494–4497.

In Progress in Controlled Radical Polymerization: Materials and Applications; Matyjaszewski, K., et al.;
ACS Symposium Series; American Chemical Society: Washington, DC, 2012.

Chapter 11

Polymer−Inorganic Hybrid Materials Using Controlled Radical Polymerization

A. O. Patil,[*] H. Dong, A. H. Tsou, and S. Bodige

**Corporate Strategic Research Laboratory,
ExxonMobil Research & Engineering Company,
Route 22 East, Annandale, New Jersey 08801
[*]E-mail: Abhimanyu.o.patil@exxonmobil.com**

This chapter deals with the synthesis and characterization of novel polymer composite materials, with an emphasis on the control of molecular and nanoscale structure to enable the design of specific properties that are otherwise inaccessible. The particular interest is in compatabilizing interfaces between organic and inorganic matter as a route to combine the advantageous properties of both components. Recent developments in polymer chemistry offer the synthetic chemist a wide range of tools to prepare well-defined, highly functional building blocks. Controlled Radical Polymerization (CRP) has been shown to be suitable for the preparation of organic/inorganic hybrid materials with varying structural complexity. Atom transfer radical polymerization (ATRP) has been particularly successful for the synthesis and preparation of nanocomposite structures since inorganic particles and substrates can be easily functionalized with initiating alkyl halides. The resulting functional inorganic material is suitable for use in the CRP of organic vinyl monomers.

The ATRP of octadecyl acrylate (ODA) (monomer with long hydrophobic side chains to obtain comb polymers) has been investigated and optimized to produce polymers with

In Progress in Controlled Radical Polymerization: Materials and Applications; Matyjaszewski, K., et al.;
ACS Symposium Series; American Chemical Society: Washington, DC, 2012.

predetermined molecular weights and narrow polydispersities. The soluble alkyl substituted 2,2-bipyridine was used with Cu(I)Br and ethyl-2-bromoisobutyrate (EBiB) as initiator for polymerization. To introduce high-density polymeric organic phase onto silica, initiator-modified silica was prepared and then surface-initiated ATRP ("grafting-from" method) was carried out with ODA. The resultant polymer-grafted silica was used to prepare polyethylene-silica nanocomposites.

Section I. Introduction

Radical polymerization, as with any chain-growth polymerization, consists of several elementary reactions (*1*). Once initiated by creation of a radical, the chain grows by addition of monomers until eventually it terminates by interaction with a different radical. However, radical polymerization is very efficient, but is a rapid and uncontrolled process. The result is polymers that are polydisperse in molecular weight and architecture. Low density polyethylene is a classic example.

In contrast, living polymerization provides a steady addition of monomer units in a controlled manner. Commercial products based on living anionic polymerization started appearing in the 1980s, based on polymerization of a limited range of non-polar monomers such as styrene, isoprene, or butadiene. The challenge has always been to make this polymerization process broadly applicable to more monomers (*2*, *3*).

One would like to be able to combine these two strategies in a way that gives more controlled but still effective polymerization. The problem is that chain growth in a radical polymerization is very rapid; a monomer unit is added to the growing chain every millisecond (*1–3*). After perhaps 1,000 monomer units are added, the chain terminates. So the life of a propagating chain - the time during which you can control the chemistry - is only about one second. That's a very short time, and it makes radical polymerization very difficult to manage. The question was, how could one extend the life of the growing chains from one second to one day, so to provide enough time to manipulate the chemistry.

The idea behind CPR is to allow chains to add one or two monomer units and then send them to sleep. In this way, a chain grows for one or two milliseconds and then becomes inactive or dormant. Then, after a few seconds or perhaps a minute, it wakes up again, adds a couple of polymer units, and again goes back to sleep. Thus, a one-second lifetime of a propagating chain is divided into a thousand pieces of one millisecond each, and, between these one-millisecond bursts of activity, a one-minute period of dormancy is inserted. A one-second chain lifetime is now expanded to approximately 1,000 minutes, or one day. Therefore, one now may have a day to perform a number of complex chemical transformations. Moreover, one can use multifunctional initiators to prepare sophisticated structures, such as star polymers, brushes, or even dendritic or hyper-branch polymers; and one can make block copolymers, graft copolymers, or gradient copolymers (*2*, *3*). In this way, CPR approaches a "living" polymerization process.

The main advantage of radical polymerization is that one can polymerize a relatively broad range of monomers such as styrene, ethylene, acrylates. Moreover, unlike *living* anionic polymerization, which require very stringent conditions-practically zero moisture, zero air, and no impurities-radical reactions can be carried out relatively easily (*4*, *5*).

Controlled Radical Polymerization (CRP)

CRP has proved to be a versatile and robust method to prepare well-defined organic polymers. In the past decade, several CPR techniques have been developed. A major difference between conventional radical [i.e., azobis(isobutyronitrile)- or peroxide-initiated processes] and CPR is the lifetime of the propagating radical during the course of the reaction. In conventional radical processes, radicals generated by decomposition of the initiator undergo propagation and bimolecular termination reactions within a second. In contrast, the lifetime of a growing radical can be extended to several hours in a CRP, enabling the preparation of polymers with predefined molar masses, low polydispersity, controlled compositions, and functionality.

The mechanism invoked in CRP to extend the lifetime of growing radicals utilizes a dynamic equilibration between dormant and active sites with rapid exchange between the two states. Unlike conventional radical processes, CRP requires the use of persistent radical (deactivator) species, or highly active transfer agents to react with propagating radicals. These persistent radicals/transfer agents react with radicals (deactivation or transfer reactions with rate constant, K_{deact}) to form the dormant species. Conversely, propagating radicals are generated from the dormant species by an activation reaction (with rate constant, K_{act}).

Classification of CRP Systems

In the past decade, the field of CRP has seen tremendous development as evidenced by the wide range of materials that have been prepared using these techniques. In particular, three methods of considerable importance are the following:

- Stable free-radical polymerization [SFRP; e.g., nitroxide-mediated polymerization (NMP)]
- Metal-catalyzed atom transfer radical polymerization (ATRP)
- Degenerative transfer [e.g., reversible addition-fragmentation chain transfer (RAFT) polymerization].

While these three methods rely on different components, general similarities can be seen in the use of initiators, radical mediators (i.e., persistent radicals or transfer agents), and in some cases catalysts (*6*). It is important to note that while SFRP and ATRP are subject to the persistent radical effect (PRE), degenerative processes, such as RAFT, do not conform to the PRE model because of the transfer-dominated nature of the reaction (*3*).

Atom Transfer Radical Polymerization (ATRP)

Atom-transfer radical polymerization (ATRP) is one of the several techniques for controlled radical polymerizations that yields well defined (co)polymers with precisely controlled architecture and functionality. ATRP can be used to polymerize several monomers like acrylates and styrene under conditions that are much less rigorous than previously required for living ionic polymerizations. ATRP is among the most efficient and robust CRP processes (*7*, *8*).

The original ATRP system used relatively inexpensive alkyl halides as initiators and copper complexes with simple commercially available ligands as the catalytic system (*3*). ATRP adapts a known organic-chemistry reaction, atom transfer radical addition, to polymer synthesis. Other transition metals can be applied as catalysts for ATRP, most notably ruthenium (*3*).

ATRP controls free-radical polymerization by the reversible activation/ deactivation of growing chains. A small amount of the chains remain active during the reaction, whereas the majority of the chains dormant awaiting reactivation. Thus, the concentration of free-radical species is kept low and, consequently, termination processes are suppressed. It is the suppression of the termination process, particularly combination reactions that help ATRP achieve controlled molecular weights and low polydispersities in the final products. Equilibrium between active and dormant chains is most commonly maintained by the reversible cleavage of a carbon-halogen bond of an alkyl halide, mediated by the presence of a copper (I) catalyst and a suitable ligand. The cleavage results in a copper (II) complex and an alkyl radical that can either undergo deactivation, propagation with monomer units, or irreversibly terminate.

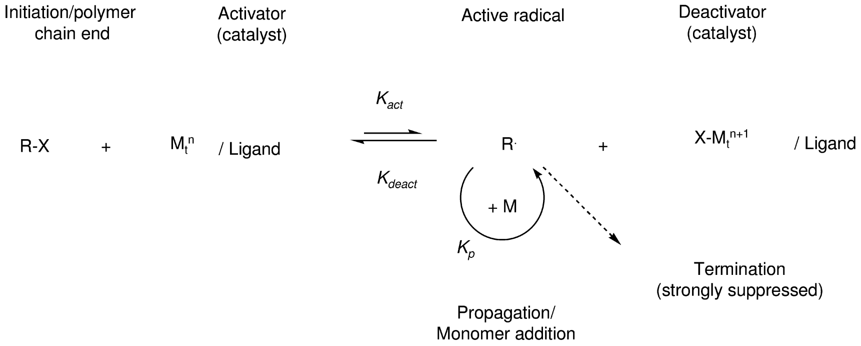
Initiation/polymer chain end
Activator (catalyst)
Active radical
Deactivator (catalyst)
K_{act}
R-X
+
M_t^n / Ligand
K_{deact}
R·
+
$X\text{-}M_t^{n+1}$ / Ligand
+ M
K_p
Termination (strongly suppressed)
Propagation/ Monomer addition

ATRP is especially well-suited for surface modification and the preparation of molecular brushes on micro- or nano-scale inorganic particles with surface hydroxyls because those surface hydroxyl groups can be easily converted to ATRP-active initiators: R-bromoesters (*9*). Additionally, the controlled nature of ATRP allows all surface polymer chains to be grown (with monomers) evenly, leading to high surface polymer coverage forming well-defined polymer brushes.

Copper-mediated ATRP has been established for over a decade and is the subject of well over a thousand publications. It is being used to prepare block copolymers, star copolymers, and polymers from surfaces. Applications being investigated are as diverse as chromatographic separation, new therapeutics, dispersants for pigments and particulates, sealants, coatings, personal care products, etc (*2*, *3*). However, ATRP is not useful for monomers like ethylene or α-olefins like 1-hexene, 1-octene, or 1-decene. Therefore, examples of ATRP to prepare polyolefins or polyolefin micro- or nano-composites are extremely limited in the literature and are mainly restricted to synthesizing copolymers of α-olefins with acrylics or styrenics.

In this study, polymers of monomers possessing long "alkyl" side chains, such as poly(octadecyl acrylate) (PODA), are synthesized. The polymerization of octadecyl acrylate (ODA) is of interest because it has a hydrophobic, crystallizable polymethylene structure in the side chain while at the same time it contains an ATRP-feasible acrylic functional group in the backbone. PODA's have been termed "comb-like" polymers and could be effective in compatibiling polar inorganic particles with non-polar polyolefins, such as polyethylene, polypropylene, ethylene-propylene copolymers or polyisobutylene. PODA could be used as a component of *smart* paints because its pendant alkyl chain segment crystallization is temperature switchable with a transition around 55-56 °C.

This chapter will be divided into 2 parts. The first part (Section II) deals with the ATRP of octadecyl acrylate (ODA), which is an acrylate monomer with long crystallizable hydrophobic side chains, to obtain comb polymers. The second part (Section III) deals tetherine a high-density PODA organic phase onto inorganic particles. The resultant polymer-grafted silica can be used to prepare polyethylene-silica nanocomposites.

Section II. Polymer Synthesis Using Controlled Radical Polymerization

Polyolefins (POs), represented by polyethylene and polypropylene, are important polymeric materials. They are high volume polymers and their worldwide use reflects the fact that POs possess excellent properties; such as good mechanical strength, flexibility, chemical stability and processability. To broaden their applications, much effort have been undertaken to create new olefinic polymers or copolymers, for instance, polyolefins that link polar (monomer/polymer) segments. This section of the chapter deals with ATRP of monomers such as acrylate or methacrylate monomers with long crystallizable hydrophobic side chains (alkyl chain length of at least 4 methylene groups).

Polymerization of octadecyl acrylate via ATRP is schematically shown below (Scheme 1) (*10*). We have polymerized octadecyl acrylate using CuBr/$CuBr_2$ as the catalyst, 4,4′-dinonyl-2,2′-dipyridyl (dNbpy) as ligand and ethyl 2-bromoisobutyrate (EBIB) as the initiator. The polymerization was carried out at 90 °C and 95 °C. To evaluate the effect of ligand on rate of reaction N,N,N′,N″,N′-pentamethyl diethylenetriamine (PMDETA) was used as a ligand. A summary of the experiments is shown in Table 1.

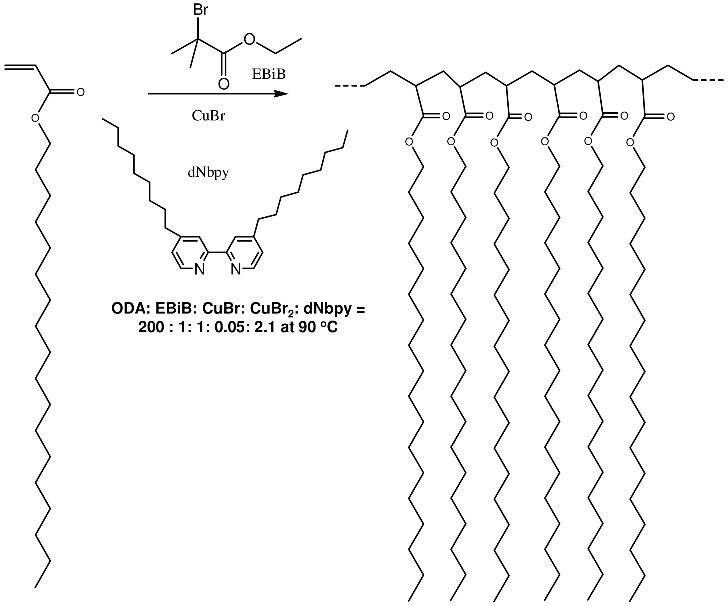
Br
O
O
EBiB
CuBr
dNbpy
N
N
O
O
ODA: EBiB: CuBr: CuBr₂: dNbpy =
200 : 1: 1: 0.05: 2.1 at 90 °C

Scheme 1. Polymerization of Octadecyl Acrylate via ATRP with 4,4'-Dinonyl-2,2'-dipyridyl (dNbpy) as a Ligand.

Table 1. ATRP of Octadecyl Acrylate Using Different Ligands

	Temp (°C)	*Ligand*	*Time (hr)*	*Conv. (%)*	*Final M_n*	*PDI*
Experiment 1	90	dNbyp	20.7	40	25K	1.11
Experiment 2	95	dNbyp	20.8	48	27K	1.12
Experiment 3	95	PMDETA	2.5	83	44K	1.42

Polymerization of octadecyl acrylate was carried out using CuBr, 4,4′-dinonyl-2,2′-dipyridyl, $CuBr_2$ with ethyl 2-bromoisobutyrate as initiator at 90 °C. The reaction solution became brown. After 4.4 h, about 0.2 mL reaction solution was taken out via syringe under N_2 protection. The sample was analyzed by ^{1}H-NMR ($CDCl_3$ as the solvent) to determine the reaction conversion, and by GPC to measure molecular weight and its polydispersity. After 4.4 h, the monomer conversion was 10.1 %, M_n was 9,190, and M_w/M_n was 1.13. After 20.7 h, the reaction was stopped by opening the flask and exposing the catalyst to air. The reaction solution became green. The final product was analyzed with results are shown in Table 1.

The Figure 1 shows (a) semilogarithmic kinetic plot and (b) dependence of molecular weights and molecular weight distributions for copper-mediated ATRP of ODA with dNbpy as a ligand (*3*). The molecular weight increased linearly with conversion and the molecular weight distribution remains low and constant. Figure 2 shows SEC traces for ATRP of ODA, with dNbpy as a ligand. It illustrates the evolution of molecular weight (increasing) and molecular weight distribution (~ constant) with increasing conversion. The molecular weight distribution remains low confirming negligible termination and transfer.

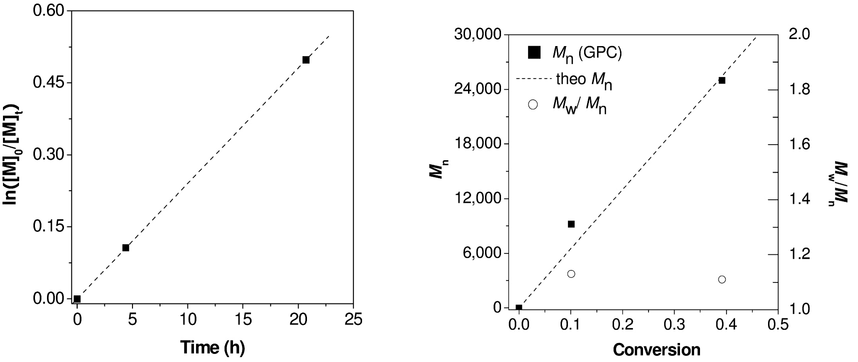

Figure 1. (a) Kinetic plot for ATRP of octadecyl acrylate (ODA) polymerization and (b) molecular weight and molecular weight distribution for ATRP of ODA as a function of conversion with dNbpy as a ligand.

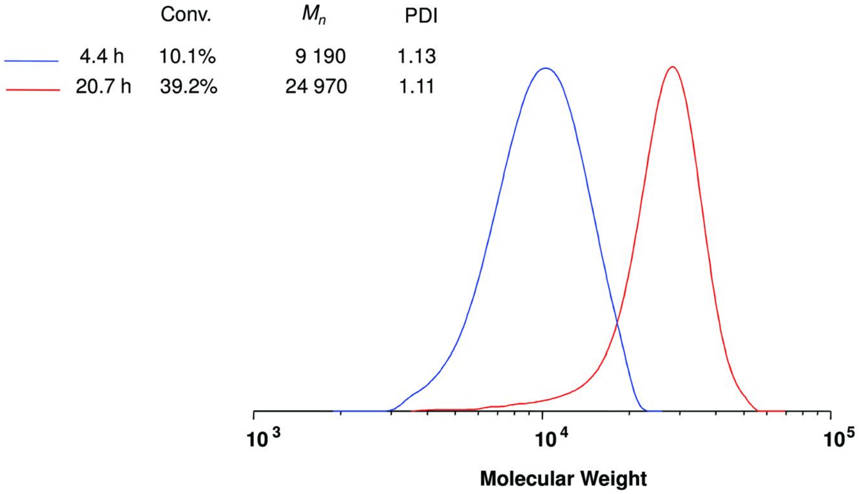

Figure 2. Evolution of SEC traces for ATRP of ODA with dNbpy as a ligand.

In experiment 2, the polymerization of octadecyl acrylate was carried out via ATRP at at 95 °C. The reaction solution became brown. After 1.5 h, about 0.2 mL reaction solution was taken out via syringe under N_2 protection. The sample was analyzed by ^{1}H-NMR ($CDCl_3$ as the solvent) to determine the reaction conversion, and by GPC to measure molecular weight and its polydispersity. Figure 3 shows SEC traces for this experiment. The product was analyzed with results are shown in Table 1. Using higher reaction temperature of 95 °C, the reaction conversion increase somewhat (39.2 % vs 48.2 % after 20 hours).

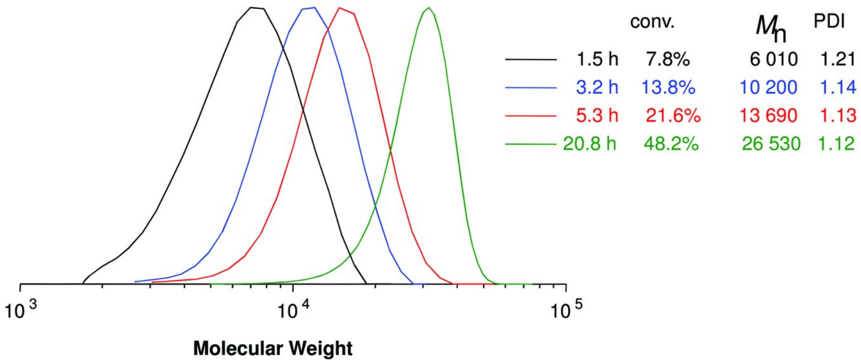

Figure 3. Evolution of SEC traces for ATRP of ODA with dNbpy as a ligand.

To evaluate the effect of ligand on rate of reaction, different ligand was used in experiment 3. The polymerization of octadecyl acrylate was carried out using N,N,N′,N″,N′-pentamethyl diethylenetriamine (PMDETA) as a ligand at 95 °C.

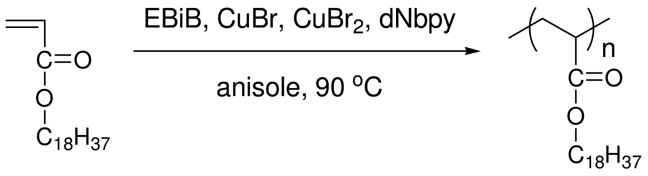

After 2.5 h, the reaction was stopped by opening the flask and exposing the catalyst to air. The sample was analyzed by ^{1}H-NMR ($CDCl_3$ as the solvent) to determine the reaction conversion, and by GPC to measure molecular weight and its polydispersity. Monomer conversion = 82.8 %. M_n = 43,980. M_w/M_n = 1.43. The reaction solution was diluted with 17 mL THF, and passed through a short basic alumina column to remove copper catalyst. The resulting solution was added drop-wise into acetone, yielding white PODA powder 1.66 g.

Figure 4 shows the evolution of SEC traces for ATRP of ODA with PMDETA as a ligand. The reaction rate was very high using this aliphatic triamine liagnd. The polymer conversion was 82.8 % in 2.5 hours. This conversion using ligand PMET was quite high compared to conversion of 39.2 % and 48.2 % in 20 hours as seem in experiments 1 and 2 using dNbby ligand. The molecular weight distribution is also become broad (M_w/M_n = 1.43) with high conversion.

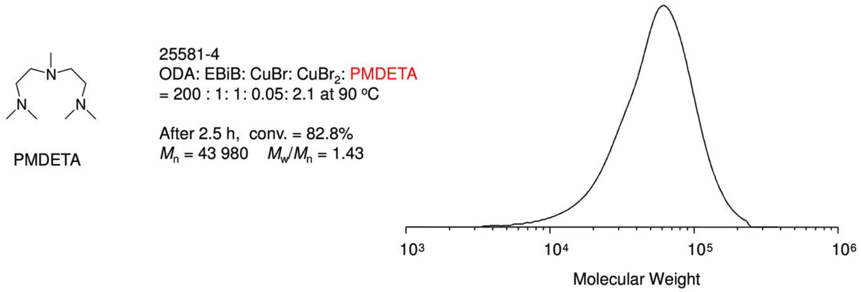

Figure 4. Evolution of SEC traces for ATRP of ODA with PMDETA as a ligand.

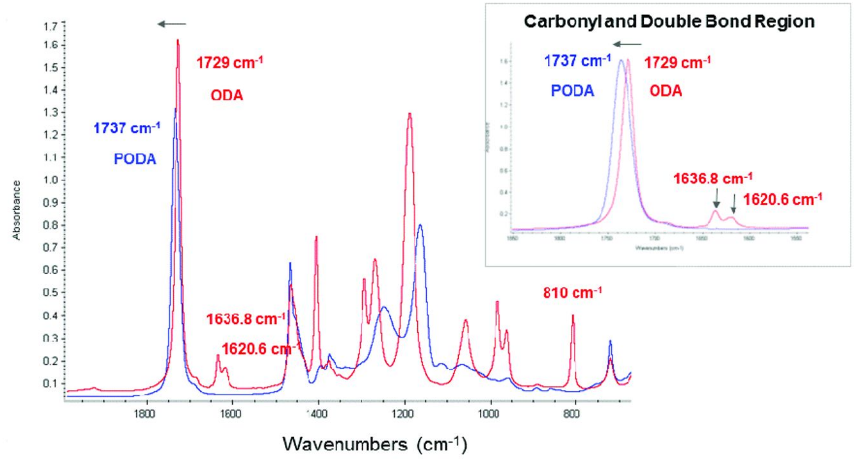

Figure 5. IR spectra of ODA and PODA.

Figure 5 showed the IR spectra of ODA monomer and PODA polymer. An IR spectrum of the ODA has an ester carbonyl absorption peak at 1729 cm^{-1} and small double bond peaks at 1637 cm^{-1}, 1621 cm^{-1} and 810 cm^{-1}. The IR spectrum of PODA polymer showed complete disappearance of double bond peaks at 1637 cm^{-1}, 1621 cm^{-1} and 810 cm^{-1} and shift in the ester peak to 1737 cm^{-1}. The shift in the ester peak to due to the change in ester nature from α,β-unsaturated carbonyl ester in monomer to saturated carbonyl ester in the polymer. Figure 6 shows the ^{1}H-NMR of PODA in $CDCl_3$. ^{1}H NMR ($CDCl_3$, δ ppm): 0.88 [broad peak, 3H, $-(CH_2)_{17}-C\underline{H}_3$], 1.26 [broad peak, 30H, $-(C\underline{H}_2)_{15}-CH_3$], 1.60 [broad peak, 4H, $-CH_2-C\underline{H}_2-(CH_2)_{15}-$, and $-C\underline{H}_2-CH-CH_2$], 3.95 [broad peak, 2H, $O-C\underline{H}_2-CH_2-$],

In contrast to a literature report (*8*) by Tsujii et al., the polymerization of ODA with a typical ATRP system was well behaved, producing low polymers with low polydispersity and excellent control in molecular weight. This may be due to a relatively high rate of deactivation compared to the rate of propagation and high rate of initiation compared to propagation.

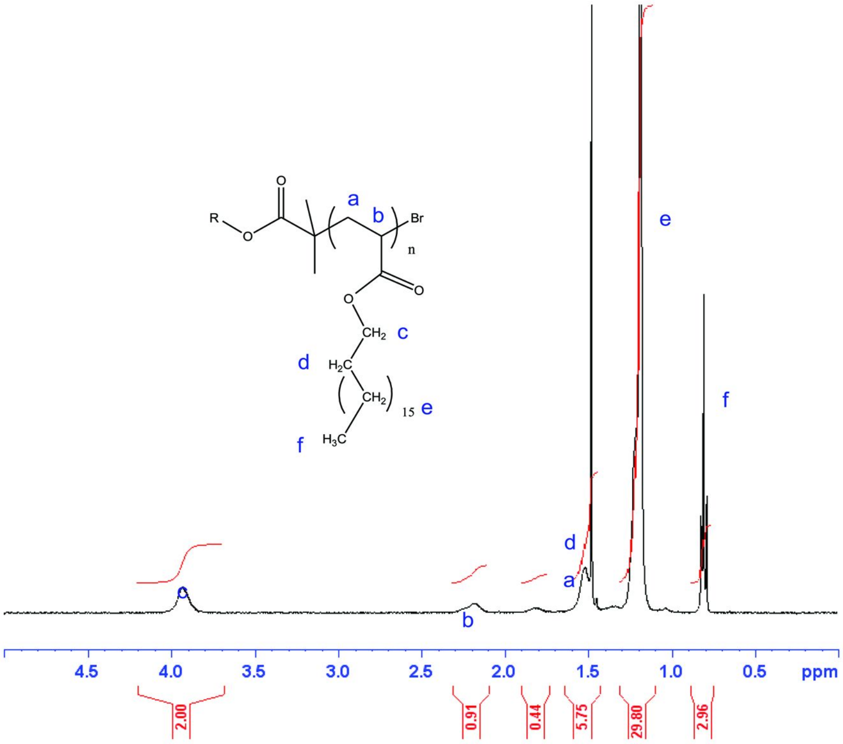

Figure 6. ^{1}H-NMR of PODA in CDCl$_3$.

High Density Polyethylene and PODA Blends

The octadecyl acrylate monomer content ATRP-feasible acrylic functional group but also content hydrophobic crystallizable long alkyl side chain of polymethylene structure. Such long alkyl chain could compatibilize polyolefins like polyethylene.

About 3 g high density polyethylene (HDPE) and 0.75 g PODA from Experiemnt 3 were blended in a DSM Micro 5 mixer at 180 °C for 2 min (a 80/20 HDPE/PODA blend ratio). The mixture was then extruded out into strand for characterization. The strand of the blended sample was immersed in liquid nitrogen for 1 min, and then broken into parts by tweezers. Freeze fracture morphology of the blend was studied by SEM (Scanning Electron Microscopy). Figure 7 shows the SEM images of fractured surfaces of a blended HDPE and PODA sample. Micron-size PODA domains appear to be uniformly distributed in polyethylene suggesting good compatibility between PODA and PE.

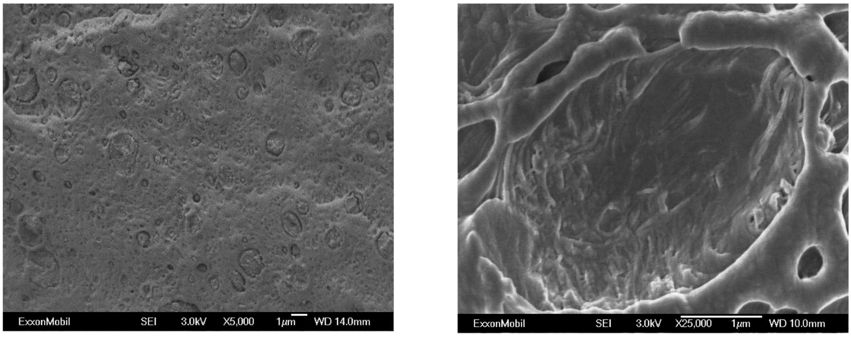
ExxonMobil SEI 3.0kV X5,000 1μm WD 14.0mm
ExxonMobil SEI 3.0kV X25,000 1μm WD 10.0mm

Figure 7. SEM images of cross section of a blended HDPE and PODA string.

Section III. Polymer–Inorganic Hybrid Materials Using Controlled Radical Polymerization

This part of the chapter deals with introducing high-density ODA polymeric organic phase onto inorganic particles. An initiator-modified silica was prepared via reacting the hydroxyl group on the surface of the silica particles with 1-(chlorodimethylsilyl)propyl 2-bromoisobutyrate hexamethyldisilazane. The ODA monomer was polymerized from the surface-initiated ATRP ("grafting-from" method) initiator. The resultant polymer-grafted silica can be used to prepare polyethylene-silica nanocomposites.

Inexpensive inorganic substances are traditional ingredients in the polymer industry. These particles are typically tenths of microns, or larger in size. They are widely used as fillers to improve mechanical and thermal properties of polymers and polymer composites: to decrease shrinkage and internal stresses during fabrication of polymer articles; to increase thermal conductivity, thermal stability, and flame resistance; and to reduce material cost. Reducing cost is often a primary motivation for using fillers - despite some deterioration in properties with large incorporation of inorganic particles (*11*).

Nanocomposites are materials that contain nanofillers or fillers of nanometer dimensions. Hybrid polymer–inorganic nanocomposite materials are promising for a variety of applications. Because of their unique electronic, optical, and mechanical properties, they have attracted the particular attention of researchers and engineers in recent decades. As a result of their nano-dimensions, extremely high interfacial areas are available in a polymer nanocomposite. Relying on these interfacial interactions, the performance of polymer nanocomposites can be enhanced tremendously with only a small amount of nanofillers. At the same time, the extremely large surface area of nanofillers render them difficult to be dispersed in polymers, especially in non-polar polyolefins. The natural aggregation tendency of nano particles is a major obstacle in developing polyolefins based nanocomposites. One approach to address this issue is to graft polymer chains that are compatible with the polymer matrix onto the surface of nanoparticles.

Surface Modification

There are two principal techniques for the modification of inorganic particles: (1) the "*grafting-to*" method, where end-functionalized polymers react with functional groups on the particle surface, and (2) the "*grafting-from*" method, where polymer chains grow from the particle surface or initiator-functionalized self-assembled monolayer. Because of the steric hindrance imposed by the grafted polymer chains, it is difficult to prepare high-density polymer-grafted particles using "*grafting to*" methods. A higher grafting density can be obtained by using the "*grafting from*" method.

Compared to small molecular stabilizers, polymeric stabilizers are able to enhance the particle's long term stability and tune the solubility and amphiphilicity for specific applications. The synthetic route to silica-polymer hybrid nanoparticles involves two steps, 1) attachment of a monolayer of ATRP initiators to the particle surface and 2) surface initiated polymerization (*12–14*, *16*, *17*). In the surface-initiated ATRP process the polymer chains grow from the initiators that have been previously anchored on to the inorganic particle surface, consequently, the grafted chains do not hinder the diffusion of the small monomers to the reaction sites, so the well-defined polymers chains with higher graft density can be obtained.

Polymer brushes are defined as dense layers of chains confined to a surface or interface where the distance between grafts is much less than the unperturbed dimensions of the tethered polymer. Due to the high steric crowding, grafted chains extend from the surface and reside in an entropically unfavorable conformation. Polymer brushes have been prepared by the end-grafting of chains to/from flat or curved surfaces that are organic or inorganic in nature. These include functional colloids, highly branched polymers and block copolymer aggregates, such as micelles or phase-separated nanostructures (*12–17*). The super high graft density that can be achieved by surface-initiated ATRP leads to the surface crowding of polymer chains and the development of polymer brushes.

Silica Particles Surface-Initiated ATRP of Polymer Brushes for Polyolefin Nanocomposites

Synthesis of ATRP Initiator

The initiator 1-(chlorodimethylsilyl)propyl 2-bromoisobutyrate was synthesized via reaction of allyl 2-bromo-2-methylpropionate and chlorodimethylsilane using Karstedt's catalyst. The conversion was determined by IR (all double bond peaks of the vinyl groups disappeared). The unreacted chlorodimethylsilane and toluene was distilled under vacuum, giving yellow oil with 100% yield. The Karsted's catalyst could be partially removed by filtration with 200 nm filter.

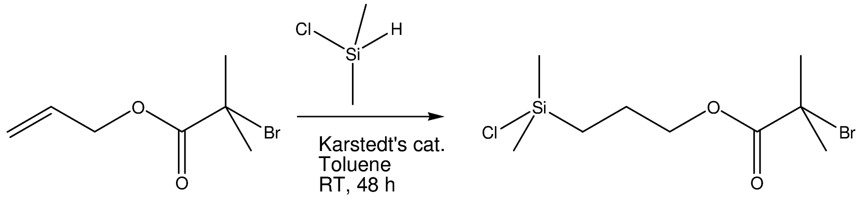
Cl
Si
H
O
Br
Karstedt's cat.
Toluene
RT, 48 h
Cl
Si
O
Br
O

Karstedt's catalyst: platinum(0)-1,3-divinyl-1,1,3,3-tetramethyldisiloxane complex solution in xylene (Pt ~ 2%).

Synthesis of 2-Bromoisobutyrate Functional Silica Colloids

The silica dispersion in methyl ethyl ketone was reacted with the 1-(chlorodimethylsilyl)propyl 2-bromoisobutyrate hexamethyldisilazane. The bromine content of the initiator-modified silica nanoparticles was determined by elemental analysis, as 1.41 wt% or 0.177 mmol Br/g SiO_2.

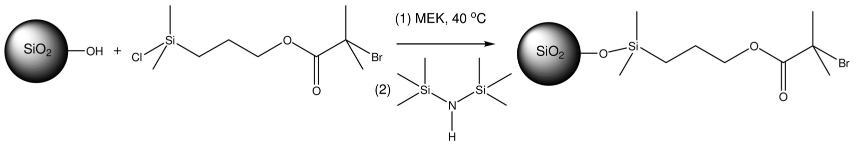
SiO2
OH
+
Cl
Si
O
Br
O
(1) MEK, 40 °C
(2)
Si
N
H
Si
SiO2
O
Si
O
Br
O

ATRP of ODA from 2-Bromoisobutyrate Functional Silica Colloids

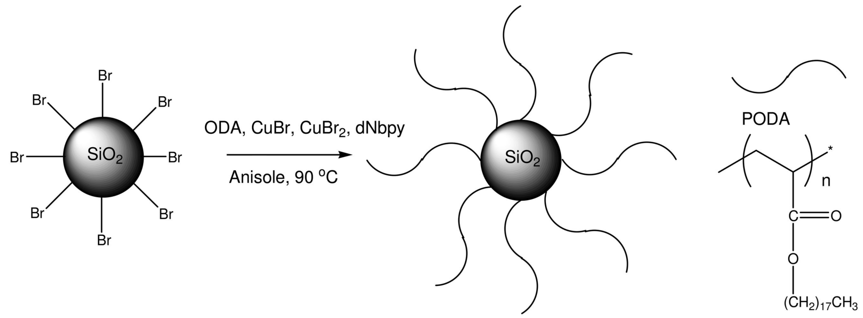
Br
SiO2
ODA, CuBr, CuBr2, dNbpy
Anisole, 90 °C
SiO2
PODA
*
n
C=O
O
(CH2)17CH3

The octadecyl acrylate was polymerized using CuBr, 4,4′-dinonyl-2,2′-dipyridyl, $CuBr_2$ was and 2-bromoisobutyrate functional silica colloids at 90 °C. After 17.5 h, about 0.2 mL reaction solution was taken out via syringe under N_2 protection. The sample was analyzed by ^1H-NMR ($CDCl_3$ as the solvent) to determine the reaction conversion. Monomer conversion = 6.8%. The oil bath temperature was increased to 105 °C at 20 h. After 24 h, monomer conversion = 7.0%. Figure 8 shows the TGA of SiO_2-PODA (25581-20-6.93%, blue scan). The TGA gave a wt. loss of 78.39% with residue of 21.61 %. After 68 h, the reaction was stopped by exposing to air. Monomer conversion = 18.7%. As shown in Figure 8 for the blue scan TGA of SiO_2-PODA (18.71%). The TGA gave a wt. loss of 87.87% with residue of 12.13 %. The reaction solution was diluted with THF, and added drop-wise into acetone, yielding white SiO_2-g-PODA powder. The potentially unreacted free initiator was washed from SiO_2 modified initiator. Hence, the only way that PODA can be obtained is via polymerization from initiator attached to silica gel.

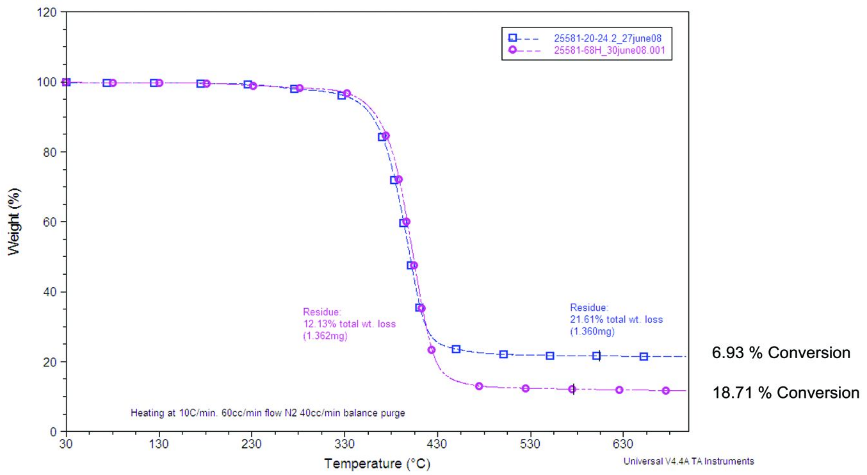

Figure 8. TGA of SiO_2-PODA.

The SiO_2-PODA sample was used for solid state ^{13}C NMR studies. Although the solid state room temperature (28 °C) NMR showed broad peaks, there was a dramatic improvement in resolution when sample was heated to 50 °C. Figure 9 shows the solid state NMR of SiO_2 modified with PODA polymer brushes. In fact, the solid state spectrum at elevated temperature was similar to the solution spectrum. We calculated the molecular weight of the PODA attached to silica using two separate procedures based on ^{13}C NMR spectrum. Relying on the signal of polymer carbons vs. dimethyl carbon attached to silica from initiator, we could estimate the molecular weight of the PODA to be 17,108. If the signal of polymer carbons (PODA) vs. dimethyl carbon, $Si(CH_3)_2$, attached to carbon from initiator was used, we estimated the molecular weight of the PODA to be 16,043. Based on ^1H NMR spectrum, the molecular weight of the PODA attached to silica was determined using signal of polymer hydrogen (PODA) vs. dimethyl hydrogen, $Si(CH_3)_2$, attached to silica from initiator to be 17,208. All these three molecular weight values are in a general agreement.

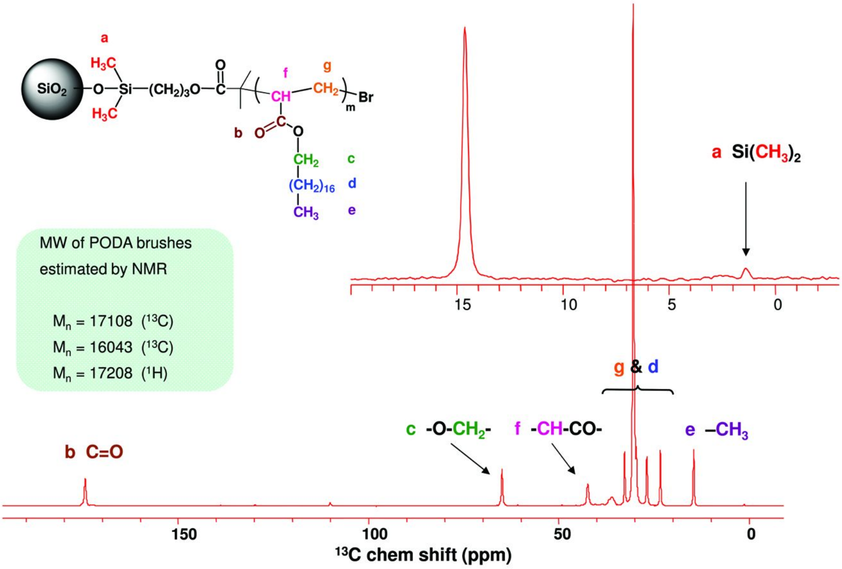

Figure 9. Solid state NMR of SiO_2 modified with PODA polymer brushes.

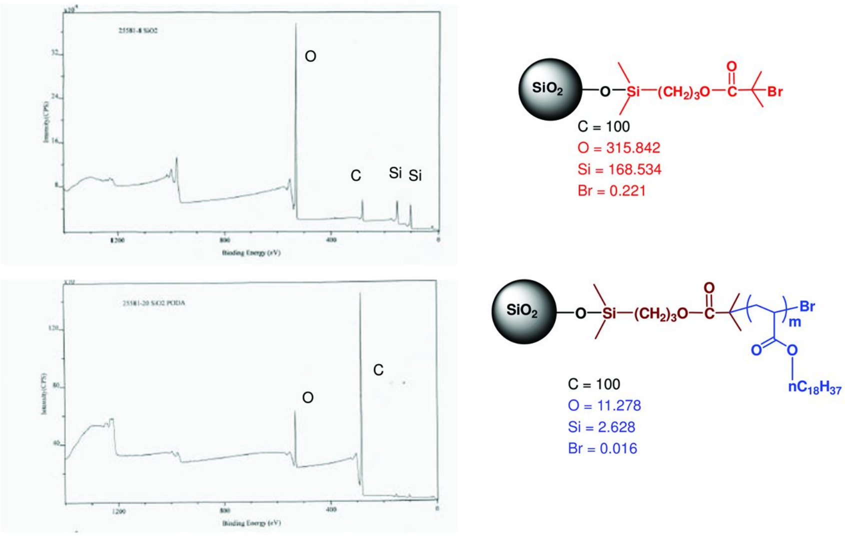

Figure 10. XPS spectra of SiO_2 modified with ATRP initiator (top spectrum) and PODA polymer brushes (bottom spectrum).

Figure 10 shows the XPS spectra of SiO_2 modified with ATRP initiator (top spectrum) and PODA polymer brushes (bottom spectrum). The top spectrum shows typical SiO_2 features with Si and oxygen peaks. The carbon peak arising from the three methylene of initiator portion of the molecule can be clearly seen. A tiny peak at extreme right from the chain end Br can also be found. The bottom spectrum shows a decrease in SiO_2 features with extremely small Si peaks and substantially reduced oxygen peak compared to the carbon peak. The carbon peak is coming from PODA polymer.

Experimental for ODA Polymerization

The detailed synthesis procedure for PODA is listed as follows. All processes were carried out under a nitrogen atmosphere with freshly dried and distilled solvents and Schlenk techniques.

Materials and Instruments

Octadecyl acrylate (Aldrich, 97%), dimethyl sulfoxide (DMSO, Aldrich, 99.5%), Anisole (Aldrich, 99.7%), 2-bromoisobutyrate (EBiB, Aldrich, 97%) was dried over 13x, 1.6mm molecular sieve pellets and degassed by nitrogen bubbling. The $CuBr_2$(Aldrich, 99%), N,N,N′N″,N′-pentamethyl diethylenetriamine (PMDETA, Aldrich, 99%), CuBr (Aldrich, 99.999%), 4,4′-dinonyl-2,2′-dipyridyl (dNbpy, Alridch, 97%) were purchased and used a received. ^1H and ^{13}C-NMR spectra was recorded on a Bruker DRX 400 spectrometer operating at 400 MHz. The IR analysis was carried out with FT-IR NEXUS 470 instrument. The Molecular weight distribution analysis was measured on waters associate GPCV2000. Morphology of blend was studied by scanning Electron Microscopy (SEM). The TGA was recorded with standard ramp method heating at 10 °C /min, 60cc/min flow nitrogen on Q 5000 differential scanning instrument (DSC) instrument.

***Experiment 1**: Polymerization of Octadecyl Acrylate via ATRP*

Octadecyl acrylate (ODA, Aldrich, 97%) (2.4 g, 7.17 mmol), CuBr (Aldrich, 99.999%) (5.2 mg, 35.9 μmol) and 4,4′-dinonyl-2,2′-dipyridyl (dNbpy, Aldrich, 97%) (31.7 mg, 75.3 μmol) were added into 100 mL round bottom flask with side arm. And then the flask was sealed with a glass stopper and purged with N_2 for about 1 h. 4.0 mg (17.9 μmol) $CuBr_2$ was dissolved in 0.1 mL dimethyl sulfoxide (DMSO), and then 1.4 mL anisole was added. The mixture was purged with N_2 for 10 min. The initiator ethyl 2-bromoisobutyrate (EBiB, Aldrich, 98%) (0.359 mmol, 53.7 μL) was then added into the $CuBr_2$ solution. About 0.15 mL of the above solution was injected into the reaction flask. The flask was placed in a thermostated oil bath at 90 °C. The reaction solution became brown. After 4.4 h, about 0.2 mL reaction solution was taken out via syringe under N_2 protection. The sample was analyzed by ^{1}H-NMR ($CDCl_3$ as the solvent) to determine the reaction conversion, and by GPC to measure molecular weight and its polydispersity. After 4.4 h, the monomer conversion was 10.1 %, M_n was 9,190, and M_w/M_n was 1.13. After 20.7 h, the reaction was stopped by opening the flask and exposing the catalyst to air. The reaction solution became green. The final product was analyzed by ^{1}H-NMR and GPC with 39.2 % monomer conversion, 24,970.M_n and 1.11 M_w/M_n.

Experiment 2: *Polymerization of Octadecyl Acrylate via ATRP at Higher Temperature*

Octadecyl acrylate (ODA, Aldrich, 97%) (2.4 g, 7.17 mmol), CuBr (Aldrich, 99.999%) (5.2 mg, 35.9 μmol) and 4,4′-dinonyl-2,2′-dipyridyl (dNbpy, Aldrich, 97%) (31.7 mg, 75.3 μmol) were added into 100 mL round bottom flask with side arm. And then the flask was sealed with a glass stopper and purged with N_2 for about 1 h. 4.0 mg (17.9 μmol) $CuBr_2$ was dissolved in 0.1 mL dimethyl sulfoxide (DMSO), and then 1.4 mL anisole was added. The mixture was purged with N_2 for 10 min. The initiator ethyl 2-bromoisobutyrate (EBiB, Aldrich, 98%) (0.359 mmol, 53.7 μL) was then added into the $CuBr_2$ solution. About 0.15 mL of the above solution was injected into the reaction flask. The flask was placed in a thermostat oil bath at 95 °C. The reaction solution became brown. After 1.5 h, about 0.2 mL reaction solution was taken out via syringe under N_2 protection. The sample was analyzed by ^{1}H-NMR ($CDCl_3$ as the solvent) to determine the reaction conversion, and by GPC to measure molecular weight and its polydispersity. After 1.5 h, monomer conversion = 7.8%. M_n = 6,010. M_w/M_n = 1.21. After 3.2 h, monomer conversion = 13.8 %. M_n = 10,190. M_w/M_n = 1.12. After 5.3 h, monomer conversion = 21.6 %. M_n = 13,690. M_w/M_n = 1.13. After 20.8 h, monomer conversion = 48.2 %. M_n = 26,530. M_w/M_n = 1.12. After 29.0 h, the reaction was stopped by opening the flask and exposing the catalyst to air. The reaction solution became green. The product was analyzed by ^{1}H-NMR and GPC. Monomer conversion = 50.0 %. M_n = 28,120. M_w/M_n = 1.15. The reaction solution was diluted with tetrahydrofuran (THF), and passed through a short basic alumina column to remove copper catalyst. The resulting solution was added drop-wise into acetone, yielding white PODA powder.

Experiment 3: *Polymerization of Octadecyl Acrylate via ATRP*

Octadecyl acrylate (ODA, Aldrich, 97%) (2.4 g, 7.17 mmol) and CuBr (Aldrich, 99.99 %) (5.2 mg, 35.9 μmol) were added into 100 mL round bottom flask with side arm. And then the flask was sealed with a glass stopper and purged with N_2 for about 1 h. 4.0 mg (17.9 μmol) $CuBr_2$ was dissolved in 0.1 mL dimethyl sulfoxide (DMSO), and then 1.4 mL anisole was added. The mixture was purged with N_2 for 10 min. The initiator ethyl 2-bromoisobutyrate (EBiB, Aldrich, 98%) (0.359 mmol, 53.7 μL) and the ligand N,N,N′,N″,N′-pentamethyl diethylenetriamine (PMDETA, Aldrich, 99%) (79.4 μL, 0.377 mmol) were then added into the $CuBr_2$ solution. The flask was placed in a thermostat oil bath at 95 °C. After 2.5 h, the reaction was stopped by opening the flask and exposing the catalyst to air. The sample was analyzed by ^{1}H-NMR ($CDCl_3$ as the solvent) to determine the reaction conversion, and by GPC to measure molecular weight and its polydispersity. Monomer conversion = 82.8 %. M_n = 43,980. M_w/M_n = 1.43. The reaction solution was diluted with 17 mL THF, and passed through a short basic alumina column to remove copper catalyst. The resulting solution was added drop-wise into acetone, yielding white PODA powder 1.66 g.

Experimental Section of Silica Particles Surface-Initiated ATRP of Polymer Brushes for Polyolefin Nanocomposites

Synthesis of ATRP Initiator (1-(Chlorodimethylsilyl)propyl 2-bromoisobutyrate)

Allyl 2-bromo-2-methylpropionate (Aldrich, 98%) (2.5 mL, 15.4 mmol) and dry toluene (30 mL) were added into a round bottom flask and purged with N_2. Chlorodimethylsilane (Aldrich, 98%) (12.2 mL, 107.8 mmol) was added drop-wise into the flask, and subsequently Karstedt's catalyst solution (300 μL) was added into the system via a syringe(Karstedt's catalyst: platinum(0)-1,3-divinyl-1,1,3,3-tetramethyldisiloxane complex solution in xylene (Pt ~ 2%)). The mixture was stirred under N_2 for over 62 h. The conversion was determined by IR. (all double bond peaks of the vinyl groups disappeared) The unreacted chlorodimethylsilane and toluene was distilled under vacuum, giving yellow oil with 100% yield. The Karsted's catalyst could be partially removed by filtration with 200 nm filter.

Synthesis of 2-Bromoisobutyrate Functional Silica Colloids

The silica dispersion (13.0 g of 30 wt% SiO_2 in methyl ethyl ketone, particle size of SiO_2 ~ 15-20 nm, Nissan) was added to a 100 mL round bottom flask, and protected with nitrogen. The 1-(chlorodimethylsilyl)propyl 2-bromoisobutyrate (1.5 mL) was then added via syringe. The orange dispersion became cloudy. The reaction mixture was stirred for 24 h at 50 °C. The mixture was cooled down to room temperature and hexamethyldisilazane (1.5 mL, Aldrich) was then added. The mixture was stirred at room temperature for 3 h, and heated at 40 °C for overnight. The precipitate was removed by centrifugation (5000 rpm for 0.5 h), and the supernatant was added drop-wise into hexane to precipitate colloids. The particles were washed with hexane for several times. And then hexane was removed by rotary evaporator, yielding 5.3 g white yellow solid. The bromine content of the initiator-modified silica nanoparticles was determined by elemental analysis, as 1.41 wt% or 0.177 mmol Br/g SiO_2.

ATRP of ODA from 2-Bromoisobutyrate Functional Silica Colloids

Octadecyl acrylate (ODA, Aldrich, 97%) (2.4 g, 7.17 mmol), 2-bromoisobutyrate functional silica colloids (100 mg, 0.0177 mmol Br), CuBr (Aldrich, 99.999%) (5.2 mg, 35.9 μmol) and 4,4′-dinonyl-2,2′-dipyridyl (dNbpy, Aldrich, 97%) (31.7 mg, 75.3 μmol) were added into 100 mL round bottom flask with side arm. And then the flask was sealed with a glass stopper and purged with N_2 for about 1 h. 4.0 mg (17.9 μmol) $CuBr_2$ was dissolved in 1 mL dimethyl sulfoxide (DMSO). And then 0.1 mL the above solution mixed with 1.4 mL anisole. The mixture was purged with N_2 for 10 min. The above mixture was injected into the reaction flask. The flask was placed in a thermostated oil bath at 90 °C. The reaction solution became brown. After 17.5 h, about 0.2 mL reaction solution was taken out via syringe under N_2 protection. The sample was analyzed by ^{1}H-NMR ($CDCl_3$ as the solvent) to determine the reaction conversion. Monomer conversion = 6.8%. The oil bath temperature was increased to 105 °C at 20 h. After 24 h, monomer conversion = 7.0%. Figure 10 shows the TGA of SiO_2-PODA (25581-20-6.93%, blue scan). The TGA gave a wt. loss of 78.39% with residue of 21.61 %. After 68 h, the reaction was stopped by exposing to air. Monomer conversion = 18.7%. As shown in Figure 10 for the blue scan TGA of SiO_2-PODA (18.71%). The TGA gave a wt. loss of 87.87% with residue of 12.13 %. The reaction solution was diluted with THF, and added drop-wise into acetone, yielding white SiO_2-g-PODA powder. The potentially unreacted free initiator was washed from SiO_2 modified initiator. Hence, the only way that PODA can be obtained is via polymerization from initiator attached to silica gel.

Summary

The ATRP of octadecyl acrylate (ODA) (monomer with long hydrophobic side chains to obtain comb polymers) has been investigated to produce PODA with predetermined molecular weights and narrow polydispersities. To introduce a high-density polymeric organic phase onto silica, initiator-modified silica was prepared and then surface-initiated ATRP ("grafting-from" method) was carried out with octadecyl acrylate. The resultant PODA-grafted silica were found to be dispersed well in polyethylene.

Acknowledgments

We would to thank Bryan Chapman, Mark W. Genowitz, Mobae Afeworki, Simon R. Kelemon, Viktor B. Buchholz, Russel R. Mueller, William A. Lamberti, David C. Calabro and Joseph A. Olkusz for their help.

References

1. Moad, G.; Solomon, D. H. *The Chemistry of Free Radical Polymerization*; Elsevier Science, Inc.: New York, 1995.
2. Matyjaszewski, K.; Davis, T. P. *Handbook of Radical Polymerization*; Wiley-Interscience: Hoboken, NJ, 2002.
3. *Advances in Controlled/Living Radical Polymerization*; Matyjaszewski, K., Ed.; ACS Symposium Series 854; American Chemical Society: Washington, DC, 2003.
4. Patten, T. E.; Xia, J.; Abernathy, T.; Matyjaszewski, K. *Science* **1996**, *272*, 866.
5. Webster, O. W. *Science* **1991**, *251*, 887.
6. Pyun, J.; Matyjaszewski, K. *Chem. Mater.* **2001**, *13*, 3436–3448.
7. Wang, J. S.; Matyjaszewski, K. *J. Am. Chem. Soc.* **1995**, *117*, 5614.
8. Matyjaszewski, K.; Xia, J. *Chem. Rev.* **2001**, *101*, 2921.
9. Tsujii, Y.; Ohno, K.; Yamamoto, S.; Goto, A.; Fukuda, T. *Adv. Polym. Sci.* **2006**, *197*, 1–45.
10. Street, G.; Illsley, D.; Holder, S. J. *J. Polym. Sci. Polym. Chem.* **2005**, *43*, 1129.
11. Tsou, A. H.; Waddell, W. H. *Kirk-Othmer Encyclopedia of Chemical Technology*; Wiley-Interscience: Hoboken, NJ, 1994; Volume 11, p 301.
12. Pyun, J.; Matyjaszewski, K. *Chem. Mater.* **2001**, *13*, 3436–3448.
13. Mallik, A. K.; Rahman, M. M.; Czaun, M.; Takafuji, M.; Ihara, H. *J. Chromatogr., A* **2008**, *1187*, 119–127.
14. Perruchot, C.; Khan, M. A.; Kamitsi, A; Armes, S. P. *Langmuir* **2001**, *17*, 4479–4481.
15. Matyjaszewski, K.; Dong, H.; Jakubowski, W.; Pietrasik, J.; Kusumo, A. *Langmuir* **2007**, *23*, 4528–4531.
16. Miller, P. J.; Matyjaszewski, K. *Macromolecules* **1999**, *32*, 8760–8767.
17. Matyjaszewski, K.; Miller, P. J.; Shukla, N.; Immaraporn, B.; Gelman, A.; Luokala, B. B.; Siclovan, T. M.; Kickelbick, G.; Vallant, T.; Hoffmann, h.; Pakula, T. *Macromolecules* **1999**, *32*, 8716–8724.

Chapter 12

Applications of Surface Initiated ATRP to the Preparation of Polyelectrolyte Brushes for Antifouling, Adhesion Control, Friction Control

**Moyotasu Kobayashi,[a] Yuki Terayama,[b] Tatsuya Ishikawa,[b]
Masami Terada,[b] Hiroe Soejima,[c] Daiki Murakami,[a]
and Atsushi Takahara*,[a,b,c]**

**[a]JST, ERATO Takahara Soft Interfaces Project, Kyushu University,
744 Motooka, Nishi-ku, Fukuoka 819-0395, Japan
[b]Graduate School of Engineering, Kyushu University, 744 Motooka,
Nishi-ku, Fukuoka 819-0395, Japan
[c]Institute for Materials Chemistry and Engineering, Kyushu University,
744 Motooka, Nishi-ku, Fukuoka 819-0395, Japan
*E-mail: takahara@cstf.kyushu-u.ac.jp**

Polyelectrolytes show unique characteristics at aqueous interfaces. High-density hydrophilic polyelectrolyte brushes were prepared on Si-wafer and various substrates by surface-initiated controlled radical polymerization. Chain dimension at liquid/solid interface was characterized by neutron reflectivity. Applications of polymer brushes to super hydrophilic surface, antifouling surface, water lubrication layer and adhesion control layer are presented.

Introduction

Surfaces and interfaces of soft materials play an important role in various functional applications such as antifouling coating, tribo-coating, adhesion layer, anti-static coating and ultrathin-insulator. Surface-grafted polymers can be classified as one of typical soft materials interfaces. The simplest way to immobilize the polymer chains on the surface is a physisorption approach involving two-component polymer chains, where one part strongly adheres to the surface and the second part extends to form the polymer layer. The tethering point can be a functional group or a diblock copolymer, both of which are strongly

In Progress in Controlled Radical Polymerization: Materials and Applications; Matyjaszewski, K., et al.;
ACS Symposium Series; American Chemical Society: Washington, DC, 2012.

adsorbed onto the surface and act as an anchor for the polymer chain. This is a typical "grafting-to" method. Although the polymer layer is thermally stable and is not released into the solvent, the graft density and film thickness are are not large because large coiled polymer chains hardly diffuse to substrate surfaces that are sterically hindered by surrounding bounded chains. The low-density grafted polymer assumes a "mushroom" conformation with a coil dimension similar to that of ungrafted chains.

In contrast, the "grafting-from" technique gives the polymer chains by polymerization from a suitable surface immobilized initiator, which are predominantly formed by self-assembled monolayers containing the desired initiating functionality (*1*, *2*). This surface-initiated polymerization technique, especially combined with a controlled radical polymerization (CRP), enables us to prepare high-density grafted polymers due to the densely immobilized initiators and the high initiator efficiency. With increasing graft densities, polymer chains will be stretched in order to avoid overlap of each polymer chain, forming a so-called "polymer brush". By definition, polymer brush can be described as polymer chains tethered to a surface or interface with a sufficiently high graft density such that the chains are forced to stretch away from the tethering site (*3*).

Polyelectrolyte brushes are soft interfaces with unique functionality due to the presence of high-density ionic groups. However, systematic studies on the structure and functionality of polyelectrolyte brushes at solid/liquid interfaces have not been done yet. Since the one end group of polymer brushes is strongly anchored on the substrate, it is expected that the polymer brush can be utilized as stable nano-coating. In this study, various polyelectrolyte brushes were prepared on the Si-wafer surface by surface initiated atom transfer radical polymerization (SI-ATRP). Adhesion, wettability and friction control utilizing various polyelectrolyte brushes immobilized onto Si-wafer are summarized.

Preparation of Polymer Brushes

Chemical structures of polymer brushes are shown in Figure 1. The surface-initiator, (2-bromo-2-methyl)propionyloxyhexyltriethoxysilane was immobilized on a silicon wafer (10 x 40 x 0.5 mm^3) by the chemical vapor adsorption method (*4*, *5*). The SI-ATRP of 2-(methacryloyloxy)ethyltrimethylammonium chloride (MTAC) using CuBr and 2,2-bipyridyl was carried out in a mixture of 2,2,2-trifluoroethanol (TFE) and 2-propanol solution at 333 K for 24 h to give a poly(MTAC) brush on the silicon wafer (*6*). Poly(3-sulfopropyl methacrylate potassium salt) (SPMK) brush was prepared by SI-ATRP in methanol aqueous solution (1.7 M of SPMK) consisting of SPMK/ CuBr/ $CuBr_2$/ 4,4′-dimehtyl-2,2′-bipyridyl (Me_2bpy) in the molar ratios of 200/2/0.4/4 at 298 K for 15 h (*7*). SI-ATRP of 2-methacryloyloxyethyl phosphorylcholine (MPC) was conducted in methanol (1.0 M of MPC) using CuBr and Me_2bpy at 303 K for 15 h (*8*). SI-ATRP of 3-(*N*-2-methacryloyloxyethyl-*N,N*-dimethyl)ammonatopropane sulfonate) (MAPS) was carried out in TFE containing a small amount of 1-hexyl-3-methylimidazolium chloride at 333 K to produce well-defined poly(sulfobetaine) brushes with predictable molecular weight and narrow polydispersity (*9*).

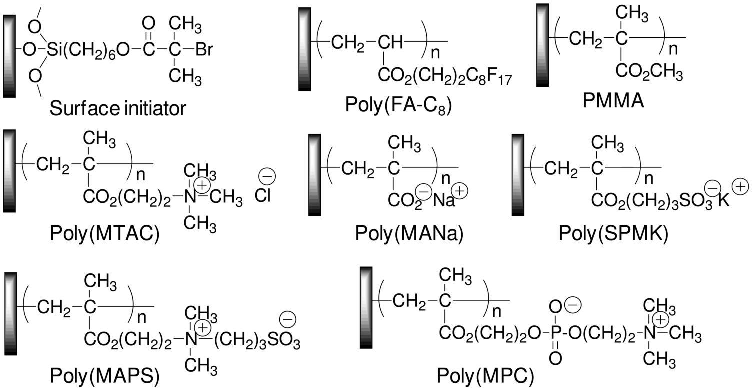

Figure 1. Chemical structures of surface initiator and polymer brushes.

After the polymerization, the silicon wafers were washed with a good solvent, such as methanol or water, using a Soxhlet apparatus for 12 h to remove the free polymer adsorbed on their surface. Thickness of the brushes on the silicon wafer was evaluated by an ellipsometer and AFM observation on the height difference between the brush surface and the scratched bare-Si wafer area.

Wettability and Antifouling Properties of Polymer Brushes

In order to evaluate the surface hydrophilicity, contact angles of water and hexadecane in air and air bubble and hexadecane in water were measured by conventional static contact angle measurement. Low water contact angle in air and large air bubble contact angle in water are measure of hydrophilicity. Surface free energies of the polymer brushes were estimated by the Owens' protocol (*10*) based on contact angle measurements. The polyelectrolyte brushes showed significantly low water contact angles below 5°, as shown in Figure 2. In particular, a water droplet was quickly spread on the poly(MPC) brush surface. The surface free energy of the poly(SPMK) and poly(MPC) brush surfaces were estimated to be 72.9 mJ m^{-2}, which is quite similar to that of water. Polyelectrolyte brush surfaces repelled both air bubble and hexadecane in water. Particularly, poly(MPC) brush showed excellent antifouling properties. On the other hand, poly(2-perfluorooctylethyl acrylate) (PFA-C_8) brush (*11*) showed very low surface free energy but hexadecane was spread at the water interface. This behavior indicated that hydrophobic surface has high affinity to alkanes.

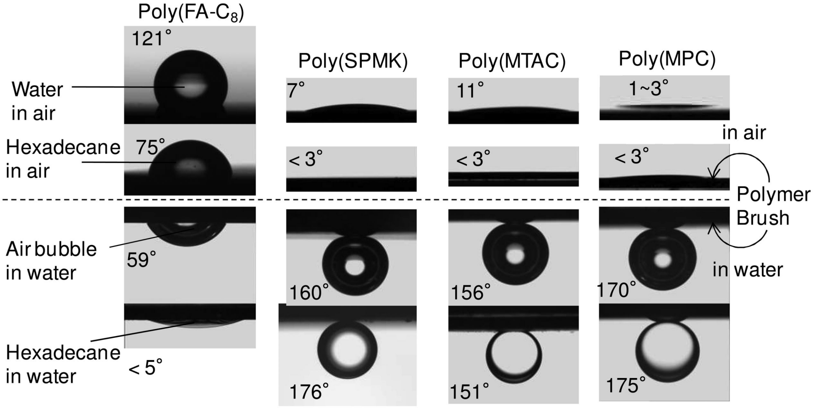

Figure 2. Photographs (side view) of water and hexadecane droplets on polymer brushes in air, and air bubbles and hexadecane droplets in contact with the brush surfaces in water. Polymer brushes consisting of poly(FA-C_8) (M_n = 93000, M_w/M_n = 1.86), poly(SPMK) (M_n = 606000, M_w/M_n = 1.85), poly(MTAC) (M_n = 312000, M_w/M_n = 1.19), poly(MPC) (M_n = 43800, M_w/M_n = 1.42) were used.

The conventional coatings of polyelectrolyte, such as spin cast films, cannot maintain these wettabilities and antifouling properties permanently, because they are easily dissolved in water to remove from the substrate. This is the large difference between the coating films and the polyelectrolyte brush, of which chain ends were densely immobilized with substrate by covalent bonds maintaining excellent hydrophilic layer.

Chain Dimension of Polymer Brushes at Liquid Interfaces

Neutron reflectivity (NR) is a powerful tool to characterize the chain dimension at the solid/water interfaces since the scattering contrast between polymer brush and water can be achieved by using heavy water (D_2O) as a solvent (*12–15*). NR measurements were carried out by a time-of-flight type reflectometer ARISA-II at BL16 in MLF/J-PARC providing 25 Hz-pulsed neutron radiation at 120 kW. Wavelength of the incident neutrons is tuned at 0.2 - 0.88 nm by a disk chopper. A neutron beam was irradiated from quartz to the interface between D_2O and the polymer brush on quartz glass. The incident slits were adjusted to maintain a 50 mm footprint size on the sample surface. The NR profiles were analyzed by fitting calculated reflectivity from the model scattering length density profiles to the data, using Parratt32 software.

The NR curves of D_2O/poly(MTAC) brush interface in Figure 3(a-c) showed a critical angle at $q = 0.11$ nm^{-1} which is attributed to the difference in neutron scattering length density (SLD) between quartz and D_2O. The neutron SLD profiles of the poly(MTAC) brush in D_2O formed in a smooth upward curve from 4.6×10^{-4} to 6.36×10^{-4} nm^{-2} along with the distance from the substrate. The gradient profile indicated that the polymer chains in D_2O were stretched to ca. 75 nm, which is larger than the brush thickness under the air (humidity = 35%) estimated to be 30 nm by ellipsometer. Therefore, the polymer chains immersed in D_2O were considerably extended to a perpendicular direction against the substrate. High osmotic pressure caused by high concentration of quaternary ammonium ions in the brush layer would have made an extended chain conformation. The gradual change in SLD was appeared due to the presence of the molecular weight dispersity in polymer brush. Polydispersity index of brush, $M_w/M_n = 1.17$, afforded a thick boundary zone to make unclear fringes in the reflectivity curve.

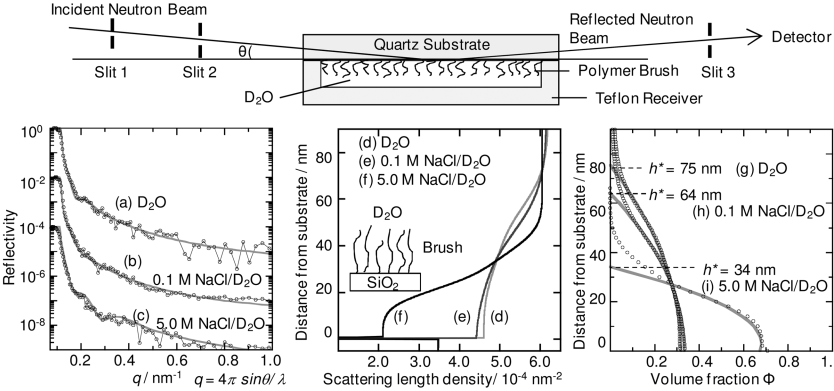

Figure 3. Schematicr epresentation of the NR experimental setup for polymer brush/D_2O interface. NR curves of (a) poly(MTAC) brush/D_2O, (b) poly(MTAC) brush/ 0.1 M NaCl in D_2O, (c) poly(MTAC) brush/5.0 M NaCl in D_2O, and their reflectivity fits (gray line) based on (d)(e)(f) their corresponding neutron SLD profiles along with the distance from quartz surface, respectively, and (g)(h)(i) volume fraction profiles of poly(MTAC) in 0 M, 0.1 M, and 5.0 M NaCl in D_2O with calculation using parabolic functions. Broken linear lines in (g)-(i) indicate swollen thickness h. Poly(MTAC) with M_n = 94,300 and M_w/M_n = 1.17 was used.*

In general, an increase in ionic strength leads to the reduction of the electrostatic repulsion. The polyelectrolyte chains in a salt solution may undergo a transition toward a more coiled state and show a volume reduction. However, quite similar reflective curve was observed from the interface of the poly(MTAC) brush in the 0.1 M NaCl/D_2O solution, indicating that the extended structure of the swelling brush chains did not change, even in a salt solution. It is a quite contrast to the fact that the unbound polyelectrolyte shrink in salt solution. We estimated the swollen brush thickness by volume fraction (φ) curve of MTAC segments as a function of the distance from the substrate (z) and the corresponding parabolic-type profile assuming a brush layer height (h*). A pure parabola equation of $\varphi = \varphi_0\{(1\text{-}z/h^*)^2\}$ is theoretically predicted by Cates et al. for polymer brush in the limit of strong stretching (*16*). Actual volume fraction curve requires the parabolic function and an additional exponential tail at larger z region to obtain better fit due to a roughness at the brush/solution interface. We regard h* as thickness of the swollen brush.

Let us assume the swollen poly(MTAC) thickness in D_2O was 75 nm, the M_n was 94,300, and grafting density was 0.21 chains/nm^2, the apparent concentration of MTAC monomers in the brush layer can be estimated to be 2.1 M, which is higher than salt concentration in the external solution. Therefore, hydrated salt ion could not diffuse into a high-density polymer brush layer due to the high local charge density, and then polyelectrolyte brush could keep an extended chain conformation in solution. Similar results have been reported by Matsuoka (*17*, *18*), Kurihara (*19*), and Tran (*20*). Huck et al. reported the swelling behavior of the poly(MTAC) brush in solution by AFM observation (*21*). They suggested that thickness of brush decreased at much lower external salt concentrations than the concentration of chemically charged monomers of the chains.

When the poly(MTAC) brush was immersed in 5.0 M NaCl/D_2O solution, the reduction in roughness and thickness of swelling brush layer was observed. The brush layer height h* was 34 nm. The hydrated salt ions in the adjacent solution with higher ionic strength than the brush layer must have screened the repulsive interaction between quaternary ammonium groups of the brush chain to moderate highly extended chain conformation. The graft area occupied with a single tethered chain was 4.7 nm^2. Considering the molecular volume per monomer unit v_0 (= 0.28 nm^3) estimated from bulk density of MTAC and the chain contour length per monomer unit l_0 (l_0= 0.25 nm for vinyl monomers), the cross-sectional area per monomer unit $a^2 = v_0/l_0$ is 1.1 nm^2. Therefore, the distance between the tethered chains on the substrate surface is around 1.2 nm, which is larger than the size of hydrated ions. Apparent hydration radius of the equivalent hydrated sphere of Na^+ and Cl^- are reported to be 0.18 and 0.20 nm (*22*). Once the concentration of added ions in solution reaches the concentration of the free counterions inside the brush, hydrated ions can enter the polyelectrolyte brush layer to screen the the electric interactions forming relatively smaller dimension and thickness. The solvent quality of NaCl aqueous solution for poly(MTAC) has not been well-understood yet, although poly(MTAC) quickly dissolves in 5.0 M NaCl aqueous solution. The second virial constant of poly(MTAC) in NaCl solution should be evaluated by light scattering measurement.

Independency on salt concentration was also observed for the swelling structure of poly(MPC) facing a pure D_2O and a NaCl/ D_2O solution, although the NR curves were not shown here. However, the negligible change in swollen brush structure was attributed to a specific property of poly(MPC). In fact, the dimension of unbound free poly(MPC) in an aqueous solution was also independent on the ionic strength of the salt solution (*23*, *24*), indicating that the poly(MPC) can be regarded as a quite unique polyelectrolyte of which chain dimension in an aqueous solution hardly changed by salt effect.

Tribological Behavior of Polymer Brushes

Macroscopic friction tests on polymer brushes (*25–27*) were carried out on a conventional ball-on-plate type reciprocating tribotester, Tribostation Type32 (Shinto Scientific Co. Ltd., Tokyo) by sliding a glass ball on the substrates along a distance of 20 mm at the sliding velocity of 10^{-4} - 10^{-1} m s^{-1} in air and in water under a normal load of 0.49 N at room temperature. The friction coefficient was determined by a strain gauge attached to the arm of the tester and was recorded as a function of time. In the case of a non-modified silicon wafer under a normal load of 50 g (0.49 N), the theoretical contact area between the glass probe and substrate can be calculated as 3.51 × 10^{-9} m^2 by Hertz's contact mechanics theory and the average pressure on the contact area was estimated to be 139 MPa.

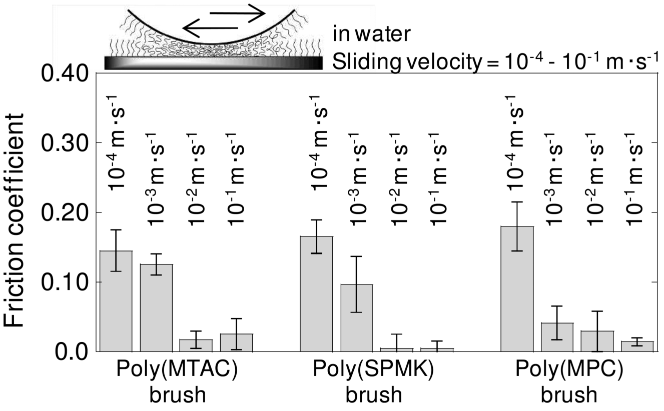

Figure 4. Sliding velocity dependence of the friction coefficient of poly(MTAC), poly(SPMK), and poly(MPC) brushes in water by sliding a glass ball (10 mm diameter) immobilized with the corresponding polymer brushes over a distance of 20 mm under a normal load of 0.49 N at 298 K. Poly(MTAC) (M_n = 312000, M_w/M_n = 1.19), poly(SPMK) (M_n = 606000, M_w/M_n = 1.85), and poly(MPC) (M_n = 618000, M_w/M_n = 1.48) brushes were used for friction test.

As mentioned in the previous section, the polyelectrolyte brushes showed low water contact angles below 7 deg and high surface free energy over 70 mJ m^{-2}. The wettability of the brush against water is an important factor for the reduction of friction coefficient in water. The friction coefficients of poly(MTAC), poly(SPMK), and poly(MPC) brushes in water were measured at a sliding velocity of 10^{-4} - 10^{-1} m s^{-1} (*8*, *28*). The polymer brushes were immobilized on both surface of silicon wafer and sliding glass ball. The friction coefficients of these brushes were 0.1 - 0.2 at the slower friction velocity of 10^{-4} - 10^{-3} m s^{-1}, whereas the friction coefficient was decreased to 0.01 - 0.03 at the higher sliding velocity over 10^{-2} - 10^{-1} m s^{-1}, as shown in Figure 4. The drastic reduction in the friction coefficients at a certain velocity could be caused by the transition of friction mode. With the low sliding velocity, the interaction between the opposite brushes and the interpenetration of brushes dominated the friction to give a large friction coefficient (boundary or interfacial friction). With an increase in the sliding velocity, a thicker liquid layer would be formed between the sliding surfaces by the hydrodynamic lubrication effect to reduce the actual contact area and the friction force (mixed lubrication region). At higher sliding velocity, we supposed that hydrodynamic lubrication partially took place between opposing swollen polyelectrolyte brushes to reduce the friction. Poly(SPMK) showed significantly low friction coefficients at the sliding velocity of 10^{-2} - 10^{-1} m s^{-1} probably because of water lubrication and the electrostatic repulsive interactions among the anionic groups

Wear track formed on the brush surface after the friction test even though the friction coefficient in water was lower than 0.02. However, XPS analysis revealed components of the brush apparently remained in the wear tracks, and low constant coefficient of friction was continuously observed during several tracking cycles of reciprocating friction. These constant values were determined as the friction coefficient in this study. For example, poly(SPMK) brush in water maintained low friction coefficient of 0.01 at the sliding velocity of 1.5 x 10^{-3} m s^{-1} until 400 tracking cycles. Wear of brush gradually proceeded keeping a low friction coefficient, but eventually, the brush was complete abraded away by sliding probe to result in much higher friction coefficient.

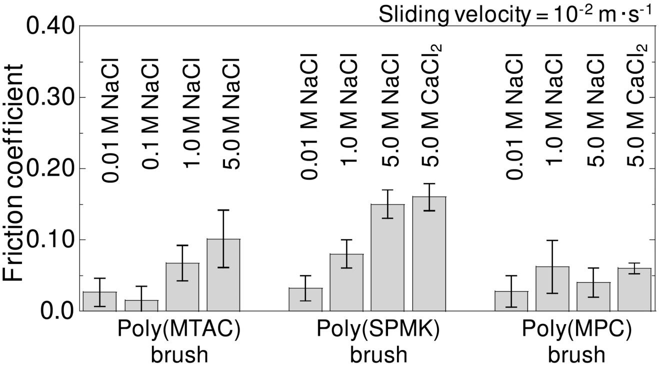

Figure 5. Friction coefficient of poly(MTAC), poly(SPMK), and poly(MPC) brushes in NaCl and $CaCl_2$ aqueous solution water by sliding a glass ball (10 mm diameter) immobilized with the corresponding polymer brushes over a distance of 20 mm at a sliding velocity of 1.0 × 10^{-2} m s^{-1} under a normal load of 0.49 N at 298 K. Poly(MTAC) (M_n = 141000, M_w/M_n = 1.19), poly(SPMK) (M_n = 606000, M_w/M_n = 1.85), and poly(MPC) (M_n = 605000, M_w/M_n = 1.68) brushes were used for friction test in salt aqueous solution.

The friction coefficients of polyelectrolyte brushes in aqueous solution are affected by a salt concentration. Figure 5 shows friction coefficient of polyelectrolyte brushes in aqueous salt solution. The poly(MTAC) brush in 0.01 M aqueous NaCl solution showed the same friction coefficient as in pure water. The friction coefficient in 1.0 – 5.0 M of $NaCl_{aq.}$ solution at the higher sliding velocity increased from 0.02 to 0.1. The low friction coefficient below 0.02 was observed in poly(SPMK) brush in 0 – 0.1 M $NaCl_{aq.}$ solution at the sliding velocity of 10^{-2} m s^{-1}, however, the friction coefficient increased to be 0.1 in a higher NaCl concentration above 1.0 M. In general, polyanion or polycation chains in aqueous solution with low ionic strength form a relatively expanded chain structures due to the intramolecular repulsive interaction. In contrast, the polyelectrolyte dissolved in solution with higher ionic strength behaves like an electrically neutral polymer to give smaller dimension because the electrostatic interactions are screened by salt ions. Therefore, an increase in salt concentration would lead to the reduction of the electrostatic repulsion among the brushes to result in a higher friction coefficient.

Poly(MPC) brush in aqueous NaCl and $CaCl_2$ solution brush showed larger friction coefficients than that in pure water at various sliding velocity. However, significant difference in friction coefficients between salt solution and water was not observed at a sliding velocity of 10^{-2} m s^{-1}. It can be related to the fact that the poly(MPC) is a quite unique polyelectrolyte of which chain conformation in a aqueous solution hardly changed by salt effect due to a weak intermolecular interaction among phosphorylcholine units and a neutral nature of zwitter ion (*24*).

Repeatable Adhesion of Polymer Brushes

Adhesion and lap shear test were carried out as follows (*29*); As shown in Figure 6, a 2 μL of deionized water was put on a brush-immobilized rectangular silicon substrate and then another substrate was pressed onto it under a constant load of 4.9 N at 298 K and 55% relative humidity. The contact area of the substrates was maintained at 5 × 10 mm^2, unless otherwise specified. After 2 h of drying time, a supporting stainless steel plate (10 × 30 × 0.2 mm^3) was bonded to both ends of the lapping substrates using a cyanoacrylate-type instant glue to prepare an easy-to-clip sample for the lap shear test. The adhesion strength was determined by measuring the lap shear adhesion force with a tensile tester (Shimadzu EZ-Graph) at 298 K in an ambient atmosphere. The sample was held at both ends of the stainless steel plates with two mechanical chucks connected to a load cell and a tester base anchor. The crosshead speed was set to 1 mm min^{-1} in tensile mode. The lap shear strength was defined as the force corresponding to the breaking point divided by an adhesion area of 50 mm^2.

In the case of poly(SPMK) and poly(MTAC) brushes pair, the average adhesion strength reached 1.52 MPa, as shown in Figure 7. This value was weaker than typical adhesion strength of commercially available adhesives (10 - 30 MPa), however, it would be sufficiently useful adhesion strength for many applications because the adhered brush substrates with 1 cm^2 adhesion area could lift up a weight of ca. 15 kg. The lap shear adhesion strength between poly(sodium methacrylate) (MANa) brush and poly(MTAC) brush substrates was 1.08 MPa. The sulfonate anion group of SPMK interacted strongly with the ammonium cation group in MTAC compared with carboxylic acid in MANa.

XPS spectrum of the poly(MTAC) brush surface after the lap shear break was similar to the virgin one maintaining consistent atomic ratio with the MTAC component, except for the K_{2s}. In the case of the poly(SPMK) brush, Cl_{2p} and N_{1s} peaks appeared after the lap shear test in addition to the original component of SPMK with carbon, oxygen, sulfur, and potassium, probably because a trace amount of poly(MTAC) from the substrate was transferred to the poly(SPMK) brush surface side when the substrates separated. Significant change was not observed in the thickness of poly(MTAC) and poly(SPMK) brushes by AFM height profile measurement before and after the lap shear test. Therefore, most of the polyelectrolyte brushes were retained on each substrate even after the lapped junction delaminated, and adhesion failure occurred predominantly at the interface of the polyanion brush and polycation brush.

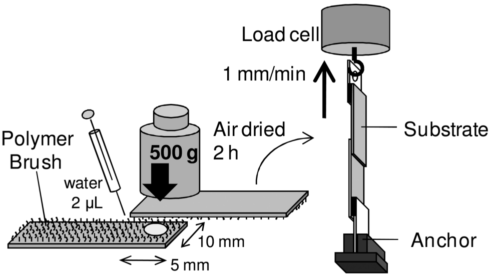

Figure 6. Schematic view of the adhesion process of the polyelectrolyte brushes and the lap shear test setup using a tensile tester. Thickness of both polymer brushes were approximately 100 nm.

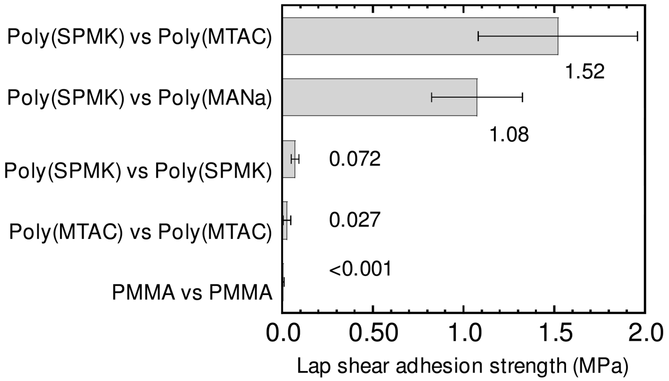

Figure 7. Lap shear adhesion strengths of pairs of polyelectrolyte brushes-immobilized on silicon substrates at 298 K in an ambient atmosphere. Poly(MTAC) (M_n = 363000, M_w/M_n = 1.18), poly(SPMK) (M_n = 606000, M_w/M_n = 1.86), and PMMA (M_n = 122000, M_w/M_n = 1.24) brushes were used for lap shear adhesion test.

Negligible adhesion was observed between two polymer brushes bearing the same polarity, such as the combination of poly(SPMK)/ poly(SPMK) brushes and poly(MTAC)/ poly(MTAC) brushes. As a control experiment, we prepared PMMA brush substrates, which also adhered to each other in the presence of a small amount of water and by successive drying at 298 K for 2 h in air. However, adhesion of the PMMA brush specimen was too weak to measure the lap shear adhesion strength. The resulting specimen debonded easily before we started the lap shear test. This result indicated that the electrostatic interaction contributed to the adhesion of anionic/cationic polymer brushes.

Since the polymer brushes remained on the substrate even after the lap shear test, a specimen combined with poly(MTAC) and poly(SPMK) brushes was rebonded several times by repeating the swelling with water and debonding in air, although the adhesive strength decreased in a stepwise fashion from 1.52 to 0.85 MPa.

To measure the debonding time, a specimen prepared by adhesion of oppositely charged polymer brushes was attached to a hanging weight of 100 g and immersed in deionized water at 298 K. Contrary to our expectation, debonding did not occur in deionized water for over 24 h. On the other hand, self-delamination took place within 10 - 60 min in 0.5 M NaCl salt aqueous solution, because the hydrated salt ions permeated the adhesion interface to screen the electrostatic interaction between brushes. After the debonded substrates were washed with deionized water to remove the salt, they readily adhered to each other again. The lap shear adhesion strength of the re-adhered substrates was 1.23 MPa, which was close to the initial adhesion strength. In this case, adhesion and debonding can be repeated without any damages to the brushes by using deionized water and salt aqueous solution.

Conclusions

Various polyelectrolyte brushes with anionic, cationic, and zwitter ionic side chains were prepared on the Si-wafer by SI-ATRP. Surface wettability and chain conformation of polymer brushes at water/solid interfaces were successfully characterized. Super hydrophilic surface, antifouling surfaces, water lubrication systems, and repeatable adhesion systems without organic solvents were realized through the polyelectrolyte brushes. The conventional coatings, such as spin cast films, cannot maintain these attractive surface properties permanently because they are easily debouched from the substrate in a good solvent or scratched off by friction. The brush structure, of which polyelectrolyte chain ends were densely immobilized with substrate, formed stable hydrated brush layer in aqueous environment to contribute to the antifouling effect, lowering friction, and reversible adhesion.

References

1. Rühe, J. Polymer Brushes on the Way to Tailor-Made Surfaces. In *P olymer Brushes: Synthesis, Characterization, Applications*; Advincula, R. C., Brittain, W. J., Caster, K. C., Rühe, J., Eds.; Wiley VCH: Weinheim, 2004; pp 1−31.
2. Tsujii, Y.; Ohno, K.; Yamamoto, S.; Goto, A.; Fukuda, T. Structure and properties of high-density polymer brushes prepared by surface-initiated living radical polymerization. *Adv. Polym. Sci.* **2006**, *197*, 1–45.
3. Zhao, B.; Brittain, W. J. Polymer brushes: Surface-immobilized macromolecules. *Prog., Polym. Sci.* **2000**, *25*, 677–710.

4. Sakata, H.; Kobayashi, M.; Otsuka, H.; Takahara, A. Tribological properties of poly(methyl methacrylate) brushes prepared by surface-initiated atom transfer radical polymerization. *Polym. J.* **2005**, *37*, 767–775.
5. Kobayashi, M.; Takahara, A. Synthesis and frictional properties of poly(2,3-dihydroxypropyl methacrylate) brush prepared by surface-initiated atom transfer radical polymerization. *Chem. Lett.* **2005**, *34*, 1582–1583.
6. Kobayashi, M.; Terada, M.; Terayama, Y.; Kikuchi, M.; Takahara, A. Direct synthesis of well-defined poly[{2-(methacryloyloxy)ethyl}trimethyl ammonium chloride] brush via surface-initiated ATRP in fluoroalcohol. *Macromolecules* **2010**, *43*, 8409–8415.
7. Masci, G.; Bontempo, D.; Tiso, N.; Diociaiuti, M.; Mannina, L.; Capitani, D.; Crescenzi, V. Atom transfer radical polymerization of potassium 3-sulfopropyl methacrylate: direct synthesis of amphiphilic block copolymers with methyl methacrylate. *Macromolecules* **2004**, *37* (20), 4464–4473.
8. Kobayashi, M.; Terayama, Y.; Hosaka, N.; Kaido, M.; Suzuki, A.; Yamada, N.; Torikai, N.; Ishihara, K.; Takahara, A. Friction behavior of high-density poly(2-methacryloyloxyethyl phosphorylcholine) brush in aqueous media. *Soft Matter* **2007**, *3*, 740–746.
9. Terayama, Y.; Kikuchi, M.; Kobayashi, M.; Takahara, A. Well-defined poly(sulfobetaine) brushes prepared by surface-initiated ATRP using a fluoroalcohol and ionic liquids as the solvents. *Macromolecules* **2011**, *44* (1), 104–111.
10. Owens, D. K.; Wendt, R. C. Estimation of surface free energy of polymers. *J. Appl. Polym. Sci.* **1969**, *13*, 1741–1747.
11. Yamaguchi, H.; Honda, K.; Kobayashi, M.; Morita, M.; Masunaga, H.; Sakata, O.; Sasaki, S.; Takahara, A. Molecular aggregation states of surface-grafted poly{2-(perfluorooctyl)ethyl acrylate} thin film analyzed by grazing incidence X-ray diffraction. *Polym. J.* **2008**, *40* (9), 854–860.
12. Kobayashi, M.; Terayama, Y.; Hino, M.; Ishihara, K.; Takahara, A. Characterization of swollen structure of high-density polyelectrolyte brushes in salt solution by neutron reflectivity. *J. Phys.: Conf. Ser.* **2009**, *184*, 012010.
13. Kobayashi, M.; Yamaguchi, H.; Terayama, Y.; Wang, Z.; Ishihara, K.; Hino, M.; Takahara, A. Structure and surface properties of high-density polyelectrolyte brushes at the interface of aqueous solution. *Macromol. Symp.* **2009**, *279*, 79–87.
14. Terayama, Y.; Kikuchi, M.; Kobayashi, M.; Hino, M.; Takahara, A. Influence of salt concentration on swelling states of poly(sulfobetaine) brush at aqueous solution interface. *J. Phys.: Conf. Ser.* **2009**, *184*, 012011.
15. Kobayashi, M.; Mitamura, K.; Terada, M.; Yamada, N. L.; Takahara, A. Characterization of swollen states of polyelectrolyte brushes in salt solution by neutron reflectivity. *J. Phys.: Conf. Ser.* **2011**, *272*, 012019.
16. Milner, S. T.; Witten, T. A.; Cates, M. E. Theory of the grafted polymer brushes. *Macromolecules* **1988**, *21*, 2610–2619.

17. Kaewsaiha, P.; Matsumoto, K.; Matsuoka, H. Synthesis and Nanostructure of strong polyelectrolyte brushes in amphiphilic diblock copolymer monolayers on a water surface. *Langmuir* **2004**, *20*, 6754–6761.
18. Kaewsaiha, P.; Matsumoto, K.; Matsuoka, H. Salt effect on the nanostructure of strong polyelectrolyte brushes in amphiphilic diblock copolymer monolayers on the water surface. *Langmuir* **2007**, *23*, 7065–7071.
19. Hayashi, S.; Abe, T.; Higashi, N.; Niwa, M.; Kurihara, K. Polyelectrolyte brush layers studied by surface forces measurement: Dependence on pH and salt concentrations and scaling. *Langmuir* **2002**, *18*, 3932–3944.
20. Sanjuan, S.; Perrin, P.; Pantoustier, N.; Tran, T. Synthesis and swelling behavior of pH-responsive polybase brushes. *Langmuir* **2007**, *23* (10), 5769–5778.
21. Moya, S. E.; Azzaroni, O.; Kelby, T.; Donath, E.; Huck, W. T. S. Explanation for the apparent absence of collapse of polyelectrolyte brushes in the presence of bulky ions. *J. Phys. Chem.* **2007**, *111*, 7034–7040.
22. Kiriukhin, M. Y.; Collins, K. D. Dynamic hydration numbers for biologically important ions. *Biophys. Chem.* **2002**, *99*, 155–168.
23. Matsuda, Y.; Kobayashi, M.; Annaka, M.; Ishihara, K.; Takahara, A. Dimension of poly(2-methacryloyloxyethyl phosphorylcholine) in aqueous solutions with various ionic strength various ionic strength. *Chem. Lett.* **2006**, *35* (11), 1310–1311.
24. Matsuda, Y.; Kobayashi, M.; Annaka, M.; Ishihara, K.; Takahara, A. Dimensions of free linear polymer and polymer immobilized on silica nano particles of a zwitter ionic polymer in aqueous solutions with various ionic strengths. *Langmuir* **2008**, *24* (16), 8772–8778.
25. Kobayashi, M.; Ishida, H.; Kaido, M.; Suzuki, A.; Takahara, A. Frictional Properties of Organosilane Monolayers and High-Density Polymer Brushes. In *Surfactants in Tribology*; Biresaw, G., Mittal, K. L., Eds.; CRC Press: Boca Raton, FL, 2008; pp 89−110.
26. Kobayashi, M.; Wang, Z.; Matsuda, Y.; Kaido, M.; Suzuki, A.; Takahara, A. Tribological Behavior of Polymer Brush Prepared by the "Grafting-from" Method. In *Polymer Tribology*; Kumar, S. S., Ed.; Imperial College Press: London, 2009; pp 582−602.
27. Ishikawa, T.; Kobayashi, M.; Takahara, A. Macroscopic frictional properties of poly(1-(2-methacryloyloxy)ethyl-3-butyl imidazolium bis(trifluoromethanesulfonyl)-imide) brush surfaces in an ionic liquid. *Appl. Mat. Interfaces* **2010**, *2* (4), 1120–1128.
28. Kobayashi, M.; Takahara, A. Tribological properties of hydrophilic polymer brushes under wet condition. *Chem. Rec.* **2010**, *10* (4), 208–216.
29. Kobayashi, M.; Terada, M.; Takahara, A. Reversible adhesive-free nanoscale adhesion utilizing oppositely charged polyelectrolyte brushes. *Soft Matter* **2011**, *7* (12), 5717–5722.

Downloaded by CORNELL UNIV on June 1, 2012 | http://pubs.acs.org
Publication Date (Web): March 20, 2012 | doi: 10.1021/bk-2012-1101.ch013

Chapter 13

Surface Intiated Atom Transfer Radical Polymerizations from Indium Tin Oxide Electrodes: Electrochemistry of Polymer Brushes

Bo Yun Kim,[†] R. Clayton Shallcross,[†] Neal R. Armstrong,[‡] Hyo-ju Kim,[§] Woo Jin Chung,[†] Rabindra Sahoo,[†] Kookheon Char,[§] Philip T. Dirlam,[‡] Philip J. Costanzo,[‡] and Jeffrey Pyun[*],[†],[§]

[†]Department of Chemistry & Biochemistry, University of Arizona, Tucson, Arizona 85721
[§]World Class University Program of Chemical Convergence for Energy & Environment, School of Chemical & Biological Engineering, Seoul National University, Seoul, Korea
[‡]Department of Chemistry and Biochemistry, California Polytechnic State University, San Luis Obispo, California 93407-0402
[*]E-mail: jpyun@email.arizona.edu

We discuss recent efforts on the modification of indium tin oxide electrodes via surface initiated atom transfer radical polymerization (SI-ATRP). In particular, we summarize our recent work on the development of model electrochemical thin films based on ferrocene functional polymethacrylate and block copolymer brushes and the use of electrochemical methods to confirm controlled brush growth.

Indium tin oxide (ITO) belongs to a class of transparent conductive oxide substrates that has been extensively utilized as for anodes in light emitting diodes (LEDs) and photovoltaics (PVs) (*1–3*). The interfacial chemistry and charge transfer properties of ITO electrodes modified with small molecule, or polymer thin films have been extensively studied to enable optimization of optoelectronic and electrochemical device performace (*4–7*). From an interface science

In Progress in Controlled Radical Polymerization: Materials and Applications; Matyjaszewski, K., et al.;
ACS Symposium Series; American Chemical Society: Washington, DC, 2012.

standpoint, ITO offers numerous surface science challenges, as the heterogeneity present on the surface complicates direct structure property correlation of surface sites and electroactivity (*8–10*). Previous studies have demonstrated that only a small fraction of surface sites are active in as received ITO substrates (*8*). Hence, a number of surface modification approaches have been investigated to modify and enhance the performance of ITO surfaces. Functionalization of ITO surfaces with various small molecule coupling agents have been investigated using carboxylic acids (*11–18*), phosphonic acids (*12*, *19–25*) and silanes (*27–29*).

Alternatively, the modification of ITO electrodes using electropolymerization techniques has been conducted to deposit polymeric thin films (*30–32*). These electropolymerization systems are very effective to deposit a wide range of organic semiconducting films onto ITO. These methods offer the advantage of depositing conjugated polymers onto ITO electrodes. We have previously reported that electropolymerizations onto modified ITO electrodes with polymerizable monolayers has enabled the generation of less corrugated conjugated polymer thin films with enhanced electrochemical “wiring” across the organic and inorganic interface (*10*, *33–35*). We have recently shown the advantages of the surface modification of ITO with thiophene ligands in the electrodeposition of PEDOT and in the preparation of hybrid nanocomposites of PEDOT with cadmium selenide (CdSe) quantum dots (*36*, *37*). While electropolymerization methods are certainly useful, there remain opportunities to develop synthetic methods to grow tethered polymers from ITO electrodes possessing well-defined interfacial chemistry, molecular weight, composition and functionality, which directly affects film thickness tunability and electrical properties.

Recent developments in controlled radical polymerizations (CRP) (*38–42*) have enabled the growth of well-defined polymers from a wide range of inorganic substrates, including both flat and curved surfaces. Of these CRP techniques, atom transfer radical polymerization (ATRP) (*43*) has been demonstrated to be a highly versatile and robust synthetic method to prepare well-defined polymers end-tethered to surfaces (*44*, *45*). In particular, the preparation of densely grafted polymer thin films (i.e., polymer brushes) has been recently reported using surface initiated ATRP (SI-ATRP) on ITO substrates. Huck and Friend *et al.* reported the controlled SI-ATRP of triarylamine functional acrylate monomers from α-halo ester silane initiating monolayers on ITO (*46*, *47*). The authors elegantly demonstrated improved hole transport properties in LED devices fabricated from the triarylamine polymer brush, which was attributed to both the enhanced alignment of tethered chains and covalent attachment to the electrode interface. Independently, Fukuda *et al.* reported the controlled SI-ATRP of a ferrocenyl methacrylate monomer from ITO and characterized the polymer brush using CV, AFM and absorption spectroscropy (*48*). Recent work by Advincula *et al.* also reported the “conventional” free radical polymerization of carbazole containing styrenic monomers from azo initiator modified ITO surfaces (*49*). Alternatively, combinations of electropolymerization and surface initiated polymerization have been developed to modify ITO. Advincula *et al.* reported surface initiated free radical polymerizations of *N*-vinylcarbazole, followed by electropolymerization to form electroactive thin films (*50*). Additionally, these authors also reported the electrodeposition of thioester RAFT containing thiophene monomers following

Downloaded by CORNELL UNIV on June 1, 2012 | http://pubs.acs.org
Publication Date (Web): March 20, 2012 | doi: 10.1021/bk-2012-1101.ch013

by surface intiated reversible addition fragmentation chain transfer polymerization (SI-RAFT) (*51*). Minko et al., utilized similar approaches to prepare stimuli responsive polymer brushes on ITO (*52*, *53*).

While these existing elegant studies on surface initiated polymerization from ITO demonstrated the feasibility of this approach, a number of fundamental challenges still exist in both the synthesis and characterization of well-defined polymer brushes on ITO. The optically transparent nature of ITO complicates the characterization of film thicknesses of polymer brushes grown on these substrates using traditional optical methods, such as ellipsometry. AFM "scratch tests" of film thickness are a convenient method to obtain these values, but suffer from reproducibility issues unless good topographic contrast between the bare surface and polymer thin films are ensured. Further correlations of polymerization kinetics with film thickness have not conclusively confirmed the "living" nature of these SI polymerizations when grown from ITO. In existing SI-ATRP derived polymer brushes, confirmation of controlled surface growth is achieved by correlation of brush film thickness with molar mass of free linear chains form in solution using "sacrificial initiators" (*39*). Thus, mechanistic confirmation of controlled SI-ATRP from ITO surfaces is still an important fundament question requiring more thorough investigation.

Herein we summarize on our recent efforts on the synthesis of polymer brushes ITO electrodes via surface initiated atom transfer radical polymerization (ATRP). The preparation of ferrocene functional polymer brushes via surface initiated atom transfer radical polymerization (SI-ATRP) on ITO will be discussed (*54*), as a model system to probe chain conformation effects on electrochemical properties and electron transfer processes.

Synthesis of Phosphonic Acid Coupling Agents and Ferrocene Containing Methacrylate Monomers

For the modification of ITO with ATRP initiators, functional phosphonic acid molecules were prepared bearing α-halo esters to enable surface initiated growth (*54*). Recent studies by Marder et al., have demonstrated that phosphonic acids form robust covalent bonds to ITO substrates and enable variation of the ITO electrode work function by variation of substituents on the molecule (*23*). The use of phosphonic acid coupling agents was desirable in comparison to silanes as Pt-catalyzed hydrosilation reactions could be circumvented to afford a hydrolytically stable coupling agent.

Phosphonic acid initiator **1** was synthesized based on established routes via esterification reaction of 6-bromo-1-hexanol with 2-bromoisobutyryl bromide and substitution reaction of 6-bromohexyl 2-bromoisobutyrate with triethyl phosphite, followed by the conversion of the phosphonate to the phosphonic acid with TMSBr via the Michaelis-Arbuzov reaction in reasonable yields (90%, Figure 1). The 2-bromoisobutyrate moiety is an efficient initiator for the SI-ATRP of methacrylates, while phosphonic acid group has been demonstrated to form robust covalent interfaces to ITO and other conductive metal oxides. FcMA monomer 2 bearing a ferrocene moiety was prepared via DCC coupling between

In Progress in Controlled Radical Polymerization: Materials and Applications; Matyjaszewski, K., et al.;
ACS Symposium Series; American Chemical Society: Washington, DC, 2012.

Downloaded by CORNELL UNIV on June 1, 2012 | http://pubs.acs.org
Publication Date (Web): March 20, 2012 | doi: 10.1021/bk-2012-1101.ch013

Downloaded by CORNELL UNIV on June 1, 2012 | http://pubs.acs.org
Publication Date (Web): March 20, 2012 | doi: 10.1021/bk-2012-1101.ch013

ferrocenecarboxylic acid and 2-hydroxyethyl methacrylate (HEMA) in over 90% yields after purification.

Earlier reports by Fukuda and Mathais reported the synthesis of ferrocene containing methacrylate monomers using a ferrocene functional methyl bromide intermediate via bromination of ferrocene methanol (*55*). FcMA was chosen due to the commercial availability of all starting materials and the ease of the esterification reaction which circumvented the use of the ferrocene functional alkyl halide intermediate which was reported to be hygroscopic and required immediate use to prepare the desired methacrylate monomer.

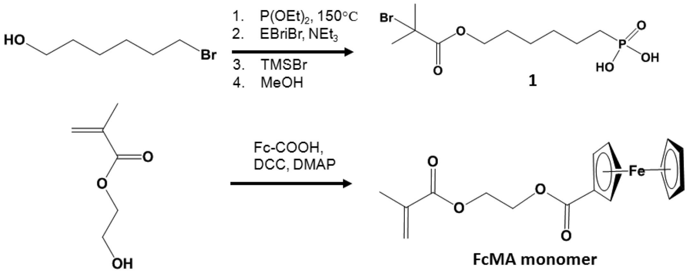

Figure 1. (a) synthesis of phosphonic acid coupling agents for surface initiated ATRP (b) synthesis of ferrocene functional methacrylate monomer (FcMA).

Surface Initiated Atom Transfer Radical Polymerization from ITO

Modification of clean ITO surfaces was conducted by solution incubation of substrates in a dry toluene solution of **1** (3 mM) for 18 hrs and rigorous washing with toluene and absolute ethanol to remove free phosphonic acid compounds from the surface. Thermal treatment of modified ITO substrates was then conducted in a vacuum oven at 100° C for an additional 24 hrs to promote anchoring of the phosphonic acid groups to the metal oxide surface. It has been observed that thermal treatment of phosphonic acid monolayer on ITO in this temperature range is essential to promote either mono-, or bidentate ligation to the surface (*56*, *57*). XPS and IRAAS of modified ITO substrates confirmed the successful deposition of phosphonic acid initiator **1** for SI-ATRP

Polymer brushes on ITO were prepared via surface initiated ATRP of FcMA, in toluene using a Cu(I)Cl/dNbpy catalyst system (10^{-2} M, Figure 2). ATRP of FcMA was conducted in toluene solutions (1 M), since the monomer was a crystalline solid and required pre-dissolution. Ethyl 2-bromoisobutyrate (10^{-3} M) was used as the sacrificial initiator with functional ITO substrate to generate free homopolymers from FcMA in solution. It is important to note that since the global concentration of sacrificial initiator was much higher in solution than of tethered initiating sites on the ITO, the overall degree of polymerization (DP) and molecular weight of the grown polymer brush could easily be controlled by adjusting the feed ratio of FcMA monomer to sacrificial initiator ($[M]_o/[I]_o$). Cu(I)Cl salts were preferred, as improved control of the SI-ATRP was observed in comparison to Cu(I)Br salts. Furthermore the presence of free linear PFcMA grown in solution enabled facile molecular weight characterization of free polymer chains via SEC and correlation with both the electrochemical activity and film thickness of ITO grafted polymer brushes (ITO-g-PFcMA). Since it has been demonstrated that free polymer chains possess similar molecular weight to grafted polymer brushes, we inferred that end-tethered PFcMA chains also exhibited comparable molar mass to free PFcMA grown in solution, which we refer to as "correlated molecular weights." While this point is generally accepted, there has been considerable controversy on the validity of this assumption. Hence, we grew polystyrene grafted ITO brushes, cleaved them from ITO using an HCl etch (conc. HCl) and confirmed that the SEC molecular weight of free polymers were comparable to cleaved-surface grown polymers. However, the HCl etching of PFcMA polymer on ITO primary lead to cleavage of ester-FcMA groups, which complicated recovery and analysis of polymers.

Downloaded by CORNELL UNIV on June 1, 2012 | http://pubs.acs.org
Publication Date (Web): March 20, 2012 | doi: 10.1021/bk-2012-1101.ch013

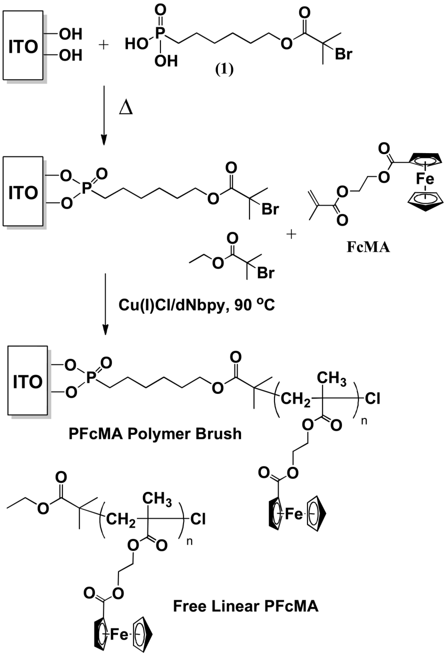

Figure 2. Synthetic scheme for the growth of PolyFcMA brushes on ITO via SI-ATRP. Reprinted with permission from Ref. (54). Copyright 2010 American Chemical Society.

Polymer brushes were found to be chemically robust to excessive solvent washing due to covalent attachment to the ITO surface. It is important to note that tethered polymer brushes contained ferrocene side chain groups in every repeating unit of the polymer. Thus, simple control of chain length, or degree of polymerization (DP) enabled systematic variation of the number of electroactive ferrocene groups into the polymer brush. Polymerization kinetics was monitored as semi-logarithmic plots of monomer conversion and observed to be linear for target $[M]_o/[I]_o$ = 200 and 400, reaching high conversions of 80% (Figure

3a). A plot of SEC determined molecular weight relative to PMMA standards vs. conversion for a range of target DPs were also found to exhibit a linear relationship and were in reasonable agreement with theoretical values with polydispersities ranging from 1.05 – 1.22 (Figure 3b).

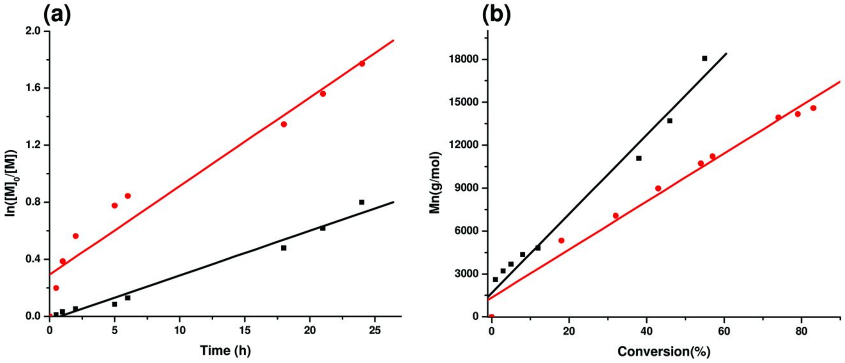

Figure 3. (a) semi-logarithmic and molecular weight vs. conversion (b) plots of the ATRP of FcMA from "sacrificial" initiators in the presence of modified ITO substrates, black squares; DP = 400 and red circles; DP = 200. Reprinted with permission from Ref. (54). Copyright 2010 American Chemical Society.

Electrochemical Characterization of Controlled SI-ATRP of FcMA from ITO

A fundamental question to address in this system was mechanistic confirmation of controlled polymerization from the modified ITO surface to enable systematic inclusion of electroactive ferrocene side chain groups. The most common approach to confirm the growth of polymer brushes via surface initiated polymerizations is the linear correlation of molecular weight (of sacrificially recovered polymers) vs. brush film thickness. As discussed previously, the optical transparency of ITO complicates the use of ellipsometry to characterize film thicknees of polymer brushes. Hence, we examined for the first time electrochemical methods via cyclic voltammetry as an approach to confirm the surface initiated growth of polymer brushes on ITO. An attractive feature of using FcMA in SI-ATRP from ITO is that every unit of tethered polymer incorporate an electroactive Fc unit with a well-established amount of charge per Fc group, which enables correlation of increasing current density (J) from CV measurements with molecular weight of grown PFcMA polymers. For PolyFcMA brushes on ITO with M_n = 4,000 to 37,000 g/mol, CV measurements at the same scan rate demonstrating increasing current density as a function of increasing brush molecular weight and thickness (Figure 4a). From these CV measurements, an electroactive surface coverage (Γ) of ferrocene groups could be calculated, which when correlated with molecular weight of recovered sacrificial polymers exhibited a linear correlation, independent of scan rate (Figure 4b). Because of the linearity of this relation, it can be inferred that a

Downloaded by CORNELL UNIV on June 1, 2012 | http://pubs.acs.org
Publication Date (Web): March 20, 2012 | doi: 10.1021/bk-2012-1101.ch013

Downloaded by CORNELL UNIV on June 1, 2012 | http://pubs.acs.org
Publication Date (Web): March 20, 2012 | doi: 10.1021/bk-2012-1101.ch013

controlled SI-ATRP proceeded. Hence, this plot of surface coverage vs. M_n should be applicable to any surface initiated polymerization conducted from an electrode substrate (e.g., Au, Pt, glassy carbon) to confirm controlled growth from the surface. The validity of this electrochemical method to characterize brush growth was confirmed by direct comparison of film thickness-M_n plots as determined from AFM measurements of patterned ITO PFcMA brushes of varying molecular weight (4,000 to 37,000 g/mol) (Figure 4c). AFM derived film thickness with molar masses of recovered sacrificially grown polymers also exhibited a linear relationship, which confirmed controlled SI-ATRP from the surface (Figure 4d). Estimations of grafting density(σ) from electrochemical methods (σ = 0.7 chains/nm^2) vs. AFM ((σ = 0.4 chains/nm^2) were in reasonable agreement, which also validated the controlled growth of PFcMA brushes from ITO. The slight higher grafting density determined from CV could be attributed to charging current contributions (i.e., non-Faradiac electrolyte diffusion into the polymer brush), which also contribute the higher current densities and are difficult to deconvalute from single-electron transfer (i.e., Faradiac) from pendant Fc groups into the ITO electrode.

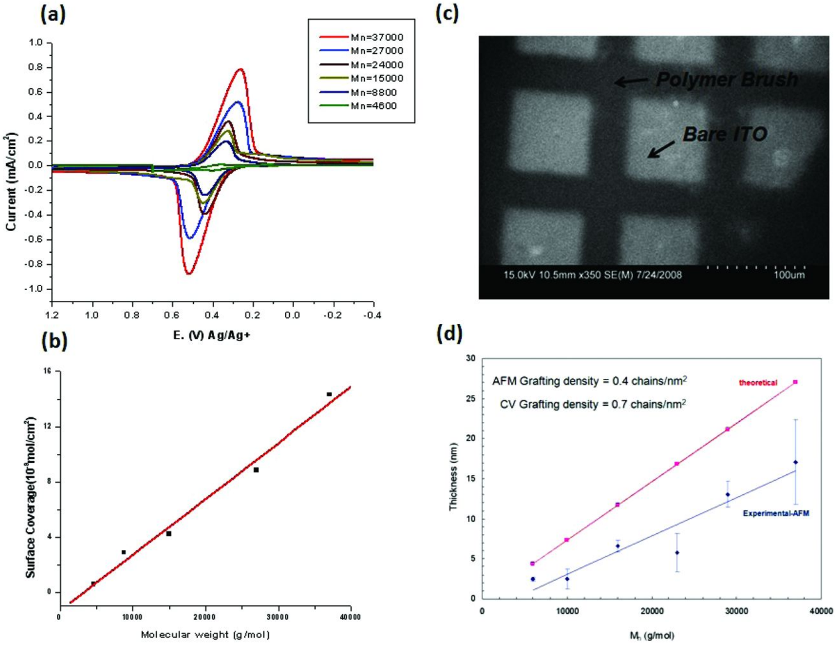

Figure 4. (a) CV of PFcMA brushes of varying MW (4000-37000) in acetonitrile with TBAHFP electrolyte, with Ag/AgNO$_3$ reference and Pt counter electrodes (b) plot of surface coverage vs. correlated MW of sacrificial PFcMA polymers (c) representative FE-SEM of patterned PFcMA brush on ITO (d) comparative plot of brush thickness vs. correlated MW of sacrificial PFcMA polymers determined from AFM. Reprinted with permission from Ref. (54). Copyright 2010 American Chemical Society.

Downloaded by CORNELL UNIV on June 1, 2012 | http://pubs.acs.org
Publication Date (Web): March 20, 2012 | doi: 10.1021/bk-2012-1101.ch013

Electrochemical Properties of PFcMA Brushes

While a number of reports have demonstrated uses of polymer brushes on ITO, fundamental electrochemical characterization of these systems have not been extensively explored, as has been conducted for electrodeposited thin films. Variation of solvents on homopolymer PFcMA brushes on ITO were conducted to examine solvation and chain conformation effects on the voltammetry of this tethered thin films. Solvents, such as, dichloromethane and tetrahydrofuran (THF) were found to be good solvents for PFcMA homopolymers, while acetonitrile (ACN) and methanol (MeOH) were found to be non-solvents for these polymers. CV done in ACN using tetrabutylammonium hexafluorophosphate (TBAHFP) as the electrolyte presumably resulted in collapse of PFcMA brushes on ITO, but still exhibited reversible, nearly symmetric voltammetry, with a progressive increase in the oxidation-reduction peak potential differences (ΔE) with increasing brush molar mass and film thickness (Figure 5a,b). However, CV measurements in THF exhibited significantly distorted oxidation-reduction voltammograms and displayed a linear correlation of increasing ΔE with increasing brush molar mass and film thickness. For polymer films in contact with THF, which is expected to solvate these tethered polymer chains, we propose that intermolecular electron transfer between Fc units was impeded, along with counter ion migration and diffusion into the polymer brush, which was required to preserve electroneutrality. The differences in voltammetric peak shapes are likely due to a combination of a) differences in electron transfer rates between adjacent Fc units (likely to be higher in ACN where collapse of the film may give rise to closer Fc-Fc contacts), and b) accessibility of counter ions to the oxidized Fc units (which again appears to be faster for films in contact with ACN).

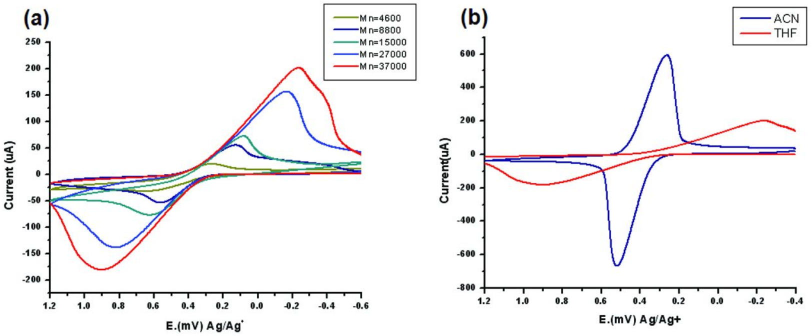

Figure 5. (a) CV of PFcMA brushes of varying MW (4000-37000) in THF with TBAHFP electrolyte, with Ag/AgNO$_3$ reference and Pt counter electrodes (b) comparison of PFcMA Brush (M_n = 37,000 g/mol) in ACN (red) vs. THF (blue). Reprinted with permission from Ref. (54). Copyright 2010 American Chemical Society.

Finally, to demonstrate the effects of controlled SI-ATRP on electrochemical properties of ITO bound brushes, block copolymers composed of poly(methyl methacrylate) and PFcMA were prepared where sequence and proximity to the

ITO electrode was compared. Block copolymers with an inner segment molar mass of 7,000-8,000 g/mol were prepared, followed by chain extension with an other block segment with molar masses of 16,000,-17,000 g/mol. In this particular study, the effects of sequencing the electroactive PFcMA segment next to the ITO electrode, or with a PMMA spacer between ITO and the PFcMA segment was investigated.

CV of the block copolymer brush of ITO-g-PFcMA-b-PMMA in ACN (i.e., “poor solvent”), for which the ferrocene functional polymer segment was attached directly to the electrode (Figure 6a) displayed reversible redox voltammetry comparable to PFcMA homopolymer brush voltammetry in ACN (Figure 4a). Conversely, a large separation in the cathodic and anodic peaks were observed for ITO-g-PMMA-b-PFcMA CV in ACN, where significant broadening of the cathodic peak was observed (Figure 6b). We inferred from this behavior that the PMMA inner segment which is non-electroactive, impeded electrochemical communication between ferrocene groups in PFcMA outer segment and ITO electrode. CV studies of both ITO-g-PFcMA-*b*-PMMA and ITO-g-PMMA-*b*-PFcMA brushes were also conducted in THF and exhibited similar, but more pronounced trends of altered voltammetric asymmetry between cathodic and anodic scans.

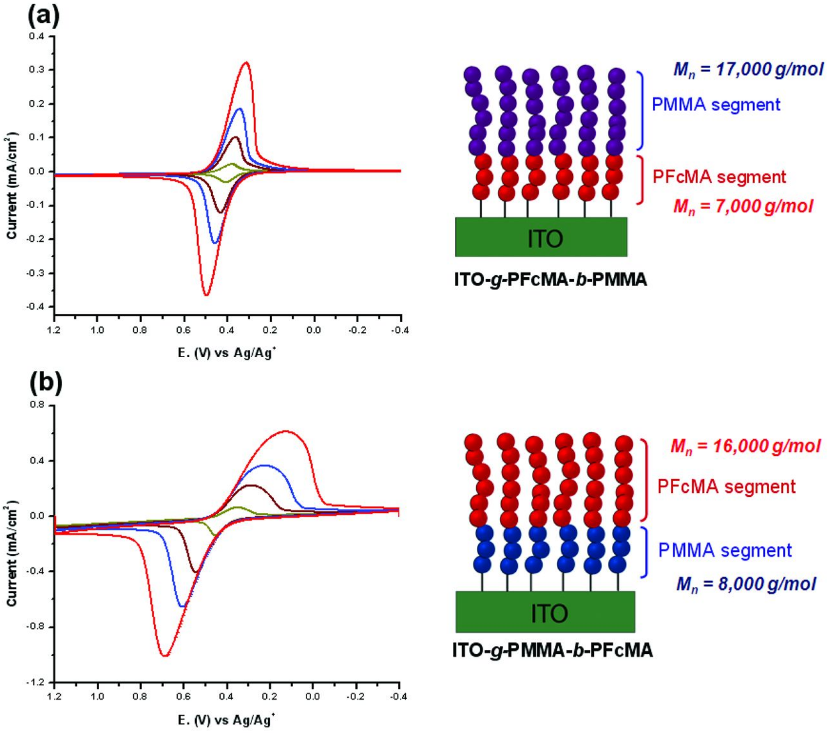

Figure 6. CV of (a) ITO-g-PFcMA-b-PMMA (Mn = 24,000 g/mol) (b) ITO-g-PMMA-b-PFcMA (Mn = 24,000 g/mol) block copolymer brushes in ACN at various scan rates; 10, 50, 100, and 200mV/s. Reprinted with permission from Ref. (54). Copyright 2010 American Chemical Society.

Downloaded by CORNELL UNIV on June 1, 2012 | http://pubs.acs.org
Publication Date (Web): March 20, 2012 | doi: 10.1021/bk-2012-1101.ch013

Downloaded by CORNELL UNIV on June 1, 2012 | http://pubs.acs.org
Publication Date (Web): March 20, 2012 | doi: 10.1021/bk-2012-1101.ch013

New Monomers for SI-ATRP

The next step in this work was the synthesis, SI-ATRP and electropolymerization of monomers carrying both free-radically and electropolymerizable groups to prepare interpenetrating brushes with conjugated polymers. In our initial work in this area, the synthesis of functional vinylic monomers based on 3-methyl-3,4-dihydro-2*H*-thieno[3,4-b][1,4]dioxepin-3-ol (ProDOT-MeOH) were prepared by esterification of the alcohol group with either methacryloyl, or acryloyl chloride to prepare methacrylate, or acrylate functional ProDOT monomers (e.g., ProDOT-MA, ProDOT-A). Additionally, ProDOT-MeOH was coupled with 4-vinylbenzoic acid using dicyclohexylcarboimide and 4-dimethylaminopyridine to prepare a styrenic functional ProDOT monomer (ProDOT-Sty) (Figure 7). It was discovered that the ProDOT-MA monomer was chemically unstable and tended to auto-polymerize rapidly (within 1 day) upon storage. However, both ProDOT-A and ProDOT-Sty monomers were found to be stable and suitable for storage and later use in polymerization. Future work is focused on evaluation of these monomers for SI-ATRP and electropolymerizations.

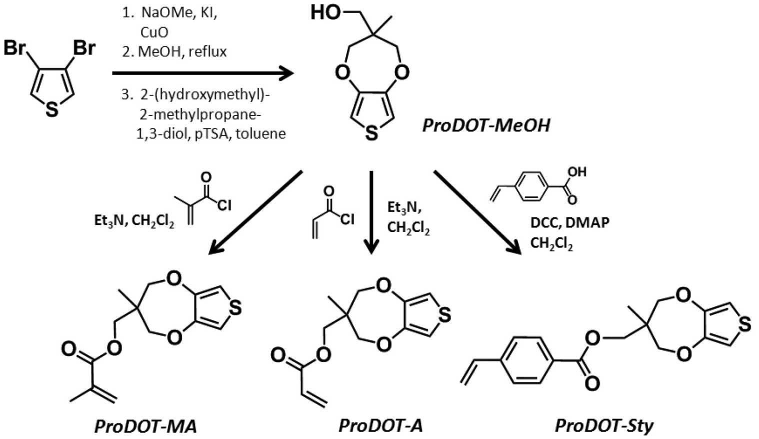

Figure 7. Synthesis of vinylic ProDOT monomers by modification of ProDOT-MeOH with methacrylate, acrylate, or styrenic groups.

Conclusions

We report on the preparation of model polymer brush systems based on FcMA that can be prepared by SI-ATRP and are amenable to both thin film and electrochemical characterization to confirm the controlled growth of brushes from ITO electrodes. By control of homo- and block copolymerizations, the electrochemical properties of these materials were controlled.

Acknowledgments

The World Class University program through the National Research Foundation of Korea funded by the Ministry of Education, Science and Technology (R31-10013), the ONR-YIP (N00014-07-1-0796), the NSF CAREER Program (DMR-0645618) and the Alfred P. Sloan Foundation are acknowledged for synthetic support of this work. The authors gratefully acknowledge the Division of Chemical Sciences, Geosciences, and Biosciences, Office of Basic Energy Sciences of the US Department of Energy through grant DE-FG03-02ER15753 for electrochemical & spectroscopic support.

Downloaded by CORNELL UNIV on June 1, 2012 | http://pubs.acs.org
Publication Date (Web): March 20, 2012 | doi: 10.1021/bk-2012-1101.ch013

References

1. Bel Hadj Tahar, R.; Ban, T.; Ohya, Y.; Takahashi, Y. *J. Appl. Phys.* **1998**, *83*, 2631.
2. Cui, J.; Wang, A.; Edleman, N. L.; Ni, J.; Lee, P.; Armstrong, N. R.; Marks, T. J. *Adv. Mater.* **2001**, *13*, 1476.
3. Armstrong, N. R.; Veneman, P. A.; Ratcliff, E.; Placencia, D.; Brumbach, M. *Acc. Chem. Res.* **2009**, *42*, 1748.
4. Armstrong, N. R.; Wang, W.; Alloway, D. M.; Placencia, D.; Ratcliff, E.; Brumbach, M. *Macromol. Rapid Commun.* **2009**, *30*, 717.
5. Koch, N. *ChemPhysChem* **2007**, *8*, 1438.
6. Kugler, T.; Loegdlund, M.; Salaneck, W. R. *Acc. Chem. Res.* **1999**, *32*, 225.
7. Wang, Y. Z.; Epstein, A. J. *Acc. Chem. Res.* **1999**, *32*, 217.
8. Donley, C.; Dunphy, D.; Paine, D.; Carter, C.; Nebesny, K.; Lee, P.; Alloway, D.; Armstrong, N. R. *Langmuir* **2002**, *18*, 450.
9. Brumbach, M.; Veneman, P. A.; Marrikar, F. S.; Schulmeyer, T.; Simmonds, A.; Xia, W.; Lee, P.; Armstrong, N. R. *Langmuir* **2007**, *23*, 11089.
10. Marrikar, F. S.; Brumbach, M.; Evans, D. H.; Lebron-Paler, A.; Pemberton, J. E.; Wysocki, R. J.; Armstrong, N. R. *Langmuir* **2007**, *23*, 1530.
11. Goebel, H. D.; Hoeber, J. K. H.; Gerber, C.; Leitner, A.; Haensch, T. W. *Ultramicroscopy* **1992**, *42-44*, 1260.
12. Gardner, T. J.; Frisbie, C. D.; Wrighton, M. S. *J. Am. Chem. Soc.* **1995**, *117*, 6927.
13. Stephan, O.; Carrier, M.; Le Bail, M.; Deronzier, A.; Moutet, J.-C. *J. Chem. Soc., Faraday Trans.* **1995**, *91*, 1241.
14. Sereno, L.; Silber, J. J.; Otero, L.; del Valle Bohorquez, M.; Moore, A. L.; Moore, T. A.; Gust, D. *J. Phys. Chem.* **1996**, *100*, 814.
15. Napier, M. E.; Thorp, H. H. *Langmuir* **1997**, *13*, 6342.
16. Berlin, A.; Zotti, G.; Schiavon, G.; Zecchin, S. *J. Am. Chem. Soc.* **1998**, *120*, 13453.
17. Zotti, G.; Schiavon, G.; Zecchin, S.; Berlin, A.; Pagani, G. *Langmuir* **1998**, *14*, 1728.
18. Armstrong, N. R.; Carter, C.; Donley, C.; Simmonds, A.; Lee, P.; Brumbach, M.; Kippelen, B.; Domercq, B.; Yoo, S. *Thin Solid Films* **2003**, *445*, 342.

19. Appleyard, S. F. J.; Day, S. R.; Pickford, R. D.; Willis, M. R. *J. Mater. Chem.* **2000**, *10*, 169.
20. Vercelli, B.; Zotti, G.; Schiavon, G.; Zecchin, S.; Berlin, A. *Langmuir* **2003**, *19*, 9351.
21. Zotti, G.; Zecchin, S.; Vercelli, B.; Berlin, A.; Grimoldi, S.; Groenendaal, L.; Bertoncello, R.; Natali, M. *Chem. Mater.* **2005**, *17*, 3681.
22. Koh, S. E.; McDonald, K. D.; Holt, D. H.; Dulcey, C. S.; Chaney, J. A.; Pehrsson, P. E. *Langmuir* **2006**, *22*, 6249.
23. Paniagua, S. A.; Hotchkiss, P. J.; Jones, S. C.; Marder, S. R.; Mudalige, A.; Marrikar, F. S.; Pemberton, J. E.; Armstrong, N. R. *J. Phys. Chem. C* **2008**, *112*, 7809.
24. Paramonov, P. B.; Paniagua, S. A.; Hotchkiss, P. J.; Jones, S. C.; Armstrong, N. R.; Marder, S. R.; Bredas, J.-L. *Chem. Mater.* **2008**, *20*, 5131.
25. Sharma, A.; Haldi, A.; Hotchkiss, P. J.; Marder, S. R.; Kippelen, B. *J. Appl. Phys.* **2009**, *105*, 074511/1.
26. Huang, Q.; Evmenenko, G. A.; Dutta, P.; Lee, P.; Armstrong, N. R.; Marks, T. J. *J. Am. Chem. Soc.* **2005**, *127*, 10227.
27. Veinot Jonathan, G. C.; Marks Tobin, J. *Acc. Chem. Res.* **2005**, *38*, 632.
28. Huang, Q.; Li, J.; Evmenenko, G. A.; Dutta, P.; Marks, T. J. *Chem. Mater.* **2006**, *18*, 2431.
29. Li, J.; Wang, L.; Liu, J.; Evmenenko, G.; Dutta, P.; Marks, T. J. *Langmuir* **2008**, *24*, 5755.
30. Groenendaal, L. B.; Jonas, F.; Freitag, D.; Pielartzik, H.; Reynolds, J. R. *Adv. Mater.* **2000**, *12*, 481.
31. Groenendaal, L. B.; Zotti, G.; Aubert, P.-H.; Waybright, S. M.; Reynolds, J. R. *Adv. Mater.* **2003**, *15*, 855.
32. Berlin, A.; Vercelli, B.; Zotti, G. *Polym. Rev.* **2008**, *48*, 493.
33. Doherty, W. J., III; Wysocki, R. J.; Armstrong, N. R.; Saavedra, S. S. *Macromolecules* **2006**, *39*, 4418.
34. Doherty, W. J., III; Wysocki, R. J., Jr.; Armstrong, N. R.; Saavedra, S. S. *J. Phys. Chem. B* **2006**, *110*, 4900.
35. Ratcliff, E. L.; Jenkins, J. L.; Nebesny, K.; Armstrong, N. R. *Chem. Mater.* **2008**, *20*, 5796.
36. Shallcross, R. C.; D'Ambruoso, G. D.; Korth, B. D.; Hall, H. K., Jr.; Zheng, Z.; Pyun, J.; Armstrong, N. R. *J. Am. Chem. Soc.* **2007**, *129*, 11310.
37. Shallcross, R. C.; D'Ambruoso, G. D.; Pyun, J.; Armstrong, N. R. *J. Am. Chem. Soc.* **2010**, *132*, 2622.
38. Patten, T. E.; Matyjaszewski, K. *Adv. Mater.* **1998**, *10*, 901.
39. Hawker, C. J.; Bosman, A. W.; Harth, E. *Chem. Rev.* **2001**, *101*, 3661.
40. Lacroix-Desmazes, P.; Lutz, J. F.; Chauvin, F.; Severac, R.; Boutevin, B. *Macromolecules* **2001**, *34*, 8866.
41. Hawker, C. J.; Wooley, K. L. *Science* **2005**, *309*, 1200.
42. Moad, G.; Rizzardo, E.; Thang, S. H. *Aust. J. Chem.* **2005**, *58*, 379.
43. Matyjaszewski, K.; Xia, J. *Chem. Rev.* **2001**, *101*, 2921.
44. Pyun, J.; Matyjaszewski, K. *Chem. Mater.* **2001**, *3436-3448*.

Downloaded by CORNELL UNIV on June 1, 2012 | http://pubs.acs.org
Publication Date (Web): March 20, 2012 | doi: 10.1021/bk-2012-1101.ch013

45. Pyun, J.; Kowalewski, T.; Matyjaszewski, K. *Macromol. Rapid Commun.* **2003**, *24*, 1043.
46. Snaith, H. J.; Whiting, G. L.; Sun, B.; Greenham, N. C.; Huck, W. T. S.; Friend, R. H. *Nano Lett.* **2005**, *5*, 1653.
47. Whiting, G. L.; Snaith, H. J.; Khodabakhsh, S.; Andreasen, J. W.; Breiby, D. W.; Nielsen, M. M.; Greenham, N. C.; Friend, R. H.; Huck, W. T. S. *Nano Lett.* **2006**, *6*, 573.
48. Sakakiyama, T.; Ohkita, H.; Ohoka, M.; Ito, S.; Tsujii, Y.; Fukuda, T. *Chem. Lett. FIELD Full Journal Title:Chemistry Letters* **2005**, *34*, 1366.
49. Fulghum, T. M.; Taranekar, P.; Advincula, R. C. *Macromolecules* **2008**, *41*, 5681.
50. Fulghum, T. M.; Taranekar, P.; Advincula, R. C. *Macromolecules* **2008**, *41*, 5681.
51. Grande, C. D.; Tria, M. C.; Jiang, G.; Ponnapati, R.; Advincula, R. *Macromolecules* **2011**, *44*, 966.
52. Motornov, M.; Sheparovych, R.; Katz, E.; Minko, S. *ACS Nano* **2008**, *2*, 41.
53. Motornov, M.; Tam, T. K.; Pita, M.; Tokarev, I.; Katz, E.; Minko, S. *Nanotechnology* **2009**, *20*, 434006/1.
54. Kim, B.-Y.; Ratcliff, E. L.; Armstrong, N. R.; Kowalewski, T.; Pyun, J. *Langmuir* **2010**, *26*, 2083.
55. Sakakiyama, T.; Ohkita, H.; Ohoka, M.; Ito, S.; Tsujii, Y.; Fukuda, T. *Chem. Lett.* **2005**, *34*, 1366.
56. Paniagua, S. A.; Hotchkiss, P. J.; Jones, S. C.; Marder, S. R.; Mudalige, A.; Marrikar, F. S.; Pemberton, J. E.; Armstrong, N. R. *J. Phys. Chem. C* **2008**, *112*, 7809.
57. Schulmeyer, T.; Paniagua, S. A.; Veneman, P. A.; Jones, S. C.; Hotchkiss, P. J.; Mudalige, A.; Pemberton, J. E.; Marder, S. R.; Armstrong, N. R. *J. Mater. Chem.* **2007**, *17*, 4563.

Downloaded by CORNELL UNIV on June 1, 2012 | http://pubs.acs.org
Publication Date (Web): March 20, 2012 | doi: 10.1021/bk-2012-1101.ch013

Chapter 14

Surface-Functionalized and Surface-Functionalizable Poly(vinylidene fluoride) Membranes via Controlled/Living Radical Polymerization and Click Chemistry

Downloaded by CORNELL UNIV on May 31, 2012 | http://pubs.acs.org
Publication Date (Web): March 20, 2012 | doi: 10.1021/bk-2012-1101.ch014

Tao Cai,[a] Koon-Gee Neoh,[a,b] and En-Tang Kang*,[a,b]

**[a]NUS Graduate School for Integrative Science and Engineering,
National University of Singapore, Kent Ridge, Singapore 117576
[b]Department of Chemical & Biomolecular Engineering,
National University of Singapore, Kent Ridge, Singapore 119260
*Tel.: +65-65162189. Fax: +65-67791936.
E-mail address: cheket@nus.edu.sg.**

Preparation of multifunctional and well-structured polymer substrates (membranes) requires a selection of the most suitable controlled/living radical polymerization (CRP) techniques in combination with appropriate click reactions. This article describes some recent research activities on poly(vinylidene fluoride) (PVDF) copolymer membranes. The synthesis strategies of PVDF membranes with functionalized and functionalizable surfaces via CRP techniques and click chemistry are described in detail. The robust and versatile CRP techniques and click chemistry have allowed the design and production of copolymers of well-defined architectures, such as telechelic, block and graft copolymers, via the "grafting from" and "grafting to" approaches. These technologies are particularly suited for the preparation of functional polymer membranes with stimuli-responsive, antifouling, antimicrobial and ion exchange surface properties. The combination of CRP techniques and click chemistry can be regarded as a revolutionary approach to the preparation of a new generation of precisely tailored specialty PVDF and related copolymer membranes.

In Progress in Controlled Radical Polymerization: Materials and Applications; Matyjaszewski, K., et al.;
ACS Symposium Series; American Chemical Society: Washington, DC, 2012.

Keywords: Poly(vinylidene fluoride); Block/Graft Copolymers; Controlled/Living Radical Polymerization; Click Chemistry; Microporous Membranes

Introduction

Downloaded by CORNELL UNIV on May 31, 2012 | http://pubs.acs.org
Publication Date (Web): March 20, 2012 | doi: 10.1021/bk-2012-1101.ch014

Poly(vinylidene fluoride) (PVDF) is a polymer of technological importance because of its excellent chemical resistance, good mechanical properties, good thermal stability, and unique ferroelectric, piezoelectric and dielectric properties (*1–3*). PVDF membranes have found applications in ultrafiltration, microfiltration, waste water treatment, protein adsorption and separation, proton conduction, stimuli-responsive and controlled deliveries, and biotechnology (*2–5*). However, the practical applications of PVDF membranes are limited to some extent by their hydrophobic and inert surface properties. Thus, the ability to manipulate and control the surface properties of PVDF membranes is of crucial importance. Among the various modification techniques, graft copolymerization has often been used to enhance the surface and bulk functionalities of the polymer. For examples, graft copolymerization of PVDF with functional monomers, such as 4-vinylpyridine (4VP), *N*-isopropylacrylamide (NIPAM), acrylic acid (AAc) and *N*,*N*′-dimethyl-(methylmethacryloyl ethyl) ammonium propanesulfonate (DMAPS) has been carried out (*6–10*). The grafted side chains can, in turn, be used to control the surface composition, morphology and pore-size distribution of the PVDF membrane during membrane casting by phase inversion, as well as to impart unique properties onto the resulting membranes.

Polymer substrates (membranes) can be functionalized via two main approaches, viz., (A) the "grafting from" and (B) the "grafting to" approaches (*11*) (Scheme 1). In the "grafting from" approach, polymerization is directly initiated from initiator-functionalized surfaces. Controlled/living radical polymerization (CRP) techniques are particularly attractive for the preparation of polymer brushes via the "grafting from" approach, as they allow control over brush thickness, chain length, composition and architecture. However, specific functional groups might have dominant effects on the polymerization rate, polydispersity index (PDI) and composition of graft chains. The most popular CRP techniques to date include atom transfer radical polymerization (ATRP), reversible addition-fragmentation chain transfer (RAFT) polymerization, nitroxide-medicated radical polymerization (NMP) and iodine transfer polymerization (ITP) (Scheme 2) (*12–21*). Each of these techniques requires the use of a selected metal/ligand complex, chain transfer agent (CTA) and nitroxide mediator, respectively, to gain control over the polymerization of various functional monomers.

Downloaded by CORNELL UNIV on May 31, 2012 | http://pubs.acs.org
Publication Date (Web): March 20, 2012 | doi: 10.1021/bk-2012-1101.ch014

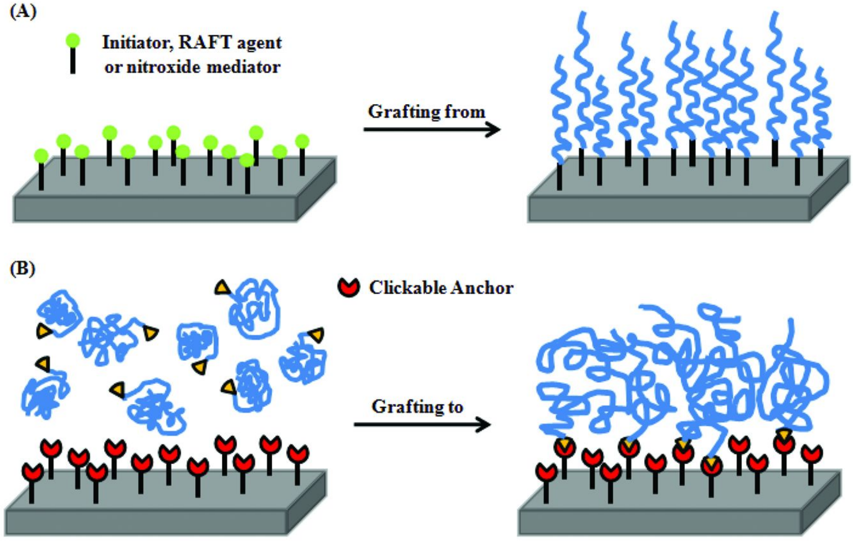

Scheme 1. Functionalization of polymer substrates (membranes) via (A) surface-initiated controlled/living radical polymerization (CRP) ("grafting from" approach) and (B) surface click reactions ("grafting to" approach). [Reprint with permission from Ref. (11), Copyright 2009 American Chemical Society.]

On the other hand, the "grafting to" approach involves the attachment of prefabricated polymer chains via covalent bonding (*11*) (Scheme 1). Although experimentally straightforward, the "grafting to" approach via conventional coupling reactions suffers from steric and reactivity limitations at the surface, making it difficult to produce homogeneous and dense polymer brushes. With increasing polymer molecular weight, the reaction between the polymer end-group and the complementary site on the substrate surface becomes less efficient. Fortunately, differing from the conventional surface coupling reactions, the Cu-catalyzed alkyne-azide click reaction (Scheme 3), introduced by Sharpless *et al* (*22–27*), holds the advantage of being modular in nature, allowing precise control over the chain length and composition of the coupled polymers prepared a priori by the CPR techniques. In addition, the ease of synthesis of alkyne and azide functionalities on polymer chains and substrates allows the direct and controlled construction of polymer substrates (membranes) via one-step surface-initiated "click" ("grafting to") reactions.

In Progress in Controlled Radical Polymerization: Materials and Applications; Matyjaszewski, K., et al.;
ACS Symposium Series; American Chemical Society: Washington, DC, 2012.

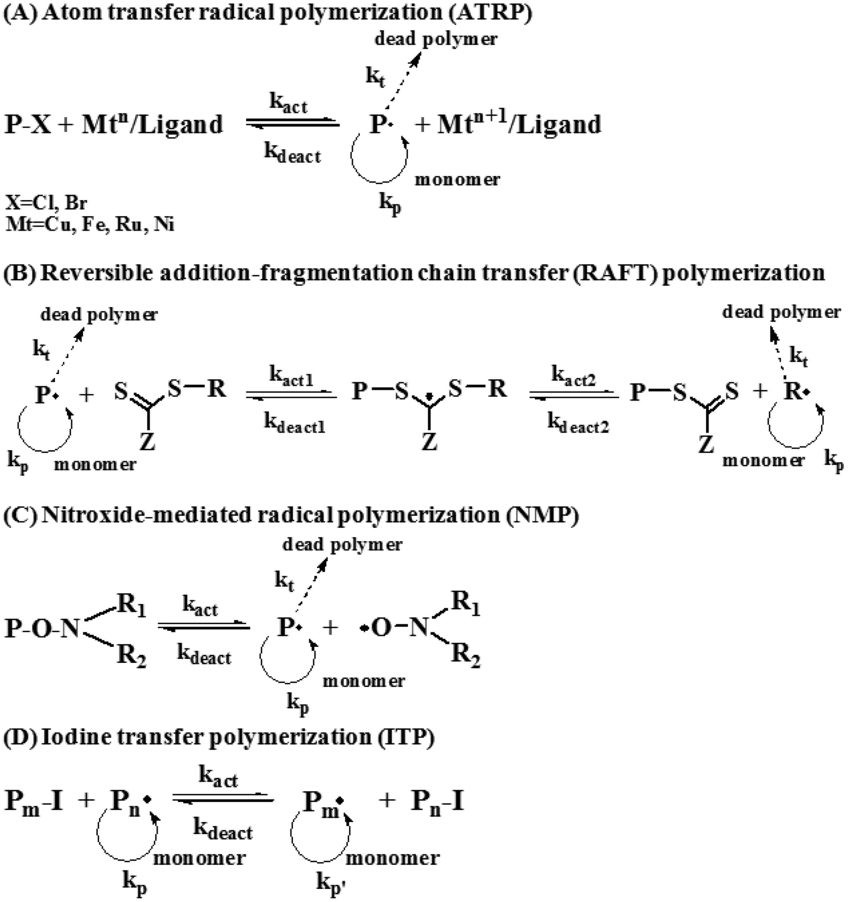
(A) Atom transfer radical polymerization (ATRP)
dead polymer
k_t
P-X + Mt^n/Ligand
k_act
k_deact
P· + Mt^{n+1}/Ligand
monomer
k_p
X=Cl, Br
Mt=Cu, Fe, Ru, Ni
(B) Reversible addition-fragmentation chain transfer (RAFT) polymerization
dead polymer
k_t
P· + S=C(Z)S−R
k_act1
k_deact1
P−S−C·(Z)−S−R
k_act2
k_deact2
P−S−C(Z)=S + R·
monomer
k_p
(C) Nitroxide-mediated radical polymerization (NMP)
dead polymer
k_t
P-O-N(R_1)(R_2)
k_act
k_deact
P· + ·O−N(R_1)(R_2)
monomer
k_p
(D) Iodine transfer polymerization (ITP)
P_m-I + P_n·
k_act
k_deact
P_m· + P_n-I
monomer
k_p
monomer
k_p'

Scheme 2. General schemes of ATRP, RAFT polymerization, NMP and ITP processes.

Several other highly efficient coupling reactions have been reported to be of ‘click’ in nature since they fulfilled all or some of the click chemistry criteria. Several types of metal-free click reactions have been developed. The more prominent ones are thiol-ene, thiol-yne, thiol-*para*-fluoro and Diels-Alder coupling reactions, and pyridyl disulfide exchange reactions (Scheme 3) (*28–30*). Each of them requires specific initiators, monomers, and/or polymerization conditions. Therefore, the synthetic route should be carefully designed to prepare the desired functional polymers or solid substrates.

The aim of this article is to provide an insight into the selection of the suitable CRP techniques and click reactions for the synthesis of PVDF microporous membranes with tailored pore and surface functionalities and morphology. The highly robust and versatile CRP techniques and click chemistry are particularly suited for the preparation of functional membranes with stimuli-responsive, antifouling, antimicrobial and ion exchange properties (*31–36*), as well as membranes with functionalizable surfaces, including pore surfaces.

Downloaded by CORNELL UNIV on May 31, 2012 | http://pubs.acs.org
Publication Date (Web): March 20, 2012 | doi: 10.1021/bk-2012-1101.ch014

Downloaded by CORNELL UNIV on May 31, 2012 | http://pubs.acs.org
Publication Date (Web): March 20, 2012 | doi: 10.1021/bk-2012-1101.ch014

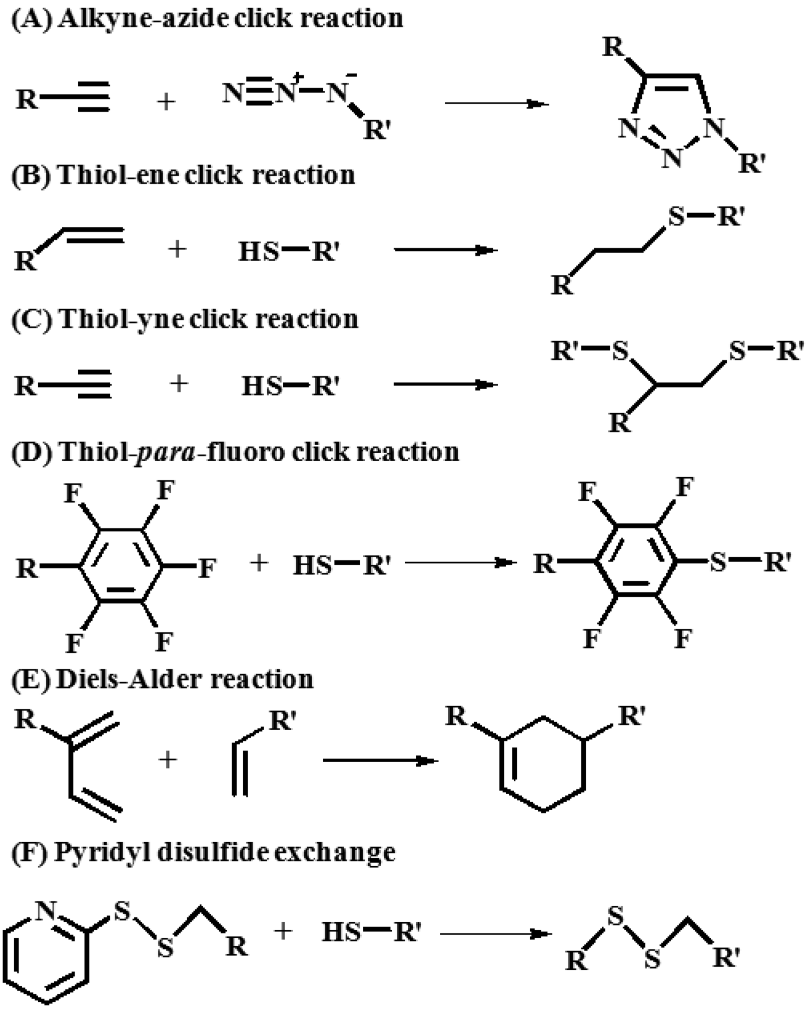
(A) Alkyne-azide click reaction
(B) Thiol-ene click reaction
(C) Thiol-yne click reaction
(D) Thiol-para-fluoro click reaction
(E) Diels-Alder reaction
(F) Pyridyl disulfide exchange
R
R'
HS—R'
N
S
F
+

Scheme 3. Schematic representation of the click reactions that have been used in combination with controlled/living radical polymerization (CRP) techniques.

Functionalization of PVDF Membrane via ATRP

ATRP has been employed to design and synthesis PVDF-based copolymers. For the ATRP process (Scheme 2), the cleavage of the carbon-halogen bond generates a free and active carbon-centered radical species at the polymer chain end. In addition to control over the molecular architecture of brushes, polymers prepared by ATRP have a dormant chain end which can be re-activated for another round of ATRP. In the functionalization of PVDF membranes via ATRP, vinylbenzyl chloride (VBC) was first graft copolymerized on the PVDF membrane surface via electron beam pre-irradiation (*37*). Subsequent ATRP of styrene

Downloaded by CORNELL UNIV on May 31, 2012 | http://pubs.acs.org
Publication Date (Web): March 20, 2012 | doi: 10.1021/bk-2012-1101.ch014

was initiated from the benzyl chloride groups on the PVDF membrane surfaces. In another study, free-radical initiated graft copolymerization of an inimer, 2-(2-bromoisobutyryloxy)ethyl acrylate (BIEA), from the ozone-pretreated PVDF in solution was carried out to produce the PVDF-*g*-PBIEA graft copolymers (*38*). Ozone pretreatment of polymers introduces certain polar groups, such as carbonyl, ketone and/or peroxide/hydroxyl peroxide groups. The peroxides are used to initiate the subsequent graft copolymerization. In general, the amount of peroxides introduced by ozone treatment can be regulated by the treatment temperature, ozone concentration and exposure time. The half-life of peroxides on the ozone-pretreated PVDF was estimated to be about 45 min at 60 °C. Thus, the thermally-induced graft copolymerizaiton time of 6 h employed in most of the studies reported should be sufficient for the complete consumption of the peroxides on the PVDF chains (*39*). Microporous membranes were fabricated from the copolymer solution by phase inversion in an aqueous medium. The tertiary C-Br groups of BIEA polymer (PBIEA) side chains allowed the initiation of ATRP of functional monomers from the copolymer or from the copolymer membrane surface. An arborescent graft copolymer was prepared via ATRP of sodium salt of 4-styrenesulfonate (NaSS) from the PVDF-*g*-PBIEA copolymer side chains (PVDF-*g*-P(BIEA-*g*-PNaSS) copolymer) (*38*). In comparison to the copolymer membrane cast in water by phase inversion, the PVDF-*g*-P(BIEA-*g*-PNaSS) copolymer membrane cast in aqueous NaCl solution have enriched PNaSS polyelectrolyte side chains on the membrane and pore surfaces and larger pore size, arising from electrostatic interactions between the PNaSS side chains and the electrolyte medium (*38*). The PVDF-*g*-P(BIEA-*g*-PPEGMA) membrane was also prepared via surface-initiated ATRP of poly(ethylene glycol) methacrylate (PEGMA) from the PVDF-*g*-PBIEA microporous membrane. Protein adsorption studies indicated that the PVDF-*g*-P(BIEA-*g*-PPEGMA) membrane exhibited substantially improved antifouling properties. These hydrophilic polymer brushes can form highly hydrated ultrathin coatings that provide an effective enthalpic and entropic barrier to non-specific protein adsorption, and impart the membrane surface with antifouling property (*38*). Thus, the PVDF-*g*-PBIEA copolymer membrane with the active ATRP inimer repeat units on the surface provides a functionalizable platform for surface molecular design.

As a simple one-step process for ATRP, direct initiation from the vinylidene fluoride (VDF) units in PVDF has also been carried out, although the reaction suffers from low initiation efficiency and requires high reaction temperature. ATRP of styrene, PEGMA, NaSS, poly(oxyethylene methacrylate) (POEM), butyl methacrylate (BMA) and 2-vinylpyridine (2VP) initiated directly from the secondary -CF_2- groups of PVDF main chains have been reported (*40–52*). PVDF with poly[2-(*N*,*N*-dimethylamino)ethyl methacrylate] (PDMAEMA) side chains were synthesized via vinylidene fluoride-initiated ATRP of 2-(*N*,*N*-dimethylamino)ethyl methacrylate (DMAEMA) (*53*). The PVDF-*g*-PDMAEMA copolymer has a highly hydrophobic PVDF main chain and hydrophilic PDMAEMA side chains, and can be cast into multi-stimuli responsive microporous membranes with surface-enriched "living" PDMAEMA graft chains. The key factors that influence membrane formation by phase inversion include the choice of solvent/non-solvent system, the composition of

In Progress in Controlled Radical Polymerization: Materials and Applications; Matyjaszewski, K., et al.;
ACS Symposium Series; American Chemical Society: Washington, DC, 2012.

Downloaded by CORNELL UNIV on May 31, 2012 | http://pubs.acs.org
Publication Date (Web): March 20, 2012 | doi: 10.1021/bk-2012-1101.ch014

the polymer solution, the composition of the coagulation bath and membrane casting conditions (*54*). The plausible process for the formation of uniform pores of PVDF-*g*-PDMAEMA microporous membrane is shown in Scheme 4. Since the hydrophobic PVDF main chains and the hydrophilic PDMAEMA side chains have good solubility in *N*-methyl-2-pyrrolidone (NMP) solution, the amphiphilic copolymer molecules remain well extended. During the process of phase inversion in an aqueous medium, the outflow of the solvent and the inflow of the nonsolvent resulted in the precipitation of hydrophobic PVDF main chains from the aqueous medium, while retaining the hydrophilic PDMAEMA side chains in the aqueous medium. Removal of the water molecules trapped within the hydrodynamic volume of the hydrophilic PDMAEMA chains produced the microporous structure. Thus the pore morphology depends on the composition, such as density and chain length, of the grafted PDMAEMA chains (*53*).

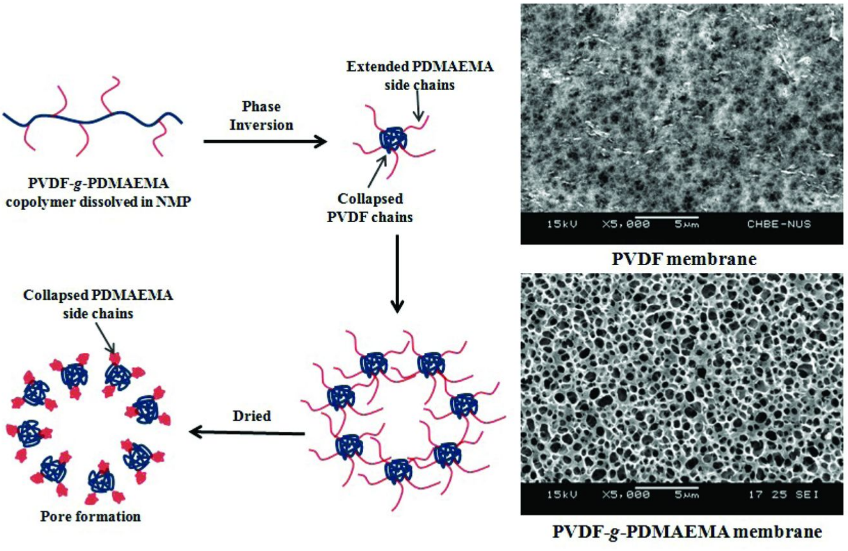
Extended PDMAEMA side chains
Phase Inversion
PVDF-g-PDMAEMA copolymer dissolved in NMP
Collapsed PVDF chains
Collapsed PDMAEMA side chains
Dried
Pore formation
15kU X5,000 5µm CHBE-NUS
PVDF membrane
15kU X5,000 5µm 17 25 SEI
PVDF-g-PDMAEMA membrane

Scheme 4. Schematic illustration of the formation of a porous membrane from the PVDF-g-PDMAEMA copolymer. [Reprint with permission from Ref. (53), Copyright 2008 American Chemical Society.]

The dimethylamine groups of PDMAEMA side chains are acid swellable. In an acidic environment, the dimethylamine groups are protonated, giving rise to internal charge repulsions among the graft chains and expansion in the overall dimensions of the graft chains. At higher pH values, reduced protonation and charge repulsion of the PDMAEMA graft chains resulted in a reduction in the overall hydrodynamic volume of the graft chains. Thus, the pH of aqueous media for phase inversion can be used to adjust the pore morphology of the PVDF-*g*-PDMAEMA membranes. In addition, the flux of aqueous solution through the PVDF-*g*-PDMAEMA membranes showed an abrupt change with the permeate temperature between 45 and 55 °C and pH between 6 and 8 (*51*). The hydrophilic nature and the quaternized ammonium groups of the PDMAEMA side chains also impart good antifouling and antibacterial properties, respectively, to the PVDF-*g*-PDMAEMA membranes. Furthermore, the dormant PDMAEMA chain ends can be reactivated for the consecutive surface-initiated ATRP of 2-naphthyl methacrylate (2NM) to produce the fluorescent PDMAEMA-*b*-P2NM diblock copolymer brushes on the PVDF membrane (*53*). PVDF-*g*-PDMAEMA graft copolymers of increasing PDMAEMA graft density with increasing polymerization time have also been observed in the ATRP of DMAEMA initiated by the -CF_2- groups of PVDF chains (Figure 1) (*55*). The ^{1}H NMR and ^{19}F NMR spectroscopy results provided direct evidence to the cleavage of C-F bond and grafting of DMAEMA monomer from the secondary -CF_2- groups of PVDF main chains (*55*).

Downloaded by CORNELL UNIV on May 31, 2012 | http://pubs.acs.org
Publication Date (Web): March 20, 2012 | doi: 10.1021/bk-2012-1101.ch014

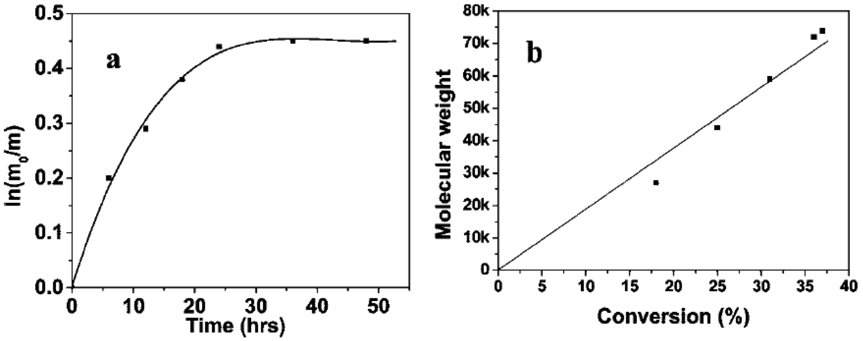

Figure 1. (a) Plot of monomer conversion (In m_0/m) against time (h) and (b) plot of molecular weight of grafted chain vs monomer conversion. [Reprint with permission from Ref. (55), Copyright 2009 American Chemical Society.]

Another ATRP technique using activators generated by electron transfer (AGET-ATRP), with the combined advantages of normal ATRP and reversed ATRP, has also been developed (*56*)–(*60*). The AGET-ATRP technique has been successfully applied to modify different substrates. In view of the inherent good biocompatibility and low toxicity of iron salts, as well as the advantages of AGET-ATRP, ATRP of methyl methacrylate (MMA) and PEGMA using activators generated by electron transfer directly from the secondary fluorine atoms on the PVDF backbone has been carried out in the presence of a limited amount of air, using $FeCl_3 \cdot 6H_2O$ as the catalyst, triphenylphosphine (PPh_3) as the ligand and L-ascorbic acid as the reducing agent (*61*). The PVDF-*g*-PPEGMA copolymers can be cast into hydrophilic microporous membranes by phase inversion in an aqueous medium. The PVDF-*g*-PPEGMA membranes displayed substantial resistance to bovine serum albumin (BSA) fouling, in comparison to the pristine hydrophobic PVDF membranes.

Downloaded by CORNELL UNIV on May 31, 2012 | http://pubs.acs.org
Publication Date (Web): March 20, 2012 | doi: 10.1021/bk-2012-1101.ch014

Functionalization of PVDF Membrane via RAFT Polymerization

In general, graft copolymerization via the conventional free-radical process usually leads to the uncontrolled size distribution of the graft chains. One of the distinct advantages of reversible addition-fragmentation chain transfer (RAFT) polymerization lies in its relative simplicity and versatility, since conventional free-radical polymerization can be readily converted into a RAFT-mediated process by the addition of an appropriate chain transfer agent (CTA), while retaining other reaction parameters. Graft copolymerization by the RAFT-mediated process can also be expected to produce well-defined side chains, which, in turn, can be expected to improve the uniformity in pore size distribution of the graft copolymer membrane during the phase inversion process. Preparation of graft copolymers via RAFT-mediated graft polymerization of PEGMA from peroxides on the ozone-pretreated PVDF has been carried out (*62*). The "living" character of the grafted PEGMA side chains was ascertained in the subsequent block copolymerization of styrene. Microporous membranes were fabricated from the PVDF-*g*-PPEGMA comb copolymers by phase inversion in an aqueous medium. Surface composition analysis of the membrane by X-ray photoelectron spectroscopy (XPS) revealed substantial surface enrichment of the PPEGMA graft chains. The pore size distribution of the resulting membranes was found to be much more uniform than that of the membranes prepared from the corresponding process without CTA. The pore size and distribution varied with the graft concentration and the density of graft points. The PVDF-*g*-PPEGMA membranes displayed substantial resistance to γ-globulin fouling, in comparison to the pristine hydrophobic PVDF membranes.

The RAFT-mediated graft copolymer approach to membrane fabrication and the resulting membrane with "living" graft chain ends on the surfaces (including pore surfaces) will allow further functionalization of the membranes via surface-initiated RAFT block copolymerization with a broad range of functional monomers. PVDF with CTA-terminated poly(acrylic acid) (PAAc) side chains (PVDF-*g*-PAAc) was initially prepared by RAFT-mediated graft copolymerization of acrylic acid (AAc) from the ozone-pretreated PVDF (*63*). The copolymer was cast into pH-sensitive microporous membranes with enriched "living" PAAc graft chains on the surface (including the pore surfaces) by phase inversion in an aqueous medium. The pore size distribution of the membranes was found to be much more uniform than that of the corresponding membranes cast from PVDF-*g*-PAAc copolymers prepared by the conventional free-radical graft copolymerization process. The microporous membranes with surface-tethered PAAc macro chain transfer agents allow the introduction of additional functionalities. The "living" membrane and pore surfaces can be further functionalized via surface-initiated block copolymerization with *N*-isopropylacrylamide (NIPAM) to obtain the pH- and temperature-responsive PVDF-*g*-PAAc-*b*-PNIPAM membranes in the presence of a radical initiator, 2,2′-azobis(2-methyl-propionitrile) (AIBN). Aqueous solutions of PNIPAM exhibit a reversible liquid-solid phase transition with a lower critical solution temperature (LCST) around 32 °C (*64*). The pK_a value of PAAc polymer is about 4.2. The flux of aqueous solutions through the PVDF-*g*-PAAc-*b*-PNIPAM membranes exhibited an increase in permeation rate in respond to the increase in permeate temperature. The temperature-dependent permeation rate was caused by the change in conformation (hydrophobic association) of the grafted PNIPAM chains on the membrane and pore surfaces. The change in permeation rate of the PVDF-*g*-PAAc-*b*-PNIPAM membranes in respond to change in pH was attributed to the change in extent of protonation of the grafted PAAc side chains. The molecular design technique thus provides an alternative approach to the preparation of multi-stimuli responsive membranes of well-defined surface structures.

Downloaded by CORNELL UNIV on May 31, 2012 | http://pubs.acs.org
Publication Date (Web): March 20, 2012 | doi: 10.1021/bk-2012-1101.ch014

Functionalization of PVDF Membranes via Combination of Controlled/Living Radical Polymerization and Click Chemistry

Although CRP techniques are characterized by a relatively high functional group tolerance, there are still a number of functional groups, such as carboxylic and amine groups, that cannot be introduced into polymer brushes via direct surface-initiated ATRP of the corresponding monomer due to the interaction of these functional groups with the metal catalyst. Such sensitive functional groups may be introduced by post-modification of precursor polymer brushes, which contain appropriate reactive groups, such as alkyne or azide groups, that are compatible with surface-initiated CRP techniques. Click reactions offer access to a multitude of complex and sophisticated polymeric architectures. This approach owes its great success to the availability of different CRP techniques which allow the introduction and transformation of specific end functional groups. Several nearly perfect combinations of polymerization techniques and clickable functionalities have evolved, providing α and/or ω-functionalized polymer backbones ideally suited for efficient and controlled coupling reactions. The halogen end groups resulting from the ATRP process react readily with sodium azide to produce the azide functionalities, which are directly applicable to the Cu-catalyzed alkyne-azide click reaction. The necessary alkyne moieties are usually obtained by using functional initiators bearing protected or unprotected terminal alkynes. The reaction conditions of ATRP and alkyne-azide click reaction are remarkable similar in terms of the catalysts and ligands used, enabling the development of one-pot synthesis approach. The combination of ATRP and alkyne-azide click reaction is thus a highly versatile synthetic strategy for obtaining complex polymeric architectures (*32–35*). The use of functionalized initiators is of course also applicable to other polymerization techniques, such as RAFT polymerization, NMP or ring-opening polymerization (ROP).

The ring-opening reaction of epoxides by nucleophiles is an efficient means for introducing click functionality into polymers (*64*). In order to introduce the azide groups on the PVDF polymer backbone for the subsequent click conjugation of functional polymer brushes, PVDF with azide-functionalized poly(glycidyl methacrylate) (PGMA) side chains (PVDF-*g*-P[GMA-(N_3)(OH)]) were synthesized via free radical-initiated graft copolymerization of glycidyl methacrylate (GMA) from ozone-pretreated

PVDF backbone, followed by reaction of the oxirane rings in the GMA side chains of the PVDF-*g*-PGMA copolymer with sodium azide (*65*). Poly(*N*-isopropylacrylamide) (PNIPAM) polymer brushes obtained from conventional radical polymerizations is often polydispersed with a broad LCST range. Preparation of linear narrow-disperse PNIPAM by ATRP is especially attractive as it can provide good control over both the molecular weight and end functionality of the polymer. In this work, alkyne-terminated PNIPAM was used for the click reaction with the azido-containing PGMA side chains of the PVDF-*g*-P[GMA-(N_3)(OH)] copolymer to generate the thermoresponsive PVDF-*g*-P[GMA-*click*-PNIPAM] copolymer. Both the PVDF-*g*-P[GMA-(N_3)(OH)] and PVDF-*g*-P[GMA-*click*-PNIPAM] copolymers can be readily cast into microporous membranes by phase inversion in an aqueous medium. The surface composition and morphology of the PVDF-*g*-P[GMA-*click*-PNIPAM] membranes can be adjusted by the temperature of casting medium. The PVDF-*g*-P[GMA-(N_3)(OH)] microporous membranes with azide-containing surfaces can thus be further functionalized via surface-initiated click grafting of alkyne-terminated PNIPAM of controlled chain lengths to obtain the PVDF-*g*-P[GMA-*click*-PNIPAM]$_{\text{surface}}$ membranes. Both types of the PNIPAM grafted membranes exhibited a reversible temperature-dependent flux, with flux variation of over an order of magnitude, as the permeate temperature was varied between 10 to 60 °C. The grafted chains acted as temperature-sensitive chemical valves in regulating the flux of aqueous solutions (*66*).

However, the necessity to use the copper catalyst in ATRP and alkyne-azide click reaction and the sensitivity of the reactions to air have limited their application under, for example, physiological conditions. Several other organic coupling reactions have been examined for their applications in polymer chemistry. Most of these reactions can be conducted in the absence of a metal catalyst and under relatively mild conditions. In particular, the thiol-ene click reaction has been of interest because of the availability of wide range of thiols and alkenes. The thiol-ene click reaction can proceed via two routes: the anti-Markovnikov radical addition and the base-catalyzed Michael addition. Thiol terminated polymers can be easily obtained by RAFT polymerization of a wide range of monomers and the subsequent reduction of the dithioester chain transfer agent to obtain the thiol groups. Alternatively, disulfide containing bifunctional ATRP initiators can be used for the preparation of thiol functionalized polymers (*32–35*). The design of polymer structures and properties in a controlled and predictable way demand mild and highly efficient coupling techniques.

The strategies discussed above can be easily extended to the preparation of PVDF membrane with "clickable" anchors. A facile synthetic approach to the preparation of PVDF-*g*-PAMA copolymers that contain well preserved allyl functionalities involved thermally-induced radical graft copolymerization of allyl methacrylate (AMA) from ozone-preactivated PVDF chains in dilute NMP solutions (*67*). Cross-linking reactions were largely prevented due to the low concentration of pendant allylic double bonds in the reaction mixture. Microporous membranes were fabricated from the PVDF-*g*-PAMA copolymers by phase inversion in an aqueous medium. The allowance of either thermal or

Downloaded by CORNELL UNIV on May 31, 2012 | http://pubs.acs.org
Publication Date (Web): March 20, 2012 | doi: 10.1021/bk-2012-1101.ch014

photochemical radical initiators is another important feature of the metal-free thiol-ene coupling reaction. To demonstrate the compatibility and efficiency of the thiol-ene reaction with different functional groups, 3-mercaptopropionic acid (MPA) was selected to incorporate carboxylic groups onto the PVDF-*g*-PAMA membrane via thermally-initiated thiol-ene click reaction. Due to pH-induced conformational transition of the P[AMA-*comb*-MPA] side chains, the permeability of aqueous solutions through the PVDF-*g*-P[AMA-*comb*-MPA] membranes displayed pronounced pH dependence. The flux increased with a decrease in pH of the permeate and vice versa. Another example is the preparation of antibacterial PVDF-*g*-P[AMA-*comb*-DMAPS] membranes. The process involved (i) click grafting of 1,6-hexanedithiol (HDT) onto the PVDF-*g*-PAMA membranes to produce PVDF-*g*-P[AMA-*comb*-HDT] membrane via UV-initiated thiol-ene click reaction, using 2,2-dimethoxy-2-phenylacetophenone (DMPA) as the photoinitiator, (ii) immobilization of the zwitterionic molecules, *N*,*N'*-dimethyl-(methylmethacryloyl ethyl) ammonium propanesulfonate (DMAPS) onto the PVDF-*g*-P[AMA-$_{\text{comb}}$-HDT] membrane to produce PVDF-*g*-P[AMA-$_{\text{comb}}$-DMAPS] membrane via thiol-Michael addition reaction. In comparison to the pristine hydrophobic PVDF membrane, a significant reduction in microbial adhesion was observed on the PVDF-*g*-P[AMA-*comb*-DMAPS] membrane in the presence of quaternary ammonium groups of the DMAPS molecules on the surfaces under continuous-flow conditions. Thus, the click strategy allows immobilization of a wide range of functional moieties onto the polymeric membranes.

Incorporation of alkyne groups on polymer surfaces is attractive because of good compatibility of alkyne groups with common addition reaction conditions. The surface alkyne moieties also provide a direct route to a diverse array of functional surfaces via the simple surface alkyne-azide click reaction or thiol-yne click reaction without the need for group-protecting chemistry. Comb-shaped polymer brushes can be prepared by first growing a polymer brush that contains clickable anchors in the side chains, followed by introduction of the side chains via click reactions. To illustrate this point, PVDF-*g*-PPMA copolymers bearing pendant propargyl groups were prepared by thermally-induced radical graft copolymerization of propargyl methacrylate (PMA) from the ozone-pretreated PVDF backbones. Microporous membranes were fabricated from the PVDF-*g*-PPMA copolymers by phase inversion in an aqueous medium (*68*). The PVDF-*g*-P[PMA-*click*-MPS] membranes were prepared via thiol-yne click reaction of 3-mercapto-1-propanesulfonic acid sodium salt (MPS) on the microporous PVDF-*g*-PPMA membranes. Due to the anti-polyelectrolyte effect, the permeability of aqueous solutions through the PVDF-*g*-P[PMA-*click*-MPS] membranes exhibited a dependence on the ionic strength, and the flow rate was observed to decrease as the ionic strength of permeate was increased. A series of commercially available thiols (Scheme 5), including 3-mercaptopropioic acid (MPA), mercaptosuccinic acid (MSA) and 2-mercaptoethylamine (MEA) were selected in order to investigate the efficiency and orthogonality of UV-initiated thiol-yne click coupling reactions and to impart the pH-responsive properties into the resulting membranes.

Downloaded by CORNELL UNIV on May 31, 2012 | http://pubs.acs.org
Publication Date (Web): March 20, 2012 | doi: 10.1021/bk-2012-1101.ch014

Downloaded by CORNELL UNIV on May 31, 2012 | http://pubs.acs.org
Publication Date (Web): March 20, 2012 | doi: 10.1021/bk-2012-1101.ch014

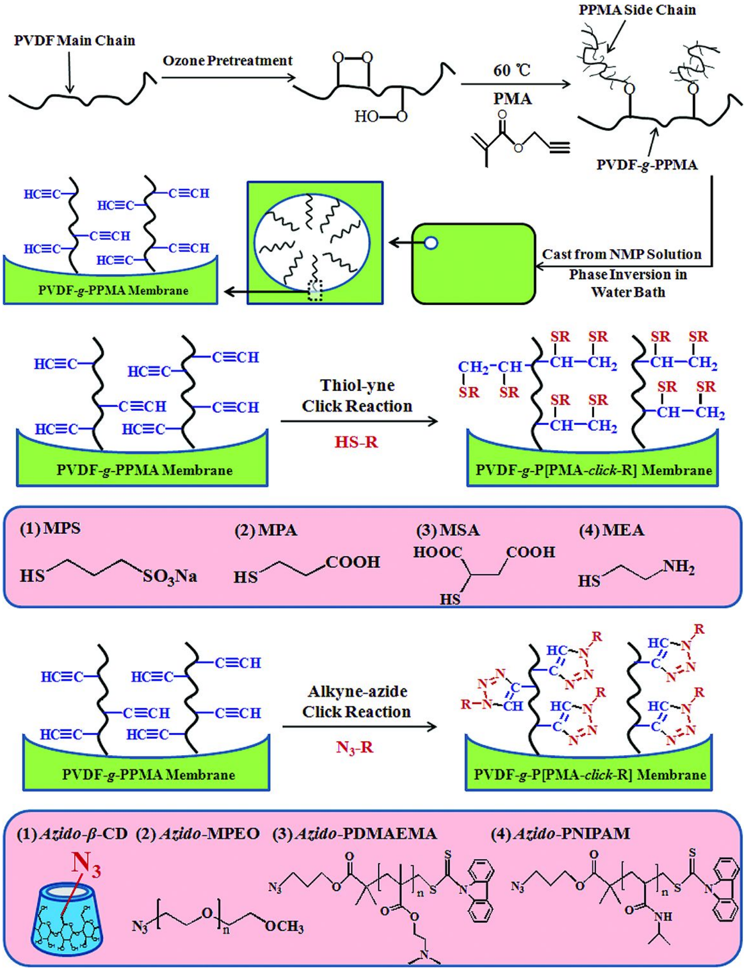
PVDF Main Chain
Ozone Pretreatment
HO—O
60 ℃
PMA
PPMA Side Chain
PVDF-g-PPMA
Cast from NMP Solution
Phase Inversion in Water Bath
PVDF-g-PPMA Membrane
HC≡C
C≡CH
Thiol-yne Click Reaction
HS-R
SR
CH₂—CH
CH—CH₂
PVDF-g-P[PMA-click-R] Membrane
(1) MPS
HS
SO₃Na
(2) MPA
COOH
(3) MSA
HOOC
COOH
HS
(4) MEA
NH₂
Alkyne-azide Click Reaction
N₃-R
R—N
HC
N
R
(1) Azido-β-CD
N₃
(2) Azido-MPEO
OCH₃
n
(3) Azido-PDMAEMA
O
S
N
(4) Azido-PNIPAM
NH

Scheme 5. Schemtic illustration of the process of ozone pretreatment, graft copolymerization of PVDF with PMA, preparation of PVDF-g-PPMA membrane with "clickable" surface by phase inversion, preparation of functional PVDF-g-P[PMA-click-R] membranes via surface thiol-yne click reaction of thiols on the PVDF-g-PPMA membrane and preparation of PVDF-g-P[PMA-click-R] membranes via surface alkyne-azide click reaction on the PVDF-g-PPMA membranes. [PVDF = poly(vinylidene fluoride); PMA = propargyl methacrylate; MPS = 3-mercapto-1-propanesulfonic acid sodium salt; MPA = 3-mercaptopropionic acid; MSA = mercaptosuccinic acid; MEA = 2-mercaptoethylamine; azido-β-CD = mono(6-azido-6-desoxy)-β-cyclodextrin; azido-MPEO = azido-poly(ethylene oxide) monoethyl ether; azido-PDMAEMA = azido-poly[2-(N,N-dimethylamino)ethyl methacrylate]; azido-PNIPAM = azido-poly(N-isopropylacrylamide)]. [Reprint with permission from Ref. (68), Copyright 2011 American Chemical Society.]

Downloaded by CORNELL UNIV on May 31, 2012 | http://pubs.acs.org
Publication Date (Web): March 20, 2012 | doi: 10.1021/bk-2012-1101.ch014

On the other hand, *β*-cyclodextrin (*β*-CD) macromolecules were covalently attached on the membranes (PVDF-*g*-P[PMA-*click*-*β*-CD] membrane) via surface-initiated alkyne-azide click reaction of mono(6-azido-6-desoxy)-*β*-cyclodextrin (*azido*-*β*-CD) on the PVDF-*g*-PPMA membranes (*69*). Then, poly(ethylene oxide) polymers (PEO) bearing both end capped adamantine groups (AD) were immobilized onto the membrane surface through the host-guest inclusion complexation between *β*-CD and AD (*70*). The hydrophilicity of PEO polymers, in turn, imparts the resulting PVDF-*g*-P[PMA-*click*-*β*-CD-*guest*-PEO] membrane with enhanced fouling resistance to protein permeates. Due to good efficiency of the alkyne-azide click reaction, polymers bearing pendant azide moieties can be tailored for a wide-range of applications, as shown in Scheme 5. Thus, surface click grafting of *azido*-poly(ethylene oxide) monomethyl ether (*azido*-MPEO), azido-poly[2-(*N*,*N*-dimethylamino)ethyl methacrylate] (*azido*-PDMAEMA) and *azido*-poly(*N*-isopropylacrylamide) (*azido*-PNIPAM) on the PVDF-*g*-PPMA membranes have allowed the preparation of, respectively, antifouling, pH-responsive and temperature-responsive membranes. These microporous membranes with “clickable” anchors on the surface (including pore surface) thus offer exciting opportunities for the direct molecular design and engineering of the membrane and pore surfaces.

Combinations of the CRP techniques and click chemistry have also been recently employed for the synthesis of functional polymeric materials and solid substrates. In an effort to combine ATRP and alkyne-azide click reaction for the synthesis of dual stimuli-responsive PVDF membrane, PVDF-*g*-[PBIEM-*co*-PPMA] graft copolymers were first prepared by thermally-induced free-radical graft copolymerization of two inimers, 2-(2-bromoisobutyryloxy)ethyl methacrylate (BIEM) and PMA, from ozone-pretreated PVDF backbones (*71*) (Scheme 6). The PVDF-*g*-[PBIEM-*co*-PPMA] copolymers were cast, by phase inversion in an aqueous medium, into microporous membranes with silutaneous presence of both inimer units on the surface. The PVDF-*g*-[PBIEM-*co*-PPMA] membranes thus provided the respective alkyl halide and alkyne functionalities for the “grafting from” process involving surface-initiated ATRP of the viologen-containing monomer, *N*-benzyl-*N*′-(4-vinylbenzyl)-4,4′-bipyridium dichloride (BVbpy), and the “grafting to” process involving alkyne-azide click reaction with azido-terminated poly(*N*-isopropylacrylamide) (PNIPAM-N_3), prepared a priori via RAFT polymerization. The as-synthesized PVDF-*g*-[P(BIEM-*g*-PBVbpy)-*co*-P(PMA-*click*-PNIPAM)] membrane exhibited both redox- and temperature-dependent permeability to aqueous solutions. The chemical interconversion of viologen moieties between the hydrophilic dicationic Vi^{2+} state and the hydrophobic radical cationic $Vi^{\cdot+}$ state provides redox-regulated permeability through the membrane (*72*). Alternatively, silver nanoparticles can be deposited on the PVDF-*g*-[P(BIEM-*g*-PBVbpy)-*co*-PPMA] membrane through UV-induced reduction of the silver ions in a salt solution (*73*). The pyridinium groups of viologen graft-copolymerized on the PVDF-*g*-[P(BIEM-*g*-PBVbpy)-*co*-PPMA] membrane surface exhibited bactericidal effects on *Staphylococcus aureus* under continuous-flow conditions. The antibacterial effect was significantly enhanced by the incorporation of silver nanoparticles on the membrane and pore surfaces (PVDF-*g*-[P(BIEM-*g*-PBVbpy)-*co*-PPMA]-Ag membrane).

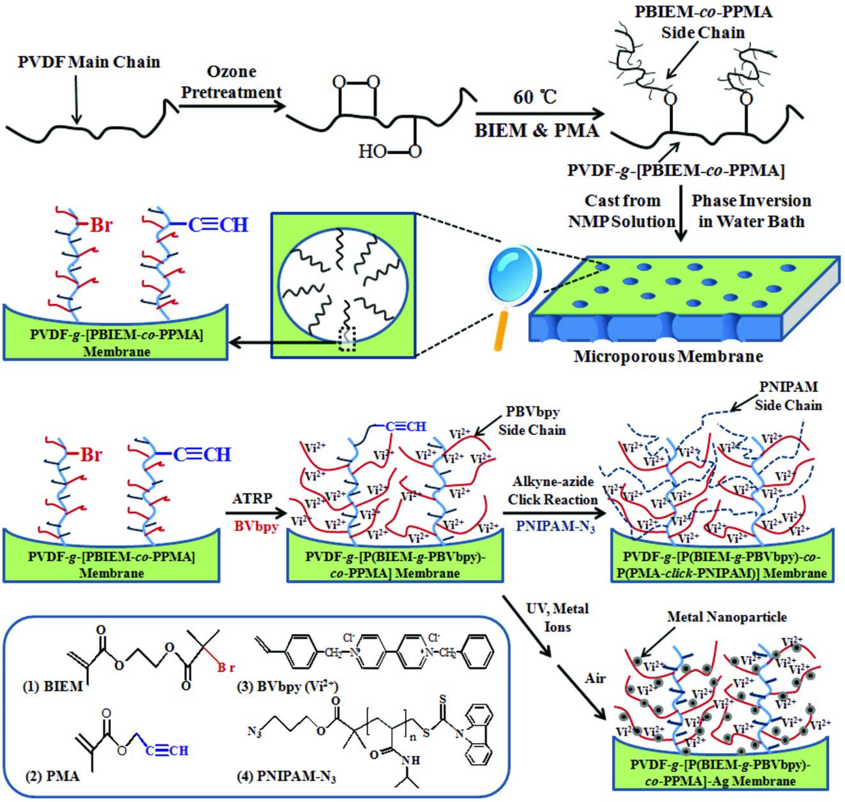
PVDF Main Chain
Ozone Pretreatment
HO—O
60 ℃
BIEM & PMA
PBIEM-*co*-PPMA Side Chain
PVDF-*g*-[PBIEM-*co*-PPMA]
Cast from NMP Solution
Phase Inversion in Water Bath
Microporous Membrane
—Br
—C≡CH
PVDF-*g*-[PBIEM-*co*-PPMA] Membrane
ATRP
BVbpy
PBVbpy Side Chain
PVDF-*g*-[P(BIEM-*g*-PBVbpy)-*co*-PPMA] Membrane
Alkyne-azide Click Reaction
PNIPAM-N₃
PNIPAM Side Chain
PVDF-*g*-[P(BIEM-*g*-PBVbpy)-*co*-P(PMA-*click*-PNIPAM)] Membrane
UV, Metal Ions
Air
Metal Nanoparticle
PVDF-*g*-[P(BIEM-*g*-PBVbpy)-*co*-PPMA]-Ag Membrane
(1) BIEM
(2) PMA
(3) BVbpy (Vi²⁺)
(4) PNIPAM-N₃

Scheme 6. Schematic illustration of the process of ozone pretreatment and graft copolymerization of PVDF with BIEM and PMA, preparation of PVDF-g-[PBIEM-co-PPMA] membrane with dual functionalities on the surface by phase inversion. Preparation of the redox-sensitive PVDF-g-[P(BIEM-g-PBVbpy)-co-PPMA] membrane via surface-initiated ATRP of BVbpy from the PVDF-g-[PBIEM-co-PPMA] membrane, preparation of the redox- and temperature-sensitive PVDF-g-[P(BIEM-g-PBVbpy)-co-P(PMA-click-PNIPAM)] membrane via surface alkyne-azide click reaction of PNIPAM-N_3 on the PVDF-g-[P(BIEM-g-PBVbpy)-co-PPMA] membrane, and depostiion of metal nanoparticles (Ag) on the PVDF-g-[P(BIEM-g-PBVbpy)-co-PPMA] membrane. [PVDF = poly(vinylidene fluoride); BIEM = 2-(2-bromoisobutyryloxy)ethyl methacrylate); PMA = propargyl methacrylate; BVbpy = N-benzyl-N'-(4-vinylbenzyl)-4,4'-bipyridium dichloride; PNIPAM-N_3 = azido-poly(N-isopropylazrylamide)]. [Reprint with permission from Ref. (71), Copyright 2011 The Royal Society of Chemistry.]

Downloaded by CORNELL UNIV on May 31, 2012 | http://pubs.acs.org
Publication Date (Web): March 20, 2012 | doi: 10.1021/bk-2012-1101.ch014

Conclusions

The advent of various controlled/living radical polymerization (CRP) techniques and click chemistry has made it possible to produce poly(vinylidene fluoride) (PVDF) and copolymer substrates (membranes) with an unprecedented level of control over composition, structure and properties. The fluoropolymer membrane structure, morphology and function can thus be tailored through polymer and (block and graft) copolymer design and controlled synthesis. The examples discussed in this article give a glance at possibilities offered by the current CRP techniques and click chemistry to impart stimuli-responsive, antifouling, antibacterial and ion exchange properties to the PVDF membrane and pore surfaces through the "grafting from" and "grafting to" approaches in both polymer/copolymer synthesis and post membrane modification. Due to the controlled character of CRP techniques and the quantitative yield of click reactions, CRP techniques in combination with click chemistry will continue to play an important role in the design and synthesis of precursor polymers and copolymers with well-defined structure and tailored properties for the preparation of functional and functionalizable platforms for a new generation of advanced polymer membranes and substrates.

Downloaded by CORNELL UNIV on May 31, 2012 | http://pubs.acs.org
Publication Date (Web): March 20, 2012 | doi: 10.1021/bk-2012-1101.ch014

References

1. Souzy, R.; Ameduri, B.; Boutevin, B. *Prog. Polym. Sci.* **2004**, *29*, 75–106.
2. Junginckel, B. J. In *The Polymeric Materials Encyclopedia*; Salamone, J. C., Ed.; CRC Press: Boca Raton, FL, 1996; Vol. 7, pp 7114−7123.
3. Seiler, D. A. In *Modern Fluoropolymers: PVDF in the Chemical Process Industry*; Scheirs, J., Ed.; Wiley: New York, 1997; Chapter 25, pp 487−506.
4. Ameduri, B. *Macromolecules* **2010**, *43*, 10163–10184.
5. Ameduri, B. *Chem. Rev.* **2009**, *109*, 6632–6686.
6. Zhai, G. Q.; Toh, S. C.; Tan, W. L.; Kang, E. T.; Neoh, K. G. *Langmuir* **2003**, *19*, 7030–7037.
7. Ying, L.; Wang, P.; Kang, E. T.; Neoh, K. G. *Macromolecules* **2002**, *35*, 673–679.
8. Zhai, G. Q.; Ying, L.; Kang, E. T.; Neoh, K. G. *J. Mater. Chem.* **2002**, *12*, 3508–3515.
9. Zhai, G. Q.; Ying, L.; Kang, E. T.; Neoh, K. G. *Macromolecules* **2002**, *35*, 9653–9656.
10. Chang, Y.; Chang, W. J.; Shih, Y. J.; Wei, T. C.; Hsiue, G. H. *ACS Appl. Mater. Interfaces* **2011**, *3*, 1228–1237.
11. Barbey, R.; Lavanant, L.; Paripovic, D.; Schuwer, N.; Sugnaux, C.; Tugulu, S.; Klok, H. A. *Chem. Rev.* **2009**, *109*, 5437–5527.
12. *Handbook of Radical Polymerization*; Barner-Kowolik, C., Ed.; Wiley-VCH: Weinheim, Germany, 2008.
13. Sciannamea, V.; Jerome, R.; Detrembleur, C. *Chem. Rev.* **2008**, *108*, 1104–1126.
14. Braunecker, W. A.; Matyjaszewski, K. *Prog. Polym. Sci.* **2007**, *32*, 93–146.

15. Boyer, C.; Bulmus, V.; Davis, T. P.; Ladmiral, V.; Liu, J. Q.; Perrier, S. B. *Chem. Rev.* **2009**, *109*, 5402–5436.
16. Kostov, G.; Boschet, F.; Buller, J.; Badache, L.; Brandsadter, S.; Ameduri, B. *Macromolecules* **2011**, *44*, 1841–1855.
17. Boyer, C.; Ameduri, B.; Hung, M. H. *Macromolecules* **2010**, *43*, 3652–3663.
18. Boyer, C.; Ameduri, B.; Boutevin, B.; Dolbier, W. R.; Winter, R.; Gard, G. *Macromolecules* **2008**, *41*, 1254–1263.
19. Boyer, C.; Valade, D.; Sauguet, L.; Ameduri, B.; Boutevin, B. *Macromolecules* **2005**, *38*, 10353–10362.
20. Valade, D.; Boyer, C.; Ameduri, B.; Boutevin, B. *Macromolecules* **2006**, *39*, 8639–8651.
21. Laruelle, G.; Nicol, E.; Ameduri, B.; Tassin, J. -F.; Ajellal, N. *J. Polym. Sci., Part A: Polym. Chem.* **2011**, *49*, 3960–3969.
22. Huisgen, R. *Angew. Chem., Int. Ed.* **1963**, *2*, 633–696.
23. Huisgen, R. *Angew. Chem., Int. Ed.* **1968**, *7*, 321–328.
24. Kolb, H. C.; Finn, M. G.; Sharpless, K. B. *Angew.Chem., Int. Ed.* **2001**, *40*, 2004–2021.
25. Lewis, W. G.; Green, L. G.; Grynszpan, F.; Radic, Z.; Carlier, P. R.; Taylor, P.; Finn, M. G.; Sharpless, K. B. *Angew. Chem., Int. Ed.* **2002**, *41*, 1053–1057.
26. Hawker, C. J.; Wooley, K. L. *Science* **2005**, *309*, 1200–1205.
27. Soules, A.; Ameduri, B.; Boutevin, B.; Calleja, G. *Macromolecules* **2010**, *43*, 4489–4499.
28. Hoyle, C. E.; Bowman, C. N. *Angew. Chem., Int. Edit.* **2010**, *49*, 1540–1573.
29. Hoyle, C. E.; Lowe, A. B.; Bowman, C. N. *Chem. Soc. Rev.* **2010**, *39*, 1355–1387.
30. Tasdelen, M. A. *Polym. Chem.* **2011**, *2*, 2133–2145.
31. Mansfeld, U.; Pietsch, C.; Hoogenboom, R.; Becer, C. R.; Schubert, U. S. *Polym. Chem.* **2010**, *1*, 1560–1598.
32. Iha, R. K.; Wooley, K. L.; Nystrom, A. M.; Burke, D. J.; Kade, M. J.; Hawker, C. J. *Chem. Rev.* **2009**, *109*, 5620–5686.
33. Golas, P. L.; Matyjaszewski, K. *Chem. Soc. Rev.* **2010**, *39*, 1338–1354.
34. Sheiko, S. S.; Sumerlin, B. S.; Matyjaszewski, K. *Prog. Polym. Sci.* **2008**, *33*, 759–785.
35. Gregory, A.; Stenzel, M. H. *Prog. Polym. Sci.* DOI: 10.1016/j.progpolymsci.2011.08.004.
36. Wandera, D.; Wickramasinghe, S. R.; Hussom, S. M. *J. Membr. Sci.* **2010**, *357*, 6–35.
37. Holmberg, S.; Holmlund, P.; Wilen, C. E.; Kallio, T.; Sundholm, G.; Sundholm, F. *J. Polym. Sci., Part A: Polym. Sci.* **2002**, *40*, 591–601.
38. Zhai, G. Q.; Kang, E. T.; Neoh, K. G. *Macromolecules* **2004**, *37*, 7240–7249.
39. Wang, P.; Tan, K. L.; Kang, E. T.; Neoh, K. G. *J. Mater. Chem.* **2001**, *11*, 783–789.
40. Sauguet, L.; Boyer, C.; Ameduri, B.; Boutevin, B. *Macromolecules* **2006**, *39*, 9087–9101.
41. Akthakul, A.; Salinaro, R. F.; Mayes, A. M. *Macromolecules* **2004**, *37*, 7663–7668.

Downloaded by CORNELL UNIV on May 31, 2012 | http://pubs.acs.org
Publication Date (Web): March 20, 2012 | doi: 10.1021/bk-2012-1101.ch014

42. Hester, J. F.; Banerjee, P.; Won, Y. Y.; Akthakul, A.; Acar, M. H.; Mayes, A. M. *Macromolecules* **2002**, *35*, 7652–7661.
43. Akthakul, A.; Hochbaum, A. I.; Stellacci, F.; Mayes, A. M. *Adv. Mat.* **2005**, *17*, 532–535.
44. Zhang, Z. C.; Chalkova, E.; Fedkin, M.; Wang, C. M.; Lvov, S. N.; Komarneni, S.; Chung, T. C. M. *Macromolecules* **2008**, *41*, 9130–9139.
45. Tsang, E. M. W.; Zhang, Z. B.; Yang, A. C. C.; Shi, Z. Q.; Peckham, T. J.; Narimani, R.; Frisken, B. J.; Holdcroft, S. *Macromolecules* **2009**, *42*, 9467–9480.
46. Tsang, E. M. W.; Zhang, Z. B.; Shi, Z. Q.; Soboleva, T.; Holdcroft, S. *J. Am. Chem. Soc.* **2007**, *129*, 15106–15107.
47. Laruelle, G.; Nicol, E.; Ameduri, B.; Tassin, J.-F.; Ajellal, N. *J. Polym. Sci., Part A: Polym. Chem.* **2011**, *49*, 3960–3969.
48. Samanta, S.; Chatterjee, D. P.; Layek, R. K.; Nandi, A. K. *Macromol. Chem. Phys.* **2011**, *212*, 134–149.
49. Chen, Y. W.; Liu, D. M.; Deng, Q. L.; He, X. H.; Wang, X. F. *J. Polym. Sci., Part A: Polym. Chem.* **2006**, *44*, 3434–3443.
50. Singh, N.; Hussom, S. M.; Zdyrko, B.; Luzinov, I. *J. Membr. Sci.* **2005**, *262*, 81–90.
51. Chang, Y.; Ko, C. Y.; Shih, Y. J.; Quemener, D.; Deratani, A.; Wei, T. C.; Wang, D. M.; Lai, J. Y. *J. Membr. Sci.* **2009**, *345*, 160–169.
52. Zhang, M. F.; Russell, T. P. *Macromolecules* **2006**, *39*, 3531–3539.
53. Xue, J.; Chem, L.; Wang, H. L.; Zhang, Z. B.; Zhu, X. L.; Kang, E. T.; Neoh, K. G. *Langmuir* **2008**, *24*, 14151–14158.
54. Guillen, G. R.; Pan, Y. J.; Li, M. H.; Hoek, E. M. V. *Ind. Eng. Chem. Res.* **2011**, *50*, 3798–3817.
55. Samata, S.; Chatterjee, D. P.; Manna, S.; Mandal, A.; Garai, A.; Nandi, A. K. *Macromolecules* **2009**, *42*, 3112–3120.
56. Jakubowski, W.; Min, K.; Matyjaszewski, K. *Macromolecules* **2006**, *39*, 39–45.
57. Zhu, W. P.; Zhong, M. J.; Li, W. W.; Dong, H. C.; Matyjaszewski, K. *Macromolecules* **2011**, *44*, 1920–1926.
58. Oh, J. K.; Min, K.; Matyjaszewski, K. *Macromolecules* **2006**, *39*, 3161–3167.
59. Luo, R.; Sen, A. *Macromolecules* **2008**, *41*, 4514–4518.
60. Zhao, H. Y.; Kang, X. L.; Liu, L. *Macromolecules* **2005**, *38*, 10619–10622.
61. Zhao, T.; Zhang, L. F.; Zhang, Z. B.; Zhou, N. C.; Cheng, Z. P.; Zhu, X. L. *J. Polym. Sci., Part A: Polym. Chem.* **2011**, *49*, 2315–2324.
62. Chen, Y. W.; Lei, Y.; Yu, W. H.; Kang, E. T.; Neoh, K. G. *Macromolecules* **2003**, *36*, 9451–9457.
63. Ying, L.; Yu, W. H.; Kang, E. T.; Neoh, K. G. *Langmuir* **2004**, *20*, 6032–6040.
64. Tsarevsky, N. V.; Bencherif, S. A.; Matyjaszewski, K. *Macromolecules* **2007**, *40*, 4439–4445.
65. Cai, T.; Kang, E. T.; Neoh, K. G.; Teo, S. L. M. *Langmuir* **2011**, *27*, 2936–2945.
66. Xia, Y.; Yin, X. C.; Burke, N. A. D.; Stover, H. D. H. *Macromolecules* **2005**, *38*, 5937–5943.

Downloaded by CORNELL UNIV on May 31, 2012 | http://pubs.acs.org
Publication Date (Web): March 20, 2012 | doi: 10.1021/bk-2012-1101.ch014

67. Cai, T.; Wang, R.; Kang, E. T.; Neoh, K. G. *Polym. Chem.* **2011**, *2*, 1849–1958.
68. Cai, T.; Kang, E. T.; Neoh, K. G. *Macromolecules* **2011**, *44*, 4258–4268.
69. Zhao, Q.; Wang, S. F.; Cheng, X. J.; Yam, R. C. M.; Kong, D. L.; Li, R. K. Y. *Biomacromolecules* **2010**, *11*, 1364–1369.
70. Harada, A.; Hashidzume, A.; Yamaguchi, H.; Takashima, Y. *Chem. Rev.* **2009**, *109*, 5974–6023.
71. Cai, T.; Wang, R.; Yang, W. J.; Lu, S. J.; Neoh, K. G.; Kang, E. T. *Soft Matter* **2011**, *7*, 11133–11143.
72. Liu, X.; Neoh, K. G.; Kang, E. T. *Macromolecules* **2003**, *36*, 8631–8637.
73. Shi, Z. L.; Neoh, K. G.; Kang, E. T. *Langmuir* **2004**, *20*, 6847–6852.

Downloaded by CORNELL UNIV on May 31, 2012 | http://pubs.acs.org
Publication Date (Web): March 20, 2012 | doi: 10.1021/bk-2012-1101.ch014

Chapter 15

Grafting of Poly(methyl methacrylate) on the Surface of Cylindrical Mesopores of Ordered Silica via Atom Transfer Radical Polymerization

Liang Cao[1,2] and Michal Kruk[*,1]

[1]Center for Engineered Polymeric Materials, Department of Chemistry, College of Staten Island, City University of New York, 2800 Victory Boulevard, Staten Island, New York 10314, and Graduate Center, City University of New York, 365 Fifth Avenue, New York, New York 10016
[2]Current address: Thermo Fisher Scientific, 1228 Titan Way, Sunnyvale, California 94085
[*]E-mail: michal.kruk@csi.cuny.edu

Downloaded by OHIO STATE UNIV LIBRARIES on June 1, 2012 | http://pubs.acs.org
Publication Date (Web): March 20, 2012 | doi: 10.1021/bk-2012-1101.ch015

Poly(methyl methacrylate) (PMMA) was grafted on the surface of ultra-large-pore SBA-15 silica using surface-initiated atom transfer radical polymerization. The silica support was synthesized using Pluronic P123 ($EO_{20}PO_{70}EO_{20}$) as a surfactant template and 1,3,5-triisopropylbenzene as a micelle swelling agent. The surface of SBA-15 was modified with bromoisobutyryl groups, which served as atom transfer radical polymerization (ATRP) initiation sites. Normal ATRP of methyl methacrylate was carried out at 40 °C in anisole. The loading of PMMA was controlled in a range from 5 to ~50 wt.% by changing the polymerization time. The pores of the SBA-15/PMMA nanocomposites were accessible for PMMA loading up to ~40 wt.% and the pore size distributions were narrow. The grafted polymers had quite low polydispersity.

In Progress in Controlled Radical Polymerization: Materials and Applications; Matyjaszewski, K., et al.;
ACS Symposium Series; American Chemical Society: Washington, DC, 2012.

Downloaded by OHIO STATE UNIV LIBRARIES on June 1, 2012 | http://pubs.acs.org
Publication Date (Web): March 20, 2012 | doi: 10.1021/bk-2012-1101.ch015

Introduction

The exploration of ordered mesoporous silicas (OMSs) (*1–3*) as high-surface-area supports for surface-initiated controlled polymerization (*4–8*) has progressed over the last eight years (*9–29*). OMSs exhibit high surface areas (~300-1200 m^2 g^{-1}) and uniform mesopores, often of cylindrical shape (diameter ~2-26 nm) (*2*, *30*, *31*). Atom transfer radical polymerization (ATRP) emerged as an especially useful method to introduce uniform polymer layers on the surfaces of OMSs (*32*, *33*), allowing one to control the polymer molecular weight (*16*, *22*) and film thickness (*16*, *19*, *22*, *23*). In some cases, narrow molecular weight distributions of the polymer graft were achieved (*12*, *16*, *22*). Polymers grafted from surfaces of OMSs (and related mesocellular foams (*34*)) via ATRP included poly(N-isopropylacrylamide) (*9*, *14*, *26*), polyacrylonitrile (*10*, *16*), polystyrene (*12*, *20*, *22*), poly(methyl methacrylate) (PMMA) (*12*, *15*, *17*, *20*, *22*), poly(styrenesulfonic acid sodium salt) (*18*, *19*, *23*), poly(glycidyl methacrylate) (*17*, *25*), and poly(sodium acrylate) (*28*). While PMMA grafting via normal ATRP (*35*, *36*) in the mesopores has been studied (*12*, *15*, *17*, *20*), demonstrating the ability to introduce appreciable polymer loadings, the ability to tailor the polymer film thickness has not been demonstrated and there was only one example of PMMA graft with narrow molecular weight distribution (*12*). On the other hand, the control of PMMA loading, film thickness and molecular weight was achieved (*22*) in the case of activators regenerated by electron transfer (ARGET) ATRP (*37–39*), the latter being carried out under less stringent conditions when compared to normal ATRP. Herein, the study of normal ATRP grafting of PMMA in ordered mesopores of ultra-large-pore SBA-15 silica (*31*) is reported. The control of polymer loading and the film thickness was clearly achieved. There was also evidence for quite low polydispersity of grafted PMMA and for the increase of molecular weight with time of the polymerization.

Materials and Methods

Materials

Methyl methacrylate (MMA, 99%) was purchased from Aldrich and purified by passing through a column filled with basic alumina. The initiator, 3-(chlorodimethylsilyl)propyl 2-bromoisobutyrate, was synthesized similarly as described elsewhere (*40*). All other chemicals, including 1,1,2,4,4-pentamethyldiethylenetriamine (PMDETA), tetraethyl orthosilicate (TEOS), 1,3,5-triisopropylbenzene (TIPB), NH_4F, CuBr, $CuBr_2$, pyridine, chlorotrimethylsilane and anisole were used as received. $EO_{20}PO_{70}EO_{20}$ block copolymer Pluronic P123 was provided by BASF as a free sample.

Synthesis of SBA-15 Support

Ultra-large-pore SBA-15 silica was synthesized as reported elsewhere (*31*). 2.4 g of Pluronic P123 surfactant and 0.027 g of NH_4F were dissolved in 84.0 mL of 1.30 M aqueous HCl solution at 12.75 °C. After about one hour

In Progress in Controlled Radical Polymerization: Materials and Applications; Matyjaszewski, K., et al.;
ACS Symposium Series; American Chemical Society: Washington, DC, 2012.

of stirring, a mixture of 5.5 mL TEOS (silica precursor) and 2.4 mL (2.0 g) TIPB (micelle swelling agent) was introduced. The solution was mechanically stirred for one day at 12.75 °C in an open container and then was transferred in a Teflon-lined autoclave and heated at 130 °C for one day. The as-synthesized surfactant-templated silica was filtered out, washed with water and dried at about 60 °C in a vacuum oven. Finally, the as-synthesized sample was calcined under air with a heating ramp 2 °C min^{-1}, and a final temperature of 550 °C (dwell time 5 hours).

Immobilization of Initiator on Surface of SBA-15

1.3 g of SBA-15, 1 mL of pyridine and 60 mL of dry toluene were stirred for 30 minutes with purging nitrogen before 1 mL of 3-(chlorodimethylsilyl)propyl 2-bromoisobutyrate was added. The solution was stirred at room temperature for two days under nitrogen and then the solid sample was isolated by filtering, washing with toluene and acetone, and drying at ~40 °C in a vacuum oven overnight. The obtained sample was added to 50 mL of dry toluene and stirred for 30 minutes under nitrogen. Then 1.0 mL pyridine and 4 mL chlorotrimethylsilane were added and stirred at room temperature for two days under nitrogen. The product was isolated by filtering, washing with toluene and acetone, and drying at about 40 °C in a vacuum oven overnight, affording 2-bromoisobutyrate-modified SBA-15 (SBA-15-BiB).

Downloaded by OHIO STATE UNIV LIBRARIES on June 1, 2012 | http://pubs.acs.org
Publication Date (Web): March 20, 2012 | doi: 10.1021/bk-2012-1101.ch015

Surface-Initiated ATRP

A typical surface-initiated polymerization of MMA was as follows: 50 mg of SBA-15-BiB, 0.25 mL of MMA, a pre-mixed solution of $CuBr_2$ (1 mg) and PMDETA ligand (11.5 µL) in 0.1 mL N,N-dimethylformamide, and 0.8 mL anisole were added into a Schlenk flask. After the mixture was deoxygenated by three freeze-pump-thaw cycles, 3.3 mg of CuBr was added under the nitrogen atmosphere and the Schlenk flask was sealed. The final molar ratio of reactants was as follows: initiator: CuBr : $CuBr_2$: PMDETA : MMA = 1 : 1 : 0.2 : 2.4 : 100, and the monomer concentration was ~2.2 mol/L. The polymerization mixture was placed in an oil bath at 40 °C for the periods of time from 2 to 9 hours. The polymerizations were terminated by opening the Schlenk flask, which introduces oxygen and converts the ATRP catalyst to the deactivator. The silica/polymer composites were isolated by filtration, washed with toluene, acetone and methanol, and dried in a vacuum oven.

Characterization

Small-angle X-ray scattering (SAXS) pattern was acquired on Bruker Nanostar U instrument equipped with a rotating anode X-ray source and Vantec-2000 2-D detector. Nitrogen adsorption measurements at -196 °C were carried out using a Micromeritics ASAP 2020 volumetric adsorption analyzer. Before the adsorption measurements, samples were outgassed under vacuum at 200 °C in the case of silicas or 80 °C in the cases of surface-modified silicas.

In Progress in Controlled Radical Polymerization: Materials and Applications; Matyjaszewski, K., et al.;
ACS Symposium Series; American Chemical Society: Washington, DC, 2012.

It should be noted that adsorption isotherms for SBA-15/PMMA composites with 41 and 47 wt.% PMMA loadings were appreciably distorted downwards because of the combination of the small sample mass and moderate/low surface area of the materials. While the isotherm for the sample with 47 wt.% loading indicated no appreciable porosity (no capillary condensation was observed) and very low surface area and pore volume, the isotherm for the other sample was suitable for the pore size analysis. However, it needed to be empirically corrected (by adjusting the free space value for the sample tube) to obtain an isotherm of a normally observed shape. This empirical adjustment did not eliminate a substantial inaccuracy in the pore volume and specific surface area, but it is expected to allow for a quite accurate pore size assessment.

The specific surface area, S_{BET}, was determined using the BET method (*41*). The total pore volume, V_t, was calculated from the amount adsorbed at a relative pressure of 0.99 (*41*). The pore size distribution (PSD) was calculated using the BJH-KJS method for cylindrical mesopores (*42*). The nominal BJH-KJS pore diameter, w_{KJS}, is defined as the position of the maximum on PSD. This nominal pore diameter is known to be systematically overestimated, and a more reliable estimate of the pore diameter, w_d, for SBA-15 silica was arrived at using a geometrical relation between structural parameters in a honeycomb pore structure, as described elsewhere (*31*). Unfortunately, this relation is not applicable to surface-modified materials, so the pore diameter changes were analyzed on the basis of the nominal BJH-KJS pore diameters. Thermogravimetric analysis (TGA) was performed under nitrogen with 5 °C/min ramping rate to 800 °C on a Hi-Res 2950 thermogravimetric analyzer from TA Instruments. The polymer loading in SBA-15/PMMA composite was calculated as a weight loss between 100 and ~800 °C after subtracting of the contribution from the decomposition of organosilane groups present prior to the polymerization. Molecular weight distributions were determined by gel permeation chromatography (GPC) on Alliance GPCV 2000 with refractive index detector using polystyrene standards. The cleavage of PMMA from the silica support was performed using 48% HF water solution mixed with THF in the volume ratio of one to ten.

Downloaded by OHIO STATE UNIV LIBRARIES on June 1, 2012 | http://pubs.acs.org
Publication Date (Web): March 20, 2012 | doi: 10.1021/bk-2012-1101.ch015

Results and Discussion

Ultra-large-pore SBA-15 silica had a (100) interplanar spacing of 21.8 nm, as determined by using SAXS (pattern not shown). As can be inferred from nitrogen adsorption data (Figure 1), the SBA-15 support had a high adsorption capacity (the corresponding total pore volume, $V_t = 1.42$ cm^3 g^{-1}, see Table I), quite high specific surface area (288 m^2 g^{-1}) and uniform large mesopores (see Figure 2). The nominal pore diameter w_{KJS} was 28.2 nm and a more accurate estimate of the pore diameter w_d was 22.1 nm. Therefore, it can be expected that the nominal pore diameters listed herein are overestimated by about 6 nm. The pore volume, specific surface area and nominal pore diameter decreased to some extent (to 1.12 cm^3 g^{-1}, 204 m^2 g^{-1} and 25.9 nm, respectively) after the modification with organosilane bearing bromoisobutyryl initiator groups (BiB) and with trimethylsilyl (TMS) groups (see

Scheme 1). Thermogravimetric weight change patterns (Figure 3) indicated the weight loss of 11.2 wt.% associated with decomposition of BiB and TMS groups.

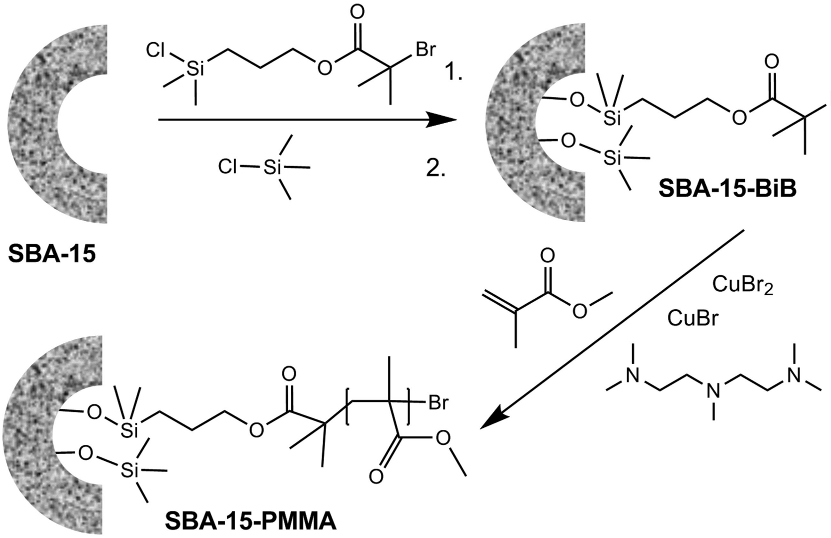

Scheme 1. ATRP grafting of methyl methacrylate in mesopores of SBA-15.

Table I. Polymer content and pore structure properties of the samples

Sample and wt.% of PMMA	*Polymerization time (h)*	*BET Specific Surface Area (m^2 g^{-1})*	*Total Pore Volume (cm^3 g^{-1})*	*KJS Pore Diameter (nm)*
SBA-15		288	1.42	28.2
SBA-15-BiB		204	1.12	25.9
SBA-15/PMMA 5%	2	197	1.00	26.3
SBA-15/PMMA 15%	3	150	0.63	24.7
SBA-15/PMMA 22%	4	120	0.47	23.1
SBA-15/PMMA 41%	6	25	0.08	~21
SBA-15/PMMA 47%	9	N/A	N/A	N/A

The polymerization of methyl methacrylate (see Scheme 1) proceeded with an appreciable rate and high loadings of PMMA were achieved in several hours. Based on TGA (see Figure 3), the polymer loadings were 5, 15, 22, 41 and 47 wt.% after 2, 3, 4, 6 and 9 hours of polymerization, respectively (see Table I). It should be noted that the highest polymer loading achieved is expected to correspond to the state in which the mesopores were nearly fully filled with the polymer. While the grafting of PMMA from the surface of ordered mesoporous silicas by normal ATRP was studied earlier (*12*, *15*, *17*, *20*), this study is first to demonstrate the control of loading of the polymer simply by adjusting the polymerization time,

Downloaded by OHIO STATE UNIV LIBRARIES on June 1, 2012 | http://pubs.acs.org
Publication Date (Web): March 20, 2012 | doi: 10.1021/bk-2012-1101.ch015

which is a signature of a living polymerization process. The present results of normal ATRP parallel our earlier findings involving ARGET ATRP (*22*), but in the latter case, the polymerization was much slower.

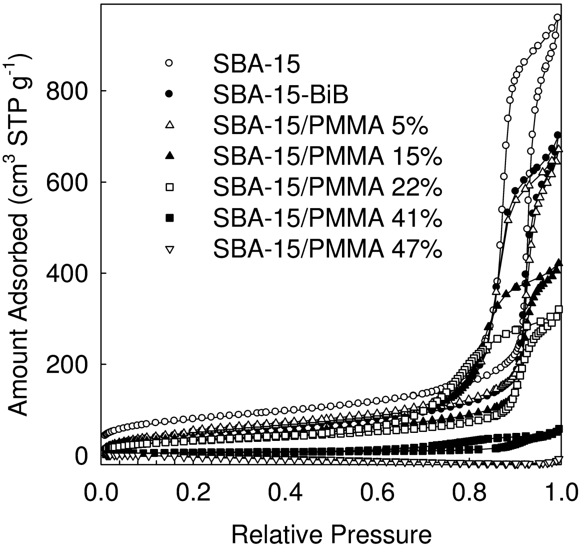

Figure 1. Nitrogen adsorption isotherms of ultra-large-pore SBA-15 silica support, the initiator-modified SBA-15 and the SBA-15/PMMA nanocomposites. The loading of the polymer is indicated in wt.%.

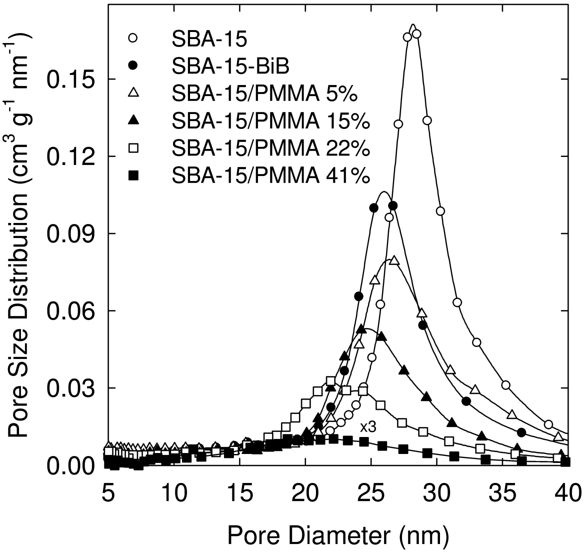

Figure 2. Pore size distributions of ultra-large-pore SBA-15 silica support, the initiator-modified SBA-15 and the SBA-15/PMMA nanocomposites. The loading of the polymer is indicated in wt.%.

Downloaded by OHIO STATE UNIV LIBRARIES on June 1, 2012 | http://pubs.acs.org
Publication Date (Web): March 20, 2012 | doi: 10.1021/bk-2012-1101.ch015

Downloaded by OHIO STATE UNIV LIBRARIES on June 1, 2012 | http://pubs.acs.org
Publication Date (Web): March 20, 2012 | doi: 10.1021/bk-2012-1101.ch015

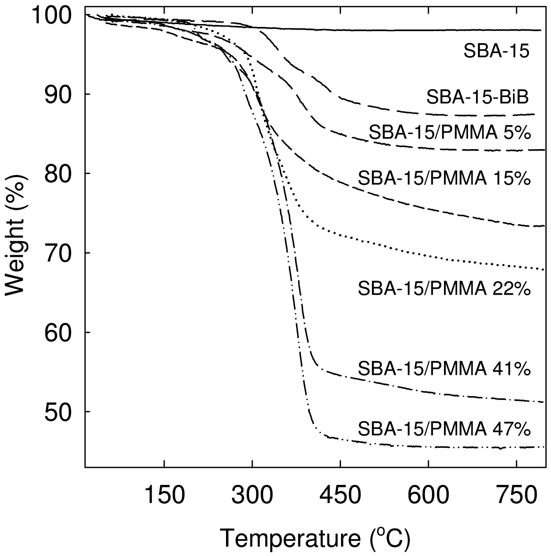

Figure 3. Weight change patterns for ultra-large-pore SBA-15 silica support, the initiator-modified SBA-15 and the SBA-15/PMMA nanocomposites. The loading of the polymer is indicated in wt.%.

As seen in Figure 1, the mesopores of the silica support were accessible for PMMA loadings up to 41 wt.%. The composites with up to 22 wt.% of PMMA had quite large pore volume and specific surface (1.00, 0.63 and 0.47 $cm^3 g^{-1}$ as well as 197, 150 and 120 $m^2 g^{-1}$ for polymer loadings of 5, 15 and 22 wt.%, respectively). On the other hand, the sample with the very high PMMA loading of 41 wt.% exhibited a small pore volume (~0.08 $cm^3 g^{-1}$) and quite low specific surface area (~25 $m^2 g^{-1}$). Anyway, it is remarkable that the mesopores were still accessible despite such a high polymer loading. As can be seen in Figure 2 and Table I, the initial pore size for initiator-modified SBA-15 (nominal w_{KJS} = 25.9 nm) did not change to any noticeable extent after the introduction of the polymer loading of 5 wt.%, assuming the value of 26.3 nm. It should be noted that the apparent pore diameter increase may be related to a change of arrangement of organic groups on the surface of the material, but more likely is an artifact related to the experimental error in the adsorption measurements or to the influence of the change in the surface properties on the capillary condensation process (which is the basis for the pore size determination). On the other hand, it is highly unlikely that the framework of SBA-15 can expand as a result of the polymerization process, thus leading to an actual pore diameter increase (*22*, *43*). The nominal pore diameter dropped to 24.7 and ~23.1 nm for PMMA loadings of 15 and 22 wt.%. Finally, the pore diameter was ~21 nm for 41 wt.% PMMA loading. Clearly, the position of peaks on pore size distributions shifted to lower pore size values as the loading of PMMA increased, indicating the increase in the polymer film thickness as the polymerization time was prolonged. On the basis of the pore radius decrease as a result of the polymerizations, one can infer that the polymer film thickness increased as the polymerization was prolonged and reached about 2 nm for the

Downloaded by OHIO STATE UNIV LIBRARIES on June 1, 2012 | http://pubs.acs.org
Publication Date (Web): March 20, 2012 | doi: 10.1021/bk-2012-1101.ch015

SBA-15/PMMA composites with accessible mesopores. The mesopores of SBA-15/PMMA sample with 47 wt.% loading of the polymer wer not accessible to nitrogen, most likely due to nearly complete filling with PMMA. Adsorption-desorption hysteresis loops did not broaden to any appreciable extent after the polymer grafting, even for 41 wt.% PMMA loading, indicating the lack of any appreciable constrictions in the pore structure and thus uniform grafting on the surface of the mesopores of the SBA-15 support (*16*). Moreover, the pore size distributions remained narrow after the polymer grafting (see Figure 3).

For the SBA-15/PMMA composites with the polymer loadings of 22 and 41 wt.%, the number-average molecular weights were determined to be 8600 and 14000 g/mol, and the corresponding polydispersity indexes (PDIs) were 1.14 and 1.16. The molecular weights of PMMA were similar to those obtained for similar polymer loadings in the case of ARGET ATRP (*22*), but PDIs were lower in the present case of normal ATRP. This is expected, as the low catalyst content used in ARGET ATRP may lead to somewhat broader molecular weight distributions (*44*).

Conclusions

Normal ATRP with bromoisobutyrate-based initiator can be used to graft uniform layers of PMMA in the mesopores of high-surface-area silica support. High loadings of PMMA were introduced within several hours in a controlled manner without blocking the mesopores. The thickness of PMMA film increased as the polymerization time was prolonged. The pore size distributions of the SBA-15/PMMA nanocomposite remained narrow even for high polymer loadings and there was no evidence of the development of any major constrictions in the mesopores. The polydispersity indexes of grafted PMMA were quite narrow.

Acknowledgments

Acknowledgment is made to the Donors of the American Chemical Society Petroleum Research Fund for partial support of this research (Award PRF #49093-DNI5). NSF is acknowledged for funding the SAXS/WAXS system through award CHE-0723028. BASF is acknowledged for providing Pluronic P123 surfactant.

References

1. Zhao, D.; Feng, J.; Huo, Q.; Melosh, N.; Frederickson, G. H.; Chmelka, B. F.; Stucky, G. D. *Science* **1998**, *279*, 548–552.
2. Beck, J. S.; Vartuli, J. C.; Roth, W. J.; Leonowicz, M. E.; Kresge, C. T.; Schmitt, K. D.; Chu, C. T. W.; Olson, D. H.; Sheppard, E. W.; McCullen, S. B.; Higgins, J. B.; Schlenker, J. L. *J. Am. Chem. Soc.* **1992**, *114*, 10834–10843.
3. Inagaki, S.; Fukushima, Y.; Kuroda, K. *J. Chem. Soc., Chem. Commun.* **1993**, 680–682.
4. Huang, X.; Wirth, M. J. *Anal. Chem.* **1997**, *69*, 4577–4580.

5. Ejaz, M.; Yamamoto, S.; Ohno, K.; Tsujii, Y.; Fukuda, T. *Macromolecules* **1998**, *31*, 5934–5936.
6. Husseman, M.; Malmstrom, E. E.; McNamara, M.; Mate, M.; Mecerreyes, D.; Benoit, D. G.; Hedrick, J. L.; Mansky, P.; Huang, E.; Russell, T. P.; Hawker, C. J. *Macromolecules* **1999**, *32*, 1424–1431.
7. Matyjaszewski, K.; Miller, P. J.; Shukla, N.; Immaraporn, B.; Gelman, A.; Luokala, B. B.; Siclovan, T. M.; Kickelbick, G.; Vallant, T.; Hoffmann, H.; Pakula, T. *Macromolecules* **1999**, *32*, 8716–8724.
8. von Werne, T.; Patten, T. E. *J. Am. Chem. Soc.* **1999**, *121*, 7409–7410.
9. Fu, Q.; Rao, G. V. R.; Ista, L. K.; Wu, Y.; Andrzejewski, B. P.; Sklar, L. A.; Ward, T. L.; Lopez, G. P. *Adv. Mater.* **2003**, *15*, 1262–1266.
10. Kruk, M.; Dufour, B.; Celer, E. B.; Kowalewski, T.; Jaroniec, M.; Matyjaszewski, K. *J. Phys. Chem. B* **2005**, *109*, 9216–9225.
11. Lenarda, M.; Chessa, G.; Moretti, E.; Polizzi, S.; Storaro, L.; Talon, A. *J. Mater. Sci.* **2006**, *41*, 6305–6312.
12. Save, M.; Granvorka, G.; Bernard, J.; Charleux, B.; Boissiere, C.; Grosso, D.; Sanchez, C. *Macromolec. Rapid Commun.* **2006**, *27*, 393–398.
13. Kruk, M.; Dufour, B.; Celer, E. B.; Kowalewski, T.; Jaroniec, M.; Matyjaszewski, K. *Polym. Mater.: Sci. Eng.* **2007**, *97*, 274–275.
14. Zhou, Z.; Zhu, S.; Zhang, D. *J. Mater. Chem.* **2007**, *17*, 2428–2433.
15. Cao, L.; Kruk, M. *Polym. Prepr.* **2008**, *49* (2), 294–295.
16. Kruk, M.; Dufour, B.; Celer, E. B.; Kowalewski, T.; Jaroniec, M.; Matyjaszewski, K. *Macromolecules* **2008**, *41*, 8584–8591.
17. Moreno, J.; Sherrington, D. C. *Chem. Mater.* **2008**, *20*, 4468–4474.
18. Calvo, A.; Yameen, B.; Williams, F. J.; Azzaroni, O.; Soler-Illia, G. J. A. A. *Chem. Commun.* **2009**, 2553–2555.
19. Li, C.; Yang, J.; Wang, P.; Liu, J.; Yang, Q. *Microporous Mesoporous Mater.* **2009**, *123*, 228–233.
20. Pasetto, P.; Blas, H.; Audouin, F.; Boissiere, C.; Sanchez, C.; Save, M.; Charleux, B. *Macromolecules* **2009**, *42*, 5983–5995.
21. Calvo, A.; Fuertes, M. C.; Yameen, B.; Williams, F. J.; Azzaroni, O.; Soler-Illia, G. J. A. A. *Langmuir* **2010**, *26*, 5559–5567.
22. Cao, L.; Kruk, M. *Polym. Chem.* **2010**, *1*, 97–101.
23. Martin, A.; Morales, G.; Martinez, F.; van Grieken, R.; Cao, L.; Kruk, M. *J. Mater. Chem.* **2010**, *20*, 8026–8035.
24. Blas, H.; Save, M.; Boissiere, C.; Sanchez, C.; Charleux, B. *Macromolecules* **2011**, *44*, 2577–2588.
25. Moreno, J.; Iglesias, J.; Melero, J. A.; Sherrington, D. C. *J. Mater. Chem.* **2011**, *21*, 6725–6735.
26. Reichhardt, N. V.; Nylander, T.; Klösgen, B.; Alfredsson, V.; Kocherbitov, V. *Langmuir* **2011**, *27*, 13838–13846.
27. Xu, L.; Ye, Z.; Cui, Q.; Gu, Z.; Mercier, L. *Polymer* **2011**, *52*, 5961–5974.
28. Zhao, Y.-H.; Shantz, D. F. *Langmuir* **2011**, *27*, 14554–14562.
29. Brunsen, A.; Cui, J.; Ceolin, M.; Campo, A. d.; Soler-Illia, G. J. A. A.; Azzaroni, O. *Chem. Commun.* **2012**, *48*, 1422–1424.
30. Zhao, D.; Huo, Q.; Feng, J.; Chmelka, B. F.; Stucky, G. D. *J. Am. Chem. Soc.* **1998**, *120*, 6024–6036.

Downloaded by OHIO STATE UNIV LIBRARIES on June 1, 2012 | http://pubs.acs.org
Publication Date (Web): March 20, 2012 | doi: 10.1021/bk-2012-1101.ch015

31. Cao, L.; Man, T.; Kruk, M. *Chem. Mater.* **2009**, *21*, 1144–1153.
32. Soler-Illia, G. J. A. A.; Azzaroni, O. *Chem. Soc. Rev.* **2011**, *40*, 1107–1150.
33. Kruk, M. *Isr. J. Chem.*in press.
34. Schmidt-Winkel, P.; Lukens, W. W., Jr.; Zhao, D.; Yang, P.; Chmelka, B. F.; Stucky, G. D. *J. Am. Chem. Soc.* **1999**, *121*, 254, 255.
35. Wang, J.-S.; Matyjaszewski, K. *J. Am. Chem. Soc.* **1995**, *117*, 5614–5615.
36. Matyjaszewski, K.; Xia, J. *Chem. Rev.* **2001**, *101*, 2921–2990.
37. Jakubowski, W.; Matyjaszewski, K. *Angew. Chem., Int. Ed.* **2006**, *45*, 4482–4486.
38. Jakubowski, W.; Min, K.; Matyjaszewski, K. *Macromolecules* **2006**, *39*, 39–45.
39. Matyjaszewski, K.; Dong, H.; Jakubowski, W.; Pietrasik, J.; Kusumo, A. *Langmuir* **2007**, *23*, 4528–4531.
40. Miller, P. J.; Matyjaszewski, K. *Macromolecules* **1999**, *32*, 8760–8767.
41. Sing, K. S. W.; Everett, D. H.; Haul, R. A. W.; Moscou, L.; Pierotti, R. A.; Rouquerol, J.; Siemieniewska, T. *Pure Appl. Chem.* **1985**, *57*, 603–619.
42. Kruk, M.; Jaroniec, M.; Sayari, A. *Langmuir* **1997**, *13*, 6267–6273.
43. Huang, L.; Dolai, S.; Raja, K.; Kruk, M. *Langmuir* **2010**, *26*, 2688–2693.
44. Listak, J.; Jakubowski, W.; Mueller, L.; Plichta, A.; Matyjaszewski, K.; Bockstaller, M. R. *Macromolecules* **2008**, *41*, 5919–5927.

Downloaded by OHIO STATE UNIV LIBRARIES on June 1, 2012 | http://pubs.acs.org
Publication Date (Web): March 20, 2012 | doi: 10.1021/bk-2012-1101.ch015

Chapter 16

Structuring of Polymer Brushes and Surface Nitroxide Exchange Reactions

Hendrik Wagner,[1] Maike Becker,[1] Lifeng Chi,[2] and Armido Studer*,[1]

**[1]Organisch-Chemisches Institut, Westfälische Wilhelms-Universität,
Corrensstraße 40, 48149 Münster, Germany
[2]Physikalisches Institut, Westfälische Wilhelms-Universität,
Wilhelm-Klemm-Straße 10, 48149 Münster, Germany, and
Center for Nanotechnology (CeNTech), Heisenbergstraße 11,
48149 Münster, Germany
*E-mail: studer@uni-muenster.de**

Alkoxyamines and nitroxides are versatile classes of compounds that show great potential for the design of new materials. The application of alkoxyamines for the preparation of polymer brushes is described. Moreover, a new method for structuring and fabrication of polymer brushes is presented. Finally, the use of alkoxyamines and nitroxides for mild surface nitroxide exchange reactions at self-assembled monolayers and zeolite L crystal surfaces is discussed.

Introduction

The design and fabrication of polymer films at surfaces and of polymer/inorganic hybrid materials have gained increased attention in various fields of research (*1–12*). By tuning surface properties via immobilization or covalent attachment of functional groups it is possible to adjust wettability, friction, adhesion or biocompatibility of a surface (*12–20*). Multiple covalent attachment of polymers via one end of the macromolecule to a surface leads to so called polymer brushes, which represent an interesting class of functional

In Progress in Controlled Radical Polymerization: Materials and Applications; Matyjaszewski, K., et al.;
ACS Symposium Series; American Chemical Society: Washington, DC, 2012.

organic/inorganic hybrid materials that show special surface properties (*1–8*). Depending on the physical properties of the attached soft polymeric material, the surface properties of the brush can be tailored at wish. Polymer brushes can be prepared by covalent attachment of a polymerization initiator onto a surface with subsequent surface-initiated polymerization (SIP) by the so-called "grafting-from" approach (*21*, *22*). If SIP is conducted using one of the available controlled radical polymerization methods, that approach enables the preparation of dense polymer brushes with well-defined brush thicknesses (*23*). Different radical polymerization techniques such as atom transfer radical polymerization (ATRP), reversible addition–fragmentation chain transfer (RAFT) and nitroxide-mediated polymerization (NMP) have been applied to the preparation of dense polymer brushes by SIP (*24–30*).

Properties of polymer brushes can be further modified and tuned by structuring the soft polymeric material with different patterning techniques, such as photolithography, electron beam chemical lithography (EBCL), dip-pen lithography, and microcontact printing (μCP) (*31–37*). All these patterning set ups belong to the "top-down" techniques. Along these lines, we have developed a complementary top-down method using mechanical surface nanoscratching which allows for the preparation of well-defined structured polymer brushes. Basically any polymeric material which is readily accessible by SIP can be structured using that method. The overall process comprises four steps: a) synthesis of a suitable initiator, b) covalent attachment of the initiator to a surface, c) SIP, and d) top-down patterning of the polymeric material by mechanical AFM-nanoscratching.

Synthesis, Structuring, and Fabrication of Polymer Brushes

We first synthesized NMP initiators **1**-**4** containing a triethoxysilylether moiety ready to be used for covalent attachment of the initiator to surface silanol groups of oxidized Si-wafers. Transsilyletherification at the surface provides a self-assembled monolayer (SAM) consisting of alkoxyamines **1**-**4**. The covalently bound alkoxyamines were then used for surface-initiated NMP (SINMP) resulting in dense polymer brushes (Scheme 1) (*13*). SINMP was conducted by placing the chemically modified surfaces bearing alkoxyamine initiators 1-4 in neat monomer in the presence of sacrificial alkoxyamines **5**-**7**. Addition of an external alkoxyamine **5**-**7** was necessary to provide a sufficient high concentration of nitroxide during SINMP which is crucial for a controlled nitroxide mediated polymerization (Scheme 1) (*30*, *38–40*).

The thickness of the brush could be readily adjusted by varying the initiator to monomer ratio and by adjusting the polymerization time. Styrene, n-butyl acrylate and *N*-isopropyl acrylamide were successfully polymerized at the Si-surface via this approach.

With these dense brushes in hand, we found that surface structuring of the soft polymeric material could be readily achieved by applying mechanical nanoscratching using atomic force microscopy (AFM) operating in contact mode (force > 7.9 μN). It is important to note that no special equipment was necessary: patterned dense brushes were obtained by using conventional AFM equipment (Figure 1a). To study whether the orientation and density of the polymer chains at the surface influence mechanical nanoscratching, we also studied scratching of spin-coated polymer films at silicon surfaces. In spin-coated systems, polymers are not covalently bound and a far lower degree of organization results. For fair comparison, polymers of about the same length were spin coated on Si-wafers and were structured by the same AFM experimental setup. The comparison of mechanical lithography on spin-coated films and polymer brushes revealed qualitative differences. AFM nanoscratching worked very well on dense polymer brushes (polystyrene (PS), poly-n-butyl acrylate (PBA) and poly-*N*-isopropylacrylamide (PNIPAM)), whereas moderate results were obtained by nanoscratching of spin-coated polymer films (the scratch borders were not well defined in the latter case, not shown) (*38*). Clearly, the major advantage of working with polymer brushes is the possibility of cleaning the sample after mechanical lithography by simple sonication of the chemically modified wafer in basically any solvent. While that washing procedure on AFM-structured spin-coated films resulted in a complete destruction of the pattern (the spin coated polymeric material was removed), sonication of the scratched brushes allowed for removal of the scratched out polymeric material, leaving a clean and well-defined lithographic pattern. We found that the patterning technique was very robust and reliable. Importantly, multiple scratching provided more complex patterns as shown in Figure 1a on a pattern design consisting of multiple single scan lines. Even a second writing over the existing scratched lines (perpendicular to the first scratch direction) was possible, resulting in the pillar structures shown in Figure 1b.

The stability of the patterned polymer brushes towards various solvents allowed for further processing of the scratched brushes using solution-based methods. This would certainly not be possible on structured spin-coated polymer films. It was obvious that the scratched areas consisting likely of surface silanol moieties and the non-scratched areas consisting of the soft polymeric material should show very different adsorption profiles towards organic molecules. To test selective recognition of the patterned brushes, immobilization of various compounds on structured brushes was investigated (*38*). For example, the pink dye lissamine rhodamine B sulfonyl chloride **8** was used along with alkyl-chain conjugated congeners (e. g. **9**) to target the brush or the scratched areas for site-selective dye deposition/immobilization. Studies were mainly conducted on structured PS-brushes. Pleasingly, the polar dye **8** did not enter the polymer brush areas. It selectively adsorbed to the scratched areas (Figure 2c). However, a derivative bearing a long hydrocarbon chain of ten carbon atoms (see **9**), that showed a higher hydrophobicity, selectively adsorbed on the PS-covered areas (Figure 2d). In this case, at the scratched areas of the wafer which are supposed to be free of any polymeric material, no dye adsorption was identified by fluorescence spectroscopy. Hence, the difference in the hydrophobicity in going from the parent dye **8** to the more hydrophobic alkyl-conjugated derivative **9** allowed for site-selective immobilization of the dye molecule either at the brush polymer regime or into the scratched out areas.

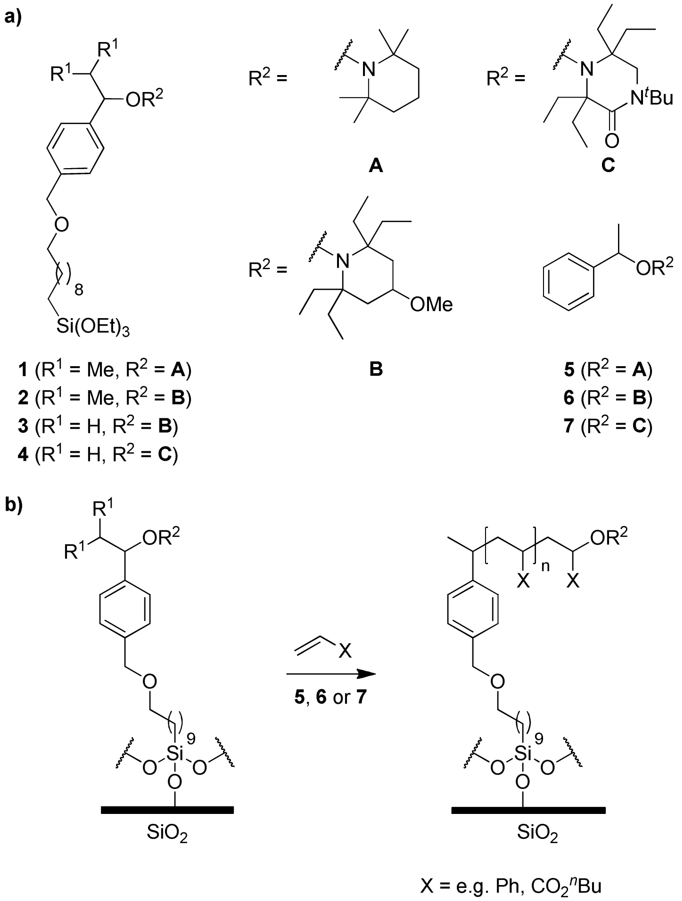
a)
R1
R1
OR2
O
8
Si(OEt)3
1 (R1 = Me, R2 = A)
2 (R1 = Me, R2 = B)
3 (R1 = H, R2 = B)
4 (R1 = H, R2 = C)
R2 =
N
A
R2 =
N
NtBu
O
C
R2 =
N
OMe
B
OR2
5 (R2 = A)
6 (R2 = B)
7 (R2 = C)
b)
R1
R1
OR2
O
9
Si
O
O
O
SiO2
X
5, 6 or 7
n
OR2
X
X
O
9
Si
O
O
O
SiO2
X = e.g. Ph, CO2nBu

Scheme 1. a) Various initiators for surface initiated polymerization and b) preparation of polymer brushes.

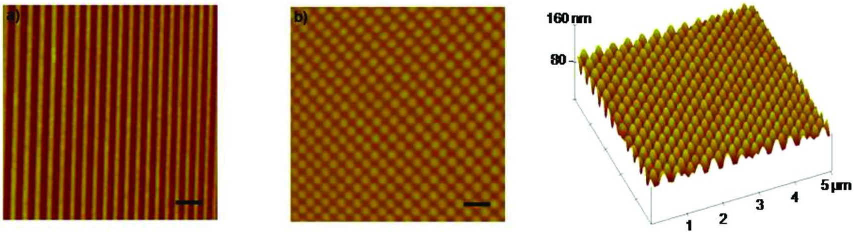
a)
b)
160 nm
80
1
2
3
4
5 µm

Figure 1. a) Multiple single scan lines with periodicity of 200 nm on a PS brush. b) Array of 200-nm-diameter pillars achieved by perpendicular writing of single scan lines with 200-nm periodicity (32-nm thickness, black bars represent 600 nm). (see color insert)

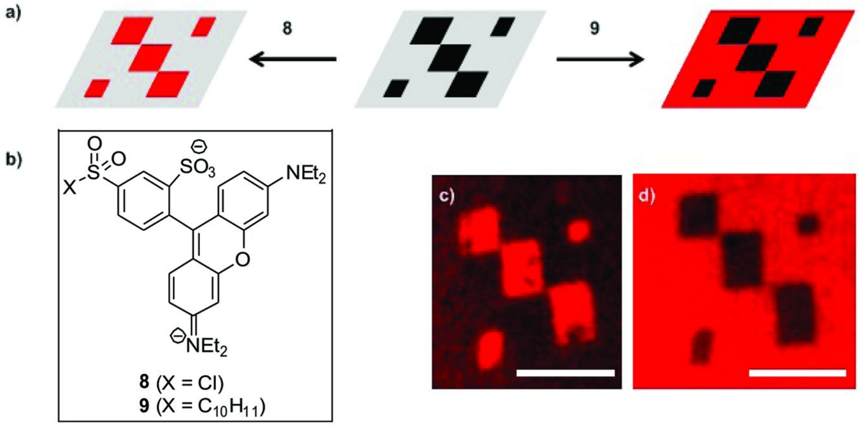

Figure 2. a) Schematic representation for selective dye adsorption onto the scratched areas (depicted in black) or polymer brush areas (depicted in grey). b) Molecular structures and fluorescence images (d and e). Scale bars: 5 µm. (see color insert)

Based on these rewarding initial experiments using dyes we decided to study far more challenging site-selective immobilization of proteins into patterned polymer brushes. The goal was the development of a novel robust method for generation of protein biochips (*41*).

Due to the fact that proteins generally adsorb to basically any hydrophobic polymeric material (*7*, *41–44*) selective immobilization of proteins into structured brushes, where the water soluble protein should address the scratched out areas, seemed to be very difficult to achieve. We therefore first investigated interactions of non-structured dense polymer brushes with various proteins. To this end, PS-brushes of defined varying thickness were prepared by SINMP. Protein adsorption on these dense PS brushes (thicknesses of 5 nm, 10 nm and 40 nm, respectively) was then investigated using fluorescent dye labeled proteins (*39*). We were pleased to find that the 40 nm thick PS-brushes showed protein repellence for ConA (Concanavalin A), streptavidin and to some extent for BSA (bovine serum albumin). However, for the 5 and 10 nm systems, the tested proteins adsorbed at the PS brushes. Importantly, PBA brushes with a thickness of 40 nm also showed protein repellent properties. It is currently not fully understood why thicker brushes show protein repellent behavior, whereas the thinner systems revealed rather strong interactions with the proteins. We are currently trying to answer that interesting question by modeling the surface properties of dense brushes as a function of brush thickness by theoretical methods. As expected, thicker spin-coated PS films at silicon surfaces did not show any protein repellent properties.

We then investigated protein adsorption on structured dense polymer brushes. Brush structuring was achieved by using mechanical AFM nanoscratching, as discussed above. As proteins belong to polar macromolecules, they should show high adsorption to the scratched areas of the wafer which likely consists of polar SiOH moieties. If thickness of the dense polymeric brush is large enough (>40 nm), the brush area should show protein repellent behavior, thus leading to site-selective protein adsorption into the scratched areas. With the help of AFM lithography, resolution down to the nanometer scale should be readily achieved. Indeed, as shown in Figure 3, three different fluorescently labeled proteins (ConA, streptavidin and BSA) were successfully site-selectively immobilized into structured PS-brushes.

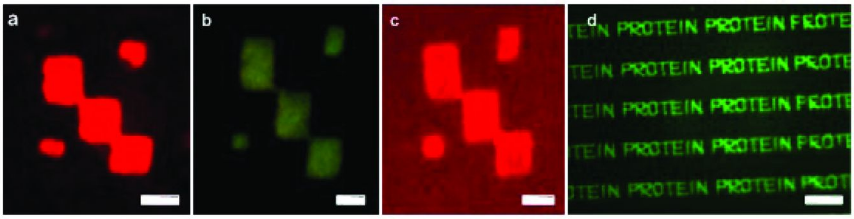

Figure 3. ConA (a), streptavidin (b) and BSA (c) immobilized at structured PS brushes. b) Immobilization of streptavidin into nanostructures generated by a cantilever array using AFM lithography towards PS brushes; scale bars for a-c: 2 μm and for d: 10 μm. (see color insert)

As expected, structured brushes with a polymer layer thickness of less than 20 nm did not show selective protein adsorption into the scratched polar regions of the wafer. For these systems, proteins were found in the scratched and also in the brush areas of the wafer. To conclude this part, we can state that our method represents an easy and robust novel approach for the preparation of protein biochips. Importantly, parallel pattern writing was achieved by an AFM cantilever array equipment resulting in structured PS and PBA polymer brushes that show highly selective protein adsorption over large areas (Figure 3d).

Radical Nitroxide Exchange Reactions at Self-Assembled Monolayers

The alkoxyamine modified Si-surfaces, which were successfully used for SINMP (see Scheme 1b), were also applied to thermal nitroxide exchange reactions at surfaces. Thermal C-O-bond homolysis of surface bound alkoxyamines leads to transient C-centered radicals covalently bound to the surface along with persistent nitroxide radicals in solution. Steered by the persistent radical effect (PRE) (*28*, *29*, *45*, *46*), little C-radical dimerization occurs and the major reaction pathway is the trapping of the C-radicals with the persistent nitroxide radicals thus reforming the starting alkoxyamines in a degenerate process. If the nitroxide exchange is conducted in the presence of an excess of an external functionalized nitroxide or alkoxyamine, exchange of the nitroxide moiety will result (Scheme 2). Reversible covalent bond formation has been applied intensively in supramolecular chemistry, yet it is not investigated well in surface chemistry (*47*, *48*). Although reversible radical exchange reactions, which belong to the class of dynamic covalent chemistry, have not been applied at SAMs to date (*49*), thermal nitroxide exchange reactions have already been utilized for the synthesis and functionalization of polymers and polymer brushes (*30*, *50–63*).

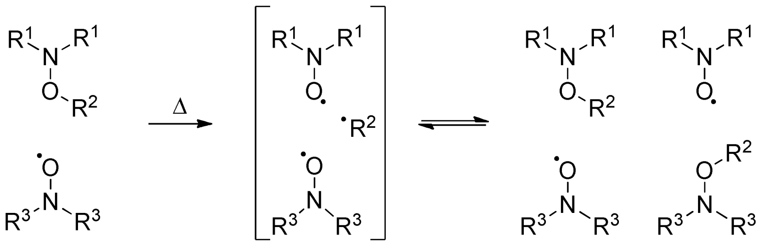

Scheme 2. Nitroxide exchange reaction by C-O bond homolysis of alkoxyamines.

We successfully used the radical nitroxide exchange reaction for reversible modification of SAMs (Figure 4a) (*64*). The radical exchange reaction turned out to be very general and many functional groups were tolerated. Reactions were conducted by subjecting SAMs, bearing alkoxyamine **1**, to a $ClCH_2CH_2Cl$ solution containing an additional functionalized alkoxyamine (large excess) under heating at 125 °C for 20 h. Surface analysis was performed by XPS, contact angle measurements and fluorescence microscopy. Our novel method allowed to reversibly functionalizing surfaces with short PEG-chains, short peptide chains and dyes. Moreover, non-protected sugars and biotin were successfully covalently bound to Si-wafers by using the corresponding sugar- and biotin-conjugated nitroxides as reagents for the thermal exchange reactions (Figure 4).

Since contact angle measurement and fluorescence microscopy offered only a qualitative picture on the efficiency of the surface nitroxide exchange reaction, we decided to properly quantify that thermal process by XPS starting with an alkoxyamine covered wafer (Figure 4a. SAM with $X = R^8$) containing a fluorinated nitroxide (*64*). Note that the C-F-bond is readily detected by XPS. The starting monolayer contained fluorine atoms, which was unambiguously verified by XPS (1.6 At%). This “fluorinated” wafer was treated with TEMPO under thermal exchange conditions and the resulting monolayer was again, after careful washing, analyzed by XPS. Indeed, fluorine could not be identified anymore at the surface after the reaction revealing that the exchange occurred with excellent yield. Since similar conditions were used for all other exchange reactions, it can be assumed that these processes generally occurred with high efficiency at the surface.

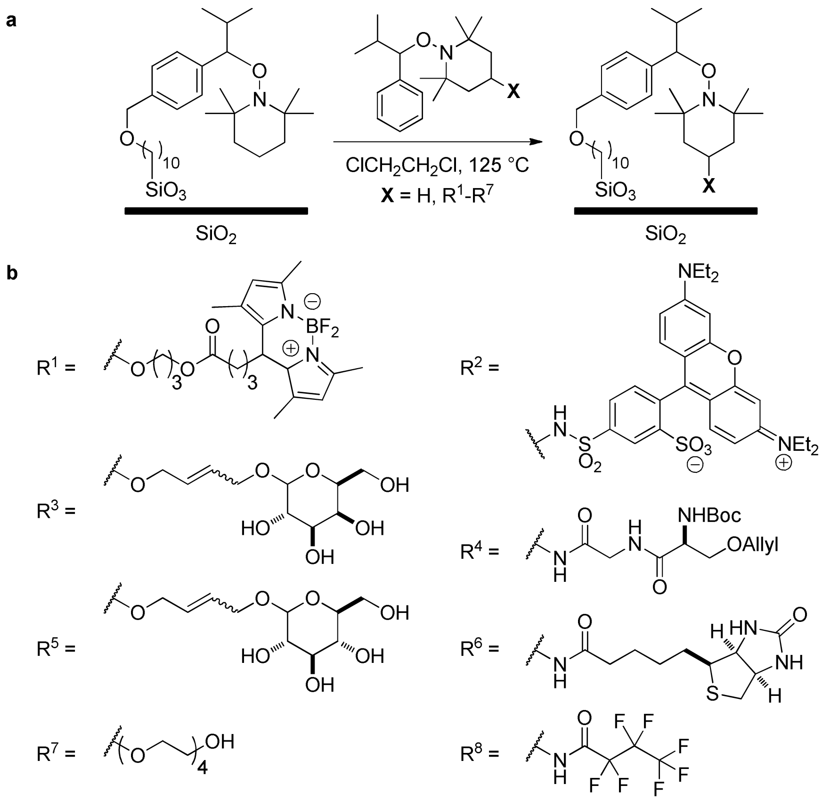

Figure 4. Surface nitroxide exchange reaction (a) Molecular structures of functionalized alkoxyamines and alkoxyamine based SAMs (b).

Self-Assembly and Modification of Zeolite L Crystals by Mild Nitroxide Exchange Reactions

Surface nitroxide exchange reactions were also successfully used to reversibly organize zeolite L nanocrystals into linear polymeric chains (*62*). Zeolite L is a crystalline aluminosilicate, which has a defined morphology and is optically transparent. Zeolite L is readily functionalized at the external and internal surface, the crystals are non-toxic and biocompatible. Moreover, it is possible to selectively functionalize the channel entrances (base area) with amine groups which can be used as linking moieties to further chemically modify the pore entrances using amide bond forming reactions (*65–68*).

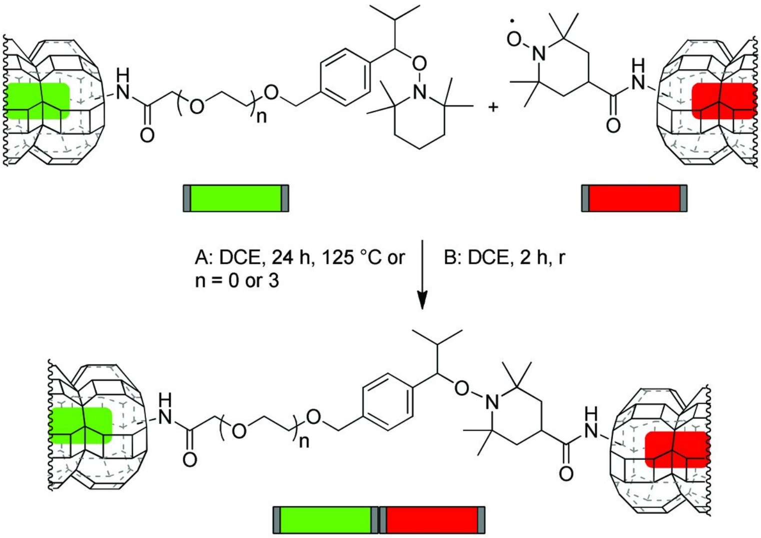

Scheme 3. Surface nitroxide exchange reaction at the pore entrances of dye labeled zeolite L. (see color insert)

For crystal assembly, the zeolite crystals (1µm zeolite L crystals were used in these studies) were first site-selectively functionalized with alkoxyamines and nitroxides at the pore entrances (Scheme 3).

To distinguish the two “complementary” hybrid materials bearing either nitroxides or alkoxyamines, the crystals were initially loaded with either green (pyronine) and red dyes (oxazine) prior to chemical entrance functionalization. Nitroxide exchange of these complementary zeolite L crystals should result in the formation of crystal chains interconnected via C-O-bonds of alkoxyamines in a strongly alternating fashion. In a first attempt, the nitroxide exchange reaction was conducted with a suspension containing equal amounts of green (alkoxyamine hybrids with n = 0) and red (nitroxide hybrids) crystals for 24 h at 125 °C in $ClCH_2CH_2Cl$ (Scheme 3).

The reaction success was verified by fluorescence microscopy and scanning electron microscopy (SEM). We were pleased to find the buildup of linear chains consisting of up to 3 color-alternating crystals. The concept worked! However, despite careful optimization of the reaction conditions, we were never able to detect any longer alternating crystal chains. In order to facilitate the surface exchange reaction between two surfaces we introduced a triethyleneglycol TEG-linker to position the reacting alkoxyamine moiety slightly farther away from the zeolite base area. Thereby the interference of surface roughness during reaction should be diminished. Experiments with this second generation hybrid material under standard conditions indeed showed linear zeolite arrangement consisting of up to 16 strongly alternating crystal types, convincingly validating our approach (Figure 5).

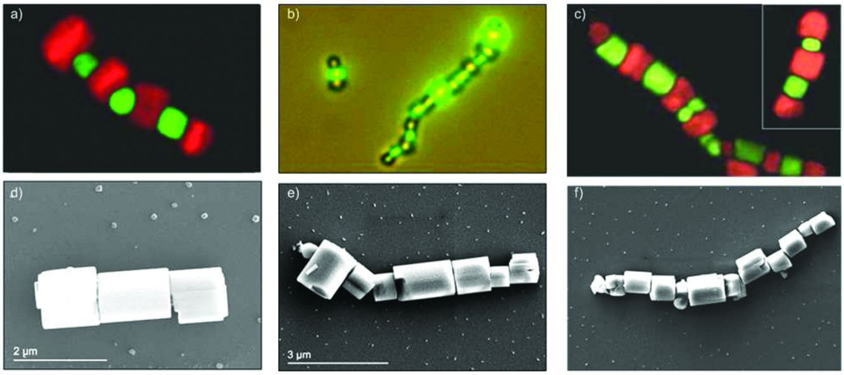

Figure 5. Confocal (a and c), fluorescence (b) and SEM (d-f) images after assembly. (see color insert)

To our surprise, we found that the surface nitroxide exchange reaction at zeolite L crystals could also be performed at room temperature. This is of great importance as nitroxide exchange reactions typically occur efficiently only at higher temperatures (above 90 °C). It is presumed that this efficient surface exchange is a result of several effects: It is known that a polar environment reduces the activation energy for the C-O bond homolysis in alkoxyamines. In addition, inter- and also intramolecular hydrogen bonding by neighboring hydroxyl groups also lead to a lowering of the activation energy (*69–72*). We therefore currently assume, that the silanol groups at the zeolite surface are involved in the activation of the surface bound alkoxyamines towards thermal C-O-bond homolysis. Further experiments to understand that unexpected behavior are currently conducted in our laboratory.

The reversibility of the assembly reaction was confirmed by the addition of excess TEMPO to the preformed zeolite crystal chains. As expected, surface nitroxide exchange reaction with a large excess of TEMPO under standard conditions led to the “destruction” of the chains: only single crystals were observed by fluorescence microscopy (Figure 6).

To study the dynamic character of the assembly, a respective 10:1 ratio of the two crystal types was reacted at room temperature in $ClCH_2CH_2Cl$. Chains formed were significantly shorter and many single crystals of the type added in excess were identified. Moreover, for the short chains (mainly three crystals) the zeolite type used in excess was always located at both termini, as expected. If the minor zeolite hybrid was then added to that mixture, chains started to grow and distribution and chain length of the experiments conducted with a 1:1 ratio of crystals were obtained.

Encouraged by these results on low temperature nitroxide surface exchange, we decided to use that process for site-selective immobilization of interesting biomolecules at the zeolite L crystal surface (mainly base area) for the preparation of novel biohybrid materials (*73*).

As a proof-of-principle, 3 µm zeolite crystals were functionalized with alkoxyamines either at the channel entrance only (Scheme 4) or at the whole crystal surface. These hybrids were reacted with a dye-labeled nitroxide. Reaction parameters such as solvent, temperature and alkoxyamine structure were carefully optimized.

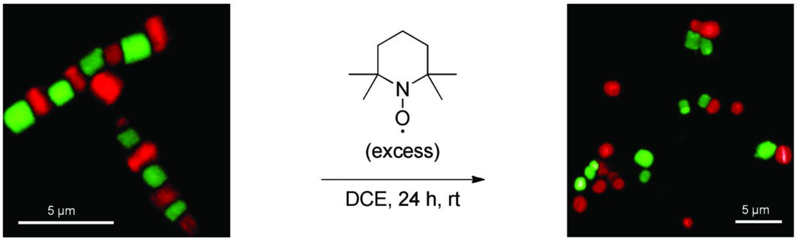

Figure 6. Reversibility of the crystal assembly reaction. (see color insert)

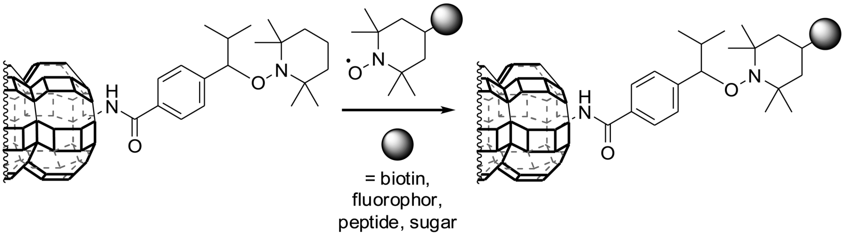

Scheme 4. Site-specific immobilization of biomolecules at the crystal surface.

The fluorescence images obtained after nitroxide exchange using rhodamine (**10**) and NBD (**11**) nitroxides clearly proved the successful site-specific surface immobilization under mild conditions (Figures 7a, b).

Again, we showed the reversible character of this process: renewed reaction of the dye-marked crystals with an excess of TEMPO resulted in crystals lacking the fluorescent dye, proving successful exchange of the dye-conjugated nitroxide by the non-fluorescent TEMPO. As radical chemistry tolerates various functional groups, this approach should also allow for the site-selective immobilization/conjugation of biomolecules and proteins at the zeolite L surface. To this end, nitroxides **12**, **13** and **14** bearing unprotected mannose, biotin and NTA (N_α,$N_{\alpha'}$bis(carboxymethyl)-L-lysine hydrate) were prepared. Nitroxide exchange was conducted under optimized conditions in $ClCH_2CH_2Cl$, H_2O or in aqueous buffer solution at room temperature. The success of the immobilization of the unprotected mannose was indirectly proven by subsequent complexation of the mannose/zeolite hybrids with rhodamine-labeled ConA which is known to strongly interact with mannose. Successful biotin conjugation was validated by postcomplexation with fluorescent streptavidin. NTA surface modification was investigated after complexation with Ni^{2+} by interaction with his-tagged eGFP (GFP = green fluorescent protein, Figures 7c-e). We repeated all experiments with crystals bearing alkoxyamine units all over the crystal surface. In these cases immobilization of the reporter moiety occurred at the whole zeolite surface. These examples clearly documented that non-selective adsorption of the tested proteins at the zeolite surface did not occur.

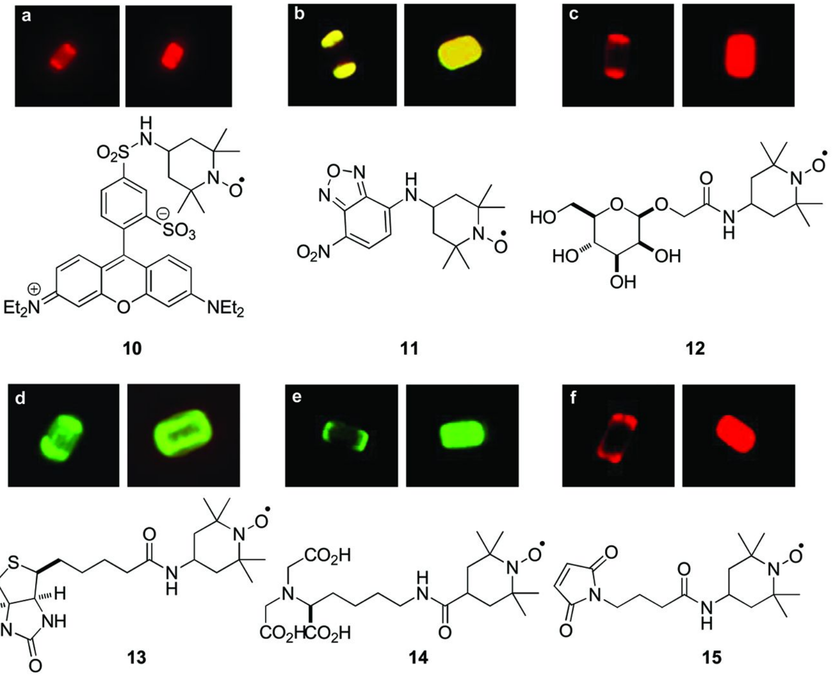

*Figure 7. Site-specific functionalization of the zeolite L surface (fluorescence microscopy images) and structures of the immobilized nitroxides: a) Rhodamine nitroxide **10**, b) NBD derivative **11**, c) unprotected mannose **12**, d) biotin nitroxide **13**, e) NTA derivative **14** and f) succinimido maleimide **15** for protein modification. (see color insert)*

In addition, succinimido maleimide nitroxide **15** was synthesized and reacted with the thiol groups of β-lactoglobulin A (LGA) or bovine serum albumin (BSA) to covalently attach the nitroxide moiety to the protein. Mass spectrometry was used to verify successful conjugation of the protein with the persistent radical. The protein nitroxide conjugate was then reacted with alkoxyamine modified zeolite L crystals in a nitroxide exchange reaction to eventually provide the corresponding protein zeolite conjugates. The successful surface functionalization was monitored by ζ potential and fluorescence measurements before and after nitroxide exchange reaction (Figure 7f).

Conclusion

To conclude we can state that readily prepared alkoxyamine modified Si-wafers are highly valuable starting materials for the preparation of dense polymer brushes by surface initiated nitroxide mediated radical polymerization. The dense brushes are further structured with mechanical AFM nanoscratching. By using cantilever array AFM equipment, patterning of large surface areas can be achieved. The thus formed structured polymer bushes consisting of soft polymeric areas (PS and PBA) and the scratched out areas consisting likely of Si-OH moieties showed site-selective adsorption of dyes and proteins into the scratched areas. However, selective protein adsorption works only if the polymer brushes are thicker than 40 nm. The selective adsorption of the proteins is likely a result of the protein repellent behavior of dense thick PS and PBA-brushes (>40 nm). Since PS and PBA brushes with thicknesses below 20 nm did not show any protein repellent properties. Our approach represents a novel reliable route towards protein biochips.

Alkoxyamine modified Si-wafers used successfully for SINMP can also be applied in thermal nitroxide exchange reactions for reversible immobilization of various functional moieties by thermal surface nitroxide exchange processes. The radical nature of the thermal nitroxide exchange tolerates many functional groups. That method is not restricted to the chemical modification of Si-wafers. This is convincingly documented for site-selective chemical manipulation of zeolite L microcrystals. Dyes, sugar derivatives, peptides and also proteins can be immobilized into the base area of the zeolite crystals with high position selectivity. In contrast to the reactions at the Si-wafer surface which are conducted at temperatures above 90 °C, thermal nitroxide exchange at the zeolite surface occurs under very mild conditions at room temperature.

Acknowledgments

We thank the Deutsche Forschungsgemeinschaft (DFG) within the programs SFB 858 and TRR61 for funding.

References

1. Bhat, R. R.; Chaney, B. N.; Rowley, J.; Liebmann-Vinson, A.; Genzer, J. *Adv. Mater.* **2005**, *17*, 2802–2807.
2. Andruzzi, L.; Senaratne, W.; Hexemer, A.; Sheets, E. D.; Ilic, B.; Kramer, E. J.; Baird, B.; Ober, C. K. *Langmuir* **2005**, *21*, 2495–2504.
3. Yoshikawa, C.; Goto, A.; Tsujii, Y.; Fukuda, T.; Kimura, T.; Yamamoto, K.; Kishida, A. *Macromolecules* **2006**, *39*, 2284–2290.

4. Charest, J. L.; Eliason, M. T.; Garcia, A. J.; King, W. P. *Biomaterials* **2006**, *27*, 2487–2494.
5. Lenhert, S.; Sesma, A.; Hirtz, M.; Chi, L. F.; Fuchs, H.; Wiesmann, H. P.; Osbourn, A. E.; Moerschbacher, B. M. *Langmuir* **2007**, *23*, 10216–10223.
6. Alves, N. M.; Pashkuleva, I.; Reis, R. L.; Mano, J. F. *Small* **2010**, *6*, 2208–2220.
7. Ahmad, S. A.; Hucknall, A.; Chilkoti, A.; Leggett, G. J. *Langmuir* **2010**, *26*, 9937–9942.
8. Chen, S.; Li, L.; Zhao, C.; Zheng, J. *Polymer* **2010**, *51*, 5283–5293.
9. Love, J. C.; Urbach, A. R.; Prentiss, M. G.; Whitesides, G. M. *J. Am. Chem. Soc.* **2003**, *125*, 12696–12697.
10. Grimsdale, A. C.; Müllen, K. *Angew. Chem., Int. Ed.* **2005**, *44*, 5592–5629.
11. Clark, T. D.; Tien, J.; Duffy, D. C.; Paul, K. E.; Whitesides, G. M. *J. Am. Chem. Soc.* **2001**, *123*, 7677–7682.
12. Hurst, S. J.; Pyne, E. K.; Qin, L.; Mirkin, C. A. *Angew. Chem., Int. Ed.* **2006**, *45*, 2672–2692.
13. Ulman, A. *Chem. Rev.* **1996**, *96*, 1533–1554.
14. Mrksich, M. *Chem. Soc. Rev.* **2000**, *29*, 267–273.
15. Chechik, V.; Crooks, R. M.; Stirling, C. J. M. *Adv. Mater.* **2000**, *12*, 1161–1171.
16. Sullivan, T. P.; Huck, W. T. S. *Eur. J. Org. Chem.* **2003**, 17–29.
17. Love, J. C.; Estroff, L. A.; Kriebel, J. K.; Nuzzo, R. G.; Whitesides, G. M. *Chem. Rev.* **2005**, *105*, 1103–1169.
18. Onclin, S.; Ravoo, B. J.; Reinhoudt, D. N. *Angew. Chem., Int. Ed.* **2005**, *44*, 6282–6304.
19. Haensch, C.; Hoeppener, S.; Schubert, U. S. *Chem. Soc. Rev.* **2010**, *39*, 2323–2334.
20. Herzer, N.; Hoeppener, S.; Schubert, U. S. *Chem. Commun.* **2010**, *46*, 5634–5652.
21. Prucker, O.; Rühe, J. *Macromolecules* **1998**, *31*, 592–601.
22. Prucker, O.; Rühe, J. *Macromolecules* **1998**, *31*, 602–613.
23. Sui, X.; Zapotoczny, S.; Benetti, E. M.; Schön, P.; Vancso, G. J. *J. Mater. Chem.* **2010**, *20*, 4981–4993.
24. Matyjaszewski, K.; Xia, J. *Chem. Rev.* **2001**, *101*, 2921–2990.
25. Kamigaito, M.; Ando, T.; Sawamoto, M. *Chem. Rev.* **2001**, *101*, 3689–3745.
26. Rizzardo, E.; Chiefari, J.; Mayadunne, R. T. A.; Moad, G.; Thang, S. H. In *Controlled/Living Radical Polymerization*; Matyjaszewski, K., Ed.; ACS Symposium Series 768; American Chemical Society: Washington, DC, 2000; p 278.
27. Hawker, C. J.; Bosman, A. W.; Harth, E. *Chem. Rev.* **2001**, *101*, 3661–3688.
28. Studer, A.; Schulte, T. *Chem. Rec.* **2005**, *5*, 27–35.
29. Studer, A. *Chem. Soc. Rev.* **2004**, *33*, 267–273.
30. Brinks, M. K.; Studer, A. *Macromol. Rapid Commun.* **2009**, *30*, 1043–1057.
31. Steenackers, M.; Lud, S. Q.; Niedermeier, M.; Bruno, P.; Gruen, D. M.; Feulner, P.; Stutzmann, M.; Garrido, J. A.; Jordan, R. *J. Am. Chem. Soc.* **2007**, *129*, 15655–15661.

32. Schmelmer, U.; Jordan, R.; Geyer, W.; Eck, W.; Golzhäuser, W.; Grunze, M.; Ulmann, A. *Angew. Chem., Int. Ed.* **2003**, *42*, 559–563.
33. Schmelmer, U.; Paul, A.; Küller, A.; Grunze, M.; Jordan, R. *Small* **2007**, *3*, 459–465.
34. Steenackers, M.; Küller, A.; Ballav, N.; Zharnikov, M.; Grunze, M.; Jordan, R. *Small* **2007**, *3*, 1764–1773.
35. Liu, X.; Guo, S.; Mirkin, C. A. *Angew. Chem., Int. Ed.* **2003**, *42*, 4785–4788.
36. Jones, D. M.; Smith, J. R.; Huck, W. T. S.; Alexander, C. *Adv. Mater.* **2002**, *14*, 1130–1134.
37. Dronavajjala, K. D.; Rajagopalan, R.; Uppili, S.; Sen, A.; Allara, D. L.; Foley, H. C. *J. Am. Chem. Soc* **2006**, *128*, 13040–13041.
38. Hirtz, M.; Brinks, M. K.; Miele, S.; Studer, A.; Fuchs, H.; Chi, L. *Small* **2009**, *5*, 919–923.
39. Wagner, H.; Li, Y.; Hirtz, M.; Chi, L.; Fuchs, H.; Studer, A. *Soft Matter* **2011**, *7*, 9854–9858.
40. For an alternative bottom up approach, see Brinks, M. K.; Hirtz, M.; Chi, L. F.; Fuchs, H.; Studer, A. *Angew. Chem., Int. Ed.* **2007**, *46*, 5231−5233.
41. Jonkheijm, P.; Weinrich, D.; Schröder, H.; Niemeyer, C. M.; Waldmann, H. *Angew. Chem., Int. Ed.* **2008**, *47*, 9618–9647.
42. Cao, Z.; Brault, N.; Xue, H.; Keefe, A.; Jiang, S. *Angew. Chem., Int. Ed.* **2011**, *50*, 6102–6104.
43. Ahmad, S. A.; Hucknall, A.; Chilkoti, A.; Leggett, G. J. *Langmuir* **2010**, *26*, 9937.
44. Cai, Y.; Newby, B.-m. Z. *Langmuir* **2008**, *24*, 5202–5208.
45. Fischer, H. *Chem. Rev.* **2001**, *101*, 3581–3610.
46. Studer, A. *Chem. Eur. J.* **2001**, *7*, 1159–1164.
47. Lehn, J. M. *Prog. Polym. Sci.* **2005**, *30*, 814–831.
48. Corbett, P. T.; Leclaire, J.; Vial, L.; West, K. R.; Wietor, J. L.; Sanders, J. K. M.; Otto, S. *Chem. Rev.* **2006**, *106*, 3652–3711.
49. Rowan, S. J.; Cantrill, S. J.; Cousins, G. R. L.; Sanders, J. K. M.; Stoddart, J. F. c *Angew. Chem., Int. Ed.* **2002**, *41*, 898–952.
50. Hawker, C. J.; Barclay, G. G.; Dao, J. L. *J. Am. Chem. Soc.* **1996**, *118*, 11467–11471.
51. Turro, N. J.; Lem, G.; Zavarine, I. S. *Macromolecules* **2000**, *33*, 9782–9785.
52. Ballesteros, O. G.; Maretti, L.; Sastre, R.; Scaiano, J. C. *Macromolecules* **2001**, *34*, 6184–6187.
53. Otsuka, H.; Aotani, K.; Higaki, Y.; Takahara, A. *Chem. Commun.* **2002**, 2838–2839.
54. Otsuka, H.; Aotani, K.; Higaki, Y.; Takahara, A. *J. Am. Chem. Soc.* **2003**, *125*, 4064–4065.
55. Higaki, Y.; Otsuka, H.; Takahara, A. *Macromolecules* **2004**, *37*, 1696–1701.
56. Yamaguchi, G.; Higaki, Y.; Otsuka, H.; Takahara, A. *Macromolecules* **2005**, *38*, 6316–6320.
57. Higaki, Y.; Otsuka, H.; Takahara, A. *Macromolecules* **2006**, *39*, 2121–2125.
58. Jhaveri, S. B.; Beinhoff, M.; Hawker, C J.; Carter, K R.; Sogah, D. Y. *ACS Nano* **2008**, *2*, 719–727.

59. Kulis, J.; Bell, C. A.; Micallef, A. S.; Jia, Z.; Monteiro, M. J. *Macromolecules* **2009**, *42*, 8218–8227.
60. Amamoto, Y.; Kikuchi, M.; Masunaga, H.; Sasaki, S.; Otsuka, H.; Takahara, A. *Macromolecules* **2010**, *43*, 1785–1791.
61. Amamoto, Y.; Kikuchi, M.; Otsuka, H.; Takahara, A. *Macromolecules* **2010**, *43*, 5470–5473.
62. Schulte, B.; Tsotsalas, M.; Becker, M.; Studer, A.; De Cola, L. *Angew. Chem., Int. Ed.* **2010**, *49*, 6881–6884.
63. Vogler, T.; Studer, A. *Synthesis* **2008**, 1979–1933.
64. Wagner, H.; Brinks, M. K.; Hirtz, M.; Schäfer, A.; Chi, L.; Studer, A. *Chem. Eur. J.* **2011**, *17*, 9107–9112.
65. Calzaferri, G.; Devaux, A. In *Supramolecular Effects in Photochemical and Photophysical Processes*; Ramamurthy, V., Inoue, Y., Eds.; Wiley: New York, 2010.
66. Megelski, S.; Calzaferri, G. *Adv. Funct. Mater.* **2001**, *11*, 277.
67. Popovic, Z.; Otter, M.; Calzaferri, G.; De Cola, L. *Angew. Chem., Int. Ed.* **2007**, *46*, 6188.
68. Busby, M.; Kerschbaumer, H.; Calzaferri, G.; De Cola, L. *Adv. Mater.* **2008**, *20*, 1614.
69. Marque, S.; Fischer, H.; Baier, E.; Studer, A. *J. Org. Chem.* **2001**, *66*, 1146–1156.
70. Beckwith, A.; Bowry, V.Ingold, K. *J. Am. Chem. Soc.* **1992**, *114*, 4983–4996.
71. Studer, A. *Angew. Chem., Int. Ed.* **2000**, *39*, 1108–1111.
72. Tebben, L.; Studer, A. *Angew. Chem., Int. Ed.* **2011**, *50*, 5034–5068.
73. Becker, M.; De Cola, L.; Studer, A. *Chem. Commun.* **2011**, *47*, 3392–3394.

Downloaded by UNIV OF GUELPH LIBRARY on June 1, 2012 | http://pubs.acs.org
Publication Date (Web): March 20, 2012 | doi: 10.1021/bk-2012-1101.ch017

Chapter 17

Surface Modification of Spherical Particles with Bioactive Glycopolymers

André Pfaff and Axel H. E. Müller[*]

Makromolekulare Chemie II, Universität Bayreuth,
95440 Bayreuth, Germany
[*]E-mail: Axel.Mueller@uni-bayreuth.de

We report the generation of novel nano- and micrometer sized glycopolymer-grafted spheres, whereby controlled radical polymerization methods, namely reversible addition fragmentation chain transfer (RAFT) and atom transfer radical polymerization (ATRP), were utilized in order to synthesize glycopolymers. The interactions of these particles with various lectins were investigated to understand the effect of the specific carbohydrate that was incorporated into the polymer chain, and the architecture of the polymer chain itself. Furthermore, carbohydrate-protein interactions facilitate the cellular uptake of carbohydrate functionalized particles that might find application as cellular imaging probes.

Introduction

Despite the enormous importance due to their appearance as food, biomass and raw materials, natural polysaccharides play a major role in many recognition effects, which is the key to a multitude of biological processes, such as embryogenesis, immune defense, microbial and viral infection and cancer metastasis (*1*, *2*). Glycopolymers, synthetic sugar-bearing macromolecules, which

In Progress in Controlled Radical Polymerization: Materials and Applications; Matyjaszewski, K., et al.;
ACS Symposium Series; American Chemical Society: Washington, DC, 2012.

display complex functionalities similar to those found in natural glycoconjugates, are attracting ever-increasing interest from the chemistry community due to their role as biomimetic analogues and their potential for commercial applications. The polymerization of glycomonomers can be carried out by a myriad of polymerization methods, such as free-radical polymerization (FRP) (*3–8*), ionic polymerization (*9*, *10*), ring-opening polymerization (ROP) (*11*, *12*), and controlled/“living” radical polymerization (CLRP). The latter include reversible addition-fragmentation chain transfer polymerization (RAFT) (*13–20*), atom transfer radical polymerization (ATRP) (*21–25*), and nitroxide mediated polymerization (NMP) (*26–30*). Applying these techniques led to a library of linear glycopolymers bearing various carbohydrate moieties that show an interesting behavior in matters of bioactivity and biorecognition towards proteins. However, their use for applications regarding biosensors or drug delivery is often limited. This prompted researchers to synthesize diblock copolymers, in particular amphiphilic diblock copolymers containing a hydrophilic glycopolymer block and a hydrophobic block that can self-assemble into more complex structures. Emphasis was put in the synthesis of block copolymers containing glycopolymers and water-insoluble (*31–34*) or pH-/temperature-responsive polymers (*35–37*) which self-assemble into micelles in aqueous solution.

Beside the self-assembly of glycocopolymers, other synthetic strategies were performed to have access to globular glycomacromolecules. Glycostars were prepared using the core-first method, either RAFT polymerization or ATRP and multiple initiator group bearing compounds (*18*, *38–42*). Furthermore, branched and hyperbranched glycopolymers have been prepared by the self-condensing vinyl copolymerization (SCVCP) of an acrylic or methacrylic initiator-monomer and glucose-containing glycomonomer (*22*, *43*), ring-opening multibranching polymerization of anhydro carbohydrates (*44*) and the ‘Strathclyde method’ (*45*). SCVCP was furthermore utilized for the modification of solid surfaces. By this, the grafting of highly branched glycopolymers from the surface of silicon wafers and multiwalled carbon nanotubes (MWCNTs) was accomplished (*46*, *47*).

The highly specific lock-and-key interactions between carbohydrates and lectins are usually weak but can be strongly increased due to the multivalent effect of clustered saccharides, known as the “glyco-cluster effect” (*48–51*). The interactions between glycopolymers and lectins are influenced by the density of the sugar molecules as well as the rigidity, architecture and molecular weight of the polymer. Therefore, micellar aggregates and other complex architectures can display a much higher binding affinity toward binding lectins which is caused by an increased surface area of spherical and three dimensional structures. Additionally, as lectins are ubiquitously present on cell surfaces and take place in recognition effects, the incorporation of carbohydrate-bearing ligands can lead to an increased cellular uptake of desired drugs or imaging tools via receptor-mediated endocytosis (*52–56*).

In the following we describe the synthesis of nano- and micrometer sized glycopolymer-grafted particles and their recognition behavior toward lectins and human lung cancer cells.

Downloaded by UNIV OF GUELPH LIBRARY on June 1, 2012 | http://pubs.acs.org
Publication Date (Web): March 20, 2012 | doi: 10.1021/bk-2012-1101.ch017

Downloaded by UNIV OF GUELPH LIBRARY on June 1, 2012 | http://pubs.acs.org
Publication Date (Web): March 20, 2012 | doi: 10.1021/bk-2012-1101.ch017

Results and Discussion

Glycopolymer-Grafted Polystyrene Nanospheres

Sugar-containing colloidal spherical polymer brushes were prepared by two different polymerization approaches. Photopolymerization and ATRP were used to attach glucose- and acetylglucosamine-displaying chains to polystyrene nanospheres by a "grafting from" approach. The synthesis of these particles was carried out in three steps: PS core particles were prepared by a conventional emulsion polymerization followed by the incorporation of an initiator and subsequent polymerization of the glycomonomer. A representative example for the synthesis of acetylglucosamine-displaying spheres is depicted in Scheme 1.

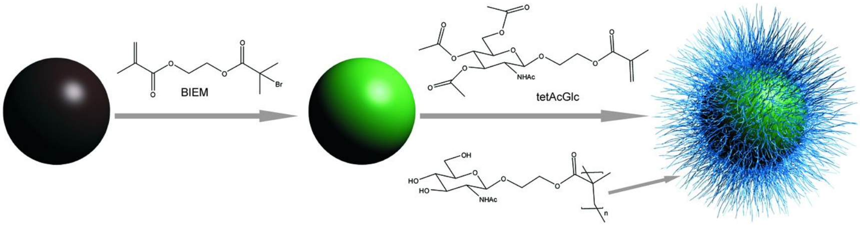

Scheme 1. Synthesis of the glucosamine-containing polymer brushes. After deprotection of the sugar moieties, hydrophilic sugar particles were obtained. (Reproduced with permission from reference (57). Copyright 2011 Wiley InterScience.)

In contrast to conventional radical polymerization, the surface initiated ATRP ensured the growth of well-defined glycopolymer chains from the particle surface (PDI = 1.12). Figure 1 shows FESEM images for pure PS-DVB particles (R_h = 50 nm) (A) and glycopolymer-grafted brushes (R_h = 102 nm) (B), respectively. The rough surface and the increase in diameter can be attributed to the grafted glycopolymer chains while the "grafting from" approach enabled a high grafting density of 0.54 chains per nm^2.

Deprotection of the sugar moieties yielded particles with a high density of hydroxy groups that could stabilize gold nanoparticles to generate carriers for catalytically active gold nanoparticles. The addition of $HAuCl_4$ to an aqueous solution of sugar containing polymer brushes and subsequent reduction of the $AuCl_4^-$ ions by $NaBH_4$ led to the formation of gold nanoparticles with an average diameter of 6.3 nm within the glycopolymer shell (Figure 1C). The catalytic reduction of *p*-nitrophenol in the presence of gold nanocomposite particles was successfully monitored by UV/vis spectroscopy (Figure 1E). The reaction follows first order rate kinetics with regard to the *p*-nitrophenol concentrations as the concentration of sodium borohydride was adjusted to largely exceed the concentration of *p*-nitrophenol. Thus, a linear relation between $\ln(c_t/c_0)$ versus time t has been obtained as shown in the inset of Figure 1E. This demonstrates the capability of the glycopolymer-displaying polymer brushes to act as biocompatible carriers for catalytically active gold nanoparticles.

Downloaded by UNIV OF GUELPH LIBRARY on June 1, 2012 | http://pubs.acs.org
Publication Date (Web): March 20, 2012 | doi: 10.1021/bk-2012-1101.ch017

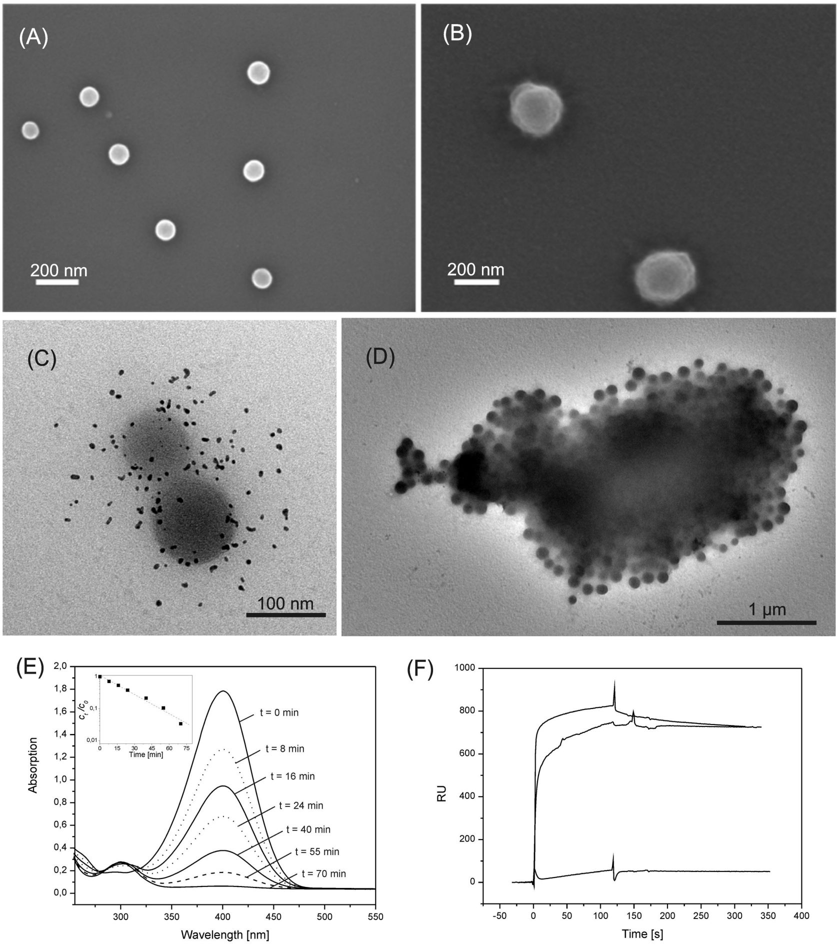

Figure 1. SEM images of (A) pure PS-DVB particles and (B) PS-DVB particles functionalized with protected glycopolymer brushes. TEM images of (C) immobilized gold nanoparticles and (D) WGA on glucosamine-displaying spheres. (E) UV/vis spectrum of catalytic reduction of p-nitrophenol in the presence of gold nanocomposite particles and $NaBH_4$. (F) SPR sensograms of the interaction between linear poly-(N-acetylglucosamine) chains (top curve), glycopolymer brushes (middle curve) and N-acetylglucosamine sugar unimer (bottom curve) with WGA. (Reproduced with permission from reference (57). Copyright 2011 Wiley InterScience.)

Investigation of the recognition properties of *N*-acetylglucosamine chains towards lectins via turbidity measurements revealed a selective binding toward the lectin wheat germ agglutinin (WGA) whereas no binding to bovine serum albumin (BSA) or peanut agglutinin (PNA) could be observed. Surface plasmon resonance (SPR) spectroscopy was performed to investigate the association behavior of linear poly(*N*-acetylglucosamine), glycopolymer brush and *N*-acetyl-glucosamine sugar unimer (Figure 1 F). In comparison to linear glycopolymers, spherical brushes show a reduced adsorption to the immobilized lectin, which can be attributed to the fact that the sugar residues next to the core are not available to bind the protein, due to steric hindrance, as well as the reduction of the total mass of sugar-units due to introduction of the polystyrene core. Nevertheless both show adsorptions magnitudes higher than the unimer.

Addition of WGA to the polymer brushes in solution led to the fast formation of large aggregates, whereby UV/vis spectroscopy measurements revealed that 1 mg of glycopolymer brush is able to precipitate 0.5 mg of wheat germ agglutinin. The lectin-polymer brush agglomerates are depicted in Figure 1D.

Downloaded by UNIV OF GUELPH LIBRARY on June 1, 2012 | http://pubs.acs.org
Publication Date (Web): March 20, 2012 | doi: 10.1021/bk-2012-1101.ch017

Surface Modification of Polymeric Microspheres Using Glycopolymers for Biorecognition

Research on core-shell microspheres covered with functional material is a topic of intense current research interest. Among others, cross-linked microspheres based on poly(divinylbenzene) (PDVB) are highly attractive because of their residual double bonds on the surface of the particle which can be easily used to attach single molecules or polymer chains to the surface by various grafting approaches. We report the synthesis of two glycopolymer-containing core-shell microspheres by grafting either 6-*O*-methacryloyl mannose (MAMan) (Scheme 2, path a) or 6-*O*-methacryloyl-1,2;3,4-di-*O*-isopropylidene-galactopyranose (MAIGal) (Scheme 2, path b) from the particle surface. In case of MAIGal, three different grafting approaches were utilised, with special emphasis being put on the resulting grafting densities.

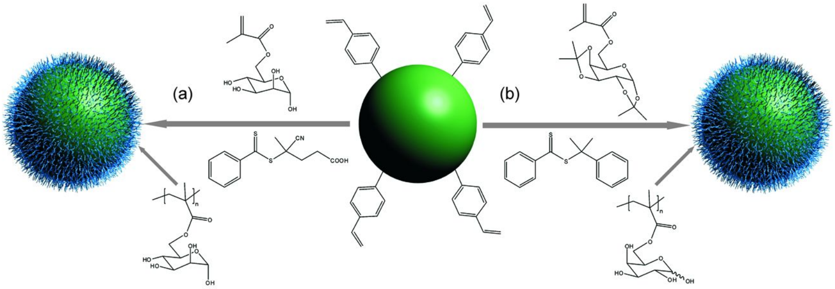

Scheme 2. Synthesis of glycopolymer-grafted DVB microspheres. (Reproduced with permission from reference (58). Copyright 2011 Elsevier.)

Without the use of protecting group chemistry, RAFT polymerization was the polymerization technique of choice to yield well-defined unprotected PMAMan glycopolymers. Applying the "grafting through" approach, PDVB microspheres (diameter = 2.4 μm) covered with a dense shell of mannose-displaying glycopolymer were achieved. Glycopolymer chains were found to be densely grafted through the microspheres (0.43 chains per nm^2 surface area). Scanning electron microscopy (SEM) was used to visualize the particles before (Figure 2, left) and after (Figure 2, right) grafting glycomonomer from the surface. A much rougher surface can be observed in the case of the mannose covered microspheres.

Downloaded by UNIV OF GUELPH LIBRARY on June 1, 2012 | http://pubs.acs.org
Publication Date (Web): March 20, 2012 | doi: 10.1021/bk-2012-1101.ch017

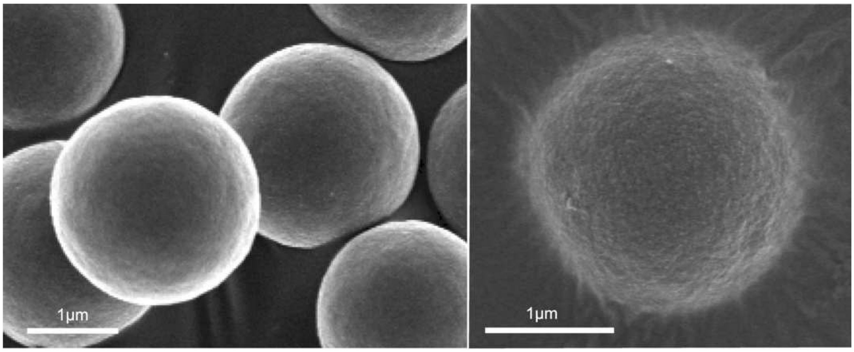

Figure 2. Scanning electron microscopy images of blank (left) and MAMan grafted (right) microspheres. (Reproduced with permission from reference (58). Copyright 2011 Elsevier.)

However, lectin interaction studies of mannose-containing polymer revealed no binding toward a series of lectins, suggesting that the esterification of the 6-carbon position of the mannose molecule to form the glycomonomer inhibited its binding to these proteins. Because of the loss of binding ability, we investigated the use of another glycomonomer based on a protected galactose unit for the preparation of sugar-containing microspheres.

For the preparation of the galactose covered spheres we performed three different approaches to affix glycopolymer chains to the particle surface, whereby RAFT polymerization has been used to prepare the glycopolymer chains. Approach 1 was conducted in a similar way to the preparation of the mannose containing microspheres. This “grafting through” technique yielded galactose-displaying particles with a grafting density of 0.22 chains per nm^2. Approach 2, a “grafting from” approach, consisted of prior modification of the particle surface by attaching the chain transfer agent. The calculation of the grafting density led to a surface coverage of 0.35 chains per nm^2, a 1.6 times higher grafting density compared to the first approach. In Approach 3, a strict “grafting onto” technique was used. The use of thiol-ene chemistry showed the lowest grafting density (0.20 chains per nm^2).

After deprotection of the sugar moieties, the galactose-displaying polymer displayed selective binding towards *Ricinus communis* agglutinin (RCA_{120}) whereas no binding to Concanavalin A (Con A) or Bovine serum albumin (BSA) occurred. UV/vis spectroscopy measurements revealed that each grafted glycopolymer chain is capable of binding to 0.7 molecules of RCA_{120}. The particles were found to have a superior binding affinity towards RCA_{120} in comparison to microspheres covered with galactose unimers (*59*). Even though galactose units next to the core are not accessible for binding, the overall amount of bound lectin is four times higher.

In Progress in Controlled Radical Polymerization: Materials and Applications; Matyjaszewski, K., et al.;
ACS Symposium Series; American Chemical Society: Washington, DC, 2012.

Hyperbranched Glycopolymer-Grafted Microspheres

To investigate the influence of the glycopolymer architecture toward the binding affinity to WGA we created core-shell particles covered with three-dimensional glycopolymer structures. The synthesis of highly branched glycopolymers was achieved by atom transfer radical polymerization (ATRP) of the methacrylic AB* initiator-monomer (inimer) 2-(2-bromoisobutyryloxy)ethyl methacrylate (BIEM) and the protected methacrylic acetylglucosamine-displaying glycomonomer 1-methacryloyloxyethyl 2-acetamido-2-deoxy-3,4,6-triacetyl-glucopyranoside (tetAcGlc) via self-condensing vinyl copolymerization (SCVCP) as depicted in Scheme 3.

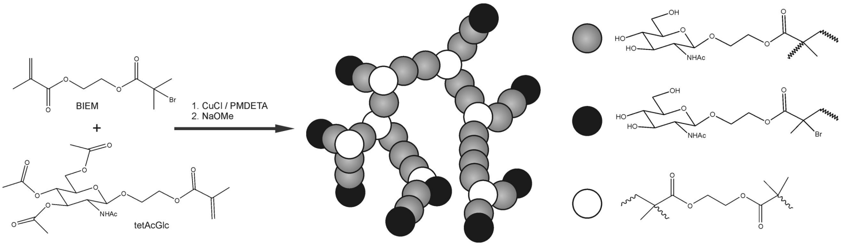

Scheme 3. General Route towards branched glycopolymers via SCVCP. (Reprinted with permission from reference (60). Copyright 2011 American Chemical Society.)

Prior to the surface grafting of hyperbranched glycopolymers to PDVB microspheres, the formation of ungrafted hyperbranched glycopolymers of different glycomonomer-to-inimer ratios (γ) via SCVCP was investigated. First-order kinetic plots of the prepared branched glycopolymers revealed a decreasing apparent rate of polymerization k_{app} with increasing content of BIEM in the feed (Figure 3). Although more initiator groups were introduced with decreasing γ, the lower k_{app} indicates a fast formation of macroinimers but slow condensation of these macroinimers with each other.

The successful pathway towards hyperbranched glycopolymers was adapted to create core-shell particles consisting of PDVB microspheres (diameter = 1.5 μm) onto which hyperbranched polymers have been grafted (Scheme 4, path b). Furthermore, microspheres covered with linear acetylglucosamine-displaying polymer have been prepared via ATRP (Scheme 4, path a) to compare the different particles in terms of surface coverage and binding affinity towards WGA.

After elemental analysis of the different polymer grafted spheres to determine the oxygen content, one can calculate the amount of grafted copolymer. It was found, that an increase in incorporated inimer, which results in more compact and branched structures, directly leads to an increase in particle coverage (1.6 – 2.4 wt.-%).

Deprotection of the sugar moieties led to acetylglucosamine-displaying spheres that could be easily dispersed in water and therefore enabled the

Downloaded by UNIV OF GUELPH LIBRARY on June 1, 2012 | http://pubs.acs.org
Publication Date (Web): March 20, 2012 | doi: 10.1021/bk-2012-1101.ch017

Downloaded by UNIV OF GUELPH LIBRARY on June 1, 2012 | http://pubs.acs.org
Publication Date (Web): March 20, 2012 | doi: 10.1021/bk-2012-1101.ch017

investigation of the binding behavior of these sugar-covered microspheres toward the lectin WGA. UV/vis spectroscopy measurements revealed that with increasing content of BIEM in the copolymer, the amount of adsorbed protein per mg of grafted acetylglucosamine on the sphere increased. The incorporation of approximately 50% of the hydrophobic linker BIEM for $\gamma = 1$ led to an increase in adsorption of 26% compared to the branched glycopolymer with $\gamma = 5$ and 16% compared to the linear glycopolymer grafted particles.

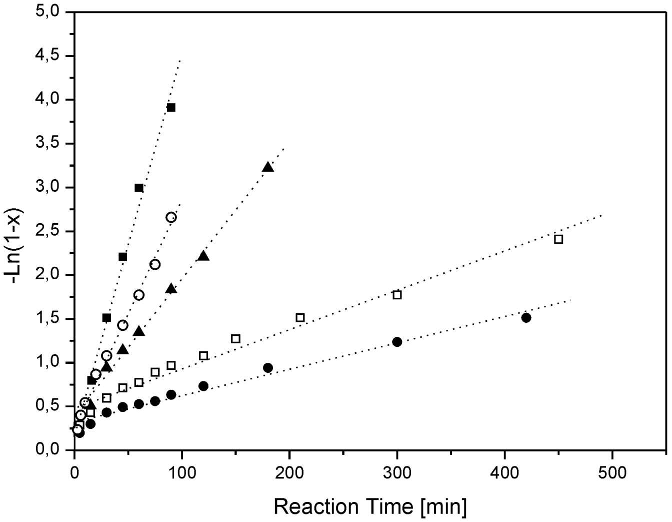

Figure 3. First-order kinetic plots for the SCVCP of BIEM and tetAcGlc at different comonomer ratios γ. Filled squares $\gamma = 15$, filled triangles: $\gamma = 5$, open squares: $\gamma = 2$ and filled circles: $\gamma = 1$. The ATRP of linear PtetAcGlc with a monomer to initiator ratio $[tetAcGlc]_0/[EBIB]_0 = 100$ is given for comparison (open circles). (Reprinted with permission from reference (60). Copyright 2011 American Chemical Society.)

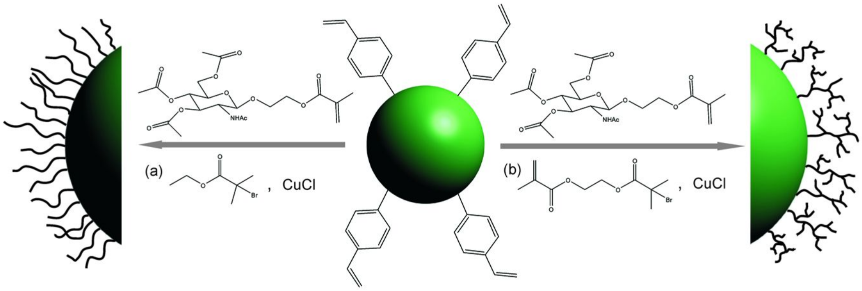

Scheme 4. Synthesis of linear (path a) and hyperbranched (path b) glycopolymer covered microspheres. (Reprinted with permission from reference (60) Copyright 2011 American Chemical Society.)

Downloaded by UNIV OF GUELPH LIBRARY on June 1, 2012 | http://pubs.acs.org
Publication Date (Web): March 20, 2012 | doi: 10.1021/bk-2012-1101.ch017

SEM images of the ungrafted and grafted microspheres are shown in Figure 4. After adsorption of wheat germ agglutinin, more organic matter covered the spheres, and marked agglutination of the spheres is clearly visible.

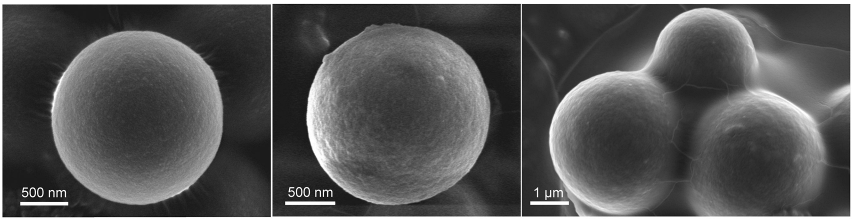

Figure 4. SEM images of (left) ungrafted and glycopolymer grafted (γ = 1) microspheres (middle) before and (right) after addition of wheat germ agglutinin. (Reprinted with permission from reference (60). Copyright 2011 American Chemical Society.)

Magnetic and Fluorescent Glycopolymer Hybrid Nanoparticles for Intranuclear Optical Imaging

The successful synthesis of fluorescent and magnetic galactose-displaying core-shell nanospheres by grafting a glycocopolymer consisting of 6-*O*-methacryloyl-galactopyranose (MAGal) and 4-(pyrenyl)butyl methacrylate (PyMA) onto silica-encapsulated iron oxide particles (diameter = 58 nm) (Scheme 5) is reported in the following. The surface modification of functional particles with carbohydrates should not only improve the biocompatibility and solubility, but also have an influence on the cellular uptake of the particles.

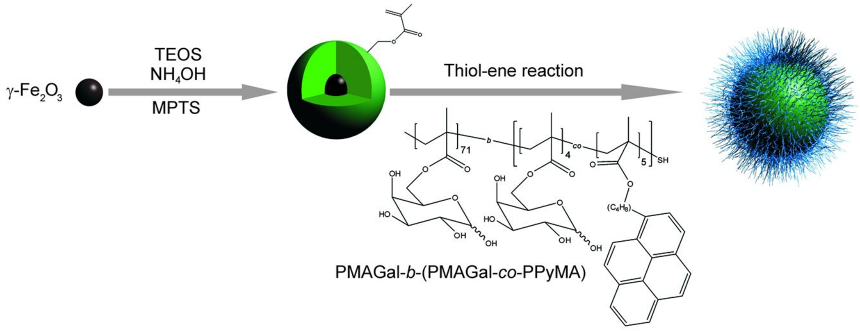

Scheme 5. Synthesis of glycopolymer-grafted magnetic, fluorescent nanoparticles. (Reprinted with permission from reference (61). Copyright 2011 American Chemical Society.)

To create a fluorescent glycopolymer that can be attached onto silica spheres, we performed sequential RAFT polymerization of a protected glycomonomer and a fluorescent pyrene-carrying methacrylate, followed by the deprotection of the sugar moieties under acidic conditions. After aminolysis of the RAFT agent, the formed thiol end group is able to react with the double-bond bearing silica particles via Michael addition. The successful attachment of the fluorescent glycocopolymer chains to the surface of the magnetic silica spheres was confirmed by UV/vis spectroscopy measurements and vibrating sample magnetometry (VSM, Figure 5). The resulting magnetization curves indicate that neither the encapsulation of the maghemite particles with silica nor the grafting of glycocopolymer chains had a significant influence on the superparamagnetic properties.

Downloaded by UNIV OF GUELPH LIBRARY on June 1, 2012 | http://pubs.acs.org
Publication Date (Web): March 20, 2012 | doi: 10.1021/bk-2012-1101.ch017

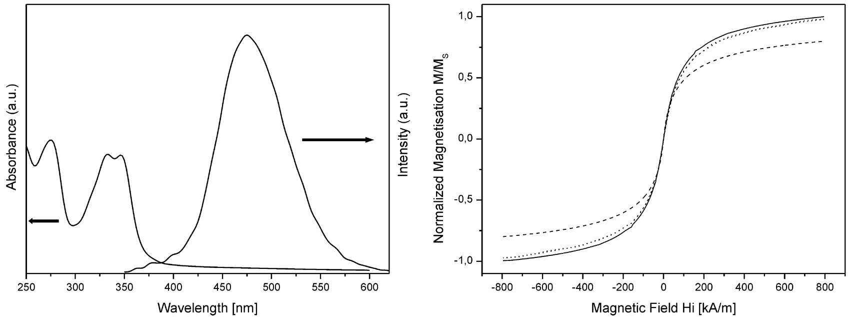

Figure 5. (Left) UV/vis absorption and fluorescence spectra of glycocoplymer-grafted nanospheres. (Right) Magnetic hysteresis curves of γ-Fe_2O_3 nanoparticles (solid line), silica encapsulated γ-Fe_2O_3 particles (dotted line) and glycocoplymer grafted nanospheres (dashed line). (Reprinted with permission from reference (61). Copyright 2011 American Chemical Society.)

The incorporation of pyrene into the core-shell particles allows their localization within cells by microscopy experiments as pyrene is a fluorescent dye with a high quantum yield and is stable against photobleaching. The cellular uptake of the silica particles in adenocarcinomic human alveolar basal epithelial cells (A549) was investigated, a cell line that expresses sugar binding proteins such as galectin. In fact the particles could be localised in A549 cells using both epifluorescence and confocal microscopy. Moreover, epifluorescence microscopy images (Figure 6, A-D) showed the preferential location of the nanospheres next to and within the cell nucleus, the membrane of which was stained with anti-NUP98-FITC (Figure 6 C and F). Confocal microscopy experiments confirmed the presence of the glycocopolymer grafted magnetic particles within the cell nucleus (Figure 6, E-G); confocal z-stacks proved that the particles were indeed located inside the cells and not stacked to the cell surface.

Downloaded by UNIV OF GUELPH LIBRARY on June 1, 2012 | http://pubs.acs.org
Publication Date (Web): March 20, 2012 | doi: 10.1021/bk-2012-1101.ch017

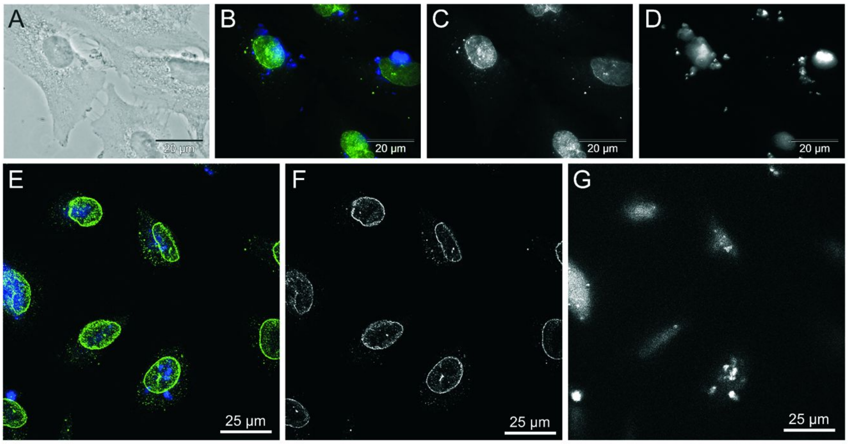

Figure 6. Microscope images of A549 cells exposed to glycopolymer-grafted nanoparticles: (A-D) epifluorescence microscope, (E-G) confocal microscope. (A) transmission image of cells, (B, E) merged fluorescence images, (C, F) fluorescence image that exclusively shows the green light emitting parts (nuclear membrane) and (D, G) blue (pyrene) emitting part (glycocopolymer covered nanospheres). (Reprinted with permission from (61). Copyright 2011 American Chemical Society.)

As both glycoconjugates and carbohydrate-binding proteins are omnipresent in the cytoplasm and the nucleus, the galactose moieties in the outer sphere of the nanoparticle could have caused their nuclear uptake. A member of the galectin family, known for its binding affinity towards β-galactosides, might be the responsible lectin in this context.

Summary

Glycopolymers containing different kinds of carbohydrates were grafted from various spherical templates, whereby the glycopolymer chains were prepared via controlled radical polymerization techniques, namely ATRP and RAFT. A library of carbohydrate-displaying spheres and their interaction with lectins is presented. The particles were not only able to stabilize gold nanoparticles to form catalytically active hybrid particles but show selective binding toward lectins whereby the binding affinity of the protein to the glycopolymer was found to be much higher than to sugar unimers. Furthermore, by creating branched architectures it was shown that the three-dimensional glycopolymer topography directly affects the strength of the key-lock interaction of sugar and sugar-binding protein. Silica particles with a carbohydrate-containing shell could furthermore be localized not only in the cytoplasm but also in the nucleus of human lung cancer cells. This cell line expresses a galactose-binding protein, galectin-1, which indicates that carbohydrate-lectin interactions are responsible for the uptake of the functionalized particles. Since the overexpression of galectin-1 in tumor tissues is considered as a sign of the malignant tumor growth, glycopolymer-covered particles might be applicable as therapeutic tools.

Acknowledgments

This work was supported by the European Science Foundation within the SONS 2 program (project BioSONS) and the Australian Research Council (ARC, Discovery Grant DP0877122). Vaishali Shinde, Yan Lu, Alexander Wittemann, Matthias Ballauff, Leonie Barner, Anthony Granville, Anja Schallon, Thomas Ruhland, Alexander Majewski, Holger Schmalz and Ruth Freitag are grateful acknowledged for their contribution to this work. We thank Marietta Böhm, Andreas Hanisch and Susanne Edinger for GPC and MALDI-ToF MS measurements, respectively. Furthermore, Markus Müllner and André Gröschel are gratefully thanked for fruitful discussions.

Downloaded by UNIV OF GUELPH LIBRARY on June 1, 2012 | http://pubs.acs.org
Publication Date (Web): March 20, 2012 | doi: 10.1021/bk-2012-1101.ch017

References

1. Dwek, R. A. *Chem. Rev.* **1996**, *96*, 683.
2. Sharon, N.; Lis, H. *Sci. Am.* **1993**, *268*, 82.
3. Furuike, T.; Nishi, N.; Tokura, S.; Nishimura, S.-I. *Macromolecules* **1995**, *28*, 7241.
4. Miura, Y.; Ikeda, T.; Kobayashi, K. *Biomacromolecules* **2003**, *4*, 410.
5. Miura, Y.; Sato, H.; Ikeda, T.; Sugimura, H.; Takai, O.; Kobayashi, K. *Biomacromolecules* **2004**, *5*, 1708.
6. Miyachi, A.; Dohi, H.; Neri, P.; Mori, H.; Uzawa, H.; Seto, Y.; Nishida, Y. *Biomacromolecules* **2009**, *10*, 1846.
7. Nagahori, N.; Nishimura, S.-I. *Biomacromolecules* **2000**, *2*, 22.
8. Yoshizumi, A.; Kanayama, N.; Maehara, Y.; Ide, M.; Kitano, H. *Langmuir* **1998**, *15*, 482.
9. Loykulnant, S.; Hirao, A. *Macromolecules* **2000**, *33*, 4757.
10. Yamada, K.; Yamaoka, K.; Minoda, M.; Miyamoto, T. *J. Polym. Sci., Part A: Polym. Chem.* **1997**, *35*, 255.
11. Aoi, K.; Tsutsumiuchi, K.; Aoki, E.; Okada, M. *Macromolecules* **1996**, *29*, 4456.
12. Tsutsumiuchi, K.; Aoi, K.; Okada, M. *Macromolecules* **1997**, *30*, 4013.
13. Albertin, L.; Cameron, N. R. *Macromolecules* **2007**, *40*, 6082.
14. Albertin, L.; Kohlert, C.; Stenzel, M.; Foster, L. J. R.; Davis, T. P. *Biomacromolecules* **2004**, *5*, 255.
15. Albertin, L.; Stenzel, M. H.; Barner-Kowollik, C.; Davis, T. P. *Polymer* **2006**, *47*, 1011.
16. Albertin, L.; Stenzel, M. H.; Barner-Kowollik, C.; Foster, L. J. R.; Davis, T. P. *Macromolecules* **2004**, 7530.
17. Albertin, L.; Stenzel, M. H.; Barner-Kowollik, C.; Foster, L. J. R.; Davis, T. P. *Polymer* **2005**, *46*, 2831.

18. Bernard, J.; Favier, A.; Zhang, L.; Nilasaroya, A.; Davis, T. P.; Barner-Kowollik, C.; Stenzel, M. H. *Macromolecules* **2005**, *38*, 5475.
19. Lowe, A. B.; Sumerlin, B. S.; McCormick, C. L. *Polymer* **2003**, *44*, 6761.
20. Ting, S. R. S.; Gregory, A. M.; Stenzel, M. H. *Biomacromolecules* **2009**, *10*, 342.
21. Ladmiral, V.; Mantovani, G.; Clarkson, G. J.; Cauet, S.; Irwin, J. L.; Haddleton, D. M. *J. Am. Chem. Soc.* **2006**, *128*, 4823.
22. Muthukrishnan, S.; Jutz, G.; Andre, X.; Mori, H.; Müller, A. H. E. *Macromolecules* **2005**, *38*, 9.
23. Muthukrishnan, S.; Nitschke, M.; Gramm, S.; Oezyuerek, Z.; Voit, B.; Werner, C.; Mueller, A. H. E. *Macromol. Biosci.* **2006**, 658.
24. Ohno, K.; Tsujii, Y.; Fukuda, T. *J. Polym. Sci., Part A: Polym. Chem.* **1998**, *36*, 2473.
25. Vazquez-Dorbatt, V.; Maynard, H. D. *Biomacromolecules* **2006**, *7*, 2297.
26. Götz, H.; Harth, E.; Schiller, S. M.; Frank, C. W.; Knoll, W.; Hawker, C. J. *J. Polym. Sci., Part A: Polym. Chem.* **2002**, *40*, 3379.
27. Narumi, A.; Kakuchi, T. *Polym. J* **2008**, *40*, 383.
28. Narumi, A.; Matsuda, T.; Kaga, H.; Satoh, T.; Kakuchi, T. *Polymer* **2002**, *43*, 4835.
29. Ohno, K.; Fukuda, T.; Kitano, H. *Macromol. Chem. Phys.* **1998**, *199*, 2193.
30. Sun, X.-L.; Faucher, K. M.; Houston, M.; Grande, D.; Chaikof, E. L. *J. Am. Chem. Soc.* **2002**, *124*, 7258.
31. Cameron, N. R.; Spain, S. G.; Kingham, J. A.; Weck, S.; Albertin, L.; Barker, C. A.; Battaglia, G.; Smart, T.; Blanazs, A. *Faraday Discuss.* **2008**, *139*, 359.
32. Ramiah, V.; Matahwa, H.; Weber, W.; McLeary, J. B.; Sanderson, R. D. *Macromol. Symp.* **2007**, *255*, 70.
33. Suriano, F.; Pratt, R.; Tan, J. P. K.; Wiradharma, N.; Nelson, A.; Yang, Y.-Y.; Dubois, P.; Hedrick, J. L. *Biomaterials* **2010**, *31*, 2637.
34. Ting, S. R. S.; Min, E. H.; Escale, P.; Save, M.; Billon, L.; Stenzel, M. H. *Macromolecules* **2009**, *42*, 9422.
35. Chen, X. M.; Dordick, J. S.; Rethwisch, D. G. *Macromolecules* **1995**, 6014.
36. Hetzer, M.; Chen, G.; Barner-Kowollik, C.; Stenzel, M. H. *Macromol. Biosci.* **2010**, *10*, 119.
37. Zhang, L.; Bernard, J.; Davis, T. P.; Barner-Kowollik, C.; Stenzel, M. H. *Macromol. Rapid Commun.* **2008**, *29*, 123.
38. Bernard, J.; Hao, X.; Davis, T. P.; Barner-Kowollik, C.; Stenzel, M. H. *Biomacromolecules* **2006**, *7*, 232.
39. Dai, X.-H.; Dong, C.-M. *J. Polym. Sci., Part A: Polym. Chem.* **2008**, *46*, 817.
40. Qiu, S.; Huang, H.; Dai, X.-H.; Zhou, W.; Dong, C.-M. *J. Polym. Sci., Part A: Polym. Chem.* **2009**, *47*, 2009.
41. Zhang, L.; Stenzel, M. H. *Aust. J. Chem.* **2009**, *62*, 813.
42. Muthukrishnan, S.; Plamper, F.; Mori, H.; Müller, A. H. E. *Macromolecules* **2005**, *38*, 10631.
43. Muthukrishnan, S.; Mori, H.; Müller, A. H. E. *Macromolecules* **2005**, *38*, 3108.

Downloaded by UNIV OF GUELPH LIBRARY on June 1, 2012 | http://pubs.acs.org
Publication Date (Web): March 20, 2012 | doi: 10.1021/bk-2012-1101.ch017

44. Satoh, T.; Kakuchi, T. *Macromol. Biosci.* **2007**, *7*, 999.
45. Besenius, P.; Slavin, S.; Vilela, F.; Sherrington, D. C. *React. Funct. Polym.* **2008**, *68*, 1524.
46. Gao, C.; Muthukrishnan, S.; Li, W.; Yuan, J.; Xu, Y.; Müller, A. H. E. *Macromolecules* **2007**, *40*, 1803.
47. Muthukrishnan, S.; Erhard, D. P.; Mori, H.; Müller, A. H. E. *Macromolecules* **2006**, *39*, 2743.
48. Kiessling, L. L.; Pohl, N. L. *Chem. Biol.* **1996**, *3*, 71.
49. Lee, Y. C. *FASEB J.* **1992**, *6*, 3193.
50. Lundquist, J. J.; Toone, E. J. *Chem. Rev.* **2002**, *102*, 555.
51. Mammen, M.; Choi, S. K.; Whitesides, G. M. *Angew. Chem., Int. Ed.* **1998**, *37*, 2754.
52. David, A.; Kopecková, P.; Kopecek, J.; Rubinstein, A. *Pharm. Res.* **2002**, *19*, 1114.
53. David, A.; Kopecková, P.; Rubinstein, A.; Kopecek, J. *Bioconjugate Chem.* **2001**, *12*, 890.
54. Montet, X.; Funovics, M.; Montet-Abou, K.; Weissleder, R.; Josephson, L. *J. Med. Chem.* **2006**, *49*, 6087.
55. Shamay, Y.; Paulin, D.; Ashkenasy, G.; David, A. *J. Med. Chem.* **2009**, *52*, 5906.
56. Sliedregt, L. A. J. M.; Rensen, P. C. N.; Rump, E. T.; van Santbrink, P. J.; Bijsterbosch, M. K.; Valentijn, A. R. P. M.; van der Marel, G. A.; van Boom, J. H.; van Berkel, T. J. C.; Biessen, E. A. L. *J. Med. Chem.* **1999**, *42*, 609.
57. Pfaff, A.; Shinde, V. S.; Lu, Y.; Wittemann, A.; Ballauff, M.; Müller, A. H. E. *Macromol. Biosci.* **2011**, *11*, 199.
58. Pfaff, A.; Barner, L.; Müller, A. H. E.; Granville, A. M. *Eur. Polym. J.* **2011**, *47*, 805.
59. Diehl, C.; Schlaad, H. *Chem.−Eur. J.* **2009**, *15*, 11469.
60. Pfaff, A.; Müller, A. H. E. *Macromolecules* **2011**, *44*, 1266.
61. Pfaff, A.; Schallon, A.; Ruhland, T. M.; Majewski, A. P.; Schmalz, H.; Freitag, R.; Müller, A. H. E. *Biomacromolecules* **2011**, *12*, 3805.

Downloaded by UNIV OF GUELPH LIBRARY on June 1, 2012 | http://pubs.acs.org
Publication Date (Web): March 20, 2012 | doi: 10.1021/bk-2012-1101.ch017

Downloaded by OHIO STATE UNIV LIBRARIES on June 1, 2012 | http://pubs.acs.org
Publication Date (Web): March 20, 2012 | doi: 10.1021/bk-2012-1101.ch018

Chapter 18

Activity Control of Mussel Glue Derived Enzymes: A Study on Thermoresponsive Tyrosinase-PNIPAM Conjugates

**Patrick Wilke,[1] William L. A. Brooks,[2] Romina Kühnle,[1]
Brent Sumerlin,[2] and Hans G. Börner*,[1]**

**[1]Humboldt-Universität zu Berlin, Department of Chemistry,
Laboratory for Organic Synthesis of Functional Systems,
Brook-Taylor-Str. 2, D-12489 Berlin, Germany
[2]Southern Methodist University, Department of Chemistry,
3215 Daniel Avenue, Dallas, Texas 75275, USA
*E-mail: h.boerner@hu-berlin.de**

Protein-polymer conjugates are promising tools for biomedical, biotechnological or chemical applications. The conjugation of responsive polymers to enzymatically active proteins leads to promising bioconjugates, combing the solubility and processability of synthetic polymers with the complexity and selectivity of enzymes. The study investigates a bioconjugate of a mussel glue derived protein tyrosinase with thermoresponsive poly(*N*-isopropylacrylamide) (PNIPAM). While the switch-ability of PNIPAM was not altered, activity of the enzyme was preserved. Synergistic effects are achieved, showing a significant increase of enzyme activity of the bioconjugate at high temperatures compared to native enzyme

Introduction

Over the past decades peptide- and protein-modifications with synthetic polymers have become a valuable strategy to access polymer systems -referred to as bioconjugates- having highly complex functions (*1–5*). Already bioconjugates of polymers and sequence-defined oligopeptides exhibit interesting properties. Frequently, these are far advanced to those of commonly established block copolymers and useful for realizing functional nanostructures or nano electronics, but also for biomedical applications, *e. g.* drug or DNA delivery and bioactive systems (*6–13*). However, protein-polymer conjugates complement the properties of synthetic polymers by providing even more complex and specific functions such as enzymatic catalysis, transport of therapeutic entities, selective gating of small molecules through barriers, or efficient luminescence (*14–19*). The conjugation of synthetic polymers to proteins often proved to enhance protein functions by increasing stability, solubility, compatibility, and bioavailability (*20*). Traditionally, the field of bioconjugates has focused primarily on protein therapeutics, which represent a promising and intensively studied class of new drugs (*16*). Therapeutic polymer-protein conjugates usually include poly(ethylene oxide) (PEO or alternatively abbreviated as PEG). PEO conjugation or "PEG*ylation*" of proteins often reduces both proteolysis and immunogenic responses as well as increased clearance times by reducing renal elimination (*21*, *22*).

Recently, the field of catalytically active materials gained increasingly attention. Advances of green and white chemistry to substitute petrochemically based product-lines highlight enzymatic transformations as capable tools (*23*, *24*). This makes enzyme-polymer conjugates of high interest. Being introduced in 1976 this class of functional polymers quickly drew attention (*25*). Up to now, bioconjugates of a large variety of enzymes, as for instance trypsine, lysozyme, papain or horseradish peroxidase were investigated (*22*, *26–30*). Depending on number and position of attached polymers on an enzyme, the activity was either positively or negatively influenced, indicating the sensitivity of proteins.

Responsive polymers promise the control of enzymatic activity in protein-polymer conjugates based on external stimuli (*31–35*). Studies on responsive enzyme-polymer conjugates have been initiated by the intriguing work of Hoffman and coworkers (*36*). Enzyme activity control by temperature was realized by conjugating thermoresponsive polymers like poly(*N*-isopropylacrylamide) (PNIPAM) or poly(2-(2-methoxyethoxy)ethyl methacrylate) (PMEO$_2$MA) onto model enzymes (*32*, *34*, *37–41*). Sumerlin *et al.* demonstrated the conjugation of well-defined PNIPAM to the enzyme lysozyme (*35*, *42*, *43*). End-group functionalized PNIPAM was produced by reversible addition chain transfer radical polymerization (RAFT). Using a "grafting onto" strategy, PNIPAM selectively reacted with amino groups presented on the surface of the enzyme. The resulting conjugates showed the typical lower critical solution temperature (LCST) transition of PNIPAM. Lutz *et al.* synthesized and studied trypsin-PMEO$_2$MA conjugates, showing that the self-digestion of the enzyme could be significantly reduced, while preserving the LCST behavior of the switchable PMEO$_2$MA (*34*, *41*). The thermo responsive PMEO$_2$MA was synthesized by atom transfer radical polymerization (ATRP) (*44*) and exhibited hysteresis free LCST transitions (*41*).

Phenolases are one class of enzymes, which have received no attention in the field of protein-polymer conjugates. The non-modified enzymes, however, were studied extensively and proved to be suitable for a wide range of applications (*45*, *46*). One particular member of the class is the polyphenoloxidase tyrosinase, which is almost ubiquitary throughout nature (*47*). Tyrosinases are responsible

Downloaded by OHIO STATE UNIV LIBRARIES on June 1, 2012 | http://pubs.acs.org
Publication Date (Web): March 20, 2012 | doi: 10.1021/bk-2012-1101.ch018

Downloaded by OHIO STATE UNIV LIBRARIES on June 1, 2012 | http://pubs.acs.org
Publication Date (Web): March 20, 2012 | doi: 10.1021/bk-2012-1101.ch018

for melanin production in mammal skin (*48*). Most importantly, phenolases have been recognized as essential enzymes occurring in marine mussels and taking action within the process of mussel adhesive production and processing (*46*). Mussel glue still outperforms in many aspects technical adhesive compounds and thus, imposes inspiration for biomimetic glues, making tyrosinase an interesting candidate to study. Figure 1 summarizes the tyrosinase-mediated oxidation of *L*-tyrosine to *L*-dopaquinone, which is formed in a two step catalytic process. The monophenolase activity of tyrosinase catalyzes the *o*-hydroxylation of *L*-tyrosine subsequently forming the corresponding quinone in a secondary 2e$^-$ oxidation step (diphenolase activity) (*49*). Further and mostly auto-catalytic reactions lead to the oligomerization and melanin biopolymer formation.

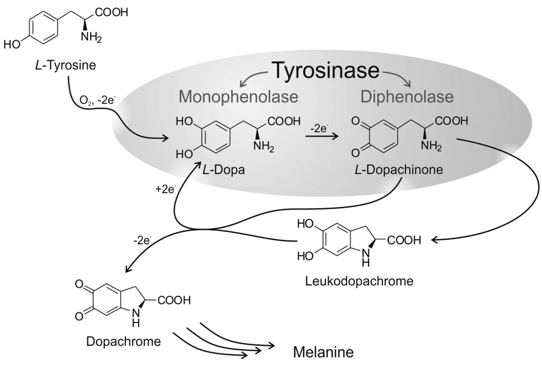

Figure 1. Role of tyrosinase in the biosynthetic pathway of melanin production.

Here, we report on the regulation of tyrosinase activity by conjugation of the thermoresponsive PNIPAM to phenolase tyrosinase. Due to the expense and sensitivity of the native enzyme, an increase in stability against thermal denaturation and the potential ease of recyclability was intended for the bioconjugate.

Experimental

Materials and Methods

Tyrosinase (≈ 4300 units/mg) from mushroom and *L*-tyrosine were purchased from Sigma-Aldrich. Tyrosinase was stored at -20°C. Azobisisobutyronitrile (AIBN, 98%, Aldrich) was recrystallized from ethanol, and *N*-isopropylacrylamide (NIPAM, TCI America) was recrystallized from hexane. *N*-hydroxysuccinimide (98%, Aldrich), and *N,N′*-dicyclohexylcarbodiimide

(DCC, PIERCE) were used as received. All other chemicals were purchased from VWR, Fisher or Sigma-Aldrich and used without further purification.

^{1}H nuclear magnetic resonance (^{1}H-NMR) spectra were recorded on a Bruker AV 500 spectrometer at 500 MHz in $CDCl_3$ at room temperature. UV-vis spectroscopy was performed on a Cary 100 Bio UV-vis spectrometer (Varian). Polymer molecular weights and molecular weight distributions were obtained by organic size exclusion chromatography (SEC) in *N,N*-dimethylformamide (DMF) with 50 mM LiBr at 55 °C using a flow rate of 1.0 mL min^{-1} (Viscotek SEC pump; columns: Agilent Technologies PolarGel-M 50 × 7.5 mm guard column and two Agilent Technologies PolarGel-M 300 × 7.5 mm mixed bed columns, for use up to 2×10^6 g/mol). Detection consisted of a Viscotek refractive index detector operating at λ = 660 nm, and a Viscotek model 270 series platform, consisting of a laser light scattering detector (operating at 3 mW, λ = 670 nm with detection angles of 7° and 90°) and a four-capillary viscometer. Molecular weights were determined by the triple detection method using a d*n*/d*c* = 0.077 mL g^{-1} for PNIPAM.

Enzymatic activity of tyrosinase and obtained bioconjugates was determined by standard activity assay according to supplier (Sigma-Aldrich) using UV-vis spectroscopy. Briefly the absorption (at 280 nm) of a 3 mL potassium phosphate (~17 mM, pH 6.5) buffered solution of 0.7 mM tyrosine containing 0.1 mL of approximately 100 units of tyrosinase in potassium phosphate buffer (50 mM, pH 6.5) was recorded for 20 min. For bioconjugate activity measurements, 50 µL (1/10 of total volume) of dissolved conjugates in potassium phosphate buffer (pH 6.5) were diluted with the same buffer to a final volume of 0.1 mL and subsequently added to 2.9 mL of 0.7 mM tyrosine. The maximal slope was determined for an interval of 3 min and used for activity calculation. Due to the lability of the enzyme, activity assays were carried out before every reaction.

Sodium dodecyl sulfate polyacrylamide gel electrophoresis (SDS Page) was carried out with commercially available Mini-Protean Precast Gels (4 –20 % Tris; Bio-Rad) using a Mini-PROTEAN® Tetra Cell (Bio-Rad) at constant 130 V for approx. 45 min. An equal concentration of the obtained conjugates was mixed with non-reducing lane marker (Fermentas) and calibrated against protein standards (10-170 kDa; Fermentas). Subsequent silver staining was carried out according to kit (Fermentas) procedure.

Temperature-dependent turbidity measurements were conducted on a TP1-J turbidimetric photometer (Tepper Analytik) operating at 670 nm. Free polymer and conjugates were dissolved (12 mg/mL) in potassium phosphate buffer (pH 6.5) and diluted with Millipore H_2O to a final concentration of 1 mg/ml. Buffer concentration was therefore set to 1/5 compared to enzymatic activity measurements. Data was obtained in a temperature range of 25-50 °C with a heating rate of 1 °C/min. For every sample, measurements were repeated twice.

Circular dichroism UV (CD) measurements were conducted on a Jasco J-710 Spectropolarimeter with a Jasco PTC-4235/15 temperature control unit. Tyrosinase (0.25 mg/mL) was dissolved in potassium phosphate buffer (17 mM, pH 6.5). The enzyme was heated to a certain temperature and incubated for 10 minutes. Spectra were recorded five times within a range of 250 - 190 nm using a sample cell with 1.0 mm width.

Downloaded by OHIO STATE UNIV LIBRARIES on June 1, 2012 | http://pubs.acs.org
Publication Date (Web): March 20, 2012 | doi: 10.1021/bk-2012-1101.ch018

Downloaded by OHIO STATE UNIV LIBRARIES on June 1, 2012 | http://pubs.acs.org
Publication Date (Web): March 20, 2012 | doi: 10.1021/bk-2012-1101.ch018

Synthesis

For polymer synthesis, NIPAM (2.0 g, 18 mmol), NHS-functionalized CTA (28 mg, 0.080 mmol), 1,3,5-trioxane (93.2 mg, 1.03 mmol, internal standard), AIBN (0.7 mg, 0.004 mmol), and 1,4-dioxane (8.0 mL) were sealed in a 20 mL vial. After purging with N_2 for 20 min, the solution was heated at 70 °C for 180 min before being quenched by exposing the polymerization solution to air. The reaction solutions were diluted with tetrahydrofuran, and polymeric product was precipitated into ether and dried under vacuum to yield succinimidyl-ester terminated PNIPAM (NHS–PNIPAM).

Conjugate synthesis was performed in Tris-buffered aqueous solution at either pH 7.5 or pH 9 according to recent literature procedures (*42*). Due to the photolability of the enzyme, experiments were carried out in the dark. Amine-reactive PNIPAM (17.7 kDa; 12 mg/mL; 10 equiv.) was dissolved at 4 °C and added to a solution of tyrosinase (4 mg/mL; 1 equiv.) in a final volume of 500 µL. The reaction mixture was then either shaken at 4 °C (2 d) or 25 °C (24 h). Isolation of the enzyme-PNIPAM conjugate was performed by temperature induced precipitation at 45 °C for 5 min. Subsequent centrifugation (at 45 °C, 10.000 U/min) and removal of excess tyrosinase solution gave the bioconjugate as a slightly brown pellet, which was redissolved in potassium phosphate buffer (pH 6.5) at 4 °C. This purification procedure was repeated three times to ensure complete removal of unreacted tyrosinase. The purified conjugate was redissolved in 500 µL of potassium phosphate buffer (pH 6.5) and stored at -20 °C. SDS page as well as temperature dependent turbidity measurements confirmed conjugate formation.

Results and Discussion

Conjugation Strategy

Due to the diversity of chemically accessible and reactive functionalities in proteins, a broad variety of conjugation strategies can be utilized (*3*, *17*, *50*). Especially free thiol groups from cysteines or amines presented at the *N*-terminus and ε-amino function of lysine residues are frequently used for more or less regio specific modifications. Thiols of cysteine residues show high reactivity and are well suited to form Michael adducts with maleimides. However, not all proteins exhibit free, accessible thiol functionalities. On the contrary, free amines are often available at the protein surface in large quantity. Therefore, most frequently, amine modification is used although it represents less specific means of protein modification.

Although the “grafting from” strategy using ATRP or RAFT has certainly several advantages (*42*, *51–54*), a “grafting onto” approach was applied to conjugate synthetic polymers to tyrosinase. One of the main reasons for the strategy was the presence of redox active, copper-containing catalytic centers of the enzyme, which are likely to interfere with the radical control systems and prohibiting the direct application of controlled radical polymerization techniques.

Downloaded by OHIO STATE UNIV LIBRARIES on June 1, 2012 | http://pubs.acs.org
Publication Date (Web): March 20, 2012 | doi: 10.1021/bk-2012-1101.ch018

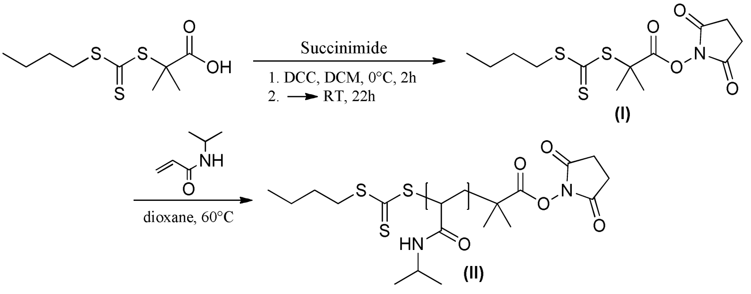

Figure 2. Synthesis of NHS-functionalized chain transfer reagent (I) and subsequent RAFT polymerization of NIPAM (II).

For the reaction with amines present on the surface of tyrosinase, thermoresponsive PNIPAM was equipped with an *N*-hydroxy succinimide (NHS) active ester moiety at one end of the polymer chain. RAFT offers probably the most straightforward access to well-defined PNIPAM with controlled chain end functionalities. The NHS entity was easily incorporated into a trithiocarbonate based chain transfer reagent (CTA) (cf. Figure 2). Subsequent RAFT polymerization of NIPAM mediated by the NHS-functional CTA yielded PNIPAM (II) with a defined NHS active ester moiety at the α-chain end. The PNIPAM was characterized by SEC (*cf.* Figure 3). The SEC trace indicated $M_n = 17{,}700$ and a low polydispersity index of $M_w/M_n = 1.14$. ^{1}H-NMR analysis confirmed the determined $M_{n,SEC}$ with $M_{n,NMR} = 18{,}300$ and showed an excellent degree of NHS chain end functionality of larger than 95% by comparing integral intensity of the characteristic resonance of succinimidyl protons ($\delta = 2.87$ ppm) with this of the methylene unit adjacent to the trithiocarbonate at the ω-chain end ($\delta = 3.34$ ppm).

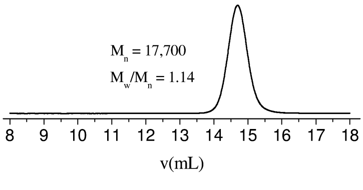

Figure 3. SEC-chromatogram of PNIPAM (II).

Prior to conjugate synthesis, the thermal stability of the enzyme was investigated. Besides its photolability (*55*) earlier studies already showed a temperature dependent decrease in enzymatic activity of different tyrosinases over time (*56*). For ease of purification, conjugation of tyrosinase with PNIPAM (II) has to include temperature induced precipitation of the bioconjugates, making the stability of the enzyme under precipitation conditions highly important. Multiple repetitions of thermal stress cycles were carried out at 45 °C for 5 minutes each. After each heating cycle the solution was cooled to 4 °C, and subsequent activity assays were carried out to determine the loss of activity. Figure 4 shows the activity curves for seven heating cycles. No loss of activity could be observed as minor variations of the traces are within the error of the experiments. Therefore, the thermal stability of tyrosinase under the given conditions was apparently sufficient.

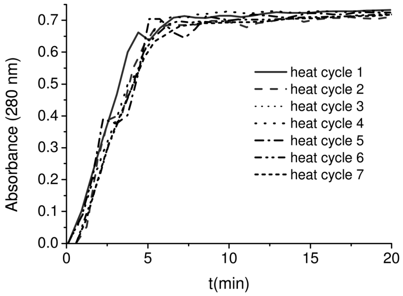

Figure 4. Tyrosinase assay of thermally stressed enzymes as proof for the stability.

To monitor the thermal stability of the secondary structure of native tyrosinase, circular dichroism measurements were carried out in a temperature range from 25 °C to 90 °C. CD spectra were recorded after equilibration for 10 minutes at each temperature. At 25 °C, the tyrosinase secondary structure is dominated by α-helical motives (Figure 5) and up to 40 °C no remarkable structural changes are visible. Obviously no loss of activity at 25 °C could be found by the application of short term heating cycles as discussed above. This suggests minor structural changes, which seem to be completely reversible. Nevertheless, longer heating periods will effect enzyme activity, as it has been shown for congener tyrosinases (*56*). It should be noted that a reduction of enzymatic activity does often not require dramatic changes in secondary structure, as minor structural distortions in the enzymatically active center are sufficient. Application of higher temperatures (50 °C – 90 °C) gradually leads to significant changes of the CD spectra, which indicate structural changes that hamper the enzymatic activity in an irreversibly manner (Figure 5).

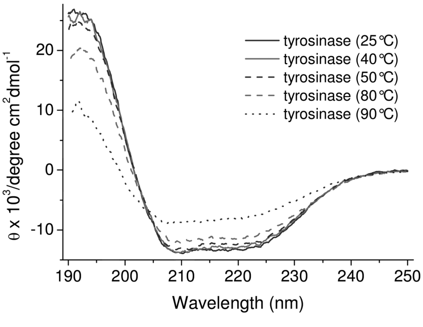

Figure 5. Circular dichroism spectra of native tyrosinase at different temperatures.

Downloaded by OHIO STATE UNIV LIBRARIES on June 1, 2012 | http://pubs.acs.org
Publication Date (Web): March 20, 2012 | doi: 10.1021/bk-2012-1101.ch018

Conjugating a chain-end-reactive polymer with a multifunctional surface of a protein might lead to ill-defined bioconjugates with distributions in number and localization of polymer modifications. The number of conjugated polymer chains per enzyme is of major importance. In an extensively conjugated enzyme it is very likely that the polymer will affect the enzymatic activity by either blocking or distorting the catalytically active site of the enzyme. To minimize this risk, a bioconjugate bearing a single PNIPAM chain-modification would be preferable.

To achieve this aim, II was conjugated to the enzyme tyrosinase under different conditions (Figure 6 and Table 1). Taking the differences in pK_a values into account, reactions of terminal amino functionalities might be favored under slightly basic conditions, whereas all amino groups, including the lysine side chain functionalities, are more reactive at higher pH (*57*). Therefore, PNIPAM conjugation may be controlled by the pH of the conjugation solution.

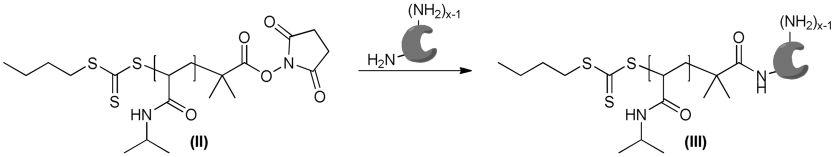

Figure 6. Conjugation of PNIPAM (II) to amine functions of tyrosinase (III).

Table 1. Reaction conditions and obtained yields of bioconjugates

conjugate	*pH*	*T [°C]*	*t [h]*	*yield [%]**
IIIa	9.0	4	48	38
IIIb	7.5	4	48	8
IIIc	7.5	25	24	14

* enzyme recovery in the bioconjugate according to UV-vis spectroscopy.

Bioconjugate synthesis was carried out at pH 7.5 and 9.0 by incubating the enzyme tyrosinase with 10 equiv. of II at 4 °C (2 d) and 25 °C (24 h), respectively (Table 1). Low reaction temperatures were favored, as they provide a higher stability of the native enzyme. Three bioconjugates were obtained, IIIa (at pH 9.0 at 4 °C), IIIb (at pH 7.5 at 4 °C) and IIIc (at pH 7.5 at 25 °C). Subsequent temperature induced precipitation of the bioconjugates was carried out at 45 °C. For complete removal of non-conjugated enzyme the purification procedure was repeated three times.

UV-vis spectroscopy served to estimate the yield of the obtained bioconjugates by Sanger test protocols (*58*). As illustrated in Table 1 strong differences in recovery were obvious, depending on the conjugation conditions. While IIIa showed approximately 40% recovery of the full enzyme reaction load in the bioconjugate fraction, conditions with lower pH lead to considerably reduced recoveries of 8% (IIIb) and 14% (IIIc). The results were expected and illustrate, that the application of pH 9.0 offers an advantage by gaining access to

Downloaded by OHIO STATE UNIV LIBRARIES on June 1, 2012 | http://pubs.acs.org
Publication Date (Web): March 20, 2012 | doi: 10.1021/bk-2012-1101.ch018

Downloaded by OHIO STATE UNIV LIBRARIES on June 1, 2012 | http://pubs.acs.org
Publication Date (Web): March 20, 2012 | doi: 10.1021/bk-2012-1101.ch018

a large number of reactive protein surface functionalities (e.g., amines), which subsequently can react with NHS-functionalized PNIPAM (II). Not surprisingly, bioconjugate synthesis at 25 °C seems to have a positive effect on the reaction yield showing an absolute increase by 6%, comparing IIIb and IIIc. Therefore, taking only the total enzyme recovery in the bioconjugate fraction into account, the application of pH 9.0 (IIIa) and 25 °C (IIIc) would offer the best reaction conditions for conjugate formation.

Influence of pH and Temperature on the Composition of the Tyrosinase-PNIPAM Conjugate

Not only the overall recovery of enzyme, but also more importantly the number of polymer chains conjugated to the enzyme is of particular interest. Gel electrophoresis of obtained bioconjugates IIIa-IIIc clearly displays severer molecular differences between the products, as seen in Figure 7. Native, non-functionalized tyrosinase (lane A) shows a strong band at apparent ~50 kDa. This is consistent with previously reported data, where the tyrosinase was stated with 45.3 kDa (*59*). Conjugate IIIa, surprisingly also shows a band at apparent ~50 kDa (lane B), although no evidence of enzyme could be found in respective wash cycles 2 and 3 (data not shown). Nevertheless, IIIa shows additional weak bands at apparent 75 kDa and at apparent 110 kDa, which might be assignable to bioconjugates with one and three PINPAM chains. The major fractions, however, are extensively conjugated enzymes appearing as strong bands at the top of lane B. These fractions exhibit large masses way out of the separation window of the used gel. This might provide an explanation for the absence of non-conjugated enzymes in the washing solutions as high molecular weight bioconjugates probably causes co-precipitation of enzyme and bioconjugates, preventing effective purification. Therefore, application of pH 9.0 for conjugation clearly results in the formation of ill-defined bioconjugates with extensively conjugated enzymes.

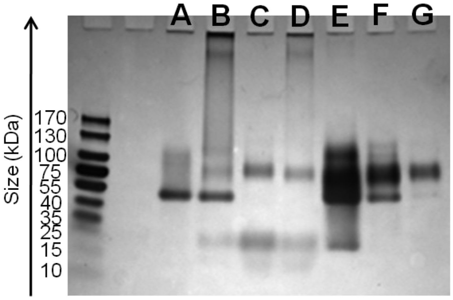

Figure 7. SDS-Page of conjugates I – III (lane A: tyrosinase; lane B: conjugate IIIa; lane C: conjugate IIIb; lane D: conjugate IIIc; lanes E-F: temperature induced wash cycles 1-3; material eluted below 25 kDa is assignable to residual PNIPAM).

Closer investigation of the product resulting from conjugation at pH 7.5 reveals remarkable differences. The bioconjugate IIIb only shows one distinct band at apparent 75 kDa (Figure 7, lane C). This clearly indicated the formation of uniformly conjugated tyrosinase. Considering the apparent molecular weight as determined from SDS page, a single polymer modification might be very likely. Taking into account that the *N*-terminal amino group is well accessible, value *N*-terminal modification shows a slight tendency to be favored at certain pH values. A reaction at the *N*-terminal amine group might be believed but has yet to be proven. Nevertheless, the results clearly demonstrate the importance of the pH in order to obtain well-defined bioconjugates, although a large loss of enzyme has to be accepted.

Attempts to increase the amount of recovered enzyme in the product include the increase of the reaction temperature from 4 °C (IIIb) to 25 °C (IIIc), while keeping the pH 7.5 constant. Changes in conjugation specificity are noticeable (cf. Figure 7, lane D). Raising the reaction temperature to 25 °C requires shortening of the reaction time to 24 h, due to the fragility of the enzyme. Conjugate IIIc shows a SDS-page band corresponding to a single conjugated system. Nevertheless, additional polymer-rich bioconjugates were detected, which cannot elute from the upper pocket. Therefore, using higher temperatures during conjugate synthesis led to higher yields but compromises the specificity of the conjugation reaction.

In order to demonstrate the separation of non-modified enzyme from the obtained bioconjugate III b, gel electrophoresis of concentrated wash solutions was performed (Figure 7, lanes E-G corresponding to washing cycles 1-3 of IIIb). A complete removal of non-conjugated tyrosinase was observed after three times precipitation (lane G). However, a partial loss of the obtained bioconjugate was evident, too. This problem might be solved easily by optimizing the length of the PNIPAM-block. Taking a single polymer modification of tyrosinase into account, PNIPAM composes approximately 26 w/w% of the bioconjugate, so it is understandable that the protein affects the conjugate properties slightly more than does PNIPAM.

To further understand these effects, temperature-dependent turbidity measurements were performed. In Figure 8 the transmittance plots of bioconjugates IIIa and IIIb in aqueous solutions are compared to those of PNIPAM (II). Free PNIPAM showed the characteristic sharp temperature transition with a precipitation at TPNIPAM = 32.9 °C. Cooling led to redissolution of PNIPAM with strong hysteresis and typical broad transition at $T'_{PNIPAM} = 29.9$ °C. Comparing this information with the transitions of the obtained bioconjugates, a shift to higher temperatures for the latter was clearly visible. While bioconjugate IIIa shows precipitation at $T_{IIIa} = 35.5$ °C and a redissolution at $T'_{IIIa} = 34.9$ °C, IIIb leads to even higher temperatures with $T_{IIIb} = 36.0$ °C and $T'_{IIIb} = 35.2$ °C. Again, this is not surprising as IIIb consists only of a single tyrosinase-PNIPAM conjugate. Interestingly, also the hysteresis of redissolution for the bioconjugates was less pronounced, if compared to free PNIPAM. As the enzyme is well soluble at precipitation temperatures, it strongly contributes to the colloidal stability and accelerates the redissolution of precipitated aggregates.

Downloaded by OHIO STATE UNIV LIBRARIES on June 1, 2012 | http://pubs.acs.org
Publication Date (Web): March 20, 2012 | doi: 10.1021/bk-2012-1101.ch018

Downloaded by OHIO STATE UNIV LIBRARIES on June 1, 2012 | http://pubs.acs.org
Publication Date (Web): March 20, 2012 | doi: 10.1021/bk-2012-1101.ch018

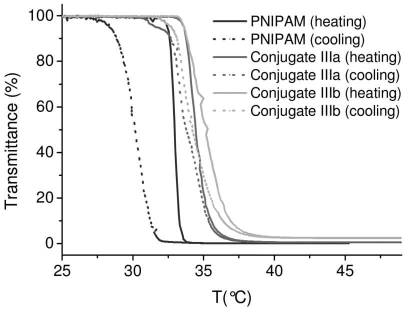

Figure 8. Temperature dependent turbidity measurements of PNIPAM (II) as well as bioconjugates IIIa and IIIb.

Activity and Thermal Stability of the Bioconjugates

After careful analysis of the conjugation process and temperature dependent solution properties of the bioconjugates, enzymatic activity of the obtained bioconjugates was determined. This analysis makes the real differences between the conjugate batches visible. Activity data for each bioconjugate batch (IIIa-IIIc) was determined by UV-vis spectroscopy (cf. Figure 9). These results can be correlated to the data presented above. As already discussed, a conjugation at pH 9.0 (IIIa) resulted in a high yield compared to reactions at pH 7.5 (IIIb or IIIc). Nevertheless, mainly extensively conjugated enzymes were obtained, where the enzymatic activity was strongly reduced by the PNIPAM. In contrary to this, conjugates obtained at lower pH (e.g. IIIb) show lower yields, but the formation of the desired well-defined single conjugated product was evident, which gives higher activity.

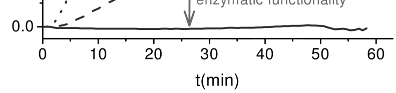

Figure 9. Activity measurements of bioconjugates IIIa-IIIc.

Figure 9 exhibits the enzymatic activities for equal amounts of bioconjugates IIIa-c. As a slope defines the conjugate catalytic activity, the tendencies are clearly visible. Extensive conjugation results in bioconjugates with no activity (IIIa). Well-defined bioconjugates exhibiting a single PNIPAM modification (IIIb) proved to be most active with an apparent activity of ~ 50 % as compared to the activity of non-modified tyrosinase. Bioconjugate IIIc, with an ill-defined mixture of single and extensive conjugations shows enzymatic activity, though much lower compared to IIIb. These results highlight the disadvantages of multiple conjugations to tyrosinase, as a deactivation of the enzymatic properties of tyrosinase occurs. Only the well-defined stoichiometric tyrosinase-PNIPAM bioconjugate proved to exhibit the desired activity.

Well-defined bioconjugate IIIb showed high enzymatic activity and sufficient thermoresponsive properties. The behavior of the enzymatic function on different temperatures was investigated. For this purpose, temperature dependent activity measurements were performed, comparing IIIb with native tyrosinase controls.

Downloaded by OHIO STATE UNIV LIBRARIES on June 1, 2012 | http://pubs.acs.org
Publication Date (Web): March 20, 2012 | doi: 10.1021/bk-2012-1101.ch018

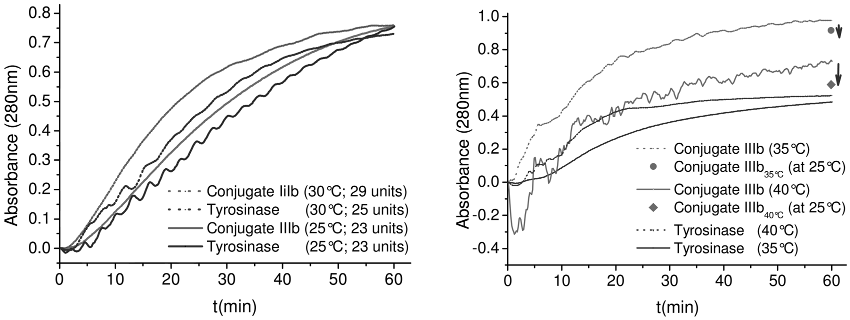

Figure 10. Temperature gradient measurements of conjugate IIIb.

An equal amount of units for both tyrosinase and bioconjugate were used and the activity was determined initially at 25 °C. Figure 10 (left) suggests an activity of ~ 23 units for both samples at 25 °C. Subsequent measurements at 30, 35, and 40 °C were carried out, keeping the other conditions constant. In Figure 10 the activities obtained for the natural enzyme at temperatures 25 °C and 30 °C indicated no significant difference in enzymatic activity, and the absorbance at 280 nm rises to approximately 0.75 within 60 minutes. An increase in temperature to 35 °C leads to a slightly decreased activity value. Noteworthy, the final absorption reached in the assays at 35 °C or 40 °C was with ~0.5 significantly lower as compared to the experiments at 25 °C or 30 °C. Apparently tyrosinase at higher temperatures is not capable of reaching similar tyrosine conversion as seen at lower temperatures. Elevated temperatures should increase reaction rates. However, the result might be explained by a partial reversible denaturation of the enzymatic center at increased temperatures of the experiment as it has been described for congener tyrosinases (*56*).

On the contrary, bioconjugate IIIb clearly showed an increase of enzymatic activity on temperature rise. While at 30 °C an increase to 29 units (Δactivity$_{25\text{-}30°C}$ ~ 5 units) was found, the activity at 35 °C was found to be even 41 units. This represents a significant activity increase of ~80 % with respect to the activity of IIIb at 25 °C. Furthermore, the substrate conversion at 60 minutes was compared to that of the native enzyme. Partial precipitation of conjugate at 35 °C or 40 °C though resulted in a higher end point absorption. Therefore, data had to be normalized by a subsequent absorption measurement after rapid cooling to 25 °C (Figure 10). At 35 °C the final absorption meets approximately 0.9, suggesting an even higher substrate conversion yield obtained by the bioconjugate, if compared to the native enzyme. At 40°C also a decrease of the final absorption can be noticed. This was contributed to the fact that most of the bioconjugate was precipitated at this temperature. Therefore, a higher thermal stability of tyrosinase or enhancement of its catalytic center by polymer conjugation with PNIPAM can be anticipated. While the accurate mechanism of conjugated PNIPAM to enhance the protein function remains to be proven, it occurs rather feasible that the PNIPAM chain reduces protein aggregation and potentially stabilizes important protein structure parts against reversible thermal denaturation due to partial hydrophobic stabilization or excluded volume effects. Moreover, the highest activity of IIIb was observed close to the precipitation temperature. These interesting stability effects are consistent with the literature, where polymer often improves protein properties (*34*). For instance, bioconjugates composed of trypsine and copolymers of 2-(2-methoxyethoxy)ethyl methacrylate and oligo(ethylene glycol) methacrylates led to higher enzymatic activity as compared to non-modified trypsine.

Although activity assays at 35 °C showed no or minor disturbances due to partial precipitation of the bioconjugate, measurements at 40 °C were clearly effected. Therefore, no activity could be calculated from the obtained data sets due to scattering. Nevertheless, enzymatic activity at this temperature is expected to decrease, since precipitation of the bioconjugates progressively hinders accessibility of the catalytically active centers.

Downloaded by OHIO STATE UNIV LIBRARIES on June 1, 2012 | http://pubs.acs.org
Publication Date (Web): March 20, 2012 | doi: 10.1021/bk-2012-1101.ch018

Conclusion

In summary, tyrosinase-PNIPAM conjugates can readily be obtained by grafting onto approach with *N*-succinimide endfunctional PNIPAM as amine reactive polymer. These conjugates showed the thermo responsiveness of the polymer. Only the selective formation of a defined stoichiometric tyrosinase-PNIPAM conjugate lead to an enzyme-polymer conjugates with the desired activity. On the contrary, ill-defined bioconjugates being extensively modified showed an inactivation of the enzymatic properties. Enzyme activity assays in a temperature range of 25 – 40 °C exhibited an increased thermostability of the bioconjugate. Enzymatic activity of the conjugate at 35 °C was increased by ~80 % with respect to the activity at 25 °C, whereas native tyrosinase exhibited practically only half the activity at this point. This clearly shows the high potential of phenolase-polymer conjugates, as the natural enzymes are more sensitive. Increased thermostability of the obtained conjugates also provides a high potential for recyclability, which dramatically reduces the costs of enzymatic transformations. Therefore, potentials of these enzymes for both industrial processes or in applied products occur feasible.

References

1. Börner, H. G. *Prog. Polym. Sci.* **2009**, *34*, 811.
2. Broyer, R.; Grover, G.; Maynard, H. D. *Chem. Commun.* **2011**, *47*, 2212.
3. Canalle, L. A.; Lowik, D. W. P. M.; van Hest, J. C. M. *Chem. Soc. Rev.* **2010**, *39*, 329.
4. Börner, H. G.; Kühnle, H.; Hentschel, J. *J. Polym. Sci., Part A: Polym. Chem.* **2010**, *48*–1.
5. Gauthier, M. A.; Klok, H.-A. *Chem. Commun.* **2008**, 2591.
6. Klok, H. A. *J. Polym. Sci., Part A: Polym. Chem.* **2005**, *43*, 1.
7. Loschonsky, S.; Shroff, K.; Woerz, A.; Prucker, O.; Ruhe, J.; Biesalski, M. *Biomacromolecules* **2008**, *9*, 543.
8. Hentschel, J.; Bleek, K.; Ernst, O.; Lutz, J.-F.; Börner, H. G. *Macromolecules* **2008**, *41*, 1073.
9. Börner, H. G. *Macromol. Rapid Commun.* **2011**, *32*, 115.
10. Gentsch, R.; Pippig, F.; Schmidt, S.; Cernoch, P.; Polleux, J.; Börner, H. G. *Macromolecules* **2011**, *44*, 453.
11. Verch, A.; Hahn, H.; Krause, E.; Cölfen, H.; Börner, H. G. *Chem. Commun.* **2010**, *46*, 8938.
12. Jahnke, E.; Severin, N.; Kreutzkamp, P.; Rabe, J. P.; Frauenrath, H. *Adv. Mater.* **2008**, *20*, 409.
13. Shaytan, A.; Schillinger, E.-K.; Khalatur, P.; Mena-Osteritz, E.; Hentschel, J.; Börner, H. G.; Baeuerle, P.; Khokhlov, A. *ACS Nano* **2011**, *5*, 6894.
14. Hoffman, J. M.; Ebara, M.; Lai, J. J.; Hoffman, A. S.; Folch, A.; Stayton, P. S. *Lab Chip* **2010**, *10*, 3130.
15. Kim, K. T.; Meeuwissen, S. A.; Nolte, R. J. M.; van Hest, J. C. M. *Nanoscale* **2010**, *2*, 844.
16. Alconcel, S. N.; Baas, A. S.; Maynard, H. D. *Polym. Chem.* **2011**, *2*, 1442.
17. Gauthier, M. A.; Klok, H.-A. *Polym. Chem.* **2010**, *1*, 1352.
18. Chen, G.; Felgner, P. L.; Guan, Z. *Biomacromolecules* **2008**, *9*, 1745.
19. Hartmann, L.; Börner, H. G. *Adv. Mater.* **2009**, *21*, 3425.
20. Ryan, S. M.; Mantovani, G.; Wang, X.; Haddleton, D. M.; Brayden, D. J. *Exp. Op. Drug Delivery* **2008**, *5*, 371.
21. Veronese, F. M.; Pasut, G. *Drug Discovery Today* **2005**, *10*, 1451.
22. Nicolas, J.; Mantovani, G.; Haddleton, D. M. *Macromol. Rapid Commun.* **2007**, *28*, 1083.
23. Octave, S.; Thomas, D. *Biochimie* **2009**, *91*, 659.
24. Teeuwen, R. L. M.; Zuilhof, H.; de Wolf, F. A.; van Hest, J. C. M. *Soft Matter* **2009**, *5*, 2261.
25. Smith, R. A. G. *Nature* **1976**, *262*, 519.
26. Gaertner, H. F.; Puigserver, A. J. *Enzyme Microb. Technol.* **1992**, *14*, 150.
27. Miyamoto, D.; Watanabe, J.; Ishihara, K. *Biomaterials* **2004**, *25*, 71.
28. van Hest, J. C. M.; Tirrell, D. A. *Chem. Commun.* **2001**, 1897.
29. Heredia, K. L.; Maynard, H. D. *Org. Biomol. Chem.* **2007**, *5*, 45.
30. Kiick, K. L.; Saxon, E.; Tirrell, D. A.; Bertozzi, C. R. *Proc. Natl. Acad. Sci. U.S.A.* **2002**, *99*, 19.

Downloaded by OHIO STATE UNIV LIBRARIES on June 1, 2012 | http://pubs.acs.org
Publication Date (Web): March 20, 2012 | doi: 10.1021/bk-2012-1101.ch018

Downloaded by OHIO STATE UNIV LIBRARIES on June 1, 2012 | http://pubs.acs.org
Publication Date (Web): March 20, 2012 | doi: 10.1021/bk-2012-1101.ch018

31. Hoffman, A. S.; Stayton, P. S. *Prog. Polym. Sci.* **2007**, *32*, 922.
32. Chang, C.-W.; Nguyen, T. H.; Maynard, H. D. *Macromol. Rapid Commun.* **2011**, *31*, 1691.
33. Lowik, D. W. P. M.; Leunissen, E. H. P.; van den Heuvel, M.; Hansen, M. B.; van Hest, J. C. M. *Chem. Soc. Rev.* **2010**, *39*, 3394.
34. Zarafshani, Z.; Obata, T.; Lutz, J. F. *Biomacromolecules* **2010**, *11*, 2130.
35. De, P.; Li, M.; Gondi, S. R.; Sumerlin, B. S. *J. Am. Chem. Soc.* **2008**, *130*, 11288.
36. Park, T. G.; Hoffman, A. S. *J. Biomater. Sci., Polym. Ed.* **1993**, *4*, 493.
37. Chen, G. H. H. A. S. *Bioconjugate Chem.* **1993**, *4*, 509.
38. Kulkarni, S.; Schilli, C.; Müller, A. H. E.; Hoffman, A. S.; Stayton, P. S. *Bioconjugate Chem.* **2004**, *15*, 747.
39. Kulkarni, S.; Schilli, C.; Grin, B.; Müller, A. H. E.; Hoffman, A. S.; Stayton, P. S. *Biomacromolecules* **2006**, *7*, 2736.
40. Margolin, A. L. I. V. A.; Svedas, V. K.; Zezin, A. B. *Biotechnol. Bioeng.* **1982**, *24*, 237.
41. Lutz, J.-F. *Adv. Mater.* **2011**, *23*, 2237.
42. Li, M.; Li, H. M.; De, P.; Sumerlin, B. S. *Macromol. Rapid Commun.* **2011**, *32*, 354.
43. Li, H. M.; Bapat, A. P.; Li, M.; Sumerlin, B. S. *Polym. Chem.* **2011**, *2*, 323.
44. Braunecker, W. A.; Matyjaszewski, K. *Prog. Polym. Sci.* **2007**, *32*, 93.
45. Parvez, S.; Kang, M.; Chung, H. S.; Bae, H. *Phytother. Res.* **2007**, *21*, 805.
46. Lee, B. P.; Messersmith, P. B.; Israelachvili, J. N.; Waite, J. H. *Ann. Rev. Mater. Res.* **2011**, *41*, 99.
47. Olivares, C.; Solano, F. *Pigm. Cell Melanoma Res.* **2009**, *22*, 750.
48. Cooksey, C. J.; Garratt, P. J.; Land, E. J.; Ramsden, C. A.; Riley, P. A. *Biochem. J.* **1998**, *333*, 685.
49. Solomon, E. I.; Chen, P.; Metz, M.; Lee, S. K.; Palmer, A. E. *Angew. Chem., Int. Ed.* **2001**, *40*, 4570.
50. Lutz, J.-F.; Börner, H. G. *Prog. Polym. Sci.* **2008**, *33*, 1.
51. Lele, B. S.; Murata, H.; Matyjaszewski, K.; Russell, A. J. *Biomacromolecules* **2005**, *6*, 3380.
52. Grover, G. N.; Maynard, H. D. *J. Polym. Sci., Part A: Polym. Chem.* **2010**, *14*, 818.
53. Broyer, R. M.; Quaker, G. M.; Maynard, H. D. *J. Am. Chem. Soc.* **2008**, *130*, 1041.
54. Peeler, J. C.; Woodman, B. F.; Averick, S.; Miyake-Stoner, S. J.; Stokes, A. L.; Hess, K. R.; Matyjaszewski, K.; Mehl, R. A. *J. Am. Chem. Soc.* **2010**, *132*, 13575.
55. Fry, D. C.; Strothkamp, K. G. *Biochemistry* **1983**, *22*, 4949.
56. Horowitz, N. H.; Fling, M. *Genetics* **1953**, *38*, 360.
57. Selo, I.; Negroni, L.; Creminon, C.; Grassi, J.; Wal, J. M. *J. Immunol. Methods* **1996**, *199*, 127.
58. Summer, K. H.; Goggelmann, W. *Mutat. Res.* **1980**, *70*, 173.
59. Ismaya, W. T.; Rozeboom, H. J.; Weijn, A.; Mes, J. J.; Fusetti, F.; Wichers, H. J.; Dijkstra, B. W. *Biochem.* **2011**, *50*, 5477.

Chapter 19

New Design of Thiol-Responsive Degradable Block Copolymer Micelles as Controlled Drug Delivery Vehicles

Qian Zhang, Samuel Aleksanian, Alexander Cunningham, and Jung Kwon Oh*

Department of Chemistry and Biochemistry, Concordia University,
7141 Sherbrooke St. W., Montreal, Quebec, Canada H4B 1R6
***E-mail: joh@alcor.concordia.ca**

Stimuli-responsive degradation of amphiphilic block copolymer (ABP) micelles is highly desired in the development of multifunctional nanomaterials. For polymer-based drug delivery applications, the degradation enables fast and controlled release of encapsulated therapeutics from the delivery vehicles in targeted cells. It also ensures clearance of the empty device after drugs are delivered in the body. This chapter reviews the recent development of new methods to synthesize three types of reductive (thiol-responsive) degradable ABP micelles having different numbers and types of disulfides positioned at various locations. These new ABPs were prepared by a combination of atom transfer radical polymerization (ATRP) with polycondensation or anionic ring opening polymerization (ROP). Due to the amphiphilic nature, these ABPs formed, through aqueous self-assembly, colloidally stable micelles with hydrophobic cores surrounded with hydrophilic coronas. The micelles exhibit rapid and controlled response to reductive reactions, enhancing the release of encapsulated model drugs as well as leading to the significant change in morphologies. In a biomedical perspective, the micelles were non-toxic to various cell lines, and hence biocompatible.

In Progress in Controlled Radical Polymerization: Materials and Applications; Matyjaszewski, K., et al.;
ACS Symposium Series; American Chemical Society: Washington, DC, 2012.

Introduction

The design and development of multifunctional nanoscale devices able to interface with biological processes are centered in current cancer nanobiotechnology. In recent years the design and development of multifunctional polymer-based drug delivery systems (DDS) have been extensively explored as promising nano-vehicles in the area of pharmaceutics, biomedicine, and nanotechnology (*1–3*). Polymer-based DDS have been demonstrated to have a great potential in treating numerous diseases, including cancer. In particular, active (or specific) targeting strategies of polymer-based DDS conjugated with tumor-targeting biomolecules significantly reduce side effect of anticancer drugs, thus enhancing the efficiency of anticancer therapeutics. Typical examples of polymer-based DDS include polymer-drug conjugates (prodrugs) (*4–6*), dendrimers (*7*), submicron-sized hydrophobic particulates (*8*, *9*), crosslinked microgels/nanogels (*10–14*), vesicles (*15*), and nanocapsules (*16*, *17*). In particular, micelles based on ABPs enable the physical encapsulation of hydrophobic biomolecules and metal nanoparticles for multifunctional drug delivery and cellular imaging platforms (*18–20*).

Well-defined ABPs consist of two different building blocks: hydrophobic and hydrophilic blocks. When the concentration of ABPs is higher than their critical micellar concentration (CMC), the hydrophobic blocks tend to aggregate in an aqueous solution, resulting in the formation of core/shell structured micelles. These stable micelles consist of hydrophobic cores, enabling the encapsulation of therapeutics and imaging agents, surrounded with hydrophilic coronas, ensuring colloidal stability and biocompatibility (*21*). The self-assembled micelles possess a number of features as drug delivery carriers. These features include colloidal stability with low CMC, tunable sizes with narrow size distribution, high physical loading efficiency of drugs without chemical modification, and protection of drugs from possible deactivation during circulation, transportation to targeted organ or tissue, and intercellular trafficking (*1*, *3*). However, the control over several properties is still required for the present and future design and development of block copolymer micelles as effective DDS.

A desired property of micellar carriers for effective DDS is the controlled (or programed) release of encapsulated biomolecules in targeted cells. The bioconjugation with tumor-targeting species such as folic acid, peptides, proteins, and antibodies can promote active targeting to specific cancer cells through, for example, specific ligand-receptor interactions (*22*, *23*). However, the controlled release of encapsulates from the micellar cores is a tremendous challenge to be overcome. A passive method involves diffusion-controlled release through nanopores of micellar cores. This method is simple, but control of the release rate is difficult. Other methods include flow-controlled release by variation of osmotic pressure and size-controlled release by changes in volume. For the latter, the typical examples include thermoresponsive polymer-based micelles, which are swollen below the lower critical solution temperature (LCST), facilitating drug loading; whereas above the LCST, they are shrunken, enhancing drug release (*24*, *25*).

The promising method is the degradation in response to external stimuli (called stimuli-responsive degradation, SRD). In general, degradable linkages (or cleavable groups) are incorporated into micelles, and then cleaved in response to low pH, light, or ultrasound as well as reductive, oxidative, or enzymatic reactions. The degradation causes micelles to dissociate, thus leading to rapid and controlled release of encapsulated biomolecules (Figure 1) (*26*). Many strategies to synthesize stimuli-responsive degradable ABP micelles have been developed (*27–29*). These degradable micelles are designed with different chemical structures, cleavable linkages, and degradation mechanisms. While these strategies have been widely explored, it is a necessity to design new types of degradable micelles in order to gain a better understanding of the structure-property relationship between morphological variance and stimuli-responsive degradation.

This chapter describes the design and development of three distinct thiol-responsive degradable block copolymer micelles having different numbers and types of disulfides positioned at various locations. These new micelles include 1) multi-cleavable $A_{(ss)n}$-B type polyester-based block copolymer micelles with multiple disulfides, 2) sheddable A-ss-B type biodegradable block copolymer micelles with thiol-responsive sheddable coronas, and 3) mono-cleavable BA-ss-AB type triblock copolymer micelles with single disulfides at the center. These block copolymers were prepared by ATRP combined with polycondensation or ROP. ATRP (*30*, *31*), a controlled radical polymerization (*32*, *33*), has proven to be useful for the construction of well-controlled ABPs as effective delivery carriers (*34–36*). Thiol-responsive (or reductive) degradable disulfide linkages were selected as the degradable platform in the preliminary studies. Disulfides are cleaved into corresponding thiols in a reducing environment or through a disulfide-thiol exchange (*37*, *38*). For example, glutathione (GSH, a tripeptide containing cysteine) exists at different levels between intracellular and extracellular environments (*39*, *40*), and moreover at elevated level in cancer cells (*41*).

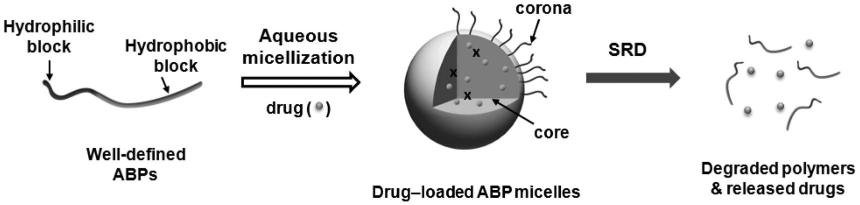

Figure 1. Schematic illustration of aqueous micellization of well-defined ABPs in the presence of drugs and stimuli-responsive degradation of micelles for controlled release of encapsulated drugs. The x denotes cleavable linkage.

Overview of Strategies To Develop Stimuli-Responsive Degradable Micelles

Stimuli-responsive polymers can undergo physical or chemical changes in response to external changes in the environment. These smart polymers are promising as effective building blocks in the construction of complex nanostructured materials for multifunctional applications (*42*). Particularly, these nanomaterials as polymer micelles and nanogels offer a number of applications in the area of nanoscience, pharmaceutics, and biomedicine (*43*). One of the desired conformational and dimensional changes of stimuli-responsive polymers is the degradation in response to external stimuli. Figure 2 summarizes the strategies to synthesize stimuli-responsive degradable block copolymer micelles. The strategies can be classified with five different types of micelles, based on the number and location of cleavable linkage (x). For the number of x linkages, the micelles can be either multi-cleavable (A, B, and C) or mono-cleavable (D and E). For the location of x linkages, micelles can have x linkages either in their micellar cores (A, B, C, and D) or at interface between the cores and coronas (E).

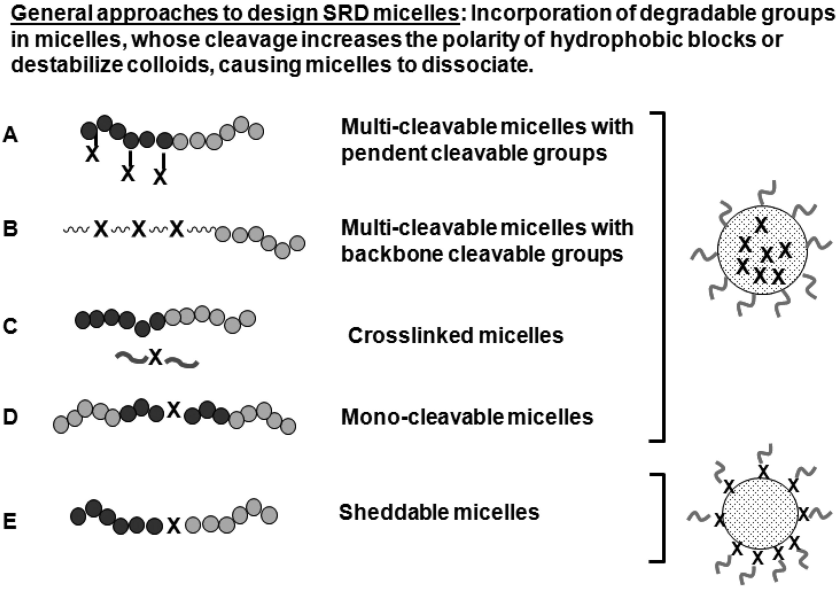
General approaches to design SRD micelles: Incorporation of degradable groups in micelles, whose cleavage increases the polarity of hydrophobic blocks or destabilize colloids, causing micelles to dissociate.
A
Multi-cleavable micelles with pendent cleavable groups
B
Multi-cleavable micelles with backbone cleavable groups
C
Crosslinked micelles
D
Mono-cleavable micelles
E
Sheddable micelles
X

Figure 2. Schematic illustration of various strategies to synthesize stimuli-responsive degradable block copolymer micelles. The dark and grey colors represent hydrophobic and hydrophilic blocks, respectively (x: cleavable group).

The general approaches to the degradation of ABP-based micelles are to tune the polarity of hydrophobic blocks and to remove the hydrophilic or hydrophobic blocks (*27*). Strategy A involves the multiple cleavable linkages positioned in the pendent chains of hydrophobic blocks. The cleavage of the degradable groups increases the polarity of the hydrophobic blocks, causing the micelles to disintegrate. For example, acid-responsive degradable micelles were prepared by self-assembly of well-defined ABPs having pendent acetals or orthoesters in side chains of hydrophobic blocks (*44–47*). These acid-labile linkages were hydrolyzed to the corresponding hydroxyl groups in acidic conditions. For light-responsive degradable micelles, photocleavable groups such as pyrenylmethyl ester (*48*), coumarin dimer (*49*), and 2-diazo-1,2-naphthoquinone (DNQ) (*50*, *51*), and o-nitrobenzyl (*52*) linkages were incorporated into the hydrophobic blocks, and then cleaved by irradiation of UV or visible light. In addition, ultrasound-responsive degradable micelles have been reported (*53*).

Strategy B involves the multiple cleavable linkages positioned on the polymer backbones. The cleavage of the degradable groups destabilizes the micelles. Examples include enzyme-responsive micelles of polycaprolactone (PCL)-containing ABPs (*54*) and pH-responsive micelles labeled with oxime (*55*) and 5,6-benzo-2-methylene-1,3-dioxepane (BMDO) (*56*). Recent examples include diselenide (*57*) and photo-cleavable (*58*) ABP micelles consisting of hydrophilic poly(ethylene oxide) (PEO) and a hydrophobic polyurethane block synthesized by polycondensation. The dissociation of these micelles upon oxidative reaction and photodegradation results in fast degradation; however, the synthesis of diols bearing diselenide and nitrobenzyl groups is required.

Strategy C involves the introduction of cleavable crosslinkers during micellization or post-micellization to yield crosslinked micelles (*59*). The crosslinkers contain disulfide (*60–62*), acid-labile acetal (*63–65*), and imine (*66*) linkages. Strategy D involves the synthesis of mono-cleavable ABPs having single cleavage groups in the middle of triblock copolymers (*67*). Strategy E involves the synthesis of ABPs having cleavable linkages at the junction of hydrophilic and hydrophobic blocks. These self-assembled micelles have cleavable linkages positioned at the interface of the hydrophobic core and hydrophilic coronas. An approach involves the immobilization of cleavable groups on poly(ethylene oxide) chains, followed by chain extension using controlled radical polymerizations (*68*, *69*). The general approach for the strategy utilizes a coupling reaction of hydrophobic and hydrophilic polymers having terminal functional groups. Examples include sheddable micelles having disulfide (*70–72*), acid-labile hydrazone (*73*), and photo-cleavable groups (*74*). However, the coupling method requires extra separation steps to remove excess homopolymers from targeted ABPs.

New Thiol-Responsive Degradable Block Copolymer Micelles

In this section, we summarize the synthesis, aqueous micellization, and degradation of three thiol-responsive degradable block copolymer micelles that have been recently developed. These micelles include polyester-based block copolymer micelles with multiple disulfides, sheddable biodegradable block copolymer micelles, and monocleavable micelles. The biological functions of these micelles were preliminarily evaluated to be non-cytotoxic through cell culture assays.

Multi-Cleavable $A_{(ss)n}$-B Type Block Copolymer: Polyester-Based Block Copolymer Micelles with Multiple Disulfides (*75*)

A new method to synthesize thiol-responsive degradable ABPs with multiple disulfides positioned repeatedly on the hydrophobic main chain was developed. These well-defined ABPs, consisting of hydrophobic disulfide-labeled polyesters (ssPESs) and water-soluble polymethacrylates were prepared by a combined facile carbodiimide coupling polycondensation and ATRP. The new method consists of three synthetic steps (Figure 3). These include 1) polycondensation of commercially available diols and diacids through a carbodiimide coupling process to synthesize degradable polyesters with disulfides labeled on the main chain at regular intervals (ssPES-OH), 2) bromination of ssPES-OH to ssPES-Br, and 3) ATRP for chain extension of ssPES-Br with water-soluble poly(oligo (ethylene glycol) monomethyl ether methacrylate) (POEOMA), yielding well-controlled ssPES-b-POEOMA block copolymers (ssABPs).

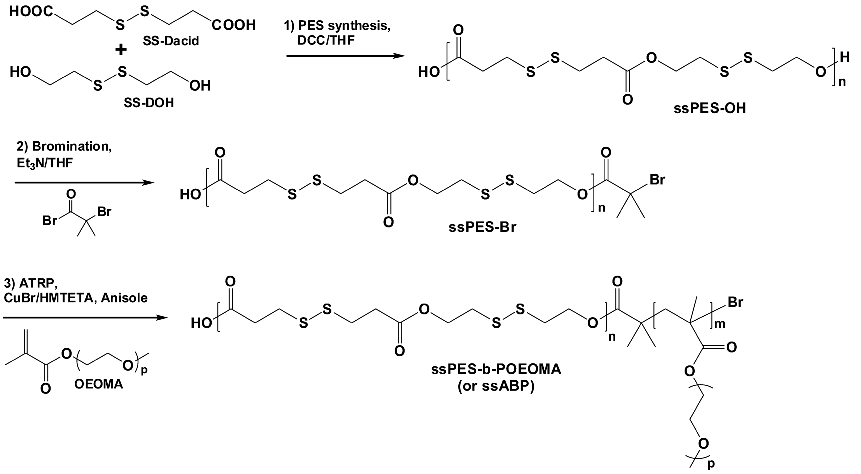
HOOC
COOH
SS-Dacid
+
HO
OH
SS-DOH
1) PES synthesis, DCC/THF
ssPES-OH
2) Bromination, Et3N/THF
Br
ssPES-Br
3) ATRP, CuBr/HMTETA, Anisole
OEOMA
ssPES-b-POEOMA (or ssABP)
n
m
p

Figure 3. Synthetic route for reductively-degradable ssABP consisting of hydrophobic ssPES block labeled repeatedly with disulfides along the main chains and a water-soluble POEOMA block. Reprinted with permission from ref. (75). Copyright 2011 Royal Society of Chemistry.

For the synthesis of ssPES-OH, 3,3′-dithiodipropionic acid (SS-Diacid) reacted with 2-hydroxyethyl disulfide (SS-DOH) in the presence of dicyclohexyl carbodiimide (DCC) at 0 °C. After precipitation from MeOH, the purified product was characterized with M_n = 1,750 g/mol with M_w/M_n = 2.1 by gel permeation chromatography (GPC) and the structure determined by ^{1}H-NMR. The availability of terminal hydroxyl (-OH) group of ssPES-OH was found to be 84% ssPES having terminal OH and COOH groups, determined by acid-base titration in a mixture of 1/2 v/v MeOH/THF. After successful synthesis and characterization, the purified, dried ssPES-OH was brominated with α-bromoisobutyryl bromide in the presence of triethylamine and a catalytic amount of 4-dimethylaminopyridine. After precipitation from MeOH, the molecular weight of ssPES-Br increased to M_n = 2,400 g/mol with M_w/M_n = 1.5.

In the presence of ssPES-Br, a series of ATRP of OEOMA in anisole at 47 °C was conducted while varying the ratio of $[OEOMA]_0/[ssPES\text{-}Br]_0$ = 50/1 and 100/1, as well as varying the ligands, either 2,2′-bipyridine (bpy) or 1,1,4,7,10,10-hexamethyltriethylenetetramine (HMTETA). Figure 4 and Table 1 summarize the results. All three polymerizations were relatively fast, reaching >80% conversion within 2 – 3 hr. ATRP-1 with 50/1 and HMTETA was slightly faster than ATRP-2 with 50/1 and bpy, but slower than ATRP-3 with 100/1 and HMTETA. The three polymerizations were first-order kinetics, indicating a constant concentration of active centers during the polymerization process. Molecular weight increased with conversion and the polydispersity remained low, M_w/M_n < 1.4 up to 60% monomer conversion (Figure 4).

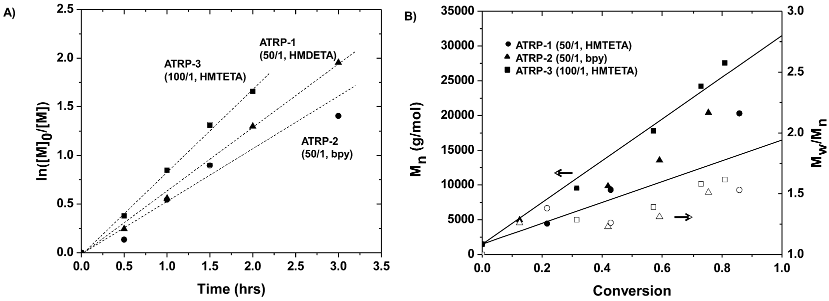

Figure 4. First-order kinetic plot (A) and evolution of molecular weight and molecular weight distribution with conversion (B) for ATRP of OEOMA in the presence of ssPES-Br in anisole at 47 °C. The dotted lines in (A) are linear fits, and the straight lines in (B) are the theoretically predicted molecular weight over conversion. Reprinted with permission from ref. (75). Copyright 2011 Royal Society of Chemistry.

Table 1. A *series of ATRP of OEOMA in the presence of ssPES-Br macroinitiator*

Sample	*$[OEOMA]_0$/ $[ssPES\text{-}Br]_0$*	*Ligand*	*Time (hrs)*	*Con (%)*	*M_n (g/mol)*	*M_w/M_n*
ATRP-1	100/1	HMTETA	2	81	27,500	1.62
ATRP-2	50/1	HMTETA	3	86	20,300	1.53
ATRP-3	50/1	bpy	3	82	22,600	1.35

Conditions: $[ssPES\text{-}Br]_0/[CuBr]_0/[HMTETA\text{ or }bpy]_0$ = 1/0.5/x where x = 0.5 for HMTETA and 1 for bpy and OEOMA/anisole = 54 wt%.

The recipe of ATRP-2 was used to synthesize well-defined ssABP with M_n = 11,000 g/mol and M_w/M_n = 1.3. ^{1}H NMR suggests successful block copolymerization. The amphiphilicity of ssABP was characterized with CMC determined by tensiometry. A stock solution of ssABP at 1.0 mg/ml was prepared in water and then diluted with water to prepare a series of solutions with various concentrations ranging from 1.0 to 10^{-5} mg/ml. The CMC was 12 μg/mL (Figure 5A). Next, the aqueous micellization by solvent evaporation method resulted in stable micellar colloids having ssPES cores surrounded with POEOMA coronas at 10 mg/ml, above the CMC. Dynamic light scattering (DLS) suggests bimodal distribution of micelles with 138 nm in diameter and a small population with a diameter <22 nm. The latter can be attributed to the presence of unimers (Figure 5B). Further, the particle size can be adjusted by varying the size of the hydrophilic corona and the concentration of the block copolymer.

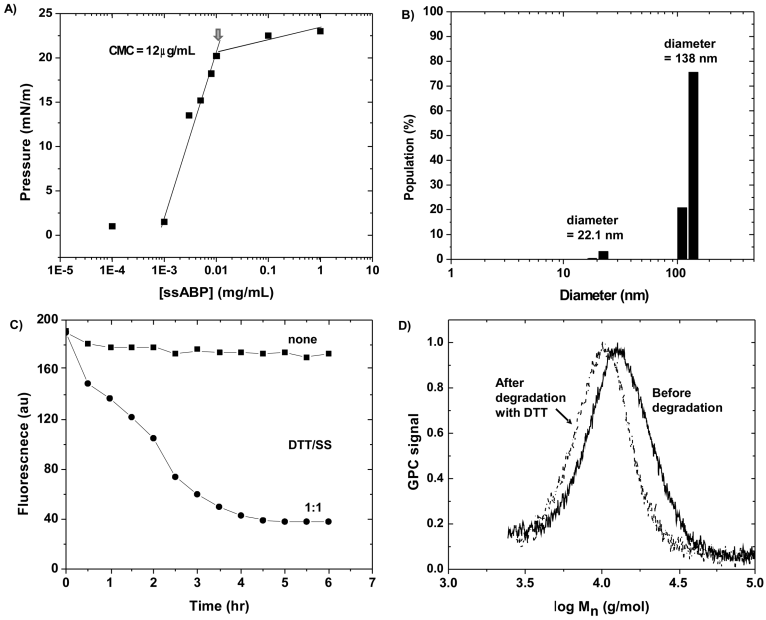

Figure 5. With ssABP, pressure vs concentration in tensiometry (A), DLS diagram based on %intensity (B), release profile of NR from NR-loaded micelles over degradation time (C), and GPC traces before and after degradation (D). Reprinted with permission from ref. (75). Copyright 2011 Royal Society of Chemistry.

The degradation of ssPES and ssPES-containing ssABP in the presence of tributyl phosphine (Bu_3P) was rapid; >90% degradation was obtained within 30 min. Such rapid thiol-responsive degradation enhances the release of encapsulated model drugs. To verify this, Nile Red (NR) as a hydrophobic model drug was mixed with ssABP in a water/THF mixture (82/18 w/w). Non-dissolved NR was removed by centrifugation and supernatant containing NR-loaded micelles was divided equally into two aliquots: one without DTT as a control and the other with DTT defined as the mole ratio of DTT/disulfide = 1/1 (DTT: dithiothreitol). Degradation was measured by monitoring the fluorescence intensity of NR at λ_{em} = 641 nm. As seen in Figure 5C, in the absence of DTT, NR can be either confined in small micellar cores or dissolved in water/THF mixture. No significant change of fluorescence intensity was observed over 6 hr, suggesting no release as well as no photobleaching of significant amount of NR. Upon an addition of DTT, the disulfides are cleaved and the micelles are disrupted to release NR. The fluorescence of NR is then quenched immediately by water, resulting in decreased intensities. In the presence of DTT, >85% NR was released within 3 hrs. Moreover, the decrease in the molecular weight of ssABP in the presence of DTT evidenced that the release of NR in the presence of DTT is attributed to the degradation of micelles upon the cleavage of disulfides in the micellar cores (Figure 5D).

Sheddable A-ss-B Type Biodegradable Block Copolymer Micelles with Thiol-Responsive Sheddable Coronas (*76*)

A new method to synthesize sheddable micelles having hydrophilic POEOMA coronas capable of being shed from biodegradable polylactide (PLA) cores by cleavage of disulfide linkages at the interface was developed. These micelles consist of well-defined ABPs with disulfide at block junctions (Shed-SS-ABP), synthesized by the combination of anionic ROP and ATRP in the presence of a double-head initiator having terminal OH and Br groups.

As illustrated in Figure 6, the approach is centered on the synthesis of new 2-hydroxyethyl-2′-(bromoisobutyryl)ethyl disulfide (OH-SS-iBuBr) initiator. Its structure was confirmed by ^{1}H-, ^{13}C-NMR, and high-resolution mass spectrometry. In the presence of OH-SS-iBuBr, a series of ROP of LA with $[Sn(Oct)_2]_0/[OH\text{-}SS\text{-}iBuBr]_0$ = 0.14/1 was conducted with varying the target DP_n (degree of polymerization) of 70, 40, and 20. All polymerizations yielded well-controlled hydrophobic PLA-ss-iBuBr homopolymers with highly preserved Br end groups and low polydispersity (M_w/M_n <1.2). After purification, PLA-SS-iBuBr was used as a macroinitiator in the ATRP of OEOMA to synthesize well-defined Shed-SS-ABP with M_n = 18,400 g/mol and M_w/M_n < 1.2. ^{1}H-NMR results indicate the DP_n = 45 for PLA block and the DP_n = 43 for POEOMA block.

After the successful synthesis of well-defined PLA-SS-POEOMA, the aqueous micellization and thiol-responsive degradation was studied. The CMC was measured to be 3 μg/mL. The low CMC value is advantageous as it can confer better colloidal stability to the micelle upon dilution under physiological conditions. Solvent evaporation process was used to prepare colloidally stable micelles at 1.0 mg/mL. DLS indicates the diameter = 30.5 nm, in good agreement with the diameter = 32.2 ± 6.5 nm by transmission electron microscopy (TEM) (Figure 7A). These results suggest that the ABP self-assembled in aqueous solution to form spherical micelles with narrow and monomodal size distribution. To study thiol-responsive degradation, a micellar dispersion was treated with a 1/1 ratio of DTT/disulfide. Shedding of the POEOMA corona, as a result of the cleavage of disulfides at interfaces, resulted in the loss of colloidal stability, accumulating PLA precipitates (Figure 7B).

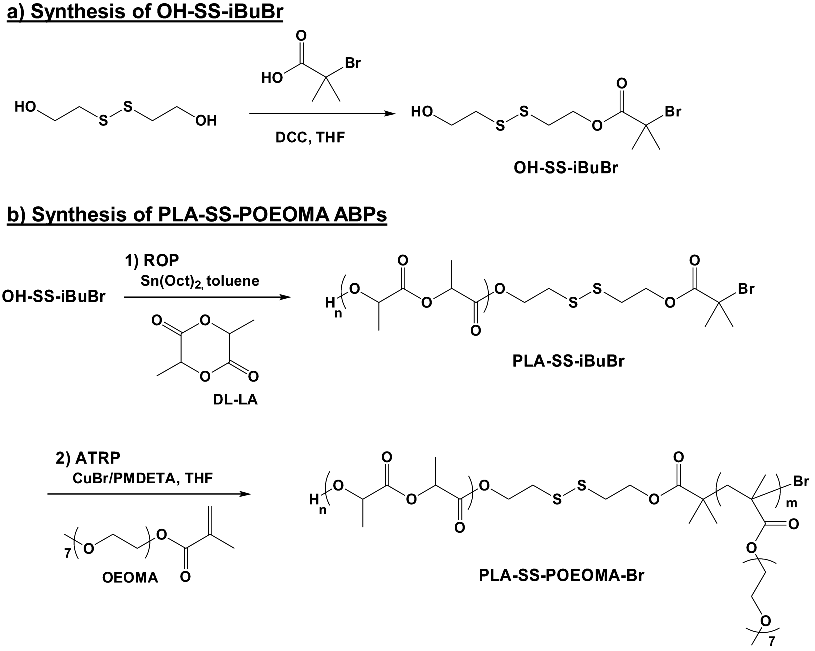
a) Synthesis of OH-SS-iBuBr
DCC, THF
OH-SS-iBuBr
b) Synthesis of PLA-SS-POEOMA ABPs
OH-SS-iBuBr
1) ROP
Sn(Oct)2, toluene
DL-LA
PLA-SS-iBuBr
2) ATRP
CuBr/PMDETA, THF
OEOMA
PLA-SS-POEOMA-Br

Figure 6. Synthesis of OH-SS-iBuBr double-head initiator and PLA-SS-POEOMA Shed-SS-ABPs. Reprinted with permission from ref. (77). Copyright 2011 American Chemical Society.

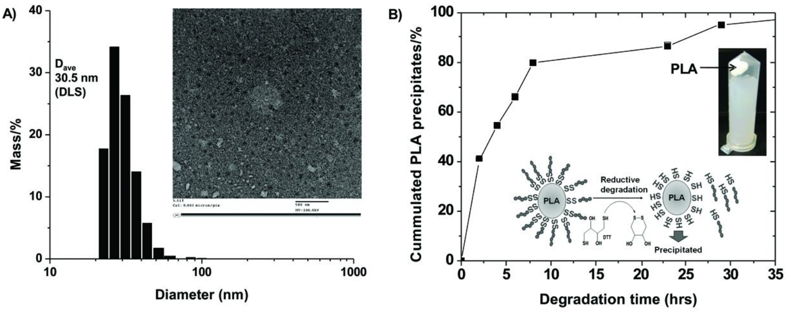

Figure 7. DLS diagram and TEM image with scale bar = 100 nm (A) and degradation (B) of Shed-SS-ABP micelles in the presence of DTT over time. Reprinted with permission from ref. (77). Copyright 2011 American Chemical Society.

Monocleavable BA-ss-AB Type Triblock Copolymer Micelles with Single Disulfides (*67*)

Aqueous micellization of amphiphilic, brush-like triblock copolymers having single disulfides in the symmetric center formed monocleavable micelles with disulfides within the core. The cleavage of disulfides in response to water-soluble thiols caused the dissociation of micelles to smaller-sized assembled structures in water.

Figure 8 shows the synthetic scheme of AB-ss-BA triblock copolymers having single disulfides. First, bis[2-(2-bromoisobutyryloxy)ethyl] disulfide (SS-DBr), a difunctional ATRP initiator was synthesized by a carbodiimide coupling reaction of 2-hydroxyethyl disulfide with α-bromoisobutyric acid as described elsewhere (*78*). In the presence of SS-DBr, AGET (activators generated by electron transfer) ATRP of hydrophobic oligo(propylene oxide) monononylphenyl ether acrylate (AP) with M = 419 g/mol and pendent propylene oxide (PO) units DP≈3 was conducted to synthesize well-controlled ss-$(PAP_{12}\text{-}Br)_2$ with M_n = 12,000 g/mol and M_w/M_n = 1.2 at 24% conversion. For block copolymerization of OEOMA in the presence of ss-$(PAP\text{-}Br)_2$, a halogen exchange process (*79*) was required to synthesize well-defined ss-$(PAP_{12}\text{-}POEOMA_5\text{-}Cl)_2$ ABPs with M_n = 15,200 g/mol and M_w/M_n = 1.2 at 10% conversion. ^{1}H-NMR results also indicate the successful synthesis of ss-ABP_2 block copolymer.

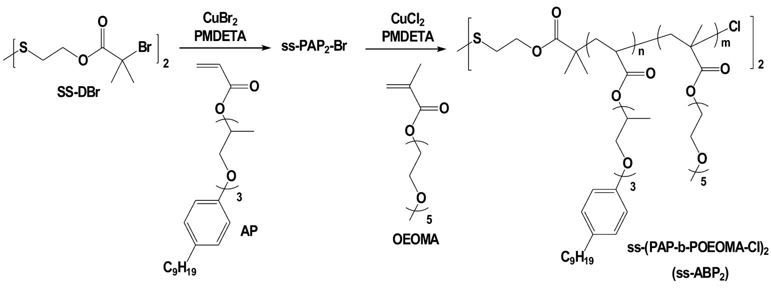

Figure 8. Synthesis of mono-cleavable brush-like symmetric triblock copolymers featured with single disulfides in the middle of hydrophobic blocks. Reprinted with permission from ref. (67). Copyright 2011 Wiley.

Due to amphiphilic nature, the resulting ss-ABP_2 with single disulfides formed stable micelles having the hydrodynamic diameter = 109.3 nm determined by DLS and the CMC = 0.32 mg/mL determined by tensiometry. In the presence of Bu_3P whose amount is defined as the mole ratio of Bu_3P/disulfide = 1/1, ss-ABP_2 was degraded in THF. GPC results show that the molecular weight decreased from 14,500 g/mol to 5,500 g/mol, suggesting significant cleavage of disulfides in reducing conditions. Stable micelles of ss-ABP_2 were mixed with DTT for 1 day. As seen in Figure 9, the hydrodynamic diameter of micelles in water significantly decreased from 109.3 nm to 70.4 nm upon degradation of micelles. AFM images also show a significant change in morphologies. In the absence of DTT, large particles along with small ones were observed. The average diameter was 255.5 ± 128.7 nm. In the presence of DTT, fairly uniform distribution of small particles was observed, with average diameter = 97.8 ± 21.8 nm. The results suggest that DTT cleaved the disulfides in the micellar core, yielding thiol-terminated degraded products (HS-PAP_{12}-$POEOMA_5$-Cl) which remained amphiphilic though shorter than the original ss-ABP_2, and thus re-aggregated to form smaller-sized assembled structures in water.

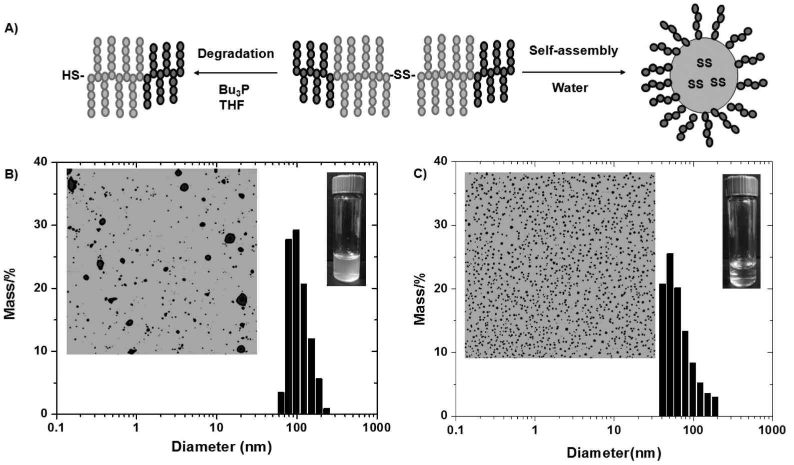

Figure 9. Schematic illustration of micellization and degradation of ss-ABP_2 (A), and DLS diagrams and AFM images (10 µm x 10 µm) of ss-ABP_2-based micelles before (B) and after (C) addition of DTT defined as DTT/disulfide = 1/1 in water (insets: digital images of micellar dispersions in water). Reprinted with permission from ref. (67). Copyright 2011 Wiley.

Cell Viability Using MTS Assay: Noncytotoxicity of New Micellar Carriers

To preliminary assess the newly developed micelles toward biomedical applications, particularly as controlled drug delivery vehicles, *in vitro* cell viability of the micelles was examined using MTS assay (a standard colorimetric method to measure cytotoxicity). Several cell lines including human embryonic kidney HEK293T cells and HeLa cancer cells were cultured with different concentrations of the micelles. Cells without polymers were also included as controls. After a 24 hrs incubation time, absorbance was measured using an absorbance-based plate reader and corrected for an increase due to the presence of micelles. Figure 10 is an example of cell viability results with HeLa cells cultured with Shed-SS-ABP up to 1.0 mg/mL. The results indicate that these micelles, including polyester-based ABP and mono-cleavable micelles, were nontoxic to cells, and thus biocompatible up to 1.0 mg/mL.

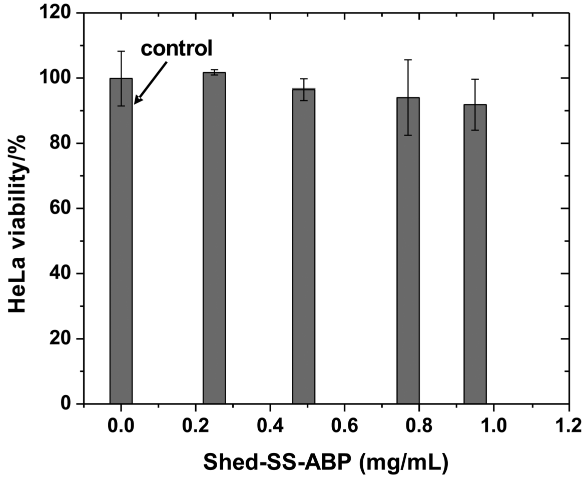

Figure 10. Viability of HeLa cells cultured with Shed-SS-ABP micelles for 24 hrs. Reprinted with permission from ref. (77). Copyright 2011 American Chemical Society.

Summary and Outlook

Thiol-responsive (reductive) degradable disulfides have been explored as an effective degradation platform, because of the existence of biological glutathione in cancer cells at higher levels (10-20 mM) than in normal ones. Three novel thiol-responsive degradable block copolymer micelles were developed. They were designed to be degraded in response to reductive reactions either in the presence of reducing agent or through thiol-disulfide exchange reactions. The degradation rate was varied with different numbers of disulfides positioned at various locations, enhancing the precise control over the release of encapsulated model drugs. These promising results allow a better understanding of the structure-property relationships between structure variance and stimuli-responsive degradation. Ultimately, they can be leveraged into optimizing degradable micelles offering tunable release of encapsulated anticancer therapeutics inside cancer cells.

Acknowledgments

Financial supports from Concordia University Start-Up, NSERC Canada Discovery Grant, FQRNT Equipment Grant, and CRC Award are greatly appreciated. Authors thank B. Khorsand, A. Nelson-Mendez, P. Pinnel, and N. R. Ko for their great contribution to experiments. JKO is Tier II Canada Research Chair (CRC) in Nanobioscience as well as a member of Centre Québécois sur les Matériaux Fonctionnels (CQMF) funded by FQRNT and of Concordia Composite (CONCOM) Center at Concordia University.

References

1. Nishiyama, N.; Kataoka, K. *Adv. Polym. Sci.* **2006**, *193*, 67–101.
2. Mailander, V.; Landfester, K. *Biomacromolecules* **2009**, *10*, 2379–400.
3. Harada, A.; Kataoka, K. *Prog. Polym. Sci.* **2006**, *31*, 949–982.
4. Khandare, J.; Minko, T. *Prog. Polym. Sci.* **2006**, *31*, 359–397.
5. Liu, S.; Maheshwari, R.; Kiick, K. L. *Macromolecules* **2009**, *42*, 3–13.
6. Du, J.-Z.; Du, X.-J.; Mao, C.-Q.; Wang, J. *J. Am. Chem. Soc.* **2011**, *133*, 17560–17563.
7. Tomalia, D. A. *Prog. Polym. Sci.* **2005**, *30*, 294–324.
8. Farokhzad, O. C.; Cheng, J.; Teply, B. A.; Sherifi, I.; Jon, S.; Kantoff, P. W.; Richie, J. P.; Langer, R. *Proc. Natl. Acad. Sci. U.S.A.* **2006**, *103*, 6315–6320.
9. Kim, S. H.; Jeong, J. H.; Chun, K. W.; Park, T. G. *Langmuir* **2005**, *21*, 8852–8857.
10. Oh, J. K.; Lee, D. I.; Park, J. M. *Prog. Polym. Sci.* **2009**, *34*, 1261–1282.
11. Oh, J. K.; Drumright, R.; Siegwart, D. J.; Matyjaszewski, K. *Prog. Polym. Sci.* **2008**, *33*, 448–477.
12. Hamidi, M.; Azadi, A.; Rafiei, P. *Adv. Drug Delivery Rev.* **2008**, *60*, 1638–1649.
13. Raemdonck, K.; Demeester, J.; De Smedt, S. *Soft Matter* **2009**, *5*, 707–715.
14. Liu, Z.; Jiao, Y.; Wang, Y.; Zhou, C.; Zhang, Z. *Adv. Drug Delivery Rev.* **2008**, *60*, 1650–1662.
15. Wu, J.; Eisenberg, A. *J. Am. Chem. Soc.* **2006**, *128*, 2880–2884.
16. Li, W.; Yoon, J. A.; Matyjaszewski, K. *J. Am. Chem. Soc.* **2010**, *132*, 7823–7825.
17. Kim, E.; Kim, D.; Jung, H.; Lee, J.; Paul, S.; Selvapalam, N.; Yang, Y.; Lim, N.; Park, C. G.; Kim, K. *Angew. Chem., Int. Ed.* **2010**, *49*, 4405–4408.
18. Mikhail, A. S.; Allen, C. *J. Controlled Release* **2009**, *138*, 214–223.
19. Xiong, X.-B.; Falamarzian, A.; Garg, S. M.; Lavasanifar, A. *J. Controlled Release* **2011**, *155*, 248–261.
20. Bae, Y.; Kataoka, K. *Adv. Drug Delivery Rev.* **2009**, *61*, 768–784.
21. Abetz, V. *Block Copolymers*; Springer: New York, Vol. II.
22. Byrne, J. D.; Betancourt, T.; Brannon-Peppas, L. *Adv. Drug Delivery Rev.* **2008**, *60*, 1615–1626.
23. Veiseh, O.; Gunn, J. W.; Zhang, M. *Adv. Drug Delivery Rev.* **2010**, *62*, 284–304.
24. Motornov, M.; Roiter, Y.; Tokarev, I.; Minko, S. *Progress in Polymer Science* **2010**, *35*, 174–211.
25. Meng, F.; Zhong, Z.; Feijen, J. *Biomacromolecules* **2009**, *10*, 197–209.
26. Loomis, K.; McNeeley, K.; Bellamkonda, R. V. *Soft Matter* **2011**, *7*, 839–856.
27. Rijcken, C. J. F.; Soga, O.; Hennink, W. E.; van Nostrum, C. F. *J. Controlled Release* **2007**, *120*, 131–148.
28. Wang, Y.; Xu, H.; Zhang, X. *Adv. Mater.* **2009**, *21*, 2849–2864.
29. Schumers, J.-M.; Fustin, C.-A.; Gohy, J.-F. *Macromol. Rapid Commun.* **2010**, *31*, 1588–1607.
30. Kamigaito, M.; Ando, T.; Sawamoto, M. *Chem. Rev.* **2001**, *101*, 3689–3745.

31. Matyjaszewski, K.; Xia, J. *Chem. Rev.* **2001**, *101*, 2921–2990.
32. Davis, K. A.; Matyjaszewski, K. *Adv. Polym. Sci.* **2002**, *159*, 1–166.
33. Matyjaszewski, K.; Davis, T. P. *Handbook of Radical Polymerization*; John Wiley & Sons, Inc.: 2002.
34. Siegwart, D. J.; Oh, J. K.; Matyjaszewski, K. *Prog. Polym. Sci.* **2012**, *37*, 18–37.
35. Blanazs, A.; Armes, S. P.; Ryan, A. J. *Macromol. Rapid Commun.* **2009**, *30*, 267–277.
36. Oh, J. K. *Soft Matter* **2011**, *7*, 5096–5108.
37. Tsarevsky, N. V.; Matyjaszewski, K. *Macromolecules* **2002**, *35*, 9009–9014.
38. Li, C.; Madsen, J.; Armes, S. P.; Lewis, A. L. *Angew. Chem., Int. Ed.* **2006**, *45*, 3510–3513.
39. Carelli, S.; Ceriotti, A.; Cabibbo, A.; Fassina, G.; Ruvo, M.; Sitia, R. *Science* **1997**, *277*, 1681–4.
40. Saito, G.; Swanson, J. A.; Lee, K.-D. *Adv. Drug Delivery Rev.* **2003**, *55*, 199–215.
41. Russo, A.; DeGraff, W.; Friedman, N.; Mitchell, J. B. *Cancer Res.* **1986**, *46*, 2845–8.
42. Rapoport, N. *Prog. Polym. Sci.* **2007**, *32*, 962–990.
43. Alexander, C.; Shakesheff, K. M. *Adv. Mater.* **2006**, *18*, 3321–3328.
44. Huang, X.; Du, F.; Ju, R.; Li, Z. *Macromol. Rapid Commun.* **2007**, *28*, 597–603.
45. Huang, X.; Du, F.; Cheng, J.; Dong, Y.; Liang, D.; Ji, S.; Lin, S.-S.; Li, Z. *Macromolecules* **2009**, *42*, 783–790.
46. Huang, X.-N.; Du, F.-S.; Zhang, B.; Zhao, J.-Y.; Li, Z.-C. *J. Polym. Sci., Part A: Polym. Chem.* **2008**, *46*, 4332–4343.
47. Chen, W.; Meng, F.; Li, F.; Ji, S.-J.; Zhong, Z. *Biomacromolecules* **2009**, *10*, 1727–1735.
48. Jiang, J.; Tong, X.; Zhao, Y. *J. Am. Chem. Soc.* **2005**, *127*, 8290–8291.
49. Babin, J.; Pelletier, M.; Lepage, M.; Allard, J.-F.; Morris, D.; Zhao, Y. *Angew. Chem., Int. Ed.* **2009**, *48*, 3329–3332.
50. Chen, C.-J.; Liu, G.-Y.; Shi, Y.-T.; Zhu, C.-S.; Pang, S.-P.; Liu, X.-S.; Ji, J. *Macromol. Rapid Commun.* **2011**, *32*, 1077–1081.
51. Goodwin, A. P.; Mynar, J. L.; Ma, Y.; Fleming, G. R.; Frechet, J. M. J. *J. Am. Chem. Soc.* **2005**, *127*, 9952–9953.
52. Fomina, N.; McFearin, C.; Sermsakdi, M.; Edigin, O.; Almutairi, A. *J. Am. Chem. Soc.* **2010**, *132*, 9540–9542.
53. Wang, J.; Pelletier, M.; Zhang, H.; Xia, H.; Zhao, Y. *Langmuir* **2009**, *25*, 13201–13205.
54. Du, J.-Z.; Chen, D.-P.; Wang, Y.-C.; Xiao, C.-S.; Lu, Y.-J.; Wang, J.; Zhang, G.-Z. *Biomacromolecules* **2006**, *7*, 1898–1903.
55. Jin, Y.; Song, L.; Su, Y.; Zhu, L.; Pang, Y.; Qiu, F.; Tong, G.; Yan, D.; Zhu, B.; Zhu, X. *Biomacromolecules* **2011**, *12*, 3460–8.
56. Lutz, J.-F.; Andrieu, J.; Uezguen, S.; Rudolph, C.; Agarwal, S. *Macromolecules* **2007**, *40*, 8540–8543.
57. Ma, N.; Li, Y.; Xu, H.; Wang, Z.; Zhang, X. *J. Am. Chem. Soc.* **2010**, *132*, 442–443.

58. Han, D.; Tong, X.; Zhao, Y. *Macromolecules* **2011**, *44*, 437–439.
59. van Nostrum, C. F. *Soft Matter* **2011**, *7*, 3246–3259.
60. Zhang, L.; Liu, W.; Lin, L.; Chen, D.; Stenzel, M. H. *Biomacromolecules* **2008**, *9*, 3321–3331.
61. Li, Y.; Lokitz, B. S.; Armes, S. P.; McCormick, C. L. *Macromolecules* **2006**, *39*, 2726–2728.
62. Dai, J.; Lin, S.; Cheng, D.; Zou, S.; Shuai, X. *Angew. Chem., Int. Ed.* **2011**, *50*, 9404–9408.
63. Zhang, L.; Bernard, J.; Davis, T. P.; Barner-Kowollik, C.; Stenzel, M. H. *Macromol. Rapid Commun.* **2008**, *29*, 123–129.
64. Li, Y.; Du, W.; Sun, G.; Wooley, K. L. *Macromolecules* **2008**, *41*, 6605–6607.
65. Duong, H. T. T.; Marquis, C. P.; Whittaker, M.; Davis, T. P.; Boyer, C. *Macromolecules* **2011**, *44*, 8008–8019.
66. Xu, X.; Flores, J. D.; McCormick, C. L. *Macromolecules* **2011**, *44*, 1327–1334.
67. Khorsand Sourkohi, B.; Schmidt, R.; Oh, J. K. *Macromol. Rapid Commun.* **2011**, *32*, 1652–1657.
68. Kang, M.; Moon, B. *Macromolecules* **2009**, *42*, 455–458.
69. Schumers, J.-M.; Gohy, J.-F.; Fustin, C.-A. *Polym. Chem.* **2010**, *1*, 161–163.
70. Ren, T.-B.; Feng, Y.; Zhang, Z.-H.; Li, L.; Li, Y.-Y. *Soft Matter* **2011**, *7*, 2329–2331.
71. Klaikherd, A.; Nagamani, C.; Thayumanavan, S. *J. Am. Chem. Soc.* **2009**, *131*, 4830–4838.
72. Liu, J.; Pang, Y.; Huang, W.; Huang, X.; Meng, L.; Zhu, X.; Zhou, Y.; Yan, D. *Biomacromolecules* **2011**, *12*, 1567–1577.
73. Brinkhuis, R. P.; Visser, T. R.; Rutjes, F. P. J. T.; van Hest, J. C. M. *Polym. Chem.* **2011**, *2*, 550–552.
74. Katz, J. S.; Zhong, S.; Ricart, B. G.; Pochan, D. J.; Hammer, D. A.; Burdick, J. A. *J. Am. Chem. Soc.* **2010**, *132*, 3654–3655.
75. Nelson-Mendez, A.; Aleksanian, S.; Oh, M.; Lim, H.-S.; Oh, J. K. *Soft Matter* **2011**, *7*, 7441–7452.
76. Khorsand Sourkohi, B.; Cunningham, A.; Zhang, Q.; Oh, J. K. *Biomacromolecules* **2011**, 3819–3825.
77. Khorsand, S. B.; Cunningham, A.; Zhang, Q.; Oh, J. K. *Biomacromolecules* **2011**, 3819–3825.
78. Tsarevsky, N. V.; Matyjaszewski, K. *Macromolecules* **2005**, *38*, 3087–3092.
79. Shipp, D. A.; Wang, J.-L.; Matyjaszewski, K. *Macromolecules* **1998**, *31*, 8005–8008.

Chapter 20

(Nitrilotriacetic Acid)-End-Functionalized Polystyrenes Synthesized by ATRP

Mohammad Abdul Kadir,[1] Hong Y. Cho,[1] Bong-Soo Kim,[1]
Young-Rok Kim,[2] Sun-Gu Lee,[3] Unyong Jeong,[4]
and Hyun-jong Paik*,[1]

[1]Department of Polymer Science & Engineering, Pusan National University,
San 30 Jangjeon 2-dong Geumjeong-gu, Busan 609-735, Korea
[2]Department of Food Science, and Biotechnology & Institute
of Life Sciences and Resources, College of Life Sciences,
Kyung Hee University, Yongin, Korea
[3]Department of Chemical Engineering, Pusan National University,
San 30 Jangjeon 2-dong Geumjeong-gu, Busan 609-735, Korea
[4]Department of Materials Science and Engineering, Yonsei University,
134 Shinchon-dong, Seoul, Korea
***E-mail: hpaik@pusan.ac.kr**

Downloaded by UNIV OF GUELPH LIBRARY on June 1, 2012 | http://pubs.acs.org
Publication Date (Web): March 20, 2012 | doi: 10.1021/bk-2012-1101.ch020

The synthesis of nitrilotriacetic acid end-functionalized polystyrenes (NTA-PS) using *t*-butyl protected NTA initiators via atom transfer radial polymerization (ATRP) of styrene is described. The protected *t*-butyl group is subsequently removed at the α-chain end of polystyrene. After complexation of NTA chain ends of the polystyrenes with Ni^{2+} to produce Ni-NTA-PS, conjugation with (six histidine-tagged green fluorescent protein) His_6-GFP via Ni^{2+}/histidine (His) interaction and the self-assembly of the resulted bioconjugate are studied. Highly mesoporous NTA-PS fibers are also produced by taking advantage of interpenetrating phase separation between PS and poly(ethylene oxide) (PEO) during electrospinning. The specific interaction of Ni^{2+}-complexed NTA-PS fibers with His enables to immobilize and purify only target proteins from highly heterogeneous protein mixtures.

In Progress in Controlled Radical Polymerization: Materials and Applications; Matyjaszewski, K., et al.;
ACS Symposium Series; American Chemical Society: Washington, DC, 2012.

Downloaded by UNIV OF GUELPH LIBRARY on June 1, 2012 | http://pubs.acs.org
Publication Date (Web): March 20, 2012 | doi: 10.1021/bk-2012-1101.ch020

Introduction

Bioconjugation of synthetic polymers with modified proteins have potential applications in biotechnology as improving the solubility, biocompatibility, and stability of hydrid materials (*1*). Generally polymer-protein bioconjugates are prepared by the reaction of pre-synthesized end-functional polymers with proteins (*2*). Recent advances in polymer synthesis, in particular, controlled radical polymerizations (CRPs), provided avenues to polymers with well-defined composition, molecular shape, chain length, and α,ω-functionality (*3*). The reactive chain-ends has been used to conjugate functional proteins. For example, using CRPs (*4*), well-defined polymers with *N*-succinimide ester (*5*, *6*), aldehyde (*7*), thiol, maleimide (*8*, *9*) or pyridyl disulfide (*10*) chain-ends have been used to conjugate with targeted proteins.

Nitrilotriacetic acid (NTA) is a tetradentate ligand which occupies four of the six binding sites of Ni^{2+}, leaving two free sites for histidine-tagged proteins (His-tagged proteins) to bind. The magnetism of the use of NTA and Ni^{2+} complexes is the selective binding due to the strong coordination with histidines. The NTA chelating chemistry with His-tagged proteins offers several advantages of biochemical recognition elements (*11*). First, fast and reversible reaction of Ni^{2+} with histidines, where competitor ligand, such as imidazole could relocate the histidine-tagged proteins. Second, Ni^{2+}-NTA chemistry is a very well defined and efficient immobilization system in biology. NTA chelated with transition metals were successfully applied for protein purification (*12*) and detection (*11*, *13*), as well as for surface immobilizations (*14–18*) and for tethering to lipid membranes (*19–21*).

Conjugation of protein with polymers via NTA chemistry has been widly studied on selective protein binding. Kiessling *et al.* synthesized poly (*N*-methacryloxysuccinimide), where NTA derivatives were appended to the polymer backbone. After nickel complexation, histidine-tagged fibroblast growth factor 8b (His-tag FGF-8b) was clustered with NTA moiety through noncovalent interaction (*22*). Ober *et al.* polymerized acrylamide monomer with an NTA moiety, which was incorporated into 2-hydroxyethyl methacrylate (HEMA) hydrogels in a controlled fashion for the specific protein immobilization (*23*) Ramstedt *et al.* prepared NTA functionalized protein-resistant poly(oliogoethylene glycol methacrylate) (POEGMA) polymer brushes (*24*). POEGMA brush-coated surface prevent nonspecific interactions with original substrate.

In this chapter, we will review the synthesis and characterization of NTA functionalized polystyrenes prepared by atom transfer radical polymerization (ATRP), one of CRPs technique, and their applications in bioconjugation and protein purification based on our recent publications (*25*, *26*).

Downloaded by UNIV OF GUELPH LIBRARY on June 1, 2012 | http://pubs.acs.org
Publication Date (Web): March 20, 2012 | doi: 10.1021/bk-2012-1101.ch020

Synthesis and Characterization of NTA End-Functionalized Polystyrenes

The NTA end-functionalized polystyrenes can be synthesized using initiators (**2a** or **2b**) by ATRP in the presence of CuCl catalyst system (Scheme 1). The use of 4,4′-di(5-nonyl)-2,2′-bipyridine (dNbpy) instead of *N,N,N′,N′,N″*-pentamethyldiethylenetriamine (PMDETA) and employing halogen exchange technique (*27*) provide better control on polymerizations (Table I).

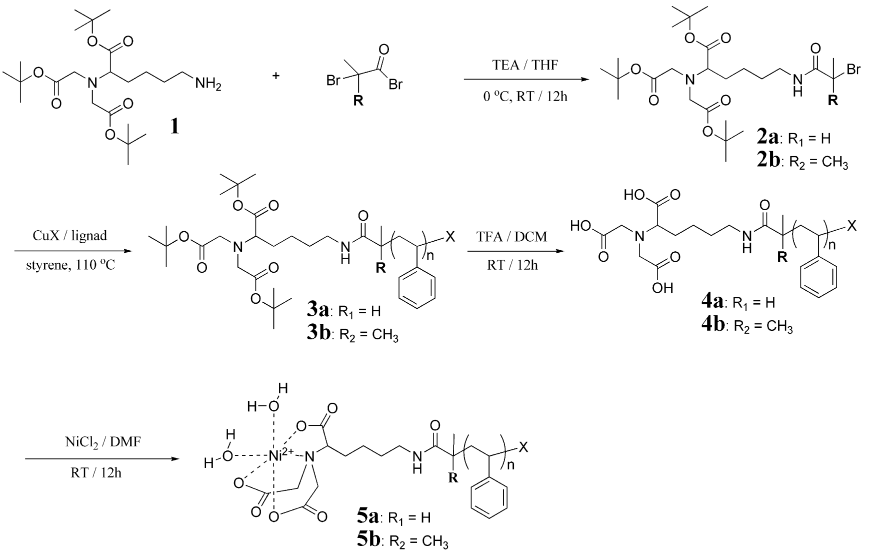

Scheme 1. Preparation of Ni²⁺-complexed-NTA end-functionalized polystyrene (Ni-NTA-PS). (Reproduced with permission from reference (25). Copyright 2011.)

Polymerization with initiator **2b** together with dNbpy yields well-defined polystyrene, **5** (entries 4-6 in Table I) as **2b** initiator shows fast activation rate. In addition, fast deactivation rate with bpy based catalyst also contributes to the improvement of initiation efficiency (*28*).

The polymerization of styrene with **2b** along with CuCl/dNbpy catalyst system shows typical characteristics of living polymerization. The first order kinetic plot is linear and the rate of radical generation is faster than that of **2a**. The molecular weight increases linearly with conversion, which shows good agreement with theoretical molecular weight. The molecular weight distribution is as narrow as 1.09 (Figure 1 and Figure 2).

Table I. ATRP of styrene using NTA derivative initiators at 110 °C. (Reproduced with permission from reference (*25*). Copyright 2011.)

No.	*$[M]_0$ /$[I]_0$*	*$[I]_0$*	*Catalyst*	*Time [hr]*	*Conv. [%]*	*$M_{n,}$ GPC [10^3]*	*M_w /M_n*	*$M_{n,}$ theory^a [10^3]*
1	672	**2a**	CuBr/PMDETA	17	34	154	1.45	24.7
2	672	**2a**	CuCl/PMDETA	7	26	170	1.67	18.7
3	196	**2a**	CuCl/2dNbpy	5.75	27	11.0	1.26	6.1
4	196	**2b**	CuCl/2dNbpy	14	55	13.5	1.21	11.8
5	48	**2b**	CuCl/2dNbpy	14	72	4.9	1.09	4.2
6	29	**2b**	CuCl/2dNbpy	20	70	3.9	1.08	2.7

1: $[M]_0$=7.9 M, $[I]_0$=$[CuBr/PMDETA]_0$=1.2 × 10^{-2} M, anisole=7.8 × 10^{-1} mL.
2: $[M]_0$=4.3 M, 2$[I]_0$=$[CuCl/PMDETA]_0$ = 1.3 × 10^{-2} M, anisole = 7.8 mL.
3: $[M]_0$=4.3 M, 2$[I]_0$=$[CuCl/2dNbpy]_0$ = 4.5 × 10^{-2} M, anisole = 1.5 mL.
4: $[M]_0$=4.3 M, 2$[I]_0$=$[CuCl/2dNbpy]_0$ = 4.5 × 10^{-2} M, anisole = 1.5 mL.
5: $[M]_0$=4.3 M, 2$[I]_0$=$[CuCl/2dNbpy]_0$ = 1.8 × 10^{-1} M, anisole = 1.0 mL.
6: $[M]_0$=4.3 M, $[I]_0$=$[CuCl/2dNbpy]_0$ = 1.5 × 10^{-1} M, anisole = 3.0 mL.
^{a} $M_{\text{n, theory}}$ = conversion × ($[M]_0/[I]_0$) × M_{monomer} + $M_{\text{initiator}}$.

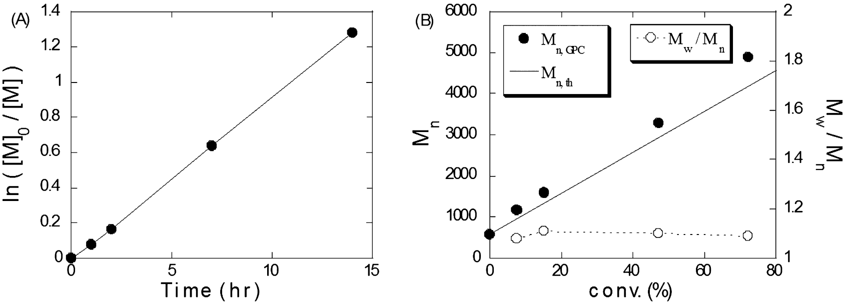

*Figure 1. Results of styrene ATRP using **2b** (entry 5, Table I); (A) first-order kinetic plots, (B) M_n and M_w/M_n evolution on monomer conversion. (Reproduced with permission from reference (25). Copyright 2011.)*

Downloaded by UNIV OF GUELPH LIBRARY on June 1, 2012 | http://pubs.acs.org
Publication Date (Web): March 20, 2012 | doi: 10.1021/bk-2012-1101.ch020

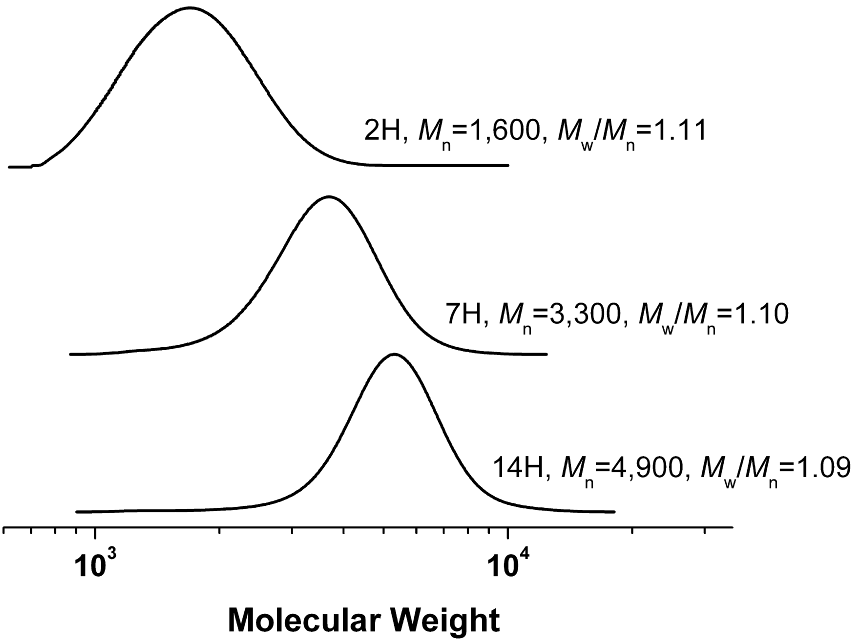

Figure 2. Gel permeation chromatogram traces of NTA-PS (entry 5, Table I). (Reproduced with permission from reference (25). Copyright 2011.)

Downloaded by UNIV OF GUELPH LIBRARY on June 1, 2012 | http://pubs.acs.org
Publication Date (Web): March 20, 2012 | doi: 10.1021/bk-2012-1101.ch020

The presence of NTA moiety in PS (entry 6 in Table I) can be verified by ^{1}H NMR (Figure 3). Peaks at 1.33 (a, $(CH_3)_3$-) and 1.35 ppm (b, $(CH_3)_3$-) are assigned to *t*-butyl protons and peaks at 2.71 (h, -CH_2-), 3.15 (d, -CH-), 3.38 (c, -CH_2-) 4.25 (n, -CH-Cl) and 5.17 (i, -NH-) ppm are clearly assigned to NTA moiety in Figure 3 (A). Based on the integral ratio of peak h (2.6-2.8 ppm), to the phenyl ring proton (6.2-7.4 ppm), the M_n of **3b** is calculated to be 4,750 g/mol. M_n calculated from ^{1}H NMR agrees well with those from GPC ($M_{n,\ \mathrm{GPC}}$ = 4,900).

Downloaded by UNIV OF GUELPH LIBRARY on June 1, 2012 | http://pubs.acs.org
Publication Date (Web): March 20, 2012 | doi: 10.1021/bk-2012-1101.ch020

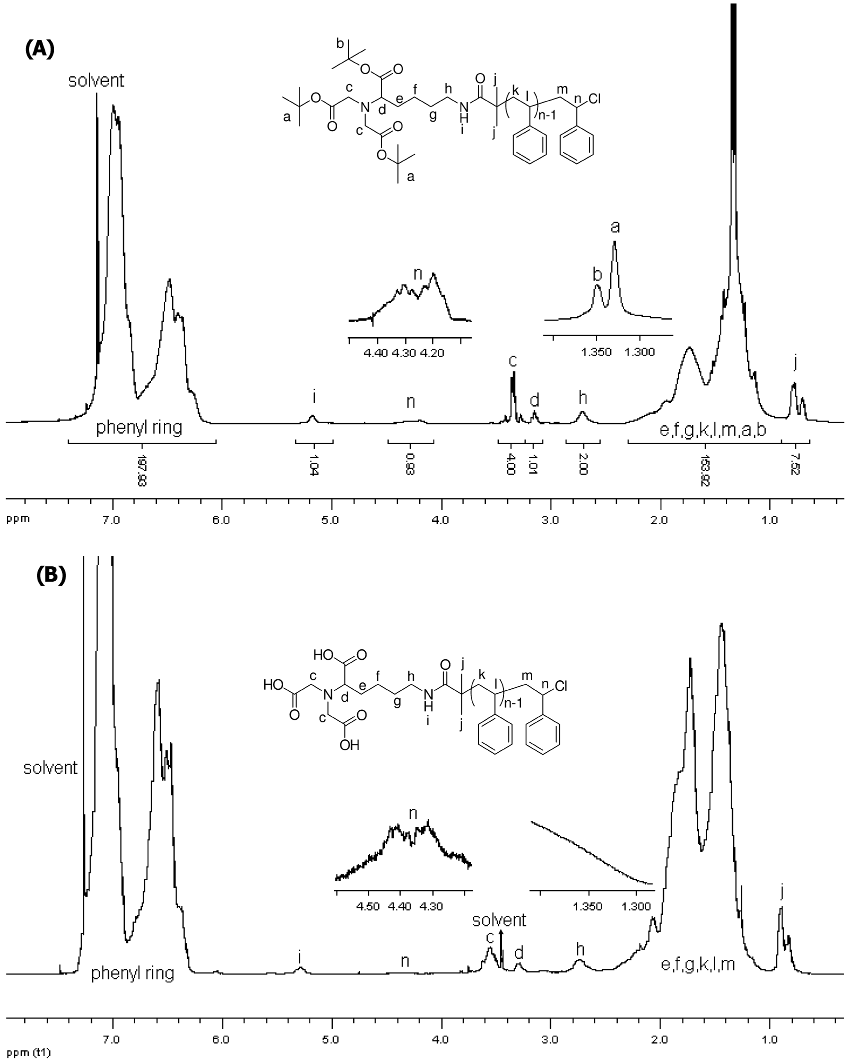

*Figure 3. (A) ^{1}H NMR spectra of α–(p-NTA)-polystyrene, **3b**, ($M_{n,\,GPC}$ = 3,900; M_w/M_n = 1.08,), $CDCl_3$ 100%, and (B) α-(NTA)-polystyrene, **4b**, ($M_{n,\,GPC}$ = 3,500; M_w/M_n = 1.18), mixed solvent system ($CDCl_3$/MeOH-d_4 = 99/1 by vol. %). (Reproduced with permission from reference (25). Copyright 2011.)*

Applications of NTA End-Functionalized Polystyrenes

NTA-modified polystyrene and its chemistry to complex with Ni^{2+}; which was explained in introduction part, enable NTA-PS to become a functional material. Accordingly it has applications in bioconjugation and bioseparation.

Downloaded by UNIV OF GUELPH LIBRARY on June 1, 2012 | http://pubs.acs.org
Publication Date (Web): March 20, 2012 | doi: 10.1021/bk-2012-1101.ch020

Formation of Micellar Aggregates and Conjugation with Protein

NTA-PS has an amphiphilic property due to hydrophilic NTA moiety and hydrophobic PS chain. Therefore, it produces micellar aggregates when water is added to THF solution containing **4b** (without Ni^{2+}) and **5b** (with Ni^{2+}), respectively. SEM and TEM studies show that the size of aggregates is ~500 nm (Figure 4). Aggregates are spherical and relatively uniform in size. Energy dispersive x-ray (EDX) fluorescence analysis confirms the presence of Ni^{2+} in the aggregates.

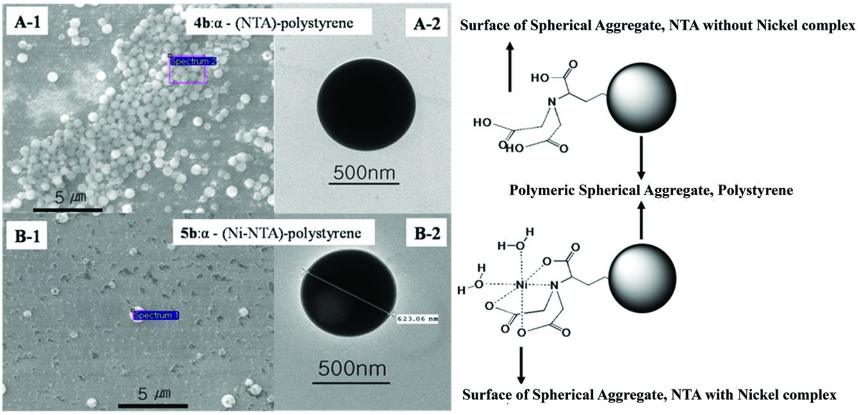
A-1
4b:α - (NTA)-polystyrene
A-2
Spectrum 2
5 μm
500nm
B-1
5b:α - (Ni-NTA)-polystyrene
B-2
Spectrum 1
623.06 nm
500nm
5 μm
Surface of Spherical Aggregate, NTA without Nickel complex
HO
O
N
HO
O
HO
O
Polymeric Spherical Aggregate, Polystyrene
H
H–O
O
O
H
H–O
Ni
N
O
O
O
O
Surface of Spherical Aggregate, NTA with Nickel complex

Figure 4. SEM and TEM images of the aggregates from the α-(NTA)-polystyrene; A-1 and A-2 are without nickel, B-1 and B-2 are with nickel. (Reproduced with permission from reference (25). Copyright 2011.)

His_6-GFP binding property on the spherical aggregates produced from **4b** (without Ni^{2+}) and **5b** (with Ni^{2+}) is observed with fluorescence microscopy (Figure 5). The fluorescence intensity of **4b** (A-1) is weaker than that of **5b** (B-1), which is due to the absence of nickel for chelating between His_6-GFP and NTA on the surface of spherical aggregates specifically (**4b**). According to Figure 5, the adsorption of His_6-GFP on the surface of spherical aggregates of **4b** is irreversible and non-specific, because the fluorescence intensity is rarely reduced even after treating with excess imidazole. However, in the case of **5b**, the fluorescence intensity decreases from 100 (before rinsing with imidazole, Figure 5, B-1) to 14 (after rinsing with imidazole, Figure 5, B-2) due to the specific and reversible binding of nickel on the surface of **5b** with His_6-GFP.

Downloaded by UNIV OF GUELPH LIBRARY on June 1, 2012 | http://pubs.acs.org
Publication Date (Web): March 20, 2012 | doi: 10.1021/bk-2012-1101.ch020

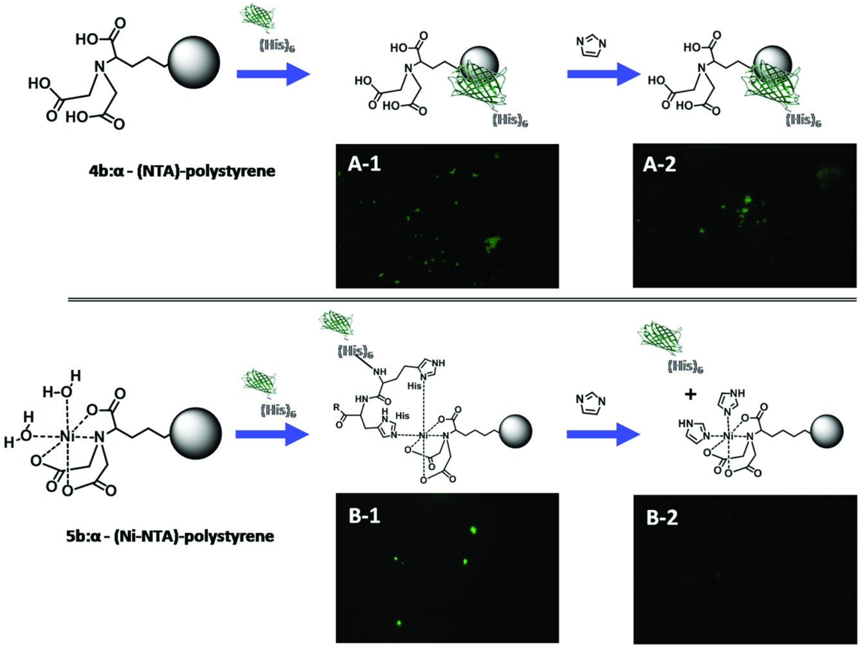

*Figure 5. Fluorescence microscope images of the aggregates from the α-(NTA)-polystyrene; A-1; non-specific binding of His$_6$-GFP with **4b**, A-2; after rinse with excess imidazole, B-1; Specific binding of His$_6$-GFP to NTA of **5b** in presence of Ni, B-2; after rinse with excess imidazole. (Reproduced with permission from reference (25). Copyright 2011.)*

On the other hand, slow addition of Ni-NTA-PS (M_n=21,800) dissolved in DMF (4 vol. % of water) to deionized water containing His$_6$-GFP produces well defined micelles due to specific interaction between polymer and protein via NTA-Ni^{2+}/His$_6$-tag interaction and amphiphilic nature of the resulted bioconjugate. The size of micelles decreases when competitor ligand (e.g.; imidazole) is added to the polymer-protein micellar solution due to the release of GFP by imidazole as is evidenced by TEM and DLS studies (Figure 6).

We also studied the effect of solvents (DMF and THF) on self-assembly structures of resulted bioconjugate following the slow addition of polymer (Ni-NTA-PS, M_n=21,800) dissolved in respective solvents to deionized water containing His$_6$-GFP under stirring. We observed that H_2O/DMF system produced well defined micellar aggregates, while H_2O/THF produced ill defined and larger aggregates (Figure 7). This might be due to poor solubility of His$_6$-GFP in THF.

Downloaded by UNIV OF GUELPH LIBRARY on June 1, 2012 | http://pubs.acs.org
Publication Date (Web): March 20, 2012 | doi: 10.1021/bk-2012-1101.ch020

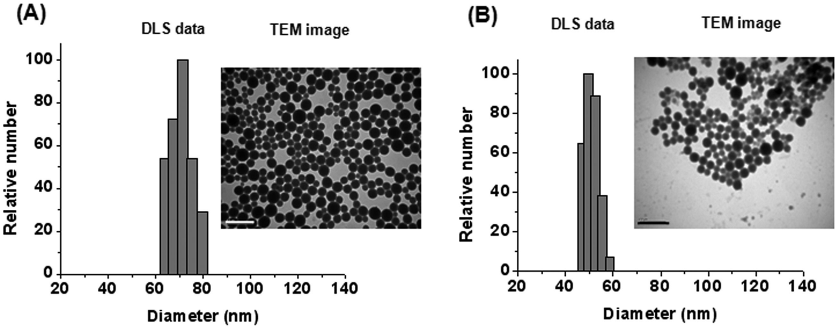

Figure 6. TEM and DLS data of Ni-NTA-PS (M_n=21,800) with His_6-GFP in water/DMF: (A) after conjugation (B) after addition of excess imidazole. Scale bar of TEM images = 500 nm. (Reproduced with permission from reference (25). Copyright 2011.)

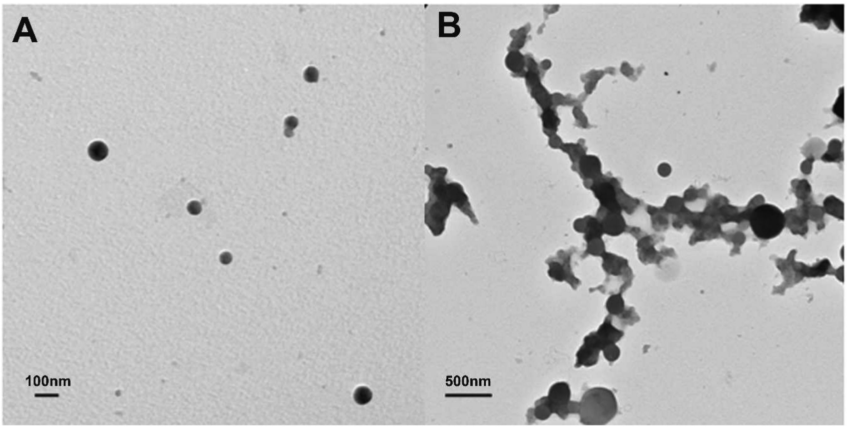

Figure 7. TEM images of Ni-NTA-PS (M_n=21,800) with His_6-GFP: (A) in water/DMF (B) in water/THF.

Formation of Mesoporous Fibres for Protein Purification

Highly mesoporous NTA-PS fibers could be produced by employing the phase separation between NTA-PS and polyethyleneoxide (PEO) during electrospinning. A mixture solution of PEO and NTA-PS was electrospun on a collector substrate. The polymer solution in chloroform (9 wt % polymer in total solution) was accelerated through a metal needle at 12 kV. Diameter of the as-spun fibers was about 1 μm (Figure 8(A)). Due to the poor miscibility between the two polymers, the polymers phase separated as the concentration increased during electrospinning. The equivalent mixture of the two polymers (1:1, w/w) forms a bicontinuous network structure inside the as-spun fibers. The porous feature on the fiber surfaces is shown in Figure 8(B). The pore size on the fiber surfaces ranged from 50 to 300 nm. The fractured cross-sectional image in Figure 8(C) displays the interpenetrating mesopores. The TEM image in Figure 8(D) clearly visualizes the mesoporous structure of the fibers. The mesoporous structure creates a lot of surfaces and helps the diffusion of proteins, which is effective for a rapid binding-and-elution response.

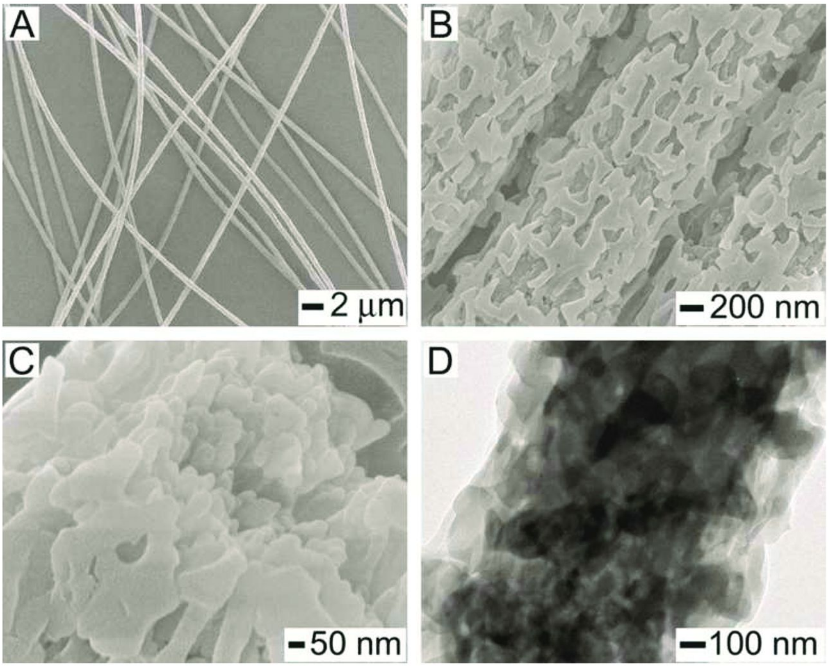

Figure 8. SEM and TEM images showing the mesoporous structure of NTA-PS fibers. (A,B) Low and high magnification of mesopores on the fiber surfaces, (C) cross-sectional SEM image of a fractured fiber, and (D) TEM image showing 3D interpenetrating pores. (Reproduced with permission from reference (26). Copyright 2010.)

These highly mesoporous NTA-PS fibers could be utilized for the functionalized microfluidic channels. The PDMS molds were directly placed on mesoporous fiber mats. The top and bottom were covered with slide glasses and tightly pressed (Scheme 2). The pressurized nanofibers by the molds were densified and did not allow water penetration. Meanwhile, the unpressurized area maintained the loose structure of the as-spun fibers so that water absorption was immediate. The unpressurized region could play as the microfludic channels. The specific affinity of Ni to imidazole moieties in histidines enabled large amount of specific binding to the recombinant proteins. Supplying pure imidazole replaced the binding and released the proteins.

Downloaded by UNIV OF GUELPH LIBRARY on June 1, 2012 | http://pubs.acs.org
Publication Date (Web): March 20, 2012 | doi: 10.1021/bk-2012-1101.ch020

Downloaded by UNIV OF GUELPH LIBRARY on June 1, 2012 | http://pubs.acs.org
Publication Date (Web): March 20, 2012 | doi: 10.1021/bk-2012-1101.ch020

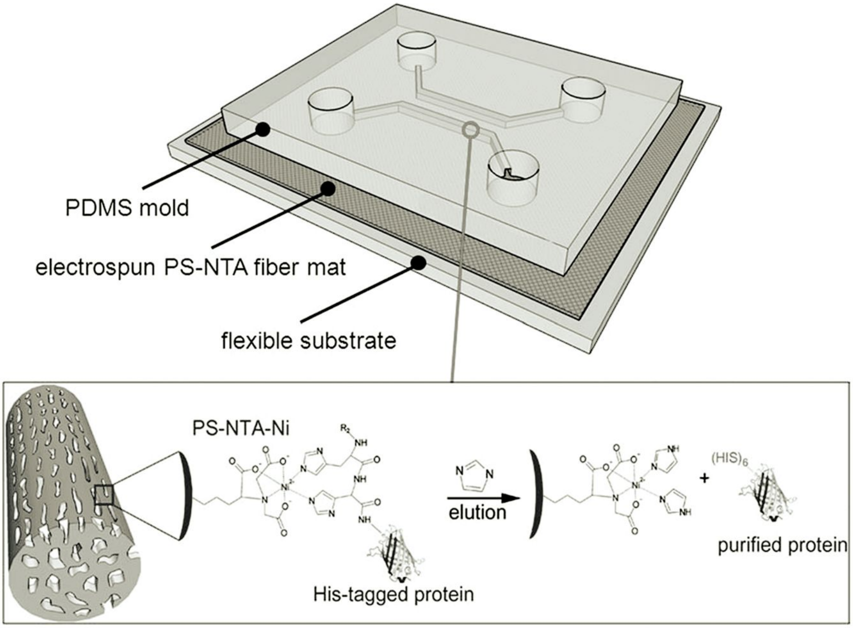

Scheme 2. Layout of the microfluidic device and illustration of purification of histidine-tagged proteins using the mesoporous NTA-PS fibers. (Reproduced with permission from reference (26). Copyright 2010.)

Conclusions

The synthesis of nitrilotriacetic acid end-functionalized polystyrenes (NTA-PS) using *t*-butyl protected NTA initiators via atom transfer radial polymerization (ATRP) of styrene is described. Due to presence of NTA moiety, NTA-PS has potential applications in bioconjugation and protein purification.

Acknowledgments

This work was supported by the Active Polymer Center for Pattern Integration (R11-2007-050-02002-0) and WCU (World Class University) program (R33-10035-0) through the National Research Foundation (NRF) grant funded by the Korea government (MEST).

References

1. Lutz, J.-F.; Börner, H. G. *Prog. Polym. Sci.* **2008**, *33*, 1–39.
2. Nicolas, J.; Mantovani, G.; Haddleton, D. M. *Macromol. Rapid Comm.* **2007**, *28*, 1083–1111.
3. Braunecker, W. A.; Matyjaszewski, K. *Prog. Polym. Sci.* **2007**, *32*, 93–146.
4. Le Droumaguet, B.; Nicolas, J. *Polym. Chem.* **2010**, *1*, 563–598.

Downloaded by UNIV OF GUELPH LIBRARY on June 1, 2012 | http://pubs.acs.org
Publication Date (Web): March 20, 2012 | doi: 10.1021/bk-2012-1101.ch020

5. Lecolley, F.; Tao, L.; Mantovani, G.; Durkin, I.; Lautru, S.; Haddleton, D. M. *Chem. Comm.* **2004**, 2026–2027.
6. Li, H.; Bapat, A. P.; Li, M.; Sumerlin, B. S. *Polym. Chem.* **2011**, *2*, 323–327.
7. Tao, L.; Mantovani, G.; Lecolley, F.; Haddleton, D. M. *J. Am. Chem. Soc.* **2004**, *126*, 13220–13221.
8. Mantovani, G.; Lecolley, F.; Tao, L.; Haddleton, D. M.; Clerx, J.; Cornelissen, J. J. L. M.; Velonia, K. *J. Am. Chem. Soc.* **2005**, *127*, 2966–2973.
9. Li, M.; De, P.; Li, H.; Sumerlin, B. S. *Polym. Chem.* **2010**, *1*, 854–859.
10. Bontempo, D.; Heredia, K. L.; Fish, B. A.; Maynard, H. D. *J. Am. Chem. Soc.* **2004**, *126*, 15372–15373.
11. Ueda, E. K. M.; Gout, P. W.; Morganti, L. *J. Chromatogr., A* **2003**, *988*, 1–23.
12. Mattiasson, B.; Kumar, A.; Ivanov, A. E.; Galaev, I. Y. *Nat. Protoc.* **2007**, *2*, 213–220.
13. Hart, C.; Schulenberg, B.; Diwu, Z.; Leung, W.-Y.; Patton, W. F. *Electrophoresis* **2003**, *24*, 599–610.
14. Sigal, G. B.; Bamdad, C.; Barberis, A.; Strominger, J.; Whitesides, G. M. *Anal. Chem.* **1996**, *68*, 490–7.
15. Gershon, P. D.; Khilko, S. *J. Immunol. Method.* **1995**, *183*, 65–76.
16. Schmid, E. L.; Keller, T. A.; Dienes, Z.; Vogel, H. *Anal. Chem.* **1997**, *69*, 1979–1985.
17. Xu, C.; Xu, K.; Gu, H.; Zhong, X.; Guo, Z.; Zheng, R.; Zhang, X.; Xu, B. *J. Am .Chem. Soc.* **2004**, *126*, 3392–3393.
18. Schmitt, L.; Ludwig, M.; Gaub, H. E.; Tampe, R. *Biophys. J.* **2000**, *78*, 3275–3285.
19. Schmitt, L.; Dietrich, C.; Tampe, R. *J. Am. Chem. Soc.* **1994**, *116*, 8485–91.
20. Dietrich, C.; Schmitt, L.; Tampe, R. *Proc. Natl. Acad. Sci. U.S.A.* **1995**, *92*, 9014–18.
21. Dorn, I. T.; Eschrich, R.; Seemuller, E.; Guckenberger, R.; Tampe, R. *J. Mol. Biol.* **1999**, *288*, 1027–1036.
22. Griffith, B. R.; Allen, B. L.; Rapraeger, A. C.; Kiessling, L. L. *J. Am. Chem. Soc.* **2004**, *126*, 1608–1609.
23. Yu, T.; Wang, Q.; Johnson, D. S.; Wang, M. D.; Ober, C. K. *Adv. Funct. Mater.* **2005**, *15*, 1303–1309.
24. Gautrot, J. E.; Huck, W. T. S.; Welch, M.; Ramstedt, M. *ACS Appl. Mater. Interfaces* **2009**, *2*, 193–202.
25. Cho, H. Y.; Kadir, M. A.; Kim, B.-S.; Han, H. S.; Nagasundarapandian, S.; Kim, Y.-R.; Ko, S. B.; Lee, S.-G.; Paik, H.-j. *Macromolecules* **2011**, *44*, 4672–4680.
26. Jo, E.; Lim, M.-C.; Kim, H.-N.; Paik, H.-J.; Kim, Y.-R.; Jeong, U. *J. Polym. Sci., Part B: Polym. Phys* **2011**, *49*, 89–95.
27. Shipp, D. A.; Wang, J.-L.; Matyjaszewski, K. *Macromolecules* **1998**, *31*, 8005–8008.
28. Matyjaszewski, K.; Paik, H.-j.; Zhou, P.; Diamanti, S. J. *Macromolecules* **2001**, *34*, 5125–5131.

Subject Index

A

Adhesion process, polyelectrolyte brushes preparation, 192*f*
Alcohol esterification, 89*s*
Antifouling properties, polyelectrolyte brushes preparation, 185
Arm number determination, 157
ATRP kinetics, 30*f*

B

Bioactive glycopolymers
  BIEM, SCVCP, 264*f*
  branched glycopolymers via SCVCP, 263*s*
  fluorescent glycopolymer hybrid nanoparticles, 265
  glucosamine-containing polymer brushes synthesis, 259*s*
  glycocoplymer-grafted nanoparticles, 267*f*
  glycocoplymer-grafted nanospheres, 266*f*
  glycopolymer brushes, 260*f*
  glycopolymer-grafted DVB microspheres synthesis, 261*s*
  glycopolymer-grafted polystyrene nanospheres, 259
  grafted microspheres, 265*f*
  hyperbranched glycopolymer covered microspheres, 264*s*
  hyperbranched glycopolymer-grafted microspheres, 263
  magnetic glycopolymer hybrid nanoparticles, 265
  MAMan grafted microspheres, 262*f*
  nanoparticle synthesis, 265*s*
  overview, 257
  polymeric microsphere surface modification, 261
  ungrafted microspheres, 265*f*
Biomolecule immobilization, polymer brushes, 251*s*
Block copolymer phase separation analysis, 118
Block copolymers
  BC1 – BC5, 131*f*
  BC1 – BC5 characterization, 130*t*
  component peaks, 137*t*
  film parameters, 133*t*
  film preparation, 132
    nanostructured polymer films preparation, 132
    XPS studies, 135
  films, AFM phase images, 134*f*
  films, high-resolution C1s spectra, 136*f*
  films, XPS wide-scan, 136*f*
  morphologies, 132*t*
  overview, 127
  phase separation behaviour, 131
  SAXS diagrams, 132*f*
  synthesis, 118, 128
  synthesized block copolymers, 129*c*
Borate, 28
  synthesis, 29*s*
Borate block copolymer micelles, 32*f*
Boronic acid, 28
  synthesis, 29*s*
Boronium block copolymers, 28
  synthesis, 29*s*
Branched glycopolymers via SCVCP, 263*s*
Butyl trithiocarbonate end group removal, 16, 18

C

CFStar1, 3 arm star PMMA, 93*f*
CFStar2, 5 arm star PMMA, 93*f*
CFStar3, 8-arm star PMMA, 94*f*
CFStar4, 21 arm star PMMA, 94*f*
Chain dimension, polyelectrolyte brushes preparation, 186
Characterization, 145
$CN(CH_3)_2C\text{-}PSt_n$, DSC curves, 23*f*
$CN(CH_3)_2C\text{-}PSt_n$, radical-induced reduction, 20*t*
Controlled radical polymerization (CRP)
  polymer primary structure control, 1
  polymer-inorganic hybrid materials, 163
  sequence-controlled CRP processes, 6
Core first PMMA star, dilute solution properties, 92
Core first PMMA star synthesis, 89
Core first star polymers, arms number quantification, 95
Core-functionalized star polymers, Ru-catalyzed living radical polymerization, 66*s*

Downloaded by 89.163.35.42 on May 30, 2012 | http://pubs.acs.org
Publication Date (Web): March 20, 2012 | doi: 10.1021/bk-2012-1101.ix002

Downloaded by 89.163.35.42 on May 30, 2012 | http://pubs.acs.org
Publication Date (Web): March 20, 2012 | doi: 10.1021/bk-2012-1101.ix002

CRP. *See* controlled radical polymerization (CRP)
CRP system classification, polymer-inorganic hybrid materials, 165
Crystal assembly reaction, polymer brushes, 251*f*

D

Diblock copolymers, Mark-Houwink plots, 54*f*
Direct Ru-encapsulation, microgel-core star polymers, 67*s*
DSC characterization, PE-b-POEGMA copolymers, 56
DSC curves
  block copolymers BC1 – BC5, 131*f*
  $CN(CH_3)_2C$-PSt$_n$, 23*f*
  CPDB-P*n*BA$_n$, 21*f*
  H-P*n*BA$_n$, 21*f*
  PABTC-P*n*BA$_n$, 21*f*
  PABTC-PSt$_n$, 22*f*
  PGMA macro initiator, 122*f*
  PGMA-b-PS block copolymer, 122*f*
DSC thermograms, 56*f*

F

Fabrication, polymer brushes, 242
FeCl2, PPh3-Star, 70*f*
Ferrocene containing methacrylate monomers synthesis, 199
Film preparation, block copolymers, 132
  nanostructured polymer films
    preparation, 132
  XPS studies, 135
Fluorescent glycopolymer hybrid nanoparticles, 265
Fluorine-condensed star polymers, 76
Fluorine-condensed star polymers, ruthenium-catalyzed living radical polymerization, 76*f*
Fluorous Molecular Recognition, 77
Friction coefficient, polyelectrolyte brushes preparation, 190*f*
Functionality determination, 87

G

Glucosamine-containing polymer brushes synthesis, 259*s*
Glycidyl methacrylate-containing resist polymer synthesis, 119
Glycocoplymer-grafted nanoparticles, 267*f*
Glycocoplymer-grafted nanospheres, 266*f*
Glycopolymer brushes, 260*f*
Glycopolymer-grafted DVB microspheres synthesis, 261*s*
Glycopolymer-grafted polystyrene nanospheres, 259
GPC elution curves, MIs, 59*f*
GPC elution traces, 50*f*
GPC elution traces, run 2, 60*f*
Graft copolymerization, PVDF, 223*s*, 225*s*
Grafted microspheres, bioactive glycopolymers, 265*f*
Gyration contraction factor, 85

H

^{1}H NMR characterization, PE-b-POEGMA copolymers, 55
1H NMR spectra, MI2, 59*f*
Hexadecane droplets, polyelectrolyte brushes preparation, 186*f*
High density polyethylene, 172
H-P*n*BA$_n$, DSC curves, 21*f*
H-P*n*BA$_n$, radical-induced reduction, 19*t*
Hyperbranched glycopolymer covered microspheres, 264*s*
Hyperbranched glycopolymer-grafted microspheres, 263
Hyperbranched/linear polyethylene macroinitiators, 46*t*

I

Indium tin oxide (ITO), SI-ATRP, 200
Intrinsic viscosity shrink factor, 86
Intrinsic viscosity study, PE-b-POEGMA copolymers, 54
ITO. *See* indium tin oxide (ITO), SI-ATRP
ITO-g-PFcMA-b-PMMA, SI-ATRP, 205*f*

K

Ketones
  Ru-PEG star-catalyzed transfer
    hydrogenation, 72*f*
  transfer hydrogenation, 72, 73*f*

Downloaded by 89.163.35.42 on May 30, 2012 | http://pubs.acs.org
Publication Date (Web): March 20, 2012 | doi: 10.1021/bk-2012-1101.ix002

L

- Lap shear adhesion strengths, polyelectrolyte brushes preparation, 192*f*
- Linear PMMA, Mark-Houwink plot, 94*f*
- Linear synthetic polymer chains, 9*f*
- Living radical polymerization, 74
- Log[η].M vs. elution volume, polymers, 83*f*

M

- M1 polymerization, 34*f*
- Magnetic glycopolymer hybrid nanoparticles, 265
- MALDI-TOF MS spectra
  - ω-allyl PMMA 3e, 110*f*
  - ω-benzoyl PBA 6, 111*f*
  - ω-benzoyl PMMA 3d, 109*f*
  - ω-benzoyl PNIPAM 8, 112*f*
  - ω-(δ-lacton)-substituted PMMA 4, 110, 111*f*
  - ω-methylester PMMA 3c, 109*f*
- MALLS, SEC, 84
- MAMan grafted microspheres, bioactive glycopolymers, 262*f*
- Mark-Houwink plots, 86
- Mark-Houwink plots, diblock copolymers, 54*f*
- Metal encapsulation, 69
- Metal-bearing star polymers, microgel-core catalysis, 71*f*
- Methyl methacrylate 3 arm star polymer synthesis, 89
- MI, GPC elution curves, 59*f*
- MI2, 1H NMR spectra, 59*f*
- Micelle behaviors, aqueous solution, 57
- Micelle size distributions, 57*f*
- Micelle solution preparation, PE-b-POEGMA copolymers, 44
- Microgel-core catalysis, 70
- Microgel-core catalysis, metal-bearing star polymers, 71*f*
- Microgel-core star polymers
  - fluorine-condensed star polymers, 76
  - fluorous molecular recognition, 77
  - ketones, transfer hydrogenation, 72
  - living radical polymerization, 74
  - metal encapsulation, 69
  - microgel-core catalysis, 70
  - overview, 65
  - Ru-bearing microgel-core star polymers, 66
  - sec-alcohols oxidation, 71
  - tandem catalyst interchange, 69
  - thermoregulated phase-transfer catalysis, 73
- MMA polymerisation, 90*s*
- MMA polymerisation, 3 arm initiator, 90*f*
- Monocleavable BA-ss-AB type triblock copolymer micelles, 297
- Mono-cleavable brush-like symmetric triblock copolymer synthesis, 297*f*
- Monomer conversion, PVDF, 218*f*
- M_p, various linear calibration standards, 82*f*
- Multi detector SEC, 87
- Multi-cleavable $A_{(ss)n}$-B type block copolymer, 292
- Multiple single scan lines, polymer brushes, 244*f*
- Mussel glue derived enzymes
  - bioconjugates, 281, 281*f*
  - conjugate IIIb, 282*f*
  - conjugation strategy, 275
  - NHS-functionalized chain transfer reagent synthesis, 276*f*
  - overview, 271
  - PNIPAM, 276*f*, 281*f*
  - synthesis, 275
  - tyrosinase, 273*f*, 278*f*
  - tyrosinase, circular dichroism spectra, 277*f*
  - tyrosinase assay, 277*f*
  - tyrosinase-PNIPAM conjugate, 279

N

- Nanoparticle synthesis, bioactive glycopolymers, 265*s*
- nBA polymerization, 15
- New monomers, SI-ATRP, 206
- NHS-functionalized chain transfer reagent synthesis, 276*f*
- Nitrilotriacetic acid end-functionalized polystyrenes (NTA-PS)
  - applications, 308
  - ATRP, 306*f*, 306*t*
  - characterization, 305
  - DLS data, 311*f*
  - fluorescence microscope images, 310*f*
  - gel permeation chromatogram, 307*f*
  - ^{1}H NMR spectra, 308*f*
  - mesoporous fibres formation, 311
  - micellar aggregates formation, 309
  - overview, 303
  - preparation, 305*s*
  - SEM images, 309*f*, 312*f*

Downloaded by 89.163.35.42 on May 30, 2012 | http://pubs.acs.org
Publication Date (Web): March 20, 2012 | doi: 10.1021/bk-2012-1101.ix002

  synthesis, 305
  TEM images, 309*f*, 311*f*, 312*f*
Nitroxide exchange reaction, polymer brushes, 247*s*
NMP initiator syntheses, 147
Number-average molecular weight dependencies, 61*f*

O

Octadecyl acrylate (ODA), 167
Octadecyl acrylate, ATRP, 168*t*, 169*f*, 170*f*, 171*f*
Octadecyl acrylate, IR spectra, 171*f*
Octadecyl acrylate polymerization, 168*s*
Octadecyl acrylate polymerization, ATRP, 169*f*
2-Octanone, transfer hydrogenation, 74*f*
ODA. *See* octadecyl acrylate (ODA)
ODA polymerization, polymer-inorganic hybrid materials, octadecyl acrylate polymerization, 178, 179
OEGMA, ATRP, 47
OEGMA, GPC curves, 48*f*
OEGMA conversion vs. kinetic plots, 49*f*
OEGMA conversion vs. polymerization time, 49*f*, 60*f*
OH-SS-iBuBr double-head initiator synthesis, 296*f*
Oligomers synthesis, 17
Organoboron polymers
  borate, 28
  boronic acid, 28
  boronium block copolymers, 28
  organoboron quinolate block copolymers, 33
  overview, 27
  star polymers, 33
Organoboron quinolate block copolymers, 33
Organoboron quinolate monomers, RAFT polymerization, 34*s*
Ozone pretreatment, PVDF, 223*s*, 225*s*

P

PABTC-PSt$_n$, DSC curves, 22*f*
PABTC-PSt$_n$, radical-induced reduction, 20*t*
PE MI synthesis, PE-b-POEGMA copolymers, 43, 45
PE-b-POEGMA copolymers. *See* polyethylene-block-poly[oligo(ethylene glycol) methacrylate] (PE-b-POEGMA) copolymers
PE-b-POEGMA synthesis, 52*t*
Perfluorinated compounds, fluorous recognition, 77*f*
PFcMA brushes, electrochemical properties of, 204
PGMA macro-initiator, 122*f*
PGMA macro-initiator, GPC traces, 120*f*
PGMA synthesis, 117. *See* poly(glycidyl methacrylate), ATRP macro initiator (PGMA) synthesis
PGMA-b-PS block copolymer, 122*f*
PGMA-b-PS block copolymer BCP1, 121*f*
PGMA-b-PS block copolymer phase separation, 123
PGMA-b-PS block copolymer synthesis, 119*s*
PGMA-b-PS photoresist block copolymers, photolithography, 123*s*
PGMA-b-PS photoresist films, 123*f*
PGMA-b-PS thin films, 124*f*
Phosphonic acid coupling agent synthesis, SI-ATRP, 199, 200*f*
Photolithographic patterning, 122
Photolithography, PGMA-b-PS photoresist block copolymers, 123*s*
Photolithography patterning, 118
PM1-b-PEO, 34*f*
PM2-b-PEO, 34*f*
PMMA 3-arm star polymer, 95*f*
PMMA 5-arm star polymer, 95*f*
PMMA 8-arm star polymer, 96*f*
PMMA 21-arm star polymer, 96*f*
PMMA arms, SEC curves, 68*f*
PMMA stars, Mark-Houwink plot, 94*f*
PMMA stars, SEC results, 92*t*
PnBA thermal properties, 20
PnBA$_n$ oligomers synthesis, 17*t*
PNIPAM-b-PS star polymers, 36*f*
PODA. *See* poly(octadecyl acrylate) (PODA)
PODA blends, 172
Polyelectrolyte brushes preparation
  adhesion process, 192*f*
  antifouling properties, 185
  chain dimension, 186
  chemical structures, 185*f*
  friction coefficient, 190*f*
  hexadecane droplets, 186*f*
  lap shear adhesion strengths, 192*f*
  overview, 183
  repeatable adhesion, 191
  schematic representation, 187*f*
  sliding velocity dependence, 189*f*
  tribological behavior, 188

Downloaded by 89.163.35.42 on May 30, 2012 | http://pubs.acs.org
Publication Date (Web): March 20, 2012 | doi: 10.1021/bk-2012-1101.ix002

  water, 186*f*
  wettability, 185
Polyethylene-block-poly[oligo(ethylene glycol) methacrylate] (PE-b-POEGMA) copolymers
  DSC characterization, 56
  ^{1}H NMR characterization, 55
  intrinsic viscosity study, 54
  materials, 43
  micelle behaviors, aqueous solution, 57
  micelle solution preparation, 44
  OEGMA, ATRP, 47
  overview, 39
  PE MI synthesis, 43, 45
  PE-b-POEGMA synthesis, ATRP, 43
  synthesis, 42*s*
PolyFcMA brushes, SI-ATRP, 201*f*, 203*f*, 204*f*
Poly(glycidyl methacrylate), ATRP, 120*t*
Poly(glycidyl methacrylate), ATRP macro initiator (PGMA) synthesis, 117
Poly(glycidyl methacrylate-block-styrene)
  ATRP, 120*t*
  block copolymer phase separation analysis, 118
  block copolymer synthesis, 118
  glycidyl methacrylate-containing resist polymer synthesis, 119
  overview, 115
  PGMA synthesis, 117
  PGMA-b-PS block copolymer phase separation, 123
  photolithographic patterning, 122
  photolithography patterning, 118
Polyhedral ogligomeric silsequioxane-core star polystyrene
  arm number determination, 157
  characterization, 145
  materials, 144
  NMP initiator syntheses, 147
  overview, 141
  POSS-MAMA-SG1, 2, 146
  POSS-NH_3+Cl^-, 145
  POSS-PS star polymer cleavage, 147
  star polystyrene, 146
  star PS, DSC studies, 159
  star PS synthesis, 150
Polymer brushes
  biomolecule immobilization, 251*s*
  crystal assembly reaction, 251*f*
  fabrication, 242
  multiple single scan lines, 244*f*
  nitroxide exchange reaction, 247*s*
  overview, 241
  polyolefin nanocomposites
    ATRP initiator synthesis, 174, 180
    2-bromoisobutyrate functional silica colloids synthesis, 175, 180
    ODA, ATRP, 175, 181
  radical nitroxide exchange reactions, 246
  schematic representation, 245*f*
  streptavidin, 246*f*
  structuring, 242
  surface initiated polymerization, 244*s*
  surface nitroxide exchange reaction, 248*f*
  synthesis, 242
  zeolite L crystals, 248, 249*s*, 252*f*
Polymer primary structure control
  overview, 1
  sequence-controlled CRP processes, 6
  sequence-defined polymer synthesis, 3
Polymer synthesis, polymer-inorganic hybrid materials, 167
Polymeric microsphere surface modification, 261
Polymer-inorganic hybrid materials
  ATRP, 166
  CRP, 165
  CRP system classification, 165
  high density polyethylene, 172
  ODA polymerization, octadecyl acrylate polymerization, 178, 179
  overview, 163
  PODA blends, 172
  polymer brushes, polyolefin nanocomposites
    ATRP initiator synthesis, 174, 180
    2-bromoisobutyrate functional silica colloids synthesis, 175, 180
    ODA, ATRP, 175
  polymer synthesis, 167
  surface modification, 174
Polymers, log[η].M *vs.* elution volume, 83*f*
Poly(methyl methacrylate) (PMMA) grafting
  ATRP grafting, 235*s*
  characterization, 233
  nitrogen adsorption isotherms, 236*f*
  overview, 231
  pore size distributions, 236*f*
  SBA-15 initiator immobilization, 233
  SBA-15 synthesis, 232
  surface-initiated ATRP, 233
  weight change patterns, 237*f*
Poly(methyl methacrylate) star polymers
  core first PMMA star, dilute solution properties, 92
  core first PMMA star synthesis, 89
  core first star polymers, arms number quantification, 95
  functionality determination, 87

Downloaded by 89.163.35.42 on May 30, 2012 | http://pubs.acs.org
Publication Date (Web): March 20, 2012 | doi: 10.1021/bk-2012-1101.ix002

    gyration contraction factor, 85
    intrinsic viscosity shrink factor, 86
    MALLS, SEC, 84
    Mark-Houwink plots, 86
    methyl methacrylate 3 arm star polymer synthesis, 88
    multi detector SEC, 87
    overview, 81
    1,1,1-tris(methyl-o-isobutyryl bromide) ethane synthesis, 88
Poly(*n*-butyl acrylate) (PBA) functionalization, 105*s*
Poly(*N*-isopropylacrylamide) (PNIPAM), MALDI-TOF MS spectra, 106*f*
Poly(*N*-isopropylacrylamide) (PNIPAM) functionalization, 105*s*
Poly(octadecyl acrylate) (PODA), 167
Poly(octadecyl acrylate), ^{1}H-NMR, 172*f*
Poly(octadecyl acrylate), IR spectra, 171*f*
Poly(octadecyl acrylate), SEM, 173*f*
Poly(vinylidene fluoride) (PVDF)
    functionalization via ATRP, 214*s*, 215
    functionalization via click chemistry, 220
    functionalization via CRP, 213*s*, 215*s*, 220
    functionalization via RAFT polymerization, 214*s*, 219
    graft copolymerization, 223*s*, 225*s*
    monomer conversion, 218*f*
    overview, 211
    ozone pretreatment, 223*s*, 225*s*
POSS-based alkoxyamine, 150*f*
POSS-MAMA-SG1, 148*f*, 149*f*, 152*f*, 153*f*, 156*f*, 157*f*, 158*f*
POSS-MAMA-SG1, 2, 146
POSS-MAMA-SG1 alkoxyamine 2, 151*t*
POSS-(MAMA-SG1)$_n$, 150*f*
POSS-NH$_3$+Cl$^-$, 144*s*, 145
POSS-PS star polymer cleavage, 147
POSS-(SG1)$_8$, 144*s*
PS star polymer synthesis, 154*f*
PSBA-b-PS self- assembly, 32*f*
PSBBr$_2$-b-PS, 31*f*
PSt thermal properties, 22
PSTMS-b-PS, 31*f*
PSt$_n$ oligomers synthesis, 18*t*
PVDF-g-PDMAEMA copolymer, 217*s*

R

Radical nitroxide exchange reactions, polymer brushes, 246
Radical-induced reduction
    CN(CH$_3$)$_2$C-PSt$_n$, 20*t*
    H-P*n*BA$_n$, 19*t*
    PABTC-PSt$_n$, 20*t*
RAFT polymerization. *See* reversible addition fragmentation chain transfer (RAFT) polymerization
Repeatable adhesion, polyelectrolyte brushes preparation, 191
Reversible addition fragmentation chain transfer (RAFT) polymerization
    analyses, 15
    butyl trithiocarbonate end group removal, 16, 18
    materials, 14
    nBA polymerization, 15
    oligomers synthesis, 17
    overview, 13
    PnBA thermal properties, 20
    PSt thermal properties, 22
    styrene polymerization, 16
Ru-bearing microgel-core star polymers, 66
Ru-catalyzed living radical polymerization
    core-functionalized star polymers, 66*s*
    microgel-core star polymers, 67*s*
RuCpCl-star-catalyzed living radical (co)polymerization, 75*t*
Run 2, GPC elution traces, 60*f*
Run 5 sample, 6 ^{1}H NMR spectra, 55*f*
Ru-PEG star-catalyzed transfer hydrogenation, ketones, 72*f*
Ru-star polymers, SEC curves, 68*f*

S

Schematic representation
    polyelectrolyte brushes preparation, 187*f*
    polymer brushes, 245*f*
Sec-alcohol oxidation, 71, 71*f*
Sequence-controlled CRP processes, 6
Sequence-controlled polymers, 2, 7*f*
Sequence-defined oligomers synthesis, 4*f*
Sequence-defined polymer, 2
Sequence-defined polymer synthesis, 3
Sheddable A-ss-B type biodegradable block copolymer micelles, 295
SI-ATRP. *See* surface initiated atom transfer radical polymerization (SI-ATRP)
SiO$_2$, PODA polymer brushes, 177*f*
SiO$_2$-PODA, TGA, 176*f*
Sliding velocity dependence, polyelectrolyte brushes preparation, 189*f*

Star polymer-catalyzed living radical polymerization, 74*f*
Star polymers, 33
  schematic representation, 83*f*
  SEC traces, 155*f*
  synthesis, 35*s*
  synthesis, ATRP, 91*f*
Star polystyrene, 146, 160*f*
Star PS, DSC studies, 159
Star PS synthesis, 150
Stimuli-responsive degradable block copolymer micelles, 290*f*
Streptavidin, 246*f*
Structuring, polymer brushes, 242
Styrene polymerization, 16, 156*f*, 157*f*
Surface initiated atom transfer radical polymerization (SI-ATRP)
  electrochemical characterization, 202
  ferrocene containing methacrylate monomers synthesis, 199
  ITO, 200
  ITO-g-PFcMA-b-PMMA, 205*f*
  new monomers, 206
  overview, 197
  phosphonic acid coupling agents synthesis, 199, 200*f*
  polyFcMA brushes, 201*f*, 203*f*, 204*f*
  vinylic ProDOT monomers synthesis, 206*f*
Surface initiated polymerization, 244*s*
Surface modification, polymer-inorganic hybrid materials, 174
Surface nitroxide exchange reaction, polymer brushes, 248*f*

T

Tandem catalyst interchange, 69
Tellurium-metal transmetallation reaction, ω-end functionalized polymers, 101
Thermoregulated phase-transfer catalysis, 73, 74*f*
Thiol-responsive degradable block copolymer micelles
  aqueous micellization, 289*f*
  cell viability, 298
  development strategies, 290
  monocleavable BA-ss-AB type triblock copolymer micelles, 297
  mono-cleavable brush-like symmetric triblock copolymer synthesis, 297*f*
  multi-cleavable $A_{(ss)n}$-B type block copolymer, 292
  OEOMA, 293*t*
  OH-SS-iBuBr double-head initiator synthesis, 296*f*
  overview, 287
  sheddable A-ss-B type biodegradable block copolymer micelles, 295
  ssABP, 292*f*, 294*f*, 296*f*, 298*f*, 299*f*
  stimuli-responsive degradable block copolymer micelles, 290*f*
Tribological behavior, polyelectrolyte brushes preparation, 188
Triple-detector GPC, 51*f*
1,1,1-Tris(methyl-o-isobutyryl bromide) ethane synthesis, 88
Tyrosinase, 273*f*, 278*f*

V

Vinylic ProDOT monomers synthesis, SI-ATRP, 206*f*

W

ω-alkynylated PNIPAM 9, 112
ω-allyl PMMA 3e, 110, 110*f*
ω-benzoyl PBA 6, 110, 111*f*
ω-benzoyl PMMA 3d, 108, 109*f*
ω-benzoyl PNIPAM 8, 112, 112*f*
ω-carboxylic acid PMMA 3b, 108
ω-deuterated PMMA 3a synthesis, 108
ω-(δ-lacton)-substituted PMMA 4, 110, 111*f*
ω-end functionalized polymers
  MALDI-TOF MS spectra, 103*f*
  overview, 99
  synthesis, 101*s*, 102*t*, 104
  tellurium-metal transmetallation reaction, 101
ω-end functionalized polymers synthesis, 108
Wettability, polyelectrolyte brushes preparation, 185
ω-methylester PMMA 3c, 108, 109*f*

Z

Zeolite L crystals, 248, 249*s*, 252*f*

Downloaded by 89.163.35.42 on May 30, 2012 | http://pubs.acs.org
Publication Date (Web): March 20, 2012 | doi: 10.1021/bk-2012-1101.ix002